BIOMATERIALS FOR ENGINEERING CELLULAR ENVIRONMENTS IN TISSUE ENGINEERING

EDITED BY: Hon Fai Chan, Hae-Won Kim and Xin Zhao
PUBLISHED IN: Frontiers in Bioengineering and Biotechnology

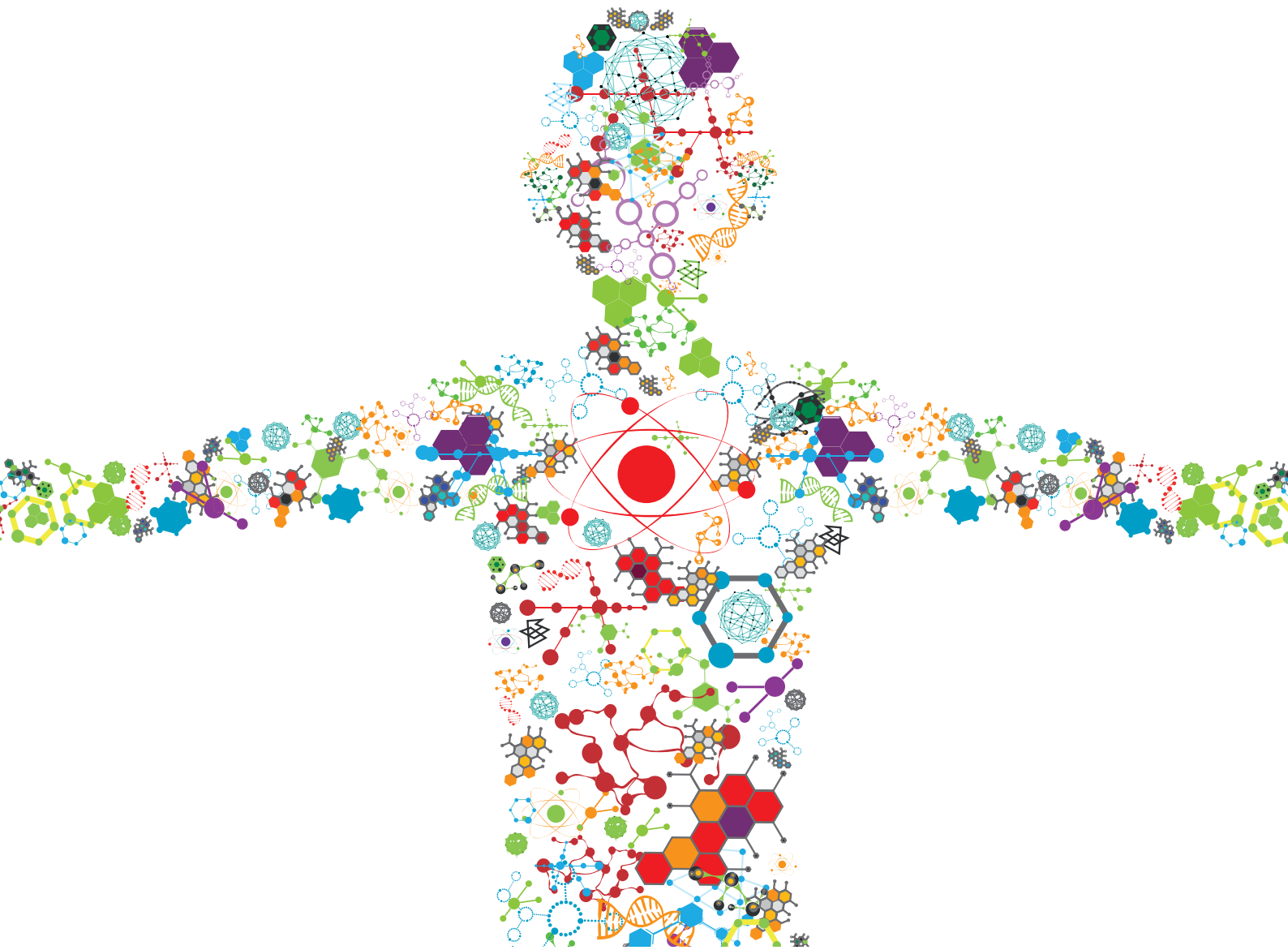

frontiers Research Topics

frontiers

ISSN 1664-8714
ISBN 978-2-88971-630-2
DOI 10.3389/978-2-88971-630-2

About Frontiers

Frontiers is more than just an open-access publisher of scholarly articles: it is a pioneering approach to the world of academia, radically improving the way scholarly research is managed. The grand vision of Frontiers is a world where all people have an equal opportunity to seek, share and generate knowledge. Frontiers provides immediate and permanent online open access to all its publications, but this alone is not enough to realize our grand goals.

Frontiers Journal Series

The Frontiers Journal Series is a multi-tier and interdisciplinary set of open-access, online journals, promising a paradigm shift from the current review, selection and dissemination processes in academic publishing. All Frontiers journals are driven by researchers for researchers; therefore, they constitute a service to the scholarly community. At the same time, the Frontiers Journal Series operates on a revolutionary invention, the tiered publishing system, initially addressing specific communities of scholars, and gradually climbing up to broader public understanding, thus serving the interests of the lay society, too.

Dedication to Quality

Each Frontiers article is a landmark of the highest quality, thanks to genuinely collaborative interactions between authors and review editors, who include some of the world's best academicians. Research must be certified by peers before entering a stream of knowledge that may eventually reach the public - and shape society; therefore, Frontiers only applies the most rigorous and unbiased reviews.
Frontiers revolutionizes research publishing by freely delivering the most outstanding research, evaluated with no bias from both the academic and social point of view. By applying the most advanced information technologies, Frontiers is catapulting scholarly publishing into a new generation.

What are Frontiers Research Topics?

Frontiers Research Topics are very popular trademarks of the Frontiers Journals Series: they are collections of at least ten articles, all centered on a particular subject. With their unique mix of varied contributions from Original Research to Review Articles, Frontiers Research Topics unify the most influential researchers, the latest key findings and historical advances in a hot research area! Find out more on how to host your own Frontiers Research Topic or contribute to one as an author by contacting the Frontiers Editorial Office: frontiersin.org/about/contact

BIOMATERIALS FOR ENGINEERING CELLULAR ENVIRONMENTS IN TISSUE ENGINEERING

Topic Editors:
Hon Fai Chan, The Chinese University of Hong Kong, China
Hae-Won Kim, Institute of Tissue Regeneration Engineering (ITREN), South Korea
Xin Zhao, Hong Kong Polytechnic University, Hong Kong, SAR China

Citation: Chan, H. F., Kim, H.-W., Zhao, X., eds. (2021). Biomaterials for Engineering Cellular Environments in Tissue Engineering.
Lausanne: Frontiers Media SA. doi: 10.3389/978-2-88971-630-2

Table of Contents

frontiers in Bioengineering and Biotechnology

ORIGINAL RESEARCH
published: 23 June 2020
doi: 10.3389/fbioe.2020.00616

A Polydopamine-Functionalized Carbon Microfibrous Scaffold Accelerates the Development of Neural Stem Cells

Yanru Yang[1], *Yuhua Zhang*[2], *Renjie Chai*[2,3,4,5]* *and Zhongze Gu*[1]*

[1] State Key Laboratory of Bioelectronics, Southeast University, Nanjing, China, [2] Key Laboratory for Developmental Genes and Human Disease, Ministry of Education, Institute of Life Sciences, Southeast University, Nanjing, China, [3] Co-innovation Center of Neuroregeneration, Nantong University, Nantong, China, [4] Institute for Stem Cell and Regeneration, Chinese Academy of Science, Beijing, China, [5] Jiangsu Province High-Tech Key Laboratory for Bio-Medical Research, Southeast University, Nanjing, China

Neuroregenerative medicine has witnessed impressive technological breakthroughs in recent years, but the currently available scaffold materials still have limitations regarding the development of effective treatment strategies for neurological diseases. Electrically conductive micropatterned materials have gained popularity in recent years due to their significant effects on neural stem cell fate. Polydopamine (PDA)—modified materials can also enhance the differentiation of neurons. In this work, we show that PDA-modified carbon microfiber skeleton composites have the appropriate conductivity, three-dimensional structure, and microenvironment regulation that are crucial for the growth of neural stem cells. The design we present is low-cost and easy to make and shows great promise for studying the growth and development of mouse neural stem cells. Our results show that the PDA-mediated formation of electrically conductive and viscous nanofiber webs promoted the adhesion, organization, and intercellular coupling of neural stem cells relative to the control group. PDA induced massive proliferation of neural stem cells and promoted the expression of Ki-67. Together, our results suggest that the composite material can be used as a multifunctional neural scaffold for clinical treatment and *in vitro* research by improving the structure, conductivity, and mechanical integrity of the regenerated tissues.

Keywords: three-dimensional scaffolds, biomaterials, polydopamine, carbon microfiber, neural stem cell

OPEN ACCESS

Edited by:
Xin Zhao,
Hong Kong Polytechnic University,
Hong Kong

Reviewed by:
Baolin Guo,
Xi'an Jiaotong University, China
Yun Qian,
Shanghai Jiao Tong University, China

***Correspondence:**
Renjie Chai
renjiec@seu.edu.cn
Zhongze Gu
gu@seu.edu.cn

Specialty section:
This article was submitted to Biomaterials, a section of the journal Frontiers in Bioengineering and Biotechnology

Received: *24 February 2020*
Accepted: *20 May 2020*
Published: *23 June 2020*

Citation:
Yang Y, Zhang Y, Chai R and Gu Z (2020) A Polydopamine-Functionalized Carbon Microfibrous Scaffold Accelerates the Development of Neural Stem Cells. Front. Bioeng. Biotechnol. 8:616. doi: 10.3389/fbioe.2020.00616

INTRODUCTION

Neurodegenerative diseases lead to severe sensory and motor damage in the human body and are among the leading causes of social disability and death globally, and the lack of transplantable nerve tissue is the prime hindrance to clinical nerve repair. Due to their multipotency and self-renewal, neural stem cell (NSC) transplantation therapy is one of the most promising strategies for treating traumatic injuries and neurodegenerative disorders. *In vitro* NSC expansion (to increase NSC resources) through nerve tissue engineering (NTE) methods might provide the most effective way to solve this clinical shortage. The ideal tissue engineered nerves are composed of scaffold materials, a microenvironment that induces or promotes cell growth, and NSCs. Biomaterials and

their biocompatible modifications, for example, oriented substrates like electrospun microfibers, conductive materials such as graphene, and ordered materials like photonic crystals are gaining widespread use in the field of NTE applications because the scaffolds have shown the unique characteristics of topological cues and bioelectric properties for mimicking the extracellular matrix (ECM) or for performing other functions (Martino and Pluchino, 2006; He et al., 2012; Limongi et al., 2018).

In recent years, electrospinning technology has generated considerable interest in fabricating tissue engineering biomaterials, mainly due to the morphological and structural properties of such materials, which almost perfectly mimic the fibrillary 3D architecture of the natural ECM (Carlberg et al., 2009; Zhu et al., 2018). Furthermore, an increasing body of evidence suggests that NSC fate—including cell adhesion, differentiation, migration, and proliferation—is greatly affected by the pattern of biochemical, physical, and topographical properties that constitute the essential elements of their niches *in vivo* (Kam et al., 2008; Heo et al., 2011; Yang et al., 2012; Ma et al., 2016). The electrospun scaffolds with aligned fibers display the versatility of ECM mimicry, which required in NTE, and several studies have been performed using this feature of electrospun fibers to induce the differentiation of NSCs. Gregory et al. fabricated electrospun polyethersulfone fiber mesh to study the influence of different fiber diameters of electrospun substrates on rat hippocampus-derived adult NSC differentiation and proliferation (Christopherson et al., 2009). Qi et al. produced a versatile substrate for insulin-like growth factor 1 delivery in a graphene oxide-incorporated poly (lactic-co-glycolic acid) electrospun nanofibrous mat and found improved NSC survival, diffusion, and differentiation (Qi et al., 2019). The electrospun micro- or nanofibers that the cells are interfacing with influence NSC growth, and the physical properties of the spun materials (such as electrical conductivity, mechanical strength, etc.) guide the development of NSCs. Neurons are electroactive cells, and cell dysfunction is also closely related to electrical activity. Electrical stimulation can induce depolarization of excitatory cell membranes and induce functional neuronal responses, and thus conductive materials could be a promising option for applications in NTE. To date, conductive biomaterials have been widely used for tissue engineering, such as they can apply in skin wound healing (He et al., 2000), 3D myoblast guidance (Wang et al., 2015), peripheral nerve tissue engineering (Wu et al., 2016) and engineered 3D cardiac anisotropy (Wu et al., 2017) and so on. Neuronal cells are quickly excited and transmit electrical signals in one direction, and the use of conductive electrospun nerve scaffolds to promote autologous nerve repair has become a trend in recent years. The electrical stimulation on theses scaffolds might also be an important factor for facilitating neurite extension and differentiation (Koppes et al., 2016; Granato et al., 2018; Uz and Mallapragada, 2019). Cellulose has excellent conductivity after carbonization, so it is a great original material for conductive electrospinning technology.

Polydopamine (PDA) is a highly viscous and highly adsorbent polymer membrane alkaline formed by the self-polymerization of the neurotransmitter dopamine. PDA has the characteristics of a polyelectrolyte in a primary environment due to the deprotonation of the catechol group. Thus, in the presence of alkaline *p*H, an electrostatic interaction is generated between the PDA and cationic polyelectrolytes. Alternating deposition on the surface of the material allows PDA to self-assemble the biomaterials layer by layer (Lee et al., 2007; Wei et al., 2010; Faure et al., 2013). PDA can form a tightly adhering composite layer on the surface of almost any solid material, and this one-step modification is efficient, versatile, cost-effective, and environmentally friendly. Thus, PDA-mediated surface coating methods can be used to modify a wide variety of biomaterials for a diverse array of functional applications in stem cell-based tissue engineering. As an example, Wu et al. demonstrated that a PDA-based coiled polycaprolactone scaffold could promote mesenchymal stem cell differentiation (Shin et al., 2011). Another group studied the combined effects of PDA functionalization and collagen on micro-grated polydimethylsiloxane and showed that the material improved the culture of human mesenchymal stem cells (Sharma et al., 2019). These studies have shown that PDA-modified biomaterials can stimulate neurons and guide axonal extension even in the absence of some functions such as conductivity, topography, and microenvironment control. However, as Yang et al. (2018) proposed, the existing studies have not considered adding such factors together to regulate NSC growth behavior and thus identify more efficient and economical methods for use in NTE. Therefore, the combination of a PDA functionalized scaffold and carbonized electrospun fiber with unique electrochemical properties might be a new strategy for the design of biomaterials and microenvironments for NTE.

The goal of this study was to develop an electrically conductive and adherent 3D scaffold and to examine the effect on NSC development by combining the effects of PDA functionalization and electrical stimulation with 3D structures. Our results indicate that compared to the untreated carbon fiber (CF) group, the PDA-mediated collection of electrically conductive and viscous microfiber webs improved the adhesion, organization, and intercellular coupling of NCSs. The presence of PDA resulted in a significantly increased proliferation of NSCs and increased expression of Ki-67. Representative 3D reconstructions of confocal microscope images demonstrated that NSCs quickly grew into the interior of the PDA-CF but only accumulated across the surface of the CF scaffold. The expression of vinculin by NSCs was also significantly enhanced in NSCs grown on PDA-CF compared to those grown on CF. These results indicate that PDA promotes the adherence and proliferation of NSCs on the conductive 3D CF skeleton and thus that PDA-CF might be used to prepare multifunctional neuron scaffolds for both treatments and for *in vitro* research.

MATERIALS AND METHODS

Fibrous Scaffold Fabrication

To prepare microfibers, surgical cotton batting (DP of 1140) was ultrasonically washed with absolute ethanol for at least 2 h and dried under vacuum at 50°C and then ground into a powder. The electrospinning solution (1.1 wt%) was prepared

by dissolving the fine cellulose particles in lithium chloride/N, N-dimethylacetamide (Kim et al., 2005) for 12 h at room temperature. The cellulose solution was loaded into a 30 ml syringe and pushed through a 0.86 mm inner diameter stainless-steel needle with a set flow rate of 0.2 ml/min and a 20-kV high-voltage source. The distance between the needle and the collector was set at 20 cm. The electrospun fibrous scaffolds were finally peeled off from the screen (the aluminum foil), run through a solid-phase extraction column (Dong qi Bio-technology Co., China), and dehydrated in a CO_2 critical point dryer (HCP-2, Hitachi Ltd) before subsequent carbonization.

Characterization of the CF Scaffold

The physicochemical properties of the surfaces of the tested materials were determined by Raman spectrometry (RAMAN, inVia, Renishaw Inc.) with a 532 nm laser. To conduct the wettability test, the samples were placed on a microscope slide and pressed slightly to smooth the surface and the contact angle was measured (JC2000D, Powereach, China). The morphological features of the materials were determined by sputter coating with a gold layer using a Hitachi E-1010 ion sputter (Hitachi, Ltd., Japan) and then imaging by scanning electron microscopy (SEM, Zeiss Ultra Plus, Germany). The elemental composition of the material was determined in real-time using an X-Max Energy Dispersive Spectrometer (EDS). The particular PDA-CF and CF groups of the sample were identified by Vertex 70-type Fourier-transform infrared spectroscopy (FT-IR). A 5–10 mg sample was mixed with potassium bromide and pressed into thin slices, and the test was performed in transmissive mode with 32 scans.

Isolation and Culture of NSCs

The NSCs were isolated from the hippocampus zones of embryonic day 18.5 wild-type mouse brains. The hippocampus was removed and collected in a 1.5 ml centrifuge tube and then dissociated by Accutase (Gibco, USA) for 25 min in a 37°C incubator. The tissue was triturated mechanically by using pipet tips. NSCs were suspended in DMEM-F12 medium (Gibco, USA) containing 2% B-27, 20 ng/ml EGF, and 20 ng/ml FGF (R&D Systems, USA) and cultured in a humidified atmosphere with 5% CO_2 at 37°C. The passage of NSCs was performed every 7 days during culturing. Before seeding, the CF and PDA-CF scaffolds were coated with laminin (10 μg/ml, 37°C overnight). After purifying three generations, the NSCs for the proliferation studies were seeded at a concentration of 5 × 105 cells/ml in proliferation medium consisting of DMEM-F12 medium with 2% B-27 supplemented with 20 ng/ml EGF and 20 ng/ml FGF. For the differentiation studies, NSCs were seeded at a similar concentration in DMEM-F12 medium containing 2% B-27 supplemented with fetal bovine serum (GIBCO, USA) and 1 μM retinoic acid (Sigma). The care and use of animals in these experiments followed the guidelines and protocols approved by the Care and Use of Animals Committee of Southeast University. All efforts were made to minimize the number of animals used and their suffering.

SEM Observation of NSCs Cultured on PDA-CF

After culturing for 5 days, NSC cultures were washed with PBS two times and then fixed with 2.5% glutaraldehyde overnight at 4°C. The samples were dehydrated by an ethanol gradient series (30, 50, 70, 80, and 90%), lyophilized, sputter-coated with gold for 2 min, and then analyzed by SEM (Zeiss Ultra Plus, Germany).

Cell Viability/Proliferation Assay

Cell viability and proliferation were assessed by CCK-8 assay. After culturing in proliferation media for 3 days, NSCs were incubated with CCK-8 reagent (diluted 20-fold in culture medium) for 2 h before the media were collected. The tetrazolium salt in CCK-8 is reduced by dehydrogenase in the cytoplasm to produce a yellow color. The intensity of the yellow color—which corresponds to the number of viable cells—was analyzed by a plate reader at 450 nm.

At the same time, after 5 days of culture cell viability was tested using the LIVE/DEAD viability/cytotoxicity kit for mammalian cells (Invitrogen, USA) according to the manufacturer's instructions. The percentage of living cells was calculated by determining the percentage of calcein-AM–positive cells out of the total cell number.

Immunofluorescence Staining of Cultured NSCs

NSCs were washed with PBS and fixed in 4% paraformaldehyde (PFA) for 30 min at room temperature, followed by blocking with PBS (pH 7.4) containing 5% donkey serum, 0.1% Triton X-100, 0.02% sodium azide (NaN_3), and 1% bovine serum albumin for 1 h at room temperature. This was followed by overnight incubation with primary antibodies at 4°C. Immunostaining was resumed by washing with PBS and incubating with secondary antibody (Invitrogen) for 1 h at room temperature followed by washing and then mounting in antifade fluorescence mounting medium (DAKO). The antibodies used in this study were anti-Ki-67, anti-TuJ1, and anti-nestin (Abcam, USA). Cell proliferation was measured with the Click-it EdU imaging kit (Invitrogen). Three independent experiments were repeated for each assay.

RNA Extraction and RT-PCR

The RNA isolation, reverse transcription, and PCR analysis were performed following standard protocols. Briefly, total cellular RNA was isolated using TRIzol reagent (Life Technologies), 1 μg of RNA was reverse transcribed using TaqMan Reverse Transcription Reagents (Applied Biosystems), and the mRNA levels of the indicated genes were measured in triplicate using the SYBR Green master mixture (Applied Biosystems) and a Chromo-4 real-time RT-PCR instrument (MJ Research). The mRNA levels were normalized to GAPDH (internal control), and gene expression was presented as fold changes (Ct method).

Statistical Analysis

All experiments were repeated three times in triplicate for each assessment, and all data are expressed as the mean ± standard deviation. Data were analyzed by one-way by Tukey's tests, and a p of <0.05 was considered statistically significant.

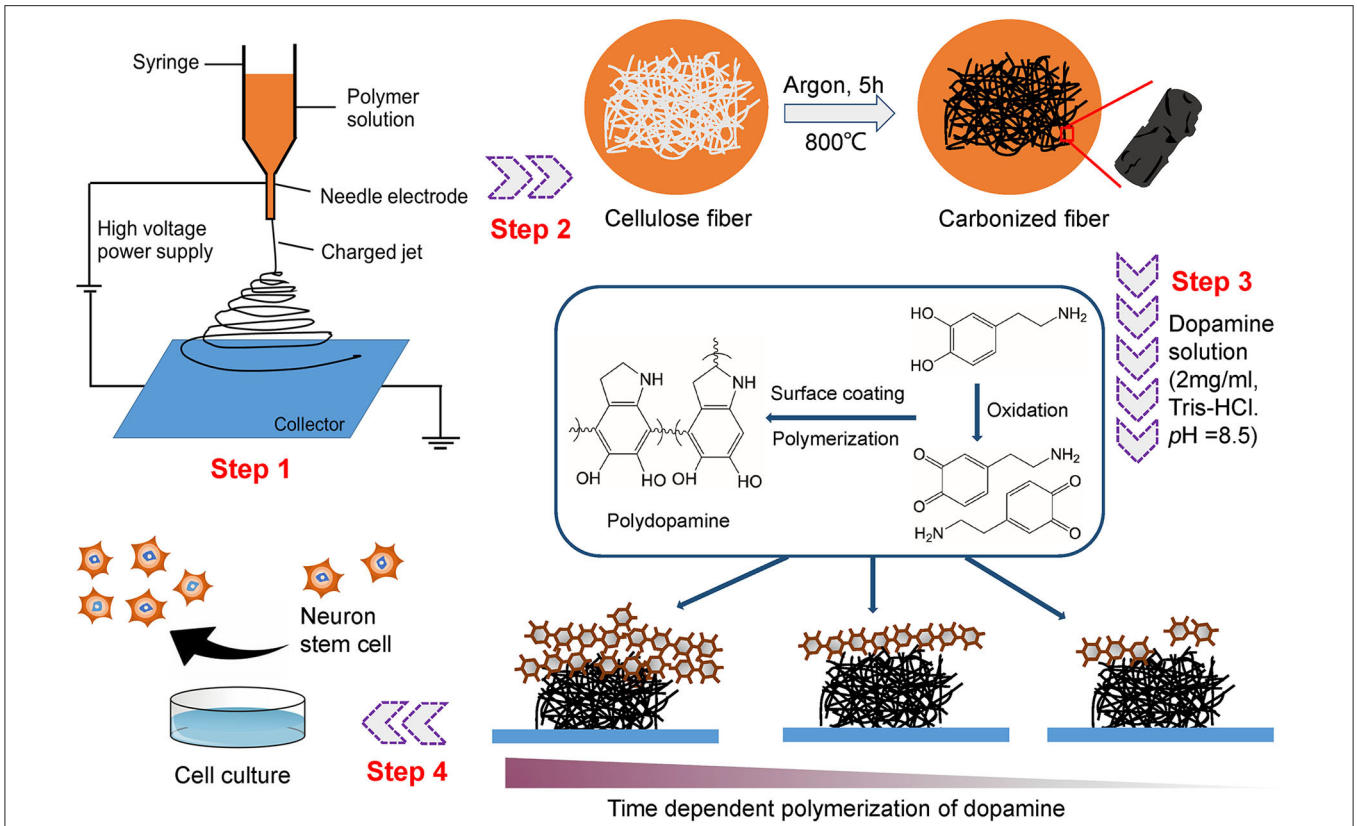

FIGURE 1 | Schematic diagram illustrating the preparation of the 3D PDA-CF used for NSC culture.

RESULTS AND DISCUSSION

Fabrication and Characterization of the PDA-CF Scaffold

Figure 1 shows the overall procedure for the fabrication of the PDA-CF scaffold and its application in NSC culture. First, the cellulose microfibers were fabricated from natural cellulose by electrospinning, and the cellulose fibers formed carbon aerogels after high-temperature carbonization (heat treatment in the tube furnace at 800°C for 5 h). The synthesis of PDA is depicted in step 3. Dopamine (2.0 mg/ml) was used as the precursor, and CFs doped with PDA self-assembled under alkaline conditions. The carbonized fibers show excellent flexibility which can be bent into different angles and folded as Li et al. (2016) presented in their study, the material was finally fixed on a circular cover glass with a diameter of 1 cm (**Figure 2A**).

The morphological features of the tested materials before and after dopamine treatment were characterized by SEM. The CFs (**Figure 3A**) retained almost all the topological cues from electrospinning before thermal annealing. In the image of PDA-CF (**Figure 3B**), it can be seen that the CF surface was very rough and that the fibers were covered with clusters of particles that we speculated were the PDA layer. Further evidence for this came from the EDS analysis and images (**Figures 2C,D**). The carbon content of the untreated CF was 99.84%, and the nitrogen content was only 0.16%. After dopamine treatment, the nitrogen content increased to 16.97%, and because the additional nitrogen mainly derived from the PDA layer, this indicated that PDA had effectively been deposited onto the CF.

FT-IR (**Figure 2E**) also illustrated this point. The analysis of the material by infrared spectroscopy showed a straight line for CF with no absorption vibration peaks. This result is consistent with the characteristics of the material itself because the cotton cellulose material is a pure carbon sample after high-temperature carbonization. The infrared absorption of PDA-CF varied between 1200 and 1600 cm^{-1}. According to the literature, 1512 cm^{-1} is the absorption peak of N–H, and 1284 cm^{-1} is the tensile vibration peak of a typical polymer C=O, both of which are characteristic absorption peaks in the PDA structure (Kim et al., 2005; Wang et al., 2008; Tang et al., 2015; Li et al., 2016). Taken together the results of SEM, EDS, and FI-IR analysis confirmed that PDA successfully coated the surface of the CFs.

The Raman analysis (**Figure 2F**) showed two peaks for graphite, one at 1,596 cm^{-1} corresponding to the G band and one at 1,350 cm^{-1} corresponding to the D band (Li et al., 2016). The conductivity test (**Figure 2B**) showed that the PDA-CF was electrophysiologically functional. Furthermore, we calculated the resistance from the I-V curve of the CF and PDA-CF scaffolds and found that the PDA-CF had a greater resistance (around 1,200 Ω in an area of 500 mm × 500 mm) compared to the

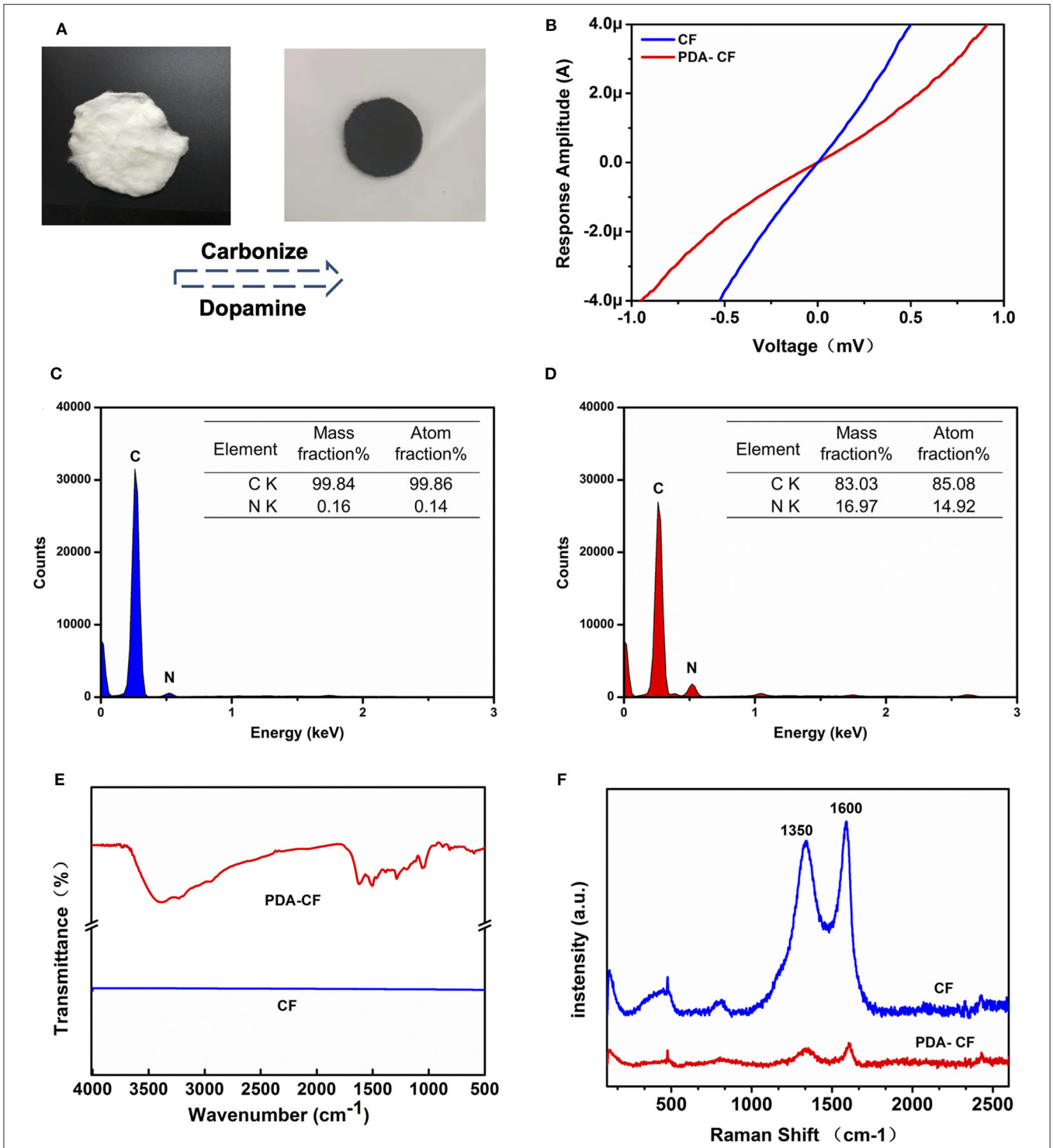

FIGURE 2 | Characterization of the PDA-CF scaffold. **(A)** Cellulose fiber (left) and the fixed PDA-CF (right) after carbonization and dopamine polymerization treatment. **(B)** I-V curve indicated that the PDA-CF has advanced electrophysiological function. **(C,D)** The EDS spectral analysis. **(E)** FT-IR spectra of the samples. **(F)** Raman spectra of the samples using an incident laser wavelength of 632.8 nm.

CF (540 Ω). The main reason for this difference might be that the adhesion of the PDA reduces the conductivity of the material. As carbonized cellulose microfibers are in highly dense and hydrophobic before PDA modification, the solution is not entirely covering the surface, leading to the PDA layer coat on CF as particle clusters, which is the best method to protects the

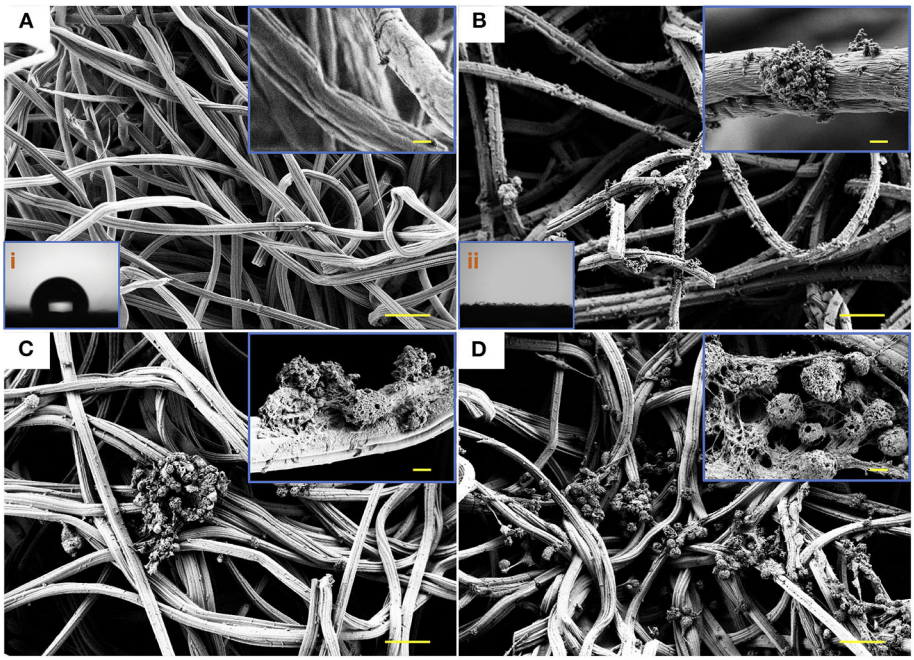

FIGURE 3 | SEM micrographs and water contact angle. SEM images illustrating the networked surfaces of CF **(A)** and PDA-CF **(B)** and the water contact angle (i and ii) of the two materials. The growth of NSCs cultured on CF **(C)** and PDA-CF **(D)**. Scale bars in the high-magnification images are 20 μm, and in the low-magnification images are 0.5 μm.

conductive properties of the materials. We further analyzed the water contact angle [**Figures 3A**(i),**B**(ii)] on the CF and PDA-CF substrates. Due to the hydrophobic nature of the CF material itself, the water does not wet it and instead forms beads on the surface of the sample. In contrast, water droplets on the PDA-CF surface quickly penetrate the sample layer, and no beads of water are visible on the surface of the sample. Thus, the PDA modification transforms the relatively hydrophobic CF material into a highly hydrophilic material, which is beneficial for the adhesion and growth of cells.

The Biocompatibility of PDA-CF

We isolated and amplified NSCs from the hippocampus of fetal mice and seeded them on the PDA-CF and CF scaffolds. In most of the SEM observations, as illustrated in **Figures 3C,D**, the PDA-CF scaffold seemed to enhance NSC proliferation. The calcein acetoxymethyl ester (calcein-AM) and ethidium homodimer-1 (EthD-1) staining assays were used to evaluate the cytotoxicity of PDA-CF. As shown in **Supplementary Figure 1A**, almost 83% of the cells cultured on PDA-CF for 5 days were alive, and there were significant differences between PDA-CF and CF in terms of cell viability (**Supplementary Figures 1B,C**), thus suggesting that PDA-CF has exceptional biocompatibility.

The cells were stained with DAPI after culturing on the scaffolds for 1 day, 5 days, and 10 days, and representative 3D reconstructions were made of the confocal microscope images with different colors showing cells at different depths. From the z-axis, we found that NSCs grew quickly into the interior of the PDA-CF after 5 days of cell culturing (**Figure 4A**), while NSCs primarily expanded along the surface of the CF scaffold. We also measured the cell infiltration depth on the two materials (**Figure 4B**), and the results were consistent with what we observed directly from the images. The greater infiltration of NSCs grown on PDA-CF suggests that PDA-CF might promote cell migration and cell viability.

NSC Proliferation on PDA-CF

The effect of PDA-CF on NSC proliferation was assessed by Ki-67, nestin, and 5-ethynyl-2′-deoxyuridine (EdU) immunofluorescence staining. The Ki-67 protein, which is required for cell division, is an active mitotic marker of proliferating cells during neurogenesis. Nestin is the intermediate filament protein for labeling and identifying NSCs. EdU is a thymidine analog that is incorporated into replicating chromosomal DNA during the S phase of the cell cycle and is widely employed to measure cell proliferation in the nervous system (Scholzen and Gerdes, 2000; Chehrehasa et al., 2009; Park et al., 2010). The expression of Ki-67 protein after 5 days of culture is presented in **Figure 5A**, and quantification (**Figure 5B**) showed that NSCs cultured on PDA- CF had a greater number of Ki-67–positive cells. The CCK-8 results (**Figure 5C**) suggested that PDA-CF could promote cell proliferation better than CF.

The percentage of EdU-positive cells (**Figure 6A**) also showed that NSCs grew better on the PDA-functionalized scaffold. After the NSCs were cultured for 1 day, the NSCs were treated with 10 μM EdU to label the mitotic cells. To quantify the proliferating NSCs, we stained the NSCs for the stem cell marker nestin.

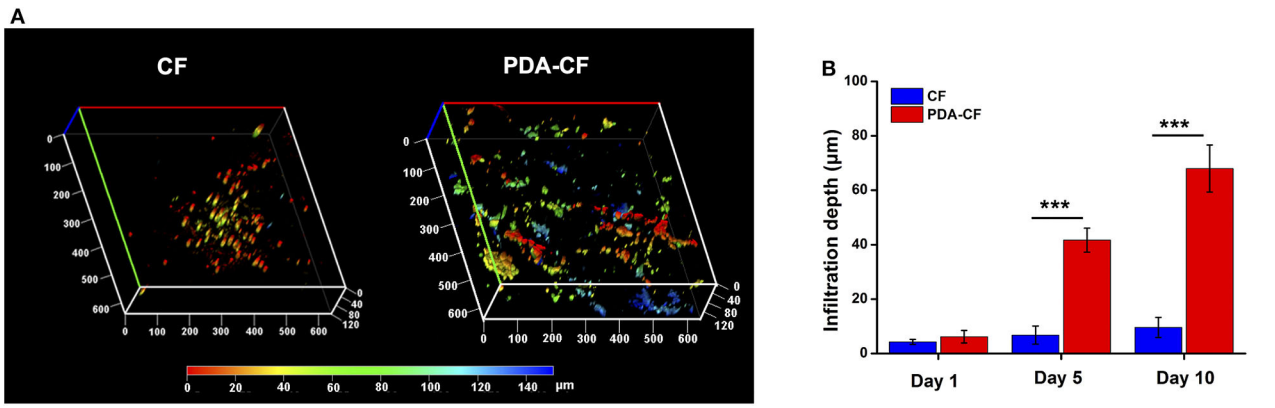

FIGURE 4 | Representative 3D reconstructions of confocal laser scanning microscopy mapping **(A)** after 5 days of culture. The depth of cell growth on the materials can be seen from the z-axis. **(B)** Mean infiltration depths on the CF and PDA-CF scaffolds (*$p < 0.05$; **$p < 0.005$; ***$p < 0.0005$).

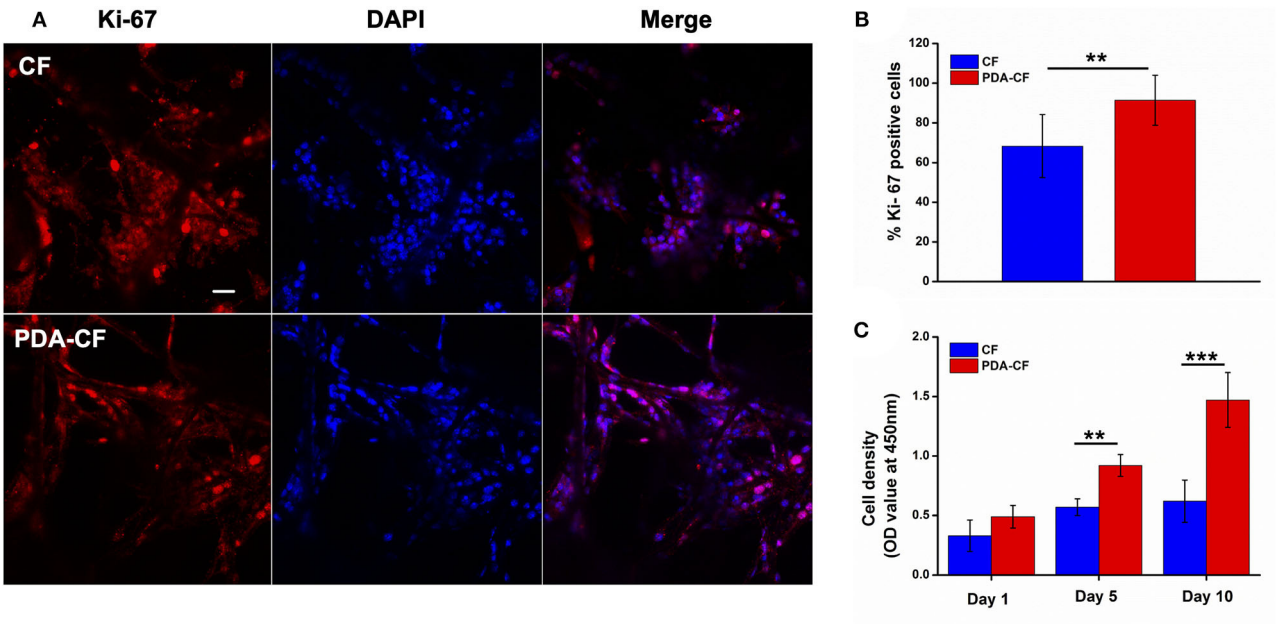

FIGURE 5 | PDA-CF increased the proliferation of NSCs compared to the CF control. **(A)** Laser scanning confocal microscopy in NSCs showing immunostaining of Ki-67 and DAPI staining. **(B)** The proportions of Ki-67–positive cells after 5 days of culture. **(C)** CCK-8 analysis of relative cell viability. Scale bar is 50 μm (**$p < 0.005$; ***$p < 0.0005$).

After 3 days, the number of EdU-positive NSCs on the PDA-CF scaffold was significantly greater than on the CF scaffold. Quantification of the EdU-positive cells (**Figure 6B**) showed that the mean proportion of EdU-positive cells on the PDA-CF scaffold was 87.43%, but was only 68.9% on the CF scaffold. These results suggested that PDA-CF could substantially promote the proliferation of NSCs.

Change in Expression of Adhesion Factors

Cell adhesion plays an essential role in regulating cell proliferation, differentiation, migration, and apoptosis. The SEM micrographs in **Figure 3D** show that NSCs adhered well to the scaffold surface. The association between NSCs proliferation processes and adhesion factor expression needs to be verified. To assess NSC adhesion, the gene expression of paxillin, focal adhesion kinase (FAK), integrin β, and vinculin was measured by quantitative real-time PCR using GAPDH as the control. Vinculin is a cytoskeletal protein associated with focal adhesion that regulates cell proliferation (Bays and DeMali, 2000). For NSCs cultured on PDA-CF for 3 days, immunohistochemistry showed increased expression of vinculin protein (**Figure 7A**), and quantification of vinculin (**Figure 7B**) showed increased expression compared to the CF group, which suggests that PDA might promote NSC proliferation by regulating the expression of vinculin. The interaction between integrins and the ECM induces the expression of paxillin, which is a central component

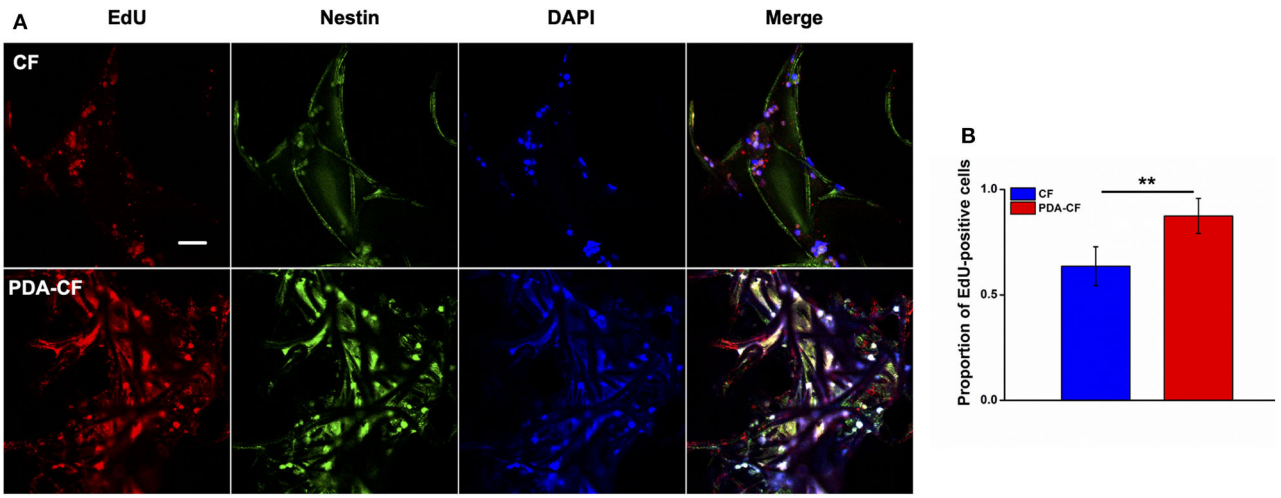

FIGURE 6 | Immunofluorescence staining of EdU and nestin in NSCs cultured for 3 days on the CF and PDA-CF scaffolds. **(A)** The proliferation of NSCs assessed by EdU staining (red), with nestin (green) indicating NSCs. **(B)** Quantification of the EdU-positive NSCs cultured on CF and PDA-CF. Scale bar is 50 μm. The data are presented as the mean ± SD; $^{*}p < 0.05$, $^{**}p < 0.01$.

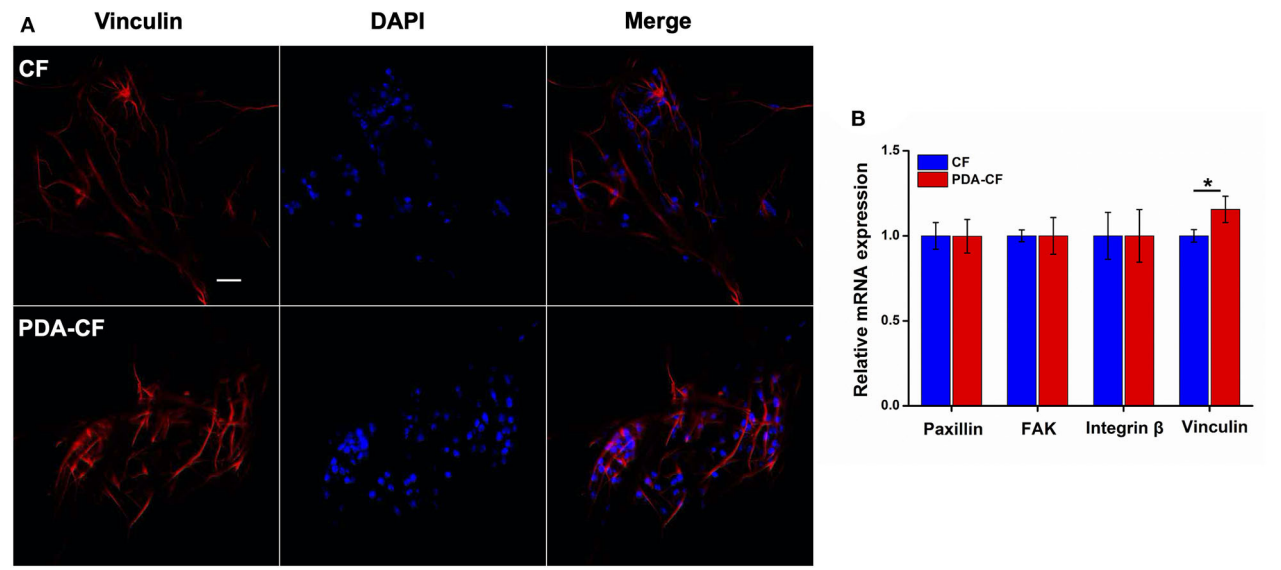

FIGURE 7 | Immunofluorescence images and adhesion molecule gene expression in NSCs cultured on CF and PDA-CF for 3 days. **(A)** NSCs were stained with vinculin (red) and DAPI (blue), and the images were merged. **(B)** mRNA expression of paxillin, FAK, integrin, and vinculin in NSCs cultured on CF and PDA-CF. Only vinculin was significantly up-regulated after culturing on PDA-CF. Scale bar is 50 μm. The data are presented as the mean ± SD; $^{*}p < 0.05$, $n = 3$.

of focal adhesion complexes and plays a vital role in cell attachment, spreading, and migration through the transduction of extracellular signals into intracellular responses (Lo'pez-Colome et al., 2017; Ma and Hammes, 2018). Cells attach to the ECM through trans-membrane integrin proteins and use these interactions to sense their environment (Kechagia et al., 2019). We measured the expression of integrin β by quantitative real-time PCR, and we found no significant changes between the two groups, which means that the proliferation of NSC on PDA-CF has no relationship with this biomolecule synthesis. In addition, we also assayed the expression of FAK, which is a cytoplasmic non-receptor tyrosine kinase that enables activation by growth factor receptors or integrins in various types of human cancers. It is a critical regulator in promoting cancer proliferation (Bullard Dunn et al., 2010; Tai et al., 2015). While from the results, the characteristics of PAD-CF scaffold seems to have no effect on the expression of FAK. In conclusion, PDA-CF might influence vinculin protein and thus regulate NSC proliferation.

In addition, we explored the effect of the PDA-CF scaffold material on the differentiation of NSCs using βIII-tubulin (TuJ1),

the expression of which has been widely used as a marker of early neuron development (Ambasudhan et al., 2011). We measured the immunofluorescence staining of TuJ1 at 1 day, 5 days, and 10 days after NSC seeding, and during the period of differentiation detection TuJ1 was expressed weakly in both the PDA-CF and CF groups and there was no significant difference between the two groups (**Supplementary Figure 2A**). Meanwhile, quantitative analysis of the NSC differentiation-related genes *Gap*, *Map2*, and *TuJ1* indicated that there was no significant difference in the expression levels between the various genes in cells grown on the two scaffolds (**Supplementary Figure 2B**). As a result, NSCs did not differentiate into neural cells on the PDA-CF scaffold any more so than on the CF control scaffold.

CONCLUSION

The difficulty in achieving functional recovery after nerve injury results in overwhelming medical costs and psychological burden, and thus there is a great need for methods to prevent neuronal cell loss and to promote nerve repair. The replacement of autologous nerves by nerve cells generated through NTE is a current research focus, and the development of biomimetic ECM is also of great importance. In addition, electrical stimulation of neurons in the absence of topographical features has been shown to guide axonal extension. In this paper, we have developed a low-cost and straightforward method for modifying 3D carbon microfibrous scaffolds with PDA to create a microenvironment that is more conducive to cell growth.

The first aim of this research was to fabricate and characterize a PDA-functionalized carbon microfibrous electrospun scaffold. The cellulose was made into a 3D network structure by electrospinning, and it maintained its electrical conductivity and mechanical flexibility and biocompatibility after heat treatment. The second part of this research was to evaluate the material's effects on the proliferation and differentiation of NSCs from the hippocampus of fetal mice. Our results suggest that PDA-CF acts as a neural scaffold that promotes the maturation of NSCs by accelerating cell development and adhesion as indicated by increased Ki-67 expression. Representative 3D reconstruction of confocal microscope images showed that NSCs grew quickly into the interior of the PDA-CF, while only expanding on the surface of the CF scaffold. In addition, the expression of vinculin was significantly enhanced on PDA-CF compared with the CF control group. This is very interesting, in some way, PDA seems to accelerating the development of NSCs by promoting the expression of adhesion protein vinculin.

These results indicated that PDA plays an essential role in promoting the spread of NSCs on the electrically conductive 3D CF skeleton and that the viscous microfibrous networks formed by PDA-CF are key for improving NSC attachment and development. However, the molecular mechanisms behind these effects need to be studied further. NSCs did not differentiate into neural cells on PDA-CF any more so than they did on the CF control material, and we suspect that the reason for this is that NSCs maintained a state of self-renewal in the short time for which they were cultured on PDA-CF. Future work should extend the incubation time of NSCs to 3 weeks in order to further explore the differentiation of cells cultured on PDA-CF scaffolds. This method can be used to prepare multifunctional neuron scaffolds for nerve transplantation treatment and *in vitro* research, and these hybrid materials are also likely to find use with myocardial and other muscle cells to create tissue constructs with improved organization, electroactivity, and mechanical integrity.

DATA AVAILABILITY STATEMENT

The raw data supporting the conclusions of this article will be made available by the authors, without undue reservation, to any qualified researcher.

ETHICS STATEMENT

The studies involving animal experiments were reviewed and approved by Care and Use of Animals Committee of Southeast University. The study does not involve any human sample or human data.

AUTHOR CONTRIBUTIONS

RC, ZG, and YY designed experiments. YY and YZ carried out experiments and analyzed experimental results. YY wrote the manuscript. All authors contributed to the article and approved the submitted version.

FUNDING

This work was supported by grants from National Key R&D Program of China (No. 2017YFA0103903), Strategic Priority Research Program of the Chinese Academy of Science (XDA16010303), National Natural Science Foundation of China (No. 81970882), the 111 Project of the Ministry of Education of China (No. B17011), Natural Science Foundation from Jiangsu Province (BE2019711), Boehringer Ingelheim Pharma GmbH, K. C. Wong Education Foundation, and Postgraduate Research & Practice Innovation Program of Jiangsu Province (KYCX19_0057).

SUPPLEMENTARY MATERIAL

The Supplementary Material for this article can be found online at: https://www.frontiersin.org/articles/10.3389/fbioe.2020.00616/full#supplementary-material

REFERENCES

Ambasudhan, R., Talantova, M., Coleman, R., Yuan, X., Zhu, S., Lipton, S. A., et al. (2011). Direct reprogramming of adult human fibroblasts to functional neurons under defined conditions. *Cell Stem Cell* 9, 113–118. doi: 10.1016/j.stem.2011.07.002

Bays, J. L., and DeMali, K. A. (2000). Vinculin in cell-cell and cell-matrix adhesions. *Cell Mol Life Sci.* 74, 2999–3009. doi: 10.1007/s00018-017-2511-3

Bullard Dunn, K., Heffler, M., M., and Golubovskaya, V. (2010). Evolving therapies and FAK inhibitors for the treatment of cancer. *Anti- Cancer Agents Med Chem*. 10, 722–734. doi: 10.2174/187152010794728657

Carlberg, B., Axell, M. Z., Nannmark, U., Liu, J., and Kuhn, H. G. (2009). Electrospun polyurethane scaffolds for proliferation and neuronal differentiation of human embryonic stem cells. *Biomed. Mater*. 4:045004. doi: 10.1088/1748-6041/4/4/045004

Chehrehasa, F., Meedeniya, A. C., Dwyer, P., Abrahamsen, G., and Mackay-Sim, A. (2009). EdU, a new thymidine analogue for labelling proliferating cells in the nervous system. *J. Neurosci. Methods* 177, 122–130. doi: 10.1016/j.jneumeth.2008.10.006

Christopherson, G. T., Song, H., and Mao, H. Q. (2009). The influence of fiber diameter of electrospun substrates on neural stem cell differentiation and proliferation. *Biomaterials* 30, 556–564. doi: 10.1016/j.biomaterials.2008.10.004

Faure, E., Falentin-Daudre,' C., Jérôme, C., Lyskawa, J., Fournier, D., Woisel, P., et al. (2013). Catechols as versatile platforms in polymer chemistry. *Prog. Polymer Sci*. 38, 236–270. doi: 10.1016/j.progpolymsci.2012.06.004

Granato, A. E., Ribeiro, A. C., Marciano, F. R., Rodrigues, B. V., Lobo, A. O., and Porcionatto, M. (2018). Polypyrrole increases branching and neurite extension by neuro2a cells on pbat ultrathin fibers. *Nanomedicine* 14, 1753–1763. doi: 10.1016/j.nano.2018.05.004

He, J., Liang, Y., Shi, M., and Guo, B. (2000). Anti-oxidant electroactive and antibacterial nanofibrous wound dressings based on poly(ε-caprolactone)/quaternized chitosan-graft-polyaniline for full-thickness skin wound healing. *Chem. Eng. J*. 385:123464. doi: 10.1016/j.cej.2019.123464

He, J., Wang, X. M., Spector, M., and Cui, F. Z. (2012). Scaffolds for central nervous system tissue engineering. *Front. Mater. Sci*. 6, 1–25. doi: 10.1007/s11706-012-0157-5

Heo, C., Yoo, J., Lee, S., Jo, A., Jung, S., Yoo, H., et al. (2011). The control of neural cell-to-cell interactions through non-contact electrical field stimulation using graphene electrodes. *Biomaterials* 32, 19–27. doi: 10.1016/j.biomaterials.2010.08.095

Kam, N. W., Jan, E., and Kotov, N. A. (2008). Electrical stimulation of neural stem cells mediated by humanized carbon nanotube composite made with extracellular matrix protein. *Nano Lett*. 9, 273–278. doi: 10.1021/nl802859a

Kechagia, J. Z., Ivaska, J., and Roca-Cusachs, P. (2019). Integrins as biomechanical sensors of the microenvironment. *Nat. Rev. Mol. Cell Biol*. 457–473. doi: 10.1038/s41580-019-0134-2

Kim, C. W., Frey, M. W., Marquez, M., and Joo, Y. L. (2005). Preparation of submicron-scale, electrospun cellulose fibers via direct dissolution. *J. Polymer Sci. Part B* 43, 1673–1683. doi: 10.1002/polb.20475

Koppes, A., Keating, K., McGregor, A., Koppes, R., Kearns, K., Ziemba, A., et al. (2016). Robustneurite extension following exogenous electrical stimulation within single walled carbon nanotube-composite hydrogels. *Acta Biomater*. 39, 34–43. doi: 10.1016/j.actbio.2016.05.014

Lee, H., Dellatore, S. M., Miller, W. M., and Messersmith, P. B. (2007). Mussel-inspired surface chemistry for multifunctional coatings. *Science* 318, 426–430. doi: 10.1126/science.1147241

Li, L., Zhong, Q., Kim, N. D., Ruan, G., Yang, Y., Gao, C., et al. (2016). Nitrogen-doped carbonized cotton for highly flexible supercapacitors. *Carbon* 105, 260–267. doi: 10.1016/j.carbon.2016.04.031

Limongi, T., Rocchi, A., Cesca, F., Tan, H., Miele, E., Giugni, A., et al. (2018). Delivery of brain-derived neurotrophic factor by 3D biocompatible polymeric scaffolds for neural tissue engineering and neuronal regeneration. *Mol. Neurobiol*. 55, 8788–8798. doi: 10.1007/s12035-018-1022-z

Lo'pez-Colome,' A. M., Lee-Rivera, I., Benavides-Hidalgo, R., and Lo'pez, E. (2017). Paxillin: a crossroad in pathological cell migration. *J. Hematol. Oncol*. 10:50. doi: 10.1186/s13045-017-0418-y

Ma, Q., Yang, L., Jiang, Z., Song, Q., Xiao, M., Zhang, D., et al. (2016). Three-dimensional stiff graphene scaffold on neural stem cells behavior. *ACS Appl. Mater. Interf*. 8, 34227–34233. doi: 10.1021/acsami.6b12305

Ma, X., and Hammes, S. R. (2018). Paxillin actions in the nucleus. *Steroids* 133, 87–92. doi: 10.1016/j.steroids.2017.10.012

Martino, G., and Pluchino, S. (2006). The therapeutic potential of neural stem cells. *Nat. Rev. Neurosci*. 7:395. doi: 10.1038/nrn1908

Park, D., Xiang, A. P., Mao, F. F., Zhang, L., Di, C. G., Liu, X. M., et al. (2010). Nestin is required for the proper self- renewal of neural stem cells. *Stem Cells* 28, 2162–2171. doi: 10.1002/stem.541

Qi, Z., Guo, W., Zheng, S., Fu, C., Ma, Y., Pan, S., et al. (2019). Enhancement of neural stem cell survival, proliferation and differentiation by IGF-1 delivery in graphene oxide-incorporated PLGA electrospun nanofibrous mats. *RSC Adv*. 9, 8315–8325. doi: 10.1039/C8RA10103E

Scholzen, T., and Gerdes, J. (2000). The Ki- 67 protein: from the known and the unknown. *J. Cell. Physiol*. 182, 311–322. doi: 10.1002/(SICI)1097-4652(200003)182:3<311::AID-JCP1>3.0.CO;2-9

Sharma, D., Jia, W., Long, F., Pati, S., Chen, Q., Qyang, Y., et al. (2019). Polydopamine and collagen coated micro- grated polydimethylsiloxane for human mesenchymal stem cell culture. *Bioactive Mater*. 4, 142–150. doi: 10.1016/j.bioactmat.2019.02.002

Shin, Y. M., Lee, Y. B., and Shin, H. (2011). Time-dependent mussel-inspired functionalization of poly (l-lactide-co-ε-caprolactone) substrates for tunable cell behaviors. *Colloids Surfaces B* 87, 79–87. doi: 10.1016/j.colsurfb.2011.05.004

Tai, Y. L., Chen, L. C., and Shen, T. L. (2015). Emerging roles of focal adhesion kinase in cancer. *BioMed Res. Int*. 20, 457–473. doi: 10.1155/2015/690690

Tang, J., Shi, Z., Berry, R. M., and Tam, K. C. (2015). Mussel-inspired green metallization of silver nanoparticles on cellulose nanocrystals and their enhanced catalytic reduction of 4-nitrophenol in the presence of β-cyclodextrin. *Industr. Eng. Chem. Res*. 54, 3299–3308. doi: 10.1021/acs.iecr.5b00177

Uz, M., and Mallapragada, S. K. (2019). Conductive polymers and hydrogels for neu-ral tissue engineering. *J. Indian Institute Sci*. 99, 489–510. doi: 10.1007/s41745-019-00126-8

Wang, L., Wu, Y., Guo, B., and Ma, P. X. (2015). Nanofiber yarn/hydrogel core-shell scaffolds mimicking native skeletal muscle tissue for guiding 3d myoblast alignment, elongation, and differentiation. *ACS Nano*. 9, 9167–9179. doi: 10.1021/acsnano.5b03644

Wang, Y., Su, F., Wood, C. D., Lee, J. Y., and Zhao, X. S. (2008). Preparation and characterization of carbon nanospheres as anode materials in lithium-ion secondary batteries. *Industr. Eng. Chem. Res*. 47, 2294–2300. doi: 10.1021/ie071337d

Wei, Q., Zhang, F., Li, J., Li, B., and Zhao, C. (2010). Oxidant-induced dopamine polymerization for multifunctional coatings. *Polymer Chem*. 1, 1430–1433. doi: 10.1039/c0py00215a

Wu, Y., Wang, L., Guo, B., and Ma, P. X. (2017). Interwoven aligned conductive nanofiber yarn/hydrogel composite scaffolds for engineered 3d cardiac anisotropy. *ACS Nano*. 11, 5646–5659. doi: 10.1021/acsnano.7b01062

Wu, Y., Wang, L., Guo, B., Shao, Y., and Ma, P. X. (2016). Electroactive biodegradable polyurethane significantly enhanced schwann cells myelin gene expression and neurotrophin secretion for peripheral nerve tissue engineering. *Biomaterials* 87, 18–31. doi: 10.1016/j.biomaterials.2016.02.010

Yang, K., Lee, J. S., Kim, J., Lee, Y. B., Shin, H., Um, S. H., et al. (2012). Polydopamine-mediated surface modification of scaffold materials for human neural stem cell engineering. *Biomaterials* 33, 6952–6964. doi: 10.1016/j.biomaterials.2012.06.067

Yang, Y., Zhang, Y., Chai, R., and Gu, Z. (2018). Designs of Biomaterials and Microenvironments for Neuroengineering. *Neural Plasticity* 2018:1021969. doi: 10.1155/2018/1021969

Zhu, W., Ye, T., Lee, S. J., Cui, H., Miao, S., Zhou, X., et al. (2018). Enhanced neural stem cell functions in conductive annealed carbon nanofibrous scaffolds with electrical stimulation. *Nanomedicine* 14, 2485–2494. doi: 10.1016/j.nano.2017.03.018

Conflict of Interest: The authors declare that the research was conducted in the absence of any commercial or financial relationships that could be construed as a potential conflict of interest.

frontiers in Bioengineering and Biotechnology

MINI REVIEW
published: 07 October 2020
doi: 10.3389/fbioe.2020.591467

Building Osteogenic Microenvironments With Strontium-Substituted Calcium Phosphate Ceramics

Ben Wan, Renxian Wang, Yuyang Sun, Jingjing Cao, Honggang Wang, Jianxun Guo and Dafu Chen**

Laboratory of Bone Tissue Engineering, Beijing Laboratory of Biomedical Materials, Beijing Research Institute of Traumatology and Orthopaedics, Beijing Jishuitan Hospital, Beijing, China

Bioceramics have experienced great development over the past 50 years. Modern bioceramics are designed to integrate bioactive ions within ceramic granules to trigger living tissue regeneration. Preclinical and clinical studies have shown that strontium is a safe and effective divalent metal ion for preventing osteoporosis, which has led to its incorporation in calcium phosphate-based ceramics. The local release of strontium ions during degradation results in moderate concentrations that trigger osteogenesis with few systemic side effects. Moreover, strontium has been proven to generate a favorable immune environment and promote early angiogenesis at the implantation site. Herein, the important aspects of strontium-enriched calcium phosphate bioceramics (Sr-CaPs), and how Sr-CaPs affect the osteogenic microenvironment, are described.

Keywords: calcium phosphate ceramics, strontium substitution, microenvironment, bone regeneration, biomaterials

OPEN ACCESS

Edited by:
Xin Zhao,
Hong Kong Polytechnic University,
Hong Kong

Reviewed by:
Lunguo Xia,
Shanghai Jiaotong University, China
Zhipeng Gu,
Sichuan University, China

****Correspondence:***
Dafu Chen
chendafujst@126.com
Renxian Wang
wrxpumc@126.com

Specialty section:
This article was submitted to Biomaterials, a section of the journal Frontiers in Bioengineering and Biotechnology

Received: *04 August 2020*
Accepted: *16 September 2020*
Published: *07 October 2020*

Citation:
Wan B, Wang R, Sun Y, Cao J, Wang H, Guo J and Chen D (2020) Building Osteogenic Microenvironments With Strontium-Substituted Calcium Phosphate Ceramics. Front. Bioeng. Biotechnol. 8:591467. doi: 10.3389/fbioe.2020.591467

INTRODUCTION

Bone is a metabolically active specialized connective tissue with the capacity for continuous resorption and reformation, but the reconstruction process requires extra support in large bone defect cases, for example, injury, tumor excision, and age-related diseases (Loi et al., 2016; Ginebra et al., 2018). Clinically, autografts still remain the most common strategy to support and stimulate bone growth. While biologically desirable, the supply of autografts from a patient's own body cannot meet the amount required for large-sized bone defects (Wang and Yeung, 2017). Grafts from bone banks or other animal species can provide a vast range of grafting forms by virtue of their relatively easy availability (Wang and Yeung, 2017). Nevertheless, they are still subject to attenuated osteointegration and disease transmission.

Synthetic bioactive ceramics can overcome these limitations. They are obtained by chemical reagent deposition through a controlled process that allows their properties to be adapted to the specific requirements of different clinical situations. Calcium phosphate ceramics (CaPs) are basic bone repair materials with excellent osteoinductive and osteoconductive features; examples include hydroxyapatite (HAP), β-tricalcium phosphate (β-TCP), calcium polyphosphate (CPP), and biphasic calcium phosphate (BCP). They have been widely used in clinical applications in the form of implant surface coatings, the composition of cements, and scaffolds (Jeong et al., 2019). Moreover, CaPs encapsulated with pharmacologics and biologics in scaffolds have shown

multiple abilities, such as enhanced osteointegration, angiogenesis, and antibacterial properties (Bose and Tarafder, 2012; Marques et al., 2016). However, these biologically active molecules are only surface-loaded and show explosive release effects with little long-term benefit (Wu et al., 2014). This raises some concerns about their safety. For example, recombinant human bone morphogenetic protein-2 (rhBMP-2) is the first commercial synthetic osteoinductive molecule, and the combined use of rhBMP-2 and calcium phosphate ceramics has achieved many clinical successes. But it is worth noting that serious side effects related to ectopic or unwanted bone formation in certain situations have made the FDA increasingly resistant to approving the use of such materials (Vavken et al., 2016).

An alternative long-lasting and potentially safer strategy is the incorporation of trace metallic elements into CaPs. The mineral composition of our bone itself is not a homogenous and bioinert calcium phosphate-based material (Von Euw et al., 2019). Bone incorporates and releases various trace elements (such as Mg^{2+}, Zn^{2+}, and Sr^{2+}) into the microenvironment during bone metabolism (Bose et al., 2013). Previous studies have confirmed that CaPs modified with these bivalent trace metallic ions can lead to controlled degradation, increase the mechanical strength of the materials, and enhance bioactive properties. But among these bioactive ions, strontium (Sr) has gained great attention since strontium ranelate (SrRan) has been approved as an anti-osteoporotic drug for post-menopausal osteoporosis since it increases bone strength (Neves et al., 2017; Marx et al., 2020). Recent findings suggest that oral administration of SrRan may have no anabolic action on bone formation in humans, and even inhibits osteogenic differentiation under the *in vitro* experiment conditions (Wornham et al., 2014; Marx et al., 2020). However, the comprehensively described SrCaPs do exert positively influence on new bone formation and accelerate the healing process (Neves et al., 2017). These discrepancies may be partially due to the implant microenvironments where biomaterials interact with various cells. The local delivery of Sr ions from SrCaPs implanted in bone changes local microenvironment, which is involved in several biological processes such as osteogenesis, angiogenesis, osteoimmunomodulation.

Consequently, in this review, we present recent developments in strontium-substituted calcium phosphate ceramics (SrCaPs) and offer insights into how Sr ions released from implants influence the immune response, angiogenesis, and osteoblastic differentiation of bone marrow stromal cells (bMSCs).

Sr-CaPs: CURRENT STATE OF THE ART

In the 1960s, surgeons valued the inertness of surgical materials in the human tissue environment, and first-generation bioceramics (alumina, zirconia, diverse forms of carbon) were developed as bone substitutes, mainly for femoral head fabrication (Smith, 1963). However, they elicited a foreign body reaction, forming fibrous capsules that isolated them from the body. In the 1980s, Larry Hench invented a bioactive glass with the ability to bond to living tissue, and Heughebaert reported that CaPs could induce bone formation (Hench and Wilson, 1984; Heughebaert et al., 1988). Since then, osteoinductive and tissue-inducing materials have become the mainstream of biomaterial science and engineering (Hench and Polak, 2002). CaPs are the most studied and implanted bioactive ceramics in the clinic because of their cost-effective preparation from chemical regents or natural resources. Various calcium phosphate compounds are in different crystalline phases and often classified on the basis of the Ca/P ratio. Of great interest is the subgroup of apatite compounds, which exhibit similarities to vertebrate hard tissues. Indeed, both bone and teeth are well-crystallized apatites (hydroxyapatite), and this structure can easily accommodate many cations and anions for substitution, thereby achieving adaptive biophysical functions (Drouet et al., 2017).

Strontium (Sr) is naturally deposited in the mineral phase of bones via consuming a normal diet, and it replaces approximately 0.035% of Ca content (International Programme on Chemical and Inter-Organization Programme for the Sound Management, 2010). The majority of *in vitro* experiments support a dual-acting mechanism in which Sr stimulates bone formation and hinders bone resorption (Saidak and Marie, 2012). The exact mechanism of the role of Sr in bone remains unclear, but it has been proposed that Sr acts on similar cellular targets as Ca^{2+} by activating the calcium sensing receptor (CaSR), thus interacting with Ca-driven signaling pathways related to bone metabolism regulation (Saidak and Marie, 2012). Furthermore, small animal trials and clinical trials have produced overwhelming evidence that Sr benefits bone remodeling and increases bone-mineral density, especially in the treatment of osteoporosis (Meunier et al., 2004; Reginster et al., 2012; Marx et al., 2020). Taking these beneficial effects into consideration, it is likely that local Sr ion delivery will enhance osteoinduction and osseointegration at the bone-implant interface, contributing to a faster healing microenvironment.

Recently, Sr has been widely incorporated into calcium phosphate-based materials for biomedical applications. Krishnan reported using Sr doped hydroxyapatite (SrHAP) particles to repair dental enamel with the potential to treat white spot lesions and incipient carious lesions (Krishnan et al., 2016). It is also an effective additive for toothpaste in the prevention of cariogenesis (Surdacka et al., 2007). These particles cannot only be used as a raw material, but also associated with other biomaterial compounds to facilitate new functions. Sr-CaPs are fabricated as coatings on the surfaces of metallic implants in order to accelerate bone healing at early implantation times (Li et al., 2010; Arcos and Vallet-Regí, 2020). Titanium and titanium-based alloys are commonly used for load-bearing applications (such as total joint replacement and fracture fixation elements), but carry a risk of loosening, especially when implanted in osteoporotic bones. Tao et al. (2016a) conducted an *in vivo* study on rats with ovariectomy-induced osteoporosis and reported that a strontium-containing HAP coating on shaped titanium implants was better than an Sr-free HAP coating in terms of new bone formation and push-out force. Furthermore, they conducted an comparative study that found that under the same the molar ratio [Zn, Mg, Sr/(Zn, Mg, Sr+Ca) = 10%], the SrHAP coating exhibited better osseointegration than zinc- and magnesium-substituted HAP coatings (Tao et al., 2016b).

SrCaP cements (SrCPC) consist of a combination of a precursor powder and liquid phase, allowing it to fill and heal bone defects during minimally invasive procedures. Kuang et al. (2015) prepared pre-set SrCPC for a metaphyseal defect in Sprague-Dawley rats and found early endochondral ossification at 2 weeks post-operation. Thormann et al. (2013) further demonstrated that Sr was deposited at newly formed tissues around the implanted SrCPC as visualized by Time-of-flight secondary ion mass spectrometry (ToF-SIMS) imaging and found a significant increase of mineralized extracellular matrix in the SrCPC group compared to the Sr-free calcium phosphate cement (CPC) and empty defect groups. Sr-CaP scaffolds can be further modified with drugs, especially antibiotics and growth factors. The chemical composition of SrHAP provides strong surface adsorption capacity and increases surface area, allowing drug release for a longer period of time (Xu et al., 2018). Lin et al. (2013) reported that SrHAP microspheres with 3D hierarchically mesoporous structures not only promoted an osteogenic response, but exhibited sustained vancomycin release. Yan et al. (2018) developed an Sr-nHAP/SF-Hep-BMP-2 scaffold system with controlled BMP-2 release that supported critical size calvarial defect healing in Sprague-Dawley rats. Tao et al. (2018) revealed synergistic bioactive properties of BMP-2 and Sr released from CPC composites, which achieved rapid bone healing in osseous defects in an ovariectomized rat model. These new applications for strontium-containing calcium phosphate extends their biomedical potential.

FAVORABLE POST-IMPLANTATION ENVIRONMENTS FOR Sr-CaPs

Sr is chemically and physically close to calcium but has a larger ionic radius (112 vs. 99 pm). The partial substitution of Ca by Sr results in higher solubility when compared with Sr-free CaPs owning to the enlargement of the unit cell (Zhu et al., 2018). The surfaces of SrCaPs are reactive and biodegradable, and bone-like apatite forms on them through continuous dissolution and precipitation. The newly formed apatite creates a strong bond between the living tissues and implants. However, it degrades over time when in contact with bodily fluids and it elevates the local concentrations of Sr^{2+}, Ca^{2+}, and PO_4^{3-} ions. These released ions affect important components of the bone microenvironment, including the mineral deposited layer phase, the cellular phase (osteoblasts, macrophages, and vascular endothelial cells), and the soluble factor phase (growth factors and/or cytokines) and provide an extracellular osteogenic signaling network. The incorporation of an appropriate proportion of Sr into CaPs allows them to build an osteogenic microenvironment via modulating the inflammatory response, stimulating osteogenic differentiation of bone marrow mesenchymal stem cells, and promoting early angiogenesis (**Figure 1**).

EFFECTS ON OSTEOGENESIS

SrCaPs is a promising biomaterial to help bone reconstruction. Mounting evidence shows that Sr replacement of Ca in CaPs leads to increased solubility due to the expansion of the crystal structure, and the high local Sr^{2+}, Ca^{2+}, and PO_4^{3-} ionic concentrations are believed to be of great importance for osteoinduction and osteoconduction (Bose et al., 2013; Neves et al., 2017). Current research shows that both Sr and Ca mediate key cellular functions in osteogenesis-related cells via Ca-sensing receptor (CaSR)-dependent mechanisms (Marx et al., 2020). In the extracellular microenvironment, a high Ca concentration is

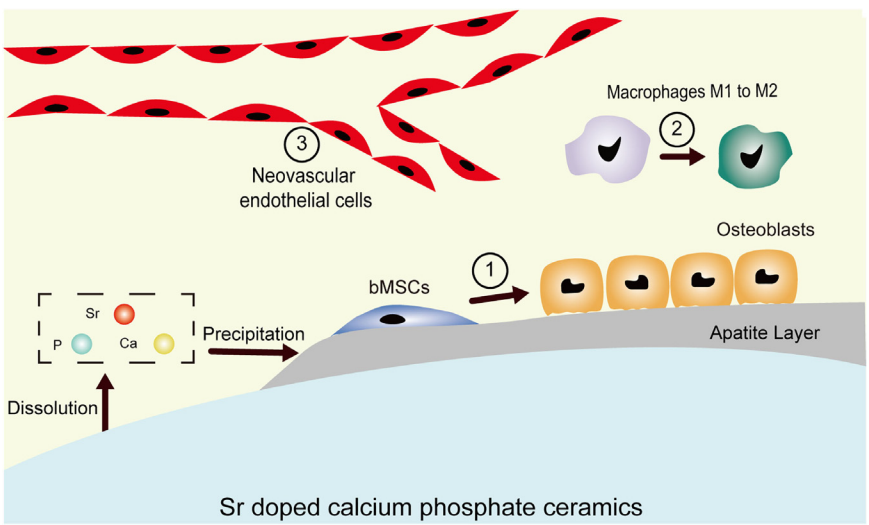

FIGURE 1 | Schematic demonstrating the microenvironment of the host bone-implant interface. The degradation-precipitation reactions of bioactive Sr-CaPs modulate local ion concentrations and influence peripheral physiological processes, including ① hMSC osteogenic differentiation, ② immune responses such as macrophage polarization to M2, and ③ revascularization processes.

a potent chemical signal for bMSCs osteogenic differentiation (Dvorak and Riccardi, 2004; Barradas et al., 2012). A lack of calcium significantly retards cell growth and differentiation (Dvorak et al., 2004; Barradas et al., 2012). Interestingly, CaPs with Sr modification tend to have decreased Ca concentrations around the material due to induced apatite precipitation, though lower concentrations of Ca do not impair the proliferation or osteogenic differentiation of bMSCs (Schumacher et al., 2013; Kruppke et al., 2019b). In an *in vitro* study, Kruppke et al. (2019a) confirmed that Sr may compensate for the adverse effects of lowered Ca ion concentrations to a certain degree and potentially stimulate bone regeneration. They investigated the effect of varied Ca and Sr ion concentrations, respectively, on proliferation and differentiation of bMSCs and concluded that under low calcium concentrations culture conditions (0.3–0.4 mM due to the addition of fetal calf serum), Sr at 0.4–0.9 mM promoted differentiation of bMSCs while 0.9–1.8 mM stimulated the highest proliferation. And in a second study exploring the relationship between Sr and Ca on bone formation, they conducted *in vitro* and *in vivo* experiments to evaluate the osteogenesis effects of Sr together with two concentration gradients of Ca (normal calcium of 1.8 mM or high calcium of 9 mM) and concluded that Sr (1 mM) enhanced mineralization and ALP expression of MC3T3-E1 pre-osteoblast cells under a high dose of calcium (9 mM) (Xie et al., 2018). This may explain the results by Wornham et al. (2014) in which concentrations of Sr ranging from 10 μM to 1 mM inhibit the mineralization ability of primary rat osteoblasts under 1.8 mM Ca present in the culture system. These experiments illustrate the importance of the implant microenvironment because bone has higher Ca levels than plasma. It also suggests that both Sr and Ca from ion-leaching SrCaPs may interact to promote bone regeneration at the bone-implant interface. In addition, the phosphate ion is a basic component in the human body and accumulates in bone minerals in the form of calcium phosphates along with calcium ions (Khoshniat et al., 2011). When phosphate ions are not present in high quantities, the generation of new bone will be blocked due to insufficient formation of hydroxyapatite (Penido and Alon, 2012).

Sr-rich CaPs consistently outperform Sr-free CaPs in *in vitro* and *in vivo* studies (Neves et al., 2017; Marx et al., 2020). In the absence of doping with other osteogenic ions, the local release of Sr is sufficient to promote bone formation, but it is difficult to ignore the effects that surface morphology, porosity, hydrophilicity, dissolution process, and local pH changes may have on osteogenesis regulation at the implantation site.

EFFECTS ON ANGIOGENESIS

Increased angiogenesis can relieve the symptoms of ischemia and facilitate the transport nutrients, which is essential for bone repair/regeneration. Sr-CaPs have been found to increase neovascularization in many convincing experiments (Liu et al., 2011; Gu et al., 2013; Wang et al., 2014). Endothelial cells are the major seed cells that drive angiogenesis. Chen et al. (2008) observed that degradation products of Sr doped calcium polyphosphate (SCPPs) promote the proliferation, migration, and tube-like structure formation of endothelial cells (ECV304). It has been reported that *in situ* production of angiogenic growth factors, such as vascular endothelial growth factor (VEGF) and basic fibroblast growth factor (bFGF), can promote more cell infiltration, extracellular matrix synthesis, and faster angiogenesis (Saberianpour et al., 2018).

TABLE 1 | The osteogenic differentiation function of various Sr concentrations.

Cell lines	Strontium salt	Sr concentration	Function	References
C3H10T1/2 and mice primary bone marrow mesenchymal stem cells	Strontium chloride	1.0 mM, 3.0 mM	Promote osteogenic differentiation	Peng et al., 2009
Ovariectomy bone marrow mesenchymal stem cells	Strontium ranelate	0.25–0.5 mM	Promote osteogenic differentiation	Guo et al., 2016
Primary fetal mouse calvaria cells	Strontium ranelate	0.1–1 mM	Promote osteogenic differentiation	Bonnelye et al., 2008
Human bone marrow mesenchymal stem cells	Strontium ranelate	2.4–240 μM	Promote osteogenic differentiation	Sila-Asna et al., 2007
Human adipose-derived stem cells	Strontium ranelate	25–500 μM	Promote osteogenic differentiation	Aimaiti et al., 2017
	Strontium ranelate	1–3 mM	Apoptosis and inhibit osteogenic differentiation	
MC3T3-E1 pre-osteoblast cells	Strontium chloride	1 mM	Inhibit osteogenic differentiation	Xie et al., 2018
Rat bone marrow mesenchymal stem cells	Strontium ranelate	0.1 mM, 1 mM	Inhibit proliferation and promote osteogenic differentiation	Li et al., 2012
Primary rat osteoblastic cells	Strontium ranelate; strontium chloride	0.1–1 mM	Inhibit mineral deposition	Wornham et al., 2014

Liu et al. (2011) directly seeded osteoblasts (ROS17/2.8) on SCPP scaffolds with various amounts of Sr and found increased secretion of VEGF and bFGF in the culture medium. Wang et al. (2014) observed the stimulating effects of SCPP on protein secretion and mRNA expression of VEGF, bFGF, and MMP-2 from endothelial cells *in vitro*. Gu et al. (2014) co-cultured umbilical vein endothelial cells and osteoblasts on SCPP scaffolds *in vitro* and demonstrated higher VEGF and bFGF protein production compared with CPP and HAP. Furthermore, Ye et al. (2019) fabricated Sr-doped calcium phosphate/polycaprolactone/chitosan (Sr-CaP/PCL/CS) nanohybrid fibrous membranes and demonstrated high VEGF secretion from bMSCs. In the future, more experiments are needed to test the ability of SrCaPs to promote blood vessel formation *in vivo*, and more attention should be paid to the impact of the immune response.

EFFECTS ON OSTEOIMMUNOMODULATION

Every implantable material must be biocompatible, meaning that only a limited inflammatory response occurs in the host body. Huang et al. (2020) reported the incorporation of fish-derived nano CaPs (Ca/P molar ratio was 2.35) into gelatin methacrylate generated a suitable immune microenvironment by inducing the secretion of cytokines and promoting macrophage phenotype conversion. The controllable inflammation may promote the osteogenic differentiation and angiogenesis (Zhao et al., 2018; Huang et al., 2020). The local release of Sr from implants to the adjacent host bone can reduce unfavorable inflammatory responses (Renaudin et al., 2008), and Sr has been proven to be an anti-inflammatory agent (Wang et al., 2020). Buache et al. (2012) first verified that Sr-BCP can decrease the production of pro-inflammatory cytokines (TNF-α and IL-6) and the chemokine interleukin 8 in human monocytes. Braux et al. (2016) demonstrated the downregulating effect of Sr-BCP on inflammatory mediator production (MCP-1 and Gro-α) by human primary osteoblasts. Sr has also been shown to suppress the expression of proinflammatory cytokines (IL-6 and TNF-α) in periodontal ligament cells and macrophages (Römer et al., 2012; Gu et al., 2014). Among various immune-related cells, macrophages play a significant role in regulating bone healing after trauma or the implantation of biomaterials (Alexander et al., 2011; Batoon et al., 2019). At the early time of bone repair, resident or infiltrating monocyte-derived macrophages mostly present the pro-inflammatory M1 phenotype, and a timely switch from M1 to M2 (anti-inflammatory phenotype) leads to osteogenic cytokine release, including that of IL-10, TGFβ, and VEGF. Interestingly, prolonged M1 polarization leads to an increased release of fiber-enhancing cytokines from M2 macrophages, which leads to the formation of fibrous capsules (Chen et al., 2016). Previous evidence suggests that Sr-integrated implants elicit more pro-regenerative M2 macrophages; examples include Sr-doped calcium polyphosphate particles, Sr-substituted bioactive glass, and Ca- and Sr-modified titanium implant surfaces (Gu et al., 2014; Lee et al., 2016; Zhao et al., 2018). The incorporation of Sr into CaPs endows traditional CaPs with osteoimmunomodulation properties and positively regulates cytokine production and immune cell functions for better bone remodeling.

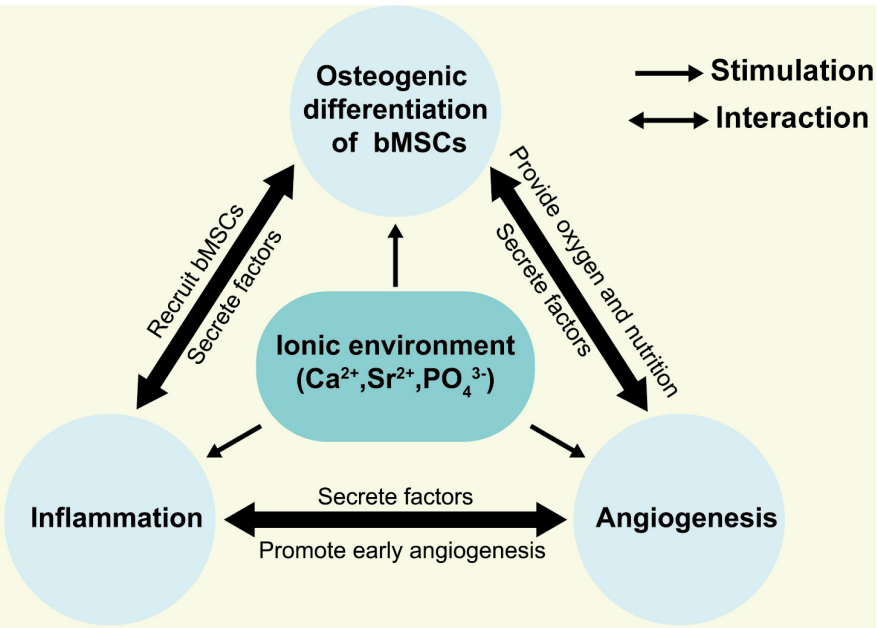

FIGURE 2 | Hypothesis for osteogenic microenvironments of SrCaPs. The local ionic environment not only stimulates the osteoblastic differentiation of bMSCs but interacts with the inflammatory cells and vascular endothelial cells.

CONTROVERSY OVER THE EFFECTIVE STRONTIUM CONCENTRATION

Local Sr release is a critical property of SrCaPs, but the optimal concentration remains to be determined. Evidence from *in vitro* studies shows that Sr promotes osteogenic differentiation in a dose-dependent manner, and different cell lineages respond differently to Sr at similar concentrations (**Table 1**). Peng et al. (2009) showed that 1 mM can promote osteogenic differentiation of C3H10T1/2 or mice primary bMSCs, while Aimaiti et al. (2017) reported that 1 mM induces apoptosis and inhibits osteogenic differentiation in human primary adipose-derived stem cells. Moreover, inhibition at this concentration also occurs for primary rat osteoblastic cells and MC3T3-E1 cells (Wornham et al., 2014; Xie et al., 2018). However, the maximum circulating concentrations of Sr in the serum of patients treated with strontium ranelate (2 g per day for 3 years) is about 0.1 mM (Meunier et al., 2004). Although several *in vitro* studies have shown that Sr concentration above 1 mM can stimulate osteogenesis, it is preferable to take clinical trial results into consideration, and the effective range (below 500 mM) is recommended here (Bonnelye et al., 2008; Peng et al., 2009; Guo et al., 2016). To the best of our knowledge, no *in vivo* study on the local administration of Sr with the use of modified CaPs has reported adverse effects on bone formation and osseointegration. The reasons may be that, first, the implantation microenvironment in the body is dynamically changing, and a high dose of Sr does not last for a long time. Second, the degradation product is not only Sr, but also Ca, which matters because of the equilibrium effect of Ca to Sr (Xie et al., 2018). Third, Sr positively modulates the microenvironment via regulating immune cells and endothelial cells in the process of bone formation.

CONCLUSION

In summary, integrating Sr ions into CaPs offers an alternative to biologics in the design of bioactive materials. It is of low cost, has a longer shelf life, and presents low systemic risk compared to growth factors. These added benefits make Sr as therapeutic agent attractive in tissue engineering and regenerative medicine applications (Jiménez et al., 2019; Prabha et al., 2019; Mao et al., 2020). However, the mechanism of osteoinduction of SrCaPs remains complicated because inflammation and angiogenesis accompany the entire process of bone healing. In light of the previous studies, we propose a hypothesis for the osteoinduction mechanism of SrCaPs: SrCaPs build the osteoinductive microenvironment of the host bone-implant interface (**Figure 2**). Functional ion release and apatite layer formation on the surfaces of SrCaP ceramics allow them to interact with cells and extracellular matrices in the host system, providing bioactive bonding to bone. Specifically, a higher local concentration of Sr stimulates the osteoblastic differentiation of MSCs (1 in **Figure 1**), induces macrophage polarization toward a pro-regenerative M2 phenotype (2 in **Figure 1**), and contributes to angiogenesis (3 in **Figure 1**). Collectively, understanding the biological microenvironment of implant-to-tissue interactions at the bone site is important for the development of high-performance bioceramics.

AUTHOR CONTRIBUTIONS

BW was the first author and drafted the manuscript. DC and RW designed the work. YS, JG, JC, and HW summarized related publications. All authors approved the final version to be published.

FUNDING

This work was financially supported by the National Natural Science Foundation of China (51973021 and 51932002), the Beijing Natural Science Foundation (7192027), and the Beijing Municipal Health Commission (BMHC-2019-9, BMHC-2018-4, and PXM2020_026275_000002).

REFERENCES

Aimaiti, A., Maimaitiyiming, A., Boyong, X., Aji, K., Li, C., and Cui, L. (2017). Low-dose strontium stimulates osteogenesis but high-dose doses cause apoptosis in human adipose-derived stem cells via regulation of the ERK1/2 signaling pathway. *Stem Cell Res. Ther.* 8:282.

Alexander, K. A., Chang, M. K., Maylin, E. R., Kohler, T., Müller, R., Wu, A. C., et al. (2011). Osteal macrophages promote in vivo intramembranous bone healing in a mouse tibial injury model. *J. Bone Miner. Res.* 26, 1517–1532. doi: 10.1002/jbmr.354

Arcos, D., and Vallet-Regí, M. (2020). Substituted hydroxyapatite coatings of bone implants. *J. Mater. Chem. B* 8, 1781–1800. doi: 10.1039/c9tb02710f

Barradas, A. M. C., Fernandes, H. A. M., Groen, N., Chai, Y. C., Schrooten, J., Van De Peppel, J., et al. (2012). A calcium-induced signaling cascade leading to osteogenic differentiation of human bone marrow-derived mesenchymal stromal cells. *Biomaterials* 33, 3205–3215. doi: 10.1016/j.biomaterials.2012.01.020

Batoon, L., Millard, S. M., Wullschleger, M. E., Preda, C., Wu, A. C.-K., Kaur, S., et al. (2019). CD169+ macrophages are critical for osteoblast maintenance and promote intramembranous and endochondral ossification during bone repair. *Biomaterials* 196, 51–66. doi: 10.1016/j.biomaterials.2017.10.033

Bonnelye, E., Chabadel, A., Saltel, F., and Jurdic, P. (2008). Dual effect of strontium ranelate: stimulation of osteoblast differentiation and inhibition of osteoclast formation and resorption in vitro. *Bone* 42, 129–138. doi: 10.1016/j.bone.2007.08.043

Bose, S., Fielding, G., Tarafder, S., and Bandyopadhyay, A. (2013). Understanding of dopant-induced osteogenesis and angiogenesis in calcium phosphate ceramics. *Trends Biotechnol.* 31, 594–605. doi: 10.1016/j.tibtech.2013.06.005

Bose, S., and Tarafder, S. (2012). Calcium phosphate ceramic systems in growth factor and drug delivery for bone tissue engineering: a review. *Acta Biomater.* 8, 1401–1421. doi: 10.1016/j.actbio.2011.11.017

Braux, J., Velard, F., Guillaume, C., Jourdain, M.-L., Gangloff, S. C., Jallot, E., et al. (2016). Strontium-substituted bioceramics particles: a new way to modulate MCP-1 and Gro-α production by human primary osteoblastic cells. *Materials* 9:985. doi: 10.3390/ma9120985

Buache, E., Velard, F., Bauden, E., Guillaume, C., Jallot, E., Nedelec, J. M., et al. (2012). Effect of strontium-substituted biphasic calcium phosphate on

inflammatory mediators production by human monocytes. *Acta Biomater.* 8, 3113–3119. doi: 10.1016/j.actbio.2012.04.045

Chen, Y. W., Feng, T., Shi, G. Q., Ding, Y. L., Yu, X. X., Zhang, X. H., et al. (2008). Interaction of endothelial cells with biodegradable strontium-doped calcium polyphosphate for bone tissue engineering. *Appl. Surface Sci.* 255, 331–335. doi: 10.1016/j.apsusc.2008.06.154

Chen, Z., Klein, T., Murray, R. Z., Crawford, R., Chang, J., Wu, C., et al. (2016). Osteoimmunomodulation for the development of advanced bone biomaterials. *Mater. Today* 19, 304–321. doi: 10.1016/j.mattod.2015.11.004

Drouet, C., Leriche, A., Hampshire, S., Kashani, M., Stamboulis, A., Iafisco, M., et al. (2017). "2 - types of ceramics: material class," in *Advances in Ceramic Biomaterials*, eds P. Palmero, F. Cambier, and E. De Barra (Cambridge, MA: Woodhead Publishing), 21–82.

Dvorak, M. M., and Riccardi, D. (2004). Ca2+ as an extracellular signal in bone. *Cell Calcium* 35, 249–255. doi: 10.1016/j.ceca.2003.10.014

Dvorak, M. M., Siddiqua, A., Ward, D. T., Carter, D. H., Dallas, S. L., Nemeth, E. F., et al. (2004). Physiological changes in extracellular calcium concentration directly control osteoblast function in the absence of calciotropic hormones. *Proc. Natl. Acad. Sci. U.S.A.* 101, 5140–5145. doi: 10.1073/pnas.0306141101

Ginebra, M.-P., Espanol, M., Maazouz, Y., Bergez, V., and Pastorino, D. (2018). Bioceramics and bone healing. *EFORT Open Rev.* 3, 173–183. doi: 10.1302/2058-5241.3.170056

Gu, Z., Xie, H., Huang, C., Peng, H., Tan, H., Li, L., et al. (2014). Effects of strontium-doped calcium polyphosphate on angiogenic growth factors expression of co-culturing system in vitro and of host cell in vivo. *RSC Adv.* 4, 2783–2792. doi: 10.1039/c3ra44323j

Gu, Z., Zhang, X., Li, L., Wang, Q., Yu, X., and Feng, T. (2013). Acceleration of segmental bone regeneration in a rabbit model by strontium-doped calcium polyphosphate scaffold through stimulating VEGF and bFGF secretion from osteoblasts. *Mater. Sci. Eng. C* 33, 274–281. doi: 10.1016/j.msec.2012.08.040

Guo, X., Wei, S., Lu, M., Shao, Z., Lu, J., Xia, L., et al. (2016). Dose-dependent effects of strontium ranelate on ovariectomy rat bone marrow mesenchymal stem cells and human umbilical vein endothelial cells. *Int. J. Biol. Sci.* 12, 1511–1522. doi: 10.7150/ijbs.16499

Hench, L. L., and Polak, J. M. (2002). Third-generation biomedical materials. *Science* 295, 1014–1017. doi: 10.1126/science.1067404

Hench, L. L., and Wilson, J. (1984). Surface-active biomaterials. *Science* 226, 630–636. doi: 10.1126/science.6093253

Heughebaert, M., Legeros, R. Z., Gineste, M., Guilhem, A., and Bonel, G. (1988). Physicochemical characterization of deposits associated with HA ceramics implanted in nonosseous sites. *J. Biomed. Mater. Res.* 22, 257–268. doi: 10.1002/jbm.820221406

Huang, L., Zhang, J., Hu, J., Zhao, T., and Gu, Z. (2020). Biomimetic gelatin methacrylate/nano fish bone hybrid hydrogel for bone regeneration via osteoimmunomodulation. *ACS Biomater. Sci. Eng.* 6, 3270–3274. doi: 10.1021/acsbiomaterials.0c00443

International Programme on Chemical and Inter-Organization Programme for the Sound Management (2010). *Strontium and Strontium Compounds*. Geneva: World Health Organization.

Jeong, J., Kim, J. H., Shim, J. H., Hwang, N. S., and Heo, C. Y. (2019). Bioactive calcium phosphate materials and applications in bone regeneration. *Biomater. Res.* 23:4.

Jiménez, M., Abradelo, C., San Román, J., and Rojo, L. (2019). Bibliographic review on the state of the art of strontium and zinc based regenerative therapies. Recent developments and clinical applications. *J. Mater. Chem. B* 7, 1974–1985. doi: 10.1039/c8tb02738b

Khoshniat, S., Bourgine, A., Julien, M., Weiss, P., Guicheux, J., and Beck, L. (2011). The emergence of phosphate as a specific signaling molecule in bone and other cell types in mammals. *Cell. Mol. Life Sci.* 68, 205–218. doi: 10.1007/s00018-010-0527-z

Krishnan, V., Bhatia, A., and Varma, H. (2016). Development, characterization and comparison of two strontium doped nano hydroxyapatite molecules for enamel repair/regeneration. *Dental Mater.* 32, 646–659. doi: 10.1016/j.dental.2016.02.002

Kruppke, B., Heinemann, C., Wagner, A.-S., Farack, J., Wenisch, S., Wiesmann, H.-P., et al. (2019a). Strontium ions promote in vitro human bone marrow stromal cell proliferation and differentiation in calcium-lacking media. *Dev., Growth Diff.* 61, 166–175. doi: 10.1111/dgd.12588

Kruppke, B., Wagner, A.-S., Rohnke, M., Heinemann, C., Kreschel, C., Gebert, A., et al. (2019b). Biomaterial based treatment of osteoclastic/osteoblastic cell imbalance – Gelatin-modified calcium/strontium phosphates. *Mater. Sci. Eng. C* 104:109933. doi: 10.1016/j.msec.2019.109933

Kuang, G.-M., Yau, W. P., Wu, J., Yeung, K. W. K., Pan, H., Lam, W. M., et al. (2015). Strontium exerts dual effects on calcium phosphate cement: accelerating the degradation and enhancing the osteoconductivity both in vitro and in vivo. *J. Biomed. Mater. Res. A* 103, 1613–1621. doi: 10.1002/jbm.a.35298

Lee, C.-H., Kim, Y.-J., Jang, J.-H., and Park, J.-W. (2016). Modulating macrophage polarization with divalent cations in nanostructured titanium implant surfaces. *Nanotechnology* 27:085101. doi: 10.1088/0957-4484/27/8/085101

Li, Y., Li, J., Zhu, S., Luo, E., Feng, G., Chen, Q., et al. (2012). Effects of strontium on proliferation and differentiation of rat bone marrow mesenchymal stem cells. *Biochem. Biophys. Res. Commun.* 418, 725–730. doi: 10.1016/j.bbrc.2012.01.088

Li, Y., Li, Q., Zhu, S., Luo, E., Li, J., Feng, G., et al. (2010). The effect of strontium-substituted hydroxyapatite coating on implant fixation in ovariectomized rats. *Biomaterials* 31, 9006–9014. doi: 10.1016/j.biomaterials.2010.07.112

Lin, K., Liu, P., Wei, L., Zou, Z., Zhang, W., Qian, Y., et al. (2013). Strontium substituted hydroxyapatite porous microspheres: surfactant-free hydrothermal synthesis, enhanced biological response and sustained drug release. *Chem. Eng. J.* 222, 49–59. doi: 10.1016/j.cej.2013.02.037

Liu, F., Zhang, X., Yu, X., Xu, Y., Feng, T., and Ren, D. (2011). In vitro study in stimulating the secretion of angiogenic growth factors of strontium-doped calcium polyphosphate for bone tissue engineering. *J. Mater. Sci. Mater. Med.* 22, 683–692. doi: 10.1007/s10856-011-4247-1

Loi, F., Córdova, L. A., Pajarinen, J., Lin, T.-H., Yao, Z., and Goodman, S. B. (2016). Inflammation, fracture and bone repair. *Bone* 86, 119–130. doi: 10.1016/j.bone.2016.02.020

Mao, Y., Pan, M., Yang, H., Lin, X., and Yang, L. (2020). Injectable hydrogel wound dressing based on strontium ion cross-linked starch. *Front. Mater. Sci.* 14, 232–241. doi: 10.1007/s11706-020-0508-6

Marques, C. F., Lemos, A., Vieira, S. I., Da Cruz, E., Silva, O. A. B., Bettencourt, A., et al. (2016). Antibiotic-loaded Sr-doped porous calcium phosphate granules as multifunctional bone grafts. *Ceram. Int.* 42, 2706–2716. doi: 10.1016/j.ceramint.2015.11.001

Marx, D., Rahimnejad Yazdi, A., Papini, M., and Towler, M. (2020). A review of the latest insights into the mechanism of action of strontium in bone. *Bone Rep.* 12:100273. doi: 10.1016/j.bonr.2020.100273

Meunier, P. J., Roux, C., Seeman, E., Ortolani, S., Badurski, J. E., Spector, T. D., et al. (2004). The effects of strontium ranelate on the risk of vertebral fracture in women with postmenopausal osteoporosis. *New Engl. J. Med.* 350, 459–468.

Neves, N., Linhares, D., Costa, G., Ribeiro, C. C., and Barbosa, M. A. (2017). In vivo and clinical application of strontium-enriched biomaterials for bone regeneration. *Bone Joint Res.* 6, 366–375. doi: 10.1302/2046-3758.66.bjr-2016-0311.r1

Peng, S., Zhou, G., Luk, K. D. K., Cheung, K. M. C., Li, Z., Lam, W. M., et al. (2009). Strontium promotes osteogenic differentiation of mesenchymal stem cells through the Ras/MAPK signaling pathway. *Cell. Physiol. Biochem.* 23, 165–174. doi: 10.1159/000204105

Penido, M. G. M. G., and Alon, U. S. (2012). Phosphate homeostasis and its role in bone health. *Pediatr. Nephrol.* 27, 2039–2048. doi: 10.1007/s00467-012-2175-z

Prabha, R. D., Nair, B. P., Ditzel, N., Kjems, J., Nair, P. D., and Kassem, M. (2019). Strontium functionalized scaffold for bone tissue engineering. *Mater. Sci. Eng. C* 94, 509–515. doi: 10.1016/j.msec.2018.09.054

Reginster, J., Kaufman, J., Goemaere, S., Devogelaer, J., Benhamou, C., Felsenberg, D., et al. (2012). Maintenance of antifracture efficacy over 10 years with strontium ranelate in postmenopausal osteoporosis. *Osteoporosis Int.* 23, 1115–1122. doi: 10.1007/s00198-011-1847-z

Renaudin, G., Laquerrière, P., Filinchuk, Y., Jallot, E., and Nedelec, J. M. (2008). Structural characterization of sol–gel derived Sr-substituted calcium phosphates with anti-osteoporotic and anti-inflammatory properties. *J. Mater. Chem.* 18, 3593–3600. doi: 10.1039/b804140g

Römer, P., Desaga, B., Proff, P., Faltermeier, A., and Reicheneder, C. (2012). Strontium promotes cell proliferation and suppresses IL-6 expression in human PDL cells. *Ann. Anat. Anatomischer Anzeiger* 194, 208–211. doi: 10.1016/j.aanat.2011.09.008

Saberianpour, S., Heidarzadeh, M., Geranmayeh, M. H., Hosseinkhani, H., Rahbarghazi, R., and Nouri, M. (2018). Tissue engineering strategies for the induction of angiogenesis using biomaterials. *J. Biol. Eng.* 12:36.

Saidak, Z., and Marie, P. J. (2012). Strontium signaling: molecular mechanisms and therapeutic implications in osteoporosis. *Pharmacol. Ther.* 136, 216–226. doi: 10.1016/j.pharmthera.2012.07.009

Schumacher, M., Lode, A., Helth, A., and Gelinsky, M. (2013). A novel strontium(II)-modified calcium phosphate bone cement stimulates human-bone-marrow-derived mesenchymal stem cell proliferation and osteogenic differentiation in vitro. *Acta Biomater.* 9, 9547–9557. doi: 10.1016/j.actbio.2013.07.027

Sila-Asna, M., Bunyaratvej, A., Maeda, S., Kitaguchi, H., and Bunyaratavej, N. (2007). Osteoblast differentiation and bone formation gene expression in strontium-inducing bone marrow mesenchymal stem cell. *Kobe J. Med. Sci.* 53, 25–35.

Smith, L. (1963). Ceramic-plastic material as a bone substitute. *Arch. Surg.* 87, 653–661. doi: 10.1001/archsurg.1963.01310160115023

Surdacka, A., Stopa, J., and Torlinski, L. (2007). In Situ effect of strontium toothpaste on artificially decalcified human enamel. *Biol. Trace Elem. Res.* 116, 147–153. doi: 10.1007/s12011-007-9024-0

Tao, Z., Zhou, W., Jiang, Y., Wu, X., Xu, Z., Yang, M., et al. (2018). Effects of strontium-modified calcium phosphate cement combined with bone morphogenetic protein-2 on osteoporotic bone defects healing in rats. *J. Biomater. Appl.* 33, 3–10. doi: 10.1177/0885328218765847

Tao, Z.-S., Bai, B.-L., He, X.-W., Liu, W., Li, H., Zhou, Q., et al. (2016a). A comparative study of strontium-substituted hydroxyapatite coating on implant's osseointegration for osteopenic rats. *Med. Biol. Eng. Comput.* 54, 1959–1968. doi: 10.1007/s11517-016-1494-9

Tao, Z.-S., Zhou, W.-S., He, X.-W., Liu, W., Bai, B.-L., Zhou, Q., et al. (2016b). A comparative study of zinc, magnesium, strontium-incorporated hydroxyapatite-coated titanium implants for osseointegration of osteopenic rats. *Mater. Sci. Eng. C* 62, 226–232. doi: 10.1016/j.msec.2016.01.034

Thormann, U., Ray, S., Sommer, U., Elkhassawna, T., Rehling, T., Hundgeburth, M., et al. (2013). Bone formation induced by strontium modified calcium phosphate cement in critical-size metaphyseal fracture defects in ovariectomized rats. *Biomaterials* 34, 8589–8598. doi: 10.1016/j.biomaterials.2013.07.036

Vavken, J., Mameghani, A., Vavken, P., and Schaeren, S. (2016). Complications and cancer rates in spine fusion with recombinant human bone morphogenetic protein-2 (rhBMP-2). *Eur. Spine J.* 25, 3979–3989. doi: 10.1007/s00586-015-3870-9

Von Euw, S., Wang, Y., Laurent, G., Drouet, C., Babonneau, F., Nassif, N., et al. (2019). Bone mineral: new insights into its chemical composition. *Sci. Rep.* 9:8456.

Wang, R., Wang, R., Chen, D., Qin, G., and Zhang, E. (2020). Novel CoCrWNi alloys with Cu addition: microstructure, mechanical properties, corrosion properties and biocompatibility. *J. Alloys Compounds* 824:153924. doi: 10.1016/j.jallcom.2020.153924

Wang, W., and Yeung, K. W. K. (2017). Bone grafts and biomaterials substitutes for bone defect repair: a review. *Bioactive Mater.* 2, 224–247. doi: 10.1016/j.bioactmat.2017.05.007

Wang, X., Wang, Y., Li, L., Gu, Z., Xie, H., and Yu, X. (2014). Stimulations of strontium-doped calcium polyphosphate for bone tissue engineering to protein secretion and mRNA expression of the angiogenic growth factors from endothelial cells in vitro. *Ceram. Int.* 40, 6999–7005. doi: 10.1016/j.ceramint.2013.12.027

Wornham, D. P., Hajjawi, M. O., Orriss, I. R., and Arnett, T. R. (2014). Strontium potently inhibits mineralisation in bone-forming primary rat osteoblast cultures and reduces numbers of osteoclasts in mouse marrow cultures. *Osteoporosis Int.* 25, 2477–2484. doi: 10.1007/s00198-014-2791-5

Wu, Y., Hou, J., Yin, M., Wang, J., and Liu, C. (2014). Enhanced healing of rabbit segmental radius defects with surface-coated calcium phosphate cement/bone morphogenetic protein-2 scaffolds. *Mater. Sci. Eng. C* 44, 326–335. doi: 10.1016/j.msec.2014.08.020

Xie, H., Gu, Z., He, Y., Xu, J., Xu, C., Li, L., et al. (2018). Microenvironment construction of strontium–calcium-based biomaterials for bone tissue regeneration: the equilibrium effect of calcium to strontium. *J. Mater. Chem. B* 6, 2332–2339. doi: 10.1039/c8tb00306h

Xu, Y., An, L., Chen, L., Xu, H., Zeng, D., and Wang, G. (2018). Controlled hydrothermal synthesis of strontium-substituted hydroxyapatite nanorods and their application as a drug carrier for proteins. *Adv. Powder Technol.* 29, 1042–1048. doi: 10.1016/j.apt.2018.01.008

Yan, S., Feng, L., Zhu, Q., Yang, W., Lan, Y., Li, D., et al. (2018). Controlled release of BMP-2 from a heparin-conjugated strontium-substituted nanohydroxyapatite/silk fibroin scaffold for bone regeneration. *ACS Biomat. Sci. Eng.* 4, 3291–3303. doi: 10.1021/acsbiomaterials.8b00459

Ye, H., Zhu, J., Deng, D., Jin, S., Li, J., and Man, Y. (2019). Enhanced osteogenesis and angiogenesis by PCL/chitosan/Sr-doped calcium phosphate electrospun nanocomposite membrane for guided bone regeneration. *J. Biomater. Sci. Polym. Ed.* 30, 1505–1522. doi: 10.1080/09205063.2019.1646628

Zhao, F., Lei, B., Li, X., Mo, Y., Wang, R., Chen, D., et al. (2018). Promoting in vivo early angiogenesis with sub-micrometer strontium-contained bioactive microspheres through modulating macrophage phenotypes. *Biomaterials* 178, 36–47. doi: 10.1016/j.biomaterials.2018.06.004

Zhu, H., Guo, D., Sun, L., Li, H., Hanaor, D. A. H., Schmidt, F., et al. (2018). Nanostructural insights into the dissolution behavior of Sr-doped hydroxyapatite. *J. Eur. Ceram. Soc.* 38, 5554–5562. doi: 10.1016/j.jeurceramsoc.2018.07.056

Conflict of Interest: The authors declare that the research was conducted in the absence of any commercial or financial relationships that could be construed as a potential conflict of interest.

frontiers in Bioengineering and Biotechnology

MINI REVIEW
published: 21 October 2020
doi: 10.3389/fbioe.2020.590998

Applications of Polydopamine-Modified Scaffolds in the Peripheral Nerve Tissue Engineering

Ji Yan[1,2,3†], Ruoyin Wu[3,4†], Sisi Liao[1,2,3], Miao Jiang[1,2,3] and Yun Qian[1,3]*

[1] Department of Orthopedics, Shanghai Jiao Tong University Affiliated Sixth People's Hospital, Shanghai, China, [2] Shanghai Jiao Tong University School of Medicine, Shanghai, China, [3] Youth Science and Technology Innovation Studio, Shanghai Jiao Tong University School of Medicine, Shanghai, China, [4] School of Pharmacy, Shanghai Jiao Tong University, Shanghai, China

OPEN ACCESS

Edited by:
Xin Zhao,
The Hong Kong Polytechnic University, Hong Kong

Reviewed by:
Chen Huang,
Donghua University, China
Jing Wang,
Chinese Academy of Sciences (CAS), China

****Correspondence:***
Yun Qian
lollipopcloudland@foxmail.com

[†] These authors have contributed equally to this work

Specialty section:
This article was submitted to Biomaterials, a section of the journal Frontiers in Bioengineering and Biotechnology

Received: *03 August 2020*
Accepted: *17 September 2020*
Published: *21 October 2020*

Citation:
Yan J, Wu R, Liao S, Jiang M and Qian Y (2020) Applications of Polydopamine-Modified Scaffolds in the Peripheral Nerve Tissue Engineering. Front. Bioeng. Biotechnol. 8:590998. doi: 10.3389/fbioe.2020.590998

Peripheral nerve injury is a common and complicated traumatic disease in clinical neurosurgery. With the rapid advancement and development of medical technologies, novel tissue engineering provides alternative therapies such as nerve conduit transplantation. It has achieved significant outcomes. The scaffold surface modification is vital to the reconstruction of a pro-healing interface. Polydopamine has high chemical activity, adhesion, hydrophilicity, hygroscopicity, stability, biocompatibility, and other properties. It is often used in the surface modification of biomaterials, especially in the peripheral nerve regeneration. The present review discusses that polydopamine can promote the adhesion, proliferation, and differentiation of neural stem cells and the growth of neuronal processes. Polydopamine is widely used in the surface modification of nerve conduits and has a potential application prospect of repairing peripheral nerve injury. Polydopamine-modified scaffolds are promising in the peripheral nerve tissue engineering.

Keywords: polydopamine, surface modification, peripheral nerve repair, nerve conduit, tissue engineering

INTRODUCTION

Peripheral nerve injury can lead to partial or total nerve rupture and result in paralysis, neuropathic pain, and even sensory loss. It severely impairs the patients' limb functions and reduces their qualities of life. Although autologous transplantation is the current gold standard of clinical treatment, it also has many defects, such as limited sources, mismatched diameters, and sensory dysfunction in the donor region (Samadian et al., 2020). Given these problems, the clinical application of nerve conduits is being constantly explored. To fabricate an ideal nerve conduit, the material selection and other important scaffold properties must be considered, such as pro-adhesive interface, conductivity, degradability, biocompatibility, and mechanical stability. Among them, surface modification is a common and vital tool to improve the microenvironment of the cell/scaffold interface to support an adhesive surface. Immobilized bioactive molecules play a

significant role in this process (Chen et al., 2016). Studies have shown that physical and chemical properties of the scaffold interface affect the adhesion, proliferation, and differentiation of cells on the biomaterial surface (Wozniak et al., 2004; Bettinger et al., 2009).

Hsiao et al. (2009) attached the synthetic hybrid DNA strands to the plasma membrane of living cells to allow the modification of the cell surface directly. This technique is more suitable for modifying primary cells because prolonged cell culture is not required. A study revealed that the Arg-Gly-Asp (RGD) peptide functionalized bilayers could support neural stem cells (NSCs) attachment and proliferation. The bilayers were prepared through physical absorption. However, this method was inefficient (Ananthanarayanan et al., 2010; Georgiou et al., 2013). Conducting polymers, such as polypyrrole (PPY) and poly(3,4-ethylenedioxythiophene), have been used to facilitate the growth and differentiation of neural cells, based on their electroactivity and electrical conductivity (Rim et al., 2013). However, the mechanical stability is reduced substantially. It also becomes difficult to calculate the exact density and distribution (Green et al., 2009; Gelmi et al., 2010). Besides, it was demonstrated that surface modification was necessary for Schwann cell's response and polycaprolactone (PCL) could improve biocompatibility (Luca et al., 2014).

Dopamine is a dopa derivative containing catechin groups. Catechol and amino groups in its molecular structure have high chemical activity and play an important role in the adhesion process through covalent bonds and non-covalent forces. Polydopamine (PDA), formed by oxidative self-polymerization of dopamine in weak basic Buer solution, has no special requirements on the properties of materials and can stick to almost any object surface even Teflon (Miller et al., 2017). In 2007, Lee et al. (2007) first discovered a simplified method to apply PDA for material surface modification based on the mussel adhesion protein inspiration. Since then, PDA has been widely used in surface modification of various inorganic or organic materials due to its unique properties, especially in the field of biomedicine. It mainly includes adhesion of organic templates in the biomineralization and preparation of nanocapsules for drug delivery. The biocompatibility and hydrophilicity of the materials were improved as well as the immunogenicity was reduced (Ryu et al., 2010; Cui et al., 2012). In the study of Bhang et al. (2013), it was verified that when the pheochromocytoma (PC) 12 cells were cultured on the PDA-coated surfaces, the expression of marker proteins would be enhanced in the neuronal differentiation, compared to that on the gelatin-modified surfaces. The length of the neurites extended more effectively. Compared with traditional surface modification strategies, PDA coatings have significant advantages. PDA deposition is non-specific, whereas grafting depends on specific sites on the membrane surface. The process of PDA modification is under simple and mild conditions so that it can avoid potential damage in the process of irradiation. The PDA coatings keep scaffolds moist in the plasma treatment that affects the surface permeability of the materials (Miller et al., 2017).

In recent years, the application of PDA in the nerve tissue engineering has become a research hotspot. In this review, the physicochemical properties, biocompatibility, and effects on neuronal activity of PDA as well as its applications in the peripheral nerve tissue engineering are reviewed (**Figure 1**).

PHYSICOCHEMICAL PROPERTIES OF PDA

Reactions of PDA

Properties of PDA such as adhesion are based on its chemical activity. Chemically active catechol can form hydrogen bonds with hydroxyl and chelate metal ions (Lee et al., 2007). Covalent bonds are commonly formed between catechol and many groups including sulfhydryl and amidogen (Lee et al., 2006).

Polydopamine acts as either oxidant or reductant in a reaction because of its oxidizing quinonyl and the reductive catechol (Miller et al., 2017). Chelation reactions take place when PDA meets metal ions with every valence (Fe^{3+}, Zn^{2+}, Mn^{2+}, Cu^{2+}) (Ye et al., 2017). Noble metal ions can be reduced by PDA because the electrons that are released during the oxidation of catechol stimulate the reduction of positive ions (Ball et al., 2011).

When it comes to proteins representative of biomolecules, nucleophilic ones react with carbon on the benzene ring (Michael addition), and the primary amino groups in proteins react with PDA in the quinone form (Schiff base reactions) (Lee et al., 2009). Thiol and amino groups also react with PDA. In alkaline conditions, phenolic groups in PDA are first oxidized to homologous quinone and then react with amino groups by Schiff base reaction or Michael addition. While thiol groups often react with PDA by Michael addition, amino and imino groups in PDA make it more likely to crosslink some organic molecules on PDA (Hu and Mi, 2013; Wang et al., 2013; Liu et al., 2014). Moreover, since PDA hardly bonds to chemical reagents except for water and solutions with metal ions, it shows the advantage when it comes to deposition (Miller et al., 2017).

Adhesion of PDA

Polydopamine deposits on organic or inorganic materials, regardless of whether the surface is hydrophilic or hydrophobic, and surface properties of composite materials are dominated (Miller et al., 2017). Although adhesion mechanisms are not clear, it is closely related to chemical compositions. There are mainly two kinds of adhesion processes: covalent bindings and non-covalent bindings. Covalent bindings involve Michael addition and Schiff base reaction, and non-covalent bindings include metal coordination, hydrogen bonds, π - π stack, and Van der Waals' force (Yu et al., 1999; Dalsin et al., 2005; Anderson et al., 2010; Li et al., 2010; Ye et al., 2011; Pop-Georgievski et al., 2012; Liu et al., 2014). The more the non-covalent bonds are, the stronger the adhesion is (Miller et al., 2017). In addition, a high concentration of SO_4^{2-}, NO_3^-, and Cl^- interrupted deposition. It indicates that adhesion of PDA is selective (Zhang et al., 2018).

After PDA is attached to materials, it performs as a secondary platform for functional molecules (drugs or growth factors, silver

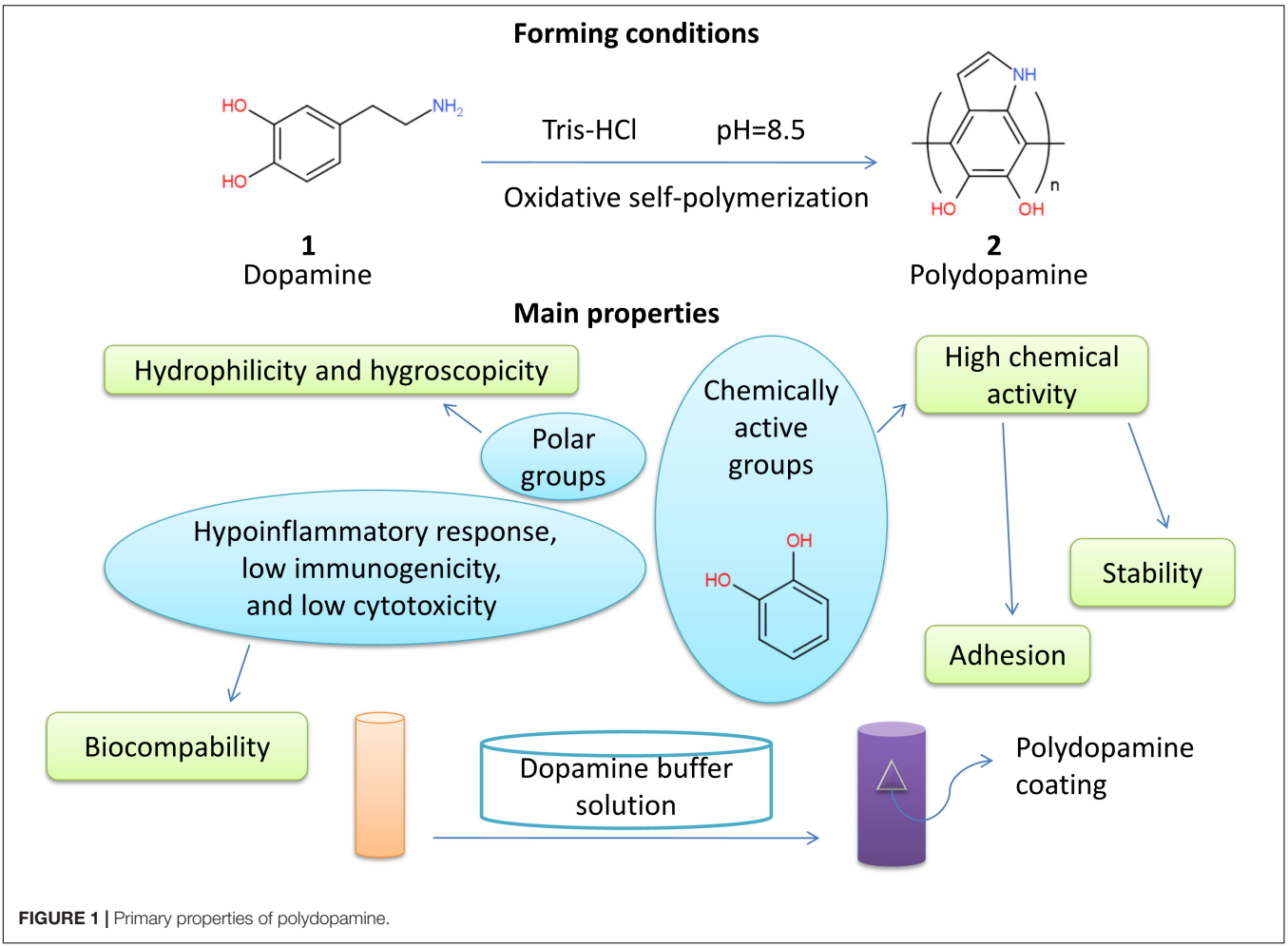

FIGURE 1 | Primary properties of polydopamine.

nanoparticles, and proteins) binding to the surface (Lee et al., 2009; Ball et al., 2011; Liang et al., 2019). In addition, thicker layers of PDA can bind more drugs with much longer release time (several hundred days), which endows the drugs with sustained release (Yang et al., 2018).

Hydrophilicity and Hygroscopicity of PDA

Many phenolic and amino groups increase the hydrophilicity of PDA, so that PDA-adhered materials are more hydrophilic, and hydrophobic materials covered by PDA have even much better hydrophilicity (Miller et al., 2017). Because of the existence of strong hydrophilic groups of PDA, such as amino, imino, and catechol groups, the ability of materials to absorb water was improved (Chen et al., 2019).

Stability of PDA

Stability of PDA depends on synthetic methods. For instance, PDA layers synthesized by air oxidation are heterogeneous and insufficient. They are unstable in polar organic solvents, and acidic and alkaline water solutions. However, PDA layers synthesized by $CuSO_4/H_2O_2$ in alkaline conditions have better homogeneity and pH stability. They also show strong polarity in organic solvents (Zhang et al., 2016). PDA coatings in water solutions often possess excellent mechanical strength and structural stability (Shen et al., 2015; Fang et al., 2019).

BIOCOMPATIBILITY OF PDA

Polydopamine displays high cellular and tissue biocompatibility characteristics (Han et al., 2017). PDA coatings can reduce inflammation, immune reaction, and cytotoxicity (Hong et al., 2011). Oxidative polymerization of dopamine could promote cell adhesion and proliferation on substrates [polylactic acid, poly(lactic-co-glycolic acid) (PLGA), polyurethane(PU), PCL, hydrophobic materials (poly-ethylene, poly-tetrafluoroethylene, and poly-dimethyl-siloxane)] (Ku et al., 2010; Tsai et al., 2011; Rim et al., 2012). Hydrogel directly applied to skin can reduce inflammation if it contains PDA in synthesis (Han et al., 2017). For example, polystyrene/silver/PDA nanoparticles show no cytotoxicity at low concentration and slight cytotoxicity at high concentration, which guarantees a higher cell survival rate (Cong et al., 2014). H_2O_2 can degrade PDA nanoparticles effectively, which has also been proved *in vivo* (Liu et al., 2014). Biodegradability strengthens PDA safety.

PDA AND THE ACTIVITY OF NEURON AND NEURON-LIKECELLS

NSC Adhesion Enhanced by PDA

In recent years, PDA has been widely used in the modification of biomaterials due to its desirable cell adhesion. Neural stem cells have the ability of division and self-renewal. Under appropriate conditions, neural stem cells can differentiate into different types of cells, including neurons, to repair and replace damaged nerve cells. Many experiments have proved that NSCs can effectively adhere to the surface of the composites modified by PDA, indicating it is beneficial to repair injured nerves. However, the molecular mechanism of PDA promoting NSC adhesion is still unclear. The addition of PDA can enhance the hydrophilicity (Cheng et al., 2016). It was reported that enhanced hydrophilicity can promote cell adhesion and other cell behaviors (Lin and Fu, 2016). PDA contains many hydrophilic functional groups, such as hydrophilic amino group and hydroxyl group, which can provide hydrophilic group for hydrophobic surface, thus improving the hydrophilicity of the nerve conduits. In addition, vincristine, a kind of cytoskeleton protein, is closely related to local adhesion and regulates cell proliferation. The expression of vincristine in NSCs cultured with PDA was enhanced significantly, and it showed that NSCs were much more proliferative than the non-PDA treatment group (Yang et al., 2020).

NSC Proliferation and Differentiation Improved by PDA

Postsynaptic density protein-95(PSD-95) protein exists in the postsynaptic membrane. Its content can reflect the development and maturity of synapses. Beta III tubulin is a specific microtubulin of neurons. Glial fibrillary acidic protein (GFAP) is a specific intermediate filament protein in astrocytes. Microtubule-associated protein 2(MAP2) only exists in the skeleton of mature nerve cells. The gradual increase in PSD-95, MAP2, and beta III tubulin and decrease in GFAP can be regarded as the process of neuronal maturation and neuronal development (Hendrickson et al., 2011). Some studies have shown that the PDA modification can increase the hydrophilicity of the scaffold and then enhance the cell adhesion, leading to the increase in cell proliferation (Lin and Fu, 2016).

Neurite Outgrowth Induced by PDA

The PDA-modified PLGA nanofiber membrane can effectively adsorb IGF-1 without damaging the growth factor activity and has an obvious slow-release effect on IGF-1. It is beneficial to maintain the long-term and stable accumulation of IGF-1 at the nerve injury site. Thus, it can maximize the function of IGF-1 (Qi et al., 2019). IGF-1stimulates the growth of neurite, promotes the proliferation and differentiation of nerve cells, inhibits the apoptosis of nerve cells, and promotes the repair of injured nerve tissues (**Table 1**).

PDA-RELATED BIOENGINEERING IN THE PERIPHERAL NERVE REGENERATION

Polydopamine has been widely applied in the field of biomedicine because of its excellent biological characteristics. Several recent studies have focused on the application of PDA in the repair

TABLE 1 | Functions and properties of different polydopamine-modified biomaterials.

Cell type	Adhesion	Viability	Proliferation	Differentiation	Substrate	Surface modification	Author/year
Hippocampal neurons	(+)	(+)	/	/	Electrode, insulators	PDA/PLL	Kang et al., 2011
HSCs	(+)	/	(+)	(+)	PU/PDA/ECM	/	Chen et al., 2019
RSCs	(+)	(+)	(+)	/	SG-PCL, MG-PCL	PDA/RGD	Qian et al., 2018a
Mouse C2C12 myoblasts, PC12 neuronal cells	/	(+)	(+)	(+)	Electrodes	PDA/PPY	Kim et al., 2018
PC12 cells	(+)	(+)	(+)	(+)	/	PDA	Bhang et al., 2013
HNSCs	/	/	(+)	(+)	PS, PLGA	NGF, GDNF, YIGSR, RGD-PDA	Yang et al., 2012
RSCs	(+)	/	(+)	(+)	PCL	dECM/PDA	Chen C. et al., 2018
Primary postnatal mouse cerebellar neurons	(+)	(+)	/	(+)	PNF	PDA	Sieste et al., 2018
RNSCs	(+)	(+)	(+)	(+)	PDA-PLGA	NGF	Pan et al., 2018
RSCs	(+)	(+)	/	/	PLLA	PDA/CGO/PPY	Li et al., 2020
Rat PC12 cells, primary rat DRG neurons	/	(+)	/	/	Fe_3O_4·Rhodamine 6G	PDA	Wang et al., 2020
Rat PC12 cells	(+)	(+)	(+)	(+)	PLGA/CNT	PDA-lam	Nazeri et al., 2020
Rat PC12 cells	(+)	/	(+)	/	CC	PDA	Chen X. et al., 2018
Rat BMSCs and SCs	(+)	(+)	(+)	(+)	PCL/gold	PDA	Qian et al., 2018b

"(+)", presentation of characteristics; PDA, polydopamine; PLL, poly-L-lysine; HSCs, human Schwann cells; PU, polyurethane; ECM, extracellular matrix; RSCs, rat Schwann cells; SG, single-layered graphene; MG, multi-layered graphene; PCL, polycaprolactone; RGD, arginyl glycylaspartic acid; PC12, pheochromocytoma 12; PPY, polypyrrole; HNSCs, human neural stem cells; PS, polystyrene; PLGA, poly(lactic-co-glycolic acid); dECM, decellularized extracellular matrix; PNF, peptide nanofiber; RNSCs, rat neural stem cells; NGF, nerve growth factor; PLLA, poly-l-lactic acid; CGO, carboxylic graphene oxide; DRG, dorsal root ganglia; CNT, carbon nanotube; lam, laminin; CC, carbonized cotton; BMSCs, bone marrow mesenchymal stem cells; SCs, Schwann cells.

of peripheral nerve injuries in order to develop suitable nerve conduit scaffolds.

Polydopamine has influenced the bioactivities of nerve conduits and the adhesion, growth, and differentiation of neural cells *in vitro*. Novel decellularized extracellular matrix (dECM) and PDA-coated 3D printed PCL-based conduits were created for nerve regeneration. The presence of PDA significantly improved the hydrophilicity and mechanical properties of conduits, as well as cellular behaviors and neuronal differentiation of Schwann cells (Chen C. et al., 2018). Similarly, the PDA coating significantly improved the hydrophilicity and cytocompatibility of fabricated carbon scaffolds. Proliferation and differentiation of nerve cells were significantly accelerated under the electrical stimulation (Chen X. et al., 2018). Nazeri et al. (2020) noted longer neuronal adhesion and growth on PLGA/carbon nanotube scaffolds modified via PDA coating. Meanwhile, PDA coating has been demonstrated to facilitate the efficient immobilization of NGF and adhesion peptides onto substrates. The growth factor or peptide-immobilized substrates enhanced the proliferation and differentiation of human NSCs (Yang et al., 2012). Another study also confirmed enhanced neuronal differentiation of nerve growth factor stimulated PC12 cells on the PDA-coated scaffolds (Bhang et al., 2013). As a mussel-inspired bioactive substance, PDA shows good prospects for the modification of nerve conduits, which may be applied in further preclinical studies and clinical trials.

Not only PDA coating on the nerve conduits plays an important role, but PDA combined with other materials contributes to the cell proliferation and the property improvement of nerve conduits. The manufactured PU/PDA/ECM nerve conduits exhibited significantly enhanced hydrophilicity, biodegradability, cell proliferation, and viability (Chen et al., 2019). The joint effect of PDA and RGD was reported to benefit the adhesion and proliferation of Schwann cells and mediate the process of cell signaling for nerve repair (Qian et al., 2018a). Robust copolymerization of PDA and PPY also showed its capability of enhancing the growth and proliferation of neuronal cells and stimulating neurogenesis (Kim et al., 2018).

Aside from *in vitro* work, PDA has also been explored in some *in vivo* studies. Qian et al. (2018a) showed notable locomotor and sensory function recovery in SD rats due to implantation of graphene-based nerve conduit coated with PDA/RGD. In another study, nerve regenerative capacity of PDA-gold/PCL nanoscaffolds in improving myelin sheath growth and functional recovery was observed on SD rats with sciatic nerve defects (Qian et al., 2018b). More sensitive signals from tibia muscles were demonstrated on the rat sciatic nerve when using PDA/PPY-coated electrodes than bare or PPY-coated electrodes (Kim et al., 2018).

Although there are limitations in *in vivo* researches on PDA-based repair of peripheral nerve injury, existing studies have shown its potential in the long-term clinical effect of peripheral nerve regeneration. More pre-clinical researches are in urgent need to translate PDA-dependent peripheral nerve repair into the clinical work.

DISCUSSION

Reliable and valid treatment with time sensitivity is of great importance. Autologous nerve transplantation has reduced its clinical outcomes due to its limitations. The immune rejection of allotransplantation also affects the normal life and recovery process of patients. It remains an urgent and unsolved problem on how to prepare nerve grafts with excellent biomimetic performance (Pfister et al., 2011; Tamaki, 2014). The substrate materials used for the preparation of nerve conduits range from macromolecular materials to nanomaterials, from non-degradable materials to degradable materials, such as chitosan, the copolymer of lactic acid-hydroxy acetic acid, and silk fibroin. Nerve conduits prepared by composite materials often include polymer materials for surface modification or strength support to promote cell adhesion and nerve repair (Ekdahl et al., 2011). Luca et al. (2014) carried out surface treatment on PCL film and improved its hydrophilicity by hydrolysis and amino hydrolysis. An *in vitro* cell test showed that the adhesion and proliferation of Schwann cells on the film was improved significantly during a short period of time, indicating the importance of surface treatment for the preparation of nerve conduits. Zhang et al. (2019) cross-linked the natural copolymer silk fibroin protein with the regenerated directional silk fibroin solution to form a high-strength mechanical scaffold. In this way, the neurons and Schwann cells of the dorsal root ganglion could migrate with the uniform positioning of the scaffold. Mecobalamine-loaded silk fibroin scaffold could promote the survival and growth of neurons which indicated its high biocompatibility. Since the surface modification method of PDA films was proposed, this polymer material has been widely used in the surface modification of metals, semiconductors, ceramics, and other materials. It gradually develops from functionalization to diversification, especially in the field of biomedical advantages (Liu et al., 2014). As is shown above, due to its unique properties, PDA can promote the adhesion, proliferation, and differentiation of nerve cells, thus supporting the promotion of peripheral nerve injury repair. Although the experimental evidence for the actual application of PDA in the surface modification of nerve conduit is not sufficient, it is believed that PDA has a broad prospect in the peripheral nerve repair.

CONCLUSION

Polydopamine based on mussel inspiration has high hydrophilicity, durable anti-corrosion ability, strong adhesion, and high biocompatibility. It has a broad application prospect in tissue engineering and biomedicine. Catecholamine functional groups can be quickly and effectively coated on the surface of various materials for function improvement through DA oxidation and polymerization reaction triggered by alkali. PDA improves the hydrophilicity and stability of the material surface. PDA-modified biomaterials promote cell adhesion, proliferation, and diffusion. The application of PDA in the nerve tissue engineering is developing rapidly. Although the current research on peripheral nerve repair by PDA is mainly based on

in vitro cell experiments, abundant existing experimental results indicate that PDA plays an important role in this field. Future experimental and translational work is necessary in order to obtain more findings of PDA on the level of clinical applications.

AUTHOR CONTRIBUTIONS

YQ, JY, and SL conceptualized and designed the manuscript. RW, JY, and MJ drafted the manuscript, designed the table, and reviewed the literature. SL designed the figure. YQ revised the manuscript. All authors approved the final version.

FUNDING

The study was sponsored by the Shanghai Sailing Program (No. 20YF1436000) and the 14th undergraduate training programs for innovation of Shanghai Jiao Tong University School of Medicine (No. 1420X001).

ACKNOWLEDGMENTS

We appreciate the support from Youth Science and Technology Innovation Studio of Shanghai Jiao Tong University School of Medicine.

REFERENCES

Ananthanarayanan, B., Little, L., Schaffer, D. V., Healy, K. E., and Tirrell, M. (2010). Neural stem cell adhesion and proliferation on phospholipid bilayers functionalized with RGD peptides. *Biomaterials* 31, 8706–8715. doi: 10.1016/j.biomaterials.2010.07.104

Anderson, T. H., Yu, J., Estrada, A., Hammer, M. U., Waite, J. H., and Israelachvili, J. N. (2010). The contribution of dopa to substrate-peptide adhesion and internal cohesion of mussel-inspired synthetic peptide films. *Adv. Funct. Mater.* 20, 4196–4205. doi: 10.1002/adfm.201000932

Ball, V., Nguyen, I., Haupt, M., Oehr, C., Arnoult, C., Toniazzo, V., et al. (2011). The reduction of Ag^{+} in metallic silver on pseudomelanin films allows for antibacterial activity but does not imply unpaired electrons. *J. Colloid Interface Sci.* 364, 359–365. doi: 10.1016/j.jcis.2011.08.038

Bettinger, C. J., Langer, R., and Borenstein, J. T. (2009). Engineering substrate topography at the micro-nanoscale to control cell function. *Angew. Chem. Int. Ed.* 48, 5406–5415. doi: 10.1002/anie.200805179

Bhang, S. H., Kwon, S., Lee, S., Kim, G. C., Han, A. M., Kwon, Y. H. K., et al. (2013). Enhanced neuronal differentiation of pheochromocytoma 12 cells on polydopamine-modified surface. *Biochem. Biophys. Res. Commun.* 430, 1294–1300. doi: 10.1016/j.bbrc.2012.11.123

Chen, C., Kong, X., and Lee, I. (2016). Modification of surface/ neuron interfaces for neural cell-type specific responses: a review. *Biomed. Mater.* 11:014108. doi: 10.1088/1748-6041/11/1/014108

Chen, C., Yu, J., Ng, H., Lee, K., Chen, C., Chen, Y., et al. (2018). The physicochemical properties of decellularized extracellular matrix-coated 3D printed poly(ε-caprolactone) nerve conduits for promoting Schwann cell proliferation and differentiation. *Materials* 11:1665. doi: 10.3390/ma11091665

Chen, Q., Ng, H. Y., and Shie, M. (2019). Additive manufacturing of nerve decellularized extracellular matrix-contained polyurethane conduits for peripheral nerve regeneration. *Polymers* 11:1612. doi: 10.3390/polym11101612

Chen, X., Wu, Y., Ranjan, V. D., and Zhang, Y. (2018). Three-dimensional electrical conductive scaffold from biomaterial-based carbon microfiber sponge with bioinspired coating for cell proliferation and differentiation. *Carbon* 134, 174–182. doi: 10.1016/j.carbon.2018.03.064

Cheng, Y., Chen, Y., Wang, K., and Shie, M. (2016). Enhanced adhesion and differentiation of human mesenchymal stem cell inside apatite-mineralized/poly(dopamine)-coated poly(ε- caprolactone) scaffolds by stereolithography. *J. Mater. Chem. B* 4, 6307–6315. doi: 10.1039/C6TB01377E

Cong, Y., Xia, T., Zou, M., Li, Z., Peng, B., Guo, D., et al. (2014). Mussel-inspired polydopamine coating as a versatile platform for synthesizing polystyrene/Ag nanocomposite particles with enhanced antibacterial activities. *J. Mater. Chem. B* 2, 3450–3461. doi: 10.1039/c4tb00460d

Cui, J., Yan, Y., Such, G. K., Liang, K., Ochs, C. J., Postma, A., et al. (2012). Immobilization and intracellular delivery of an anticancer drug using mussel-inspired polydopamine capsules. *Biomacromolecules* 13, 2225–2228. doi: 10.1021/bm300835r

Dalsin, J. L., Lin, L., Tosatti, S., Vörös, J., Textor, M., and Messersmith, P. B. (2005). Protein resistance of Titanium oxide surfaces modified by biologically inspired mPEG-DOPA. *Langmuir* 21, 640–646. doi: 10.1021/la048626g

Ekdahl, K. N., Lambris, J. D., Elwing, H., Ricklin, D., Nilsson, P. H., Teramura, Y., et al. (2011). Innate immunity activation on biomaterial surfaces: a mechanistic model and coping strategies. *Adv. Drug Deliv. Rev.* 63, 1042–1050. doi: 10.1016/j.addr.2011.06.012

Fang, Q., Zhang, J., Bai, L., Duan, J., Xu, H., Leung, K. C. F., et al. (2019). In situ redox-oxidation polymerization for magnetic core-shell nanostructure with polydopamine-encapsulated-Au hybrid shell. *J. Hazard. Mater.* 367, 15–25. doi: 10.1016/j.jhazmat.2018.12.059

Gelmi, A., Higgins, M., and Wallace, G. G. (2010). Physical surface and electromechanical properties of doped polypyrrole biomaterials. *Biomaterials* 31, 1974–1983. doi: 10.1016/j.biomaterials.2009.11.040

Georgiou, M., Bunting, S. C., Davies, H. A., Loughlin, A. J., Golding, J. P., and Phillips, J. B. (2013). Engineered neural tissue for peripheral nerve repair. *Biomaterials* 34, 7335–7343. doi: 10.1016/j.biomaterials.2013.06.025

Green, R. A., Lovell, N. H., and Poole-Warren, L. A. (2009). Cell attachment functionality of bioactive conducting polymers for neural interfaces. *Biomaterials* 30, 3637–3644. doi: 10.1016/j.biomaterials.2009.03.043

Han, L., Lu, X., Liu, K., Wang, K., Fang, L., Weng, L., et al. (2017). Mussel-inspired adhesive and tough hydrogel based on nanoclay confined dopamine polymerization. *ACS Nano* 11, 2561–2574. doi: 10.1021/acsnano.6b05318

Hendrickson, M. L., Rao, A. J., Demerdash, O. N. A., and Kalil, R. E. (2011). Expression of nestin by neural cells in the adult rat and human brain. *PLoS One* 6:e18535. doi: 10.1371/journal.pone.0018535

Hong, S., Kim, K. Y., Wook, H. J., Park, S. Y., Lee, K. D., Lee, D. Y., et al. (2011). Attenuation of the in vivo toxicity of biomaterials by polydopamine surface modification. *Nanomedicine* 6, 793–801. doi: 10.2217/nnm.11.76

Hsiao, S. C., Shum, B. J., Onoe, H., Douglas, E. S., Gartner, Z. J., Mathies, R. A., et al. (2009). Direct cell surface modification with DNA for the capture of primary cells and the investigation of myotube formation on defined patterns. *Langmuir* 25, 6985–6991. doi: 10.1021/la900150n

Hu, M., and Mi, B. (2013). Enabling graphene oxide nanosheets as water separation membranes. *Environ. Sci. Technol.* 47, 3715–3723. doi: 10.1021/es400571g

Kang, K., Choi, I. S., and Nam, Y. (2011). A biofunctionalization scheme for neural interfaces using polydopamine polymer. *Biomaterials* 32, 6374–6380. doi: 10.1016/j.biomaterials.2011.05.028

Kim, S., Jang, L. K., Jang, M., Lee, S., Hardy, J. G., and Lee, J. Y. (2018). Electrically conductive polydopamine-polypyrrole as high performance biomaterials for cell stimulation in vitro and electrical signal recording in vivo. *ACS Appl. Mater. Interfaces* 10, 33032–33042. doi: 10.1021/acsami.8b11546

Ku, S. H., Ryu, J., Hong, S. K., Lee, H., and Park, C. B. (2010). General functionalization route for cell adhesion on non-wetting surfaces. *Biomaterials* 31, 2535–2541. doi: 10.1016/j.biomaterials.2009.12.020

Lee, H., Dellatore, S. M., Miller, W. M., and Messersmith, P. B. (2007). Mussel-inspired surface chemistry for multifunctional coatings. *Science* 318, 426–430. doi: 10.1126/science.1147241

Lee, H., Rho, J., and Messersmith, P. B. (2009). Facile conjugation of biomolecules onto surfaces via mussel adhesive protein inspired coatings. *Adv. Mater.* 21, 431–434. doi: 10.1002/adma.200801222

Lee, H., Scherer, N. F., and Messersmith, P. B. (2006). Single-molecule mechanics of mussel adhesion. *Proc. Natl. Acad. Sci. U.S.A.* 103, 12999–13003. doi: 10.1073/pnas.0605552103

Li, S., Chu, L., Gong, X., and Diebold, U. (2010). Hydrogen bonding controls the dynamics of catechol adsorbed on a TiO_2(110) surface. *Science* 328, 882–884. doi: 10.1126/science.1188328

Li, Y., Huang, Z., Pu, X., Chen, X., Yin, G., Wang, Y., et al. (2020). Polydopamine/carboxylic graphene oxide-composited polypyrrole films for promoting adhesion and alignment of Schwann cells. *Colloids Surf. B* 191:110972. doi: 10.1016/j.colsurfb.2020.110972

Liang, Y., Zhao, X., Hu, T., Chen, B., Yin, Z., Ma, P. X., et al. (2019). Adhesive hemostatic conducting injectable composite hydrogels with sustained drug release and photothermal antibacterial activity to promote full-thickness skin regeneration during wound healing. *Small* 15:e1900046. doi: 10.1002/smll.201900046

Lin, C. C., and Fu, S. J. (2016). Osteogenesis of human adipose-derived stem cells on poly(dopamine)-coated electrospun poly(lactic acid) fiber mats. *Mater. Sci. Eng. C* 58, 254–263. doi: 10.1016/j.msec.2015.08.009

Liu, Y., Ai, K., and Lu, L. (2014). Polydopamine and its derivative materials: synthesis and promising applications in energy, environmental and biomedical fields. *Chem. Rev.* 114, 5057–5115. doi: 10.1021/cr400407a

Luca, A. C., Terenghi, G., and Downes, S. (2014). Chemical surface modification of poly-ε- caprolactone improves Schwann cell proliferation for peripheral nerve repair. *J. Tissue Eng. Regen. Med.* 8, 153–163. doi: 10.1002/term.1509

Miller, D. J., Dreyer, D. R., Bielawski, C. W., Paul, D. R., and Freeman, B. D. (2017). Surface modification of water purification membranes. *Angew. Chem. Int. Ed.* 17, 4662–4711. doi: 10.1002/anie.201601509

Nazeri, N., Karimi, R., and Ghanbari, H. (2020). The effect of surface modification of poly-lactide-co-glycolide/ carbon nanotube nanofibrous scaffolds by laminin protein on nerve tissue engineering. *J. Biomed. Mater. Res.* 2020, 1–11. doi: 10.1002/jbm.a.37013

Pan, S., Zhao, Y., Qiao, X., Qi, Z., Fu, C., Kong, W., et al. (2018). PLGA porous scaffolds by polydopamine-assisted immobilization of NGF for spinal cord injury repair. *Mater. Res. Express* 6:045024. doi: 10.1088/2053-1591/aafa8a

Pfister, B. J., Gordon, T., Loverde, J. R., Kochar, A. S., Mackinnon, S. E., and Cullen, D. K. (2011). Biomedical engineering strategies for peripheral nerve repair: surgical applications, state of the art, and future challenges. *Crit. Rev. Biomed. Eng.* 39, 81–124. doi: 10.1615/CritRevBiomedEng.v39.i2.20

Pop-Georgievski, O., Verreault, D., Diesner, M. O., Proks, V., Heissler, S., and Rypáček, F. (2012). Nonfouling poly(ethylene oxide)layers end-tethered to polydopamine. *Langmuir* 28, 14273–14283. doi: 10.1021/la3029935

Qi, Z., Yang, L., Pan, S., Ma, Y., Fu, C., and Chen, X. (2019). The effect of polydopamine modified nanofibers combined with insulin-like growth factors-1 on neural stem cells. *Chin. J. Exp. Surg.* 36:1492. doi: 10.3760/cma.j.issn.1001-9030.2019.08.050

Qian, Y., Song, J., Zheng, W., Zhao, X., Ou-yang, Y., Yuan, W., et al. (2018a). 3D manufacture of gold nanocomposite channels facilitates neural differentiation and regeneration. *Adv. Funct. Mater.* 28:1707077. doi: 10.1002/adfm.201707077

Qian, Y., Zhao, X., Han, Q., Chen, W., Li, H., and Yuan, W. (2018b). An integrated multi-layer 3D-fabrication of PDA/RGD coated graphene loaded PCL nanoscaffold for peripheral nerve restoration. *Nat. Commun.* 9:323. doi: 10.1038/s41467-017-02598-7

Rim, N. G., Kim, S. J., Shin, Y. M., Jun, I., Lim, D. W., Park, J. H., et al. (2012). Mussel-inspired surface modification of poly(L-lactide) electrospun fibers for modulation of osteogenic differentiation of human mesenchymal stem cells. *Colloids Surf. B* 91, 189–197. doi: 10.1016/j.colsurfb.2011.10.057

Rim, N. G., Shin, C., and Shin, H. (2013). Current approaches to electrospun nanofibers for tissue engineering. *Biomed. Mater.* 8:014102. doi: 10.1088/1748-6041/8/1/014102

Ryu, J., Ku, S. H., Lee, H., and Park, C. B. (2010). Mussel-inspired polydopamine coating as a universal route to hydroxyapatite crystallization. *Adv. Funct. Mater.* 20, 2132–2139. doi: 10.1002/adfm.200902347

Samadian, H., Maleki, H., Fathollahi, A., Salehi, M., Gholizadeh, S., Derakhshankhah, H., et al. (2020). Naturally occurring biological macromolecules-based hydrogels: potential biomaterials for peripheral nerve regeneration. *Int. J. Biol. Macromol.* 154, 795–817. doi: 10.1016/j.ijbiomac.2020.03.155

Shen, H., Guo, J., Wang, H., Zhao, N., and Xu, J. (2015). Bioinspired modification of h-BN for high thermal conductive composite films with aligned structure. *ACS Appl. Mater. Interfaces* 7, 5701–5708. doi: 10.1021/am507416y

Sieste, S., Mack, T., Synatschke, S. V., Schilling, C., Reckendorf, C. M., Pendi, L., et al. (2018). Water-dispersible polydopamine-coated nanofibers for stimulation of neuronal growth and adhesion. *Adv. Healthcare Mater.* 7:1701485. doi: 10.1002/adhm.201701485

Tamaki, T. (2014). Bridging long gap peripheral nerve injury using skeletal muscle-derived multipotent stem cells. *Neural Regen. Res.* 14, 1333–1336. doi: 10.4103/1673-5374.137582

Tsai, W. B., Chen, W. T., Chien, H. W., Kuo, W. H., and Wang, M. J. (2011). Poly(dopamine) coating of scaffolds for articular cartilage tissue engineering. *Acta Biomater.* 7, 4187–4194. doi: 10.1016/j.actbio.2011.07.024

Wang, L., Wang, D., Dong, Z., Zhang, F., and Jin, J. (2013). Interface chemistry engineering for stable cycling of reduced GO/SnO_2 nanocomposites for lithium ion battery. *Nano Lett.* 13, 1711–1716. doi: 10.1021/nl400269d

Wang, Y., Li, B., Xu, H., Du, S., Liu, T., Ren, J., et al. (2020). Growth and elongation of axons through mechanical tension mediated by fuorescent-magnetic bifunctional Fe_3O_4·Rhodamine 6G@PDA superparticles. *J. Nanobiotechnol.* 18:64. doi: 10.21203/rs.2.21261/v2

Wozniak, M. A., Modzelewska, K., Kwong, L., and Keely, P. J. (2004). Focal adhesion regulation of cell behavior. *BBA Mol. Cell Res.* 1692, 103–119. doi: 10.1016/j.bbamcr.2004.04.007

Yang, K., Lee, J. S., Kim, J., Lee, Y. B., Shin, H., Um, S. H., et al. (2012). Polydopamine-mediated surface modification of scaffold materials for human neural stem cell engineering. *Biomaterials* 33, 6952–6964. doi: 10.1016/j.biomaterials.2012.06.067

Yang, Y., Li, X., Qiu, H., Li, P., Qi, P., Maitz, M. F., et al. (2018). Polydopamine modified TiO_2 nanotube arrays for long-term controlled elution of bivalirudin and improved hemocompatibility. *ACS Appl. Mater. Interfaces* 10, 7649–7660. doi: 10.1021/acsami.7b06108

Yang, Y., Zhang, Y., Chai, R., and Gu, Z. (2020). A polydopamine-functionalized carbon microfibrous scaffold accelerates the development of neural stem cells. *Front. Bioeng. Biotechnol.* 8:616. doi: 10.3389/fbioe.2020.00616

Ye, Q., Zhou, F., and Liu, W. (2011). Bioinspired catecholic chemistry for surface modification. *Chem. Soc. Rev.* 40, 4244–4258. doi: 10.1039/C1CS15026J

Ye, Z., Wu, S., Zheng, C., Yang, L., Zhang, P., and Zhang, Z. (2017). Self-etching of metal-organic framework templates during polydopamine coating: nonspherical polydopamine capsules and potential intracellular trafficking of metal ions. *Langmuir* 33, 12952–12959. doi: 10.1021/acs.langmuir.7b02811

Yu, M., Hwang, J., and Deming, T. J. (1999). Role of L-3,4-dihydroxyphenylalanine in mussel adhesive proteins. *J. Am. Chem. Soc.* 121, 5825–5826. doi: 10.1021/ja990469y

Zhang, C., Ou, Y., Lei, W., Wan, L., Ji, J., and Xu, Z. (2016). $CuSO_4/H_2O_2$-induced rapid deposition of polydopamine coatings with high uniformity and enhanced stability. *Angew. Chem. Int. Ed.* 55, 3054–3057. doi: 10.1002/ange.201510724

Zhang, L., Xu, L., Li, G., and Yang, Y. (2019). Fabrication of high-strength mecobalamin loaded aligned silk fibroin scaffolds for guiding neuronal orientation. *Colloids Surf. B* 173, 689–697. doi: 10.1016/j.colsurfb.2018.10.053

Zhang, Q., Li, Y., Yang, Q., Chen, H., Chen, X., Jiao, T., et al. (2018). Distinguished Cr(VI) capture with rapid and superior capability using polydopamine microsphere: behavior and mechanism. *J. Hazard. Mater.* 342, 732–740. doi: 10.1016/j.jhazmat.2017.08.061

Conflict of Interest: The authors declare that the research was conducted in the absence of any commercial or financial relationships that could be construed as a potential conflict of interest.

frontiers in Bioengineering and Biotechnology

REVIEW
published: 04 November 2020
doi: 10.3389/fbioe.2020.586406

Toward Biomimetic Scaffolds for Tissue Engineering: 3D Printing Techniques in Regenerative Medicine

Justin J. Chung[1†], Heejung Im[1†], Soo Hyun Kim[1,2], Jong Woong Park[3] and Youngmee Jung[1,4]*

[1] Center for Biomaterials, Korea Institute of Science and Technology, Seoul, South Korea, [2] KU-KIST Graduate School of Converging Science and Technology, Korea University, Seoul, South Korea, [3] Department of Orthopedic Surgery, Korea University Anam Hospital, Seoul, South Korea, [4] School of Electrical and Electronic Engineering, Yonsei University, Seoul, South Korea

OPEN ACCESS

Edited by:
Hon Fai Chan, The Chinese University of Hong Kong, China

Reviewed by:
Fatemeh Kabirian, KU Leuven, Belgium
Jiacan Su, Second Military Medical University, China
Changchun Zhou, Sichuan University, China

****Correspondence:***
Youngmee Jung
winnie97@kist.re.kr

[†] These authors have contributed equally to this work

Specialty section:
This article was submitted to Biomaterials, a section of the journal Frontiers in Bioengineering and Biotechnology

Received: *23 July 2020*
Accepted: *05 October 2020*
Published: *04 November 2020*

Citation:
Chung JJ, Im H, Kim SH, Park JW and Jung Y (2020) Toward Biomimetic Scaffolds for Tissue Engineering: 3D Printing Techniques in Regenerative Medicine. Front. Bioeng. Biotechnol. 8:586406. doi: 10.3389/fbioe.2020.586406

Three-dimensional (3D) printing technology allows fabricating complex and precise structures by stacking materials layer by layer. The fabrication method has a strong potential in the regenerative medicine field to produce customizable and defect-fillable scaffolds for tissue regeneration. Plus, biocompatible materials, bioactive molecules, and cells can be printed together or separately to enhance scaffolds, which can save patients who suffer from shortage of transplantable organs. There are various 3D printing techniques that depend on the types of materials, or inks, used. Here, different types of organs (bone, cartilage, heart valve, liver, and skin) that are aided by 3D printed scaffolds and printing methods that are applied in the biomedical fields are reviewed.

Keywords: 3D printing, tissue engineering, bioink, scaffold, regenerative medicine

INTRODUCTION

Three-dimensional (3D) printing, also known as additive manufacturing, is a method that can fabricate objects with complex structures by depositing materials, i.e., metals, polymers, and ceramics, layer by layer (He et al., 2014; Hung et al., 2014). A 3D object can be produced through 3D scanning technology, such as computed tomography (CT) and computer-aided design (CAD) software (Hollister, 2005; Melchels et al., 2010). After image file of an object is acquired; it is converted to an STL file format that can be sliced into layers to create a 3D model (Melchels et al., 2010; Zorlutuna et al., 2012). Charles W. Hull, the president of 3D SYSTEMS, invented the first 3D printer, which was based on a stereolithography apparatus (SLA) technique (Melchels et al., 2010; Murphy and Atala, 2014; Schubert et al., 2014). The SLA printing method obtained issued a patent in 1986 (Gross et al., 2014). In 1990, a fused deposition modeling (FDM)-type printer was developed by Scott Crump, chairman of STRATASYS (Rengier et al., 2010; Gross et al., 2014). These 3D printing techniques sent shockwaves throughout multiple industries, such as automotive, aerospace, architecture, fashion, as well as bio-medicine (Duoss et al., 2014; Gross et al., 2014), since complex 3D structures can be precisely controlled and easily produced compared to subtractive methods (He et al., 2014; Choi and Kim, 2015).

In the medical fields, 3D printing technology is a promising tool for personalized treatments (Choi and Kim, 2015; Jakus et al., 2015; Kim et al., 2016). 3D models of a patient's damaged organ can be produced to serve as a visual aid for the surgeons and to help the patient to understand his or her conditions (Melchels et al., 2010; Gross et al., 2014). Additionally, 3D printing techniques

are applied to produce scaffolds and implants for regenerative medicine (He et al., 2014; Torres-Rendon et al., 2015; Kim et al., 2018, Lee et al., 2019). For example, Mankovich et al. (1994) used additive manufacturing to fabricate calvarial bone grafts, and Morrison et al. (2015) designed 3D printed scaffolds to treat tracheobronchomalacia. There are various 3D printing techniques that are classified by the types of materials and printing methods that are used to create an object (**Table 1**; Sachlos and Czernuszka, 2003; Childers et al., 2015). FDM is the most common 3D printing method. Thermoplastic filaments are melted by a heating block, and then a nozzle head directs the extrusion of the melted filaments to deposit thin layers (Azari and Nikzad, 2009; Gross et al., 2014). One of the advantages of FDM is that there are wide ranges of biodegradable and biocompatible materials, or filaments, which can be printed. Additionally, toxic organic solvents are not required to dissolve the polymeric filaments for printing (Yang et al., 2002; Leong et al., 2003). For example, Hutmacher et al. (2001) fabricated poly(ε-caprolactone) (PCL) scaffolds with a honeycomb-like porous structure using an FDM-type printer. Fibroblasts were able to proliferate and differentiate on the scaffold. However, the high temperature applied during the melt-extrusion stage can change the inherent material properties, and high-resolution printing is challenging (Yang et al., 2002). SLA type is based on solidification of liquid resin through photo-crosslinking (Melchels et al., 2010). A stage, or a base plate, for an object is immersed in liquid resin, and then the laser beam is applied to cure the resin on the stage. After the first layer is produced, the stage moves downward and the second layer is cured to deposit on the first layer (Gross et al., 2014). A selective laser sintering (SLS) printer follows a similar process to the SLA type, but the high-powered laser is applied to sinter solid powders (Leong et al., 2003). SLA-type printers can produce objects with high resolution and design more precise structures compared to the FDM technique. However, they are limited to photo-polymerizing resins, and the resins are often toxic for biomedical applications. The SLS method does not require liquid resins or toxic organic solvents to dissolve polymers, yet the sintering process can damage materials that are biodegradable (Yang et al., 2002; Williams et al., 2005). 3D plotting is an extrusion-based technology, which expels materials from a chamber by pneumatics (Sachlos and Czernuszka, 2003). Typically, plotting pastes and viscose materials are used as printing inks (Luo et al., 2013), which are either directly printed or melted in a feeding channel before they are extruded by a pneumatic pump (Ragaert et al., 2010). Due to the mild printing conditions, various soft materials (i.e., hydrogels, biocompatible polymers, and cell spheroids) can be printed with the 3D plotting method, and it is also referred to as bioprinting when cells are printed with hydrogel inks (Murphy and Atala, 2014). Haberstroh et al. (2010) were able to fabricate 3D plotted cell-seeded scaffolds of poly(L-lactide-co-glycolide) (PLGA), tricalcium phosphate (TCP)/collagen, and TCP/collagen/chitosan successfully for bone regeneration. The bioactivity of scaffolds and bone formation in calvarial defect model were evaluated. Lee et al. (2019) developed a new type of 3D bioprinting method, which allows printing a more precise and complex organ structure using hydrogel inks. The collagen ink was printed within a thermo-reversible support bath of gelatin microparticles to reproduce patient-specific cardiac ventricles. Inkjet printing is also widely used in regenerative medicine. It is a droplet-based extrusion printing technique, where droplets from the supplied fluid are deposited layer by layer, or patterned to desired shapes with biomolecules (Xu et al., 2013). Inkjet printing methods are cost-effective and applied in various fields from drug screening to tissue engineering (Boland et al., 2006); however, it is challenging to print viscous materials and cells (Koch et al., 2010). The laminated object manufacturing (LOM) process builds polymeric and metallic layers that are sequentially fed from a roller (Park et al., 2000). Laminates are cut with CO2 laser, and then layers are bonded by a heated roller. This rapid prototyping process can fabricate large objects with low cost (Murr(ed.)., 2015); however, it is challenging to make small and precise structures (Yang et al., 2002).

Every year, millions of patients are waiting organ donors and suffer from long transplant waiting lists. Tissue engineering has a potential not only to solve the current complications in organ shortage but also to improve the current level of the biomedical technology (Khademhosseini et al., 2006; Slaughter et al., 2009). Vacanti et al. (1988) established seminal work in the field of tissue engineering in the 1980s, and it is still one of the most researched fields. Conventionally, most scaffolds for tissue engineering were fabricated through a "top-down" approach, where scaffolds are designed with biocompatible polymeric materials in porous structures to biomimic the host tissue. However, for cell attachment and proliferation, the scaffolds were coated with bioactive substances, or surface modification was necessary. In contrast, the "bottom-up" approach aims to encapsulate cells in hydrogels to allow self-assembly of cell aggregation and 3D print cells directly in the form of a scaffold (**Figure 1**). An ideal scaffold has to possess a surface that is suitable for cell attachment and 3D inter-connected porous structures for extracellular matrix (ECM) formation and vascularization. 3D printing allows fabricating scaffolds with more controlled and precise structures (Derby, 2012; Do et al., 2015) compared to electro-spinning (Poologasundarampillai et al., 2011), foaming (Mahony et al., 2010), freeze-drying (Connell et al., 2014), and salt-leaching (Woodard et al., 2017) techniques. Here, we review 3D printing technologies for regenerative medicine, from 3D printed polymeric scaffolds to bio-artificial tissues, and promising outlooks for advanced treatments through 3D printing.

3D PRINTED SCAFFOLDS FOR TISSUE ENGINEERING

There have been numerous types of 3D printing techniques used and developed by researchers in the field of tissue engineering. In this section, 3D printing techniques and 3D printed biomaterials are categorized into subsections by tissues and organs that they were designed to aid. They are also summarized in **Table 2**.

Bone

The bone regeneration process involves migration and recruitment of osteoprogenitor cells to a defect region, which will then differentiate to osteoblasts to form bone minerals or

TABLE 1 | Different types of 3D printing techniques, and their pros and cons.

Types	Advantage	Limitations	References
FDM	Thermoplastic polymers are extruded without toxic organic solvents	Melting process can affect inherent material properties	Cornejo et al., 2000; Hutmacher et al., 2001; Yang et al., 2002; Zein et al., 2002; Leong et al., 2003; Woodfield et al., 2004; Azari and Nikzad, 2009; Gross et al., 2014; Hung et al., 2014, 2016; Kwon et al., 2015
SLA	High-resolution objects can be printed with complex structures	Printable materials are limited to liquid resins, which can be toxic	Rimell and Marquis, 2000; Leong et al., 2003; Tsang and Bhatia, 2004; Jiankang et al., 2009; Melchels et al., 2010; Gross et al., 2014; Melchiorri et al., 2016
SLS	Powdered materials are sintered through a similar process as SLA. No liquid resins are needed	Sintering can modify material properties	Yang et al., 2002; Seitz et al., 2005; Williams et al., 2005; Gbureck et al., 2007; Khalyfa et al., 2007; Morrison et al., 2015; Pei et al., 2017; Zhang et al., 2019
3D plotting	Bioceramics can be printed in mild conditions. 3D cell printing is possible by seeding cells into hydrogels	Post-sintering or curing is necessary. Constrained by temperature and complex multi-layer fabrication is challenging for bioprinting	Sachlos and Czernuszka, 2003; Wang et al., 2006; Lee et al., 2009, 2014b, 2019; Haberstroh et al., 2010; Ragaert et al., 2010; Fu et al., 2011; Wu et al., 2011; Hockaday et al., 2012; Bose et al., 2013; Gao et al., 2013; Luo et al., 2013; Mannoor et al., 2013; Duan et al., 2014; Inzana et al., 2014; Murphy and Atala, 2014; Markstedt et al., 2015; Kim et al., 2018; Nommeots-Nomm et al., 2018; Tallia et al., 2018; Li et al., 2020; Shi et al., 2020
Inkjet	Precise and controlled placement printing for small volume biological materials	Difficult to print viscose materials/cells. Large volume construct fabrication is challenging	Boland et al., 2006; Cui and Boland, 2009; Koch et al., 2010; Xu et al., 2013
LOM	Ideal for fabricating large 3D objects	Lamination coatings can be toxic and vulnerable when fabricating small constructs	Park et al., 2000; Yang et al., 2002; Murr(ed.)., 2015

hydroxyapatite (HA). There are various methods to enhance bioactive properties to bone tissue engineering scaffolds, such as incorporating growth factors and gene/drug deliveries. An ideal bone scaffold should be made with biocompatible materials that act as a temporary template to withstand mechanical forces in the defect site until the host tissue is fully recovered. Specifically, biodegradation rate should be similar to the duration of bone formation process, and inter-connected porous structure for vascularization is essential for the scaffold design (Bose et al., 2012; Jones, 2013).

Synthetic biodegradable polymers, such as poly(caprolactone) (PCL), poly(glycolic acid) (PGA), poly(lactic acid) (PLA), and their copolymers, have received high attention in the biomedical field since ester linkages can be degraded by hydrolysis and their by-products are non-toxic. These biodegradable polymers have also been 3D printed to produce scaffolds for tissue engineering (**Figure 2A**). Williams et al. (2005) fabricated PCL scaffold with similar mechanical properties to that of human trabecular bone using the SLS printing technique. Bone morphogenetic protein-7 (BMP-7) was seeded to enhance the bioactivity of the scaffold, and subcutaneous implantation has shown bone formation within 4 weeks. Additionally, the scaffold was fabricated to replicate a CT-scanned minipig condyle structure, which showed a possibility of producing patient-specific scaffolds (**Figures 2B,C**). Kwon et al. (2015) synthesized PCL containing PLGC [methoxy poly(ethylene glycol)-co-L-lactide-co-glycolide-co-ε-caprolactone] copolymer scaffold through the FDM process. Human dental pulp stem cell (hDPSC)-loaded PLGC scaffold instigated bone regeneration, and the degradation rate of the scaffold was comparable to the bone formation rate.

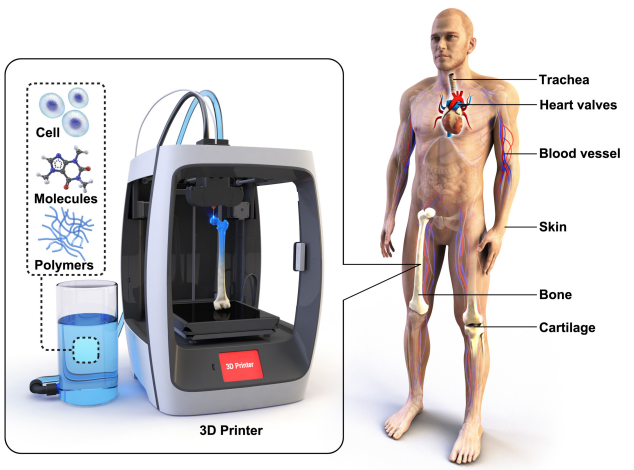

FIGURE 1 | Various scaffolds for tissues and organs have been 3D printed in the regenerative medicine field. 3D scaffolds are typically made of biocompatible polymers. Cells and bioactive molecules are often incorporated with the scaffolds to enhance bioactive properties.

Calcium phosphate-based ceramics have similar compositions to bone mineral; therefore, they have been widely used as bone substitutes. Since bioceramics are in powder form, the SLS method is often used to produce grid-like scaffold structures (Seitz et al., 2005; Gbureck et al., 2007; Khalyfa et al., 2007). 3D plotting is also practiced with a post-sintering process when binders and sacrificial polymers are mixed with bioceramics to produce printable inks (Pei et al., 2017; Zhang et al., 2019).

TABLE 2 | Summary of materials, cell types, and molecules used for 3D printed scaffolds for tissue engineering.

Organs	Materials	Cell type/Molecules	Printer type	References
Bone	PCL	BMP-2	SLS	Williams et al., 2005
	PLGA, TCP, Collagen, Chitosan	–	FDM and 3D plotting	Haberstroh et al., 2010
	PLGC		FDM	Kwon et al., 2015
	TTCP, β-TCP, Calcium sulfate	–	SLS	Khalyfa et al., 2007
	TCP	–	SLS	Gbureck et al., 2007; Zhang et al., 2019
	HA	–	SLS	Seitz et al., 2005; Pei et al., 2017; Zhang et al., 2019
	Calcium phosphate, Type I collagen	–	3D plotting	Inzana et al., 2014
	PCL, Type I collagen, Alginate, Gelatin	DPSCs/VEGF, BMP-2	FDM and 3D plotting	Park et al., 2015
	Bioactive glasses	–	3D plotting	Fu et al., 2011; Nommeots-Nomm et al., 2018; Shi et al., 2020
	Bioglass–gelatin hybrid	–	3D plotting	Gao et al., 2013
Cartilage	PU, PEO	–	FDM	Hung et al., 2014, 2016
	PEGT/PBT block copolymer	–	FDM	Woodfield et al., 2004
	Cellulose, Alginate	Human nasoseptal chondrocytes	3D plotting	Markstedt et al., 2015
	PCL, PEG, Alginate	Chondrocytes, Adipocytes	FDM and 3D plotting	Lee et al., 2014a
	Silicon, Alginate, Silver nanoparticle	Calf articular chondrocyte	3D plotting	Mannoor et al., 2013
	Silica-Poly(tetrahydrofuran)-PCL-hybrid	–	3D plotting	Tallia et al., 2018; Li et al., 2020
Heart valve	PEG-DA, Alginate	PAVIC	3D plotting	Hockaday et al., 2012
	Me-HA, Me-Gel	HAVIC	3D plotting	Duan et al., 2014
	Collagen	Human embryonic stem cell-derived cardiomyocytes	3D plotting	Lee et al., 2019
Blood vessel	Pluronic F127-DA	–	3D plotting	Wu et al., 2011
	Poly(propylene fumarate)	–	SLA	Melchiorri et al., 2016
	Type I collagen, Gelatin	HUVECs, ECs	3D plotting	Lee et al., 2014b
	Fibrinogen, Thrombin, $CaCl_2$	HMVECs	Inkjet	Cui and Boland, 2009
Trachea	PCL, Hydroxyapatite	–	SLS	Morrison et al., 2015
	PCL	–	FDM	Chang et al., 2014
	Silk fibroin	Chondrocytes	3D plotting	Kim et al., 2018
Liver	Gelatin	Hepatocytes	3D plotting	Wang et al., 2006
	PDMS	–	SLA	Jiankang et al., 2009
	PCL, Collagen	Hepatocytes, HUVECs, HLFs	FDM and 3D plotting	Lee et al., 2016
Skin	Type I collagen	hDFB, hEKC	3D plotting	Lee et al., 2009
	Collagen	NIH-3T3, HaCaT	Inkjet	Koch et al., 2012

Although bioactive glasses are not commercially successful as bioceramics, they are known to be more bioactive, and 45S5 composition (Bioglass®) was the first artificial material that formed a chemical bond to bone (Hench, 2006; Jones, 2013; Cai et al., 2018). Various compositions of bioactive glasses were also 3D printed to biomimic the porous structure of bone (Fu et al., 2011; Nommeots-Nomm et al., 2018; Shi et al., 2020). However, inorganic scaffolds (i.e., bioceramics and bioactive glasses) are too brittle for repairing defect sites that are exposed to constant loading. Flexibility and toughness of bioactive glasses can be enhanced by introducing flexible polymers to the silica network with covalent bonding, termed inorganic–organic hybrids. This is possible since glasses can be fabricated through a sol-gel process that prevents oxidization of polymers (Sanchez et al., 2005; Jones et al., 2006; Valliant and Jones, 2011; Chung et al., 2017). Gao et al. (2013) were able to 3D print a gelatin–bioactive glass hybrid to a grid-like structure. MC3T3-E1 osteoblast precursor cells were able to adhere and proliferate on the printed hybrid scaffold.

Bone is a nanocomposite composed of HA (50–70%) and organic matrix (20–40%), which is primarily composed of type I collagen (Clarke, 2008; Jones, 2013). Collagen is widely used as biomaterials for tissue engineering in skin (Powell et al., 2008), bone (Rodrigues et al., 2003), tendon (Young et al., 1998), and blood vessel (Zorlutuna et al., 2008) applications due to its tough mechanical properties and biocompatibility. Inzana et al. (2014) 3D printed collagen and calcium phosphate composite for bone regeneration. The scaffold was implanted in a murine femur with critical defect size, and osteoconductivity was confirmed

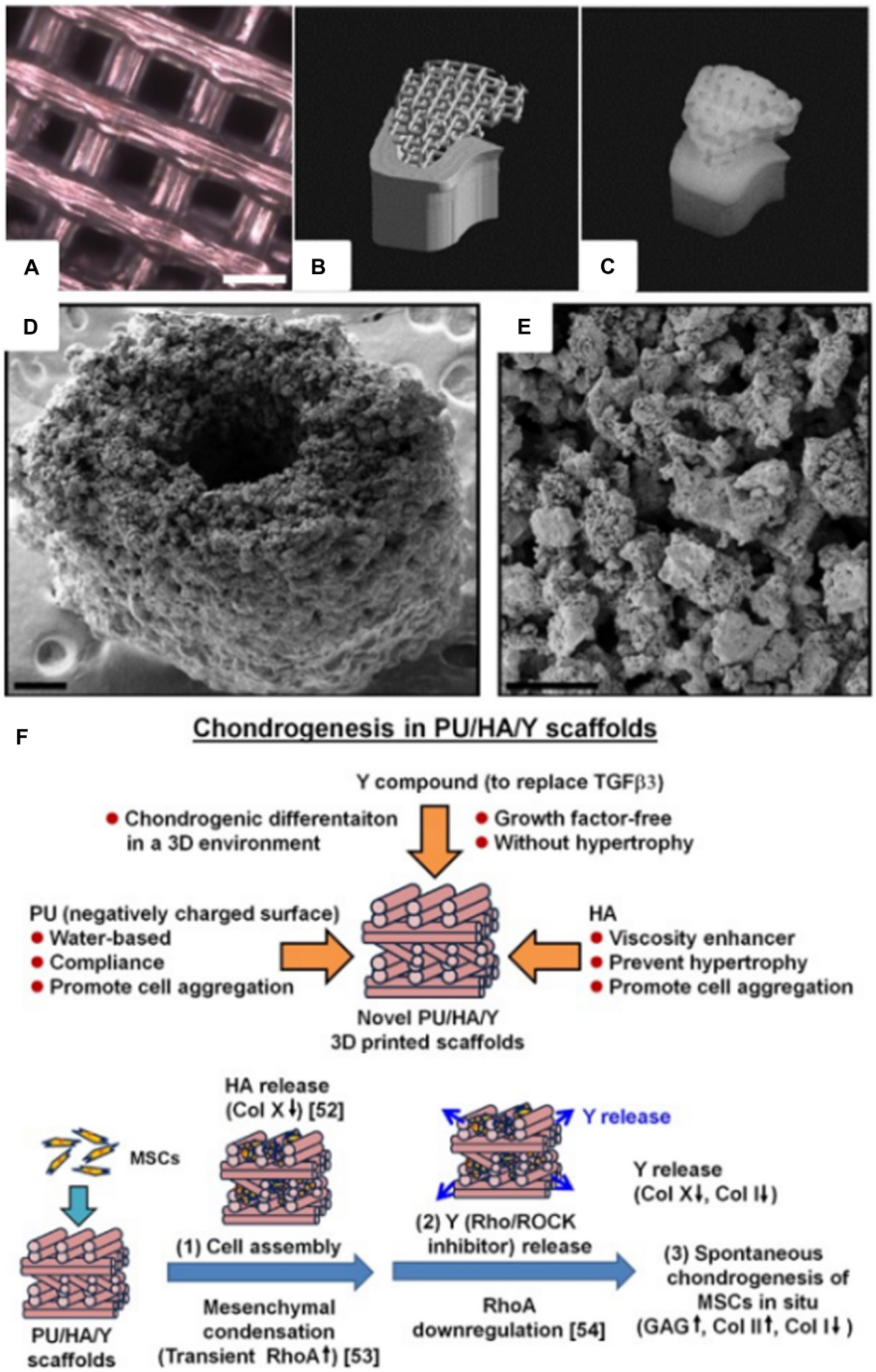

FIGURE 2 | (A) Optical microscope image of a 3D printed poly(l-lactide-co-ε-caprolactone) scaffold for adipose tissue engineering (courtesy of YJ, scale bar = 2 mm). **(B)** STL image of a pig condyle scaffold. **(C)** Front view of the 3D printed PCL scaffold (Williams et al., 2005). **(D)** SEM image of a 3D printed murine-sized scaffold for femoral mid-diaphysis regeneration (scale bar = 250 μm). **(E)** Micro-porosity of the calcium phosphate-collage composite scaffold with pore sizes of 20–50 μm (scale bar = 100 μm) (Inzana et al., 2014). **(F)** 3D printed PU/HA-based scaffold design, and possible mechanism of spontaneous chondrogenesis *in situ* (Hung et al., 2016) (Reproduced with permission from Williams et al., 2005; Inzana et al., 2014; Hung et al., 2016).

(**Figures 2D,E**). 3D bioprinting technique is one of the most recent methods of printing biomaterials; it renders 3D tissue constructs with cells embedded in hydrogels (Mironov et al., 2009; Kang et al., 2013; Levato et al., 2014). Park et al. (2015) were able to demonstrate the multi-head bioprinting method. Vascular endothelial growth factor (VEGF) and BMP-2 were loaded to various blends of hydrogels with hDPSC. The hydrogels were 3D plotted to a PCL scaffold framework, and this fabrication method

was shown to produce large volume scaffolds, which is one of the major limitations in the tissue engineering field.

Cartilage

The ECM of cartilage is composed of type II collagen and glycosaminoglycan (GAG), which allows to regulate expression of chondrocyte phenotype and instigate chondrogenesis (Suh and Matthew, 2000). In contrast to bone, cartilage has limited ability to naturally heal itself, since avascular structure inhibits nutrients and progenitor cells to migrate toward the defect region. Articular cartilage covers end of bones in synovial joints, which allows the bones to glide over each other; therefore, it should withstand load-bearing forces while providing low-friction surfaces. Osteoarthritis and high-impact injuries can cause articular cartilage defects, and it is one of the most challenging tissues to repair (Temenoff and Mikos, 2000; Huey et al., 2012).

Poly(ethylene glycol) terephthalate/poly(butylene terephthalate) (PEGT/PBT) block copolymer was 3D printed through the FDM technique to fabricate grid-like structured scaffold. The scaffold was seeded with bovine articular chondrocytes (bACs), which developed cartilage-like tissue *in vivo* while having mechanical properties similar to the native articular cartilage (Woodfield et al., 2004). Hung et al. (2014, 2016) were able to 3D print cartilage scaffolds with water as a printing ink solvent, which allowed incorporation of biomolecules, i.e., growth factors, with higher biocompatibility compared to inks that require organic solvents. Polyurethane (PU) particles, hyaluronic acid (HA), and TGFβ3 containing ink were 3D printed through a customized low-temperature FDM-type printer. Then, the scaffold was seeded with mesenchymal stem cells (MSCs) to improve cartilage regeneration *in vivo* (**Figure 2F**). Markstedt et al. (2015) developed a nanocellulose-alginate scaffold using the 3D bioprinting technique. The rheological properties of the composite bioink, which required low pressure to extrude at room temperature, allowed the production of precise 3D grid, disc, human ear, and sheep meniscus constructs. The cytotoxicity and live/dead cell-imaging assay confirmed that the scaffold was suitable for cartilage regeneration.

Other researchers have also reported 3D printing of ear-shaped structures for cartilage regeneration. Lee et al. (2014a) fabricated a human ear scaffold by printing both articular cartilage and fat tissue. Poly(ethylene glycol) (PEG) was used as a sacrificial layer since it is soluble in aqueous solutions, and PCL was printed as a main framework of the scaffold. Alginate hydrogel was used as a bioink to print chondrocyte and adipocyte. It was printed along with PCL to fabricate an ear scaffold with two distinct regions, which included a main ear part (chondrocyte) and an earlobe area (adipocyte). Additionally, co-printing of cell-seeded alginate scaffold confirmed that gene expression of both chondrocyte and adipocyte were remarkably enhanced compared to that of the control group. Mannoor et al. (2013) were able to integrate 3D biological tissue and electronic components. Alginate hydrogel with chondrocyte and silver nanoparticles was printed to structurally mimic human ears. Then, cochlea-shaped electrodes for hearing were inserted into the hydrogel construct, which was referred to as "cyborg ears." Cell viability of the cyborg ear was 91.3 ± 3.9%, which is an adequate biocompatibility for the application.

Recently, an inorganic–organic hybrid of silica-poly(tetrahydrofuran)/PCL was 3D printed to fabricate scaffolds for articular cartilage regeneration (Tallia et al., 2018; Li et al., 2020). The silica network and organic component was forming co-networks via covalent bonding, which displayed elasticity, self-healing ability, and bioactivity. The scaffold with a grid-like structure mimicked the compressive behavior of cartilage, and *in vitro* chondrogenic differentiation was observed.

Heart Valve

Heart is one of the essential organs in human physiology, which consists of various muscles to pump blood in the circulatory system. Heart valves, two in atria and the other two in ventricle chambers, are important for the blood circulation since they prevent backward flow (Dasi et al., 2009). In 2000, the American Heart Association announced that 87,000 replacement surgeries occurred (Flanagan and Pandit, 2003). Specifically, aortic valve disease is one of the serious cardiovascular diseases that are usually treated by replacement of the valves. Many researchers have studied artificial heart valves using various polymeric materials, such as PGA, PLA, collagen, and fibrin. Similar to the scaffolds described in the previous sections, inherent structures and mechanical properties are also important for designing heart valve conduits. Therefore, a 3D printing technique has been applied to this research field for several years (Hockaday et al., 2012). For heart valve engineering, hydrogels are promising materials due to their physicochemical and mechanical stability while they are hydrated. Furthermore, hydrogels are permeable for nutrients and waste transportation. Duan et al. (2014) fabricated human aortic valvular interstitial cell (HAVIC)-encapsulated heart valve conduits with photo-crosslinkable methacrylated hyaluronic acid (Me-HA) and methacrylated gelatin (Me-Gel) hydrogels. The viscosity of the hydrogel conduits was optimized and tuned by applying different hydrogel concentrations. The 3D bioprinted hydrogel conduits confirmed cell viability and remodeling potential for initial collagen and glycosaminoglycan matrix formation (**Figures 3A–G**). Hockaday et al. (2012) printed heart valve scaffolds with photo-crosslinkable poly(ethylene glycol)-diacrylate (PEG-DA). The scaffold was fabricated with two types of PEG-DA with different molecular weights in order to meet the heterogeneous mechanical properties of aortic valves. The conduit had high elastic modulus and nearly 100% cell viability (**Figures 3H–J**).

Blood Vessel/Trachea

In the United States, coronary artery bypass grafting surgeries are performed more than 400,000 per year. Critical drawbacks of the surgeries are graft damages during harvesting procedure, poor long-term patency, and donor morbidity. Therefore, there are high demands for the development of artificial blood vessels that can overcome the current shortcomings. An ideal artificial blood vessel should be biocompatible, anti-thrombogenic, and durable, and have comparable compliance with structural density

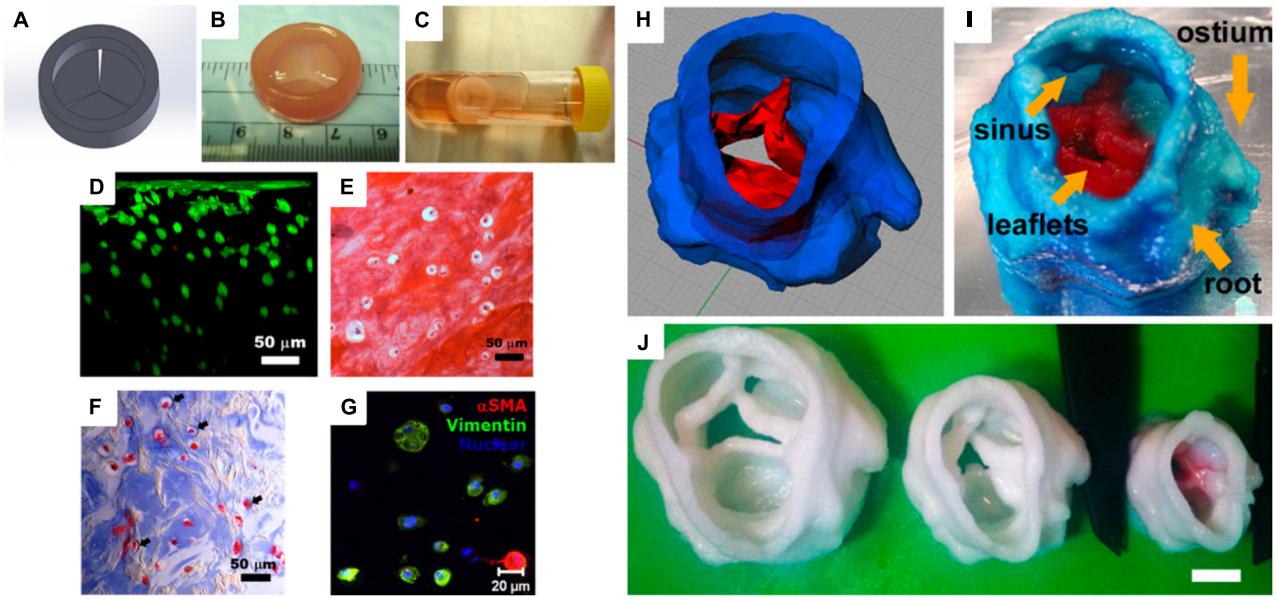

FIGURE 3 | (A) Computer-aided design (CAD) model of a heart valve. **(B)** Bioprinted methacrylated hyaluronic acid/gelatin heart valve conduit. **(C)** The hydrogel hybrid conduit after 7 days of static culture, and **(D)** cross-sectional view of a live/dead cell viability assay. **(E)** Safranin-O staining image and **(F)** Masson's Trichrome staining images showed that the heart valve conduit was composed of collagen type II and GAG. **(G)** Representative immunohistochemical staining image of αSMA, vimentin, and nuclei (Duan et al., 2014). **(H)** Porcine aortic valve model and **(I)** 3D printed scaffold with two types of PEG-DA inks [root: 700 molecular weight (MW) PEG-DA and leaflets: 700/8000 MW PEG-DA]. **(J)** Scaffolds were printed with 700 MW PEG-DA at different scales for fidelity analysis. The inner diameters (ID) were 22, 17, and 12 mm. Scale bar = 1 cm (Hockaday et al., 2012) (Reproduced with permission from Hockaday et al., 2012; Duan et al., 2014).

to that of the native blood vessels (Mosadegh et al., 2015). Wu et al. (2011) fabricated a biomimetic 3D microvascular network based on hydrogel matrix. The blood vessel's branching pattern was designed by omnidirectional printing of sacrificial ink in a photo-crosslinkable hydrogel matrix. The authors suggested that this technique can be applied to 3D cell culture; however, there were no cell tests performed. Similar work was performed by Lee et al. (2014b); functional vascular channels with perfused open lumen were fabricated through 3D bioprinting of collagen matrix with liquefying fugitive ink. Gelatin with endothelial cell (EC) was used as a fugitive ink, which protected from plasma protein and dextran molecule. Additionally, human umbilical vein endothelial cells (HUVECs) were cultured in the vascular channel, which was successfully aligned along the flow direction. The gene expression analysis confirmed that the 3D printed vascular channels had high potential for tissue engineering application.

Fibrin is a natural polymer formed by polymerization of fibrinogen and thrombin. It is present in human blood and involved in the wound healing process. Cui and Boland (2009) 3D printed human microvascular endothelial cell (HMVEC)-seeded bioink of thrombin and Ca^{2+} solution into a fibrinogen substrate. The scaffold was composed of fibrin channels with aligned HMVECs, and 21 days of cell culture confirmed tubular structure formation inside the channels. Poly(propylene fumarate)-based aorta graft was synthesized via digital light stereolithography technique (Melchiorri et al., 2016). The biodegradable polymer was 3D printed to an MRI/CT scanned structure, which showed a possibility to design patient-specific aorta grafts. Additionally, the scaffold was able to confirm bioactive properties *in vivo* with comparable mechanical strength to that of human aorta.

Tracheal structure restoration and scaffold fabrications are also in great demand. Forty-three percent of pediatric patients who went through tracheostomy experience respiratory arrest due to tube occlusion (Carr et al., 2001; Berry et al., 2010). However, if the pediatric patients are supported by a temporary scaffold for 24 to 36 months, the airway growth can naturally resolve the disease. Morrison et al. (2015) were able to produce a personalized and biodegradable tracheal splint through the SLS technique. PCL powders were mixed with hydroxyapatite, which was used as a flowing agent for the laser sintering process. PCL splints were successfully implanted to pediatric patients, and they were able to expand over time with airway growth (**Figures 4A,B**). Chang et al. (2014) 3D printed PCL scaffolds through an FDM-type printer for tracheal regeneration. The scaffold was coated with MSC-seeded fibrin to enhance bioactivity. *In vivo* study confirmed that the scaffolds were mechanically stable and able to reconstruct trachea within 8 weeks of implantation. Kim et al. (2018) produced a ring-like cartilaginous trachea scaffold through 3D bioprinting with digital light processing technique. Chondrocytes were encapsulated in methacrylated silk fibroin, which made cross-linking possible through UV light exposure. This cell-loaded hydrogel scaffold showed homogeneously distributed cells and cartilage tissue formation *in vitro*. The chemically modified silk fibroin ink was also printed

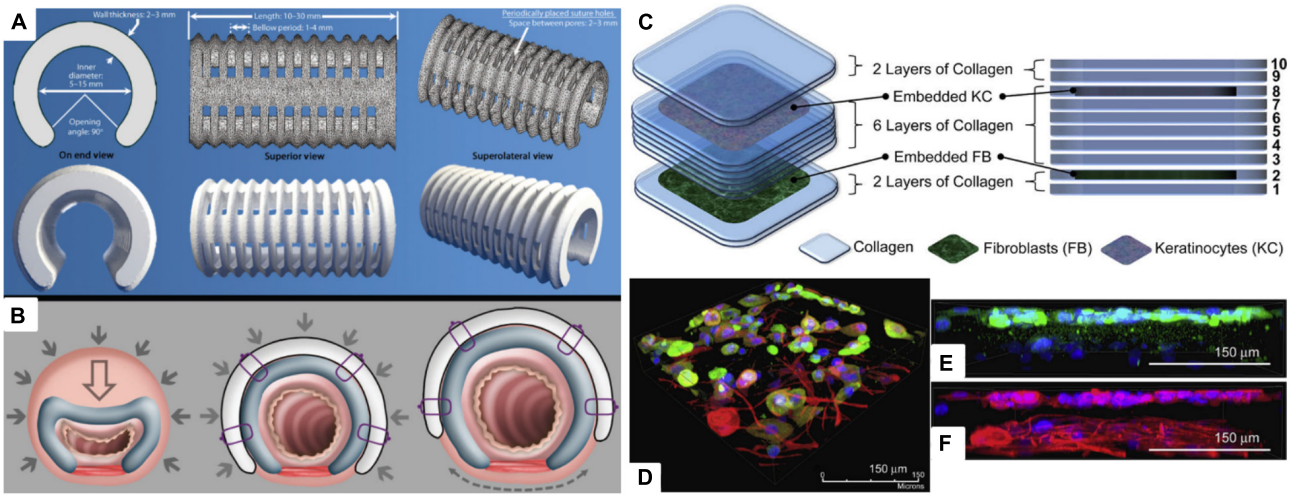

FIGURE 4 | (A) Virtual rendering of tracheobronchial splint STL file in top, bottom, and side views. Inner diameter, length, thickness, and suture hole spacing were patient-specifically designed, and then it was placed over an airway through the 90° opening angle. **(B)** The mechanism of the tracheobronchial splint. Filled arrows signify intrathoracic pressure when breathing out, and empty arrows represent reducing vector values. Dashed arrow indicates the vector movement of a splint according to the airway growth (Morrison et al., 2015). **(C)** Representative scheme of a multi-layered collagen scaffold for tissue regeneration. Primary adult human dermal fibroblast-seeded collagen is printed in the 2nd layer, and primary adult human epidermal keratinocyte embedded collagen layer is deposited in the 8th layer. **(D)** Immunofluorescent image of the 3D printed multi-layered scaffold with fibroblast and keratinocyte on a tissue culture dish. **(E)** Keratinocyte layer with keratin, and **(F)** keratinocyte and fibroblast layer with β-tubulin (Lee et al., 2009) (Reproduced with permission from Lee et al., 2009; Morrison et al., 2015).

to heart, lung, and vascular shapes, which confirmed that the bioink and printing method can be applied to various tissue engineering applications.

Liver

The liver is a fundamental organ that is responsible for multifunctional metabolic activities. Although liver transplant has been practiced for a long time, the procedure is costly, patient survival rate is poor, and there is a shortage of organ donors (Wang et al., 2007). Wang et al. (2006) made a 3D construct of gelatin hydrogel with hepatocyte as an ECM and 2.5% glutaraldehyde as a cross-linking agent. They were able to confirm that hepatocytes in gelatin construct can survive over 2 months in *in vitro* cell culture and retain their 3D structure for a month. A chitosan–gelatin hybrid scaffold was developed to biomimic the architecture of natural liver. A highly porous and well-organized structure was fabricated by a combination of 3D printing, micro-replication, and freeze-drying techniques. The novel scaffold was also composed of intrinsic fluidic channels and hepatic chambers. Firstly, a resin mold was fabricated by the SLA technique to cast polydimethylsiloxane (PDMS) for creating a micro-replication mold. Chitosan–gelatin solution was cast in the PDMS mold followed by freeze-drying to produce a porous structure. Biodegradability and hepatocyte growth were confirmed through 7-day cell culture. More importantly, albumin secretion and urea synthesis were evident, which are representative evaluation for hepatocyte functionality (Jiankang et al., 2009). Lee et al. (2016) 3D printed PCL to a grid-like structure as a primary framework to mechanically support collagen bioinks. HUVECs, human lung fibroblasts (HLFs), and hepatocytes were encapsulated in collagen inks, printed in between PCL struts for angiogenesis. The authors also evaluated albumin secretion and urea synthesis for confirming hepatocytes functionality and angiogenesis. Specifically, hepatocyte-, HLF-, and HUVEC-containing constructs showed highest albumin secretion and urea formation compared to that of hepatocytes only and hepatocyte- and HLF-containing groups.

Skin

Skin is the largest organ in our body that is responsible for various functions, such as preventing loss of body fluid, acting as a barrier against pathogenic bacterium and thermotaxis, and regulating body temperature (Bonvallet et al., 2015; Ojeh et al., 2015). Severe acute and chronic wounds (i.e., burns, diabetic ulcer, pressure sores, and lesion) effect loss of dermal tissues. Skin grafts have limitations in antigenicity and shortage of transplantable tissues; therefore, there are high demands for skin regeneration (Tchemtchoua et al., 2011; Wang et al., 2013). Lee et al. (2009) used a 3D bioprinter with four-channel dispensers to print stratified skin layers. PDMS substrate was first coated with sodium bicarbonate, a pH-altering cross-linking agent. Then, collagen was printed layer by layer to fabricate a multi-layered skin construct. Specifically, among the 10 layers of skin construct, the 2nd and 8th collagen layers were embedded with cells, fibroblast and keratinocyte, respectively. Several advantages of this fabrication method include the following: the scaffold can be made on irregular surfaces, as long as cross-linking agent coating is possible, and other types of hydrogels can substitute collagen, if they are cross-linkable. Additionally, this was the first study to 3D print both keratinocyte and fibroblast for skin regeneration (**Figures 4C–F**). Koch et al. (2010, 2012) also 3D printed keratinocyte- and fibroblast-embedded collagen for

skin tissue engineering. Laser-assisted bioprinting (LaBP) with laser-induced forward transfer technique was used to produce 3D scaffolds. The LaBP method is advantageous over other bioprinting techniques since higher-resolution cell printing is possible with greater cell density. Also, various hydrogels can be printed regardless of their viscosity. The skin scaffold, which was printed in micro-scale, confirmed that each cell layer did not blend into each other. Ten days of culture confirmed the cell vitality of the cells embedded in the scaffold, and collagen layers did not intermix with each other.

CONCLUSION AND PERSPECTIVES

Three-dimensional printing is one of the most promising technologies in tissue engineering and regenerative medicine to fabricate advanced 3D scaffolds. It allows to produce more defined and biomimetic scaffolds with bioactive factors to enhance their functionalities. Although there have been numerous studies in 3D printing for biomedical applications, there are still much room for improvement (Jakus et al., 2016; Zhu et al., 2016). Optimization of printable inks, standardization of printing methods, and higher reproducibility with mass production are major challenges. 4D printing, an integration of 3D printing with time, has emerged recently. This technology allows the printed materials to change their physical forms or functionalities when excited by an external stimulus, such as temperature, water, magnetism, and pH (Gao et al., 2016; Gladman et al., 2016). Since human body is a complex environment with various stimuli, 4D printing technology is receiving a lot of attention for medical implant surgeries. 3D bioprinting of stem cells has shown unprecedented possibilities for producing tissue constructs from bone to skin. As bioprinting technology advances, printing induced pluripotent stem (iPS) cells could take current bioactive scaffolds a step closer to regenerate patient-specific tissues and organs. iPS cells are known to have advantages over embryonic stem cells since they can be derived from patients for autologous cell treatment. However, the reprogramming process is not fully understood so far (Yamanaka, 2009). 3D bioprinting is an encouraging technology for future regenerative medicine. It allows to deliver, or mount, cells and physicochemical factors that are essential for tissue regeneration. Furthermore, patient-specific therapies are one of the essential technologies for hospital factory, where damaged organ rendering is produced by medical imaging, and defect regenerating construct is printed with patient's cells, plasma, and tissues in the operating theater. The authors are confident that the progress in 3D printing technology will foster and enhance personalized regenerative medicine.

AUTHOR CONTRIBUTIONS

JC and HI drafted the initial manuscript with guidance by YJ. SK, YJ, and JP made contributions and modifications according to their field of expertise. All authors reviewed and approved the manuscript.

FUNDING

This research was supported by the KIST Institutional Program (2V08550). This work was partially supported by the Nano-Material Technology Development Program (NRF-2018M3A7B4071106) through the National Research Foundation of Korea and a National Research Foundation of Korea grant (NRF-2020R1C1C1012881) funded by the Ministry of Science and ICT (MSIT).

REFERENCES

Azari, A., and Nikzad, S. (2009). The evolution of rapid prototyping in dentistry: a review. *Rapid Prototyp. J.* 15, 216–225. doi: 10.1108/13552540910961946

Berry, J. G., Graham, R. J., Roberson, D. W., Rhein, L., Graham, D. A., Zhou, J., et al. (2010). Patient characteristics associated with in-hospital mortality in children following tracheotomy. *Arch. Dis. Child.* 95, 703–710. doi: 10.1136/adc.2009.180836

Boland, T., Xu, T., Damon, B., and Cui, X. (2006). Application of inkjet printing to tissue engineering. *Biotechnol. J.* 1, 910–917. doi: 10.1002/biot.200600081

Bonvallet, P. P., Schultz, M. J., Mitchell, E. H., Bain, J. L., Culpepper, B. K., Thomas, S. J., et al. (2015). Microporous dermal-mimetic electrospun scaffolds pre-seeded with fibroblasts promote tissue regeneration in full-thickness skin wounds. *PLoS One* 10:e0122359. doi: 10.1371/journal.pone.0122359

Bose, S., Roy, M., and Bandyopadhyay, A. (2012). Recent advances in bone tissue engineering scaffolds. *Trends Biotechnol.* 30, 546–554. doi: 10.1016/j.tibtech.2012.07.005

Bose, S., Vahabzadeh, S., and Bandyopadhyay, A. (2013). Bone tissue engineering using 3D printing. *Mater. Today* 16, 496–504. doi: 10.1016/j.mattod.2013.11.017

Cai, L., Zhang, J., Qian, J., Li, Q., Li, H., Yan, Y. G., et al. (2018). The effects of surface bioactivity and sustained-release of genistein from a mesoporous magnesium-calcium-silicate/PK composite stimulating cell responses in vitro, and promoting osteogenesis and enhancing osseointegration in vivo. *Biomater. Sci.* 6, 842–853. doi: 10.1039/c7bm01017f

Carr, M. M., Poje, C. P., Kingston, L., Kielma, D., and Heard, C. (2001). Complications in pediatric tracheostomies. *Laryngoscope* 111(11 Pt 1), 1925–1928. doi: 10.1097/00005537-200111000-00010

Chang, J. W., Park, S. A., Park, J. K., Choi, J. W., Kim, Y. S., Shin, Y. S., et al. (2014). Tissue-engineered tracheal reconstruction using three-dimensionally printed artificial tracheal graft: preliminary report. *Artif. Organs* 38, E95–E105. doi: 10.1111/aor.12310

Childers, E. P., Wang, M. O., Becker, M. L., Fisher, J. P., and Dean, D. (2015). 3D printing of resorbable poly(propylene fumarate) tissue engineering scaffolds. *MRS Bull.* 40, 119–126. doi: 10.1557/mrs.2015.2

Choi, J. W., and Kim, N. (2015). Clinical application of three-dimensional printing technology in craniofacial plastic surgery. *Arch. Plast. Surg.* 42, 267–277. doi: 10.5999/aps.2015.42.3.267

Chung, J. J., Sum, B. S. T., Li, S., Stevens, M. M., Georgiou, T. K., and Jones, J. R. (2017). Effect of comonomers on physical properties and cell attachment to silica-methacrylate/acrylate hybrids for bone substitution. *Macromol. Rapid Commun.* 28:1700168. doi: 10.1002/marc.201700168

Clarke, B. (2008). Normal bone anatomy and physiology. *Clin. J. Am. Soc. Nephrol.* 3(Suppl. 3), S131–S139. doi: 10.2215/CJN.04151206

Connell, L. S., Romer, F., Suarez, M., Valliant, E. M., Zhang, Z. Y., Lee, P. D., et al. (2014). Chemical characterisation and fabrication of chitosan-silica hybrid

scaffolds with 3-glycidoxypropyl trimethoxysilane. *J. Mater. Chem. B* 2, 668–680. doi: 10.1039/c3tb21507e

Cornejo, I., McNulty, T. F., Lee, S., Bianchi, E., Danforth, S. C., and Safari, A. (2000). "Development of bioceramic tissue scaffolds via fused deposition of ceramics," in *Bioceramics: Materials and Applications III*, ed. L. George (Westerville, OH: American Ceramic Society), 183–195.

Cui, X. F., and Boland, T. (2009). Human microvasculature fabrication using thermal inkjet printing technology. *Biomaterials* 30, 6221–6227. doi: 10.1016/j.biomaterials.2009.07.056

Dasi, L. P., Simon, H. A., Sucosky, P., and Yoganathan, A. P. (2009). Fluid mechanics of artificial heart valves. *Clin. Exp. Pharmacol. Physiol.* 36, 225–237. doi: 10.1111/j.1440-1681.2008.05099.x

Derby, B. (2012). Printing and prototyping of tissues and scaffolds. *Science* 338, 921–926. doi: 10.1126/science.1226340

Do, A. V., Khorsand, B., Geary, S. M., and Salem, A. K. (2015). 3D printing of scaffolds for tissue regeneration applications. *Adv. Healthc. Mater.* 4, 1742–1762. doi: 10.1002/adhm.201500168

Duan, B., Kapetanovic, E., Hockaday, L. A., and Butcher, J. T. (2014). Three-dimensional printed trileaflet valve conduits using biological hydrogels and human valve interstitial cells. *Acta Biomater.* 10, 1836–1846. doi: 10.1016/j.actbio.2013.12.005

Duoss, E. B., Weisgraber, T. H., Hearon, K., Zhu, C., Small, W., Metz, T. R., et al. (2014). Three-dimensional printing of elastomeric, cellular architectures with negative stiffness. *Adv. Funct. Mater.* 24, 4905–4913. doi: 10.1002/adfm.201400451

Flanagan, T. C., and Pandit, A. (2003). Living artificial heart valve alternatives: a review. *Eur. Cell Mater.* 6, 28–45; discussion 45.

Fu, Q. A., Saiz, E., and Tomsia, A. P. (2011). Bioinspired strong and highly porous glass scaffolds. *Adv. Funct. Mater.* 21, 1058–1063. doi: 10.1002/adfm.201002030

Gao, B., Yang, Q., Zhao, X., Jin, G., Ma, Y., and Xu, F. (2016). 4D bioprinting for biomedical applications. *Trends Biotechnol.* 34, 746–756. doi: 10.1016/j.tibtech.2016.03.004

Gao, C., Rahaman, M. N., Gao, Q., Teramoto, A., and Abe, K. (2013). Robotic deposition and in vitro characterization of 3D gelatin-bioactive glass hybrid scaffolds for biomedical applications. *J. Biomed. Mater. Res. A* 101, 2027–2037. doi: 10.1002/jbm.a.34496

Gbureck, U., Hozel, T., Klammert, U., Wurzler, K., Muller, F. A., and Barralet, J. E. (2007). Resorbable dicalcium phosphate bone substitutes prepared by 3D powder printing. *Adv. Funct. Mater.* 17, 3940–3945. doi: 10.1002/adfm.200700019

Gladman, A. S., Matsumoto, E. A., Nuzzo, R. G., Mahadevan, L., and Lews, J. A. (2016). Biomimetic 4D printing. *Nat. Mater.* 15, 413–418. doi: 10.1038/Nmat4544

Gross, B. C., Erkal, J. L., Lockwood, S. Y., Chen, C., and Spence, D. M. (2014). Evaluation of 3D printing and its potential impact on biotechnology and the chemical sciences. *Anal. Chem.* 86, 3240–3253. doi: 10.1021/ac403397r

Haberstroh, K., Ritter, K., Kuschnierz, J., Bormann, K. H., Kaps, C., Carvalho, C., et al. (2010). Bone repair by cell-seeded 3D-bioplotted composite scaffolds made of collagen treated tricalciumphosphate or tricalciumphosphate-chitosan-collagen hydrogel or PLGA in ovine critical-sized calvarial defects. *J. Biomed. Mater. Res. B Appl. Biomater.* 93, 520–530. doi: 10.1002/jbm.b.31611

He, Y., Xue, G. H., and Fu, J. Z. (2014). Fabrication of low cost soft tissue prostheses with the desktop 3D printer. *Sci. Rep.* 4:6973. doi: 10.1038/srep06973

Hench, L. L. (2006). The story of bioglass (R). *J. Mater. Sci. Mater. Med.* 17, 967–978. doi: 10.1007/s10856-006-0432-z

Hockaday, L. A., Kang, K. H., Colangelo, N. W., Cheung, P. Y. C., Duan, B., Malone, E., et al. (2012). Rapid 3D printing of anatomically accurate and mechanically heterogeneous aortic valve hydrogel scaffolds. *Biofabrication* 4:035005. doi: 10.1088/1758-5082/4/3/035005

Hollister, S. J. (2005). Porous scaffold design for tissue engineering. *Nat. Mater.* 4, 518–524. doi: 10.1038/nmat1421

Huey, D. J., Hu, J. C., and Athanasiou, K. A. (2012). Unlike bone, cartilage regeneration remains elusive. *Science* 338, 917–921. doi: 10.1126/science.1222454

Hung, K. C., Tseng, C. S., Dai, L. G., and Hsu, S. H. (2016). Water-based polyurethane 3D printed scaffolds with controlled release function for customized cartilage tissue engineering. *Biomaterials* 83, 156–168. doi: 10.1016/j.biomaterials.2016.01.019

Hung, K. C., Tseng, C. S., and Hsu, S. H. (2014). Synthesis and 3D printing of biodegradable polyurethane elastomer by a water-based process for cartilage tissue engineering applications. *Adv. Healthc. Mater.* 3, 1578–1587. doi: 10.1002/adhm.201400018

Hutmacher, D. W., Schantz, T., Zein, I., Ng, K. W., Teoh, S. H., and Tan, K. C. (2001). Mechanical properties and cell cultural response of polycaprolactone scaffolds designed and fabricated via fused deposition modeling. *J. Biomed. Mater. Res.* 55, 203–216. doi: 10.1002/1097-4636(200105)55:2<203::aid-jbm1007>3.0.co;2-7

Inzana, J. A., Olvera, D., Fuller, S. M., Kelly, J. P., Graeve, O. A., Schwarz, E. M., et al. (2014). 3D printing of composite calcium phosphate and collagen scaffolds for bone regeneration. *Biomaterials* 35, 4026–4034. doi: 10.1016/j.biomaterials.2014.01.064

Jakus, A. E., Rutz, A. L., and Shah, R. N. (2016). Advancing the field of 3D biomaterial printing. *Biomed. Mater.* 11:014102. doi: 10.1088/1748-6041/11/1/014102

Jakus, A. E., Secor, E. B., Rutz, A. L., Jordan, S. W., Hersam, M. C., and Shah, R. N. (2015). Three-dimensional printing of high-content graphene scaffolds for electronic and biomedical applications. *ACS Nano* 9, 4636–4648. doi: 10.1021/acsnano.5b01179

Jiankang, H., Dichen, L., Yaxiong, L., Bo, Y., Hanxiang, Z., Qin, L., et al. (2009). Preparation of chitosan-gelatin hybrid scaffolds with well-organized microstructures for hepatic tissue engineering. *Acta Biomater.* 5, 453–461. doi: 10.1016/j.actbio.2008.07.002

Jones, J. R. (2013). Review of bioactive glass: from Hench to hybrids. *Acta Biomater.* 9, 4457–4486. doi: 10.1016/j.actbio.2012.08.023

Jones, J. R., Ehrenfried, L. M., and Hench, L. L. (2006). Optimising bioactive glass scaffolds for bone tissue engineering. *Biomaterials* 27, 964–973. doi: 10.1016/j.biomaterials.2005.07.017

Kang, K. H., Hockaday, L. A., and Butcher, J. T. (2013). Quantitative optimization of solid freeform deposition of aqueous hydrogels. *Biofabrication* 5:035001. doi: 10.1088/1758-5082/5/3/035001

Khademhosseini, A., Langer, R., Borenstein, J., and Vacanti, J. P. (2006). Microscale technologies for tissue engineering and biology. *Proc. Natl. Acad. Sci. U.S.A.* 103, 2480–2487. doi: 10.1073/pnas.0507681102

Khalyfa, A., Vogt, S., Weisser, J., Grimm, G., Rechtenbach, A., Meyer, W., et al. (2007). Development of a new calcium phosphate powder-binder system for the 3D printing of patient specific implants. *J. Mater. Sci. Mater. Med.* 18, 909–916. doi: 10.1007/s10856-006-0073-2

Kim, J. E., Kim, S. H., and Jung, Y. (2016). Current status of three-dimensional printing inks for soft tissue regeneration. *Tissue Eng. Regen. Med.* 13, 636–646. doi: 10.1007/s13770-016-0125-8

Kim, S. H., Yeon, Y. K., Lee, J. M., Chao, J. R., Lee, Y. J., Seo, Y. B., et al. (2018). Precisely printable and biocompatible silk fibroin bioink for digital light processing 3D printing. *Nat. Commun.* 9:1620. doi: 10.1038/s41467-018-03759-y

Koch, L., Deiwick, A., Schlie, S., Michael, S., Gruene, M., Coger, V., et al. (2012). Skin tissue generation by laser cell printing. *Biotechnol. Bioeng.* 109, 1855–1863. doi: 10.1002/bit.24455

Koch, L., Kuhn, S., Sorg, H., Gruene, M., Schlie, S., Gaebel, R., et al. (2010). Laser printing of skin cells and human stem cells. *Tissue Eng. Part C Methods* 16, 847–854. doi: 10.1089/ten.TEC.2009.0397

Kwon, D. Y., Kwon, J. S., Park, S. H., Park, J. H., Jang, S. H., Yin, X. Y., et al. (2015). A computer-designed scaffold for bone regeneration within cranial defect using human dental pulp stem cells. *Sci. Rep.* 5:12721.

Lee, A., Hudson, A. R., Shiwarski, D. J., Tashman, J. W., Hinton, T. J., and Yerneni, S. (2019). 3D bioprinting of collagen to rebuild components of the human heart. *Science* 365, 482–487. doi: 10.1126/science.aav9051

Lee, J. S., Hong, J. M., Jung, J. W., Shim, J. H., Oh, J. H., and Cho, D. W. (2014a). 3D printing of composite tissue with complex shape applied to ear regeneration. *Biofabrication* 6:024103. doi: 10.1088/1758-5082/6/2/024103

Lee, J. W., Choi, Y. J., Yong, W. J., Pati, F., Shim, J. H., Kang, K. S., et al. (2016). Development of a 3D cell printed construct considering angiogenesis for liver tissue engineering. *Biofabrication* 8:015007. doi: 10.1088/1758-5090/8/1/015007

Lee, V. K., Kim, D. Y., Ngo, H., Lee, Y., Seo, L., Yoo, S. S., et al. (2014b). Creating perfused functional vascular channels using 3D bio-printing technology. *Biomaterials* 35, 8092–8102. doi: 10.1016/j.biomaterials.2014.05.083

Lee, W., Debasitis, J. C., Lee, V. K., Lee, J. H., Fischer, K., Edminster, K., et al. (2009). Multi-layered culture of human skin fibroblasts and keratinocytes through three-dimensional freeform fabrication. *Biomaterials* 30, 1587–1595. doi: 10.1016/j.biomaterials.2008.12.009

Leong, K. F., Cheah, C. M., and Chua, C. K. (2003). Solid freeform fabrication of three-dimensional scaffolds for engineering replacement tissues and organs. *Biomaterials* 24, 2363–2378. doi: 10.1016/s0142-9612(03)00030-9

Levato, R., Visser, J., Planell, J. A., Engel, E., Malda, J., and Mateos-Timoneda, M. A. (2014). Biofabrication of tissue constructs by 3D bioprinting of cell-laden microcarriers. *Biofabrication* 6:035020. doi: 10.1088/1758-5082/6/3/035020

Li, S. W., Tallia, F., Mohammed, A. A., Stevens, M. M., and Jones, J. R. (2020). Scaffold channel size influences stem cell differentiation pathway in 3-D printed silica hybrid scaffolds for cartilage regeneration. *Biomater. Sci.* 8, 4458–4466. doi: 10.1039/c9bm01829h

Luo, Y. X., Lode, A., Sonntag, F., Nies, B., and Gelinsky, M. (2013). Well-ordered biphasic calcium phosphate-alginate scaffolds fabricated by multi-channel 3D plotting under mild conditions. *J. Mater. Chem. B* 1, 4088–4098. doi: 10.1039/c3tb20511h

Mahony, O., Tsigkou, O., Ionescu, C., Minelli, C., Ling, L., Hanly, R., et al. (2010). Silica-gelatin hybrids with tailorable degradation and mechanical properties for tissue regeneration. *Adv. Funct. Mater.* 20, 3835–3845. doi: 10.1002/adfm.201000838

Mankovich, N. J., Samson, D., Pratt, W., Lew, D., and Beumer, J. III (1994). Surgical planning using three-dimensional imaging and computer modeling. *Otolaryngol. Clin. North Am.* 27, 875–889. doi: 10.1016/s0030-6665(20)30614-9

Mannoor, M. S., Jiang, Z., James, T., Kong, Y. L., Malatesta, K. A., Soboyejo, W. O., et al. (2013). 3D printed bionic ears. *Nano Lett.* 13, 2634–2639. doi: 10.1021/nl4007744

Markstedt, K., Mantas, A., Tournier, I., Martinez Avila, H., Hagg, D., and Gatenholm, P. (2015). 3D bioprinting human chondrocytes with nanocellulose-alginate bioink for cartilage tissue engineering applications. *Biomacromolecules* 16, 1489–1496. doi: 10.1021/acs.biomac.5b00188

Melchels, F. P., Feijen, J., and Grijpma, D. W. (2010). A review on stereolithography and its applications in biomedical engineering. *Biomaterials* 31, 6121–6130. doi: 10.1016/j.biomaterials.2010.04.050

Melchiorri, A. J., Hibino, N., Best, C. A., Yi, T., Lee, Y. U., Kraynak, C. A., et al. (2016). 3D-printed biodegradable polymeric vascular grafts. *Adv. Healthc. Mater.* 5, 319–325. doi: 10.1002/adhm.201500725

Mironov, V., Trusk, T., Kasyanov, V., Little, S., Swaja, R., and Markwald, R. (2009). Biofabrication: a 21st century manufacturing paradigm. *Biofabrication* 1:022001. doi: 10.1088/1758-5082/1/2/022001

Morrison, R. J., Hollister, S. J., Niedner, M. F., Mahani, M. G., Park, A. H., Mehta, D. K., et al. (2015). Mitigation of tracheobronchomalacia with 3D-printed personalized medical devices in pediatric patients. *Sci. Transl. Med.* 7:285ra264. doi: 10.1126/scitranslmed.3010825

Mosadegh, B., Xiong, G., Dunham, S., and Min, J. K. (2015). Current progress in 3D printing for cardiovascular tissue engineering. *Biomed. Mater.* 10:034002. doi: 10.1088/1748-6041/10/3/034002

Murphy, S. V., and Atala, A. (2014). 3D bioprinting of tissues and organs. *Nat. Biotechnol.* 32, 773–785. doi: 10.1038/nbt.2958

Murr, L. (ed.). (2015). "Additive manufacturing additive manufacturing: changing the rules of manufacturing," in *Handbook of Materials Structures, Properties, Processing and Performance*, (Cham: Springer International Publishing), 691–699. doi: 10.1007/978-3-319-01815-7_42

Nommeots-Nomm, A., Lee, P. D., and Jones, J. R. (2018). Direct ink writing of highly bioactive glasses. *J. Eur. Ceram. Soc.* 38, 837–844. doi: 10.1016/j.jeurceramsoc.2017.08.006

Ojeh, N., Pastar, I., Tomic-Canic, M., and Stojadinovic, O. (2015). Stem cells in skin regeneration, wound healing, and their clinical applications. *Int. J. Mol. Sci.* 16, 25476–25501. doi: 10.3390/ijms161025476

Park, J., Tari, M. J., and Hahn, H. T. (2000). Characterization of the laminated object manufacturing (LOM) process. *Rapid Prototyp. J.* 6, 36–50. doi: 10.1108/13552540010309868

Park, J. Y., Shim, J. H., Choi, S. A., Jang, J., Kim, M., Lee, S. H., et al. (2015). 3D printing technology to control BMP-2 and VEGF delivery spatially and temporally to promote large-volume bone regeneration. *J. Mater. Chem. B* 3, 5415–5425. doi: 10.1039/c5tb00637f

Pei, X., Ma, L., Zhang, B. Q., Sun, J. X., Sun, Y., Fan, Y. J., et al. (2017). Creating hierarchical porosity hydroxyapatite scaffolds with osteoinduction by three-dimensional printing and microwave sintering. *Biofabrication* 9:045008. doi: 10.1088/1758-5090/aa90ed

Poologasundarampillai, G., Yu, B. B., Jones, J. R., and Kasuga, T. (2011). Electrospun silica/PLLA hybrid materials for skeletal regeneration. *Soft Matter* 7, 10241–10251. doi: 10.1039/c1sm06171b

Powell, H. M., Supp, D. M., and Boyce, S. T. (2008). Influence of electrospun collagen on wound contraction of engineered skin substitutes. *Biomaterials* 29, 834–843. doi: 10.1016/j.biomaterials.2007.10.036

Ragaert, K., Cardon, L., Dekeyser, A., and Degrieck, J. (2010). Machine design and processing considerations for the 3D plotting of thermoplastic scaffolds. *Biofabrication* 2:014107. doi: 10.1088/1758-5082/2/1/014107

Rengier, F., Mehndiratta, A., von Tengg-Kobligk, H., Zechmann, C. M., Unterhinninghofen, R., Kauczor, H. U., et al. (2010). 3D printing based on imaging data: review of medical applications. *Int. J. Comput. Assist. Radiol. Surg.* 5, 335–341. doi: 10.1007/s11548-010-0476-x

Rimell, J. T., and Marquis, P. M. (2000). Selective laser sintering of ultra high molecular weight polyethylene for clinical applications. *J. Biomed. Mater. Res.* 53, 414–420. doi: 10.1002/1097-4636(2000)53:4<414::aid-jbm16>3.0.co;2-m

Rodrigues, C. V., Serricella, P., Linhares, A. B., Guerdes, R. M., Borojevic, R., Rossi, M. A., et al. (2003). Characterization of a bovine collagen-hydroxyapatite composite scaffold for bone tissue engineering. *Biomaterials* 24, 4987–4997. doi: 10.1016/s0142-9612(03)00410-1

Sachlos, E., and Czernuszka, J. T. (2003). Making tissue engineering scaffolds work. Review: the application of solid freeform fabrication technology to the production of tissue engineering scaffolds. *Eur. Cell Mater.* 5, 29–39; discussion 39–40.

Sanchez, C., Julian, B., Belleville, P., and Popall, M. (2005). Applications of hybrid organic-inorganic nanocomposites. *J. Mater. Chem.* 15, 3559–3592.

Schubert, C., van Langeveld, M. C., and Donoso, L. A. (2014). Innovations in 3D printing: a 3D overview from optics to organs. *Br. J. Ophthalmol.* 98, 159–161. doi: 10.1136/bjophthalmol-2013-304446

Seitz, H., Rieder, W., Irsen, S., Leukers, B., and Tille, C. (2005). Three-dimensional printing of porous ceramic scaffolds for bone tissue engineering. *J. Biomed. Mater. Res. B Appl. Biomater.* 74, 782–788. doi: 10.1002/jbm.b.30291

Shi, X., Nommeots-Nomm, A., Todd, N. M., Devlin-Mullin, A., Geng, H., Lee, P. D., et al. (2020). Bioactive glass scaffold architectures regulate patterning of bone regeneration in vivo. *Appl. Mater. Today* 20:100770. doi: 10.1016/j.apmt.2020.100770

Slaughter, B. V., Khurshid, S. S., Fisher, O. Z., Khademhosseini, A., and Peppas, N. A. (2009). Hydrogels in regenerative medicine. *Adv. Mater.* 21, 3307–3329. doi: 10.1002/adma.200802106

Suh, J. K., and Matthew, H. W. (2000). Application of chitosan-based polysaccharide biomaterials in cartilage tissue engineering: a review. *Biomaterials* 21, 2589–2598. doi: 10.1016/s0142-9612(00)00126-5

Tallia, F., Russo, L., Li, S. W., Orrin, A. L. H., Shi, X. M., Chen, S., et al. (2018). Bouncing and 3D printable hybrids with self-healing properties. *Mater. Horiz.* 5, 849–860. doi: 10.1039/c8mh00027a

Tchemtchoua, V. T., Atanasova, G., Aqil, A., Filee, P., Garbacki, N., Vanhooteghem, O., et al. (2011). Development of a chitosan nanofibrillar scaffold for skin repair and regeneration. *Biomacromolecules* 12, 3194–3204. doi: 10.1021/bm200680q

Temenoff, J. S., and Mikos, A. G. (2000). Review: tissue engineering for regeneration of articular cartilage. *Biomaterials* 21, 431–440. doi: 10.1016/s0142-9612(99)00213-6

Torres-Rendon, J. G., Femmer, T., De Laporte, L., Tigges, T., Rahimi, K., Gremse, F., et al. (2015). Bioactive gyroid scaffolds formed by sacrificial templating of nanocellulose and nanochitin hydrogels as instructive platforms for biomimetic tissue engineering. *Adv. Mater.* 27, 2989–2995. doi: 10.1002/adma.201405873

Tsang, V. L., and Bhatia, S. N. (2004). Three-dimensional tissue fabrication. *Adv. Drug Deliv. Rev.* 56, 1635–1647. doi: 10.1016/j.addr.2004.05.001

Vacanti, J. P., Morse, M. A., Saltzman, W. M., Domb, A. J., Perezatayde, A., and Langer, R. (1988). Selective cell transplantation using bioabsorbable artificial polymers as matrices. *J. Pediatr. Surg.* 23, 3–9. doi: 10.1016/s0022-3468(88)80529-3

Valliant, E. M., and Jones, J. R. (2011). Softening bioactive glass for bone regeneration: sol-gel hybrid materials. *Soft Matter* 7, 5083–5095. doi: 10.1039/c0sm01348j

Wang, H. M., Chou, Y. T., Wen, Z. H., Wang, C. Z., Chen, C. H., and Ho, M. L. (2013). Novel biodegradable porous scaffold applied to skin regeneration. *PLoS One* 8:e56330. doi: 10.1371/journal.pone.0056330

Wang, X., Yan, Y., Pan, Y., Xiong, Z., Liu, H., Cheng, J., et al. (2006). Generation of three-dimensional hepatocyte/gelatin structures with rapid prototyping system. *Tissue Eng.* 12, 83–90. doi: 10.1089/ten.2006.12.83

Wang, X., Yan, Y., and Zhang, R. (2007). Rapid prototyping as a tool for manufacturing bioartificial livers. *Trends Biotechnol.* 25, 505–513. doi: 10.1016/j.tibtech.2007.08.010

Williams, J. M., Adewunmi, A., Schek, R. M., Flanagan, C. L., Krebsbach, P. H., Feinberg, S. E., et al. (2005). Bone tissue engineering using polycaprolactone scaffolds fabricated via selective laser sintering. *Biomaterials* 26, 4817–4827. doi: 10.1016/j.biomaterials.2004.11.057

Woodard, L. N., Kmetz, K. T., Roth, A. A., Page, V. M., and Grunlun, M. A. (2017). Porous Poly(epsilon-caprolactone)-Poly(L-lactic acid) Semi-Interpenetrating networks as superior, defect-specific scaffolds with potential for cranial bone defect repair. *Biomacromolecules* 18, 4075–4083. doi: 10.1021/acs.biomac.7b01155

Woodfield, T. B., Malda, J., de Wijn, J., Peters, F., Riesle, J., and van Blitterswijk, C. A. (2004). Design of porous scaffolds for cartilage tissue engineering using a three-dimensional fiber-deposition technique. *Biomaterials* 25, 4149–4161. doi: 10.1016/j.biomaterials.2003.10.056

Wu, W., DeConinck, A., and Lewis, J. A. (2011). Omnidirectional printing of 3D microvascular networks. *Adv. Mater.* 23, H178–H183. doi: 10.1002/adma.201004625

Xu, T., Zhao, W., Zhu, J. M., Albanna, M. Z., Yoo, J. J., and Atala, A. (2013). Complex heterogeneous tissue constructs containing multiple cell types prepared by inkjet printing technology. *Biomaterials* 34, 130–139. doi: 10.1016/j.biomaterials.2012.09.035

Yamanaka, S. (2009). A fresh look at iPS cells. *Cell* 137, 13–17. doi: 10.1016/j.cell.2009.03.034

Yang, S. F., Leong, K. F., Du, Z. H., and Chua, C. K. (2002). The design of scaffolds for use in tissue engineering. Part II. Rapid prototyping techniques. *Tissue Eng.* 8, 1–11. doi: 10.1089/107632702753503009

Young, R. G., Butler, D. L., Weber, W., Caplan, A. I., Gordon, S. L., and Fink, D. J. (1998). Use of mesenchymal stem cells in a collagen matrix for Achilles tendon repair. *J. Orthop. Res.* 16, 406–413. doi: 10.1002/jor.1100160403

Zein, I., Hutmacher, D. W., Tan, K. C., and Teoh, S. H. (2002). Fused deposition modeling of novel scaffold architectures for tissue engineering applications. *Biomaterials* 23, 1169–1185. doi: 10.1016/s0142-9612(01)00232-0

Zhang, B. Q., Sun, H., Wu, L. N., Ma, L., Xing, F., Xing, F., et al. (2019). 3D printing of calcium phosphate bioceramic with tailored biodegradation rate for skull bone tissue reconstruction. *Biodes. Manuf.* 2, 161–171. doi: 10.1007/s42242-019-00046-7

Zhu, W., Ma, X., Gou, M., Mei, D., Zhang, K., and Chen, S. (2016). 3D printing of functional biomaterials for tissue engineering. *Curr. Opin. Biotechnol.* 40, 103–112. doi: 10.1016/j.copbio.2016.03.014

Zorlutuna, P., Annabi, N., Camci-Unal, G., Nikkhah, M., Cha, J. M., Nichol, J. W., et al. (2012). Microfabricated biomaterials for engineering 3D tissues. *Adv. Mater.* 24, 1782–1804. doi: 10.1002/adma.201104631

Zorlutuna, P., Hasirci, N., and Hasirci, V. (2008). Nanopatterned collagen tubes for vascular tissue engineering. *J. Tissue Eng. Regen. Med.* 2, 373–377. doi: 10.1002/term.99

Conflict of Interest: The authors declare that the research was conducted in the absence of any commercial or financial relationships that could be construed as a potential conflict of interest.

frontiers in Bioengineering and Biotechnology

ORIGINAL RESEARCH
published: 06 November 2020
doi: 10.3389/fbioe.2020.589094

Desktop-Stereolithography 3D Printing of a Polyporous Extracellular Matrix Bioink for Bone Defect Regeneration

Yunxiang Luo[1,2†], Hao Pan[3†], Jiuzhou Jiang[1,2†], Chenchen Zhao[1,2], Jianfeng Zhang[1,2], Pengfei Chen[1,2], Xianfeng Lin[1,2*] and Shunwu Fan[1,2*]*

[1] Department of Orthopaedic Surgery, Sir Run Run Shaw Hospital, Medical College of Zhejiang University, Hangzhou, China, [2] Key Laboratory of Musculoskeletal System Degeneration and Regeneration Translational Research of Zhejiang Province, Hangzhou, China, [3] Department of Orthopaedic, The First Affiliated Hospital of Wenzhou Medical University, Wenzhou, China

OPEN ACCESS

Edited by:
Xin Zhao,
The Hong Kong Polytechnic University, Hong Kong

Reviewed by:
Maria Grazia Raucci,
National Research Council (CNR), Italy
Huifang Zhou,
Shanghai Jiao Tong University, China

****Correspondence:***
Pengfei Chen
790048914@qq.com
Xianfeng Lin
xianfeng_lin@zju.edu.cn
Shunwu Fan
shunwu_fan@zju.edu.cn;
shunwu_fan@126.com

† These authors have contributed equally to this work

Specialty section:
This article was submitted to Biomaterials, a section of the journal Frontiers in Bioengineering and Biotechnology

Received: *30 July 2020*
Accepted: *19 October 2020*
Published: *06 November 2020*

Citation:
Luo Y, Pan H, Jiang J, Zhao C, Zhang J, Chen P, Lin X and Fan S (2020) Desktop-Stereolithography 3D Printing of a Polyporous Extracellular Matrix Bioink for Bone Defect Regeneration. Front. Bioeng. Biotechnol. 8:589094. doi: 10.3389/fbioe.2020.589094

Introduction: Decellularized tendon extracellular matrix (tECM) perfectly provides the natural environment and holds great potential for bone regeneration in Bone tissue engineering (BTE) area. However, its densifying fiber structure leads to reduced cell permeability. Our study aimed to combine tECM with polyethylene glycol diacrylate (PEGDA) to form a biological scaffold with appropriate porosity and strength using stereolithography (SLA) technology for bone defect repair.

Methods: The tECM was produced and evaluated. Mesenchymal stem cell (MSC) was used to evaluate the biocompatibility of PEGDA/tECM bioink *in vitro*. Mineralization ability of the bioink was also evaluated *in vitro*. After preparing 3D printed polyporous PEGDA/tECM scaffolds (3D-pPES) via SLA, the calvarial defect generation capacity of 3D-pPES was assessed.

Results: The tECM was obtained and the decellularized effect was confirmed. The tECM increased the swelling ratio and porosity of PEGDA bioink, both cellular proliferation and biomineralization *in vitro* of the bioink were significantly optimized. The 3D-pPES was fabricated. Compared to the control group, increased cell migration efficiency, up-regulation of osteogenic differentiation RNA level, and better calvarial defect repair in rat of the 3D-pPES group were observed.

Conclusion: This study demonstrates that the 3D-pPES may be a promising strategy for bone defect treatment.

Keywords: 3D printing, stereolithography, tendon extracellular matrix, polyethylene glycol diacrylate, calvarial defect

INTRODUCTION

High-energy injuries or pathological fractures, such as tumors and inflammation, are the main reasons for bone defects, which create numerous challenges in the clinical setting and require bone grafting (Campana et al., 2014; Hwang et al., 2017; Zhang H. et al., 2019). As the gold standard for bone substitution in clinical surgeries, the autogenous bone grafts application is limited by

the inadequate practicability, donor-site morbidity, and complicated surgical procedures (Sharif et al., 2016; Bez et al., 2018; Cabbad et al., 2019; Chen et al., 2019). Consequently, a more valid alternative procedure of BTE platform was proposed. BTE provides several benefits such as the rare spread of disease, lower infection or immunogenicity rate, various implantation materials, and wide availability (Hollister and Murphy, 2011). Many biomaterial substitutes have already been clinically applied due to their superior biological performance (Gibbs et al., 2016; Hassan et al., 2019).

Among all biological materials, the extracellular matrix (ECM) graft retains its natural structure and has high homology among different species, since it is derived from the biological tissue rather than the chemosynthesis materials, and it shows excellent effects in terms of the regulation of cellular adhesion, proliferation, migration, and differentiation (Pham et al., 2008). The tendon ECM (tECM) is rich in type-1 collagen, which can serve as a heterogeneous nucleation template to induce calcium and phosphorus (Ca-Pi) cluster formation (Xu et al., 2015; Thankam et al., 2018). In this biochemistry procedure, a self-assembled, pseudo-hexagonal array of collagen molecules participate and facilitate the Ca-Pi binding and nucleation (Xu et al., 2015). However, independent application of tECM to build a scaffold in BTE has several drawbacks; lack of sufficient mechanical support due to the original physical property, difficulty in forming a specific shape coinciding with the bone defect, and the lack of 3D micropore structure that is beneficial to the cell growth and differentiation (Narayanan et al., 2009).

To conquer the shortcomings that pure ECM is unable to provide, like adequate mechanical strength, the scaffold processing techniques are taken into consideration. Conventional scaffold processing techniques that fabricate various tissues, such as phase separation (Fang et al., 2019), freeze-drying (Grenier et al., 2019; Zhang L. et al., 2019), solvent casting (Ahn et al., 2018; Mao et al., 2018), gas foaming (Kaynak Bayrak et al., 2017; Catanzano et al., 2018), and electrospinning (Chan et al., 2019), cannot precisely control pore size, geometry, and interconnectivity of the scaffolds. However, 3D printing has emerged as a brand-new material processing approach, which largely overcomes these difficulties, allowing us to fabricate more bionic scaffolds for bone transplantation and to repair the bone defect in a clinical setting (Do et al., 2015). To ensure the 3D printing scaffold is built efficiently, hybridizing the natural ECM and synthetic polymer-based materials to create novel tissue-engineered scaffolds seems feasible because, in this method, the advantages, including the biocompatibility of the ECM, and the superior physical properties of the synthetic polymer-based materials, are both fully embodied (Lee et al., 2014). Though traditional 3D printing provides lots of benefits, creating a complicated 3D scaffold with natural ingredients of biological origin, such as fibrin, gelatin or hyaluronic acid, seems impractical (Knowlton et al., 2016). Stereolithography (SLA), a simple, user-friendly photo-crosslinked biomaterial printing with high resolution, gives us a brand-new solution to achieve bone regeneration (Do et al., 2015; Knowlton et al., 2016).

Here, we focus on the 3D printing-based scaffolds using the hybridization of tECM and synthetic polymer-based materials to fabricate a highly interconnected architecture bone grafts scaffold (**Scheme 1**). This 3D printed polyporous PEGDA/tECM scaffolds (3D-pPES) could promote the mesenchymal stem cell (MSCs) proliferation and migration in the defect regions. The promising bone defect regeneration could be achieved using this novel repair system.

MATERIALS AND METHODS

All animal experiments *in vivo* were conducted following the principles and procedures of the National Institutes of Health (NIH) Guide for the Care and Use of Laboratory Animals and the guidelines for animal treatment of Sir Run Shaw Affiliated Hospital of Zhejiang University School of Medicine (Hangzhou, Zhejiang).

Preparation of the tECM

First, grown pigs were purchased at a local slaughterhouse in Hangzhou, and ten porcine tendons were harvested from their hind legs. The tendons were exposed to three continuous freeze-thaw (−80–37°C) cycles. Then, the tissues were immersed in 1% Triton X-100 solution for 24 h, 1% sodium dodecyl sulfate for 3 h and 200 U mL^{-1} DNAase at 37°C for 12 h.

Next, 4′, 6-diamidino-2-phenylindole (DAPI), hematoxylin and eosin (H&E), Masson's trichrome staining and a DNA assay were performed to evaluate the decellularized efficiency. Using a Universal Genomic DNA Kit (CW Biotech, Beijing, China) and a microplate spectrophotometer (260 nm, Thermo Fisher Scientific, Waltham, MA, United States), DNA contents were measured. Meanwhile, a hydroxyproline (Hyp) assay kit (Nanjing Keygen Biotech Co., Ltd., Nanjing, China) was used to measure the collagen content. The decellularized tECM was dehydrated, ground for digestion, and adjusted to a neutral pH (7.4).

Physical Performance Measurement of the Hydrogels

The physical properties of bioinks with different compositions were determined. Exactly 10% (w/v) polyethylene glycol diacrylate (PEGDA) and 0.25% (w/v) lithium acylphosphinate photo-initiator (LAP) were added to the tECM hydrogel obtained previously, as described above, then the PEGDA/tECM pre-gel was crosslinked for 15 s at 375 nm of UV light exposure. Isostatic compression tests of the hydrogels were conducted in a dry state at 25°C using a universal testing system (Instron 5567, United States). The weight swelling ratio, Q, was calculated using the following equation:

$$Q = \frac{\text{Swelling mass (Ws)}}{\text{dry mass (Wd)}} \times 100\%$$

The coagulation time of several types of hydrogels with different tECM concentrations was tested on the print plane. The 3D microstructure of the lyophilized PEGDA/tECM hydrogels was observed using scanning electron microscopy (SEM).

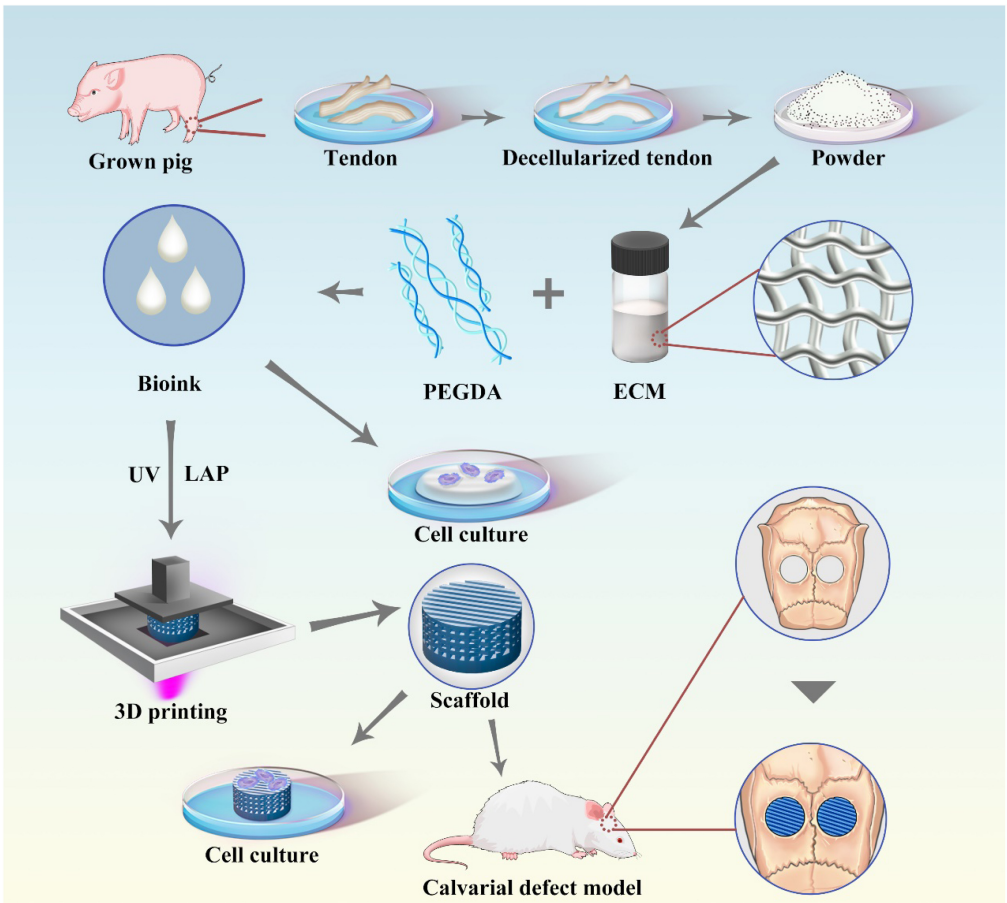

SCHEME 1 | Schematic illustration of the polyporous tECM bioink 3D printing scheme, included PEGDA/tECM bioink preparation, tECM hydrogel for cell culture *in vitro* and SLA-based PEGDA/tECM bioprinting that applied to calvarial defect implantation.

An Icon atomic force microscope (Dimension Icon, Bruker, Billerica, MA, United States) was used to observe the PEGDA hydrogel and scaffold.

Cell Viability and Metabolic Activity Assays of the Hydrogels

For all the experiments on cell viability and metabolic activity assays, C57BL/6 bone marrow-derived MSCs were used, which were purchased from Cyagen Biosciences (MUBMX-90011, Santa Clara, United States). Live-Dead Cell Staining Kit (Thermo Fisher Scientific, Waltham, MA, United States) was used to assay the MSCs viability and CCK-8 kit (Cell Counting Kit-8; Dojindo Laboratories, Kumamoto, Japan) was used to test the metabolic activity of MSCs growing on the hydrogels. Using the same experimental conditions, we also carried out the cytotoxicity test of LAP.

Spontaneous Biomineralization of the Hydrogels *In vitro*

The hydrogel specimens (pure PEGDA group and PEGDA/tECM group) were produced and merged into the modified simulated body fluid (m-SBF; 1.67×10^{-3} M $CaCl_2$, 9.5×10^{-3} M Na_2HPO4, 150×10^{-3} M NaCl, and 100 $\mu g/mL^{-1}$ polyaspartic acid) for 2 and 4 weeks. Micro-CT scanning (Siemens Inveon, Eschborn, Germany) was used following a scanning protocol of 80 kV, 500 mA, and 14.97 mm isotropic resolution. Data were obtained and analyzed using Inveon Research Workplace v. 2.2 software (Siemens, Munich, Germany).

Biofabrication of 3D-pPES Using Dynamic Projection SLA

A digital light processing (DLP) chip (Discovery 4000; Texas Instruments, Dallas, TX, United States), a replaceable UV light source at 375 nm wavelength (OmniCure S2000; EXFO, Quebec City, QC, Canada), and XYZ stages made up our SLA printing system. Pre-designed user-defined computer-aided-design (CAD) files could be read and converted into printable programs by the DLP chip. The light from the UV light source was directed onto the print plane of the bioink through an optically-specific lens (Edmunds Optics, Barrington, NJ, United States). Catalyzed by LAP, the bioink reacted rapidly in

the projected space and quickly solidified into a 3D scaffold at certain physical strength.

Cell Migration and Cytotoxicity Assay of 3D-pPES

CCK-8 kit (Cell Counting Kit-8; Dojindo Laboratories, Kumamoto, Japan) was used to test the metabolic activity of MSCs growing in the 3D-pPES lixivium. We conducted control studies using static cultures of MSCs in Transwell plates (Corning Inc., Lowell, MA, United States), containing porous polyester membrane inserts (0.33 cm^2, 0.4 μm pores), to detect cell migration ability.

Evaluation of the Osteoinductive Activity of the 3D-pPES *In vitro*

The scaffolds, containing 1% (w/v) tECM, were placed in 96-well plates, at 1×10^5 cells/well MSCs. Both DMEM supplemented with 10% FBS and 100 μg/mL streptomycin were added. Osteoblastic induction medium (Sigma Aldrich Corp., St. Louis, MO, United States) was added to incubate MSCs. On day 7, real-time quantitative polymerase chain reaction (RT-qPCR) was performed to measure the expression of *ALP, Runx2, Col1α1, OCN,* and *OPN*. *GAPDH* was referred to as a quantitative control for RNA levels. The primer sequences are listed in **Supplementary Table S1**.

Protein Mass Spectrometry of the tECM

Deformation and reduction of the protein sample were performed for proteomic experiments. Protein concentration was determined using BCA assay. Peptide samples were analyzed using nano-LC-MS/MS. Sequences were mapped based on gene ontology (GO) terms[1] to determine the biological and functional properties of all identified proteins. Meanwhile, we employed hypergeometric tests to perform GO enrichment analysis.

Repair Assay in the Rat Critical-Sized Calvarial Defect Model

Twelve one-month-old Sprague Dawley rats were purchased and raised individually in cages. After anesthesia, bilateral full-thickness critical-sized calvarial defects (4 mm in diameter) were created. Details of each group of operation are shown in **Supplementary Table S2**. The skulls were collected and embalmed in 4% paraformaldehyde. Repair assay in the rat critical-sized calvarial defect model was implemented using micro-CT scanning. The specimens were cut along the coronal plane for H&E, Masson's trichrome, and Goldner trichrome staining.

Statistical Analysis

Data are presented as mean ± standard deviation (SD) of at least three experiments with similar results. Experiments were run in triplicate unless stated otherwise. Either one−way ANOVA or Student's *t*-test was applied to assess the differences between the means. $^{*}P < 0.05$, $^{**}P < 0.01$, $^{\#}P < 0.05$, and $^{\#\#}P < 0.01$ were considered statistically significant.

[1]http://geneontology.org/

RESULTS

Preparation of a Decellularized Tendon With Potential Biological Functions

The microstructure, composition and biological functions of the decellularized tendon were carefully analyzed. After decellularization, the tendon pieces were ground into powder, which was dissolved in acid to form a gel (**Figure 1A**). The tECM mainly presented a filamentous structure observed by SEM (**Figure 1A**). DAPI and H&E staining (**Figure 1B**) showed the absence of the nucleus. Well-organized fibrous structures were observed via HE staining (**Figure 1B**). Masson trichrome staining confirmed excellent collagen retention as well (**Figure 1B**). The DNA content decreased approximately by 97% (**Figures 1C,D**) after the decellularization. There was little change in collagen content before and after decellularization (**Figure 1E**).

Physical Properties of the Hydrogels

The physical properties of the bioink and hydrogels were further observed from several aspects. Both coagulation time and Young's modulus showed no visible difference when the concentration of the tECM changed from 0 to 1% (**Figures 2A,B**). The representative curve of elastic force generated by the pressure with the displacement of compression deformation is shown in **Supplementary Figure S1**. Rapid swelling and water absorption were observed within the first 100 min, then the swelling ratio verged to extremely slow after 3 h (**Figure 2C**). Moreover, 1% tECM greatly increased the swelling ratio of the PEGDA hydrogels. As the concentration of the tECM increased, an increasing number (10%) of holes appeared, observed via SEM, which contributed to the increase of the hydrogel porosity (**Figures 2D,E**). We assumed that tECM hydrogel greatly improved the physical characteristics of the hydrogel. The data above indicated that the PEGDA/tECM hydrogel was endowed with good hygroscopicity and appropriate mechanical properties.

PEGDA/tECM Hydrogels Promote Cellular Proliferation and Biomineralization *In vitro*

The cell viability assay showed that the cell proliferation rate was significantly higher on the PEGDA/tECM hydrogel compared to the control hydrogel (**Figures 3A,B**). All groups containing tECM showed a significant difference compared to the control group; this difference was observed from day 1. Moreover, as the concentration of the tECM increased, the proliferative capacity of the cell improved (**Figures 3A,B**). To create a scaffold with a suitable cytocompatibility, we tested the cytotoxicity of LAP (**Figure 3C**). The quantitative analysis proved that high concentration (1% wt) of LAP showed more potent cytotoxicity, while the bioink, containing low concentration (0.25% wt) of LAP, met the UV crosslinking requirements of 3D printing and showed better biocompatibility (**Figure 3C**). In our following

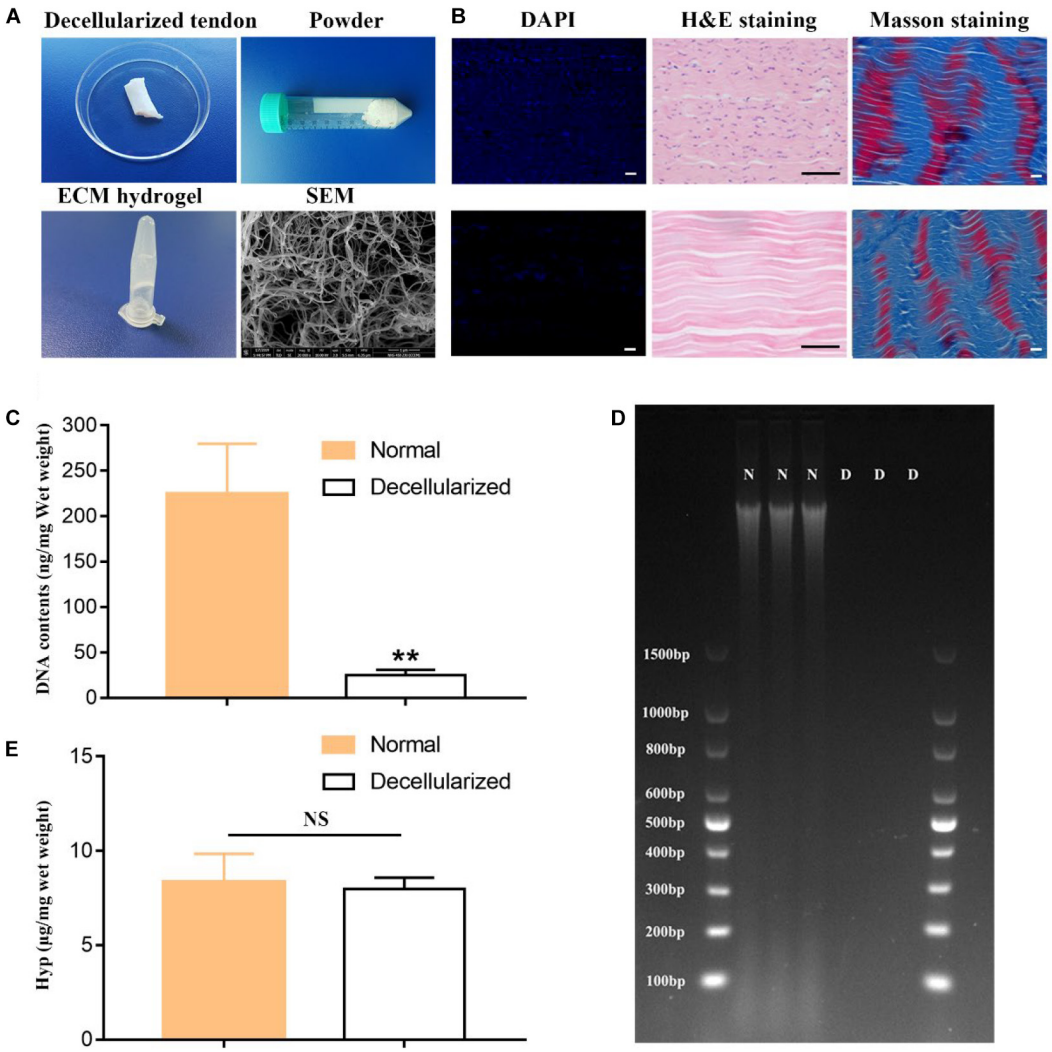

FIGURE 1 | Fabrication and characterization of the hydrogel derived from decellularized tendon. **(A)** General and SEM Images of tendon decellularization and preparation of hydrogel. **(B)** H&E and DAPI staining confirmed cell removal; Masson trichrome staining confirmed collagen retention. Scale bar = 10 μm. Quantitative detection of DNA removal retention **(C,D)** and collagen **(E)**. $^{**}P < 0.01$ compares to normal group.

experiment, the bioink that contained low concentration (0.25% wt) of LAP and high concentration of tECM (1% wt) was used uniformly. Then the PEGDA hydrogels and PEGDA/tECM hydrogels were immersed in m-SBF. Micro-CT results of the PEGDA/tECM group showed poor mineralization and relatively low BV/TV at 4 weeks, while the results at 8 weeks increased greatly ($P < 0.05$, **Figures 3D–F**). However, little change was observed in the PEGDA group due to the absence of tECM (**Figures 3D,E**). Hence, PEGDA/tECM hydrogels were better than PEGDA hydrogels at coordinating Ca-Pi deposition.

3D Printing of Polyporous PEGDA/tECM Bioink

Computer-aided-design files (**Figure 4A**) were used to produce the virtual mask and transmit UV light to the PEGDA/tECM bioink to print polyporous scaffolds. The structural formula of PEGDA and LAP are shown in **Supplementary Figure S2**. The line chart of the real-time temperature of the bioink in the printing process showed that the temperature was kept below 37°C (**Supplementary Figure S3**). The SLA-based technique successfully yielded a polyporous scaffold with abundant and dense pipelines that could be observed both by the naked eye and under a microscope (**Figure 4A**). These channels were also visible by SEM after lyophilizing the scaffold for 24 h (**Figure 4A**).

Increased Migration and Osteogenic Differentiation Triggered by the 3D-pPES

Before the MSCs were reseeded for cell differentiation, non-cytotoxicity of the 3D-pPES was confirmed (**Supplementary Figure S4**). Quantitative analysis of cell numbers showed that cell migration increased 3.6 times in the 3D-pPES group compared to the control group and PEGDA group (**Figures 4B,C**).

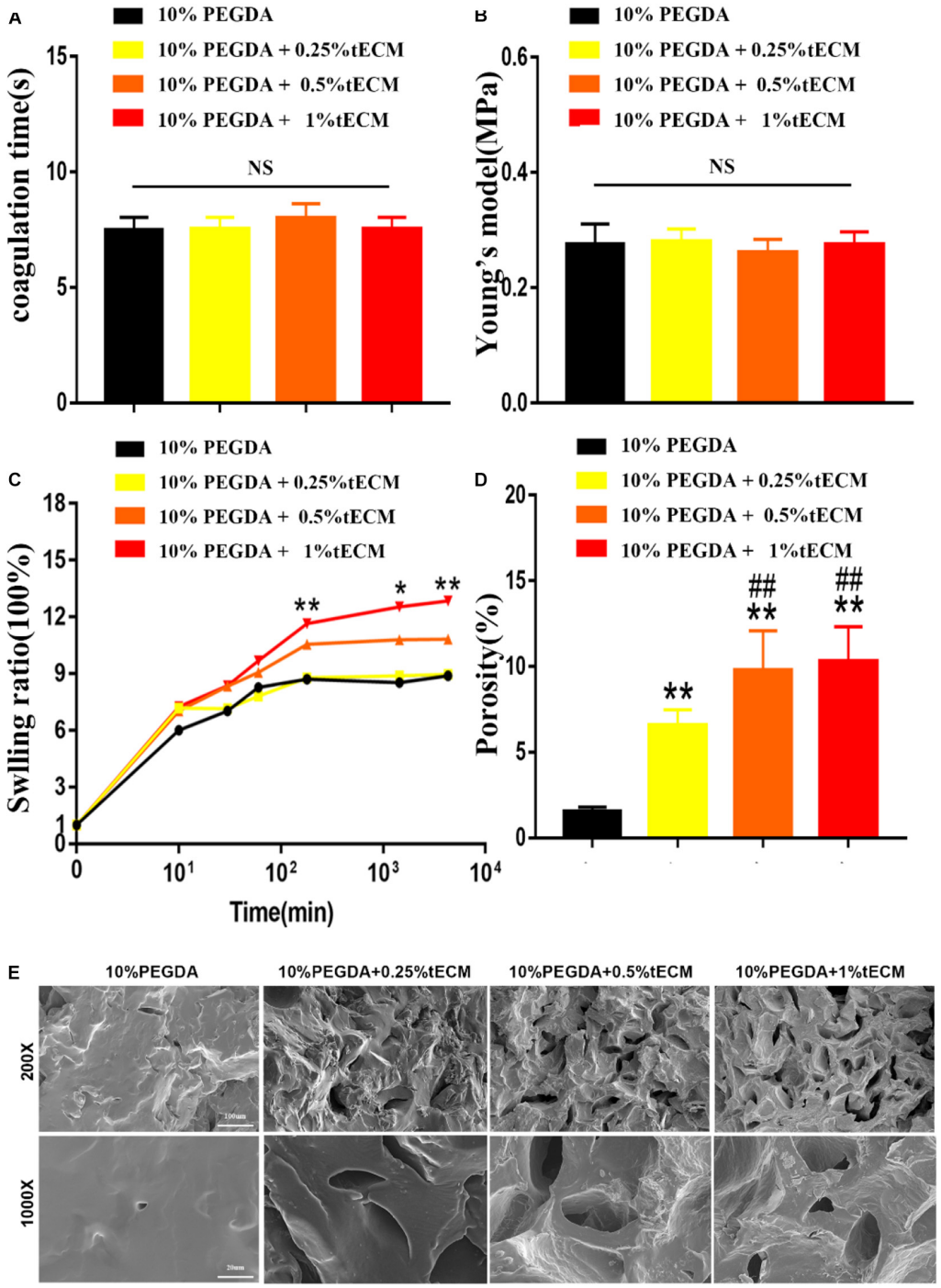

FIGURE 2 | Physical properties of the bioink and hydrogel: coagulation time **(A)**, Young's modulus **(B)**, swelling ratio **(C)** and porosity **(D,E)**. The hydrogel was observed via SEM **(E)**. $^{**}P < 0.01$ compares to 10% PEGDA group. $^{\#\#}P < 0.01$ compares to 10% PEGDA + 0.25% tECM group. $^{*}P < 0.05$ compares to 10% PEGDA group.

Roughness image showed 3D-pPES group has a rougher surface than PEGDA group (**Figures 4D,E**). It confirmed that the addition of ECM made the surface of the scaffold rougher. Proteomic analysis of tECM was also performed to divide the identified proteins into three classes (**Figures 4F–H**). GO cellular component and molecular function analysis confirmed the successful retention of various ECM structural constituents after decellularization (**Figures 4F,G**), which provided the bionic environment for cell growth. GO biological process analysis showed that the tECM contained proteins that function as

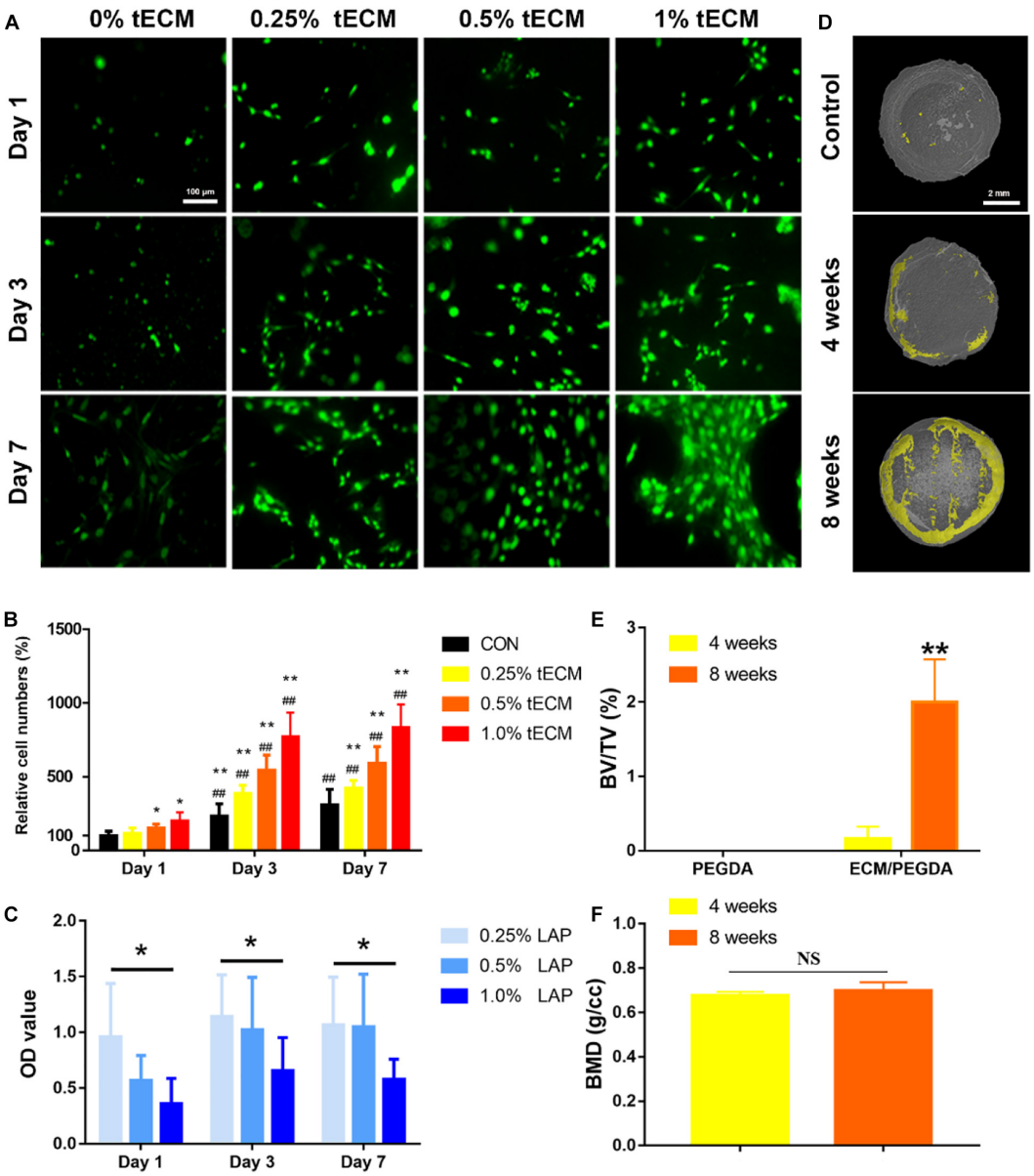

FIGURE 3 | Evaluation of Increased cellular proliferation and biomineralization *in vitro* by the PEGDA/tECM hydrogel. **(A)** Cell proliferation on the PEGDA, 0.25% tECM/ PEGDA, 0.5% tECM/ PEGDA, 1% tECM/ PEGDA hydrogels. **(B)** Quantitative analysis of Cell proliferation on the PEGDA, 0.25% tECM/ PEGDA, 0.5% tECM/ PEGDA, 1% tECM/ PEGDA scaffolds. **(C)** Quantitative analysis of Cell proliferation at different concentrations of LAP. **(D)** Representative Micro-CT scans images of PEGDA hydrogels for 8 weeks and PEGDA/tECM hydrogels for 4 and 8 weeks. Quantitative analysis of the mineralization presented in using BV/TV **(E)** and BMD **(F)** values. $^{*}P < 0.05$, $^{**}P < 0.01$ compares to control group at the same time. $^{\#\#}P < 0.01$ compares to the same group on day 1. BV/TV: trabecular bone volume fraction, BMD: Bone mineral density. Scale bars are shown in the figure.

regulation of cell adhesion and migration (**Figure 4H**), which might have contributed to the migration in **Figures 4B,C**. The result of the proteomic analysis corresponded with that of the Transwell assay. Osteogenic differentiation experiment *in vitro* showed conformably upregulated expression of genes associated with osteogenesis (Runx2, ALP, Col1α1, OCN, and OPN) after 14 days of induction (**Figure 4I**). The rougher 3D-pPES has a more pronounced effect on osteogenic differentiation than PEGDA. These findings indicated that the 3D-pPES had a positive effect on cell migration and osteogenic differentiation.

Bone Regeneration Enhancement Triggered by the 3D-pPES

The relative efficacy of PEGDA and PEGDA/tECM hydrogels in promoting new bone formation was evaluated in rats with induced critical-sized calvarial bone defects (**Figure 5A**) at 4 and

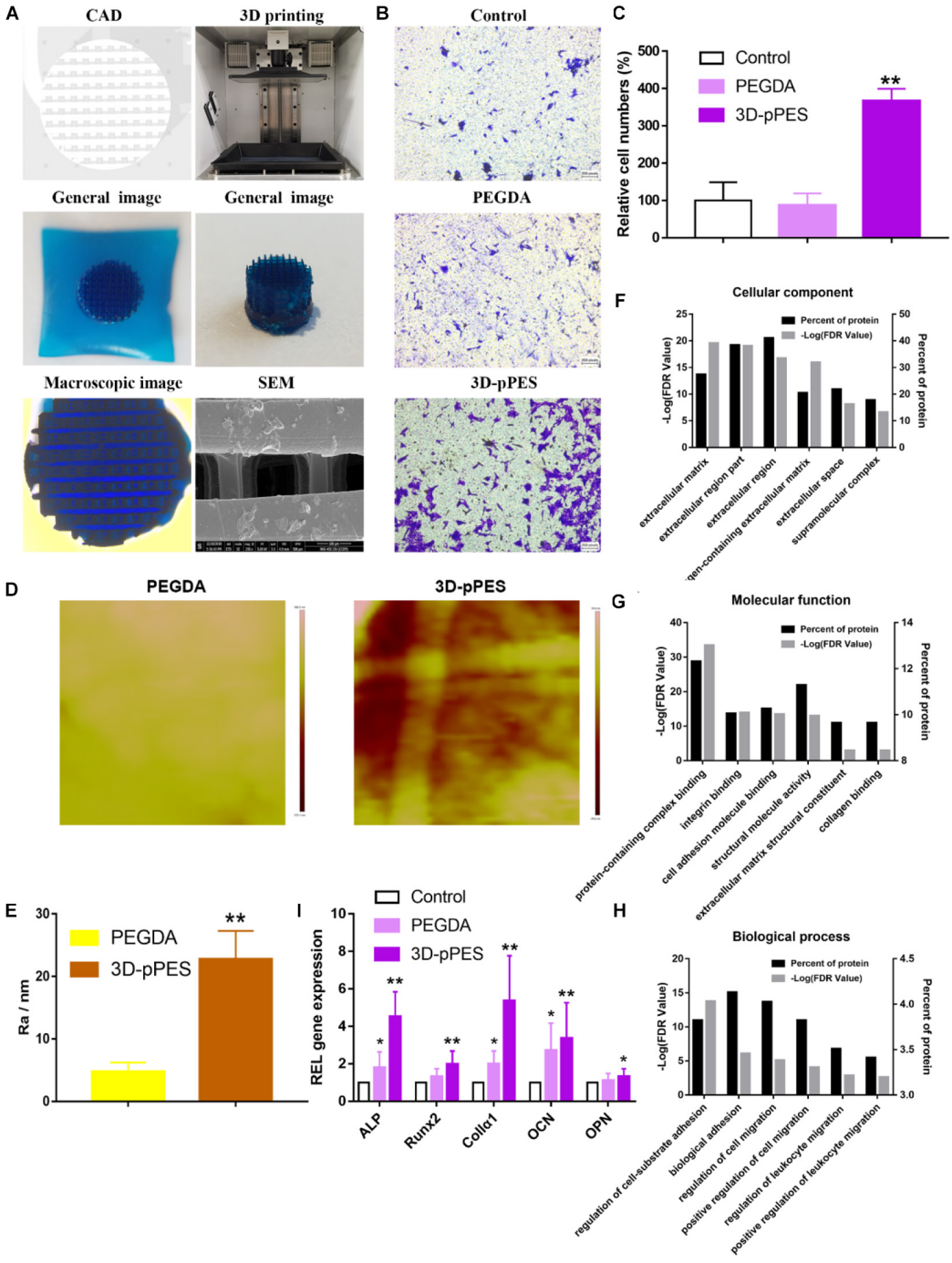

FIGURE 4 | 3D printing of polyporous tECM bioink and scaffold promoting migration and osteogenic differentiation. **(A)** CAD file, printing process, and scaffold (stained with methylene blue dye) printed by the 3D printer. The 3D-pPES was observed under microscopy and SEM. **(B)** Transwell migration assay of different treatments. Scale bars = 100 μm. **(C)** Quantitative analysis of migrating cells. **(D)** Roughness image by AFM within the scope of 1 μm^2. **(E)** Quantitative analysis of roughness value Ra (n = 5). **(F–H)** GO classification of tECM proteins. Scale bars are shown in the figure. **(I)** qPCR quantification of the relative mRNA expression of Runx2, ALP, OCN, OPN, and Col1α1 in osteoblasts cultured for 14 days on the hydrogels (n = 6). *P < 0.05 compares to control group. **P < 0.01 compares to control group.

8 weeks after surgery. Observation and analysis of the regenerated bone were successfully conducted, applying micro-CT scanning. Newly-formed bone was observed in all groups. However, the maximum amount of mineralized bone was measured in the PEGDA/tECM group (**Figure 5B**), along with the maximum value in BV/TV, Tb.Th, Tb.N, and BMD (**Figures 5C–G**). In

contrast, Tb.Sp value of the PEGDA/tECM group was the lowest since it was inversely proportional to the BMD value (**Figure 5F**). Notably, the increased value in BV/TV, Tb.Th, Tb.N, and BMD of the PEGDA group was observed. A similar conclusion could be drawn that a rigid surface of PEGDA without tECM was slightly effective in osteogenic differentiation and biomineralization.

From the H&E stained images (**Figure 6A**), it was clearly seen that the bone defects of the control groups and PEGDA groups were partly recovered, with the bone defect still unjoined. Little evidence supporting the new bone formation was found in the control group after 4 weeks. Denser new bone and more bone-like tissues near the border of the bone defect were seen in the PEGDA/tECM group. Markedly, the amount of the new bones observed in the PEGDA/tECM group were high compared to the other two groups (**Figure 6B**). Goldner's trichrome staining (**Figure 6C**) revealed that in PEGDA and PEGDA/tECM groups, immature woven bone and osteoid were formed in the defects, while the formation of mature lamellar bone, and even new bone marrow by the end of the observation period, were observed in the PEGDA/tECM group. All the evidence above showed a reasonable inference that the 3D-pPES had the best therapeutic effect in bone regeneration in the rat model. Meanwhile, degradation experiments *in vitro* (**Supplementary Figure S5**) further proved that the optimized degradation performance may further promote the function of bone repair.

DISCUSSION

Summarizing the experimental results above, our article is the first to report this innovative composite scaffold fabricated by SLA to repair bone defect that had advantage of both the biocompatibility of ECM and mechanical strength of traditional synthetic materials. The innovative scaffold was rich in various bioactive factors, had micropore structure on the surface and interconnectivity of macrostructures, attracted cells, and promoted osteogenic differentiation. Ultimately, experimental results showed that both *in vitro* and *in vivo* experiments resulted in apparent facilitation in terms of osteogenesis.

The ECM has been reported commonly in the field of bone and other parts repair (Pham et al., 2008; Pacelli et al., 2017; Matai et al., 2020). Our team has published relevant literature before. For instance, (Qiu et al., 2020) has fabricated an injectable periosteal ECM hydrogel that dynamically integrates multiple biological functions, promotes angiogenesis and osteogenesis at the defect site. The whole dynamic process contains bone formation, remodeling and repair, which involves cell migration, ECM assembly, osteocyte embedding, and bone resorption (Shiflett et al., 2019). Our experimental results have proved the effect on cell growth, migration, and differentiation. However, the physical properties and spatial structure of this original material need to be improved (Narayanan et al., 2009).

In this study, the physical and mechanical strength of the material was significantly improved by adding PEGDA. As reported previously (Engler et al., 2006), naive MSCs differentiated toward a specific lineage and committed to phenotypes with extreme sensitivity to tissue-level elasticity, and when tissue-level elasticity of the matrices mimicked a collagenous bone, the outcome was osteogenic (Engler et al., 2006; Caliari et al., 2016). PEGDA (∼0.3 MPa) improved the hardness of the material and promoted osteogenic differentiation of MSCs. In fact, in our animal experiments, there were also some weak positive results of osteogenesis in the PEGDA group.

In contrast, the addition of tECM improved the biocompatibility of traditional synthetic materials. Various parameters, including surface properties, mobility and solute diffusion, were affected by the swelling ratio, an essential material parameter in tissue engineering (Stephanopoulos et al., 2013). Microscopically, both the pore size of the polymer and the interaction between the solvent and polymer affect the value of swelling ratio (Du et al., 2008). The addition of tECM greatly improved the swelling degree of the material, and as the concentration of tECM increased, the swelling degree also increased, which was closely related to the hydrophilicity of tECM, as it contains numerous hydrophilic components. The tECM component increased the porosity of the hydrogel. The scaffold with more pores and a larger pore size creates favorable conditions for cell survival, adhesion, and migration (O'Brien et al., 2005, 2007).

To further improve the external form and internal permeability of the PEGDA/tECM hydrogel, SLA technology was applied in the fabrication of this novel scaffold. To date, A challenge that inkjet bioprinting, a traditional printing method, faces is that it is challenging to print vertical 3D structures, while SLA avoids this problem entirely (Wang et al., 2015; Bhattacharjee et al., 2018). Other drawbacks inkjet printing has include shear stress that damage cells, and print nozzle blockage (Wang et al., 2018). In contrast, the SLA printing speed is not affected by plane complexity, while the number of printing layers determines the printing time (Wang et al., 2015). Also, each printing detail may extend the printing time in traditional inkjet bioprinting. Consequently, complex 3D shapes are more likely to be created by SLA without extending the printing time (Wang et al., 2015). The printing time of a customized scaffold is extremely important since urgent surgical treatment is crucial in accidental trauma (Rauch et al., 2019).

Compared with traditional synthetic materials, 3D-pPES has been confirmed to have a rougher surface. Micro-roughness can affect the type of integrins produced by cells, promoting those subunits associated with bone proteins, such as α_2 and β_1 (Olivares-Navarrete et al., 2008). Moreover, micro-rough surface evoked accelerated gene expression of the bone matrix molecules osteopontin and osteonectin and up-regulated of bone sialoprotein, collagen III and integrins (Salvi et al., 2015). In fact, both 3D micropore architectural structure and micro-rough surface of 3D-pPES accelerate the MSCs osteogenic differentiation.

Polyethylene glycol diacrylate/tECM hydrogel showed better capability in coordinating Ca-Pi deposition, which led to high biomineralization. The cell osteogenesis induction experiment *in vitro* also proved that PEGDA/tECM hydrogels significantly and conformably upregulated the expression of genes associated with osteogenesis. There is significant evidence that endochondral (EC) ossification occurs in ECM grafts

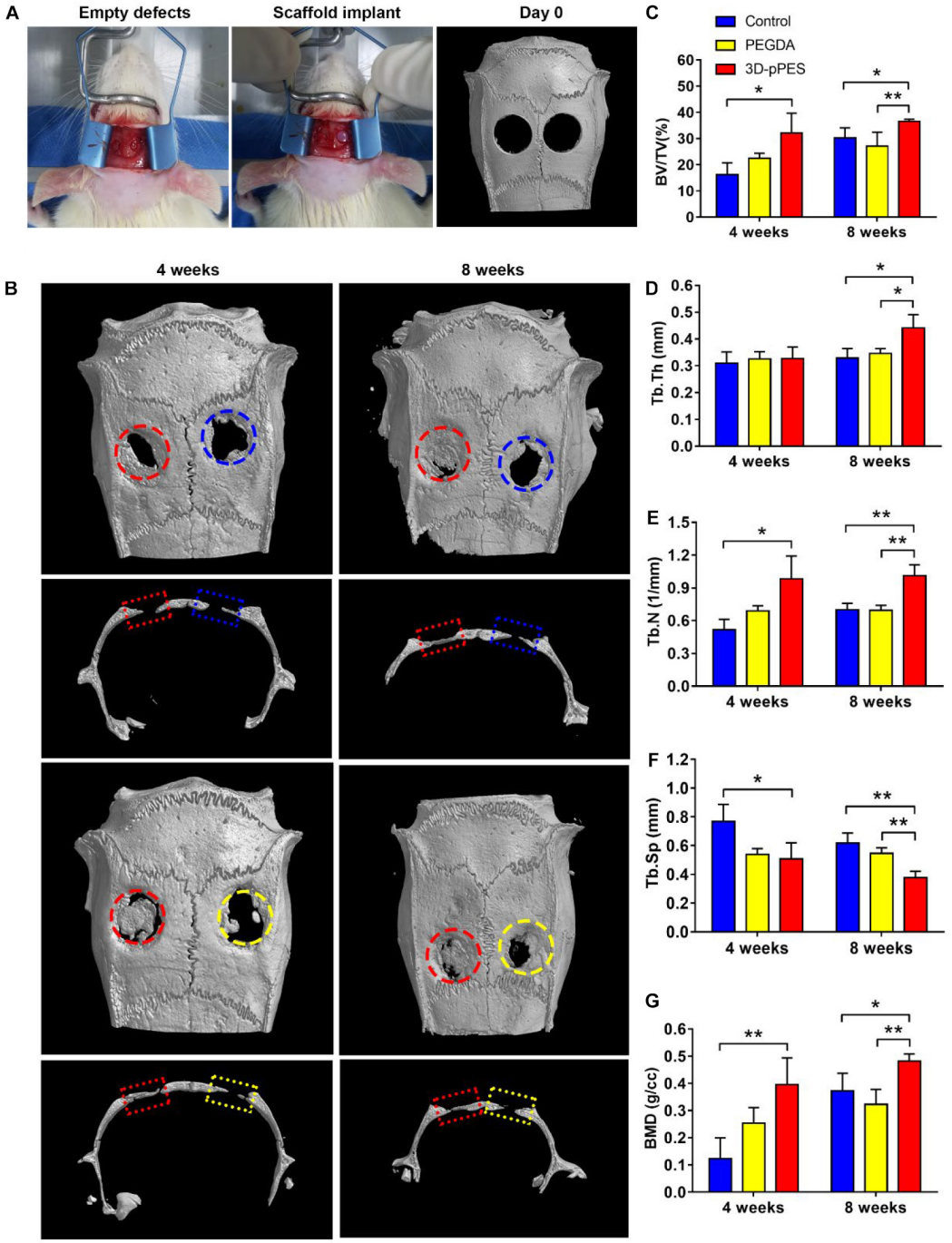

FIGURE 5 | Bone regeneration in the calvarial bone defect model. **(A)** Surgical procedure and micro-CT scanning of the calvarial defect after surgery on day 0. **(B)** Mineralization of the calvarial defect was evaluated by micro-CT and bone defect healing at 4 and 8 weeks after gel implantation was showed. **(C–G)** Quantitative analysis of **(C)** BV/TV, **(D)** Tb.Th, **(E)** Tb.N, **(F)** Tb.Sp, and **(G)** BMD new bone formation area of the regenerated bone 4 and 8 weeks after implantation. BV, bone volume; TV, total volume; Tb.Th, Trabecular thickness; Tb.N, trabecular number; Tb.Sp, Trabecular separation; BMD, bone mineral density. The blue circle/rectangle represented the original defect of control group, the yellow circle/rectangle represented the original defect of PEGDA group, the red circle/rectangle represented the original defect of 3D-pPES group.

(Dennis et al., 2015) and our results agree with this conclusion. The osteogenic properties of our 3D-pPES were proved by *in vivo* experiments. The repair of critical-sized calvarial bone defects in the 3D-pPES group showed the highest quality and the most substantial quantity of new mineralized bone formation. Meanwhile, from the results of tissue slices from animal

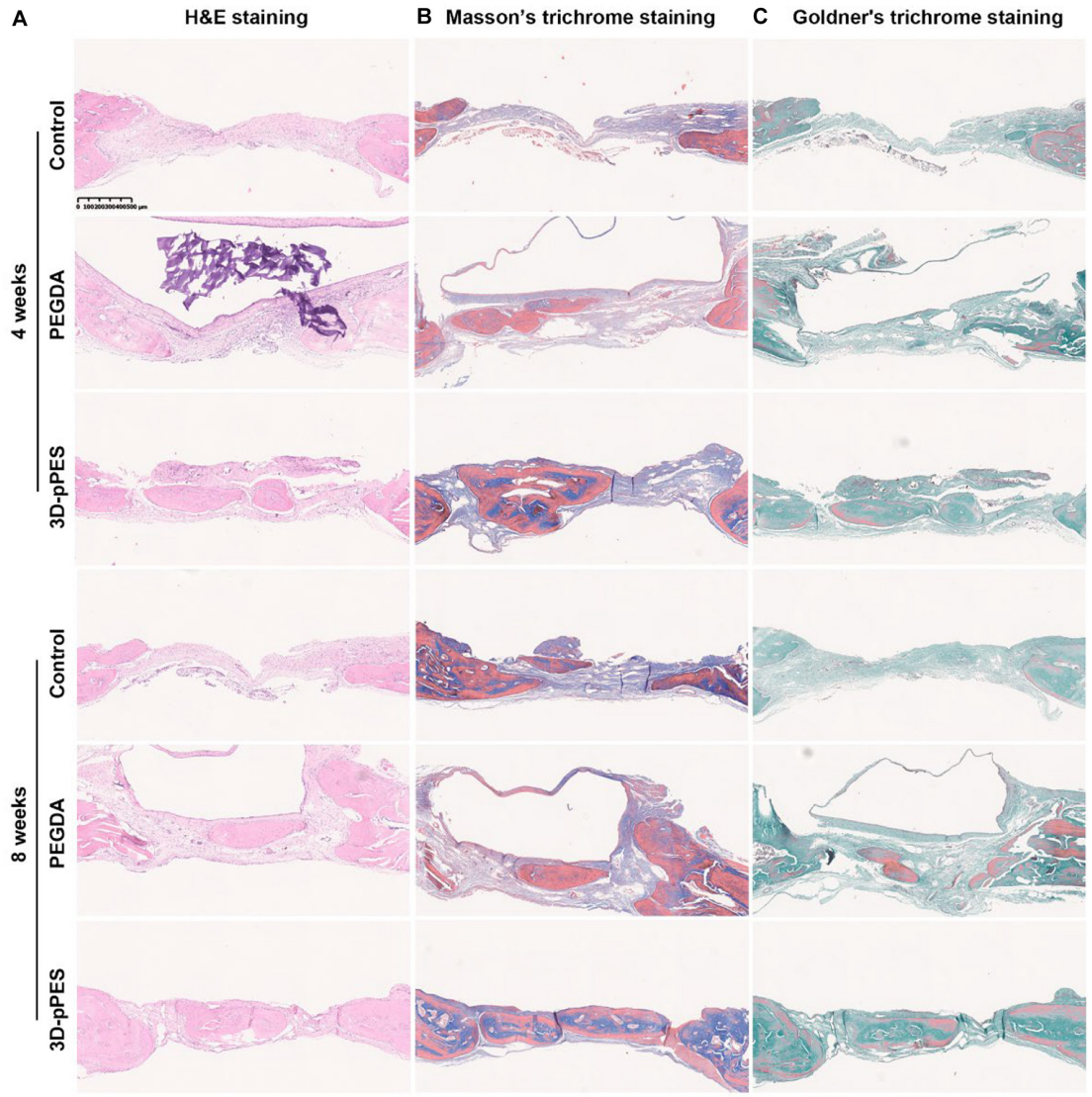

FIGURE 6 | Osteogenesis after hydrogel implantation showed by histological staining. **(A)** H&E staining of the calvarial defects at 4 and 8 weeks after hydrogel implantation. **(B)** Masson's trichrome staining of the calvarial defects at 4 and 8 weeks after hydrogel implantation, new bones were shown in dark blue. **(C)** Goldner's staining of the regenerated bone in calvarial defects, fibroblastic connective tissue was shown in light green, immature woven bone and osteoid tissue were shown in red. mature bone island (lamellar bone) was showed in dark green. Scale bar = 500 μm.

experiments, islands of new bone formation were observed in the 3D-pPES group. Moreover, denser new bone and more bone-like tissues near the border of the bone defect were observed in the 3D-pPES group.

Degradation experiment *in vitro* proved that the 3D-pPES have the advantage of faster degradation. First, ECM has multiple biological enzymes to accelerate the degradation of scaffold (Pham et al., 2008). Second, the 3D-pPES greatly increased the surface area of the material. Moreover, it has been reported that scaffold microarchitecture profoundly influences macrophage adhesion, infiltration and differentiation (Kurpinski et al., 2010). Once invading into the scaffold microarchitecture, macrophages secrete reactive oxygen species (ROS) and hydrolytic enzymes, contributing to oxidative and enzymatic biomaterial degradation, respectively (Wissing et al., 2019). Meanwhile, the scaffolds with larger pore size on the micron scale can promote the oxidative degradation of the synthetic scaffolds (Versaevel et al., 2012). Optimized by multiple factors, 3D-pPES showed superior degradation and repair performance.

We can reasonably speculate that a relatively biomimetic bone repair process has been achieved via intramembranous ossification (Dennis et al., 2015). MSCs proliferate intensively and differentiate into osteoblasts, forming ossification center. The ossification center acts as a primed template for subsequent osteoblast infiltration,

woven bone ossification, and bone remodeling restore healthy lamellar bone architecture (Dennis et al., 2015; Serra-Vinardell et al., 2020). Further work is needed to confirm the inference of these molecular mechanisms.

CONCLUSION

In this study, we revealed that PEGDA/tECM hydrogel is a greatly enriched small aperture with a traditional synthetic material surface. It overcomes the drawbacks of insufficient mechanical strength of the traditional ECM and promotes cell growth. Using SLA, our 3D-pPES promote cell migration, initiate MSCs differentiation toward osteogenesis. In conclusion, promising repair efficacy of the 3D-pPES is confirmed in a bone defect model.

DATA AVAILABILITY STATEMENT

The original contributions presented in the study are included in the article/**Supplementary Material**, further inquiries can be directed to the corresponding authors.

ETHICS STATEMENT

The animal study was reviewed and approved by Sir Run Shaw Affiliated Hospital of Zhejiang University School of Medicine.

AUTHOR CONTRIBUTIONS

All authors listed have made a substantial, direct and intellectual contribution to the work, and approved it for publication.

FUNDING

The study was supported by the National Key R&D Program of China (grant number 2018YFC1105203); the National Nature Science Fund of China (grant numbers 81802147, 81702143, and 81772387); Zhejiang Basic Public Welfare Research Project (GF19H060036), and Innovation research grant program for 8-year-system medical students at Zhejiang University (No. 119000-5405A1).

ACKNOWLEDGMENTS

We thank Mrs. Dandan Song in the Center of Cryo-Electron Microscopy (CCEM), Zhejiang University for her technical assistance on Scanning Electron Microscopy. We would like to thank Editage (www.editage.cn) for English language editing.

SUPPLEMENTARY MATERIAL

The Supplementary Material for this article can be found online at: https://www.frontiersin.org/articles/10.3389/fbioe.2020.589094/full#supplementary-material

REFERENCES

Ahn, H., Patel, R. R., Hoyt, A. J., Lin, A. S. P., Torstrick, F. B., Guldberg, R. E., et al. (2018). Biological evaluation and finite-element modeling of porous poly(para-phenylene) for orthopaedic implants. *Acta Biomater.* 72, 352–361. doi: 10.1016/j.actbio.2018.03.025

Bez, M., Kremen, T. J., Tawackoli, W., Avalos, P., Sheyn, D., Shapiro, G., et al. (2018). Ultrasound-mediated gene delivery enhances tendon allograft integration in mini-pig ligament reconstruction. *Mol. Ther.* 26, 1746–1755. doi: 10.1016/j.ymthe.2018.04.020

Bhattacharjee, N., Parra-Cabrera, C., Kim, Y. T., Kuo, A. P., and Folch, A. (2018). Desktop-stereolithography 3D-printing of a poly(dimethylsiloxane)-based material with sylgard-184 properties. *Adv. Mater.* 30:e1800001. doi: 10.1002/adma.201800001

Cabbad, N. C., Stalder, M. W., Arroyave, A., Wolfe, E. M., and Wolfe, S. A. (2019). Autogenous bone cranioplasty: review of a 42-year experience by a single surgeon. *Plast. Reconstr. Surg.* 143, 1713–1723. doi: 10.1097/PRS.0000000000005677

Caliari, S. R., Vega, S. L., Kwon, M., Soulas, E. M., and Burdick, J. A. (2016). Dimensionality and spreading influence MSC YAP/TAZ signaling in hydrogel environments. *Biomaterials* 103, 314–323. doi: 10.1016/j.biomaterials.2016.06.061

Campana, V., Milano, G., Pagano, E., Barba, M., Cicione, C., Salonna, G., et al. (2014). Bone substitutes in orthopaedic surgery: from basic science to clinical practice. *J. Mater. Sci. Mater. Med.* 25, 2445–2461. doi: 10.1007/s10856-014-5240-2

Catanzano, O., Soriente, A., La Gatta, A., Cammarota, M., Ricci, G., Fasolino, I., et al. (2018). Macroporous alginate foams crosslinked with strontium for bone tissue engineering. *Carbohydr. Polym.* 202, 72–83. doi: 10.1016/j.carbpol.2018.08.086

Chan, J. P., Battiston, K. G., and Santerre, J. P. (2019). Synthesis and characterization of electrospun nanofibrous tissue engineering scaffolds generated from in situ polymerization of ionomeric polyurethane composites. *Acta Biomater.* 96, 161–174. doi: 10.1016/j.actbio.2019.06.046

Chen, H., Zhang, J., Li, X., Liu, L., Zhang, X., Ren, D., et al. (2019). Multi-level customized 3D printing for autogenous implants in skull tissue engineering. *Biofabrication* 11:045007. doi: 10.1088/1758-5090/ab1400

Dennis, S. C., Berkland, C. J., Bonewald, L. F., and Detamore, M. S. (2015). Endochondral ossification for enhancing bone regeneration: converging native extracellular matrix biomaterials and developmental engineering in vivo. *Tissue Eng. Part B Rev.* 21, 247–266. doi: 10.1089/ten.TEB.2014.0419

Do, A. V., Khorsand, B., Geary, S. M., and Salem, A. K. (2015). 3D printing of scaffolds for tissue regeneration applications. *Adv. Healthc. Mater.* 4, 1742–1762. doi: 10.1002/adhm.201500168

Du, Y., Lo, E., Ali, S., and Khademhosseini, A. (2008). Directed assembly of cell-laden microgels for fabrication of 3D tissue constructs. *Proc. Natl. Acad. Sci. U.S.A.* 105, 9522–9527. doi: 10.1073/pnas.0801866105

Engler, A. J., Sen, S., Sweeney, H. L., and Discher, D. E. (2006). Matrix elasticity directs stem cell lineage specification. *Cell* 126, 677–689. doi: 10.1016/j.cell.2006.06.044

Fang, Y., Zhang, T., Zhang, L., Gong, W., and Sun, W. (2019). Biomimetic design and fabrication of scaffolds integrating oriented micro-pores with branched channel networks for myocardial tissue engineering. *Biofabrication* 11:035004. doi: 10.1088/1758-5090/ab0fd3

Gibbs, D. M., Black, C. R., Dawson, J. I., and Oreffo, R. O. (2016). A review of hydrogel use in fracture healing and bone regeneration. *J. Tissue Eng. Regen. Med.* 10, 187–198. doi: 10.1002/term.1968

Grenier, J., Duval, H., Barou, F., Lv, P., David, B., and Letourneur, D. (2019). Mechanisms of pore formation in hydrogel scaffolds textured by freeze-drying. *Acta Biomater.* 94, 195–203. doi: 10.1016/j.actbio.2019.05.070

Hassan, M. N., Yassin, M. A., Suliman, S., Lie, S. A., Gjengedal, H., and Mustafa, K. (2019). The bone regeneration capacity of 3D-printed templates in calvarial defect models: a systematic review and meta-analysis. *Acta Biomater.* 91, 1–23. doi: 10.1016/j.actbio.2019.04.017

Hollister, S. J., and Murphy, W. L. (2011). Scaffold translation: barriers between concept and clinic. *Tissue Eng. Part B Rev.* 17, 459–474. doi: 10.1089/ten.TEB.2011.0251

Hwang, K. S., Choi, J. W., Kim, J. H., Chung, H. Y., Jin, S., Shim, J. H., et al. (2017). Comparative efficacies of collagen-based 3D printed PCL/PLGA/beta-TCP composite block bone grafts and biphasic calcium phosphate bone substitute for bone regeneration. *Materials* 10:421. doi: 10.3390/ma10040421

Kaynak Bayrak, G., Demirtas, T. T., and Gumusderelioglu, M. (2017). Microwave-induced biomimetic approach for hydroxyapatite coatings of chitosan scaffolds. *Carbohydr. Polym.* 157, 803–813. doi: 10.1016/j.carbpol.2016.10.016

Knowlton, S., Yu, C. H., Ersoy, F., Emadi, S., Khademhosseini, A., and Tasoglu, S. (2016). 3D-printed microfluidic chips with patterned, cell-laden hydrogel constructs. *Biofabrication* 8:025019. doi: 10.1088/1758-5090/8/2/025019

Kurpinski, K. T., Stephenson, J. T., Janairo, R. R., Lee, H., and Li, S. (2010). The effect of fiber alignment and heparin coating on cell infiltration into nanofibrous PLLA scaffolds. *Biomaterials* 31, 3536–3542. doi: 10.1016/j.biomaterials.2010.01.062

Lee, J. S., Hong, J. M., Jung, J. W., Shim, J. H., Oh, J. H., and Cho, D. W. (2014). 3D printing of composite tissue with complex shape applied to ear regeneration. *Biofabrication* 6:024103. doi: 10.1088/1758-5082/6/2/024103

Mao, D., Li, Q., Bai, N., Dong, H., and Li, D. (2018). Porous stable poly(lactic acid)/ethyl cellulose/hydroxyapatite composite scaffolds prepared by a combined method for bone regeneration. *Carbohydr. Polym.* 180, 104–111. doi: 10.1016/j.carbpol.2017.10.031

Matai, I., Kaur, G., Seyedsalehi, A., McClinton, A., and Laurencin, C. T. (2020). Progress in 3D bioprinting technology for tissue/organ regenerative engineering. *Biomaterials* 226:119536. doi: 10.1016/j.biomaterials.2019.119536

Narayanan, K., Leck, K. J., Gao, S., and Wan, A. C. (2009). Three-dimensional reconstituted extracellular matrix scaffolds for tissue engineering. *Biomaterials* 30, 4309–4317. doi: 10.1016/j.biomaterials.2009.04.049

O'Brien, F. J., Harley, B. A., Waller, M. A., Yannas, I. V., Gibson, L. J., and Prendergast, P. J. (2007). The effect of pore size on permeability and cell attachment in collagen scaffolds for tissue engineering. *Technol. Health Care* 15, 3–17.

O'Brien, F. J., Harley, B. A., Yannas, I. V., and Gibson, L. J. (2005). The effect of pore size on cell adhesion in collagen-GAG scaffolds. *Biomaterials* 26, 433–441. doi: 10.1016/j.biomaterials.2004.02.052

Olivares-Navarrete, R., Raz, P., Zhao, G., Chen, J., Wieland, M., Cochran, D. L., et al. (2008). Integrin alpha2beta1 plays a critical role in osteoblast response to micron-scale surface structure and surface energy of titanium substrates. *Proc. Natl. Acad. Sci. U.S.A.* 105, 15767–15772. doi: 10.1073/pnas.0805420105

Pacelli, S., Basu, S., Whitlow, J., Chakravarti, A., Acosta, F., Varshney, A., et al. (2017). Strategies to develop endogenous stem cell-recruiting bioactive materials for tissue repair and regeneration. *Adv. Drug Deliv. Rev.* 120, 50–70. doi: 10.1016/j.addr.2017.07.011

Pham, Q. P., Kasper, F. K., Scott Baggett, L., Raphael, R. M., Jansen, J. A., and Mikos, A. G. (2008). The influence of an in vitro generated bone-like extracellular matrix on osteoblastic gene expression of marrow stromal cells. *Biomaterials* 29, 2729–2739. doi: 10.1016/j.biomaterials.2008.02.025

Qiu, P., Li, M., Chen, K., Fang, B., Chen, P., Tang, Z., et al. (2020). Periosteal matrix-derived hydrogel promotes bone repair through an early immune regulation coupled with enhanced angio- and osteogenesis. *Biomaterials* 227:119552. doi: 10.1016/j.biomaterials.2019.119552

Rauch, S., Wallner, B., Strohle, M., Dal Cappello, T., and Brodmann Maeder, M. (2019). Climbing accidents-prospective data analysis from the international alpine trauma registry and systematic review of the literature. *Int. J. Environ. Res. Public Health* 17:203. doi: 10.3390/ijerph17010203

Salvi, G. E., Bosshardt, D. D., Lang, N. P., Abrahamsson, I., Berglundh, T., Lindhe, J., et al. (2015). Temporal sequence of hard and soft tissue healing around titanium dental implants. *Periodontology* 68, 135–152. doi: 10.1111/prd.12054

Serra-Vinardell, J., Roca-Ayats, N., De-Ugarte, L., Vilageliu, L., Balcells, S., and Grinberg, D. (2020). Bone development and remodeling in metabolic disorders. *J. Inherit. Metab. Dis.* 43, 133–144. doi: 10.1002/jimd.12097

Sharif, F., Ur Rehman, I., Muhammad, N., and MacNeil, S. (2016). Dental materials for cleft palate repair. *Mater. Sci. Eng. C Mater. Biol. Appl.* 61, 1018–1028. doi: 10.1016/j.msec.2015.12.019

Shiflett, L. A., Tiede-Lewis, L. M., Xie, Y., Lu, Y., Ray, E. C., and Dallas, S. L. (2019). Collagen dynamics during the process of osteocyte embedding and mineralization. *Front. Cell. Dev. Biol.* 7:178. doi: 10.3389/fcell.2019.00178

Stephanopoulos, N., Ortony, J. H., and Stupp, S. I. (2013). Self-assembly for the synthesis of functional biomaterials. *Acta Mater.* 61, 912–930. doi: 10.1016/j.actamat.2012.10.046

Thankam, F. G., Dilisio, M. F., Gross, R. M., and Agrawal, D. K. (2018). Collagen I: a kingpin for rotator cuff tendon pathology. *Am. J. Transl. Res.* 10, 3291–3309.

Versaevel, M., Grevesse, T., and Gabriele, S. (2012). Spatial coordination between cell and nuclear shape within micropatterned endothelial cells. *Nat. Commun.* 3:671. doi: 10.1038/ncomms1668

Wang, Z., Abdulla, R., Parker, B., Samanipour, R., Ghosh, S., and Kim, K. (2015). A simple and high-resolution stereolithography-based 3D bioprinting system using visible light crosslinkable bioinks. *Biofabrication* 7:045009. doi: 10.1088/1758-5090/7/4/045009

Wang, Z., Kumar, H., Tian, Z., Jin, X., Holzman, J. F., Menard, F., et al. (2018). Visible light photoinitiation of cell-adhesive gelatin methacryloyl hydrogels for stereolithography 3D bioprinting. *ACS Appl. Mater. Interfaces* 10, 26859–26869. doi: 10.1021/acsami.8b06607

Wissing, T. B., Bonito, V., van Haaften, E. E., van Doeselaar, M., Brugmans, M., Janssen, H. M., et al. (2019). Macrophage-driven biomaterial degradation depends on scaffold microarchitecture. *Front. Bioeng. Biotechnol.* 7:87. doi: 10.3389/fbioe.2019.00087

Xu, Z., Yang, Y., Zhao, W., Wang, Z., Landis, W. J., Cui, Q., et al. (2015). Molecular mechanisms for intrafibrillar collagen mineralization in skeletal tissues. *Biomaterials* 39, 59–66. doi: 10.1016/j.biomaterials.2014.10.048

Zhang, L., Yang, G., Johnson, B. N., and Jia, X. (2019). Three-dimensional (3D) printed scaffold and material selection for bone repair. *Acta Biomater.* 84, 16–33. doi: 10.1016/j.actbio.2018.11.039

Zhang, H., Zhou, Y., Yu, N., Ma, H., Wang, K., Liu, J., et al. (2019). Construction of vascularized tissue-engineered bone with polylysine-modified coral hydroxyapatite and a double cell-sheet complex to repair a large radius bone defect in rabbits. *Acta Biomater.* 91, 82–98. doi: 10.1016/j.actbio.2019.04.024

Conflict of Interest: The authors declare that the research was conducted in the absence of any commercial or financial relationships that could be construed as a potential conflict of interest.

frontiers in Bioengineering and Biotechnology

SYSTEMATIC REVIEW
published: 26 November 2020
doi: 10.3389/fbioe.2020.587052

The Role of Paracrine Regulation of Mesenchymal Stem Cells in the Crosstalk With Macrophages in Musculoskeletal Diseases: A Systematic Review

Hongtao Xu[1†], *Chien-Wei Lee*[1,2,3†], *Yu-Fan Wang*[1], *Shuting Huang*[2], *Lih-Ying Shin*[1], *Yu-Hsuan Wang*[1], *Zihao Wan*[1], *Xiaobo Zhu*[1], *Patrick Shu Hang Yung*[1] and *Oscar Kuang-Sheng Lee*[1,2,4,5*]

[1] Department of Orthopaedics and Traumatology, Faculty of Medicine, Prince of Wales Hospital, The Chinese University of Hong Kong, Hong Kong, China, [2] Institute for Tissue Engineering and Regenerative Medicine, The Chinese University of Hong Kong, Hong Kong, China, [3] Developmental and Regenerative Biology TRP, Faculty of Medicine, School of Biomedical Sciences, The Chinese University of Hong Kong, Hong Kong, China, [4] Faculty of Medicine, Li Ka Shing Institute of Health Sciences, Prince of Wales Hospital, The Chinese University of Hong Kong, Hong Kong, China, [5] Department of Orthopadics, China Medical University Hospital, Taichung, Taiwan

OPEN ACCESS

Edited by:
Hae-Won Kim,
Institute of Tissue Regeneration Engineering (ITREN), South Korea

Reviewed by:
Kunyu Zhang,
Johns Hopkins University, United States
Jung-Hwan Lee,
Institute of Tissue Regeneration Engineering (ITREN), South Korea

***Correspondence:**
Oscar Kuang-Sheng Lee
oscarlee9203@gmail.com

[†]These authors have contributed equally to this work

Specialty section:
This article was submitted to Biomaterials, a section of the journal Frontiers in Bioengineering and Biotechnology

Received: 24 July 2020
Accepted: 28 October 2020
Published: 26 November 2020

Citation:
Xu H, Lee C-W, Wang Y-F, Huang S, Shin L-Y, Wang Y-H, Wan Z, Zhu X, Yung PSH and Lee OK-S (2020) The Role of Paracrine Regulation of Mesenchymal Stem Cells in the Crosstalk With Macrophages in Musculoskeletal Diseases: A Systematic Review. Front. Bioeng. Biotechnol. 8:587052. doi: 10.3389/fbioe.2020.587052

The phenotypic change of macrophages (Mφs) plays a crucial role in the musculoskeletal homeostasis and repair process. Although mesenchymal stem cells (MSCs) have been shown as a novel approach in tissue regeneration, the therapeutic potential of MSCs mediated by the interaction between MSC-derived paracrine mediators and Mφs remains elusive. This review focused on the elucidation of paracrine crosstalk between MSCs and Mφs during musculoskeletal diseases and injury. The search method was based on the PRISMA (Preferred Reporting Items for Systematic Reviews and Meta-Analyses) and Cochrane Guidelines. The search strategies included MeSH terms and other related terms of MSC-derived mediators and Mφs. Ten studies formed the basis of this review. The current finding suggested that MSC administration promoted proliferation and activation of $CD163^+$ or $CD206^+$ M2 Mφs in parallel with reduction of proinflammatory cytokines and increase in anti-inflammatory cytokines. During such period, Mφs also induced MSCs into a motile and active phenotype via the influence of proinflammatory cytokines. Such crosstalk between Mφs and MSCs further strengthens the effect of paracrine mediators from MSCs to regulate Mφs phenotypic alteration. In conclusion, MSCs in musculoskeletal system, mediated by the interaction between MSC paracrine and Mφs, have therapeutic potential in musculoskeletal diseases.

Keywords: mesenchymal stem cells (MeSH ID D059630), extracellular vesicles (EVs), exosomes, macrophages, musculoskeletal

INTRODUCTION

The inflammatory processes in response to musculoskeletal diseases and injury, such as bone fractures, osteoarthritis (OA), osteoporosis, tendon injuries, and muscle injuries, are essential for the correct restoration of structure and function to the affected area (Bosurgi et al., 2011; Mianehsaz et al., 2019; Pajarinen et al., 2019; Wang et al., 2019; Yang and Yang, 2019). However,

the dysregulation of inflammatory reactions can aggravate the tissue healing results (Saldana et al., 2019).

Macrophages (Mφs) are the critical regulators involved in initiation, propagation, and resolution of inflammatory response throughout the tissue regenerative process. Mφs have a broad spectrum of adaptive phenotypes and functional transitions that might exacerbate and resolve inflammation during tissue repair process (Saldana et al., 2019). In 2008, Mosser and Edwards analyzed the phenotypic changes of Mφs and robustly classified Mφs into two types: M1 and M2 (Mosser and Edwards, 2008). Proinflammatory Mφs are identified as the classic M1 Mφs, which are involved in the early stages of tissue repair, whereas the anti-inflammatory Mφs are identified as M2 Mφs, which dominated later stages of tissue repair (Murray et al., 2014; Spiller and Koh, 2017). Upon injury, the early presence of M1 Mφs initiates tissue repair, but the persistent of M1 activity can deteriorate the repair process (Krzyszczyk et al., 2018). On the other hand, the early presence of M2 can prevent cellular and vascular infiltration that impairs tissue development through ectopic secretion of fibrotic chemokines and cytokine (Stahl et al., 2013; Bility et al., 2014; Moore et al., 2015). Moreover, several different M2 subtypes have been identified, including M2a, M2b, M2c, and M2d (Stein et al., 1992; Donnelly et al., 1999; Anderson and Mosser, 2002). The undisciplined regulation of Mφ phenotypic change impairs tissue repair, and each of the subtypes might have specific functions; therefore, further investigation is needed to identify the explicit role of M2 subtypes (O'Brien et al., 2019).

In the 1980's, Arnold Caplan and his colleagues published an isolation method of fibroblast-like stromal cells from bone marrow and first identified them as mesenchymal stem cells (MSCs) because of their multilineage differentiation potential (Caplan, 1991). A rapid expansion in the field of MSC-based therapy in immunomodulation and regenerative medicine has been acknowledged (Kingery et al., 2019). It has been reported that MSCs can switch M1 Mφs or resting Mφs into M2 Mφs (Kim and Hematti, 2009; Nemeth et al., 2009; Melief et al., 2013b). Previous studies showed that prostaglandin E_2 (PGE_2), interleukin-4 (IL-4), IL-6, and IL-10 released from MSCs can induce the Mφ polarization toward M2 to accelerate tissue regeneration (da Costa Goncalves and Paz, 2019). On the other hand, such immunomodulatory ability of MSCs is adjusted by inflammatory factors released by macrophages (Waterman et al., 2010; Carrero et al., 2012). After the stimulation, MSCs would secrete anti-inflammatory factors, such as transforming growth factor β (TGF-β) and CCL-18, to further suppress activation of lymphocytes and inhibit major histocompatibility complex (MHC) class II and CD86 in lipopolysaccharide (LPS)–stimulated Mφs (Melief et al., 2013b; Cho et al., 2014). This suggested that the interplay between MSCs and Mφs is in control of inflammation, and their crosstalk may be recommended to advocate tissue healing or repair.

Besides versatile soluble proteins, MSC-derived extracellular vesicles (MSC-EVs) have raised worldwide attention in regenerative medicine because of their immunomodulation ability (Raposo and Stoorvogel, 2013). EVs represent a heterogeneous group of cell-derived membranous vesicles, such as microvesicles (MVs) and exosomes, which were first described in the 1970's (Vakhshiteh et al., 2019). MVs, ranging from 40 to 2,000 nm in diameter (Bruno et al., 2012; Kim et al., 2012), and exosomes, ranging from 30 to 150 nm in diameter (Li et al., 2013; Zhao et al., 2015), are critical mediators for intercellular communication via the delivery of the embedded RNAs, DNAs, and cytosolic proteins. Moreover, boosting the therapeutic potential of MSC-EVs by changing the intrinsic bioactive factors or modifying membrane by bioengineering approach is possible (Lu and Huang, 2020). Refining the culture condition of MSCs could significantly increase the production yield and improve the efficacy of MSC-EVs (Luan et al., 2017; Willis et al., 2017; Bagno et al., 2018; Cha et al., 2018; Ferguson et al., 2018). Also, MSC-derived EVs could serve as a promising drug delivery vector, owing to their high biocompatibility, high efficacy of delivery, and low immunogenicity (Clayton et al., 2003; Ridder et al., 2014; Zomer et al., 2015). EVs derived from different origins have preferential targeting cells due to their distinct membrane composition gained from their parental cells that impart differential effect on body systems (Luan et al., 2017; Ferguson et al., 2018), which could be addressed by exploiting the nature of EVs as natural carriers of miRNA or other molecules by considering them as drug delivery vehicles (Cheng et al., 2017). In addition, MSC-derived EVs in conjunction with other materials might provide substantial advances in both immunomodulation and tissue regeneration (Cosenza et al., 2018). And it has been reported that a variety of material's environment could affect cell's downstream response by cell–material interactions (Darnell et al., 2018). Taken together, bioengineered MSC-derived EVs are novel adjustable biomaterials for tissue regeneration.

The therapeutic effect of MSCs showed a clinical benefit in children suffering from osteogenesis imperfecta (Otsuru et al., 2012) and preclinical benefit in bone fracture (Li Y. et al., 2019), OA (Cosenza et al., 2017), tendon injury (Chamberlain et al., 2019), pulmonary hypertension (Lee et al., 2012), cancer (Silva et al., 2013), and infectious diseases (Cheng and Schorey, 2013). The mechanisms of these mentioned therapeutic potentials of MSCs need elucidation. This review aimed to expound the role of MSC paracrine, especially MSC-derived EVs, in the crosstalk with Mφs in musculoskeletal diseases. Moreover, a systemic understanding of MSC-EVs properties and activities will provide a solid foundation to boost MSC-EVs for regenerative medicine and will significantly facilitate the translation value of MSC-based therapy (Zhang et al., 2020).

METHODS

The Preferred Reporting Items for Systematic Reviews and Meta-Analyses (PRISMA) statement was used for this article. Meanwhile, the Cochrane handbook was selected as guidelines for the study protocol (Moher et al., 2009).

Search Strategy and Study Selection

Two different investigators (H.-T.X., L.-Y.S.) conducted the customized up-to-date literature search. PubMed database and EMBASE (Excerpta Medica Database) database were selected in this study.

The title and abstract field were selected to search for MeSH terms and other related terms, which pertained to "Mesenchymal Stem Cells," "Macrophages," and "Paracrine Regulation," such as "Exosomes," "Extracellular Vesicles" and "Culture Media, Conditioned." The details of selected search terms and searching procedures that were used in the individual database are available in Appendices 1–3 in **Supplementary Material**. Additional studies were also located by searching papers referenced in listed articles. Those studies identified by the search outcomes were combined, and duplicates were excluded. Then, the screening procedure of titles and abstracts was performed before elaboration on the selected full-text articles. Two investigators (H.-T.X., L.-Y.S.) screened the titles and abstracts of those identified studies individually. In cases of disagreement between the two authors, a consensus was reached by discussion with a third author (C.-W.L.). After that, the full text of screened

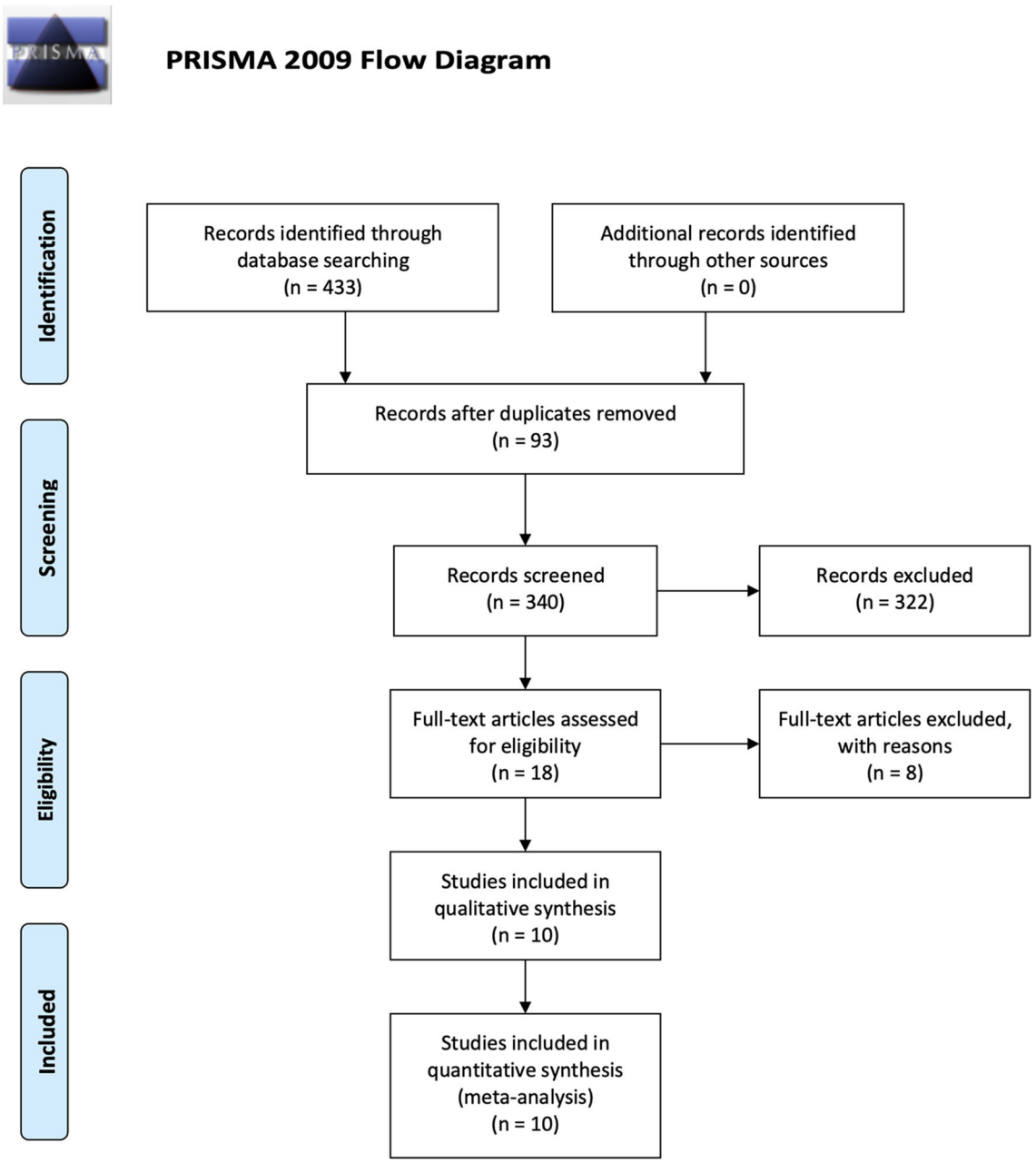

FIGURE 1 | Flowchart presenting the results of the literature search and the strategy used to select studies that relate to the crosstalk between MSCs and Mφs of musculoskeletal diseases. Study selection process. The search revealed 433 records. A total of 93 overlaps were removed between the databases. The remaining 340 records were screened by title and abstract, and 322 records were excluded. The remaining 18 studies were examined using their full texts, and finally ten eligible studies were identified.

articles were examined. Corresponding authors of the reviewed articles could be contacted with essential needs to obtain those missing data.

The search yielded 433 studies across all databases (239 studies across PubMed database and 194 studies across EMBASE database). A total of 93 duplicates were removed. According to the inclusion and exclusion criteria, all these studies were screened and reviewed by titles and abstracts first; 322 studies were excluded because they were review articles, case reports, case series, letters, chapters, or studies published more than 10 years ago. Of the 18 remaining studies, which were applied by a filter to include musculoskeletal-related studies, eight studies were excluded via reviewing full text. The 10 remaining studies underwent secondary full-text review and were confirmed as fitting the inclusion criteria. The flowchart of the selected studies selection process, which was based on the PRISMA 2009 Flow Diagram (Moher et al., 2009), is shown in **Figure 1**, and the details of inclusion and exclusion criteria are shown in **Table 1**.

TABLE 1 | Inclusion and exclusion criteria.

Criteria	
Inclusion criteria	1. Full-text available; 2. Written in English; 3. Articles published in the last 10 years; 4. Articles containing original data; 5. Studies must be related to "mesenchymal stem cells" and "macrophages"; 6. Musculoskeletal related studies.
Exclusion criteria	1. No control group; 2. Sampling method described inconsistent; 3. Case reports, case series and review articles, letter, chapter; 4. Not available in the English language.

Data Extraction

All relevant data were extracted by H.-T.X. and X.-B.Z.: author information, published journal, year of publication, sample source, target disease, study type (*in vivo*, *in vitro*, or both), cell management, and measurement instrument. The details of results extraction consisted of variable/control group descriptions, laboratory effects, proposed mechanisms, article conclusions, and research implications. After that, the selected articles were classified according to the type of target disease.

Methodological Quality Assessment

The methodological assessment should be used as an essential procedure, which could exclude articles with a large degree of bias or with a higher degree of potential bias, has been highlighted to readers (McElvany et al., 2015). Identified studies fitting all criteria were reviewed, and all included data were extracted and analyzed based on study heterogeneity and methodological quality. Because of the natural heterogeneity of measurement across studies, a meta-analysis could not be performed. Two independent authors (H.-T.X. and Z.-H.W.) separately assessed and graded the methodological quality of all selected studies. Disagreements between the two independent researchers were identified and resolved by discussion with a third reviewer (C.-W.L.). The selected studies were assessed with a quality scoring system raised by Wells and Julia (2009) (Appendix 4 in **Supplementary Material**). The quality assessment system was based on the following eight questions: Was the study hypothesis/aim/objective clearly described? Were the animal models for the study well-described? Were the methods well-described? Were the data collection time point clearly defined? Were the main outcome measures clearly defined? Were the experiment group well-compared with the control group? Were the results well-described? Were the articles discussed the limitation? For each question, 1 point was allocated for "yes," and 0 point was allocated for "no." The number of "yes" answers was counted for each selected study to give a total score out of 8. A study's rating was considered as excellent with a score ranging from 6 to 8, good with a score ranging from 4 to 6, poor with a score ranging from 2 to 4, and bad with a score ranging from 0 to 2.

RESULTS

Study Methodology Quality Assessment

The scoring system was used to calculate all ten selected studies in Appendix 5 in **Supplementary Material**. The mean score is 6.6 (range, 5–8), including eight studies exceeding 6 points (Cosenza et al., 2017; Lo Sicco et al., 2017; Hyvarinen et al., 2018; Zhang et al., 2018; Chamberlain et al., 2019; Li Y. et al., 2019; Shi et al., 2019; Shen et al., 2020).

Study Characteristics

Of the ten selected studies, one study was published in 2015 (Chang et al., 2015), two were published in 2017 (Cosenza et al., 2017; Lo Sicco et al., 2017), two studies were published in 2018 (Hyvarinen et al., 2018; Zhang et al., 2018), four studies were published in 2019 (Chamberlain et al., 2019; Li Y. et al., 2019; Pacienza et al., 2019; Shi et al., 2019), and the final one was published in 2020 (Shen et al., 2020) (**Figure 2A**). All selected studies were related to the musculoskeletal system. For details of target diseases, two studies were bone fracture–related studies (Chang et al., 2015; Li Y. et al., 2019), two studies were OA-related studies (Cosenza et al., 2017; Zhang et al., 2018), one study was a muscle damage–related study (Lo Sicco et al., 2017), three studies were tendon injury–related studies (Chamberlain et al., 2019; Shi et al., 2019; Shen et al., 2020), and the other two studies were included without targeting disease (Hyvarinen et al., 2018; Pacienza et al., 2019) (**Figure 2B**). Six studies used a mice model (Cosenza et al., 2017; Lo Sicco et al., 2017; Chamberlain et al., 2019; Li Y. et al., 2019; Pacienza et al., 2019; Shen et al., 2020), two studies used a rat model (Zhang et al., 2018; Shi et al., 2019), and two studies performed *in vitro* experiments only (Chang et al., 2015; Hyvarinen et al., 2018) (**Figure 2C**). Three paracrine factors were extracted from the results: MSC-derived exosomes (Cosenza et al., 2017; Zhang et al., 2018; Pacienza et al., 2019; Shen et al., 2020), MSC-derived EVs (Lo Sicco et al., 2017; Hyvarinen et al., 2018; Chamberlain et al.,

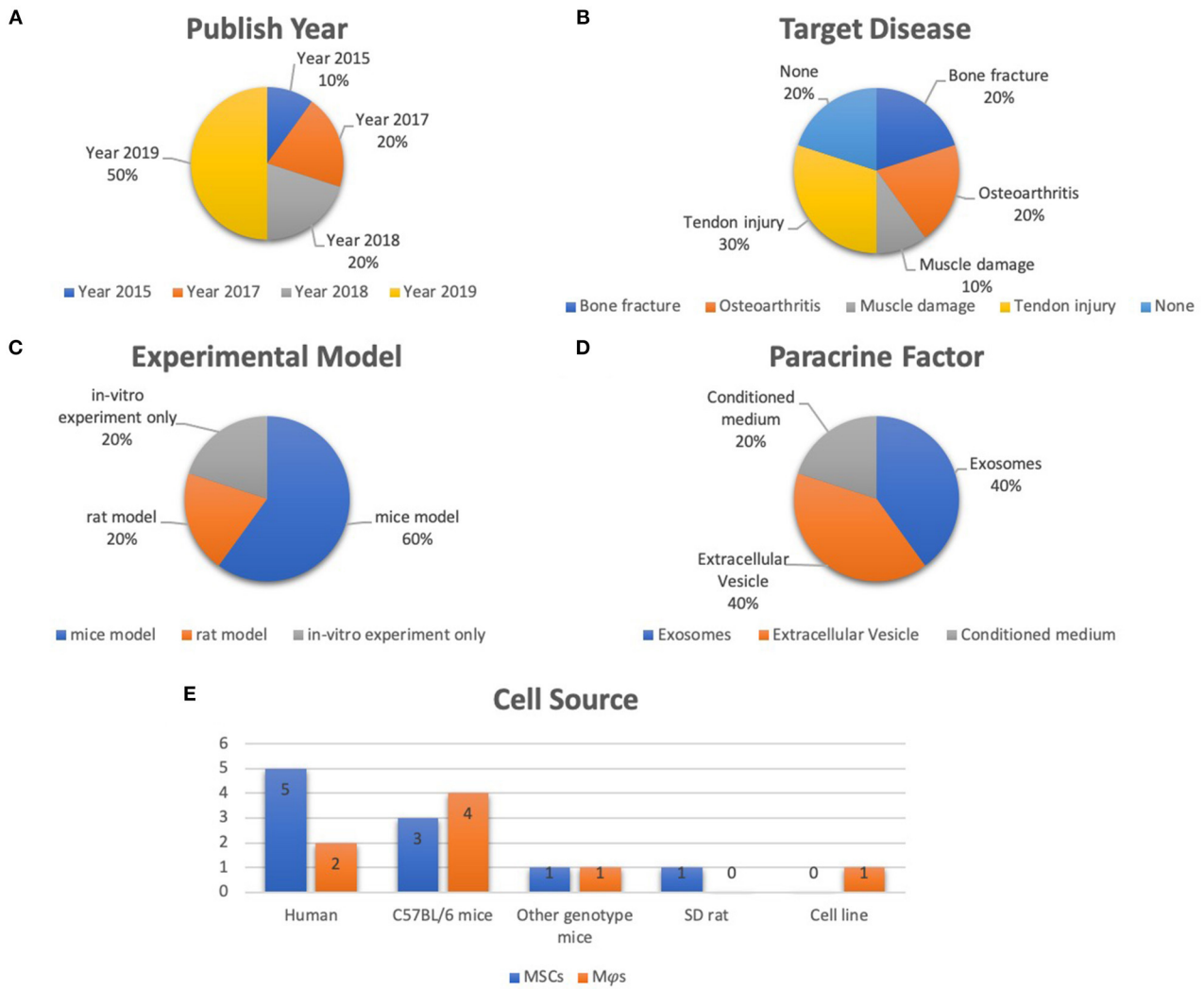

FIGURE 2 | Representative graph of the included studies presented in the articles reviewed. **(A)** Publication year of included studies (range from 2015 to 2020). **(B)** Target disease of included studies (include bone fracture, OA, muscle damage, tendon injury). **(C)** Experimental model of included studies (including mice model, rat model, *in vitro* experiment only). **(D)** Paracrine factors (including extracellular vesicle, exosomes, CM). **(E)** Cell source of included studies (including human, C57Bl/6 mice, other genotype mice, SD rat, cell line).

2019; Shi et al., 2019), and MSC-derived conditioned medium (CM) (Chang et al., 2015; Li Y. et al., 2019) (**Figure 2D**). Five MSC and Mφs cell sources for EVs isolation were described in these selected studies: human (Lo Sicco et al., 2017; Hyvarinen et al., 2018; Zhang et al., 2018; Chamberlain et al., 2019; Pacienza et al., 2019), cell lines (Pacienza et al., 2019), Sprague–Dawley rats (Shi et al., 2019), C57BL/6 mice (Chang et al., 2015; Cosenza et al., 2017; Lo Sicco et al., 2017; Li Y. et al., 2019), and transgenic mice [scleraxis–green fluorescent protein (GFP) tendon reporter mice, nuclear factor (NF-κB)–GFP–luciferase transgenic reporter mice, and wild-type FVB/NJ (FVB) mice] (Shen et al., 2020). The detailed data are graphically shown in **Figure 2E**.

Target Diseases and Experimental Animal Models

In the bone fracture–related studies (Chang et al., 2015; Li Y. et al., 2019), Li Y. et al. (2019) established a cylindrical bone defect mice model by using an electric drill to make a defect with 1-mm diameter and 1-mm depth at the bone callus of the femur. Chang et al. (2015) studied only *in vitro* experiments, and they cocultured bone marrow–derived mesenchymal stem cells (BMSCs) with Mφs. Two studies selected OA as the target disease (Cosenza et al., 2017; Zhang et al., 2018). Cosenza et al. (2017) established a collagenase-induced arthritis mouse model by intra-articularly injecting 1U type VII collagenase (in 5 μL saline) into the knee joint of 10-week-old C57BL/6 mice at days

0 and 2. Zhang et al. (2018) generated an osteochondral defect model in an 8-week-old Sprague–Dawley rat. Osteochondral defects, with 1.5-mm diameter and 1-mm depth, were generated on the trochlear grooves of the distal femurs by a drill bit. For muscle injury study, cardiotoxin-induced muscle injury was applied in 8-week-old male C57BL/6 mice by intramuscular administration of cardiotoxin into the Tibialis Anterior (TA) muscle (Lo Sicco et al., 2017). Three tendon injury models were used in the selected studies (Chamberlain et al., 2019; Shi et al., 2019; Shen et al., 2020). Chamberlain et al. (2019) established a surgically transected Achilles tendon mouse model. After superficial digital flexor tendon was removed, the Achilles tendon was completely transected at the midpoint. Then tendon was sutured together by using 5-0 Vicryl suture. In Shen et al. (2020) study, Achilles tendon was two-thirds transected at the midpoint part between calcaneal insertion and the musculotendinous junction and then was sutured with a two-strand modified Kessler technique. Shi et al. (2019) applied the Sprague–Dawley rat patellar tendon defect model. Briefly, the central one-third of the patellar tendon was removed from the distal apex of the patellar to the insertion of the tibial tuberosity to achieve a tendon structural defect condition. In addition, Pacienza et al. (2019) established a mouse endotoxemia model by injecting LPS via tail vein, which was used to study the crosstalk between MSC-derived exosomes and Mφs. Hyvarinen et al. (2018) only cocultured BMSCs and BMSC-derived EVs with Mφs without preforming animal study. The target diseases and experimental models are represented in **Table 2** in detail.

Cell Sources and Cell Management

Five of 10 studies used human source cells (Lo Sicco et al., 2017; Hyvarinen et al., 2018; Zhang et al., 2018; Chamberlain et al., 2019; Pacienza et al., 2019). Human adipose-derived mesenchymal stem cells (ADSCs) were used for *in vitro* experiments in Lo Sicco's research; the EVs derived from ADSCs were cocultured with mouse Mφs and intralesionally injected into the mouse muscle injury model (Lo Sicco et al., 2017). In Hyvarinen et al. (2018) study, they used human BMSCs or BMSC-derived EVs to coculture with human Mφs. Zhang et al. (2018) intra-articularly injected exosomes from human embryonic stem cell–derived MSCs into rat with osteochondral defect. Chamberlain et al. (2019) also used human BMSCs and Mφs for the *in vitro* experiment. BMSCs, $CD14^+$ Mφs and exosome-educated Mφs were intralesionally injected in the mice with Achilles tendon injury. Pacienza et al. (2019) used human BMSCs and RAW 264.7 for the *in vitro* experiment. Exosomes derived from BMSCs were intravenously injected into the endotoxemia mouse model. The *in vitro* experiment cell sources were all C57BL/6 mice in Chang et al. (2015), Cosenza et al. (2017) and Li Y. et al. (2019) studies. Fibrin containing Sprague–Dawley rat BMSC-derived EVs was intralesionally injected into the patellar tendon defect rat in Shi et al. (2019) study. Shen et al. (2020) used an *in vitro* model whose cell source was isolated from specific transgenic mice. The details of cell management are summarized in **Table 2**.

Boosting Approaches for MSC-Paracrine Mediators

Lo Sicco et al. (2017) isolated ADSC-derived EVs from normoxic and hypoxic culture condition. Li Y. et al. (2019) used a Transwell coculture system of ADSCs and Mφs without extra management of MSCs paracrine mediators. The other eight studies collected and purified EVs or other paracrine mediators from MSC-derived CM by differential centrifugation approaches (Chang et al., 2015; Cosenza et al., 2017; Lo Sicco et al., 2017; Hyvarinen et al., 2018; Zhang et al., 2018; Chamberlain et al., 2019; Pacienza et al., 2019; Shi et al., 2019; Shen et al., 2020). The detailed methods are described in **Table 2**.

Measurement Instruments

For classifications on the results, the measurement instruments, including immunohistochemistry, reverse transcriptase–polymerase chain reaction analysis, Western blot analysis, enzyme-linked immunosorbent assay, flow cytometry analysis, multiplex cytokine assay, confocal laser scanning, micro–computed tomography, and mechanical testing, were used. Also, fractal analysis (Chamberlain et al., 2019) and bone parameter analysis (Cosenza et al., 2017) were applied. Detailed results are listed in **Table 2**.

Experimental Variables and Controls

For two bone fracture–related studies, Li Y. et al. (2019) locally injected a total of 1×10^6 ADSCs at the injury site of their cylindrical bone defect model; the therapeutic efficacy of ADSCs was compared to the non-injected group. In the *in vitro* experiment, the bone marrow–derived Mφs were cocultured with 1×10^5 ADSCs in the upper chamber of Transwell under with high-glucose Dulbecco modified eagle medium containing 10% fetal bovine serum (FBS). Chang et al. (2015) planted 1×10^5 bone marrow–derived Mφs into six-well plates and cultured 24 h. Then, 1×10^5 BMSCs or apoptotic BMSCs (exposed to UV light treatment for 30 min) were placed on the Mφs in α-minimum essential medium containing 10% FBS. For each time point, Mφs cultured alone, apoptotic BMSCs cultured alone, and BMSCs cultured alone served as control groups.

For the OA-related studies, Cosenza et al. (2017) applied the *in vitro* OA-like chondrocytes model to investigate the effect of microparticles, BMSC-derived exosomes, BMSC-derived CM, and BMSCs on Mφs in a Transwell system. For their *in vivo* experiment, BMSCs, microparticles, and exosomes were intra-articularly injected into the arthritis model. Those OA mice without treatment served as a control group. In Zhang et al. (2018) study, exosomes and phosphate-buffered saline (PBS) (used as control) were intra-articularly injected into the rat osteochondral defect model after surgery, respectively.

For three tendon injury–related studies, two of them (Chamberlain et al., 2019; Shen et al., 2020) reported the coculture results of EVs and Mφs, and the another one study reported *in vivo* experiment (Shi et al., 2019). Chamberlain et al. (2019) reported that exosome-educated Mφs could be generated by MSC-derived EVs, and Mφs treated with PBS served as control groups in their *in vitro* experiment. To compare the therapeutic potential on tendon healing, the authors intralesionally injected

TABLE 2 | Study characteristics and outcomes.

Author	Journal	Year	Cell source	Target disease	Study type	Cells management	Bioengineering method for MSCs paracrine mediators	Measurement instrument
Chang J	Bone Res	2015	C57BL/6 mice	Bone fracture	*In-vitro*	BMSC CM and Mφs cell contract co-culture	BMSCs intrinsic bio-activation: the supernatants from BMSCs cultures were collected and stored at −80 °C until used as conditioned medium.	Scratch assay, BMSCs migration assay, IL-6 ELISA assay, cell growth assay, Gene expression by RT-PCR, Western blot
Cosenza et al., 2017	Sci Rep	2017	C57BL/6 mice	Osteoarthritis	*In-vitro* and *in-vivo*	*In-vitro:* BMSC Exos and Mφs *In-vivo* (arthritis model): IA injections of BM-MSCs, MPs or Exos.	BMSCs intrinsic bio-activation: BMSC-CM was centrifuged at 300 g for 10 min to eliminate cells and 2,500 g for 25 min to remove debris and apoptotic bodies. For MP isolation, CM was centrifuged at 18,000 g for 1 h in polyallomer tubes; the pellet was then suspended in PBS and submitted to a second round of centrifugation. For Exos, supernatant from MP fraction was filtered on 0.22 μm porous membrane and centrifuged at 100,000 g for 2 h.	Flow cytometry analysis, Bone parameter analyses, Confocal laser scanning microscopy, Histological analysis
Lo Sicco	Stem Cells Transl Med	2017	Human-ADSCs; C57BL/6 mice–Mφs	Muscle damage	*In-vitro* and *in-vivo*	*In-vitro:* ADSC EVs and Mφs *In-vivo* (muscle injury model): IL injection of ADSCs EVs	ADSCs extrinsic modification: ADSC EVs were isolated from normoxic- and hypoxic-conditioned media by differential centrifugation at 300 g for 10 min, 2,000 g for 20 min, 10,000 g for 30 min at 4°C to eliminate cells and debris	Protein quantification and immunoblot analysis, Flow cytometry analysis, qRT-PCR, Immunofluorescence analysis, Histology and morphometric analysis
HyvÃ¤rinen K	Front Immunol	2018	Human	/	*In-vitro*	BMSCs or BMSC-EVs and Mφs co-culture	BMSCs intrinsic bio-activation: BMSCs media were collected and centrifuged at 2,000 g for 10 min to remove cell debris. The supernatant was ultracentrifuged with Optima^{TM} MAX-XP Ultracentrifuge (Beckman Coulter) at 100,000 g 1.5 h +4°C with MLA-50 rotor (k-factor = 92, Beckman Coulter), and the pelleted EVs were combined. For the second EV collection, the cell starvation was continued in 200 ml α-MEM at 37°C, 5% CO_2 for 2 days followed by replication of EV centrifugation steps.	Flow cytometry analysis, cytokine (IL-10, IL-23, IL-22) and LMs measurements
Zhang S	Biomaterials	2018	Human embryonic stem cell derived MSCs	Osteoarthritis	*In-vivo*	Sprague-Dawley rat osteochondral defect model: IA injection of MSCs-Exos	BMSCs intrinsic bio-activation: MSCs were grown in a chemically defined medium for 3 days and exosomes were purified from the CM.	Histology and immunohistochemistry, Multiplex cytokine assay (IL-1β, IL-6, TNF-β)
Chamberlain CS	Stem Cells	2019	Human	Tendon injury	*In-vitro* and *in-vivo*	*In-vitro*: BMSC-EVs and Mφs; *In-vivo* (Foxn1nu mouse model of Achilles tendon injury): IL injection of BMSCs, CD14+ Mφs or EEMs	BMSCs intrinsic bio-activation: BMSCs CM was centrifuged using a Beckman Coulter Allegra X-15R centrifuge at 2,000 g at 4°C for 20 min. Clarified supernatant CM was then centrifuged in a Beckman Coulter Optima L-80 XP Ultracentrifuge at 100,000 g at 4°C for 2 h with a swinging bucket SW 28 rotor to pellet EVs.	Flow cytometry analysis, IHC/Immunofluorescence/Histology; Fractal analysis; Mechanical testing

(Continued)

TABLE 2 | Continued

Author	Journal	Year	Cell source	Target disease	Study type	Cells management	Bioengineering method for MSCs paracrine mediators	Measurement instrument
Pacienza N	Mol Ther Methods Clin Dev	2019	Human–BMSCs; RAW 264.7–Mφs cell	/	*In-vitro* and *in-vivo*	*In-vitro*: LPS in combination with Exos and Mφs; *In-vivo* (endotoxemia mouse model): IV injection of Exos	BMSCs intrinsic bio-activation: BMSCs CM was applied directly at room temperature to a column containing the anion exchange resin (Q Sepharose Fast Flow, GE Healthcare, Chicago, IL, USA) that had been equilibrated with 50 mM NaCl in 50 mM phosphate buffer (pH 7.5). The column resin was washed with 100 mM NaCl in 50 mM phosphate buffer (pH 7.5) and then eluted with 500 mM NaCl in 50 mM phosphate buffer (pH 7.5).	qRT-PCR, Quantitation of TNF-a, IL-1β, and IL-6 by ELISA
Shi Z	J Transl Med	2019	Sprague-Dawley rats–BMSCs	Tendon injury	*In-vivo*	Sprague-Dawley rat patellar tendon defect model: injection of fibrin containing EVs	BMSCs CM was centrifuged sequentially at 300 g for 10 min followed by 2,000 g for 10 min to remove cellular debris. The supernatants were then ultracentrifuged at 100,000 g for 2 h to obtain a pellet containing the EVs, which was resuspended in 200 μL of PBS. EVs-enriched fraction was centrifuged at 1,500 g, 30 min with 100-kDa molecular weight cut off (MWCO) hollow fiber membrane (Millipore, Billerica, MA, USA). Then, EVs were passed through a 0.22-μm filter.	Histology and immunohistochemistry, Gene expression, Histological analysis
Li Y	J Cell Biochem	2019	C57BL/6 mice	Bone fracture	*In-vitro* and *in-vivo*	*In-vitro*: ADSCs and Mφs cell contract co-culture; *In-vivo* (a cylindrical bone defect model): IL injection of ADSCs	/	Immunohistochemistry, Western-blot analysis, RT-PCR, Enzyme-linked immunosorbent assay, micro-CT
Shen H	J Orthop Res	2020	Scleraxis-GFP tendon reporter mice or NF-κB-GFP-luciferase transgenic reporter mice–ADSCs Wild type FVB/NJ (FVB) –Mφs	Tendon injury	*In-vitro* and *in-vivo*	*In-vitro:* Exos and Mφs co-culture; *In-vivo* (NGL mouse model of Achilles tendon injury and repair): collagen sheet loaded with EVs from naÃ¨ve ASCs or IFNγ-primed ASCs	ADSCs intrinsic bio-activation: ADSCs were cultured in an EV collection medium (2% EV-free FBS in α-MEM) for 48 h. CM from ASC culture (150 ml from ∼2.5 E+07 cells per isolation) with or without IFNγ pre-treatment was collected and centrifuged at 500 g for 10 min and 10,000 g for 30 min at 4°C to remove large vesicles. After passing through a 0.22 μm filter, the medium was further centrifuged at 100,000 g for 90 min at 4°C.	Mφs assays, NF-κB-Luciferase Imaging *in-vivo*, RT-PCR, Histology

Both the methodology employed and the results obtained by each article are represented in this table. BMSCs, bone marrow stem cells; ADSCs, adipose tissue derived stem cells; Mφs, macrophages; Exos, exosomes; MPs, microparticles; EVs, extracellular vesicles; CM, conditioned medium; IA, intra-articularly; IL, intralesional; IV, intravenous; LMs, lipid mediators; EEMs, exosome-educated macrophages; LPS, lipopolysaccharide.

1×10^6 human BMSCs, 1×10^6 $CD14^+$ Mφs, 1×10^6 exosome-educated Mφs, or Hanks balanced saline solution (used as the injured control) to the surgical sites; the contralateral intact Achilles tendon without any treatment was used as a control (Chamberlain et al., 2019). In Shen et al. (2020) study, EVs produced by IFN-γ-primed and non-primed mouse ADSC were used to treat with Mφs to evaluate the impact of EVs on the Mφs inflammatory response. And EV collection medium and EV-free CM were used as controls in the *in vitro* experiment. In Shen et al. (2020) *in vivo* experiment, collagen sheet loaded with EVs was applied around the repair sites, and the collagen sheet only was set as a control group. Shi et al. (2019) placed fibrin glue containing BMSC-EVs in the window defect of patellar tendon**.** The fibrin glue alone and non-surgical rats were designed as control groups.

In Lo Sicco et al. (2017) study, ADSC-derived EVs and PBS were intramuscularly injected into an injured TA muscle as experimental and control groups, respectively.

No target disease was mentioned in Hyvarinen et al. (2018) and Pacienza et al. (2019) studies. Mφs cocultured with MSCs and MSC-EVs served as experimental variables in Hyvarinen et al. (2018) study, and Mφs served as the control group (Hyvarinen et al., 2018). In Pacienza et al. (2019) study, LPS-stimulated Mφs treated with BMSC-derived exosomes served as the experimental group, and the three control groups were Mφs treated with complete medium alone, LPS, and LPS plus dexamethasone. In Pacienza et al. (2019) *in vivo* experiment, LPS alone or in combination with exosomes ($\sim 5 \times 10^9$ vesicles) was injected into mice through tail vein, respectively. Control group was injected with saline (Pacienza et al., 2019). Detailed results are listed in **Table 3**.

Laboratory Effects and Proposed Mechanisms

The bone fracture–related studies showed that femoral bone formation and bone volume all increased after ADSC injection. The increase in osteoblasts after ADSC injection was accompanied by increases in $CD206^+$, $CD68^+$, $CD11b^+$, and $F4/80^+$ cells, which represented a typical M2 surface phenotype. Meanwhile, the transcript and protein expression of Arg-1, M2 marker genes, were also up-regulated (Pacienza et al., 2019). Two OA-related studies reported that bone volume, cartilage thickness, hyaline cartilage formation, migration and proliferation of chondrocytes, and matrix synthesis were increased by BMSC-derived exosomes (Cosenza et al., 2017; Zhang et al., 2018). The therapeutic effect of anti-inflammation on OA was in line with a decrease in M1 Mφs ($F4/80^+$, $CD86^+$, $MHCII^+$, $CD40^+$), IL-1β, and tumor necrosis factor α (TNF-α), as well as increases in chondrocytes, M2 Mφs ($CD163^+$), and IL-10 (Cosenza et al., 2017; Zhang et al., 2018). Moreover, BMSC-derived exosomes increased type II collagen deposition, and decreased type I collagen in cartilage was reported by Zhang et al. (2018) Such protective effects on chondrocytes might be attributed to the increase in Survivin, Bcl-2, and FGF-2 by BMSC-derived exosomes administration.

Lo Sicco et al. (2017) reported that ADSC-derived EVs were internalized in Mφs at the muscle injury site, which could promote myofiber regeneration. Interestingly, a dynamic change of Mφs subpopulation was observed after transplantation of ADSC-derived EVs. ADSC-derived EVs increased M1 Mφs ($Ly6C^+$, $CD11b^+$, $CD40^+$, $CD86^+$) at 24 h post-treatment and increased M2 Mφs ($CD206^+$, $CD51^+$, $CD36^+$) at 72 h post-treatment.

Extended results could be concluded from three tendon injury–related studies (Chamberlain et al., 2019; Shi et al., 2019; Shen et al., 2020). The shift of Mφs from M1 to M2 showed consistent variation to the increase in ultimate stress, Young's modulus (Chamberlain et al., 2019), NF-κB activity (Shen et al., 2020), fiber alignment score, tendon matrix formation, tenogenesis, and tendon cell proliferation (Shi et al., 2019) and the decrease in type I/type III collagen ratio (Chamberlain et al., 2019), gap-rupture rate (Shen et al., 2020), and tendon cell apoptosis (Shi et al., 2019) by BMSC-derived or ADSC-derived exosome administration.

DISCUSSION

Nowadays, it has been emphatically contended that all newly presented clinical interventions should start with and end with a systematic review, or even meta-analysis (Clarke et al., 2007). Although the therapeutic effects of MSCs via paracrine factors have been demonstrated in many pre-clinical investigations, the substantial clinical evidence in beneficial effects of MSCs in musculoskeletal diseases is not adequately investigated (Regenberg et al., 2009; Lukomska et al., 2019). This systematic review aims to analyze the impact of MSC and MSC-derived EVs on Mφs in the treatment of musculoskeletal diseases. According to the outcomes of the included studies, MSCs could promote musculoskeletal tissue repair or healing via their paracrine regulation on Mφs.

Interactions of Predominant Mφs With MSC-EVs

Mφs are predominant myeloid cells that chronologically accumulate in musculoskeletal tissue at the onset of injury-induced inflammation and exhibit regulatory activity at all stages of the healing process (Tidball, 2011; Varol et al., 2015). Therefore, Mφs are potent triggers for tissue healing processes, including cell recruitment, proliferation, and remodeling (Artlett, 2013).

Growing evidence has demonstrated that the phenotypic switch of Mφs is critical in MSC-mediated tissue regeneration, which is presented in **Figure 3**. Moreover, M1 Mφ-released proinflammatory cytokines enhanced the migratory capacity of MSCs that facilitates the accessibility of exogenous MSCs toward the injured site. Then, the attracted MSCs would regulate Mφ phenotypes into M2 via paracrine effect to facilitate the tissue remodeling at a later stage (Le Blanc and Mougiakakos, 2012; Maxson et al., 2012; Shi et al., 2012; Bernardo and Fibbe, 2013; Ma et al., 2014). Interestingly, the secretomes of MSCs, such as EVs or exosomes, were also altered by M1 Mφ that boosts the therapeutic effect of MSCs, so-called primed MSCs (Aktas et al., 2017; Saldana et al., 2019).

TABLE 3 | Evaluations and results list of selected studies in which the therapeutic potential of the administration of MSCs for the treatment of musculoskeletal diseases.

Target disease	References	Variables	Controls	Laboratory effects	Proposed mechanisms	Conclusions	Research implications
Bone fracture	Chang et al., 2015	Seeding BM Mφs first. Then placing primary or apoptotic BMSCs. Additional validation: IL-6 KO mice.	Mφs cultured alone, apoptotic BMSCs cultured alone, and BMSCs cultured alone.	↑ BMSCs migration ↑ BMSCs proliferation	↑ IL-6 proteins and mRNA ! IL-6/gp130/STAT3 pathway	BMSCs are the main contributing cells of juxtacrine IL-6 production. Juxtacrine cultures accelerated BMSCs migration and numbers.	Increase the understanding of Mφs in bone formation.
	Li Y. et al., 2019	ADSCs and BM Mφs co-culture system; ADSCs locally injection.	Untreated control mice	↑ femoral bone formation ↑ femoral bone volume	↑ osteoblasts ↑ CD206+ cells ↑ CD68+ cells ↓ iNOS+ cells ↑ CD11b+ F4/80+ cells ↑ IL-1rα proteins ↓ TNF-α proteins and mRNA ↓ iNOS proteins and mRNA ↑ Arg-1 proteins and mRNA ↑ MR proteins and mRNA ↑ Runx-2 and osterix and OPG and ALP genes ↓ RANKL genes	ADSCs and Mφs can synergistically contribute to bone repair through mutual regulation of their differentiation and cytokine secretion.	The interactions between ADSCs and BM Mφs could be a promising therapeutic strategy in the rehabilitation of bone damage.
Osteoarthritis	Cosenza et al., 2017	Mediums of OA like chondrocytes model were replaced by medium containing MPs, Exos, BMSCs-CM or BMSCs (transwell); BMSCs, MPs or Exos intra-articularly injection.	OA control mice	Restore the anabolic equilibrium ↓ apoptotic chondrocytes ↓ macrophage activation ↑ bone volume, cartilage degradation (surface/volume ratio) and thickness	↓ MMP-13, ADAMTS5, iNOS genes ↑ ACAN, COL2B, COL1 genes ↓ F4/80+ cells ↓ CD86, MHCII or CD40 markers ↓ TNF-α proteins ↑ IL-10 proteins	Exos were more efficient than MPs and BMSCs in chondroprotective and anti-inflammatory function.	MPs and Exos help to promote re-establish chondrocyte homeostatic state.
	Zhang et al., 2018	Intra-articular injection of Exos.	Intra-articular injection of PBS	↑ neotissue formation and ECM deposition of s-GAG ↑ Wakitani score ↑ surface regularity ↑ hyaline cartilage formation ↑ percentage areal deposition of type II collagen ↓ percentage areal deposition of type I collagen ↑ chondrocyte migration, proliferation and matrix synthesis ↑ metabolic activity	↑ chondrocytic cells ↓ PCNA+ cells ↑ CD163+ cells ↓ CD86+ cells ↓ IL-1β and TNF-α ↑ Survivin, Bcl-2, FGF-2 mRNA ! AKT and ERK pathways	Exos mediate cartilage repair by mounting a coordinated, multi-faceted response of enhancing proliferation, migration and matrix synthesis, attenuating apoptosis and modulating immune reactivity.	Exso could be provided as a cell-free MSC therapeutic.
Muscle damage	Lo Sicco et al., 2017	EVs–Mφs co-culture; EVs were intramuscularly administered into muscle.	PBS were intramuscularly administered into muscle	↑ internalization of EVs in Mφs ↑ Mφs proliferation ↓ M1/M2 ↓ mononucleated myoblasts ↑ fibers containing nuclei ≥2	↑ Ly6C, CD11b, CD40, CD86 (post-treat 24h) ↑ CD206, CD51, CD36 (post-treat 72h) ↓ CD11b, CD86 (post-treat 72h) ↓ IL-6/IL-10 ↑ Arg-1, Ym-1markers ↓ Nos-2 markers ↑ CD206+ cells ↓ Ly6C+ cells ↑ MCP-1 ↑ Pax-7, MyoD genes (activated satellite cells); eMyhc gene (regenerating fibers)	EVs co-cultured with responding BM-derived Mφs, shifting the balance toward a M2 phenotype.	Establish an alternative cell-free approach of EVs for the induction of regenerative processes.

(Continued)

TABLE 3 | Continued

Target disease	References	Variables	Controls	Laboratory effects	Proposed mechanisms	Conclusions	Research implications
Tendon injury	Chamberlain et al., 2019	EVs–Mφs co-culture; BMSCs, CD14+ Mφs or EEMs locally injection.	Mφs controls were treated with PBS; Contralateral controls	↑ EVs educated Mφs ↑ ultimate stress and Young's modulus ↓ M1/M2 ratio ↓ type I collagen ↓ type I/type III collagen ratio	↑ CD206 mean fluorescence intensity and cells ↑ PD-L1 mean fluorescence intensity and cells ↑ M2 Mφs ↓ M1 Mφs ↑ endothelial cells	EVs-educated Mφs treatments improve mechanical properties for tendon function as shown by reduce endogenous M1/M2 ratio indicating less inflammation.	EEMs treatment provides a novel strategy in musculoskeletal injuries.
	Shen et al., 2020	EVs–Mφs co-culture; Collagen sheet loaded with EVs was applied around the repair site.	EVs collection medium and EV-free conditioned medium controls; Collagen sheet only control. IL-1 (EVs from IFNγ-primed ASCs)	↑ NF-κB activity ↑/↓ Matrix gene expression ↓ gap-rupture rate	↓ IL-1 gene (only EVs from IFNγ-primed ASCs) ↑ IFNγ gene (only EVs from IFNγ-primed ASCs) ↑ MMP-1, Sox-9 genes ↑ Col-1α1, Col-2α1 and Col-3α1 genes (only EVs from IFNγ-primed ASCs) ↑ collagen staining (only EVs from IFNγ-primed ASCs)	EVs from ASCs can shift the Mφs phenotypic response to tendon injury from a default M1 to a M2 phenotype.	EVs could be a new cell-free therapy, for tendon repair with the potential for improved therapeutic efficacy and safety.
	Shi et al., 2019	Fibrin glue containing EVs was placed in the window defect	Fibrin glue alone and untreated controls	↑ Fiber alignment score ↑ anti-inflammatory response ↑ tendon matrix formation ↑ tenogenesis ↓ tendon cell apoptosis ↑ tendon cell proliferation	↑ CD163 marker ↑ IL-4, IL-10 mRNA and + cells ↓ IFNγ, IL-1β, IL-6, CCR7 + cells ↑ SCX, TNMD, Col-1α1, Col-3α1 genes ↑ CD146+ cells ↓ cleaved caspase 3 signals	EVs derived from BMSCs can help to improve the quality of tendon healing by promoting an anti-inflammatory environment.	These findings provide a basis for the potential clinical use of BMSC-EVs in tendon repair.
None	Hyvarinen et al., 2018	MSCs–Mφs coculture; MSC-EVs–Mφs coculture	Mφs only control	↓ FRI of CD163 ↓ cytokine levels of Mreg-CM ↑ LMs level and pathway markers ↑ phagocytic ability	↓ CD163+ cells ↓ IL-10, IL-22, IL-23, TNF-α proteins ↑ arachidonic acid-derived PGE2, 15-HETE, docosahexaenoic acid-derived 17-HDHA ↑ CD206 Mregs and receptors	Both MSCs and MSC-EVs decrease IL-23 and IL-22 while increasing PGE2 production.	MSC-EVs may potentiate tolerance-promoting proresolving phenotype of human Mregs.
	Pacienza et al., 2019	LPS in combination with Exos–Mφs coculture; Tail vein injection of LPS	FBS medium alone control, containing LPS control, and LPS plus dexamethasone control; Tail vein injection of saline control	↑ anti-inflammatory activity ↑ predictive efficacy	↓ IL-6, IL-1β levels ↓ iNOS mRNA	Exos could suppress LPS-induced inflammation.	*In-vitro* Mφs assay predicts the *in-vivo* anti-inflammatory potential of Exos

Both the methodology employed and the results obtained by each article are represented in this table. Apoptotic BMSCs (exposed to UV light treatment for 30 min); !, activation; KO, knockout; TNF-α, tumor necrosis factor-α; RANKL, receptor activator of nuclear factor κB ligand; iNOS, inducible nitric oxide synthase; MR, mannose receptor; Arg-1, Antibodies against arginase 1; Runx-2, runt-related transcription factor 2; OPG, osteoprotegerin; ALP, alkaline phosphatase; Mregs, regulatory macrophages; MPs, microparticles; Exos, exosomes; EVs, extracellular vesicles; EEMs, exosome-educated macrophages; OA, osteoarthritis; ECM, extracellular matrix; FRI, fluorescence intensity; LMs, lipid mediators; LPS, lipopolysaccharide.

The cross-talk between Mφs and MSC-derived EVs regulates a shift in Mφs subtypes from M1 into M2 (Galli et al., 2011). An increasing number of musculoskeletal tissue injury models showed that Mφs phenotypic alteration mediated MSC-based therapy (Lo Sicco et al., 2017; Chu et al., 2019). M1 Mφs promote recruitment of inflammatory immune cells and release extracellular matrix (ECM) degrading proteins to allow quick migration to inflamed sites. As the Mφs shift to M2 subtypes, the release of proinflammatory cytokines is inhibited, angiogenesis is stimulated, and fibroblasts are activated to produce and restore more ECM. Also, Mφs induced MSCs into a motile phenotype with increased secretion of IL-6 and IL-10, which benefit MSCs to migrate to injury site (Anton et al., 2012; Wolfe et al., 2016). Typically, MSC-EVs impact the maturation of Mφs by decreasing the expression levels of IL-12 and TNF-α and increasing IL-6 and IL-10 in Mφs (Kim and Hematti, 2009; Cosenza et al., 2017; Lo Sicco et al., 2017; Hyvarinen et al., 2018; Shi et al., 2019). PGE_2 and TNF-α inducible gene 6 (TSG-6) embedded in MSC-EVs can promote M2 polarization in inflammatory microenvironment (Nemeth et al., 2009; Maggini et al., 2010; Melief et al., 2013b). EVs, which were released from proinflammatory cytokines–activated MSCs, could enhance anti-inflammatory properties to suppress MHC class II and CD86 signaling in LPS-stimulated Mφs (Melief et al., 2013a,b; Cho et al., 2014). Lo Sicco et al. (2017) and Chamberlain et al. (2019) reported the MSC-EVs change the M1-to-M2 Mφs ratio. And Lo Sicco et al. (2017) demonstrated that MSC-EVs could be efficiently internalized by responding cells, inducing an increase in their proliferation rate, and shifting the balance toward an alternatively anti-inflammatory M2 phenotype. M2 Mφs phenotype could be commonly associated with the secretion of the anti-inflammatory cytokine IL-10 and scavenger receptors CD206 and CD163 (Sica and Mantovani, 2012; Mantovani et al., 2013).

In this review, we found consistent results suggesting that an M2 phenotype could be induced from M1 Mφs upon coculture with MSCs, MSC-EVs, and CM. The enrichment of M1 Mφs appears at early phases (1–3 days) during bone remodeling (Chang et al., 2015; Li Y. et al., 2019), muscle regeneration (Lo Sicco et al., 2017), and tendon healing (Chamberlain et al., 2019; Harvey et al., 2019; Shi et al., 2019; Shen et al., 2020) and is later replaced by M2 Mφs (4–7 days). As Mφ polarization and tissue repair by MSC-EVs are highly associated, MSC-EVs–mediated Mφs phenotypic transformation must play a significant role during tissue healing. However, the molecular action of MSC-EVs in such Mφ polarization and tissue regeneration needs further investigation (Chen et al., 2008; Rodero and Khosrotehrani, 2010).

Although studies have provided evidence of immunosuppressive effects of MSCs in clinical trials for graft-vs.-host disease and Crohn disease (Godoy et al., 2019), the transplanted MSCs have not been proven in the persistence after injection and the contribution in tissue regeneration (Pittenger, 2009; Parekkadan and Milwid, 2010; Caplan and Correa, 2011). It is likely that the main immunosuppressive effects of MSCs resulted from paracrine regulation through secreted mediators, including EVs (Raposo and Stoorvogel, 2013). The immune modulation effect of MSC has been generalized as

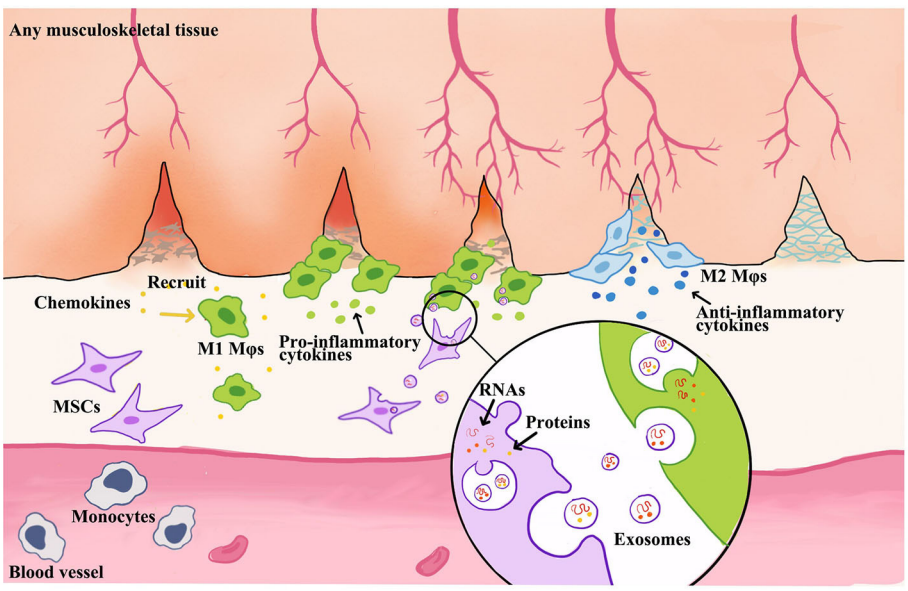

FIGURE 3 | Schematic illustration of MSC-derived exosome-guided macrophage reprogramming. MSC-derived exosomes can induce a conversion of M1 to M2 Mφs and accelerate musculoskeletal tissue healing. Mφs could be activated by inflammatory chemokines and then to produce proinflammatory factors. This creates a feedback loop whereby proinflammatory cytokines produced by Mφs stimulate MSC to produce immune modulators, such as exosomes or EVs. Therefore, the formation of exosomes begins with membrane invagination in the form of endosomes, leading to the development of the early endosomes. Upon maturation, the endosomes become multivesicular endosomes, which release their contents in the form of exosomes.

the inhibition of both innate and adaptive immunity and also derives inflammatory, autoimmune, and infectious disease pathology (Le Blanc and Mougiakakos, 2012; English, 2013). However, increasing analysis in animal models of inflammation demonstrated that MSC-EVs suppressed immune response through the transfer of RNAs and protein (Cantaluppi et al., 2012; Arslan et al., 2013). The inflammatory signals are essential to initiate and maintain the MSC- or EV-mediated tissue repair process; afterward, MSC-derived EVs could manipulate the niche by switching Mφ phenotype to facilitate tissue repair.

Functional MSC-EVs Cargo and Boosting Approaches

Recently, the use of MSC-based therapies has emerged. The therapeutic benefits of MSC transplantation have been attributed into two types, EVs and soluble factors. Soluble components include a wide variety of secreted chemokines, growth factors, and hormones with immunomodulatory activity. For example, PGE_2 and TGF-β are vital mediators of anti-inflammatory in therapeutic therapy of MSCs (Yoo et al., 2013). And lots of anti-inflammatory proteins also represent tissue protection, such as TSG-6, which has been reported with healing ability by reducing the influx of neutrophils to the tissue injury site (Oh et al., 2010). The studies regarding MSC-derived EVs have grown exponentially since it has been recognized that EVs containing mRNA, miRNA, and protein could exchange intracellular information and act as sophisticated mediators of recipient cell behavior, particularly in immunomodulation (Wolfers et al., 2001; Valadi et al., 2007; Skog et al., 2008). MSC-derived EVs contain not only more than 200 mRNA and 60 miRNA, but also more than 800 proteins (Bruno et al., 2009; Chen et al., 2010; Lai et al., 2012). These EV-derived proteins have been reported with an integral role in activating anti-inflammatory responses and regulating the cascade of tissue healing process in various injury models (Lee et al., 2012; Zhang et al., 2018; Li et al., 2019).

It has been demonstrated that genetically modified MSCs possess great prosurvival, proangiogenic, and anti-inflammatory properties not only by the altering release of soluble proteins, but also EVs (Huang et al., 2013; Wang et al., 2016; Lou et al., 2017; Ma et al., 2017; Qu et al., 2017; Tao et al., 2017). MSC-derived EVs are engineered at the cellular level under natural conditions, and it further highlighted the unique advantage of EV-based nanoplatforms for cargo delivery (Luan et al., 2017). For clinical applications, some advantages of MSC-derived EVs include easier injection, reduced Mφs phagocytosis and vascular occlusion (EL Andaloussi et al., 2013), innate biocompatibility, high physicochemical stability, high penetrability, and long-distance communication (Clayton et al., 2003; Ridder et al., 2014; Zomer et al., 2015).

Many strategies have been applied to modify EVs, including cell modification and direct EV modification (Armstrong and Perriman, 2016). Because EVs are secreted from cells, they can intrinsically express some lipids or cell adhesion molecules and ligands that naturally target certain types of recipient cells (Luan et al., 2017). Undoubtedly, it was inevitable that genetic engineering has been used to modify EVs. Overexpression of mRNA or miRNA in cells could be assembled into EVs, which could be fused to target cells to introduce or inhibit gene expression (Kosaka et al., 2010; Akao et al., 2011; Ridder et al., 2014; Zomer et al., 2015). For a significant amount of time, researchers have explored non-native biomaterials to cells to augment therapeutic function (Armstrong et al., 2015; Correia Carreira et al., 2016). Therefore, biomaterials delivered to the membrane could also naturally be incorporated into budding EVs, while internalized material may be packaged into exosomes for secretion (Armstrong et al., 2017). Taking advantage of these methods allows cellular processes and cell engineering techniques to be specifically adapted to EV functionalization.

Because only a small fraction of material could be packaged into EVs, the efficiency issue results in a low-yielding ending. And besides the widely explored cancer cells, the yield of exosomes derived from MSCs is one of the major factors that limits the expansion of cell-free therapeutic productions (Phan et al., 2018). Functional EVs could be derived from native ECM (Huleihel et al., 2016; Du et al., 2017), and three-dimensional environment for cell attachment and growth has been particularly attracted because it can mimic the ECM structure and function (Phan et al., 2018). Such structure has been reported with the effects of influencing EV secretion. For example, Tao et al. reported that Avitene Ultrafoam collagen hemostat caused the BMSCs to release 2-fold of exosomes compared to the plastic surface culture based on protein assay (Tao et al., 2017). Besides, a bioactive artificial ECM that was modified by adding molecules has been used to imitate native ECM mimicking structures and to improve yield of MSC exosomes by presenting specific functional ligands (Hao et al., 2017).

Moreover, an essential and urgent solution can provide an approach to improve the yield without sacrificing the functionality or with enhancing the efficacy simultaneously. Therefore, researchers tried to purify EVs, which could ensure that all modified sites or encapsulated species could be localized at the vesicle (Armstrong et al., 2017). As non-living entities, EVs have a major advantage over cells when they received membrane surface modification. It has been reported that excessive pressures, temperature, chemical induction, or hypoxia environment exposure could cause membrane disruption, vesicle aggregation, and surface protein denaturation (Smyth et al., 2014; Armstrong et al., 2017; Lo Sicco et al., 2017). Also, multivalent electrostatic interactions, receptor–ligand binding, and hydrophobic insertion have been commonly applied as methods of biological membrane modifications (Nakase and Futaki, 2015; Correia Carreira et al., 2016; Lee et al., 2016). In addition, electroporation, which is an alternative approach to EV active loading strategies, has been reported to transiently permeabilize the EV membrane to enhance the absorptivity of small molecules (Tian et al., 2014; Fuhrmann et al., 2015). Taken together, the engineered EVs will open up exciting opportunities in EV-based therapies

by boosting therapeutic capability, which is beyond their native functions.

STRENGTHS AND LIMITATIONS

This systematic review poses several advantages compared to other attempts to summarize the experimental results of MSC-derived paracrine mediators for musculoskeletal diseases. First, the up-to-date literature search has been yielded by two widely used databases: PubMed and EMBASE. The search strategies included MeSH terms and other related terms. Therefore, we could identify a number of eligible studies, which might remain relatively unnoticed. Second, the quality of included studies and risk of bias, including publication bias, were assessed. Third, study heterogeneity had been explored to point out potential explanatory variables. Fourth, to standardize the spontaneous recovery in the control groups, we analyzed the variables and controls specifically. And studies without scientific controls have been excluded during full-text screening procedure.

There were several limitations to this study. The first limitation is the small number of included studies. The second limitation is that we could not standardize the effectiveness of Mφs depletion among different studies. Moreover, the depletion is not permanent and, once subsided, could result in a reactive increase in Mφs numbers with unknown consequences. Third, these studies utilized different cell sources and delivery methods. Different types of animals were selected for *in vivo* studies. Fourth, the assessment methods also widely varied among studies; therefore, it was impossible to perform a quantitative analysis or a meta-analysis with the included studies.

CONCLUSION

This review demonstrated that MSC and MSC-EVs are authentic biomaterials to treat musculoskeletal problems. The broad therapeutic effect of MSC and MSC-EVs attribute to the management of Mφ polarization, at least in part. A further understanding in the molecular mechanism of how MSCs regulate Mφ polarization will facilitate the development of bioengineering approach to boost the therapeutic capacity of MSCs and their clinical application. However, more pre-clinical studies are needed to understand how EVs and their subcomponent play a role in musculoskeletal tissue healing process.

DATA AVAILABILITY STATEMENT

All datasets generated for this study are included in the article/**Supplementary Material**.

AUTHOR CONTRIBUTIONS

HX: conception and design, manuscript writing, and data analysis and interpretation. C-WL: conception and design, financial support, and manuscript writing. Y-FW: manuscript writing. L-YS, Y-HW, ZW, and XZ: data analysis and interpretation. PY and OL: administrative support and final approval of manuscript. SH: revisions to scientific content of manuscripts. All authors contributed to the article and approved the submitted version.

FUNDING

This work was supported by MWLC Associate Member Programme, Ming Wai Lau Centre for Reparative Medicine of Karolinska Institute to OL; CUHK Research Committee Direct Grant for Research (Reference no. 2018.020) and Hong Kong Government Research Grant Council, General Research Fund (Reference no. 14104620) to CW-L.

SUPPLEMENTARY MATERIAL

The Supplementary Material for this article can be found online at: https://www.frontiersin.org/articles/10.3389/fbioe.2020.587052/full#supplementary-material

REFERENCES

Akao, Y., Iio, A., Itoh, T., Noguchi, S., Itoh, Y., Ohtsuki, Y., et al. (2011). Microvesicle-mediated RNA molecule delivery system using monocytes/macrophages. *Mol. Ther.* 19, 395–399. doi: 10.1038/mt.2010.254

Aktas, E., Chamberlain, C. S., Saether, E. E., Duenwald-Kuehl, S. E., Kondratko-Mittnacht, J., Stitgen, M., et al. (2017). Immune modulation with primed mesenchymal stem cells delivered via biodegradable scaffold to repair an achilles tendon segmental defect. *J. Orthop. Res.* 35, 269–280. doi: 10.1002/jor.23258

Anderson, C. F., and Mosser, D. M. (2002). A novel phenotype for an activated macrophage: the type 2 activated macrophage. *J. Leukoc. Biol.* 72, 101–106.

Anton, K., Banerjee, D., and Glod, J. (2012). Macrophage-associated mesenchymal stem cells assume an activated, migratory, pro-inflammatory phenotype with increased IL-6 and CXCL10 secretion. *PLoS ONE* 7:e35036. doi: 10.1371/journal.pone.0035036

Armstrong, J. P., Holme, M. N., and Stevens, M. M. (2017). Re-engineering extracellular vesicles as smart nanoscale therapeutics. *ACS Nano* 11, 69–83. doi: 10.1021/acsnano.6b07607

Armstrong, J. P., and Perriman, A. W. (2016). Strategies for cell membrane functionalization. *Exp. Biol. Med.* 241, 1098–1106. doi: 10.1177/1535370216650291

Armstrong, J. P. K., Shakur, R., Horne, J. P., Dickinson, S. C., Armstrong, C. T., Lau, K., et al. (2015). Artificial membrane-binding proteins stimulate oxygenation of stem cells during engineering of large cartilage tissue. *Nat. Commun.* 6:7405. doi: 10.1038/ncomms8405

Arslan, F., Lai, R. C., Smeets, M. B., Akeroyd, L., Choo, A., Aguor, E. N., et al. (2013). Mesenchymal stem cell-derived exosomes increase ATP levels, decrease oxidative stress and activate PI3K/Akt pathway to enhance myocardial viability and prevent adverse remodeling after myocardial ischemia/reperfusion injury. *Stem Cell Res.* 10, 301–312. doi: 10.1016/j.scr.2013.01.002

Artlett, C. M. (2013). Inflammasomes in wound healing and fibrosis. *J. Pathol.* 229, 157–167. doi: 10.1002/path.4116

Bagno, L., Hatzistergos, K. E., Balkan, W., and Hare, J. M. (2018). Mesenchymal stem cell-based therapy for cardiovascular disease: progress and challenges. *Mol. Ther.* 26, 1610–1623. doi: 10.1016/j.ymthe.2018.05.009

Bernardo, M. E., and Fibbe, W. E. (2013). Mesenchymal stromal cells: sensors and switchers of inflammation. *Cell Stem Cell* 13, 392–402. doi: 10.1016/j.stem.2013.09.006

Bility, M. T., Cheng, L., Zhang, Z., Luan, Y., Li, F., Chi, L., et al. (2014). Hepatitis B virus infection and immunopathogenesis in a humanized mouse model: induction of human-specific liver fibrosis and M2-like macrophages. *PLoS Pathog.* 10:e1004032. doi: 10.1371/journal.ppat.1004032

Bosurgi, L., Manfredi, A. A., and Rovere-Querini, P. (2011). Macrophages in injured skeletal muscle: a perpetuum mobile causing and limiting fibrosis, prompting or restricting resolution and regeneration. *Front. Immunol.* 2:62. doi: 10.3389/fimmu.2011.00062

Bruno, S., Grange, C., Collino, F., Deregibus, M. C., Cantaluppi, V., Biancone, L., et al. (2012). Microvesicles derived from mesenchymal stem cells enhance survival in a lethal model of acute kidney injury. *PLoS ONE* 7:e33115. doi: 10.1371/journal.pone.0033115

Bruno, S., Grange, C., Deregibus, M. C., Calogero, R. A., Saviozzi, S., Collino, F., et al. (2009). Mesenchymal stem cell-derived microvesicles protect against acute tubular injury. *J. Am. Soc. Nephrol.* 20, 1053–1067. doi: 10.1681/ASN.2008070798

Cantaluppi, V., Gatti, S., Medica, D., Figliolini, F., Bruno, S., Deregibus, M. C., et al. (2012). Microvesicles derived from endothelial progenitor cells protect the kidney from ischemia-reperfusion injury by microRNA-dependent reprogramming of resident renal cells. *Kidney Int.* 82, 412–427. doi: 10.1038/ki.2012.105

Caplan, A. I. (1991). Mesenchymal stem cells. *J. Orthop. Res.* 9, 641–650. doi: 10.1002/jor.1100090504

Caplan, A. I., and Correa, D. (2011). The MSC: an injury drugstore. *Cell Stem Cell* 9, 11–15. doi: 10.1016/j.stem.2011.06.008

Carrero, R., Cerrada, I., Lledo, E., Dopazo, J., Garcia-Garcia, F., Rubio, M. P., et al. (2012). IL1beta induces mesenchymal stem cells migration and leucocyte chemotaxis through NF-kappaB. *Stem Cell Rev. Rep.* 8, 905–916. doi: 10.1007/s12015-012-9364-9

Cha, J. M., Shin, E. K., Sung, J. H., Moon, G. J., Kim, E. H., Cho, Y. H., et al. (2018). Efficient scalable production of therapeutic microvesicles derived from human mesenchymal stem cells. *Sci. Rep.* 8:1171. doi: 10.1038/s41598-018-19211-6

Chamberlain, C. S., Clements, A. E. B., Kink, J. A., Choi, U., Baer, G. S., Halanski, M. A., et al. (2019). Extracellular vesicle-educated macrophages promote early achilles tendon healing. *Stem Cells* 37, 652–662. doi: 10.1002/stem.2988

Chang, J., Koh, A. J., Roca, H., and McCauley, L. K. (2015). Juxtacrine interaction of macrophages and bone marrow stromal cells induce interleukin-6 signals and promote cell migration. *Bone Res.* 3:15014. doi: 10.1038/boneres.2015.14

Chen, L., Tredget, E. E., Wu, P. Y., and Wu, Y. (2008). Paracrine factors of mesenchymal stem cells recruit macrophages and endothelial lineage cells and enhance wound healing. *PLoS ONE* 3:e1886. doi: 10.1371/journal.pone.0001886

Chen, T. S., Lai, R. C., Lee, M. M., Choo, A. B., Lee, C. N., and Lim, S. K. (2010). Mesenchymal stem cell secretes microparticles enriched in pre-microRNAs. *Nucleic Acids Res.* 38, 215–224. doi: 10.1093/nar/gkp857

Cheng, L., Zhang, K., Wu, S., Cui, M., and Xu, T. (2017). Focus on mesenchymal stem cell-derived exosomes: opportunities and challenges in cell-free therapy. *Stem Cells Int.* 2017:6305295. doi: 10.1155/2017/6305295

Cheng, Y., and Schorey, J. S. (2013). Exosomes carrying mycobacterial antigens can protect mice against *Mycobacterium tuberculosis* infection. *Eur. J. Immunol.* 43, 3279–3290. doi: 10.1002/eji.201343727

Cho, D. I., Kim, M. R., Jeong, H. Y., Jeong, H. C., Jeong, M. H., Yoon, S. H., et al. (2014). Mesenchymal stem cells reciprocally regulate the M1/M2 balance in mouse bone marrow–derived macrophages. *Exp. Mol. Med.* 46:e70. doi: 10.1038/emm.2013.135

Chu, S. Y., Chou, C. H., Huang, H. D., Yen, M. H., Hong, H. C., Chao, P. H., et al. (2019). Mechanical stretch induces hair regeneration through the alternative activation of macrophages. *Nat. Commun.* 10:1524. doi: 10.1038/s41467-019-09402-8

Clarke, M., Hopewell, S., and Chalmers, I. (2007). Reports of clinical trials should begin and end with up-to-date systematic reviews of other relevant evidence: a status report. *J. R. Soc. Med.* 100, 187–190. doi: 10.1177/014107680710011415

Clayton, A., Harris, C. L., Court, J., Mason, M. D., and Morgan, B. P. (2003). Antigen-presenting cell exosomes are protected from complement-mediated lysis by expression of CD55 and CD59. *Eur. J. Immunol.* 33, 522–531. doi: 10.1002/immu.200310028

Correia Carreira, S., Armstrong, J. P., Seddon, A. M., Perriman, A. W., Hartley-Davies, R., and Schwarzacher, W. (2016). Ultra-fast stem cell labelling using cationised magnetoferritin. *Nanoscale* 8, 7474–7483. doi: 10.1039/C5NR07144E

Cosenza, S., Ruiz, M., Toupet, K., Jorgensen, C., and Noel, D. (2017). Mesenchymal stem cells derived exosomes and microparticles protect cartilage and bone from degradation in osteoarthritis. *Sci. Rep.* 7:16214. doi: 10.1038/s41598-017-15376-8

Cosenza, S., Toupet, K., Maumus, M., Luz-Crawford, P., Blanc-Brude, O., Jorgensen, C., et al. (2018). Mesenchymal stem cells-derived exosomes are more immunosuppressive than microparticles in inflammatory arthritis. *Theranostics* 8, 1399–1410. doi: 10.7150/thno.21072

da Costa Goncalves, F., and Paz, A. H. (2019). Cell membrane and bioactive factors derived from mesenchymal stromal cells: cell-free based therapy for inflammatory bowel diseases. *World J. Stem Cells* 11, 618–633. doi: 10.4252/wjsc.v11.i9.618

Darnell, M., O'Neil, A., Mao, A., Gu, L., Rubin, L. L., and Mooney, D. J. (2018). Material microenvironmental properties couple to induce distinct transcriptional programs in mammalian stem cells. *Proc. Natl. Acad. Sci. U.S.A.* 115, E8368–E8377. doi: 10.1073/pnas.1802568115

Donnelly, R. P., Dickensheets, H., and Finbloom, D. S. (1999). The interleukin-10 signal transduction pathway and regulation of gene expression in mononuclear phagocytes. *J. Interferon Cytokine Res.* 19, 563–573. doi: 10.1089/107999099313695

Du, W., Zhang, K., Zhang, S., Wang, R., Nie, Y., Tao, H., et al. (2017). Enhanced proangiogenic potential of mesenchymal stem cell-derived exosomes stimulated by a nitric oxide releasing polymer. *Biomaterials* 133, 70–81. doi: 10.1016/j.biomaterials.2017.04.030

EL Andaloussi, S., Mager, I., Breakefield, X. O., and Wood, M. J. (2013). Extracellular vesicles: biology and emerging therapeutic opportunities. *Nat. Rev. Drug Discov.* 12, 347–357. doi: 10.1038/nrd3978

English, K. (2013). Mechanisms of mesenchymal stromal cell immunomodulation. *Immunol. Cell Biol.* 91, 19–26. doi: 10.1038/icb.2012.56

Ferguson, S. W., Wang, J., Lee, C. J., Liu, M., Neelamegham, S., Canty, J. M., et al. (2018). The microRNA regulatory landscape of MSC-derived exosomes: a systems view. *Sci. Rep.* 8:1419. doi: 10.1038/s41598-018-19581-x

Fuhrmann, G., Serio, A., Mazo, M., Nair, R., and Stevens, M. M. (2015). Active loading into extracellular vesicles significantly improves the cellular uptake and photodynamic effect of porphyrins. *J. Control. Release* 205, 35–44. doi: 10.1016/j.jconrel.2014.11.029

Galli, S. J., Borregaard, N., and Wynn, T. A. (2011). Phenotypic and functional plasticity of cells of innate immunity: macrophages, mast cells and neutrophils. *Nat. Immunol.* 12, 1035–1044. doi: 10.1038/ni.2109

Godoy, J. A. P., Paiva, R. M. A., Souza, A. M., Kondo, A. T., Kutner, J. M., and Okamoto, O. K. (2019). Clinical translation of mesenchymal stromal cell therapy for graft versus host disease. *Front Cell Dev Biol.* 7:255. doi: 10.3389/fcell.2019.00255

Hao, D., Xiao, W., Liu, R., Kumar, P., Li, Y., Zhou, P., et al. (2017). Discovery and characterization of a potent and specific peptide ligand targeting endothelial progenitor cells and endothelial cells for tissue regeneration. *ACS Chem. Biol.* 12, 1075–1086. doi: 10.1021/acschembio.7b00118

Harvey, T., Flamenco, S., and Fan, C. M. (2019). A Tppp3(+)Pdgfra(+) tendon stem cell population contributes to regeneration and reveals a shared role for PDGF signalling in regeneration and fibrosis. *Nat. Cell Biol.* 21, 1490–1503. doi: 10.1038/s41556-019-0417-z

Huang, F., Zhu, X., Hu, X. Q., Fang, Z. F., Tang, L., Lu, X. L., et al. (2013). Mesenchymal stem cells modified with miR-126 release angiogenic factors and activate Notch ligand Delta-like-4, enhancing ischemic angiogenesis and cell survival. *Int. J. Mol. Med.* 31, 484–492. doi: 10.3892/ijmm.2012.1200

Huleihel, L., Hussey, G. S., Naranjo, J. D., Zhang, L., Dziki, J. L., Turner, N. J., et al. (2016). Matrix-bound nanovesicles within ECM bioscaffolds. *Sci Adv.* 2:e1600502. doi: 10.1126/sciadv.1600502

Hyvarinen, K., Holopainen, M., Skirdenko, V., Ruhanen, H., Lehenkari, P., Korhonen, M., et al. (2018). Mesenchymal stromal cells and their extracellular vesicles enhance the anti-inflammatory phenotype of regulatory macrophages by downregulating the production of interleukin (IL)-23 and IL-22. *Front. Immunol.* 9:771. doi: 10.3389/fimmu.2018.00771

Kim, H. S., Choi, D. Y., Yun, S. J., Choi, S. M., Kang, J. W., Jung, J. W., et al. (2012). Proteomic analysis of microvesicles derived from human mesenchymal stem cells. *J. Proteome Res.* 11, 839–849. doi: 10.1021/pr200682z

Kim, J., and Hematti, P. (2009). Mesenchymal stem cell-educated macrophages: a novel type of alternatively activated macrophages. *Exp. Hematol.* 37, 1445–1453. doi: 10.1016/j.exphem.2009.09.004

Kingery, M. T., Manjunath, A. K., Anil, U., and Strauss, E. J. (2019). Bone marrow mesenchymal stem cell therapy and related bone marrow-derived orthobiologic therapeutics. *Curr. Rev. Musculoskelet. Med.* 12, 451–459. doi: 10.1007/s12178-019-09583-1

Kosaka, N., Iguchi, H., Yoshioka, Y., Takeshita, F., Matsuki, Y., and Ochiya, T. (2010). Secretory mechanisms and intercellular transfer of microRNAs in living cells. *J. Biol. Chem.* 285, 17442–17452. doi: 10.1074/jbc.M110.107821

Krzyszczyk, P., Schloss, R., Palmer, A., and Berthiaume, F. (2018). The role of macrophages in acute and chronic wound healing and interventions to promote pro-wound healing phenotypes. *Front. Physiol.* 9:419. doi: 10.3389/fphys.2018.00419

Lai, R. C., Tan, S. S., Teh, B. J., Sze, S. K., Arslan, F., de Kleijn, D. P., et al. (2012). Proteolytic potential of the MSC exosome proteome: implications for an exosome-mediated delivery of therapeutic proteasome. *Int. J. Proteomics* 2012:971907. doi: 10.1155/2012/971907

Le Blanc, K., and Mougiakakos, D. (2012). Multipotent mesenchymal stromal cells and the innate immune system. *Nat. Rev. Immunol.* 12, 383–396. doi: 10.1038/nri3209

Lee, C., Mitsialis, S. A., Aslam, M., Vitali, S. H., Vergadi, E., Konstantinou, G., et al. (2012). Exosomes mediate the cytoprotective action of mesenchymal stromal cells on hypoxia-induced pulmonary hypertension. *Circulation* 126, 2601–2611. doi: 10.1161/CIRCULATIONAHA.112.114173

Lee, J., Lee, H., Goh, U., Kim, J., Jeong, M., Lee, J., et al. (2016). Cellular engineering with membrane fusogenic liposomes to produce functionalized extracellular vesicles. *ACS Appl. Mater. Interfaces* 8, 6790–6795. doi: 10.1021/acsami.6b01315

Li, T., Yan, Y., Wang, B., Qian, H., Zhang, X., Shen, L., et al. (2013). Exosomes derived from human umbilical cord mesenchymal stem cells alleviate liver fibrosis. *Stem Cells Dev.* 22, 845–854. doi: 10.1089/scd.2012.0395

Li, Y., Kong, N., Li, Z., Tian, R., Liu, X., Liu, G., et al. (2019). Bone marrow macrophage M2 polarization and adipose-derived stem cells osteogenic differentiation synergistically promote rehabilitation of bone damage. *J. Cell. Biochem.* 120, 19891–19901. doi: 10.1002/jcb.29297

Li, Z., Liu, F., He, X., Yang, X., Shan, F., and Feng, J. (2019). Exosomes derived from mesenchymal stem cells attenuate inflammation and demyelination of the central nervous system in EAE rats by regulating the polarization of microglia. *Int. Immunopharmacol.* 67, 268–280. doi: 10.1016/j.intimp.2018.12.001

Lo Sicco, C., Reverberi, D., Balbi, C., Ulivi, V., Principi, E., Pascucci, L., et al. (2017). Mesenchymal stem cell-derived extracellular vesicles as mediators of anti-inflammatory effects: endorsement of macrophage polarization. *Stem Cells Transl. Med.* 6, 1018–1028. doi: 10.1002/sctm.16-0363

Lou, G., Yang, Y., Liu, F., Ye, B., Chen, Z., Zheng, M., et al. (2017). MiR-122 modification enhances the therapeutic efficacy of adipose tissue-derived mesenchymal stem cells against liver fibrosis. *J. Cell. Mol. Med.* 21, 2963–2973. doi: 10.1111/jcmm.13208

Lu, M., and Huang, Y. (2020). Bioinspired exosome-like therapeutics and delivery nanoplatforms. *Biomaterials* 242:119925. doi: 10.1016/j.biomaterials.2020.119925

Luan, X., Sansanaphongpricha, K., Myers, I., Chen, H., Yuan, H., and Sun, D. (2017). Engineering exosomes as refined biological nanoplatforms for drug delivery. *Acta Pharmacol. Sin.* 38, 754–763. doi: 10.1038/aps.2017.12

Lukomska, B., Stanaszek, L., Zuba-Surma, E., Legosz, P., Sarzynska, S., and Drela, K. (2019). Challenges and controversies in human mesenchymal stem cell therapy. *Stem Cells Int.* 2019:9628536. doi: 10.1155/2019/9628536

Ma, J., Zhao, Y., Sun, L., Sun, X., Zhao, X., Sun, X., et al. (2017). Exosomes derived from Akt-modified human umbilical cord mesenchymal stem cells improve cardiac regeneration and promote angiogenesis via activating platelet-derived growth factor D. *Stem Cells Transl. Med.* 6, 51–59. doi: 10.5966/sctm.2016-0038

Ma, S., Xie, N., Li, W., Yuan, B., Shi, Y., and Wang, Y. (2014). Immunobiology of mesenchymal stem cells. *Cell Death Differ.* 21, 216–225. doi: 10.1038/cdd.2013.158

Maggini, J., Mirkin, G., Bognanni, I., Holmberg, J., Piazzon, I. M., Nepomnaschy, I., et al. (2010). Mouse bone marrow-derived mesenchymal stromal cells turn activated macrophages into a regulatory-like profile. *PLoS ONE* 5:e9252. doi: 10.1371/journal.pone.0009252

Mantovani, A., Biswas, S. K., Galdiero, M. R., Sica, A., and Locati, M. (2013). Macrophage plasticity and polarization in tissue repair and remodelling. *J. Pathol.* 229, 176–185. doi: 10.1002/path.4133

Maxson, S., Lopez, E. A., Yoo, D., Danilkovitch-Miagkova, A., and Leroux, M. A. (2012). Concise review: role of mesenchymal stem cells in wound repair. *Stem Cells Transl. Med.* 1, 142–149. doi: 10.5966/sctm.2011-0018

McElvany, M. D., McGoldrick, E., Gee, A. O., Neradilek, M. B., and Matsen, F. A. 3rd (2015). Rotator cuff repair: published evidence on factors associated with repair integrity and clinical outcome. *Am. J. Sports Med.* 43, 491–500. doi: 10.1177/0363546514529644

Melief, S. M., Geutskens, S. B., Fibbe, W. E., and Roelofs, H. (2013a). Multipotent stromal cells skew monocytes towards an anti-inflammatory interleukin-10-producing phenotype by production of interleukin-6. *Haematologica* 98, 888–895. doi: 10.3324/haematol.2012.078055

Melief, S. M., Schrama, E., Brugman, M. H., Tiemessen, M. M., Hoogduijn, M. J., Fibbe, W. E., et al. (2013b). Multipotent stromal cells induce human regulatory T cells through a novel pathway involving skewing of monocytes toward anti-inflammatory macrophages. *Stem Cells* 31, 1980–1991. doi: 10.1002/stem.1432

Mianehsaz, E., Mirzaei, H. R., Mahjoubin-Tehran, M., Rezaee, A., Sahebnasagh, R., Pourhanifeh, M. H., et al. (2019). Mesenchymal stem cell-derived exosomes: a new therapeutic approach to osteoarthritis? *Stem Cell Res. Ther.* 10:340. doi: 10.1186/s13287-019-1445-0

Moher, D., Liberati, A., Tetzlaff, J., Altman, D. G., and Group, P. (2009). Preferred reporting items for systematic reviews and meta-analyses: the PRISMA statement. *PLoS Med* 6:e1000097. doi: 10.1371/journal.pmed.1000097

Moore, J. P., Vinh, A., Tuck, K. L., Sakkal, S., Krishnan, S. M., Chan, C. T., et al. (2015). M2 macrophage accumulation in the aortic wall during angiotensin II infusion in mice is associated with fibrosis, elastin loss, and elevated blood pressure. *Am. J. Physiol. Heart Circ. Physiol.* 309, H906–917. doi: 10.1152/ajpheart.00821.2014

Mosser, D. M., and Edwards, J. P. (2008). Exploring the full spectrum of macrophage activation. *Nat. Rev. Immunol.* 8, 958–969. doi: 10.1038/nri2448

Murray, P. J., Allen, J. E., Biswas, S. K., Fisher, E. A., Gilroy, D. W., Goerdt, S., et al. (2014). Macrophage activation and polarization: nomenclature and experimental guidelines. *Immunity* 41, 14–20. doi: 10.1016/j.immuni.2014.06.008

Nakase, I., and Futaki, S. (2015). Combined treatment with a pH-sensitive fusogenic peptide and cationic lipids achieves enhanced cytosolic delivery of exosomes. *Sci. Rep.* 5:10112. doi: 10.1038/srep10112

Nemeth, K., Leelahavanichkul, A., Yuen, P. S., Mayer, B., Parmelee, A., Doi, K., et al. (2009). Bone marrow stromal cells attenuate sepsis via prostaglandin E(2)-dependent reprogramming of host macrophages to increase their interleukin-10 production. *Nat. Med.* 15, 42–49. doi: 10.1038/nm.1905

O'Brien, E. M., Risser, G. E., and Spiller, K. L. (2019). Sequential drug delivery to modulate macrophage behavior and enhance implant integration. *Adv. Drug Deliv. Rev.* 149–150, 85–94. doi: 10.1016/j.addr.2019.05.005

Oh, J. Y., Roddy, G. W., Choi, H., Lee, R. H., Ylostalo, J. H., Rosa, R. H. Jr., et al. (2010). Anti-inflammatory protein TSG-6 reduces inflammatory damage to the cornea following chemical and mechanical injury. *Proc. Natl. Acad. Sci. U.S.A.* 107, 16875–16880. doi: 10.1073/pnas.1012451107

Otsuru, S., Gordon, P. L., Shimono, K., Jethva, R., Marino, R., Phillips, C. L., et al. (2012). Transplanted bone marrow mononuclear cells and MSCs impart clinical benefit to children with osteogenesis imperfecta through

different mechanisms. *Blood* 120, 1933–1941. doi: 10.1182/blood-2011-12-400085

Pacienza, N., Lee, R. H., Bae, E. H., Kim, D. K., Liu, Q., Prockop, D. J., et al. (2019). *In vitro* macrophage assay predicts the *in vivo* anti-inflammatory potential of exosomes from human mesenchymal stromal cells. *Mol. Ther. Methods Clin. Dev.* 13, 67–76. doi: 10.1016/j.omtm.2018.12.003

Pajarinen, J., Lin, T., Gibon, E., Kohno, Y., Maruyama, M., Nathan, K., et al. (2019). Mesenchymal stem cell-macrophage crosstalk and bone healing. *Biomaterials* 196, 80–89. doi: 10.1016/j.biomaterials.2017.12.025

Parekkadan, B., and Milwid, J. M. (2010). Mesenchymal stem cells as therapeutics. *Annu. Rev. Biomed. Eng.* 12, 87–117. doi: 10.1146/annurev-bioeng-070909-105309

Phan, J., Kumar, P., Hao, D., Gao, K., Farmer, D., and Wang, A. (2018). Engineering mesenchymal stem cells to improve their exosome efficacy and yield for cell-free therapy. *J. Extracell. Vesicles* 7:1522236. doi: 10.1080/20013078.2018.1522236

Pittenger, M. (2009). Sleuthing the source of regeneration by MSCs. *Cell Stem Cell* 5, 8–10. doi: 10.1016/j.stem.2009.06.013

Qu, Y., Zhang, Q., Cai, X., Li, F., Ma, Z., Xu, M., et al. (2017). Exosomes derived from miR-181-5p-modified adipose-derived mesenchymal stem cells prevent liver fibrosis via autophagy activation. *J. Cell. Mol. Med.* 21, 2491–2502. doi: 10.1111/jcmm.13170

Raposo, G., and Stoorvogel, W. (2013). Extracellular vesicles: exosomes, microvesicles, and friends. *J. Cell Biol.* 200, 373–383. doi: 10.1083/jcb.201211138

Regenberg, A. C., Hutchinson, L. A., Schanker, B., and Mathews, D. J. (2009). Medicine on the fringe: stem cell-based interventions in advance of evidence. *Stem Cells* 27, 2312–2319. doi: 10.1002/stem.132

Ridder, K., Keller, S., Dams, M., Rupp, A. K., Schlaudraff, J., Del Turco, D., et al. (2014). Extracellular vesicle-mediated transfer of genetic information between the hematopoietic system and the brain in response to inflammation. *PLoS Biol.* 12:e1001874. doi: 10.1371/journal.pbio.1001874

Rodero, M. P., and Khosrotehrani, K. (2010). Skin wound healing modulation by macrophages. *Int. J. Clin. Exp. Pathol.* 3, 643–653.

Saldana, L., Bensiamar, F., Valles, G., Mancebo, F. J., Garcia-Rey, E., and Vilaboa, N. (2019). Immunoregulatory potential of mesenchymal stem cells following activation by macrophage-derived soluble factors. *Stem Cell Res. Ther.* 10:58. doi: 10.1186/s13287-019-1156-6

Shen, H., Yoneda, S., Abu-Amer, Y., Guilak, F., and Gelberman, R. H. (2020). Stem cell-derived extracellular vesicles attenuate the early inflammatory response after tendon injury and repair. *J. Orthop. Res.* 38, 117–127. doi: 10.1002/jor.24406

Shi, Y., Su, J., Roberts, A. I., Shou, P., Rabson, A. B., and Ren, G. (2012). How mesenchymal stem cells interact with tissue immune responses. *Trends Immunol.* 33, 136–143. doi: 10.1016/j.it.2011.11.004

Shi, Z., Wang, Q., and Jiang, D. (2019). Extracellular vesicles from bone marrow-derived multipotent mesenchymal stromal cells regulate inflammation and enhance tendon healing. *J. Transl. Med.* 17:211. doi: 10.1186/s12967-019-1960-x

Sica, A., and Mantovani, A. (2012). Macrophage plasticity and polarization: *in vivo* veritas. *J. Clin. Invest.* 122, 787–795. doi: 10.1172/JCI59643

Silva, A. K., Kolosnjaj-Tabi, J., Bonneau, S., Marangon, I., Boggetto, N., Aubertin, K., et al. (2013). Magnetic and photoresponsive theranosomes: translating cell-released vesicles into smart nanovectors for cancer therapy. *ACS Nano* 7, 4954–4966. doi: 10.1021/nn400269x

Skog, J., Wurdinger, T., van Rijn, S., Meijer, D. H., Gainche, L., Sena-Esteves, M., et al. (2008). Glioblastoma microvesicles transport RNA and proteins that promote tumour growth and provide diagnostic biomarkers. *Nat. Cell Biol.* 10, 1470–1476. doi: 10.1038/ncb1800

Smyth, T., Petrova, K., Payton, N. M., Persaud, I., Redzic, J. S., Graner, M. W., et al. (2014). Surface functionalization of exosomes using click chemistry. *Bioconjug. Chem.* 25, 1777–1784. doi: 10.1021/bc500291r

Spiller, K. L., and Koh, T. J. (2017). Macrophage-based therapeutic strategies in regenerative medicine. *Adv. Drug Deliv. Rev.* 122, 74–83. doi: 10.1016/j.addr.2017.05.010

Stahl, M., Schupp, J., Jager, B., Schmid, M., Zissel, G., Muller-Quernheim, J., et al. (2013). Lung collagens perpetuate pulmonary fibrosis via CD204 and M2 macrophage activation. *PLoS ONE* 8:e81382. doi: 10.1371/journal.pone.0081382

Stein, M., Keshav, S., Harris, N., and Gordon, S. (1992). Interleukin 4 potently enhances murine macrophage mannose receptor activity: a marker of alternative immunologic macrophage activation. *J. Exp. Med.* 176, 287–292. doi: 10.1084/jem.176.1.287

Tao, S. C., Guo, S. C., Li, M., Ke, Q. F., Guo, Y. P., and Zhang, C. Q. (2017). Chitosan wound dressings incorporating exosomes derived from MicroRNA-126-overexpressing synovium mesenchymal stem cells provide sustained release of exosomes and heal full-thickness skin defects in a diabetic rat model. *Stem Cells Transl. Med.* 6, 736–747. doi: 10.5966/sctm.2016-0275

Tian, Y., Li, S., Song, J., Ji, T., Zhu, M., Anderson, G. J., et al. (2014). A doxorubicin delivery platform using engineered natural membrane vesicle exosomes for targeted tumor therapy. *Biomaterials* 35, 2383–2390. doi: 10.1016/j.biomaterials.2013.11.083

Tidball, J. G. (2011). Mechanisms of muscle injury, repair, and regeneration. *Compr. Physiol.* 1, 2029–2062. doi: 10.1002/cphy.c100092

Vakhshiteh, F., Atyabi, F., and Ostad, S. N. (2019). Mesenchymal stem cell exosomes: a two-edged sword in cancer therapy. *Int. J. Nanomedicine* 14, 2847–2859. doi: 10.2147/IJN.S200036

Valadi, H., Ekstrom, K., Bossios, A., Sjostrand, M., Lee, J. J., and Lotvall, J. O. (2007). Exosome-mediated transfer of mRNAs and microRNAs is a novel mechanism of genetic exchange between cells. *Nat. Cell Biol.* 9, 654–659. doi: 10.1038/ncb1596

Varol, C., Mildner, A., and Jung, S. (2015). Macrophages: development and tissue specialization. *Annu. Rev. Immunol.* 33, 643–675. doi: 10.1146/annurev-immunol-032414-112220

Wang, B., Yao, K., Huuskes, B. M., Shen, H. H., Zhuang, J., Godson, C., et al. (2016). Mesenchymal stem cells deliver exogenous MicroRNA-let7c via exosomes to attenuate renal fibrosis. *Mol. Ther.* 24, 1290–1301. doi: 10.1038/mt.2016.90

Wang, Y., He, G., Guo, Y., Tang, H., Shi, Y., Bian, X., et al. (2019). Exosomes from tendon stem cells promote injury tendon healing through balancing synthesis and degradation of the tendon extracellular matrix. *J. Cell. Mol. Med.* 23, 5475–5485. doi: 10.1111/jcmm.14430

Waterman, R. S., Tomchuck, S. L., Henkle, S. L., and Betancourt, A. M. (2010). A new mesenchymal stem cell (MSC) paradigm: polarization into a pro-inflammatory MSC1 or an Immunosuppressive MSC2 phenotype. *PLoS ONE* 5:e10088. doi: 10.1371/journal.pone.0010088

Wells, K., and Julia, H. L. (2009). Study quality assessment in systematic reviews of research on intervention effects. *Res. Soc. Work Pract.* 19, 52–62. doi: 10.1177/1049731508317278

Willis, G. R., Kourembanas, S., and Mitsialis, S. A. (2017). Toward exosome-based therapeutics: isolation, heterogeneity, and fit-for-purpose potency. *Front. Cardiovasc. Med.* 4:63. doi: 10.3389/fcvm.2017.00063

Wolfe, A. R., Trenton, N. J., Debeb, B. G., Larson, R., Ruffell, B., Chu, K., et al. (2016). Mesenchymal stem cells and macrophages interact through IL-6 to promote inflammatory breast cancer in pre-clinical models. *Oncotarget* 7, 82482–82492. doi: 10.18632/oncotarget.12694

Wolfers, J., Lozier, A., Raposo, G., Regnault, A., Thery, C., Masurier, C., et al. (2001). Tumor-derived exosomes are a source of shared tumor rejection antigens for CTL cross-priming. *Nat. Med.* 7, 297–303. doi: 10.1038/85438

Yang, D. H., and Yang, M. Y. (2019). The Role of Macrophage in the pathogenesis of osteoporosis. *Int. J. Mol. Sci.* 20:2093. doi: 10.3390/ijms20092093

Yoo, S. W., Chang, D. Y., Lee, H. S., Kim, G. H., Park, J. S., Ryu, B. Y., et al. (2013). Immune following suppression mesenchymal stem cell transplantation in the ischemic brain is mediated by TGF-beta. *Neurobiol. Dis.* 58, 249–257. doi: 10.1016/j.nbd.2013.06.001

Zhang, S., Chuah, S. J., Lai, R. C., Hui, J. H. P., Lim, S. K., and Toh, W. S. (2018). MSC exosomes mediate cartilage repair by enhancing proliferation, attenuating apoptosis and modulating immune reactivity. *Biomaterials* 156, 16–27. doi: 10.1016/j.biomaterials.2017.11.028

Zhang, Z., Dombroski, J. A., and King, M. R. (2020). Engineering of exosomes to target cancer metastasis. *Cell. Mol. Bioeng.* 13, 1–16. doi: 10.1007/s12195-019-00607-x

Zhao, Y., Sun, X., Cao, W., Ma, J., Sun, L., Qian, H., et al. (2015). Exosomes derived from human umbilical cord mesenchymal stem cells relieve acute myocardial ischemic injury. *Stem Cells Int.* 2015:761643. doi: 10.1155/2015/761643

Zomer, A., Maynard, C., Verweij, F. J., Kamermans, A., Schafer, R., Beerling, E., et al. (2015). *In vivo* imaging reveals extracellular vesicle-mediated phenocopying of metastatic behavior. *Cell* 161, 1046–1057. doi: 10.1016/j.cell.2015.04.042

Conflict of Interest: The authors declare that the research was conducted in the absence of any commercial or financial relationships that could be construed as a potential conflict of interest.

frontiers in Bioengineering and Biotechnology

MINI REVIEW
published: 03 December 2020
doi: 10.3389/fbioe.2020.602009

Cell-Derived Extracellular Matrix for Tissue Engineering and Regenerative Medicine

*Marisa Assunção[1,2], Dorsa Dehghan-Baniani[2], Chi Him Kendrick Yiu[1,2], Thomas Später[3], Sebastian Beyer[4] and Anna Blocki[1,2,5]**

[1] School of Biomedical Sciences, Faculty of Medicine, The Chinese University of Hong Kong, Shatin, Hong Kong, [2] Institute for Tissue Engineering and Regenerative Medicine, The Chinese University of Hong Kong, Shatin, Hong Kong, [3] Institute for Clinical and Experimental Surgery, University of Saarland, Saarbrücken, Germany, [4] Department of Biomedical Engineering, Faculty of Engineering, The Chinese University of Hong Kong, Shatin, Hong Kong, [5] Department of Orthopaedics and Traumatology, Faculty of Medicine, The Chinese University of Hong Kong, Shatin, Hong Kong

Cell-derived extracellular matrices (CD-ECMs) captured increasing attention since the first studies in the 1980s. The biological resemblance of CD-ECMs to their *in vivo* counterparts and natural complexity provide them with a prevailing bioactivity. CD-ECMs offer the opportunity to produce microenvironments with costumizable biological and biophysical properties in a controlled setting. As a result, CD-ECMs can improve cellular functions such as stemness or be employed as a platform to study cellular niches in health and disease. Either on their own or integrated with other materials, CD-ECMs can also be utilized as biomaterials to engineer tissues *de novo* or facilitate endogenous healing and regeneration. This review provides a brief overview over the methodologies used to facilitate CD-ECM deposition and manufacturing. It explores the versatile uses of CD-ECM in fundamental research and therapeutic approaches, while highlighting innovative strategies. Furthermore, current challenges are identified and it is accentuated that advancements in methodologies, as well as innovative interdisciplinary approaches are needed to take CD-ECM-based research to the next level.

Keywords: cell-derived extracellular matrix, stem cell niche, cell differentiation, tissue engineering, regenerative medicine, skeletal repair, cardiovascular repair, cell-extracellular matrix interactions

OPEN ACCESS

Edited by:
Xin Zhao,
Hong Kong Polytechnic University, Hong Kong

Reviewed by:
Masoud Mozafari,
University of Toronto, Canada
Katiucia Batista Silva Paiva,
University of São Paulo, Brazil

****Correspondence:***
Anna Blocki
anna.blocki@cuhk.edu.hk

Specialty section:
This article was submitted to Biomaterials, a section of the journal Frontiers in Bioengineering and Biotechnology

Received: *02 September 2020*
Accepted: *10 November 2020*
Published: *03 December 2020*

Citation:
Assunção M, Dehghan-Baniani D, Yiu CHK, Später T, Beyer S and Blocki A (2020) Cell-Derived Extracellular Matrix for Tissue Engineering and Regenerative Medicine. Front. Bioeng. Biotechnol. 8:602009. doi: 10.3389/fbioe.2020.602009

INTRODUCTION

The extracellular matrix (ECM) is the non-cellular component present in all connective tissues and has a composition specific for each tissue. It is comprised of a complex and highly organized three-dimensional macromolecular network of biomolecules. These include fibrous proteins (such as collagens) and glycosaminoglycan (GAG)-based components. Fibrous ECM components form the backbone of the polymer network, thereby providing shape/stability and tensile strength to tissues. They also regulate cell adhesion and support cell migration. GAG-based components fill the interstitial space, ensuring hydration and lubrication of tissues, and acting as a reservoir and modulator of cytokine signaling (Theocharis et al., 2016; Yong et al., 2020).

ECM-driven communication arises from a complex combination of biochemical, topological and biomechanical cues, facilitating a reciprocal dialogue with cells, which can respond via remodeling of the ECM. This multi-dimensional signaling enables the ECM to guide intricate cellular and tissue processes such as homeostasis, healing and regeneration (Kaukonen et al., 2017).

ECM AS A BIOMATERIAL

The ECM is a biomaterial designed by nature that underwent over 600 million years of material optimization (Ozbek et al., 2010). It serves as a blueprint for many man-made biomimetic biomaterials. Nonetheless, these materials represent oversimplified versions of the ECM that are not able to replicate its complex bioactivity (Kaukonen et al., 2017). As a result, ECM derived from decellularized tissues, remains one of the most successful biomaterials in clinics (Hussey et al., 2018).

Unfortunately, tissue-derived ECM faces various challenges to its clinical application. The limited availability of human cadaveric tissue leads to the use of animal tissue-derived ECM as an alternative source. Especially the incomplete decellularization of tissue carries the risk of disease transmission and immunological rejection. Some ECMs are plainly not available, since some specific tissues are hard to isolate (e.g., stem cell niches). Further, tissue-derived ECM is set in its composition, therefore cannot be customized in its bioactivity toward a specific application (Aamodt and Grainger, 2016).

As cell-derived ECM (CD-ECM) partially recapitulates the complex biological machinery of native tissue (Ahlfors and Billiar, 2007), it can address many of the tissue-derived ECM's limitations. It can be derived from human cell cultures by gentle decellularization to remove immunogenic components, while preserving its bioactivity. ECM-synthesizing cells can be standardized and pre-screened (Sharma et al., 2020), minimizing the risk of disease transmission. Deriving ECM *in vitro* provides the opportunity to select appropriate ECM-producing cell types, further modify them (e.g., genetically) and expose them to specific stimuli, thus enabling the creation of ECM with desired properties (Maia et al., 2020). CD-ECM is therefore an incredibly versatile material to be used in physiological studies and therapeutic approaches.

METHODOLOGIES TO GENERATE CD-ECM

Stromal cell-derived ECMs are rich in collagens (Antebi et al., 2015), while endothelial/epithelial CD-ECMs contain a laminin-rich basement membrane-like ECM (Davis and Senger, 2005). CD-ECM can be generated by culturing cells scaffold-free in 2D and 3D cultures (Serebriiskii et al., 2008; Hoshiba et al., 2016; Sharma et al., 2020). Alternatively, cells can also be seeded within hydrogels or scaffolds, forming hybrid CD-ECM-based materials (Sart et al., 2014; Suhaeri et al., 2018).

Facilitating ECM Deposition *in vitro*

Slow ECM assembling kinetics *in vitro* necessitate long cell culture periods up to several weeks to harvest sufficient CD-ECM amounts for the desired application (Bourget et al., 2012). This can be improved by adjusting culture conditions (Hoshiba, 2017).

The most essential supplement for robust ECM deposition is ascorbate, a cofactor of lysyl hydroxylase and prolyl hydroxylase, essential enzymes in collagen fibrillogenesis (Pinnell, 1985). Collagen type I is the most prominent ECM component and its deposition increases the overall yield of CD-ECM and improves its mechanical properties. Nonetheless, rapid degradation of ascorbate (Grinnell et al., 1989) calls for frequent media changes, thereby discarding the not-yet deposited ECM components. A stable form of ascorbate (2-phospho-L-ascorbate) can reduce the frequency of medium replacements (Chen et al., 2011).

The yield of deposited ECM can be amplified by introducing macromolecules, which emulate the crowded conditions present *in vivo*. The biophysical principle of macromolecular crowding (MMC) relies on macromolecules occupying space, thereby increasing the effective concentration of other molecules and the thermodynamic activity of the system. This has profound effects on protein folding, molecular interactions and enzyme kinetics (Chen et al., 2011). In particular, under MMC more ECM can be deposited within 1 week than after several weeks under non-crowded conditions. Most commonly used "crowders" are Ficoll, carrageenan, polyvinylpyrrolidone and dextran sulfate (Lareu et al., 2007; Lu et al., 2011; Blocki et al., 2015; Gaspar et al., 2019), albeit dextran sulfate was recently found to act as a precipitating agent, independent of MMC (Assunção et al., 2020).

Culturing cells with low serum concentration (<1% v/v) was also beneficial, as serum carries exogenous matrix metalloproteases that degrade ECM and imbalance the ECM's natural remodeling rate (Satyam et al., 2014; Kumar et al., 2015). Furthermore, hypoxia was shown to induce synthesis of ECM richer in collagenous proteins and angiogenic factors, as seen in fibroblasts (Distler et al., 2007; Kumar et al., 2018) and mesenchymal stem cells (MSCs) (Cigognini et al., 2016; Du et al., 2017).

Decellularization and Processing of CD-ECM

CD-ECMs are usually generated in a small format, permitting gentle decellularization methods with focus on maintaining architecture and bioactivity. Most methods use detergents, enzymes, chelating agents, mechanical approaches and combinations thereof (**Figure 1A**; Woods and Gratzer, 2005; Faulk et al., 2014; Levorson et al., 2014; Gilpin and Yang, 2017). Complete decellularization is further achieved by removing genetic material with nucleases to prevent host immune reaction, as can be observed in tissue-derived ECMs (Crapo et al., 2011).

Decellularized CD-ECMs can then be used in their original format, fragmented (Carvalho et al., 2019b), grinded (Wei et al., 2015) or solubilized (Decaris et al., 2012). These formats give rise to 2D ECM layers or more complex 3D structures comprising 3D scaffolds (McAllister et al., 2009), spheroids (Cheng et al., 2009), fibers (Roberts et al., 2017), and sheets (Sharma et al., 2020; **Figure 1B**).

APPLICATIONS OF CD-ECM

Numerous applications have been explored for CD-ECMs including the improvement of cellular functions, seen in tailored cellular niches, the study of ECM in a physiological

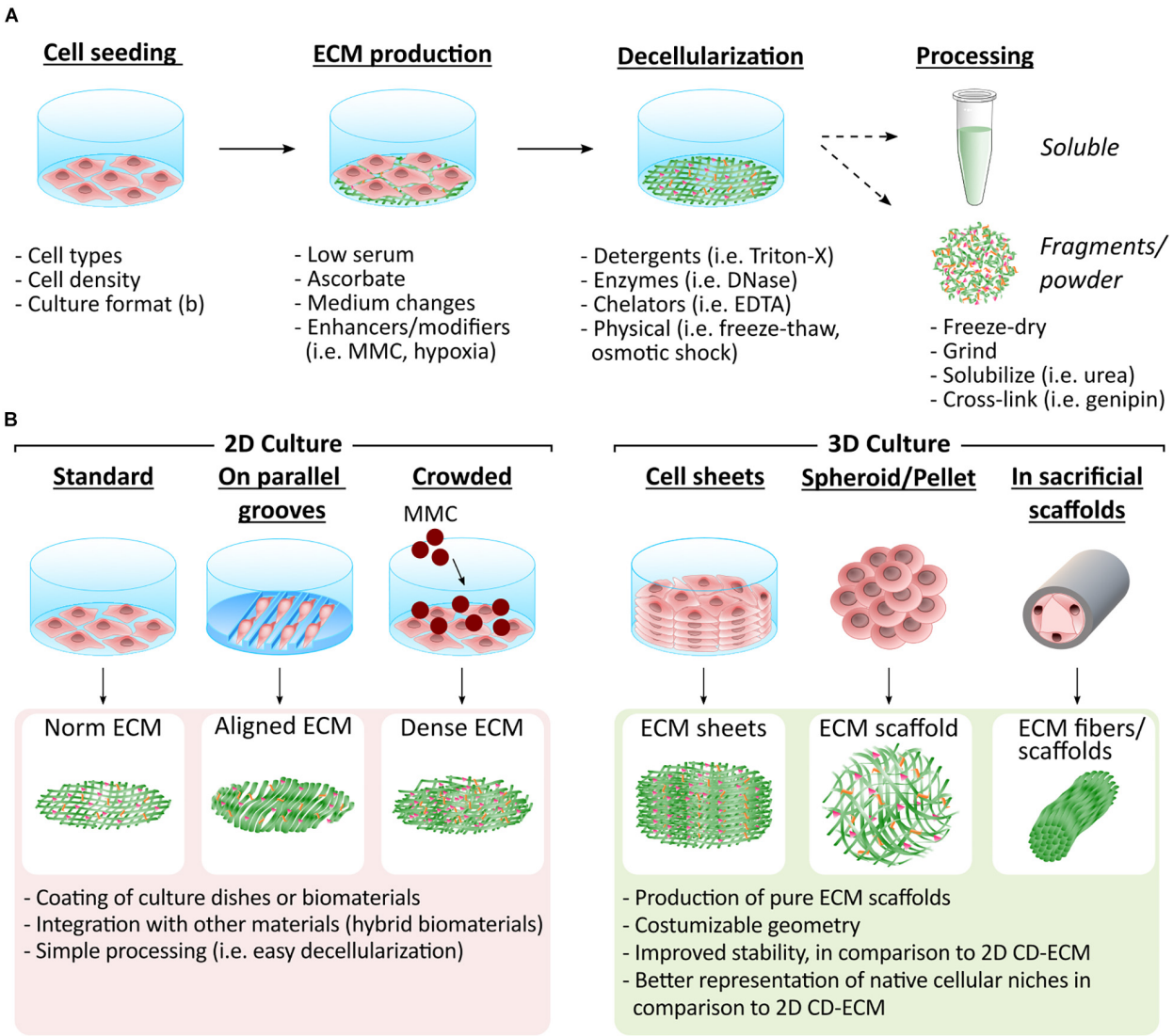

FIGURE 1 | Methodologies to generate CD-ECM in different formats. **(A)** CD-ECMs are synthesized by different cell types (i.e., MSCs and fibroblasts). Culture conditions are adjusted to facilitate ECM deposition by e.g., introducing MMC or hypoxia into cell culture. The assembled ECM is then gently decellularized, while preserving the ECM's integrity as much as possible. The resulting CD-ECM can be used in its original format or further processed. **(B)** The arrangement in which the ECM producing cells are cultured determines the format of the CD-ECM material. Which type of presentation is most advantageous depends on the desired application. Easiest decellularization can be achieved in 2D cultures. The resulting CD-ECM is suitable for coating of culture dishes and biomaterial surfaces or can be further processed and integrated with other biomaterials, such as hydrogels. Integration of CD-ECM with other materials provides the opportunity to combine the bioactivity of the ECM with desired geometries and mechanical properties. CD-ECM assembled in 3D recapitulates native cellular niches more closely. It can thus be utilized to engineer improved tissue models and ECM 3D scaffolds with desired geometries. Various techniques exist that enable the construction of 3D scaffolds based on CD-ECM.

and pathophysiological context, and the application in tissue engineering and regenerative medicine (TERM) (**Figure 2**).

Recreation of Cellular Niches

Stem Cell Niches

The emulation of the native cellular microenvironment in culture is a prerequisite to maintain the cells' phenotype and function. This is especially true for sensitive cell types, such as stem cells, which are known to undergo senescence and lose their stemness *ex vivo* (Hoshiba et al., 2016).

Various studies demonstrated that MSC-derived ECM can recapitulate the stem cell niche sufficiently to protect reseeded MSCs from oxidative stress, promote their proliferation, and conserve their stemness (Chen et al., 2007; Lai et al., 2010; Liu et al., 2016; Xing et al., 2020). CD-ECMs were also shown to maintain the native phenotype of neural progenitor cells (Yang et al., 2017; Hoshiba et al., 2018), embryonic stem cells (ESCs) (Klimanskaya et al., 2005), periodontal ligament stem cells (Xiong et al., 2019) and hematopoietic stem cells (Prewitz et al., 2013). Furthermore, ECMs derived from younger MSCs were shown

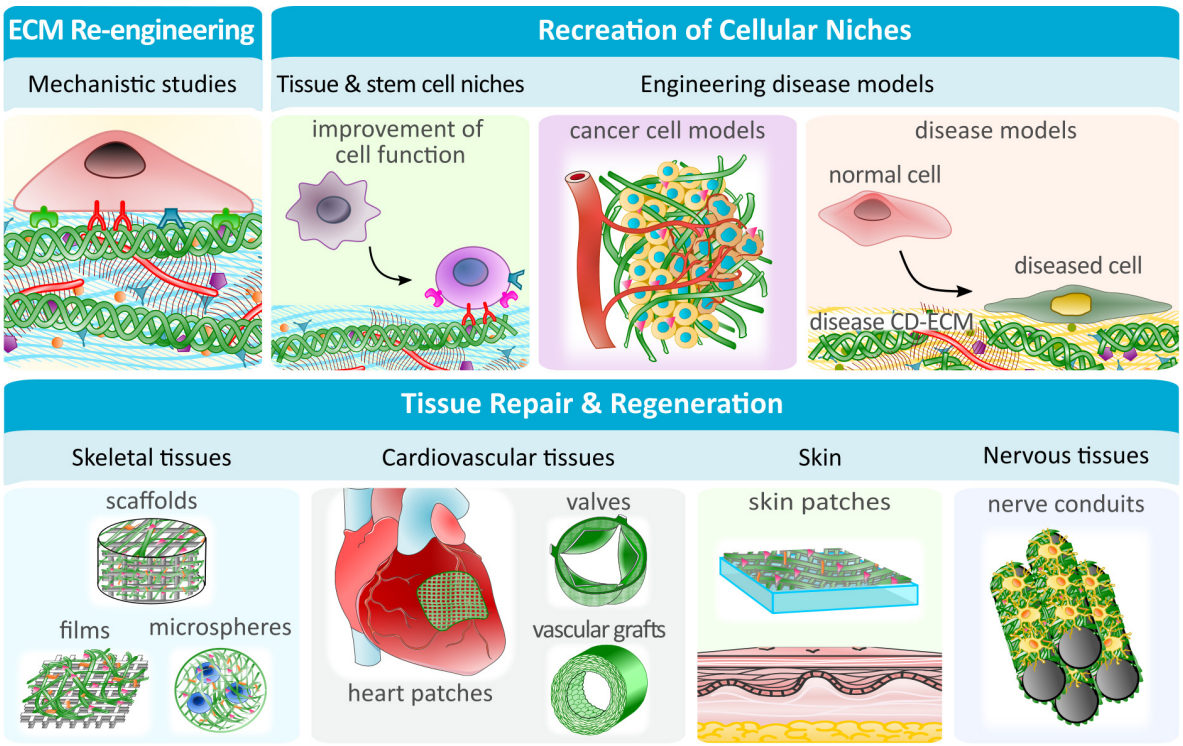

FIGURE 2 | CD-ECM applications in fundamental research, pathophysiological studies and renegerative medicine. The ease with which CD-ECM can be modified, makes it the ideal platform to study detailed ECM mechanisms or the role of cellular niches under physiological and pathophysiological conditions. Specialized engineered cellular niches can be further utilized to improve cellular functions *in vitro*, such as stemness. In TERM, CD-ECMs can be created with specific mechanical and biological properties to be used on their own (i.e., as vascular grafts) or to enhance the performance of (semi-) synthetic biomaterials.

to rejuvenate *in vitro*-aged and chronologically-aged MSCs (Pei et al., 2011; Sun et al., 2011; Lin et al., 2012). These effects were tightly linked to the biological profile of the ECM (reviewed in Sart et al., 2020).

Tissue-Specific Niches

Similar to MSC-derived ECM supporting stemness, ECMs derived from adipogenically or osteogenically induced MSCs promoted the respective lineage commitment of reseeded MSCs via integrated structural and regulatory proteins (Ang et al., 2014; Jeon et al., 2018; Carvalho et al., 2019a). Chondrogenic differentiation was best supported by chondrogenic ECM deposited in 3D (Cheng et al., 2009; Lu et al., 2011). Synovial MSC-derived ECM also protected chondrocytes from pro-inflammatory stimuli (Yan et al., 2020).

CD-ECMs from stromal, endothelial and epithelial cells could improve the function of specialized cell types, such as podocytes (Satyam et al., 2020), chondrocytes (Wei et al., 2015; Yang et al., 2018; Zhang et al., 2019), hepatocytes (Grant et al., 2017; Guo et al., 2017), Schwann cells (Xiao et al., 2016), as well as promote natural killer cell differentiation (Lee et al., 2020).

Similarly to adult stem cells, CD-ECMs synthesized by differentiating ESCs were able to promote early differentiation of ESCs, even without external factors (Goh et al., 2013). ECM produced by an endoderm-inducing cell line and ECM from liver progenitor cells promoted differentiation of pluripotent cells into insulin-expressing pancreatic β-cells (Higuchi et al., 2010) and hepatic cells (Kanninen et al., 2016), respectively.

Hence, CD-ECMs can be utilized to tailor cell and tissue-specific niches to promote cellular functions and study cell-niche interactions in detail.

Engineering ECM in Disease

The ECM has a long-implicated role in disease development and progression, although the exact mechanisms often remain elusive. While the CD-ECM platform provides the opportunity to manipulate ECM and study it in detail, few studies utilized CD-ECM to study ECM mechanisms in disease (Raghunathan et al., 2018), most of them related to cancer.

It is currently well accepted that the tumor microenvironment plays a pivotal role in cancer cell behavior, including proliferation, invasiveness, metastasis and drug resistance (Serebriiskii et al., 2008). CD-ECMs provide the prospect to improve cancer models by recreating the cancer microenvironment using standard 2D, 3D cultures or more complex, organ-on-a-chip strategies (Gioiella et al., 2016; Kaukonen et al., 2017; Hoshiba, 2018). Indeed, culture of cancer cells on tumor CD-ECMs led to more physiologically relevant cancer cell phenotypes, as observed in various carcinoma (Serebriiskii et al., 2008; Eberle et al., 2011; Kaukonen et al., 2017), breast (Castelló-Cros et al., 2009; Hoshiba and Tanaka, 2013), and colon (Hoshiba, 2018) cancer

models. Increased malignancy and drug resistance of cells was observed on invasive cancer CD-ECMs, in comparison to non-invasive cancer CD-ECMs (Hoshiba and Tanaka, 2013; Hoshiba, 2018). In contrast, upon culture on MSC-derived ECM, cancer cells proliferated less (Marinkovic et al., 2016) and showed reduced tumorgenecity upon implantation (Sun et al., 2010). Differences in cancer cell behavior were attributed not only to the biochemical composition of the tumor-associated ECM, but also to changes in stiffness (Kaukonen et al., 2016; Hoshiba, 2018) and a decreased cell adhesion (Hoshiba and Tanaka, 2013).

Engineering and Characterization of CD-ECM to Study ECM Physiology

The ease of manipulating CD-ECM *in vitro* provides the opportunity to examine the reciprocal relationship between cells and their ECM.

Biochemical ECM re-engineering could be achieved through direct addition of functional groups (Xing et al., 2015) or exogenous factors (Sart et al., 2020), genetic modification (Higuchi et al., 2010) or growth factor stimulation of ECM-synthesizing cells (Wolchok and Tresco, 2012). Other changes in culture conditions, such as hypoxic cultures, were also shown to affect ECM properties and bioactivity (Hielscher, 2013).

Mechano-physical re-engineering could be achieved by culturing ECM-secreting cells in 3D sacrificial hydrogels (Yuan et al., 2018), on micro-molds (Schell et al., 2016), and micro- and nano-grooves (Ozguldez et al., 2018; Almici et al., 2020; Yang et al., 2020), forcing cell reorganization and leading to ECM assemblies with unique architectures (i.e., parallel fiber alignment). ECM postprocessing, such as cross-linking, could further alter ECM stiffness (Subbiah et al., 2016) or the overall presentation of CD-ECM.In particular, cross-linking of pepsin-solubilized CD-ECM with genipin resulted in the formation of hydrogels (Nyambat et al., 2020), Changes in biochemical and mechano-physical properties of the ECM let to changes in gene expression and behavior of reseeded cells (Kim et al., 2015; Ozguldez et al., 2018; Sart et al., 2020).

CD-ECM characterization and correlation with specific bioactivities can contribute to the mechanistic understanding of the ECM. ECM ultrastructure can be generally studied by scanning electron microscopy or atomic force microscopy (Kaukonen et al., 2016; Raghunathan et al., 2018). The latter method can also be used for biomechanical characterization (Prewitz et al., 2013; Assunção et al., 2020). Identification of proteins of interest is best performed by antibody-based assays such as immunocytochemistry or western blotting (Sart et al., 2020). Proteomic analysis based on mass spectroscopy enables the simultaneous identification of many components, however also faces challenges based on the insolubility and high complexity of the ECM (Ragelle et al., 2017; Senthebane et al., 2018; Silva et al., 2019). Furthermore, additional methods, such as Raman microscopy, can be used for biochemical characterization (Brauchle and Schenke-Layland, 2013).

CD-ECM Applications in TERM

CD-ECM uses for TERM have been increasingly explored, either with CD-ECM alone or integrated in biomaterials. 3D scaffolds purely composed of CD-ECM were produced by decellularizing stacked cell sheets (McAllister et al., 2009) and pellets (Zwolinski et al., 2011), or depositing ECM in sacrificial materials, such as hollow tubes (ECM fibers) (Roberts et al., 2017) and foams (ECM porous scaffolds) (Wolchok and Tresco, 2010; **Figure 1B**).

For applications that require specific mechanical properties of the biomaterials, CD-ECM was integrated with synthetic materials, forming hybrid scaffolds (Schenke-Layland et al., 2009; Carvalho et al., 2019b; Sart et al., 2020). Hybrid materials met mechanical requirements, while providing adequate biochemical stimuli, thus facilitating implant integration and functionality (Silva et al., 2020). Commonly, CD-ECM was utilized as a coating by simply decellularizing cells on the biomaterial surface (Kumar et al., 2016; Junka et al., 2020), although solubilized CD-ECM was also used as a coating (Decaris et al., 2012). A more sophisticated approach introduced azide-modified monosaccharides into culture media, which subsequently were incorporated into the ECM. The CD-ECM could then be covalently "clicked" to material surfaces (Ruff et al., 2017). Alternative approaches directly incorporated CD-ECM into the biomaterial during synthesis (e.g., electro-spinning) (Schenke-Layland et al., 2009; Carvalho et al., 2019b).

CD-ECMs based biomaterials were mainly investigated for skeletal and cardiovascular repair, although other applications such as in skin (Suhaeri et al., 2018) and peripheral nerve repair (Gu et al., 2017) were also explored.

CD-ECM for Skeletal Repair

Most approaches to engineer CD-ECM-carrying bone implants utilized inorganic materials (reviewed in Zhang et al., 2016), such as meshes and scaffolds (Kang et al., 2012; Antebi et al., 2015; Kim et al., 2015; Jeon et al., 2016; Kumar et al., 2016; Noh et al., 2016; Junka et al., 2020; Silva et al., 2020). These were coated with ECM assembled by collagen I-overexpressing epithelial cells (Noh et al., 2016), fibroblasts (Kim et al., 2015), MSCs (Kang et al., 2011; Silva et al., 2020), endothelial cells (Kang et al., 2012), osteoblasts (Jeon et al., 2016; Kumar et al., 2016) and combinations thereof (Junka et al., 2020). CD-ECM coated scaffolds promoted attachment, proliferation, and bone-like tissue formation *in vitro*. In a more advanced approach, Kim et al. (2015) enhanced an PLGA/PLA-based mesh scaffold coated with CD-ECM, by covalently conjugating heparin to the ECM. The heparin then acted as a growth factor reservoir for bone morphogenic protein-2 (BMP2), thereby promoting bone healing *in vivo* (Kim et al., 2015). CD-ECM was also used to increase retention of osteogenically precommitted MSCs on biomaterial surfaces after implantation. This revitalized ECM successfully repaired mouse calvaria defects (Zeitouni et al., 2012).

Therapeutic approaches targeting cartilage repair mainly utilized 3D scaffolds purely composed of CD-ECM (Jin et al., 2007; Tang et al., 2013, 2014) or CD-ECM-loaded hydrogels (Yuan et al., 2013). Indeed, 3D scaffolds of chondrocyte- and MSC-derived ECM reseeded with chondrocytes induced ectopic

hyaline-like cartilage formation *in vivo* (Jin et al., 2007; Tang et al., 2013). When applied to an osteochondral defect together with bone marrow stimulation, autologous MSC-derived ECM could enhance cartilage repair (Tang et al., 2014). In another study, a protective effect on the degenerating cartilage could be demonstrated, when collagen I microspheres containing nucleus pulposus CD-ECM and MSCs were injected into a rabbit degenerative disc model (Yuan et al., 2013).

CD-ECM for Cardiovascular Tissue Engineering and Repair

CD-ECMs have been explored as cardiac patches for cell-delivery (Schmuck et al., 2014; Kim et al., 2019), as well as to engineer heart valves replacements (Weber et al., 2013) and blood vessel grafts (McAllister et al., 2009; Syedain et al., 2014; Xing et al., 2017).

Cardiac patches were composed of fibroblast ECM alone (Schmuck et al., 2014) or combined with a polyvinyl alcohol sheet, resulting in a stretchable scaffold for cell delivery. Application of the latter in a rat myocardial infarct model resulted in improved cardiac remodeling (Kim et al., 2019).

A cardiac valve prototype containing vein-derived fibroblast ECM was implanted in a non-human primate. Albeit valve functionality was reduced, there was a significant improvement in repopulation by host cells, when compared to decellularized human heart valves (Weber et al., 2013).

McAllister et al. (2009) utilized partially devitalized autologous fibroblast/endothelial CD-ECM sheets to form vascular access grafts for dialysis patients. Complete remodeling and repopulation of CD-ECM occurred, although diffuse dilation of the graft was observed (McAllister et al., 2009).

In order to improve this low graft resistance, Syedain et al. (2014) stimulated tubular fibroblast cultures in a pulsed-flow-stretch bioreactor. Upon implantation of the decellularized graft into the femoral artery of sheep, no dilation was observed. Once completely recellularized, the grafts resembled native vessels in terms of cellular composition, ECM architecture and mechanical properties (Syedain et al., 2014).

CONCLUSION AND OUTLOOK

Although CD-ECM was continuously explored for over three decades and many safety concerns associated with tissue-derived products can be addressed, relatively slow advancements were made over the years. This can be partially attributed to the low amounts of CD-ECM that can be harvested *in vitro*, indicating that strategies for upscaling processes as well as manufacturing of larger 3D constructs need to be developed.

In addition, most TERM approaches used unmodified ECM from MSCs or tissue-specific cell types to induce cellular responses *in vitro* and *in vivo*. And although various approaches on how to re-engineer the CD-ECM are proposed, relatively few are applied to address scientific questions or to manufacture biomaterials with enhanced desired bioactivities. The reason for the limited progress can be partially attributed to our restricted fundamental understanding of the ECM. Hence, functional studies in combination with CD-ECM characterization will have to be adopted. Another reason is that re-engineering approaches are mainly focused on biological manipulation. Research at the interface to other disciplines such as materials science is indeed required to enable further evolvement of the CD-ECM research field. Future applications could focus on bio-inks with tailor-made bioactivities for 3D bioprinting or improved biomimetic cell niches in organ-on-a-chip approaches.

In conclusion, CD-ECM based research is far from its full potential. Advancements in methodologies as well as innovative interdisciplinary approaches are needed to pave the way for an exciting next generation of CD-ECMs for basic research and therapeutic approaches.

AUTHOR CONTRIBUTIONS

All authors contributed to the elaboration of this review.

FUNDING

This study was financially supported by a laboratory start-up grant (8508266) from the Chinese University of Hong Kong (CUHK) and by the Innovation and Technology Commission—Hong Kong (Innovation and Technology Commission of Hong Kong Special Administrative Government) (ITS/116/19) and the Postdoctoral Hub for ITF projects (PiH/007/20).

ACKNOWLEDGMENTS

MA would like to acknowledge School of Biomedical Sciences (The Chinese University of Hong Kong) for her post-graduate scholarship.

REFERENCES

Aamodt, J. M., and Grainger, D. W. (2016). Extracellular matrix-based biomaterial scaffolds and the host response. *Biomaterials* 86, 68–82. doi: 10.1016/j.biomaterials.2016.02.003

Ahlfors, J.-E. W., and Billiar, K. L. (2007). Biomechanical and biochemical characteristics of a human fibroblast-produced and remodeled matrix. *Biomaterials* 28, 2183–2191. doi: 10.1016/j.biomaterials.2006.12.030

Almici, E., Caballero, D., Montero Boronat, J., and Samitier Martí, J. (2020). Engineering cell-derived matrices with controlled 3D architectures for pathophysiological studies. *Methods Cell Biol.* 156, 161–183. doi: 10.1016/bs.mcb.2019.11.022

Ang, X. M., Lee, M. H. C., Blocki, A., Chen, C., Ong, L. L. S., Asada, H. H., et al. (2014). Macromolecular crowding amplifies adipogenesis of human bone marrow-derived mesenchymal stem cells by enhancing the pro-adipogenic microenvironment. *Tissue Eng. Part A* 20, 966–981. doi: 10.1089/ten.tea.2013.0337

Antebi, B., Zhang, Z., Wang, Y., Lu, Z., Chen, X.-D., and Ling, J. (2015). Stromal-cell-derived extracellular matrix promotes the proliferation and retains the osteogenic differentiation capacity of mesenchymal stem cells on three-dimensional scaffolds. *Tissue*

Eng. Part C. Methods 21, 171–181. doi: 10.1089/ten.TEC.2014.0092

Assunção, M., Wong, C. W., Richardson, J. J., Tsang, R., Beyer, S., Raghunath, M., et al. (2020). Macromolecular dextran sulfate facilitates extracellular matrix deposition by electrostatic interaction independent from a macromolecular crowding effect. *Mater. Sci. Eng. C* 106:110280. doi: 10.1016/j.msec.2019.110280

Blocki, A., Wang, Y., Koch, M., Goralczyk, A., Beyer, S., Agarwal, N., et al. (2015). Sourcing of an alternative pericyte-like cell type from peripheral blood in clinically relevant numbers for therapeutic angiogenic applications. *Mol. Ther.* 23, 510–522. doi: 10.1038/mt.2014.232

Bourget, J.-M., Gauvin, R., Larouche, D., Lavoie, A., Labbé, R., Auger, F. A., et al. (2012). Human fibroblast-derived ECM as a scaffold for vascular tissue engineering. *Biomaterials* 33, 9205–9213. doi: 10.1016/j.biomaterials.2012.09.015

Brauchle, E., and Schenke-Layland, K. (2013). Raman spectroscopy in biomedicine - non-invasive in vitro analysis of cells and extracellular matrix components in tissues. *Biotechnol. J.* 8, 288–297. doi: 10.1002/biot.201200163

Carvalho, M. S., Silva, J. C., Cabral, J. M. S. S., da Silva, C. L., Vashishth, D., Silva, C. L., et al. (2019a). Cultured cell-derived extracellular matrices to enhance the osteogenic differentiation and angiogenic properties of human mesenchymal stem/stromal cells. *J. Tissue Eng. Regen. Med.* 13, 1544–1558. doi: 10.1002/term.2907

Carvalho, M. S., Silva, J. C., Udangawa, R. N., Cabral, J. M. S., Ferreira, F. C., da Silva, C. L., et al. (2019b). Co-culture cell-derived extracellular matrix loaded electrospun microfibrous scaffolds for bone tissue engineering. *Mater. Sci. Eng. C* 99, 479–490. doi: 10.1016/j.msec.2019.01.127

Castelló-Cros, R., Khan, D. R., Simons, J., Valianou, M., and Cukierman, E. (2009). Staged stromal extracellular 3D matrices differentially regulate breast cancer cell responses through PI3K and beta1-integrins. *BMC Cancer* 9:94. doi: 10.1186/1471-2407-9-94

Chen, C., Loe, F., Blocki, A., Peng, Y., and Raghunath, M. (2011). Applying macromolecular crowding to enhance extracellular matrix deposition and its remodeling in vitro for tissue engineering and cell-based therapies. *Adv. Drug Deliv. Rev.* 63, 277–290. doi: 10.1016/j.addr.2011.03.003

Chen, X.-D., Dusevich, V., Feng, J. Q., Manolagas, S. C., and Jilka, R. L. (2007). Extracellular matrix made by bone marrow cells facilitates expansion of marrow-derived mesenchymal progenitor cells and prevents their differentiation into osteoblasts. *J. Bone Miner. Res.* 22, 1943–1956. doi: 10.1359/jbmr.070725

Cheng, H.-W., Tsui, Y.-K., Cheung, K. M. C., Chan, D., and Chan, B. P. (2009). Decellularization of chondrocyte-encapsulated collagen microspheres: a three-dimensional model to study the effects of acellular matrix on stem cell fate. *Tissue Eng. Part C Methods* 15, 697–706. doi: 10.1089/ten.tec.2008.0635

Cigognini, D., Gaspar, D., Kumar, P., Satyam, A., Alagesan, S., Sanz-Nogués, C., et al. (2016). Macromolecular crowding meets oxygen tension in human mesenchymal stem cell culture - A step closer to physiologically relevant in vitro organogenesis. *Sci. Rep.* 6:30746. doi: 10.1038/srep30746

Crapo, P. M., Gilbert, T. W., and Badylak, S. F. (2011). An overview of tissue and whole organ decellularization processes. *Biomaterials* 32, 3233–3243. doi: 10.1016/j.biomaterials.2011.01.057

Davis, G. E., and Senger, D. R. (2005). Endothelial extracellular matrix: biosynthesis, remodeling, and functions during vascular morphogenesis and neovessel stabilization. *Circ. Res.* 97, 1093-1107. doi: 10.1161/01.RES.0000191547.64391.e3

Decaris, M. L., Binder, B. Y., Soicher, M. A., Bhat, A., and Leach, J. K. (2012). Cell-derived matrix coatings for polymeric scaffolds. *Tissue Eng. Part A* 18, 2148–2157. doi: 10.1089/ten.tea.2011.0677

Distler, J. H. W., Jüngel, A., Pileckyte, M., Zwerina, J., Michel, B. A., Gay, R. E., et al. (2007). Hypoxia-induced increase in the production of extracellular matrix proteins in systemic sclerosis. *Arthritis Rheum.* 56, 4203–4215. doi: 10.1002/art.23074

Du, H.-C., Jiang, L., Geng, W.-X., Li, J., Zhang, R., Dang, J.-G., et al. (2017). Growth factor-reinforced ecm fabricated from chemically hypoxic msc sheet with improved in vivo wound repair activity. *Biomed. Res. Int.* 2017, 1–11. doi: 10.1155/2017/2578017

Eberle, K. E., Sansing, H. A., Szaniszlo, P., Resto, V. A., and Berrier, A. L. (2011). Carcinoma matrix controls resistance to cisplatin through talin regulation of NF-kB. *PLoS One* 6:e21496. doi: 10.1371/journal.pone.0021496

Faulk, D. M. M., Carruthers, C. A. A., Warner, H. J. J., Kramer, C. R. R., Reing, J. E. E., Zhang, L., et al. (2014). The effect of detergents on the basement membrane complex of a biologic scaffold material. *Acta Biomater.* 10, 183–193. doi: 10.1016/j.actbio.2013.09.006

Gaspar, D., Fuller, K. P., and Zeugolis, D. I. (2019). Polydispersity and negative charge are key modulators of extracellular matrix deposition under macromolecular crowding conditions. *Acta Biomater.* 88, 197–210. doi: 10.1016/j.actbio.2019.02.050

Gilpin, A., and Yang, Y. (2017). Decellularization strategies for regenerative medicine: from processing techniques to applications. *Biomed. Res. Int.* 2017, 1–13. doi: 10.1155/2017/9831534

Gioiella, F., Urciuolo, F., Imparato, G., Brancato, V., and Netti, P. A. (2016). An engineered breast cancer model on a chip to replicate ECM-activation in vitro during tumor progression. *Adv. Healthc. Mater.* 5, 3074–3084. doi: 10.1002/adhm.201600772

Goh, S.-K., Olsen, P., and Banerjee, I. (2013). Extracellular matrix aggregates from differentiating embryoid bodies as a scaffold to support ESC proliferation and differentiation. *PLoS One* 8:e61856. doi: 10.1371/journal.pone.0061856

Grant, R., Hay, D. C., and Callanan, A. (2017). A drug-induced hybrid electrospun poly-capro-lactone: cell-derived extracellular matrix scaffold for liver tissue engineering. *Tissue Eng. Part A* 23, 650–662. doi: 10.1089/ten.tea.2016.0419

Grinnell, F., Fukamizu, H., Pawelek, P., and Nakagawa, S. (1989). Collagen processing, crosslinking, and fibril bundle assembly in matrix produced by fibroblasts in long-term cultures supplemented with ascorbic acid. *Exp. Cell Res.* 181, 483–491. doi: 10.1016/0014-4827(89)90105-5

Gu, Y., Li, Z., Huang, J., Wang, H., Gu, X., and Gu, J. (2017). Application of marrow mesenchymal stem cell- derived extracellular matrix in peripheral nerve tissue engineering. *J. Tissue Eng. Regen. Med.* 11, 2250–2260. doi: 10.1002/term

Guo, X., Li, W., Ma, M., Lu, X., and Zhang, H. (2017). Endothelial cell-derived matrix promotes the metabolic functional maturation of hepatocyte via integrin-Src signalling. *J. Cell. Mol. Med.* 21, 2809–2822. doi: 10.1111/jcmm.13195

Hielscher, A. (2013). Hypoxia affects the structure of breast cancer cell-derived matrix to support angiogenic responses of endothelial cells. *J. Carcinog. Mutagen* Suppl. 13:005. doi: 10.4172/2157-2518.s13-005

Higuchi, Y., Shiraki, N., Yamane, K., Qin, Z., Mochitate, K., Araki, K., et al. (2010). Synthesized basement membranes direct the differentiation of mouse embryonic stem cells into pancreatic lineages. *J. Cell Sci.* 123, 2733–2742. doi: 10.1242/jcs.066886

Hoshiba, T. (2017). Cultured cell-derived decellularized matrices: a review towards the next decade. *Royal Soc. Chem.* 5, 4322-4331. doi: 10.1039/c7tb00074j

Hoshiba, T. (2018). An extracellular matrix (ECM) model at high malignant colorectal tumor increases chondroitin sulfate chains to promote epithelial-mesenchymal transition and chemoresistance acquisition. *Exp. Cell Res.* 370, 571–578. doi: 10.1016/j.yexcr.2018.07.022

Hoshiba, T., Chen, G., Endo, C., Maruyama, H., Wakui, M., Nemoto, E., et al. (2016). *Decellularized Extracellular Matrix As an in Vitro Model to Study the Comprehensive Roles of the ECM in Stem Cell Differentiation*. New York, NY: Hindawi Publishing Corporation, doi: 10.1155/2016/6397820

Hoshiba, T., Sugano, Y., and Yokoyama, N. (2018). Murine neural stem cell (NSC) line, MEB5-derived decellularized matrix as an in vitro extracellular matrix model in NSC Niche. *Chem. Lett.* 47, 1498–1501. doi: 10.1246/cl.180788

Hoshiba, T., and Tanaka, M. (2013). Breast cancer cell behaviors on staged tumorigenesis-mimicking matrices derived from tumor cells at various malignant stages. *Biochem. Biophys. Res. Commun.* 439, 291–296. doi: 10.1016/j.bbrc.2013.08.038

Hussey, G. S., Dziki, J. L., and Badylak, S. F. (2018). Extracellular matrix-based materials for regenerative medicine. *Nat. Rev. Mater.* 3, 159–173. doi: 10.1038/s41578-018-0023-x

Jeon, H., Lee, J., Lee, H., and Kim, G. H. (2016). Nanostructured surface of electrospun PCL/dECM fibres treated with oxygen plasma for tissue engineering. *RSC Adv.* 6, 32887–32896. doi: 10.1039/C6RA03840A

Jeon, J., Lee, M. S., and Yang, H. S. (2018). Differentiated osteoblasts derived decellularized extracellular matrix to promote osteogenic

differentiation. *Biomater. Res.* 22:4. doi: 10.1186/s40824-018-0115-0

Jin, C. Z., Park, S. R., Choi, B. H., Park, K., and Min, B.-H. (2007). In vivo cartilage tissue engineering using a cell-derived extracellular matrix scaffold. *Artif. Organs* 31, 183–192. doi: 10.1111/j.1525-1594.2007.00363.x

Junka, R., Quevada, K., and Yu, X. (2020). Acellular polycaprolactone scaffolds laden with fibroblast/endothelial cell-derived extracellular matrix for bone regeneration. *J. Biomed. Mater. Res. Part A* 108, 351–364. doi: 10.1002/jbm.a.36821

Kang, Y., Kim, S., Bishop, J., Khademhosseini, A., and Yang, Y. (2012). The osteogenic differentiation of human bone marrow MSCs on HUVEC-derived ECM and β-TCP scaffold. *Biomaterials* 33, 6998–7007. doi: 10.1016/j.biomaterials.2012.06.061

Kang, Y., Kim, S., Khademhosseini, A., and Yang, Y. (2011). Creation of bony microenvironment with CaP and cell-derived ECM to enhance human bone-marrow MSC behavior and delivery of BMP-2. *Biomaterials* 32, 6119–6130. doi: 10.1016/j.biomaterials.2011.05.015

Kanninen, L. K., Porola, P., Niklander, J., Malinen, M. M., Corlu, A., Guguen-Guillouzo, C., et al. (2016). Hepatic differentiation of human pluripotent stem cells on human liver progenitor HepaRG-derived acellular matrix. *Exp. Cell Res.* 341, 207–217. doi: 10.1016/J.YEXCR.2016.02.006

Kaukonen, R., Jacquemet, G., Hamidi, H., and Ivaska, J. (2017). Cell-derived matrices for studying cell proliferation and directional migration in a complex 3D microenvironment. *Nat. Protoc.* 12, 2376–2390. doi: 10.1038/nprot.2017.107

Kaukonen, R., Mai, A., Georgiadou, M., Saari, M., De Franceschi, N., Betz, T., et al. (2016). Normal stroma suppresses cancer cell proliferation via mechanosensitive regulation of JMJD1a-mediated transcription. *Nat. Commun.* 7:12237. doi: 10.1038/ncomms12237

Kim, I. G., Hwang, M. P., Du, P., Ko, J., Ha, C., Do, S. H., et al. (2015). Bioactive cell-derived matrices combined with polymer mesh scaffold for osteogenesis and bone healing. *Biomaterials* 50, 75–86. doi: 10.1016/j.biomaterials.2015.01.054

Kim, I. G., Hwang, M. P., Park, J. S., Kim, S. S.-H., Kim, J.-H. J., Kang, H. J., et al. (2019). Stretchable ECM patch enhances stem cell delivery for Post-MI cardiovascular repair. *Adv. Healthc. Mater.* 8:e1900593. doi: 10.1002/adhm.201900593

Klimanskaya, I., Chung, Y., Meisner, L., Johnson, J., West, M. D., and Lanza, R. (2005). Human embryonic stem cells derived without feeder cells. *Lancet* 365, 1636–1641. doi: 10.1016/S0140-6736(05)66473-2

Kumar, A., Nune, K. C., and Misra, R. D. K. (2016). Biological functionality and mechanistic contribution of extracellular matrix-ornamented three dimensional Ti-6Al-4V mesh scaffolds. *J. Biomed. Mater. Res. Part A* 104, 2751–2763. doi: 10.1002/jbm.a.35809

Kumar, P., Satyam, A., Cigognini, D., Pandit, A., and Zeugolis, D. I. (2018). Low oxygen tension and macromolecular crowding accelerate extracellular matrix deposition in human corneal fibroblast culture. *J. Tissue Eng. Regen. Med.* 12, 6–18. doi: 10.1002/term.2283

Kumar, P., Satyam, A., Fan, X., Collin, E., Rochev, Y., Rodriguez, B. J., et al. (2015). Macromolecularly crowded in vitro microenvironments accelerate the production of extracellular matrix-rich supramolecular assemblies. *Sci. Rep.* 5:8729. doi: 10.1038/srep08729

Lai, Y., Sun, Y., Skinner, C. M., Son, E. L., Lu, Z., Tuan, R. S., et al. (2010). Reconstitution of marrow-derived extracellular matrix ex vivo: a robust culture system for expanding large-scale highly functional human mesenchymal stem cells. *Stem Cells Dev.* 19, 1095–1107. doi: 10.1089/scd.2009.0217

Lareu, R. R., Harve, K. S., and Raghunath, M. (2007). Emulating a crowded intracellular environment in vitro dramatically improves RT-PCR performance. *Biochem. Biophys. Res. Commun.* 363, 171–177. doi: 10.1016/j.bbrc.2007.08.156

Lee, B. J., Hegewisch Solloa, E., Shannon, M. J., and Mace, E. M. (2020). Generation of cell-derived matrices that support human NK cell migration and differentiation. *J. Leukoc. Biol* 108, MA0420–MA635. doi: 10.1002/JLB.1MA0420-635R

Levorson, E. J., Hu, O., Mountziaris, P. M., Kasper, F. K., and Mikos, A. G. (2014). Cell-derived polymer/extracellular matrix composite scaffolds for cartilage regeneration, part 2: construct devitalization and determination of chondroinductive capacity. *Tissue Eng. Part C Methods* 20, 358–372. doi: 10.1089/ten.tec.2013.0288

Lin, H., Yang, G., Tan, J., and Tuan, R. S. (2012). Influence of decellularized matrix derived from human mesenchymal stem cells on their proliferation, migration and multi-lineage differentiation potential. *Biomaterials* 33, 4480–4489. doi: 10.1016/J.BIOMATERIALS.2012.03.012

Liu, X., Zhou, L., Chen, X., Liu, T., Pan, G., Cui, W., et al. (2016). Culturing on decellularized extracellular matrix enhances antioxidant properties of human umbilical cord-derived mesenchymal stem cells. *Mater. Sci. Eng. C* 61, 437–448. doi: 10.1016/j.msec.2015.12.090

Lu, H., Hoshiba, T., Kawazoe, N., Koda, I., Song, M., and Chen, G. (2011). Cultured cell-derived extracellular matrix scaffolds for tissue engineering. *Biomaterials* 32, 9658–9666. doi: 10.1016/j.biomaterials.2011.08.091

Maia, F. R., Reis, R. L., and Oliveira, J. M. (2020). Decellularized hASCs-derived matrices as biomaterials for 3D in vitro approaches. *Methods Cell Biol.* 156, 45–58. doi: 10.1016/bs.mcb.2019.11.019

Marinkovic, M., Block, T. J., Rakian, R., Li, Q., Wang, E., Reilly, M. A., et al. (2016). One size does not fit all: developing a cell-specific niche for in vitro study of cell behavior. *Matrix Biol.* 5:426. doi: 10.1016/J.MATBIO.2016.01.004

McAllister, T. N., Maruszewski, M., Garrido, S. A., Wystrychowski, W., Dusserre, N., Marini, A., et al. (2009). Effectiveness of haemodialysis access with an autologous tissue-engineered vascular graft: a multicentre cohort study. *Lancet* 373, 1440–1446. doi: 10.1016/S0140-6736(09)60248-8

Noh, Y. K., Du, P., Kim, I. G., Ko, J., Kim, S. W., and Park, K. (2016). Polymer mesh scaffold combined with cell-derived ECM for osteogenesis of human mesenchymal stem cells. *Biomater. Res.* 20:6. doi: 10.1186/s40824-016-0055-5

Nyambat, B., Manga, Y. B., Chen, C.-H., Gankhuyag, U., Pratomo, W. P. A., Kumar Satapathy, M., et al. (2020). New insight into natural extracellular matrix: genipin cross-linked adipose-derived stem cell extracellular matrix gel for tissue engineering. *Int. J. Mol. Sci.* 21:4864. doi: 10.3390/ijms21144864

Ozbek, S., Balasubramanian, P. G., Chiquet-Ehrismann, R., Tucker, R. P., and Adams, J. C. (2010). The evolution of extracellular matrix. *Mol. Biol. Cell* 21, 4300–4305. doi: 10.1091/mbc.E10-03-0251

Ozguldez, H. O., Cha, J., Hong, Y., Koh, I., and Kim, P. (2018). Nanoengineered, cell-derived extracellular matrix influences ECM-related gene expression of mesenchymal stem cells. *Biomater. Res.* 22:32. doi: 10.1186/s40824-018-0141-y

Pei, M., He, F., and Kish, V. L. (2011). Expansion on extracellular matrix deposited by human bone marrow stromal cells facilitates stem cell proliferation and tissue-specific lineage potential. *Tissue Eng. Part A* 17, 3067–3076. doi: 10.1089/ten.TEA.2011.0158

Pinnell, S. R. (1985). Regulation of collagen biosynthesis by ascorbic acid: a review. *Yale J. Biol. Med.* 58, 553–559.

Prewitz, M. C., Seib, F. P., von Bonin, M., Friedrichs, J., Stißel, A., Niehage, C., et al. (2013). Tightly anchored tissue-mimetic matrices as instructive stem cell microenvironments. *Nat. Methods* 10, 788–794. doi: 10.1038/nmeth.2523

Ragelle, H., Naba, A., Larson, B. L., Zhou, F., Prijiæ, M., Whittaker, C. A., et al. (2017). Comprehensive proteomic characterization of stem cell-derived extracellular matrices. *Biomaterials* 128, 147–159. doi: 10.1016/j.biomaterials.2017.03.008

Raghunathan, V. K., Benoit, J., Kasetti, R., Zode, G., Salemi, M., Phinney, B. S., et al. (2018). Glaucomatous cell derived matrices differentially modulate non-glaucomatous trabecular meshwork cellular behavior. *Acta Biomater.* 71, 444–459. doi: 10.1016/j.actbio.2018.02.037

Roberts, K., Schluns, J., Walker, A., Jones, J. D., Quinn, K. P., Hestekin, J., et al. (2017). Cell derived extracellular matrix fibers synthesized using sacrificial hollow fiber membranes. *Biomed. Mater.* 13:015023. doi: 10.1088/1748-605X/aa895c

Ruff, S. M. M., Keller, S., Wieland, D. E. E., Wittmann, V., Tovar, G. E. M. E. M., Bach, M., et al. (2017). clickECM: development of a cell-derived extracellular matrix with azide functionalities. *Acta Biomater.* 52, 159–170. doi: 10.1016/j.actbio.2016.12.022

Sart, S., Jeske, R., Chen, X., Ma, T., and Li, Y. (2020). Engineering stem cell-derived extracellular matrices: decellularization, characterization, and biological function. *Tissue Eng. Part B Rev.* 26:ten.teb.2019.0349. doi: 10.1089/ten.teb.2019.0349

Sart, S., Ma, T., and Li, Y. (2014). Extracellular matrices decellularized from embryonic stem cells maintained their structure and signaling specificity. *Tissue Eng. Part A* 20, 54–66. doi: 10.1089/ten.tea.2012.0690

Satyam, A., Kumar, P., Fan, X., Gorelov, A., Rochev, Y., Joshi, L., et al. (2014). Macromolecular crowding meets tissue engineering by self-assembly:

a paradigm shift in regenerative medicine. *Adv. Mater.* 26, 3024–3034. doi: 10.1002/adma.201304428

Satyam, A., Tsokos, M. G., Tresback, J. S., Zeugolis, D. I., and Tsokos, G. C. (2020). Cell-derived extracellular matrix-rich biomimetic substrate supports podocyte proliferation, differentiation, and maintenance of native phenotype. *Adv. Funct. Mater.* 30:1908752. doi: 10.1002/adfm.201908752

Schell, J. Y., Wilks, B. T., Patel, M., Franck, C., Chalivendra, V., Cao, X., et al. (2016). Harnessing cellular-derived forces in self-assembled microtissues to control the synthesis and alignment of ECM. *Biomaterials* 77, 120–129. doi: 10.1016/J.BIOMATERIALS.2015.10.080

Schenke-Layland, K., Rofail, F., Heydarkhan, S., Gluck, J. M., Ingle, N. P., Angelis, E., et al. (2009). The use of three-dimensional nanostructures to instruct cells to produce extracellular matrix for regenerative medicine strategies. *Biomaterials* 30, 4665–4675. doi: 10.1016/j.biomaterials.2009.05.033

Schmuck, E. G., Mulligan, J. D., Ertel, R. L., Kouris, N. A., Ogle, B. M., Raval, A. N., et al. (2014). Cardiac fibroblast-derived 3D extracellular matrix seeded with mesenchymal stem cells as a novel device to transfer cells to the ischemic myocardium. *Cardiovasc. Eng. Technol.* 5, 119–131. doi: 10.1007/s13239-013-0167-1

Senthebane, D., Jonker, T., Rowe, A., Thomford, N., Munro, D., Dandara, C., et al. (2018). The role of tumor microenvironment in chemoresistance: 3d extracellular matrices as accomplices. *Int. J. Mol. Sci.* 19:2861. doi: 10.3390/ijms19102861

Serebriiskii, I., Castelló-Cros, R., Lamb, A., Golemis, E. A., and Cukierman, E. (2008). Fibroblast-derived 3D matrix differentially regulates the growth and drug-responsiveness of human cancer cells. *Matrix Biol.* 27, 573–585. doi: 10.1016/j.matbio.2008.02.008

Sharma, D., Ferguson, M., and Zhao, F. (2020). A step-by-step protocol for generating human fibroblast cell-derived completely biological extracellular matrix scaffolds. *Methods Cell Biol.* 156, 3–13. doi: 10.1016/BS.MCB.2019.10.010

Silva, J. C., Carvalho, M. S., Han, X., Xia, K., Mikael, P. E., Cabral, J. M. S., et al. (2019). Compositional and structural analysis of glycosaminoglycans in cell-derived extracellular matrices. *Glycoconj. J.* 36, 141–154. doi: 10.1007/s10719-019-09858-2

Silva, J. C., Carvalho, M. S., Udangawa, R. N., Moura, C. S., Cabral, J. M. S., da Silva, C., et al. (2020). Extracellular matrix decorated polycaprolactone scaffolds for improved mesenchymal stem/stromal cell osteogenesis towards a patient-tailored bone tissue engineering approach. *J. Biomed. Mater. Res. Part B Appl. Biomater.* 108, 2153–2166. doi: 10.1002/jbm.b.34554

Subbiah, R., Hwang, M. P., Du, P., Suhaeri, M., Hwang, J. H., Hong, J. H., et al. (2016). Tunable crosslinked cell-derived extracellular matrix guides cell fate. *Macromol. Biosci.* 16, 1723–1734. doi: 10.1002/mabi.201600280

Suhaeri, M., Noh, M. H., Moon, J., Kim, I. G., Oh, S. J., Ha, S. S., et al. (2018). Novel skin patch combining human fibroblast-derived matrix and ciprofloxacin for infected wound healing. *Theranostics* 8, 5025–5038. doi: 10.7150/thno.26837

Sun, B., Yu, K.-R. R., Bhandari, D. R., Jung, J.-W. W., Kang, S.-K. K., and Kang, K.-S. S. (2010). Human umbilical cord blood mesenchymal stem cell-derived extracellular matrix prohibits metastatic cancer cell MDA-MB-231 proliferation. *Cancer Lett.* 296, 178–185. doi: 10.1016/j.canlet.2010.04.007

Sun, Y., Li, W., Lu, Z., Chen, R., Ling, J., Ran, Q., et al. (2011). Rescuing replication and osteogenesis of aged mesenchymal stem cells by exposure to a young extracellular matrix. *FASEB J.* 25, 1474–1485. doi: 10.1096/fj.10-161497

Syedain, Z. H., Meier, L. A., Lahti, M. T., Johnson, S. L., and Tranquillo, R. T. (2014). Implantation of completely biological engineered grafts following decellularization into the sheep femoral artery. *Tissue Eng. Part A* 20, 1726–1734. doi: 10.1089/ten.TEA.2013.0550

Tang, C., Jin, C., Du, X., Yan, C., Min, B.-H., Xu, Y., et al. (2014). An autologous bone marrow mesenchymal stem cell-derived extracellular matrix scaffold applied with bone marrow stimulation for cartilage repair. *Tissue Eng. Part A* 20, 2455–2462. doi: 10.1089/ten.TEA.2013.0464

Tang, C., Xu, Y., Jin, C., Min, B.-H., Li, Z., Pei, X., et al. (2013). Feasibility of autologous bone marrow mesenchymal stem cell-derived extracellular matrix scaffold for cartilage tissue engineering. *Artif. Organs* 37, E179–E190. doi: 10.1111/aor.12130

Theocharis, A. D., Skandalis, S. S., Gialeli, C., and Karamanos, N. K. (2016). *Extracellular matrix structure*. Amsterdam: Elsevier, doi: 10.1016/j.addr.2015.11.001

Weber, B., Dijkman, P. E., Scherman, J., Sanders, B., Emmert, M. Y., Grünenfelder, J., et al. (2013). Off-the-shelf human decellularized tissue-engineered heart valves in a non-human primate model. *Biomaterials* 34, 7269–7280. doi: 10.1016/j.biomaterials.2013.04.059

Wei, B., Guo, Y., Xu, Y., Mao, F., Yao, Q., Jin, C., et al. (2015). Composite scaffolds composed of bone marrow mesenchymal stem cell-derived extracellular matrix and marrow clots promote marrow cell retention and proliferation. *J. Biomed. Mater. Res. Part A* 103, 2374–2382. doi: 10.1002/jbm.a.35373

Wolchok, J. C., and Tresco, P. A. (2010). The isolation of cell derived extracellular matrix constructs using sacrificial open-cell foams. *Biomaterials* 31, 9595–9603. doi: 10.1016/J.BIOMATERIALS.2010.08.072

Wolchok, J. C., and Tresco, P. A. (2012). Using growth factor conditioning to modify the properties of human cell derived extracellular matrix. *Biotechnol. Prog.* 28, 1581–1587. doi: 10.1002/btpr.1625

Woods, T., and Gratzer, P. F. (2005). Effectiveness of three extraction techniques in the development of a decellularized bone-anterior cruciate ligament-bone graft. *Biomaterials* 26, 7339–7349. doi: 10.1016/j.biomaterials.2005.05.066

Xiao, B., Rao, F., Guo, Z., Sun, X., Wang, Y., Liu, S.-Y., et al. (2016). Extracellular matrix from human umbilical cord-derived mesenchymal stem cells as a scaffold for peripheral nerve regeneration. *Neural Regen. Res.* 11:1172. doi: 10.4103/1673-5374.187061

Xing, H., Lee, H., Luo, L., and Kyriakides, T. R. (2020). Extracellular matrix-derived biomaterials in engineering cell function. *Biotechnol. Adv.* 42:107421. doi: 10.1016/J.BIOTECHADV.2019.107421

Xing, Q., Qian, Z., Tahtinen, M., Yap, A. H., Yates, K., and Zhao, F. (2017). Aligned nanofibrous cell-derived extracellular matrix for anisotropic vascular graft construction. *Adv. Healthc. Mater.* 6:1601333. doi: 10.1002/adhm.201601333

Xing, Q., Zhang, L., Redman, T., Qi, S., and Zhao, F. (2015). Nitric oxide regulates cell behavior on an interactive cell-derived extracellular matrix scaffold. *J. Biomed. Mater. Res. - Part A* 103, 3807–3814. doi: 10.1002/jbm.a.35524

Xiong, X., Yang, X., Dai, H., Feng, G., Zhang, Y., Zhou, J., et al. (2019). Extracellular matrix derived from human urine-derived stem cells enhances the expansion, adhesion, spreading, and differentiation of human periodontal ligament stem cells. *Stem Cell Res. Ther.* 10:396. doi: 10.1186/s13287-019-1483-7

Yan, J., Chen, X., Pu, C., Zhao, Y., Liu, X., Liu, T., et al. (2020). Synovium stem cell-derived matrix enhances anti-inflammatory properties of rabbit articular chondrocytes via the SIRT1 pathway. *Mater. Sci. Eng. C* 106:110286. doi: 10.1016/j.msec.2019.110286

Yang, L., Ge, L., and van Rijn, P. (2020). Synergistic effect of cell-derived extracellular matrices and topography on osteogenesis of mesenchymal stem cells. *ACS Appl. Mater. Interfaces* 12, 25591-25603. doi: 10.1021/ACSAMI.0C05012

Yang, L., Jiang, Z., Zhou, L., Zhao, K., Ma, X., and Cheng, G. (2017). Hydrophilic cell-derived extracellular matrix as a niche to promote adhesion and differentiation of neural progenitor cells. *RSC Adv.* 7, 45587–45594. doi: 10.1039/C7RA08273H

Yang, Y., Lin, H., Shen, H., Wang, B., Lei, G., and Tuan, R. S. (2018). Mesenchymal stem cell-derived extracellular matrix enhances chondrogenic phenotype of and cartilage formation by encapsulated chondrocytes in vitro and in vivo. *Acta Biomater.* 69, 71–82. doi: 10.1016/j.actbio.2017.12.043

Yong, I., Oh, S. W., and Kim, P. (2020). Re-engineered cell-derived extracellular matrix as a new approach to clarify the role of native ECM. *Methods Cell Biol.* 156, 205–231. doi: 10.1016/BS.MCB.2019.12.007

Yuan, M., Pai, P.-J., Liu, X., Lam, H., and Chan, B. P. (2018). Proteomic analysis of nucleus pulposus cell-derived extracellular matrix niche and its effect on phenotypic alteration of dermal fibroblasts. *Sci. Rep.* 8:1512. doi: 10.1038/s41598-018-19931-9

Yuan, M., Yeung, C. W., Li, Y. Y., Diao, H., Cheung, K. M. C. M. C., Chan, D., et al. (2013). Effects of nucleus pulposus cell-derived acellular matrix on the differentiation of mesenchymal stem cells. *Biomaterials* 34, 3948–3961. doi: 10.1016/j.biomaterials.2013.02.004

Zeitouni, S., Krause, U., Clough, B. H., Halderman, H., Falster, A., Blalock, D. T., et al. (2012). Human mesenchymal stem cell-derived matrices for enhanced osteoregeneration. *Sci. Transl. Med.* 4:132ra55. doi: 10.1126/scitranslmed.3003396

Zhang, W., Yang, J., Zhu, Y., Sun, X., Guo, W., Liu, X., et al. (2019). Extracellular matrix derived by human umbilical cord-deposited mesenchymal stem

cells accelerates chondrocyte proliferation and differentiation potential in vitro. *Cell Tissue Bank.* 20, 351–365. doi: 10.1007/s10561-019-09774-7

Zhang, W., Zhu, Y., Li, J., Guo, Q., Peng, J., Liu, S., et al. (2016). Cell-derived extracellular matrix: basic characteristics and current applications in orthopedic tissue engineering. *Tissue Eng. Part B Rev.* 22, 193–207. doi: 10.1089/ten.teb.2015.0290

Zwolinski, C. M., Ellison, K. S., DePaola, N., and Thompson, D. M. (2011). Generation of cell-derived three dimensional extracellular matrix substrates from two dimensional endothelial cell cultures. *Tissue Eng. Part C Methods* 17, 589–595. doi: 10.1089/ten.tec.2010.0619

Conflict of Interest: The authors declare that the research was conducted in the absence of any commercial or financial relationships that could be construed as a potential conflict of interest.

frontiers in Bioengineering and Biotechnology

BRIEF RESEARCH REPORT
published: 04 December 2020
doi: 10.3389/fbioe.2020.579896

Primary Extracellular Matrix Enables Long-Term Cultivation of Human Tumor Oral Mucosa Models

*Leonie Gronbach[1], Philipp Jurmeister[2,3], Monika Schäfer-Korting[1], Ulrich Keilholz[4], Ingeborg Tinhofer[3,5] and Christian Zoschke[1]**

[1] Institute of Pharmacy (Pharmacology and Toxicology), Freie Universität Berlin, Berlin, Germany, [2] Institute of Pathology, Berlin Institute of Health, Humboldt-Universität zu Berlin, Corporate Member of Freie Universität Berlin, Charité – Universitätsmedizin Berlin, Berlin, Germany, [3] Heidelberg and German Cancer Consortum Partner Site Berlin, German Cancer Research Center, Berlin, Germany, [4] Comprehensive Cancer Center, Berlin Institute of Health, Humboldt-Universität zu Berlin, Corporate Member of Freie Universität Berlin, Charité – Universitätsmedizin Berlin, Berlin, Germany, [5] Department of Radiooncology and Radiotherapy, Berlin Institute of Health, Humboldt-Universität zu Berlin, Corporate Member of Freie Universität Berlin, Charité – Universitätsmedizin Berlin, Berlin, Germany*

3D tumor models clearly outperform 2D cell cultures in recapitulating tissue architecture and drug response. However, their potential in understanding treatment efficacy and resistance development should be better exploited if also long-term effects of treatment could be assessed *in vitro*. The main disadvantages of the matrices commonly used for *in vitro* culture are their limited cultivation time and the low comparability with patient-specific matrix properties. Extended cultivation periods are feasible when primary human cells produce the extracellular matrix *in situ*. Herein, we adapted the hyalograft-3D approach from reconstructed human skin to normal and tumor oral mucosa models and compared the results to bovine collagen-based models. The hyalograft models showed similar morphology and cell proliferation after 7 weeks compared to collagen-based models after 2 weeks of cultivation. Tumor thickness and VEGF expression increased in hyalograft-based tumor models, whereas expression of laminin-332, tenascin C, and hypoxia-inducible factor 1α was lower than in collagen-based models. Taken together, the *in situ* produced extracellular matrix better confined tumor invasion in the first part of the cultivation period, with continuous tumor proliferation and increasing invasion later on. This proof-of-concept study showed the successful transfer of the hyalograft approach to tumor oral mucosa models and lays the foundation for the assessment of long-term drug treatment effects. Moreover, the use of an animal-derived extracellular matrix is avoided.

Keywords: extracellular matrix, head and neck cancer, oral mucosa, personalized medicine, tissue engineering, tumor microenvironment, long-term cultivation, Hyalograft 3D

OPEN ACCESS

Edited by:
Hon Fai Chan,
The Chinese University of Hong Kong, China

Reviewed by:
Jennifer Patterson,
Instituto IMDEA Materiales, Spain
Martin Degen,
Universität Bern, Switzerland

****Correspondence:***
Christian Zoschke
christian.zoschke@fu-berlin.de

Specialty section:
This article was submitted to Biomaterials, a section of the journal Frontiers in Bioengineering and Biotechnology

Received: *03 July 2020*
Accepted: *10 November 2020*
Published: *04 December 2020*

Citation:
Gronbach L, Jurmeister P, Schäfer-Korting M, Keilholz U, Tinhofer I and Zoschke C (2020) Primary Extracellular Matrix Enables Long-Term Cultivation of Human Tumor Oral Mucosa Models. Front. Bioeng. Biotechnol. 8:579896. doi: 10.3389/fbioe.2020.579896

INTRODUCTION

Stromal, endothelial, and immune cells create a unique environment for each individual tumor with altered paracrine signaling compared to the normal tissue (Zheng and Gao, 2019). This cellular tumor microenvironment can promote tumor growth, invasion, and dissemination (Varol, 2019) as well as treatment resistance (Jo et al., 2018). The impact of the extracellular matrix

(ECM) as the major component of the tumor microenvironment in these biological processes remains contradictory or unexplored (Pickup et al., 2014; Saggioro et al., 2020). Commonly, tumors dysregulate the composition and structure of the surrounding normal tissue toward an inflamed, hypoxic, and desmoplastic tumor microenvironment (Zheng and Gao, 2019). The effect of the tumor environment on the biology of tumors of the oral cavity remains to be investigated.

Patient-specific tumor ECMs are rarely recapitulated *ex vivo*. Tumor cells are either cultivated in scaffold-free ultra-low attachment plates or embedded in collagen of animal origin, e.g., Matrigel (Langhans, 2018). Furthermore, non-human matrices like cellulose are used as scaffolds for *ex vivo* tumor models (Nath and Devi, 2016). Major drawbacks of these approaches include poor stability, limited lifespan, and underrepresentation of patient-specific tumor microenvironment components. Initially designed to better reconstruct human skin, the hyalograft-3D is a biodegradable, non-immunogenic scaffold, which consists of esterified hyaluronic acid fibers. It is certified for medical use and allows the fibroblasts to produce and assemble their own ECM (Campoccia et al., 1998). Thereby, hyalograft-based skin models extended the life by six times, compared to collagen-based skin models (Stark et al., 2006).

Recently, we developed normal and tumor oral mucosa models emulating head and neck cancer, with a collagen scaffold (Gronbach et al., 2020) to improve non-clinical drug evaluation. The 3D model showed large similarities in morphology, grading, and protein expression profiles to patient's tumors. Moreover, the tumor models recapitulated docetaxel and cetuximab effects in line with clinical observations of head and neck-cancer. However, the cultivation of the collagen-based tumor models for a maximum of 2 weeks enabled only the investigation of short-term drug effects. This represents a major limitation for studies investigating the impact of genetic heterogeneity and therapy-driven clonal evolution in acquired drug resistance in the tumor (Magdeldin et al., 2014; Braig et al., 2017).

Herein, we assessed whether by using the hyalograft-3D approach human tumor oral mucosa models could be maintained in *ex vivo* cultures for up to 7 weeks, without major changes in tumor cell viability and proliferative activity. In addition, the impact of the ECM on tumor growth and invasion in hyalograft-based tumor oral mucosa models was compared with their collagen-based counterparts.

MATERIALS AND METHODS

Materials

Collagen G, DMEM 10× and HEPES buffer were purchased from Merck (Darmstadt, Germany). Hyalograft-3D was purchased from Anika Therapeutics (Bedford, MA, United States). The thrombin-fibrinogen-solution tisseel® was purchased from Baxter (Deerfield, IL, United States).

Human oral keratinocytes and human oral fibroblasts, as well as the respective cell culture media were purchased from ScienCell (Carlsbad, CA, United States). The tumor-cell line SCC-25 from the tongue (RRID: CVCL_1682, Rheinwald and Beckett, 1981) was a generous gift from Howard Green, Dana-Farber Cancer Institute (Boston, MA, United States). The detailed composition and origin of the construct growth and construct differentiation media were described elsewhere (Gronbach et al., 2020). Here, these media were supplemented with the transforming growth factor (TGF)-β1 and aprotinin, obtained from ThermoFisher Scientific (Waltham, MA, United States) and Merck. 12-well plates and 12-well inserts (0.4 μm pore size) were obtained from Greiner bio-one (Leipzig, Germany).

Hematoxylin, eosin, rotihistol, and rotihistokit were purchased from Carl Roth (Karlsruhe, Germany). Periodic acid was from Sigma-Aldrich and Schiff's reagent was obtained from Merck. Primary antibodies were purchased from abcam (Cambridge, United Kingdom): hypoxia-inducible factor 1α (1:200; RRID: AB_880418), Ki-67 (1:100; RRID: AB_302459), laminin-332 (1:500; RRID: AB_1566368), Tenascin C (1:1000; RRID: AB_2043021), vascular endothelial growth factor (1:200; RRID: AB_299738). Cytokeratin Pan Plus KL1 antibody (1:100; RRID: AB_2864507) was from Zytomed (Berlin, Germany). Anti-mouse and anti-rabbit IgGs (H + L), with F(ab')2 Fragment (Alexa Fluor® 488 and 594 Conjugate; RRIDs: AB_1904025, AB_2714182) were obtained from Cell Signaling Technology (Danvers, MA, United States). DAPI (4′,6-Diamidin-2-phenylindol) mounting medium was purchased from dianova (Hamburg, Germany). The *in situ* cell death detection kit (TUNEL assay) was purchased from Sigma-Aldrich (Munich, Germany).

Cell Culture

Human oral keratinocytes and human oral fibroblasts (ScienCell) were cultured in oral keratinocyte and fibroblast medium, respectively, at 37°C with 5% CO_2. The SCC-25 tumor-cell line was grown in DMEM/F-12 Ham medium, supplemented with 9% fetal calf serum, 0.9% L-glutamine, and penicillin/streptomycin. The medium was changed three times a week and the cells were passaged after reaching confluency of 80%. The cell line was tested for mycoplasm and regularly checked by single nucleotide polymorphism authentication (Multiplexion; Heidelberg, Germany). Cell culture was performed according to standard operating procedures and referred to good cell culture practice.

Multilayered Oral Mucosa Model Building

The multi-layered oral mucosa models (**Figure 1A**) were constructed as a lamina propria growing underneath an epithelium. All cultures were kept at 37°C and 5% CO_2 in a humidified atmosphere. The building of collagen-based oral mucosa models was described previously (Gronbach et al., 2020). Briefly, 1×10^5 human oral fibroblasts per model were mixed with a buffered solution and added to collagen. After solidification of the matrix, construct growth medium was added to the model and changed three times until day 7. Thereafter, either 1×10^6 human oral keratinocytes or 1×10^6 SCC-25 cells were seeded onto the lamina propria compartment for normal or tumor oral mucosa models, respectively. From day 14, the construct surface was kept medium-free to expose the epithelium to the air and the construct growth medium was supplemented

with 0.25 mmol/l ascorbic acid acting as construct differentiation medium. On day 21, the models were snap frozen and stored at −80°C.

The generation of hyalograft-3D was described previously (Stark et al., 2006). In brief, the hyalograft-3D is a fleece-like matrix, composed of recombinant human hyaluronic acid fibers, esterified with benzylic alcohol to retard its degradation. Here, hyalograft-3D was cut into disks of 10 mm in diameter to fit the size of 12-well cell culture inserts. Next, 1×10^5 human oral fibroblasts per model were resuspended in a thrombin solution (10 international units/ml), mixed with a fibrinogen solution (8 mg/ml) and subsequently added to the pre-cut hyalograft-3D pieces. During the following 7 days, the fibroblasts were allowed to replace the fibrin by *in situ* produced ECM components (Stark et al., 2006). Thereafter, either human oral keratinocytes or SCC-25 cells were seeded onto the lamina propria compartment as described above for the collagen model. The construct growth medium was supplemented with 1 ng/ml transforming growth factor-β1 and 500 international units/ml aprotinin. TGF-β1 reduces keratinocyte differentiation and growth (Dahler et al., 2001). Aprotinin, a serin-protease inhibitor was used to limit fibrinolysis and thus premature model degradation. Medium was changed three times per week. From day 14, the construct surface was kept medium-free and aprotinin was reduced to 200 international units/ml in the construct differentiation medium. At the end of the cultivation period, the models were snap frozen and stored at −80°C.

Morphology and Protein Expression

The models were cut into 7 μm thick slices using a cryotome (Leica CM 1510S; Leica, Wetzlar, Germany) and fixed with 4% paraformaldehyde. The cryosections were subjected to either hematoxylin and eosin (H&E), periodic acid-Schiff (PAS), immunofluorescence staining or immunohistochemistry (IHC). For the H&E staining, slides were successively submerged into hematoxylin (5 min), water (5 min), eosin (30 s), 70 and 99.9% ethanol (2 min) and rotihistol (2 min). Finally, the slides were fixed with the rotihistokit and a cover slide. PAS staining was performed on a Tissue-Tek Prisma Plus Automated Slide Stainer (Sakura Finetech, Staufen, Germany). Slides were incubated with periodic acid for 10 min, followed by staining with Schiff's reagent for 10 min and hematoxylin for 7 min. For immunofluorescence staining, the samples were permeabilized for 5 min by a 0.5% triton solution, blocked for 30 min with 5% goat serum and incubated over night with the primary antibody at 4°C. Afterward the slides were incubated for 1 h with the secondary antibody. In the end, DAPI mounting medium was added to stain cell nuclei and fixed the samples. IHC staining was done on a BOND MAX Automated Slide Stainer (Leica) using the HP1 program and the BOND polymer Refine Detection System (Leica). Images were taken with a fluorescence microscope (BZ-8000; Keyence, Neu-Isenburg, Germany) and analyzed using the ImageJ software (Schneider et al., 2012).

Apoptosis Quantification

For apoptosis measurements, the *in situ* cell death detection kit was used according to the manufacturer's instructions. The kit detects DNA fragments in apoptotic cells based on TdT-mediated dUTP-biotin nick end labeling (TUNEL).

Data Analysis

Data are presented as the mean + standard deviation (SD) obtained from up to three independent experiments. Due to the explorative data analysis, a level of $p \leq 0.05$, calculated using non-parametric Kruskal–Wallis tests and subsequent Dunn's *Post hoc*-tests, was considered to indicate a statistically significant difference.

RESULTS

Morphological Analysis

We extended the culture period from 2 weeks of collagen-based normal oral mucosa models (c-NOM) and tumor oral mucosa models (c-TOM) to 7 weeks in hyalograft-based h-NOM and h-TOM models. To evaluate the impact of the scaffold, we cultured also h-NOM and h-TOM for 2 weeks (**Figure 1A**).

The epithelium of c-NOM models consisted of a basal layer with rounded cells and multiple layers of spinous cells, as found in non-keratinized oral mucosa (**Figure 1B**). All TOM models depicted an unstructured, hyperproliferative, and thickened epithelial layer with atypical, enlarged, irregular tumor cells and hyperchromatic nuclei. The tumor morphology appeared desmoplastic in particular in h-TOM models after 7 weeks of culture (**Figure 1B**, inserts).

The glycogen distribution was confined to the upper epithelial layers of the h-NOM model, while glycogen was found in all epithelial layers of c-NOM models (**Figure 1C**). A similar pattern was observed in TOM models after 2 weeks of culture (**Figure 1C**, inserts). Only after 7 weeks of culture the glycogen distribution became also patchy in h-TOM models. Concurrently, cytokeratin-positive tumor cells penetrated the hyalograft-3D matrix only slightly as tumor nests, but massively invaded the lamina propria compartment as single cells (**Figure 2A**). The final tumor thickness in h-TOM models exceeded tumor thickness of c-TOM models, but the difference was not statistically significant (**Figure 2B**).

The large structures in the lamina propria of hyalograft-based models were hyaluronic ester fibers, which were unspecifically stained by hematoxylin and eosin, periodic acid-Schiff as well as DAPI. The unspecific staining might be explained by the large three-dimensional structure of the fibers and their negative charge, which prevented the washout of stains as well as monoclonal antibodies, and led to the intercalation of DAPI into the fibers.

Protein Expression

The basement membrane protein laminin-332 was expressed in particular between the epithelial layer and the lamina propria in both h-NOM and c-NOM models (**Figure 2C**). In contrast, the expression of laminin-332 was more heterogeneous in TOM models with the highest levels in h-TOM models after 2 weeks of culture (**Figure 2D**), in particular observed in the subepithelial zone in h-TOM models.

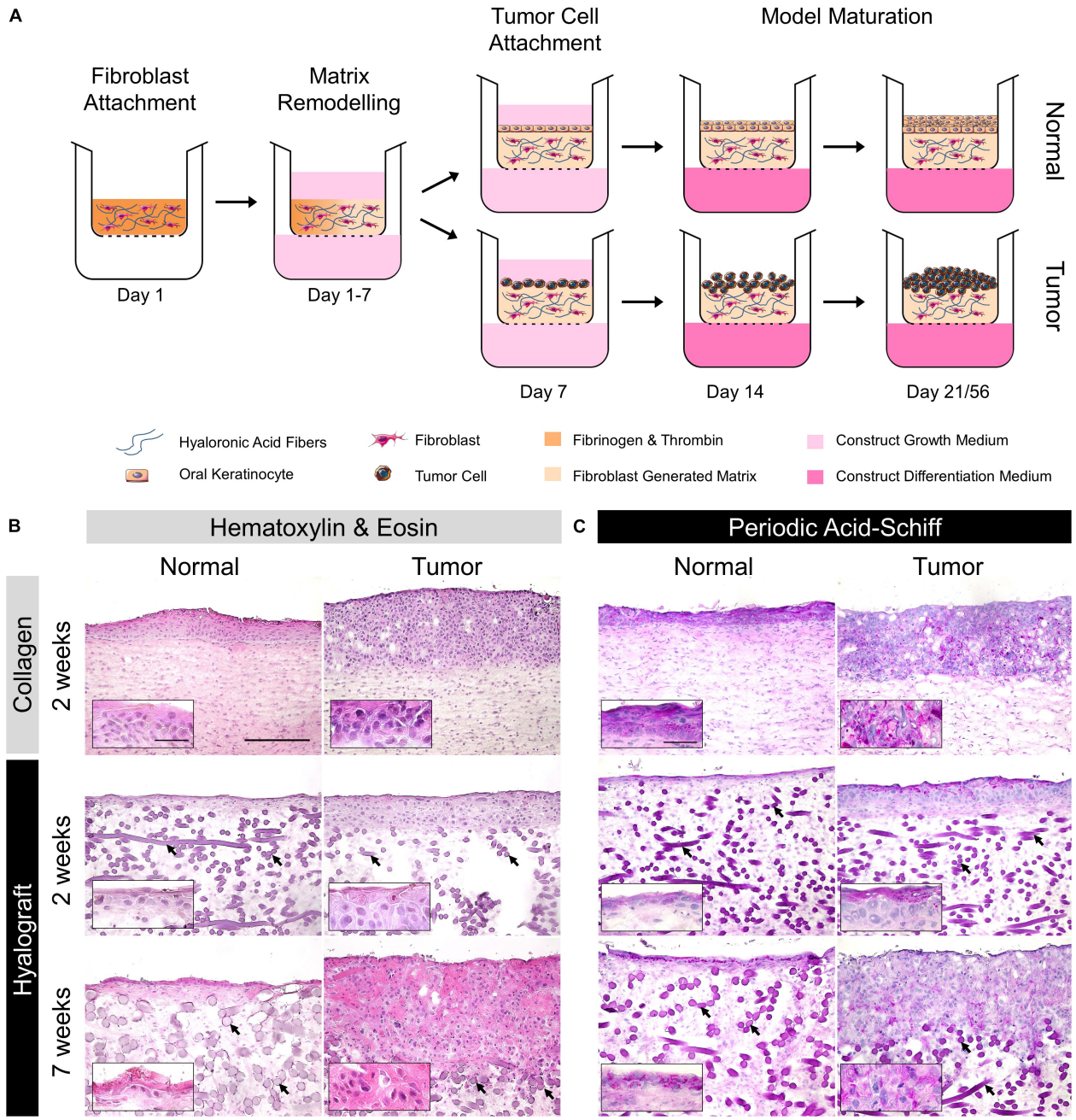

FIGURE 1 | Procedure outline and morphology of NOM and TOM models. **(A)** Human oral fibroblasts were suspended in a fibrinogen/thrombin solution and poured into a patch with esterified hyaluronic acid fibers (Hyalograft-3D). Fibroblasts replaced the fibrin gel by their own extracellular matrix (day 1–7). Normal oral keratinocytes or tumor cells were seeded on day 7 onto the matrix and grew until day 21 or 56 (2 or 7 weeks with tumor cells). **(B)** Hematoxylin and eosin and **(C)** Periodic Acid-Schiff staining. Dark purple structures in both stainings of the lamina propria were hyaluronic acid fibers of the scaffold (black arrows). The inserts show the difference between normal and tumor cell morphology by higher magnification. Representative images from the analysis of up to three batches are presented. Scale bars = 250 and 50 μm in the inserts.

The extracellular matrix protein tenascin C was most abundant in collagen-based models with no difference between NOM and TOM models (**Figure 3A**). Tenascin C expression markedly decreased in hyalograft-based models already after 2 weeks of cultivation and further declined to 33% ($p > 0.05$) after 7 weeks. Again, no relevant difference between NOM and TOM models was observed (**Figure 3B**).

The hypoxia-inducible factor (HIF)-1α was detected in the entire tumor mass of c-TOM models, and particularly in

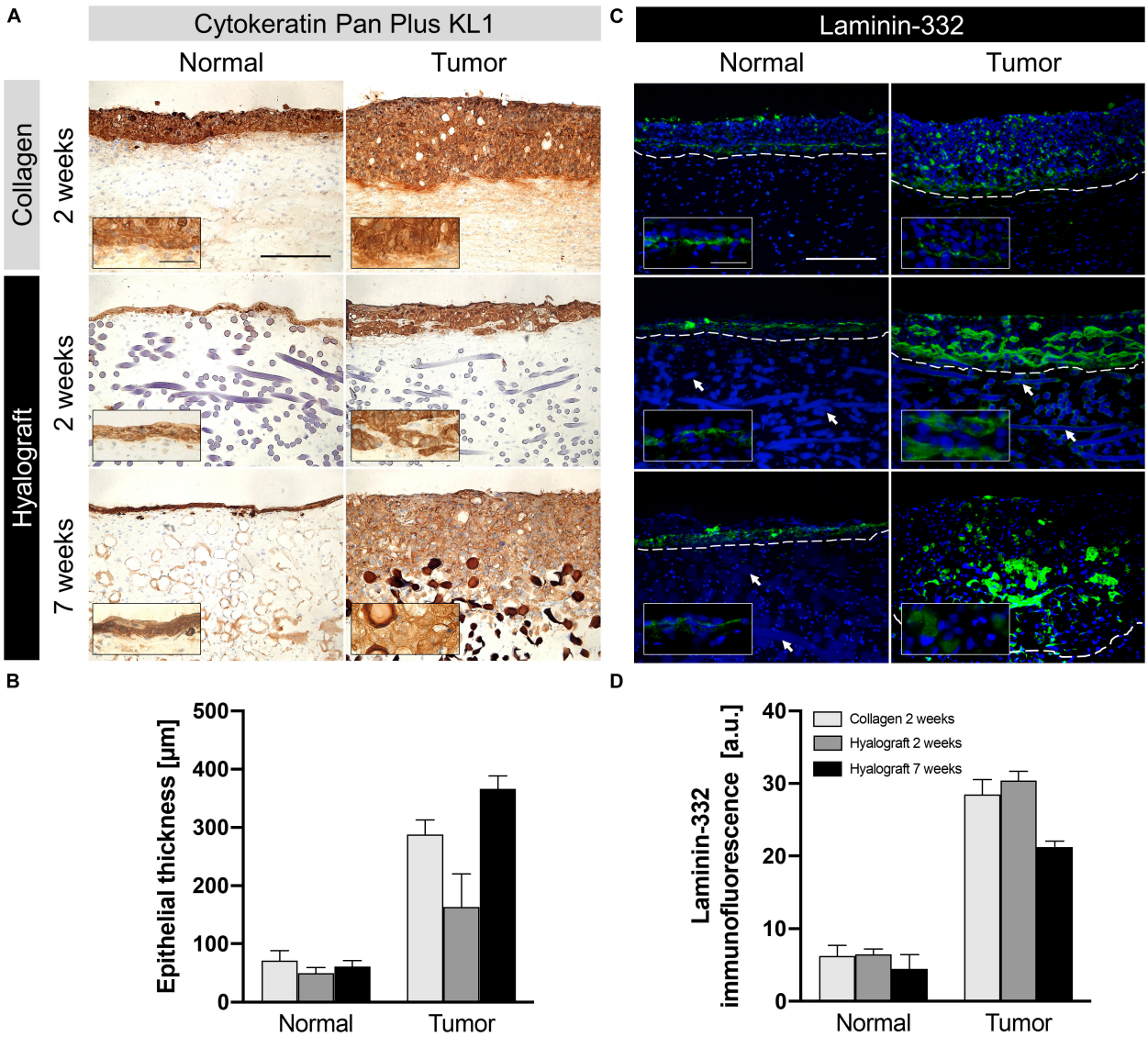

FIGURE 2 | Expression of cytokeratin and laminin-332 in NOM and TOM models. **(A)** Cytokeratin staining (brown) showed the absence of invasive growth in NOM and c-TOM models. In contrast, nests of cytokeratin positive cells started to infiltrate the lamina propria in h-TOM models after 2 weeks and markedly separated into single cells after 7 weeks. **(B)** Epithelial thickness in TOM models exceeded those in NOM models. The highest value occurred in h-TOM models after 7 weeks. **(C,D)** Laminin-332 (green) expression was restricted to a small layer in NOM models and diffusely clustered in TOM models. DAPI stained nuclei and fibers in blue, which could however be distinguished by their size and shape. The inserts show the border between epithelial cells and the matrix, with highest infiltration of the tumor cells in the 7 weeks cultured hyalograft-models, by higher magnification. White arrows highlight fibers and dashed lines indicate the border between epithelium and lamina propria. Representative images from up to three independent cultures are presented. Scale bars = 250 and 50 µm in the inserts. Bar graphs show the mean + SD from the quantitative analysis of up to six regions of interest.

central tumor areas in h-TOM models (**Figure 3C**). Very low levels of HIF-1α were detected in both c-NOM and h-NOM models (**Figure 3D**).

Overall, vascular endothelial growth factor (VEGF) was expressed at similar levels in the c-TOM and h-TOM models; however, the type of matrix interfered with its localization. While VEGF was detected in the entire tumor areas of c-TOM models, it was restricted to the border between the tumor layer and the lamina propria in h-TOM models (**Figures 4A,B**). VEGF expression further increased after 7 weeks both in NOM and TOM models ($p > 0.05$). Increased VEGF levels were particularly observed close to hyaluronic acid fibers in h-NOM models.

Proliferation and Apoptosis

Proliferation was higher in tumor compared to normal models, irrespective of the used matrix (**Figures 4C,D**). Importantly, tumor cells continued to proliferate excessively in h-TOM models until the end of the 7-week culture within all regions of the culture.

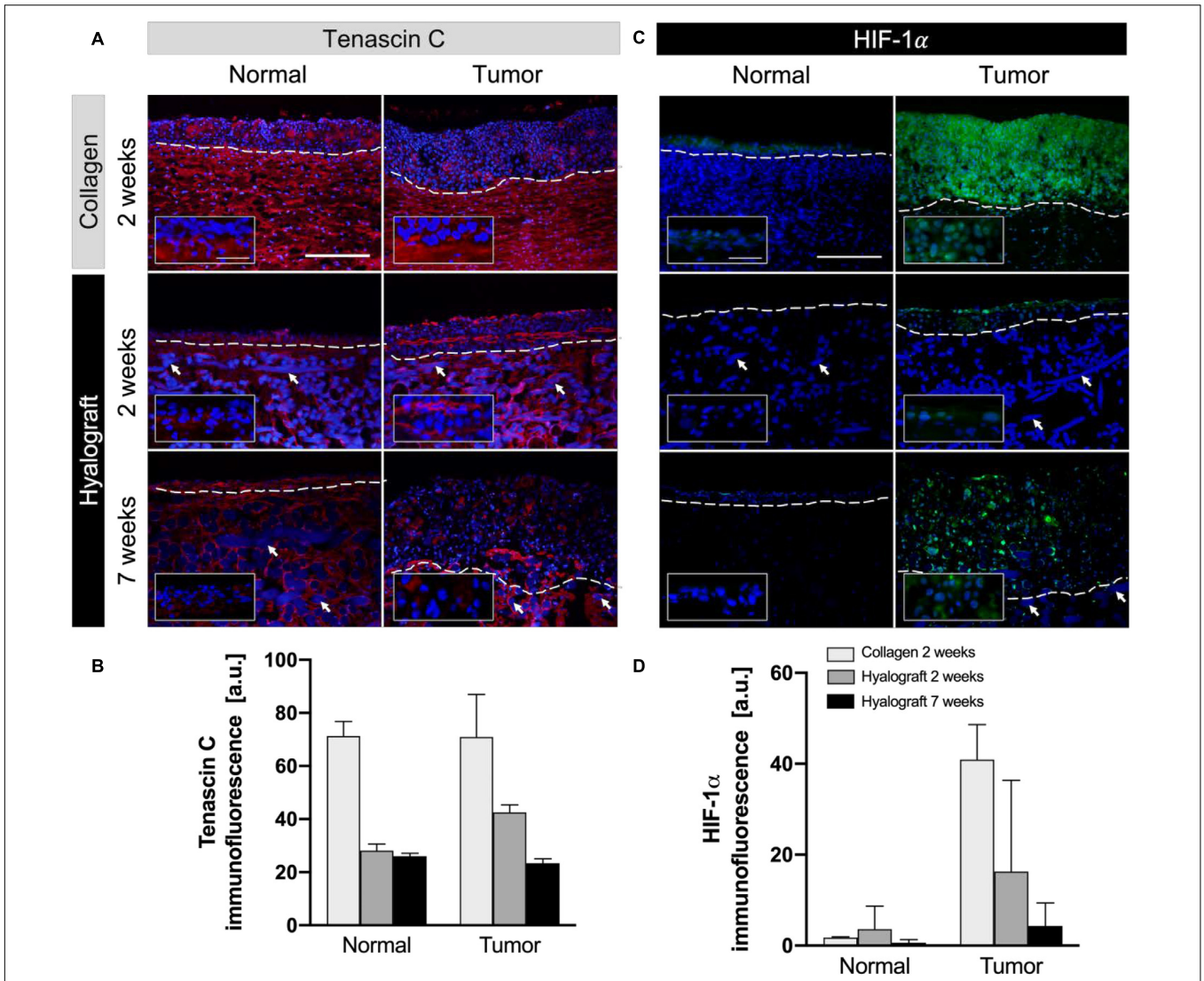

FIGURE 3 | Expression of tenascin c and HIF-1α in NOM and TOM models. **(A,B)** Tenascin c (red) was less expressed in hyalograft-based models than collagen-based models and further decreased during cultivation. **(C,D)** HIF-1α (green) showed increased expression in TOM models, with matrix-dependent differences. DAPI stained nuclei and fibers in blue. The inserts show the border between epithelial cells and the matrix for the tenascin C staining and highlights of the HIF-1α staining by higher magnification. White arrows highlight fibers and dashed lines indicate the border between epithelium and lamina propria. Representative images from up to three independent cultures are presented. Scale bar = 250 and 50 μm in the inserts. Bar graphs show the mean + SD from the quantitative analysis of up to six regions of interest of interest.

In c-NOM and the 7 weeks cultured h-NOM models, only few apoptotic cells could be detected (mean = 2.5%), while in the 2 weeks h-NOM models apoptotic cells made up to 20% of the epithelial cells (**Supplementary Figure 1**).

In TOM models, both 2 weeks cultured c-TOM and h-TOM models depicted less than 5% apoptotic cells, but the 7 weeks cultured h-TOM models showed up to 30% apoptotic cells.

DISCUSSION

We here showed that normal and tumor oral mucosa models can be successfully cultured in a hyalograft-based scaffold, allowing extended *ex vivo* cultivation. Our data corroborate previous findings showing that hyaluronic acid and its derivatives provide a well-defined and tunable scaffold for *ex vivo* tumor models (Fong et al., 2014). Moreover, hyalograft-based models are not affected by the poor adhesion of epithelial layers and the tendency to shrink of collagen-based models (Stark et al., 2004). In contrast, nylon-meshes and collagen-chitosan-sponges, which have been tested for elongated cultivation periods have the disadvantage of requiring long pre-cultivation and displaying considerable stiffness, thus complicating tissue sectioning and analysis (Michel et al., 1999; Stark et al., 2006).

Hyalograft-based tumor models contained high numbers of proliferative cells and recapitulated hallmarks of oral cancer

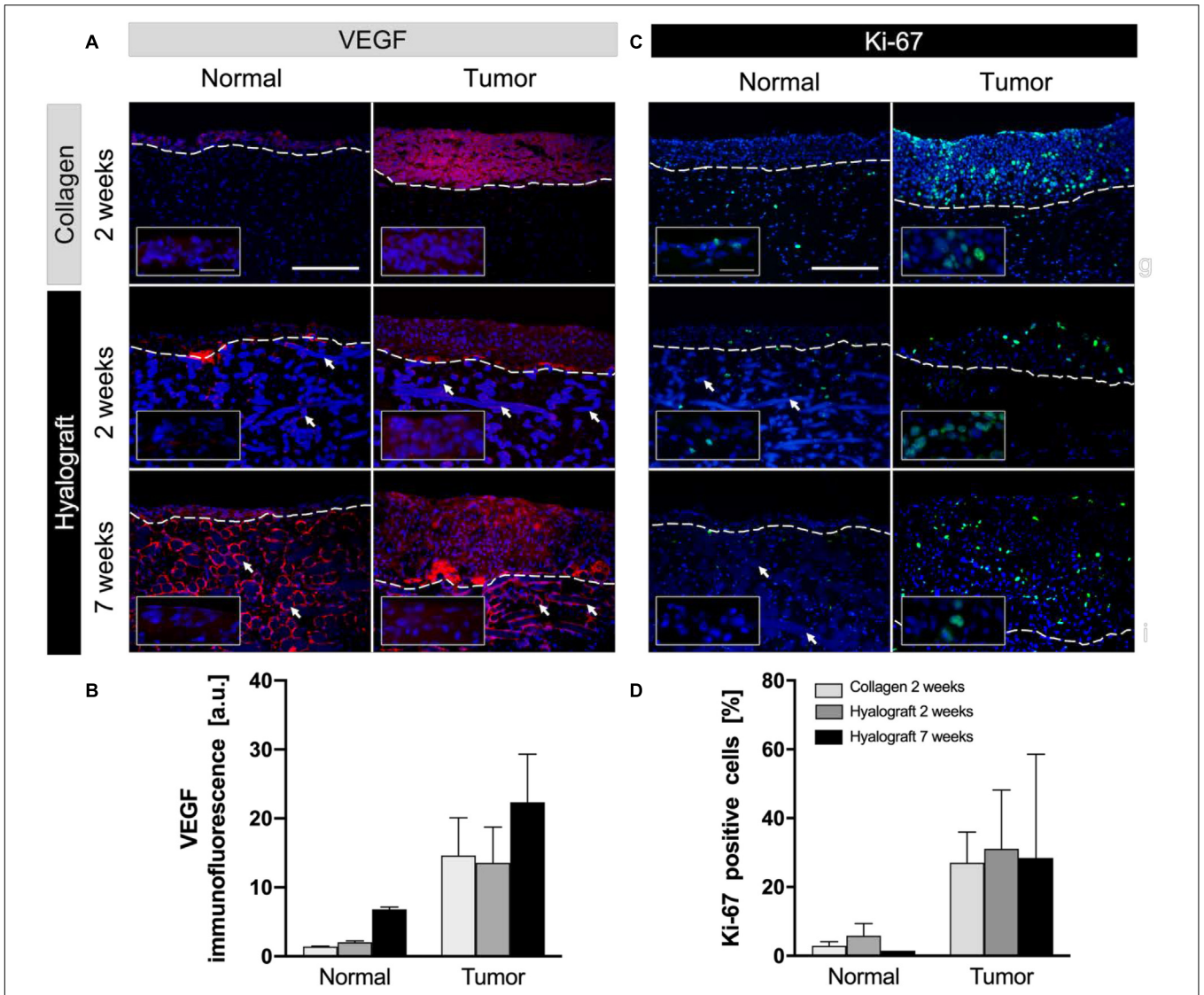

FIGURE 4 | Expression of vascular endothelial growth factor (VEGF) and proliferation (Ki-67) in NOM and TOM models. **(A,B)** Highest expression of VEGF (red) was observed in h-TOM models after 7 weeks. **(C,D)** The number of proliferative cells (Ki-67 positive, green) was increased in TOM models until the end of the cultivation period compared to NOM models. The inserts highlight detected VEGF and Ki-67 in the epithelial layers by higher magnification. Representative images from up to three independent cultures are presented. Scale bars = 250 and 50 μm in the inserts. Bar graphs show the mean + SD from the quantitative analysis of up to six regions of interest.

even after a cultivation period of 7 weeks. In particular, increased epithelial thickness, abundant cellular pleomorphism, and the altered laminin-332 expression, very well reflected the histopathological characteristics of patient tumors (Miyazaki, 2006; Bernstein et al., 2013; Jerjes et al., 2019). Thus, h-TOM models should be suitable to monitor long-term tumor progression as well as the effects of anti-proliferative drugs and the potential tumor re-growth after an initial treatment cycle. An improved understanding of the re-growth kinetics after drug treatment would help to overcome drug resistance, which is currently the major cause of treatment failure (Vasan et al., 2019).

Beside large similarities in protein expression patterns of hyalograft-and collagen-based models, there was a significant difference in tenascin C expression. The increased expression of tenascin C in collagen-based models might explain the faster growth in the epithelial layers of both c-NOM and c-TOM models, since tenascin C is known as a provisional matrix for keratinocyte growth (Pellegrini et al., 1999). Moreover, the expression of the extracellular matrix proteins tenascin c and fibronectin discriminates low- and high-risk tongue cancers (Sundquist et al., 2017). Low tenascin C expression in the h-TOM model established from SCC-25 cells is in line with the previously described poorly invasive phenotype of this cell line model (Ramos et al., 1997).

Normal oral fibroblasts better confined tumor invasion in hyalograft- than in collagen-based models after 2 weeks.

This difference might be related to paracrine signaling between fibroblasts and tumor cells which has been shown to depend on the composition of the ECM (Barcellos-Hoff and Bissell, 1989; Boudreau and Bissell, 1998). Laminin-332 appears to play a key part in the invasion process, in line with its higher expression in h-TOM compared to c-TOM models. While a well-defined laminin-332 expression is typical for normal tissues, clustered laminin-332 expression is known to promote cell survival and tumorigenesis, especially in squamous cell carcinoma (Marinkovich, 2007). In addition, the occurrence of desmoplasia in h-TOM models might contribute to delayed invasive growth and reduced hypoxia compared to c-TOM models. These differences in the ECM of collagen- and hyalograft-based models need to be considered in evaluating drug effects since hypoxia reduces the clinical efficacy of anticancer drugs (Brennan et al., 2005; Johnstone and Logan, 2006).

Although this proof-of-concept study shows the suitability of the hyalograft scaffold for the *ex vivo* cultivation of TOM models, future studies need to elucidate the scaffold effects on patient-derived tumor cells and compare these results to *in vivo* tumors. One limitation of the current h-TOM model is the relative high percentage of apoptotic tumor cells in long-term cultures. Further approaches for model improvement in the future might thus include also testing of additional supplements to the construct growth medium. Moreover, future studies will show whether the hyalograft approach better recapitulates the interaction of immune and tumor cells in an immunocompetent model of oral mucosa tumor, which seems very likely since the scaffold is non-immunogenic (Galassi et al., 2000). Given their close correlation to the individual tumor, long-term cultivation of human TOM models offer the opportunity to study tumor re-growth and alterations in the tumor stroma after initial treatment and thus will help to better understand drug resistance mechanisms.

CONCLUSION

The hyalograft-3D approach recapitulated key features of human oral squamous cell carcinoma in multi-layered *ex vivo* tumor models for up to 7 weeks. The long-term cultivation provides the basis for studying tumor re-growth and stromal alterations following an initial anti-cancer drug therapy. Moreover, the well-defined and tunable hyaluronic acid derivatives might help to better culture patient-derived cells. Finally, hyalograft-based models can be extended by the addition of further tumor stroma components and relinquish the use of animal-based scaffolds.

DATA AVAILABILITY STATEMENT

The raw data supporting the conclusions of this article will be made available by the authors on reasonable request.

AUTHOR CONTRIBUTIONS

LG and CZ: conceptualization and design. LG, PJ, and CZ: investigation. CZ: project administration. MS-K, UK, and CZ: supervision. LG and CZ: visualization. LG and CZ: writing-original draft preparation. LG, MS-K, IT, and CZ: writing-review and editing. All authors contributed to the article and approved the submitted version.

FUNDING

The authors acknowledge support by the Open Access Publication Fund of the Freie Universität Berlin.

ACKNOWLEDGMENTS

The authors highly appreciated the excellent technical assistance of Jill García-Miller and Leticia M. Cruz.

SUPPLEMENTARY MATERIAL

The Supplementary Material for this article can be found online at: https://www.frontiersin.org/articles/10.3389/fbioe.2020.579896/full#supplementary-material

REFERENCES

Barcellos-Hoff, M. H., and Bissell, M. J. (1989). "A role for the extracellular matrix in Autocrine and Paracrine regulation of tissue-specific functions," in *Autocrine and Paracrine Mechanisms in Reproductive Endocrinology*, eds L. C. Krey, B. J. Gulyas, and J. A. McCracken (Boston, MA: Springer), 137–155. doi: 10.1007/978-1-4684-5751-3_10

Bernstein, J. M., Bernstein, C. R., West, C. M., and Homer, J. J. (2013). Molecular and cellular processes underlying the hallmarks of head and neck cancer. *Eur. Arch. Otorhinolaryngol.* 270, 2585–2593. doi: 10.1007/s00405-012-2323-x

Boudreau, N., and Bissell, M. J. (1998). Extracellular matrix signaling: integration of form and function in normal and malignant cells. *Curr. Opin. Cell Biol.* 10, 640–646. doi: 10.1016/s0955-0674(98)80040-9

Braig, F., Kriegs, M., Voigtlaender, M., Habel, B., Grob, T., Biskup, K., et al. (2017). Cetuximab resistance in head and neck cancer is mediated by EGFR-K(521) Polymorphism. *Cancer Res.* 77, 1188–1199. doi: 10.1158/0008-5472.can-16-0754

Brennan, P. A., Mackenzie, N., and Quintero, M. (2005). Hypoxia-inducible factor 1alpha in oral cancer. *J. Oral Pathol. Med.* 34, 385–389. doi: 10.1111/j.1600-0714.2005.00335.x

Campoccia, D., Doherty, P., Radice, M., Brun, P., Abatangelo, G., and Williams, D. F. (1998). Semisynthetic resorbable materials from hyaluronan esterification. *Biomaterials* 19, 2101–2127. doi: 10.1016/s0142-9612(98)00042-8

Dahler, A., Cavanagh, L., and Saunders, N. (2001). Suppression of keratinocyte growth and differentiation by transforming growth factor 1 involves multiple signaling pathways. *JIDEAE* 116, 266–274. doi: 10.1046/j.1523-1747.2001.01243.x

Fong, E. L. S., Martinez, M., Yang, J., Mikos, A. G., Navone, N. M., Harrington, D. A., et al. (2014). Hydrogel-based 3D model of patient-derived prostate xenograft tumors suitable for drug screening. *Mol. Pharm.* 11, 2040–2050. doi: 10.1021/mp500085p

Galassi, G., Brun, P., Radice, M., Cortivo, R., Zanon, G. F., Genovese, P., et al. (2000). In vitro reconstructed dermis implanted in human wounds: degradation

studies of the HA-based supporting scaffold. *Biomaterials* 21, 2183–2191. doi: 10.1016/s0142-9612(00)00147-2

Gronbach, L., Wolff, C., Klinghammer, K., Stellmacher, J., Jurmeister, P., Alexiev, U., et al. (2020). A multilayered epithelial mucosa model of head neck squamous cell carcinoma for analysis of tumor-microenvironment interactions and drug development. *Biomaterials* 258:120277. doi: 10.1016/j.biomaterials.2020.120277

Jerjes, W., Hamdoon, Z., Yousif, A., Al-Rawi, N., and Hopper, C. (2019). Epithelial tissue thickness improves optical coherence tomography's ability in detecting oral cancer. *Photodiagn. Photodyn. Ther.* 28, 69–74. doi: 10.1016/j.pdpdt.2019.08.029

Jo, Y., Choi, N., Kim, K., Koo, H.-J., Choi, J., and Kim, H. N. (2018). Chemoresistance of cancer cells: requirements of tumor microenvironment-mimicking in vitro models in anti-cancer drug development. *Theranostics* 8, 5259–5275. doi: 10.7150/thno.29098

Johnstone, S., and Logan, R. M. (2006). The role of vascular endothelial growth factor (VEGF) in oral dysplasia and oral squamous cell carcinoma. *Oral Oncol.* 42, 337–342. doi: 10.1016/j.oraloncology.2005.06.020

Langhans, S. A. (2018). Three-dimensional in vitro cell culture models in drug discovery and drug repositioning. *Front. Pharmacol.* 9:6. doi: 10.3389/fphar.2018.00006

Magdeldin, T., López-Dávila, V., Villemant, C., Cameron, G., Drake, R., Cheema, U., et al. (2014). The efficacy of cetuximab in a tissue-engineered three-dimensional in vitro model of colorectal cancer. *J. Tissue Eng.* 5, 1–9.

Marinkovich, M. P. (2007). Laminin 332 in squamous-cell carcinoma. *Nat. Rev. Cancer* 7, 370–380. doi: 10.1038/nrc2089

Michel, M., L'Heureux, N., Pouliot, R., Xu, W., Auger, F. A., and Germain, L. (1999). Characterization of a new tissue-engineered human skin equivalent with hair. *Vitro Cell Dev. Biol. Anim.* 35, 318–326. doi: 10.1007/s11626-999-0081-x

Miyazaki, K. (2006). Laminin-5 (laminin-332): unique biological activity and role in tumor growth and invasion. *Cancer Sci.* 97, 91–98. doi: 10.1111/j.1349-7006.2006.00150.x

Nath, S., and Devi, G. R. (2016). Three-dimensional culture systems in cancer research: focus on tumor spheroid model. *Pharmacol. Ther.* 163, 94–108. doi: 10.1016/j.pharmthera.2016.03.013

Pellegrini, G., Ranno, R., Stracuzzi, G., Bondanza, S., Guerra, L., Zambruno, G., et al. (1999). The control of epidermal stem cells (holoclones) in the treatment of massive full-thickness burns with autologous keratinocytes cultured on fibrin. *Transplantation* 68, 868–879. doi: 10.1097/00007890-199909270-00021

Pickup, M. W., Mouw, J. K., and Weaver, V. M. (2014). The extracellular matrix modulates the hallmarks of cancer. *EMBO Rep.* 15, 1243–1253. doi: 10.15252/embr.201439246

Ramos, D. M., Chen, B. L., Boylen, K., Stern, M., Kramer, R. H., Sheppard, D., et al. (1997). Stromal fibroblasts influence oral squamous-cell carcinoma cell interactions with tenascin-C. *Int. J. Cancer* 72, 369–376. doi: 10.1002/(sici)1097-0215(19970717)72:2<369::aid-ijc28>3.0.co;2-9

Rheinwald, J. G., and Beckett, M. A. (1981). Tumorigenic keratinocyte lines requiring anchorage and fibroblast support cultured from human squamous cell carcinomas. *Cancer Res.* 41, 1657–1663.

Saggioro, M., D'Angelo, E., Bisogno, G., Agostini, M., and Pozzobon, M. (2020). Carcinoma and sarcoma microenvironment at a glance: where we are. *Front. Oncol.* 10:76. doi: 10.3389/fonc.2020.00076

Schneider, C. A., Rasband, W. S., and Eliceiri, K. W. (2012). NIH Image to ImageJ: 25 years of image analysis. *Nat. Methods* 9, 671–675. doi: 10.1038/nmeth.2089

Stark, H.-J., Boehnke, K., Mirancea, N., Willhauck, M. J., Pavesio, A., Fusenig, N. E., et al. (2006). Epidermal homeostasis in long-term scaffold-enforced skin equivalents. *J. Investig. Dermatol. Symp. Proc.* 11, 93–105. doi: 10.1038/sj.jidsymp.5650015

Stark, H. J., Willhauck, M. J., Mirancea, N., Boehnke, K., Nord, I., Breitkreutz, D., et al. (2004). Authentic fibroblast matrix in dermal equivalents normalises epidermal histogenesis and dermoepidermal junction in organotypic co-culture. *Eur. J. Cell Biol.* 83, 631–645. doi: 10.1078/0171-9335-00435

Sundquist, E., Kauppila, J. H., Veijola, J., Mroueh, R., Lehenkari, P., Laitinen, S., et al. (2017). Tenascin-C and fibronectin expression divide early stage tongue cancer into low- and high-risk groups. *Br. J. Cancer* 116, 640–648. doi: 10.1038/bjc.2016.455

Varol, C. (2019). Tumorigenic interplay between macrophages and collagenous matrix in the tumor microenvironment. *Methods Mol. Biol.* 1944, 203–220. doi: 10.1007/978-1-4939-9095-5_15

Vasan, N., Baselga, J., and Hyman, D. M. (2019). A view on drug resistance in cancer. *Nature* 575, 299–309.

Zheng, J., and Gao, P. (2019). Toward normalization of the tumor microenvironment for cancer therapy. *Integr. Cancer Ther.* 18, 1–13.

Conflict of Interest: The authors declare that the research was conducted in the absence of any commercial or financial relationships that could be construed as a potential conflict of interest.

frontiers in Bioengineering and Biotechnology

ORIGINAL RESEARCH
published: 09 December 2020
doi: 10.3389/fbioe.2020.600103

Cartilage Extracellular Matrix Scaffold With Kartogenin-Encapsulated PLGA Microspheres for Cartilage Regeneration

Yanhong Zhao[1,2†], Xige Zhao[1,2†], Rui Zhang[1,2], Ying Huang[1,2], Yunjie Li[1,2], Minhui Shan[1,2], Xintong Zhong[1,2], Yi Xing[1,2], Min Wang[1,2], Yang Zhang[3] and Yanmei Zhao[4*]*

[1] Stomatological Hospital of Tianjin Medical University, Tianjin, China, [2] Tianjin Medical University, Tianjin, China, [3] Tianjin Hospital, Tianjin, China, [4] Institute of Disaster Medicine, Tianjin University, Tianjin, China

OPEN ACCESS

Edited by:
Hon Fai Chan,
The Chinese University of Hong Kong, China

Reviewed by:
Kunyu Zhang,
Johns Hopkins University, United States
Shun Duan,
Beijing University of Chemical Technology, China

***Correspondence:**
Yanhong Zhao
leafzh@126.com
Yanmei Zhao
zhaoyanmei@126.com

† These authors have contributed equally to this work

Specialty section:
This article was submitted to Biomaterials, a section of the journal Frontiers in Bioengineering and Biotechnology

Received: 28 August 2020
Accepted: 30 October 2020
Published: 09 December 2020

Citation:
Zhao Y, Zhao X, Zhang R, Huang Y, Li Y, Shan M, Zhong X, Xing Y, Wang M, Zhang Y and Zhao Y (2020) Cartilage Extracellular Matrix Scaffold With Kartogenin-Encapsulated PLGA Microspheres for Cartilage Regeneration. Front. Bioeng. Biotechnol. 8:600103. doi: 10.3389/fbioe.2020.600103

Repair of articular cartilage defects is a challenging aspect of clinical treatment. Kartogenin (KGN), a small molecular compound, can induce the differentiation of bone marrow-derived mesenchymal stem cells (BMSCs) into chondrocytes. Here, we constructed a scaffold based on chondrocyte extracellular matrix (CECM) and poly(lactic-co-glycolic acid) (PLGA) microspheres (MP), which can slowly release KGN, thus enhancing its efficiency. Cell adhesion, live/dead staining, and CCK-8 results indicated that the PLGA(KGN)/CECM scaffold exhibited good biocompatibility. Histological staining and quantitative analysis demonstrated the ability of the PLGA(KGN)/CECM composite scaffold to promote the differentiation of BMSCs. Macroscopic observations, histological tests, and specific marker analysis showed that the regenerated tissues possessed characteristics similar to those of normal hyaline cartilage in a rabbit model. Use of the PLGA(KGN)/CECM scaffold may mimic the regenerative microenvironment, thereby promoting chondrogenic differentiation of BMSCs *in vitro* and *in vivo*. Therefore, this innovative composite scaffold may represent a promising approach for acellular cartilage tissue engineering.

Keywords: cartilage tissue engineering, decellularized cartilage extracellular matrix, poly(lactic-co-glycolic acid), composite scaffold, kartogenin

INTRODUCTION

Because of its avascular, alymphatic, and aneural properties, articular cartilage has poor spontaneous repair and regeneration capabilities (Malfait, 2016). The widespread articular cartilage injury caused by trauma, infection, osteoarthritis, tumors, and other diseases is a challenging aspect of clinical treatment (Huang et al., 2016). Traditional treatment methods (e.g., mosaicplasty, autologous chondrocyte transplantation, and microfracture surgery) have a number of limitations, including poor repair effect and additional trauma (Loeser et al., 2016). In the past decade, tissue engineering, especially cell-free tissue engineering, which involves scaffold implantation and microfracture creation to promote the recruitment of endogenous cells has been studied to overcome these limitations (Zhen et al., 2013; Trounson and McDonald, 2015).

Stimulating factors are among the most basic elements for cell-free tissue engineering. Previous studies have focused on cartilage stimulation methods that support the capacity for self-repair. Signaling molecules, such as transforming growth factor beta-3 (TGF-β3), have been widely used as chondrogenic modulators (Mi et al., 2003; van der Kraan and van den Berg, 2007; Cals et al., 2012; Almeida et al., 2014). Kartogenin (KGN), a non-toxic and stable small molecule first described by Johnson et al. (2012) is sufficiently small to avoid immune responses; it demonstrates good stability, cost-effectiveness, and ease of storage and transportation, compared to signaling molecules (e.g., TGF-β3). During mesenchymal stem cell (MSC) differentiation, KGN frees CBFβ, which binds to the transcription factor RUNX1. The resultant CBFβ-RUNX1 complex plays a critical role in the activation of cartilage matrix transcription; therefore, KGN has great potential for use in cartilage regeneration (Wu et al., 2014). Furthermore, KGN has protective effects with respect to existing cartilage tissue and reduces the decomposition of chondrogenic proteins; thus, it slows the progression of cartilage injury (Cai et al., 2019). Although KGN has been investigated as a cartilage-promoting molecule, two common models of KGN application remain problematic: (1) direct injection into the joint cavity, (Xu et al., 2015; Kwon et al., 2018) which is ineffective because most KGN is absorbed by the circulatory system and repeated injections increase both pain and risk of infection; (2) combination of KGN with drug delivery system: such as hydrogel (Wang S.J. et al., 2019), platelet-rich plasma (PRP)(Liu et al., 2019), nanoparticles, or microspheres (Kang et al., 2014). Although several drug delivery systems have been used to achieve sustained release of KGN, the potential application of KGN in cartilage tissue engineering is seldom investigated, and additional mesenchymal stem cells implantation are needed (Li et al., 2016; Wang J. et al., 2019). Therefore, methods for application of KGN would need to be further studied. Previous studies have shown that scaffolds loaded with drug-encapsulated microspheres can achieve sustained drug release and ensure that cells within the scaffold maintain high levels of activity (Gupta et al., 2017; Zhang et al., 2017). Among the most attractive polymer candidates, poly(lactic-co-glycolic acid) (PLGA)—a typical compound used in fabrication of biodegradable microspheres or nanoparticles, which has been approved for use by the Food and Drug Administration—is widely used as a vehicle for delivery of pharmaceutically relevant payloads (Danhier et al., 2012; Fernando et al., 2018). Furthermore, the amino groups of PLGA can bind covalently to the carboxyl groups of KGN, thus enhancing the permeability and retention of KGN and promoting its therapeutic effects (Kang et al., 2014; Fan et al., 2018; Chen et al., 2020).

Another critical component of cell-free tissue engineering comprises the biomaterial scaffold. Decellularized extracellular matrix (ECM) derived from cartilage (CECM) can preserve natural ECM components and avoid immune rejection. Therefore, it has been used as a scaffold for cartilage regeneration (Sutherland et al., 2015; Monibi and Cook, 2017). CECM scaffold can provide a suitable microenvironment for the cells it contains; moreover, it exhibits natural adhesion to the cells and growth factors. Notably, CECM is biodegradable, which allows the scaffold to participate in the construction of new cartilage tissue. All of these characteristics promote cell proliferation and functional expression (Yang et al., 2008; Ravindran et al., 2015; Oh et al., 2018; Wang et al., 2018). However, its rapid degradation rate and weak mechanical performance limit the application of ECM scaffold in tissue engineering (Oh et al., 2018). Recently, the introduction of composite scaffolds based on ECM and polymers has provided mechanically and chemically stable properties, while retaining biocompatibility and biodegradability; this offers a new strategy for application of the CECM scaffold. In our previous study, we designed a three-layer biomimetic porous scaffold based on CECM, nano-hydroxyapatite, and silk fibroin. PLGA microspheres encapsulating growth factor rhBMP-2 and TGF-β3 were loaded into the three-layer scaffold to form a slow-release biomimetic osteochondral scaffold. This composite scaffold was able to effectively repair osteochondral defects (Dong et al., 2020).

Here, we fabricated cartilage-derived ECM scaffolds that contained PLGA microspheres or nanoparticles for use in controlled delivery of KGN; the constructs were designed to promote cartilage repair by means of simple procedures. Without the requirement for cell transplantation, this system could recruit endogenous BMSCs from the bone marrow cavity through microfracture apertures. This study was performed to: (1) characterize the ability of the PLGA(KGN)/CECM composite scaffold to support sustained release and chondrogenic differentiation ability *in vitro*, and (2) to evaluate the effects of implantation of PLGA(KGN)/CECM composite scaffold on articular cartilage defects *in vivo*.

MATERIALS AND METHODS

Materials and Reagents

CECM was obtained from fresh porcine articular cartilage by decellularization, in accordance with methods described previously (Yang et al., 2008). Other materials, including biochemical and chemical reagents, are listed in the supporting information.

Preparation of KGN-Encapsulating PLGA Microspheres and Nanoparticles

PLGA microspheres encapsulating KGN were prepared by the solid-oil-water double solvent evaporation technique. Briefly, PLGA (MedChemexpress, NJ, United States) was dissolved in dichloromethane to approach a final mass fraction of 5%. KGN was dissolved in dimethyl sulfoxide and then mixed with 5% PLGA. The mixture was then added dropwise into 1% polyvinyl alcohol (PVA) solution at an oil phase:water phase volume ratio of 1:20 and emulsified at 16,000 rpm for 3 min, using a high-shear homogenizer in an ice bath. The suspension was then transferred to a magnetic stirrer and stirred overnight at room temperature. Finally, the suspension was centrifuged and the sediments were washed with deionizer water several times. KGN-PLGA microspheres were obtained after the sediments had been freeze-dried for 24 h and stored at −20°C. PLGA nanospheres were prepared by ultrasonication. First, 2.5% PLGA solution

containing KGN was added in a dropwise manner to 2.5% PVA solution at an oil phase: water phase volume ratio of 1:5; it was then emulsified by ultrasonication (500 W, 3 min) to prepare an oil/water emulsion. Subsequently, the ethyl acetate was extracted by adding six volumes of 0.5% PVA aqueous solution to the emulsion. Subsequent steps were performed as described for the preparation of PLGA microspheres.

Morphology Observations and Size Distribution Measurements of Microspheres and Nanoparticles

The freeze-dried PLGA microspheres Were uniformly coated on the surface of the conductive adhesive of the sample table. The shape and surface morphology of PLGA microspheres Were observed by scanning electron microscope (SEM; Quanta 200; FEI, Hillsboro, OR, United States). To determine the morphology of the PLGA nanoparticles, the nanoparticles Were resuspended by deionized water and dripped on a copper mesh and then visualized by transmission electron microscopy (TEM; HT7700 Exalens, Hitachi, Japan). The sizes of the microspheres and nanoparticles Were measured by Zetasizer Nano ZS90 (Malvern Instruments, Worcestershire, United Kingdom).

Extraction of Cartilage-Derived ECM

The cartilage used in the ECM-derived scaffold was separated with a scalpel from the femoral condyle and patellar groove. The cartilage was cut into small slices (1 mm^3) using eye scissors, then washed several times with phosphate-buffered saline (PBS). The cleaned cartilage pieces were then placed in an appropriate amount of Tris–HCl; they were disrupted and decellularized using a tissue homogenizer to create a cartilage slurry. The homogenized tissue was centrifuged at 4°C and the supernatant was removed. Next, the sediments were incubated with 1% Triton X-100 in hypotonic Tris–HCl (Solarbio, Beijing, China) with gentle agitation at 4°C for 24 h; they were rinsed several times with deionizer water, then incubated for 12 h in DNase (Sigma-Aldrich, NJ, United States) and RNase (Sigma-Aldrich, NJ, United States) with agitation at 37°C. Finally, the homogenate was centrifuged and washed as described above. The resulting sediment was freeze-dried and stored at −20°C for further use.

Fabrication of KGN-PLGA Microspheres and CECM Scaffold Composite System

Freeze-dried CECM was resuspended in deionizer water to form a 3% (w/v) suspension. An adequate amount of KGN (MedChemexpress, Rocky Hill, NJ, United States) was then added to the suspension. The mixture was poured into a cylindrical mould, frozen at −80°C for 72 h, and freeze-dried for 48 h. The resulting scaffolds were sterilized and trimmed to an appropriate size. Next, cross-linking was performed in anhydrous ethanol solution containing 50 mM 1-ethyl-3-(3-dimethylaminopropyl) carbodiimide (EDC) and 20 mM *N*-hydroxysuccinimide (NHS) for 24 h at 4°C; cross-linked scaffolds were rinsed several times with PBS. The process produced PLGA microsphere-embedded CECM composite scaffolds with diameter of approximately 5 mm and depth of approximately 3 mm. Scaffolds loaded with TGF-β3 were obtained by immersion in 400 ng/mL TGF-β3 (Peprotech, Rocky Hill, NJ, United States) solution (24 h at 4°C) and then freeze-dried.

Characterization of Scaffolds

The morphology and structure of scaffolds were characterized by scanning SEM. Briefly, the scaffold specimens were cut into thin sections and fixed on the platform. After they had been sputter-coated with gold, all sections were examined by SEM. Pore diameter distributions were determined using ImageJ software (NIH, Bethesda, MD, United States).

Determination of Encapsulation Efficiency and Drug Loading of Microspheres

First, several concentrations of KGN standard solutions were prepared and the absorption peak area was determined by high-performance liquid chromatography (HPLC). A standard curve was obtained with the concentration as the x-axis and the peak area as the y-axis. Subsequently, the KGN-PLGA microspheres were submerged in 0.1 M NaOH solution at 1 mg/mL and shaken gently at 37°C for 24 h. The peak area was determined by HPLC and the KGN content in the sample (W1) was calculated by the standard curve formula. The encapsulation rate and drug loading amount of KGN in PLGA microspheres were calculated using the following formulae:

$$\text{Encapsulation efficiency} = W_1/W_k \times 100\%$$

and

$$\text{Drug loading} = W_1/(Wp + W_1) \times 100\%,$$

where W_k represents the total volume of KGN and Wp represents the total volume of PLGA.

KGN Release From Scaffolds

First, the two scaffolds (KGN-CECM and PLGA(KGN)-CECM) were soaked in 5 mL of sterile PBS and shaken at 37°C. PBS was collected daily and replaced with 5 mL of fresh PBS. The concentration of KGN in the collected PBS was determined by HPLC, as described above. Thus, sustained-release curves of KGN-CECM and PLGA(KGN)/CECM were obtained.

Isolation and Culture of Bone Marrow Mesenchymal Stem Cells

BMSCs were isolated from 4-month-old New Zealand White rabbits. All experimental protocols were approved by the Animal Experimental Ethics Committee of Tianjin Hospital. Following injection of 30% urethane (2.2 mL/kg) into the ear vein, BMSCs were obtained from the rabbits by bone marrow aspiration. After the operative region had been shaved and disinfected, a 2-mL aliquot of bone marrow was aspirated from the femur of each rabbit and placed in a sterile centrifuge tube. Following the addition of 5 volumes of Hanks balanced salt solution, the tubes were centrifuged for 7 min at 1,000 rpm; the mixtures were then divided into three layers. The top two layers were transferred to a new tube and resuspended in 5 mL of Dulbecco's Modified Eagle Medium supplemented with penicillin and 10% fetal bovine

serum (Gibco, Grand Island, NY, United States). BMSCs were then cultured at 5 × 106 cells/cm^2 in 75-mL culture flasks under an atmosphere of 5% CO_2 at 37°C. Half of the volume of culture medium was changed after 3 days; the entire volume of culture medium was changed within 1 week. Third-generation (P3) cells were stored for further use.

Chondrogenic Induction *in vitro*

First, four scaffolds were prepared: blank CECM, CECM loaded with PLGA(KGN), CECM loaded with TGF-β3, and CECM loaded with PLGA(KGN) and TGF-β3. BMSCs were suspended at 1 × 10^7 cells/mL, then dropped into each of the scaffolds to construct cell–scaffold complexes. The cell–scaffold complexes were then incubated in chondrogenic induction media (α-Minimum Essential Medium supplemented with 10% fetal bovine serum, 100 nM dexamethasone, 50 μg/mL vitamin C, 1% ITS, 100 μg/mL sodium pyruvate, 40 μg/mL proline, 30 μg/mL L-glutamate, and 1% antibiotic-antimycotic) for 14 or 28 days under an atmosphere of 5% CO_2 at 37°C. The cell–scaffold complexes were fixed with 4% paraformaldehyde; dehydrated and embedded in paraffin wax using a tissue dehydrator; processed for histological analysis; and stained with haematoxylin and eosin (H&E), safranin O, and toluidine blue. All procedures were carried out in accordance with the instructions provided by the reagent manufacturers. For quantitative evaluation of aggrecan and type II collagen in the ECM, the cell–scaffold complexes were removed from the incubator, transferred to liquid nitrogen for several minutes, and then stored at −80°C. Aggrecan and type II collagen enzyme-linked immunosorbent assay (ELISA) kits (R&D Systems, Minneapolis, MN, United States) were used in accordance with the manufacturer's instructions.

Cytotoxicity Assay

The cytotoxicity of the scaffold resulting from the residual reagents and/or processing was determined by assessment of cell proliferation using cell counting kit-8 (CCK-8; Dojindo, Rockville, MD, United States). Briefly, the four freeze-dried scaffolds were placed in 24-well plates and pre-wetted with culture solution in an incubator for at least 12 h before cell seeding. Then, P3 BMSCs (1 × 107 cells/mL) were seeded onto each scaffold and incubated at 37°C under an atmosphere of 5% CO2 for 7 days. CCK-8 solution was added to each well at 1, 3, 5, and 7 days, in accordance with the manufacturer's instructions. The absorbances at 450 nm (A450) of the samples were recorded using a microplate reader. Six replicates of each scaffold type were studied.

Cell Adhesion and Viability Assessment

Cell adhesion and morphology of BMSCs grown on PLGA(KGN)/CECM scaffold were assessed by SEM after 48 h of cell culture. The viability of adhesive cells on the scaffold was measured using a live/dead cell viability assay kit at 1 and 3 days, in accordance with the manufacturer's instructions. Briefly, the cell–scaffold samples were incubated in a solution containing calcein (2 × 106 M) and ethidium homodimer-1 (4 × 106 M) for 15–20 min at 37°C, under an atmosphere of 5% CO2; they were then rinsed two to three times with sterile PBS. Cell viability was visualized using laser confocal microscopy (Leica). The numbers of live (green fluorescence) and dead (red fluorescence) cells were calculated using ImageJ.

Chondrogenic Induction *in vivo*

A full-layer cartilage defect model was used to evaluate the ability of the PLGA(KGN)/CECM scaffold to promote chondrogenic induction. This study was approved by the Institutional Research Ethics Committee of Tianjin Medical University. Twenty-four female New Zealand White rabbits (4–5 months old, 2.5–3.0 kg) were randomly divided into four groups and acclimatized for 1 week at Tianjin Institute of Orthopedics and Sports Medicine before the operation. Rabbits were injected with 30% urethane (2.2 mL/kg) through the ear vein. A lateral para-patellar skin incision, approximately 3 cm in length, was made in both knee joints of each rabbit. Following layer-by-layer incision, the joint capsule was opened. The femoral condyle was exposed following patellar dislocation. A corneal trephine was used to drill a full-thickness cartilage defect (diameter of 4 mm and depth of 1 mm). An acne needle was used to prepare a microfracture on the subchondral bone layer. Defect sites were treated with one of the four scaffolds: (1) CECM, (2) CECM-TGFβ3, (3) PLGA(KGN)/CECM, and (4) PLGA(KGN)/CECM-TGFβ3. The incisions were then sutured in a layer-by-layer manner. Each rabbit was intramuscularly injected with 800,000 units of penicillin once per day for 1 week postoperatively. At 4 and 12 weeks postoperatively, all rabbits were sacrificed by anesthesia overdose and whole knees were collected. Finally, the effects on chondrogenic induction *in vivo* and cartilage defect repair were evaluated by general observation, H&E staining, toluidine blue staining, safranin O staining (Solarbio, Beijing, China), and type II collagen and aggrecan Western blotting.

Statistical Analysis

Data analysis was performed with IBM SPSS Statistics, version 19.0 (IBM Corp., Armonk, NY, United States). Data are presented as the means ± standard deviations. One-way analysis of variance was performed to determine statistical significance, followed by Tukey's *post hoc* test or Dunnett's T3 *post hoc* test. For all analyses, $P < 0.05$ was considered to indicate statistical significance.

RESULTS

Characterization of PLGA(KGN) Microspheres and Microsphere-Embedded CECM-Derived Scaffolds

The prepared PLGA microspheres and nanoparticles loaded with KGN showed a spherical morphology with a smooth external surface; incorporation of KGN did not produce any meaningful changes in the PLGA scaffold structure (**Figures 1A,B**). NanoZS90 analysis indicated that the mean diameters of PLGA microspheres and nanoparticles were 2.186 μm and 288.8 nm, respectively. A standard curve was constructed to determine KGN concentration. The trapping efficiency and drug loading

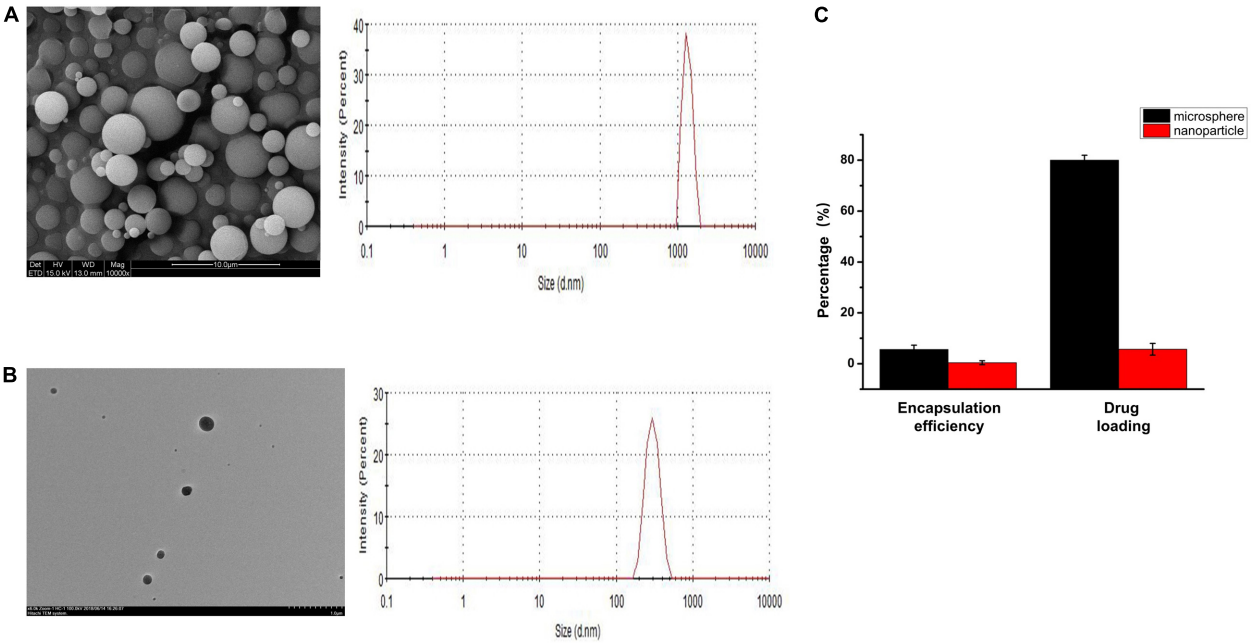

FIGURE 1 | (A) SEM image and particle size distribution of PLGA microspheres. **(B)** TEM image and particle size distribution of PLGA nanoparticles. **(C)** Drug loading and encapsulating efficiency rates of PLGA microspheres and PLGA nanoparticles.

rate of PLGA microspheres were 80 and 5.6%, respectively; for PLGA nanoparticles, those parameters were 5.7 and 0.4%, respectively (**Figure 1C**). Therefore, PLGA microspheres were selected for subsequent experiments. The morphology of the PLGA(KGN)/CECM composite scaffold is presented in **Figure 2A**. The scaffold demonstrated alveolar construction; the interconnected pores of the scaffold exhibited a uniform distribution and the apertures were generally uniform in size. Quantitative analysis revealed that the mean pore diameter was 140 μm (**Figure 2A**), which met the requirements for use in cartilage tissue engineering. This scaffold was presumed to provide sufficient space for cell adhesion and proliferation, and was considered suitable for the transport of nutritive materials and metabolic waste.

In vitro Release of KGN From Microspheres and Scaffold System

The release of KGN from the CECM/PLGA system (CKP) was monitored for 30 days and compared with the direct release of KGN from the CECM (CK) scaffold. The cumulative release curve (**Figure 2B**) clearly showed two distinct release patterns of CECM/PLGA and CECM. The release curve of CK reached a plateau after initial rapid release in the first 7 days; cumulative release during that period reached 70% of the gross release. The release curve of CKP demonstrated that there was almost no KGN release in the first 5 days and cumulative release reached approximately 45% of the gross release during the first 10 days; thereafter, it entered a sustained slow-release phase cumulative release reached approximately 45% of the gross release during the first 10 days. The results showed that the CKP displayed controlled and sustained release behavior. Therefore, it was considered suitable for long-term treatment in promoting cartilage regeneration.

Cell Viability and Proliferation Inside the CECM/PLGA Composite Scaffold

To assess the biocompatibility of PLGA(KGN)/CECM scaffolds, BMSCs were seeded in the scaffolds. The biocompatibility of scaffolds was evaluated by cell viability, cell proliferation, and cell adhesion assays. Cell viability was assessed by live/dead staining. As shown in **Figure 3A**, there were few dead cells on the scaffold, indicating that BMSCs on the scaffold exhibited good cell viability. Cell proliferation, as determined by CCK-8 assay, is shown in **Figure 3B**. The number of cells increased over time in each group; the three induced groups showed higher rates of increase than the control group, indicating that the scaffold remained safe and non-toxic after embedding of KGN-encapsulated PLGA microspheres. SEM images of cell adhesion in the PLGA(KGN)/CECM composite scaffold are shown in **Figure 3C**. BMSCs with rough morphology were attached to the inner wall surface of the scaffold; some extended pseudopods and wound through the scaffold. These results further validated that the PLGA(KGN)/CECM scaffold promoted cell adhesion, which could be beneficial for use in cartilage regeneration after *in vivo* implantation.

Isolation and Chondrogenic Differentiation of the BMSCs

BMSCs were successfully extracted and cultured to passage 3. Following chondrogenesis culture of BMSCs within the four

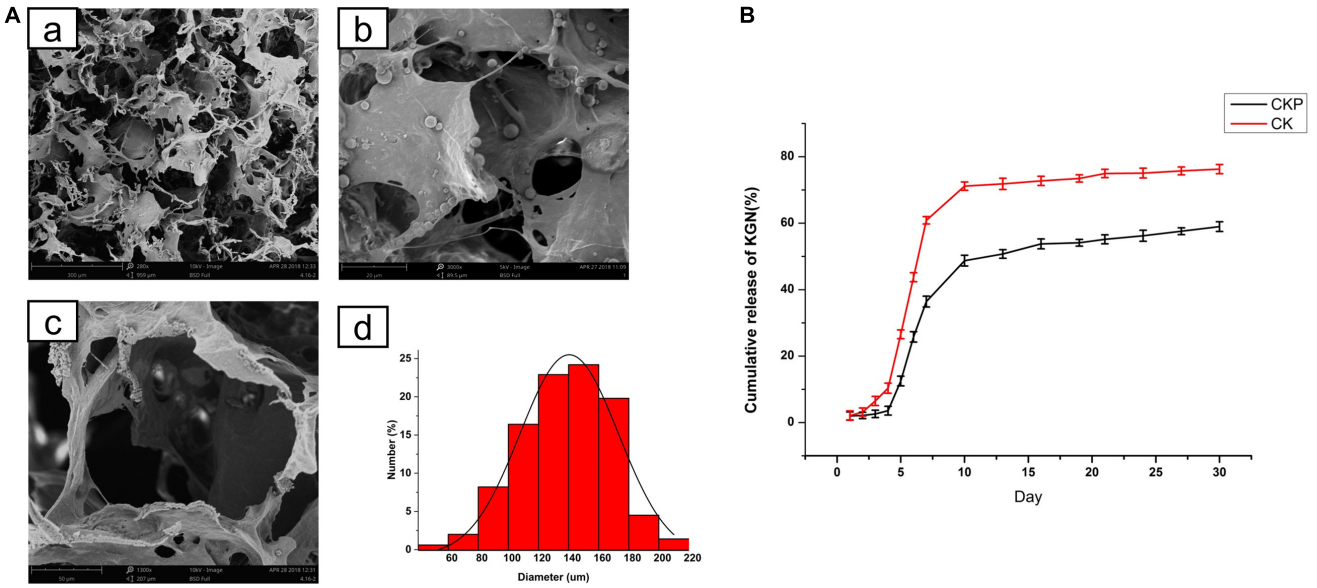

FIGURE 2 | (A) Morphology of PLGA(KGN)/CECM composite scaffold: **(a)** PLGA microsphere embedded in CECM scaffold; **(b)** low power (280×); **(c)** pore morphology (1,300×); **(d)** pore size distribution. **(B)** Comparison of release patterns between CECM/PLGA and CECM scaffolds (CKP: PLGA(KGN)/CECM; CK: CECM-KGN).

scaffolds for 4 weeks, histological staining (H&E, safranin O, and toluidine blue) and quantitative ELISA analysis of glycosaminoglycan (GAG) and type II collagen were used to compare the chondrogenesis capability of BMSCs among the four scaffolds. As shown in **Figure 4A**, H&E, toluidine blue, and safranin O staining results indicated that KGN and TGF-β3 both promoted proliferation and chondrogenic differentiation of BMSCs; the cell–scaffold complex exhibited consistent histological findings among the three staining methods. With the exception of the control group, which showed no intact cells or nuclei within CECM scaffolds, the numbers of cells in the other three induced groups (TGF-β3, KGN, and TGF-β3 + KGN) significantly increased over time. The nucleus and cytoplasm were visible by H&E staining, indicating that the cells were in good overall condition; the cell morphology changed from long fusiform to round or oval, indicating that the MSCs had differentiated into chondrocytes. Toluidine blue and safranin O staining revealed that most cells and their secretions in the three induced groups were stained, indicating the presence of type II collagen and GAG components after 28 days of culture.

Longitudinal comparison of the staining conditions of the four groups after 14 and 28 days of culture indicated no significant differences among the TGF-β3, KGN, and TGF-β3 + KGN groups. We presumed that KGN and TGF-β3 did not exhibit a synergistic effect with respect to inducing BMSC differentiation into chondrocytes. These findings were consistent with the results of quantitative analysis of two representative components of hyaline cartilage: GAG and type II collagen (**Figure 4B**). After 14 days of culture, the total amounts of type II collagen and GAG in the three induced groups did not significantly differ from the total amounts in the control group. After 28 days of culture, the total amounts of type II collagen and GAG were significantly higher in the three induced groups (TGF-β3, KGN, TGF-β3 + KGN) than the control group; however, the total amounts did not significantly differ among the three induced groups. After 14 days of culture, there were no significant differences in the enhancement of type II collagen level among the four groups, while the enhancement of GAG level in the three induced groups significantly differed from the enhancement in the control group. After 28 days of culture, the enhancement of type II collagen level in the three induced groups also significantly differed from the enhancement in the control group.

Cartilage Repair Assessment in the Rabbit Model

A cartilage defect model was successfully established, as described in the Methods section. At predetermined time points of 8 and 12 weeks, the rabbits were sacrificed and their femoral condyles were harvested. Subsequent assessments were performed to estimate the cartilage regeneration efficiency *in vivo*.

Macroscopic Observation

Macroscopic observation of repaired cartilage was performed, as shown in **Figure 5**. At 4 weeks postoperatively, the vestiges of the articular cartilage defect remained, but new tissue began to appear in the three induction groups, whereas it did not in the blank scaffold group (treatment with CECM scaffold alone). At 12 weeks postoperatively, the control group exhibited broad areas of cartilage destruction and surface denudation, while constructs induced with either KGN or TGF-β3 generally showed an intact surface. The boundary with surrounding natural cartilage was

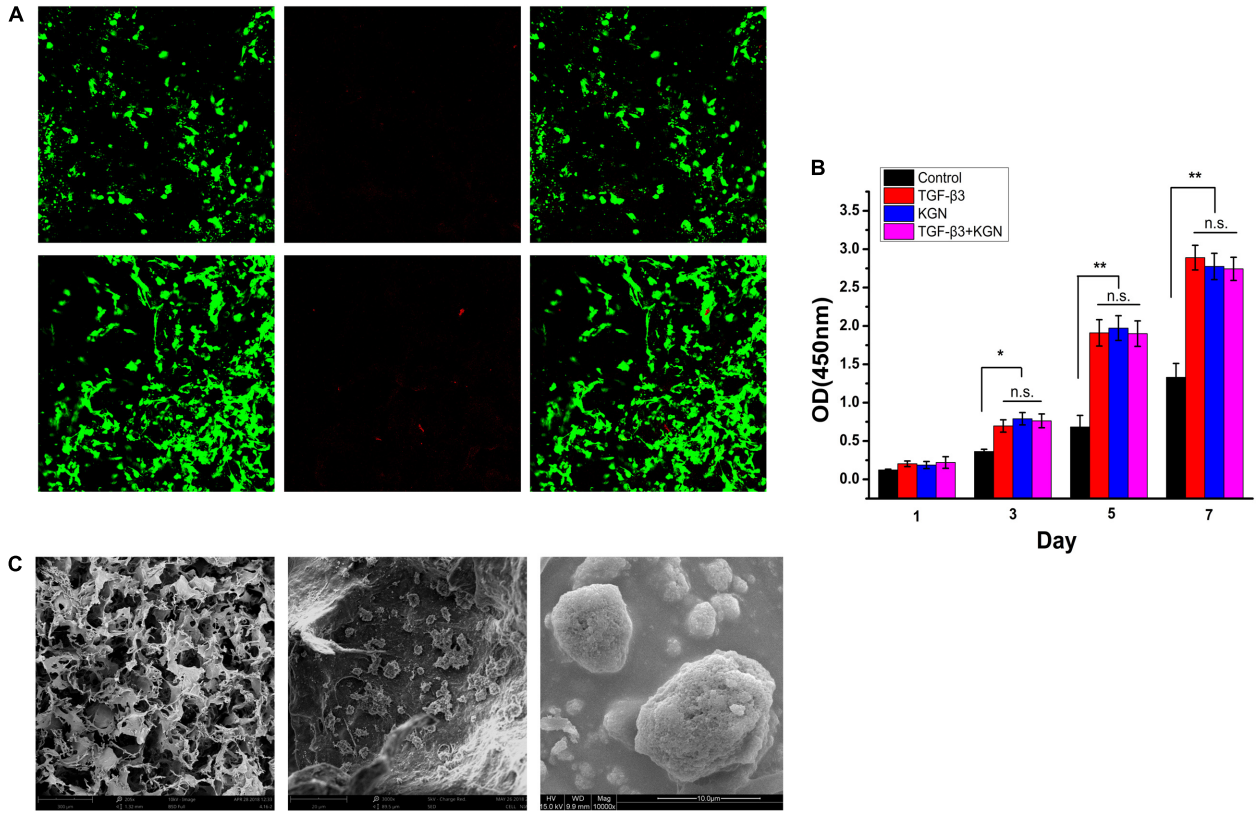

FIGURE 3 | (A) Live (green)/dead (red) assessment of BMSCs on composite scaffold. **(B)** Scaffold cytotoxicity assessment using a CCK-8 kit to assess cell proliferation (*$P < 0.05$; **$P < 0.01$; n.s., not significant). **(C)** SEM images of BMSC adherence.

less noticeable in the KGN-induced group, compared to the TGF-β3-induced group. Combined induction with both factors did not enhance the repair effect, compared to either KGN or TGF-β3 alone.

Histological Staining Analysis

H&E staining of regenerated cartilage in the four groups is depicted in **Figure 6A**. At 12 weeks postoperatively, H&E staining revealed cartilage defects in the blank scaffold group. In contrast, cartilage defect areas in the KGN, TGF-β3. and TGF-β3 + KGN groups were mostly covered with new cartilage tissue; the thickness of the new tissue was similar to that of the surrounding normal cartilage layer. The chondrocyte concentration and ECM deposition were significantly enhanced, while the number of inflammatory cells was reduced, compared with 4 weeks postoperatively. Blue dye was evident in toluidine blue staining assays (**Figure 6A**), further confirming the changes in cartilage matrix content. Compared with the other two groups, staining intensity was higher in the KGN and TGF-β3 + KGN groups that contained higher glucosamine polysaccharide content in the cartilage ECM.

Western Blotting Analysis

Type II collagen and aggrecan protein expression were further assessed by Western blotting analysis (**Figures 6B,C**). At both 4 and 8 weeks postoperatively, the three induced groups displayed much stronger bands of type II collagen and aggrecan, compared with the blank scaffold group. However, there were no visible differences among the three induced groups.

DISCUSSION

Tissue engineering offers novel and effective approaches for repairing articular cartilage defects. While numerous cell-based techniques have been applied to repair and regenerate cartilage defects, these techniques have multiple limitations, including cellular apoptosis and increased risk of disease transmission, resulting in low repair efficiency (Trounson and McDonald, 2015; Huang et al., 2016). Cell-free strategies have been proposed to repair and regenerate the injured cartilage by recruitment of endogenous stem cells, thus avoiding many of the limitations and pitfalls of cell-based strategies and allowing broader clinical application. The present study demonstrated that a cell-free scaffold based on CECM and PLGA microspheres loaded with KGN provided an optimal *in vitro* environment for the attachment and chondrogenesis of BMSCs. Following implantation into a cartilage defect in the rabbit knee joint, the scaffold supported chondrogenic differentiation of endogenous BMSCs, thus promoting the regeneration of hyaline cartilage.

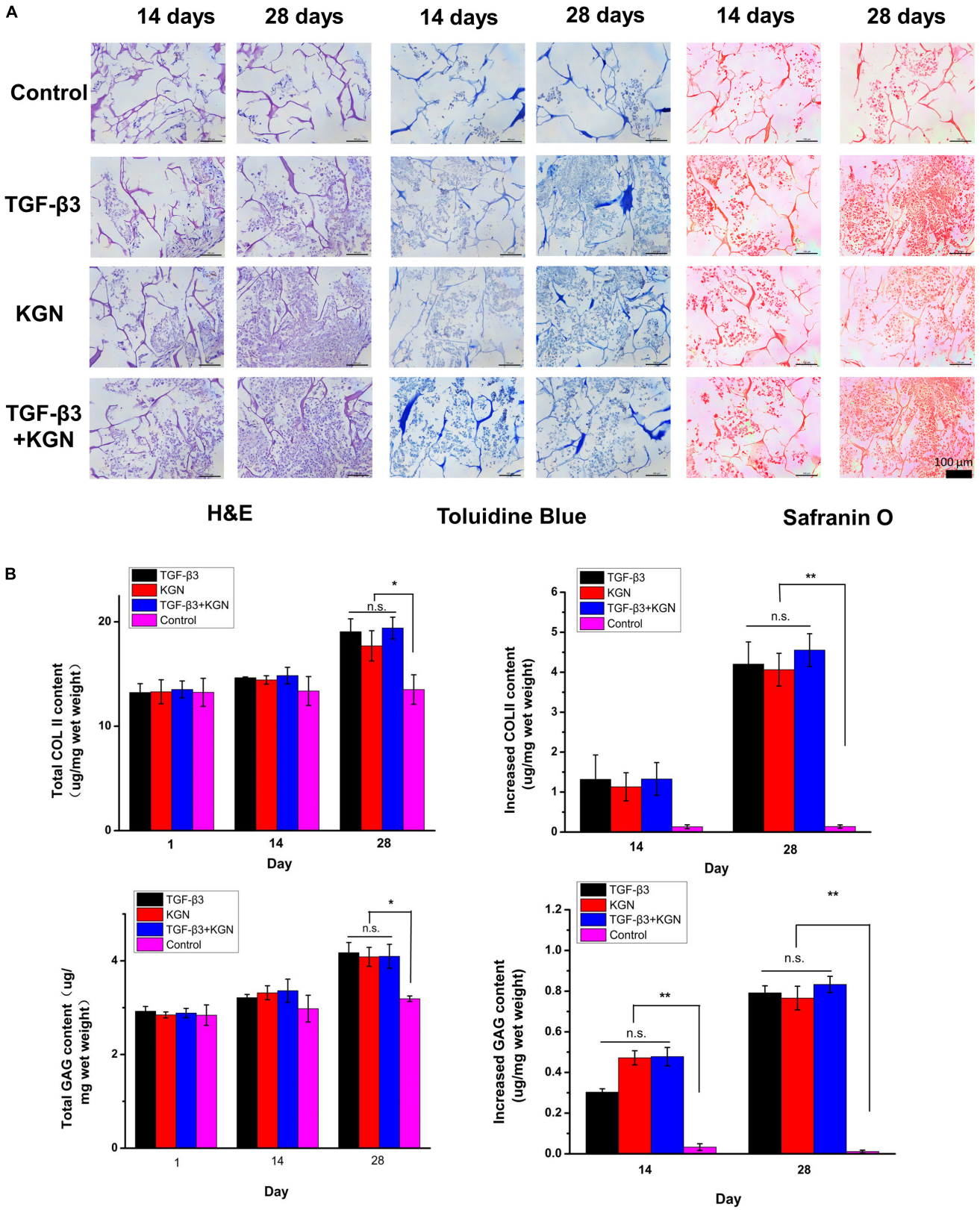

FIGURE 4 | (A) Histology of chondrogenic matrix formation within the composite scaffold. **(B)** Quantitative analysis of GAG and type II collagen by ELISA. *$p < 0.05$, **$p < 0.01$.

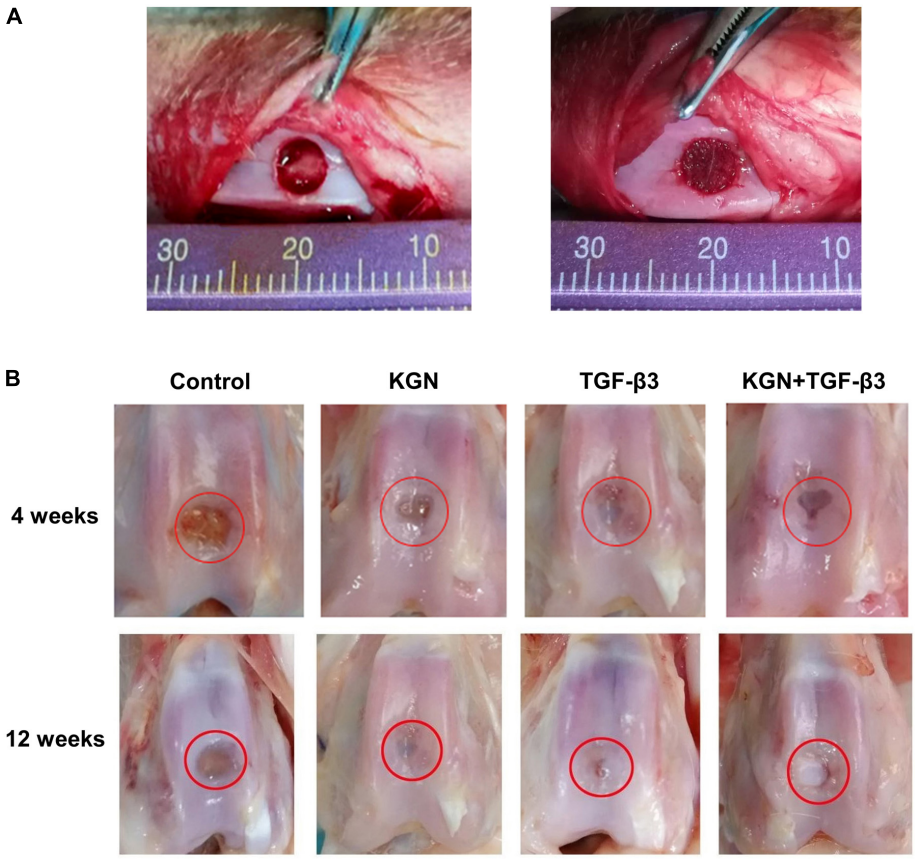

FIGURE 5 | (A) Full-thickness cartilage defect model of rabbit femoral trochlea. **(B)** Gross observation at different time points.

The fabrication of biomimetic scaffolds to recreate the structural features of native articular cartilage is crucial for successful cartilage regeneration. In our previous studies, we developed and characterized a structurally biomimetic oriented scaffold derived from CECM, which could closely mimic the natural chondrogenesis microenvironment (Yang et al., 2008, 2017). The CECM scaffold preserves multiple structural and functional proteins (e.g., fibronectin, hyaluronic acid, and GAG), which could modify the secretion of GAG and type II collagen to further induce specific cellular responses and direct new tissue formation (Sutherland et al., 2015; Ng et al., 2016). In the present study, we combined PLGA and CECM to produce composite scaffolds, which revealed the complementary benefits of the two materials. Notably, the presence of CECM provided good scaffold biocompatibility; additionally, the presence of PLGA conferred adequate mechanical support and relatively long degradation time, thereby matching the neocartilage formation rate (Lih et al., 2016). We showed that the composite scaffold with appropriate pore structure and pore diameter served as a guide for BMSC attachment, distribution, and proliferation; thus facilitating chondrogenic differentiation (**Figure 2A**). These findings indicated that we had fabricated the physiological structure of native cartilage.

The PLGA microsphere-embedded CECM scaffold can serve to mimic some features of the native ECM; it also enables sustained and localized delivery of bioactive molecules to achieve prolonged exposure of BMSCs to bioactive molecules. Previous studies have shown that the delivery effect of PLGA is related to multiple factors (Wu et al., 2013; Zhu et al., 2019) including the grain size of PLGA spheres; this parameter mainly affects the specific surface area, distribution of hydrophobic drugs in spheres, and polymer degradation rate (Chen et al., 2015; Almeida et al., 2020). Therefore, it is necessary to identify a suitable particle size range that can preserve resources and effectively control KGN release. In the present study, we fabricated PLGA microspheres and nanoparticles for encapsulation of KGN. Following multiple analyses, we chose PLGA microspheres for subsequent experiments because of their considerable advantages in terms of drug loading and encapsulating efficiency (**Figure 1C**). To evaluate the controlled release effect of the composite scaffold, we monitored the release of KGN for 30 days. The release curve of KGN loaded in the CKP group demonstrated that there was almost no KGN release in the first 5 days and cumulative release reached approximately 45% of the gross release during the first 10 days; thereafter, it entered a sustained slow-release phase (**Figure 2B**). We speculate that this is due to the protection of CECM scaffolds

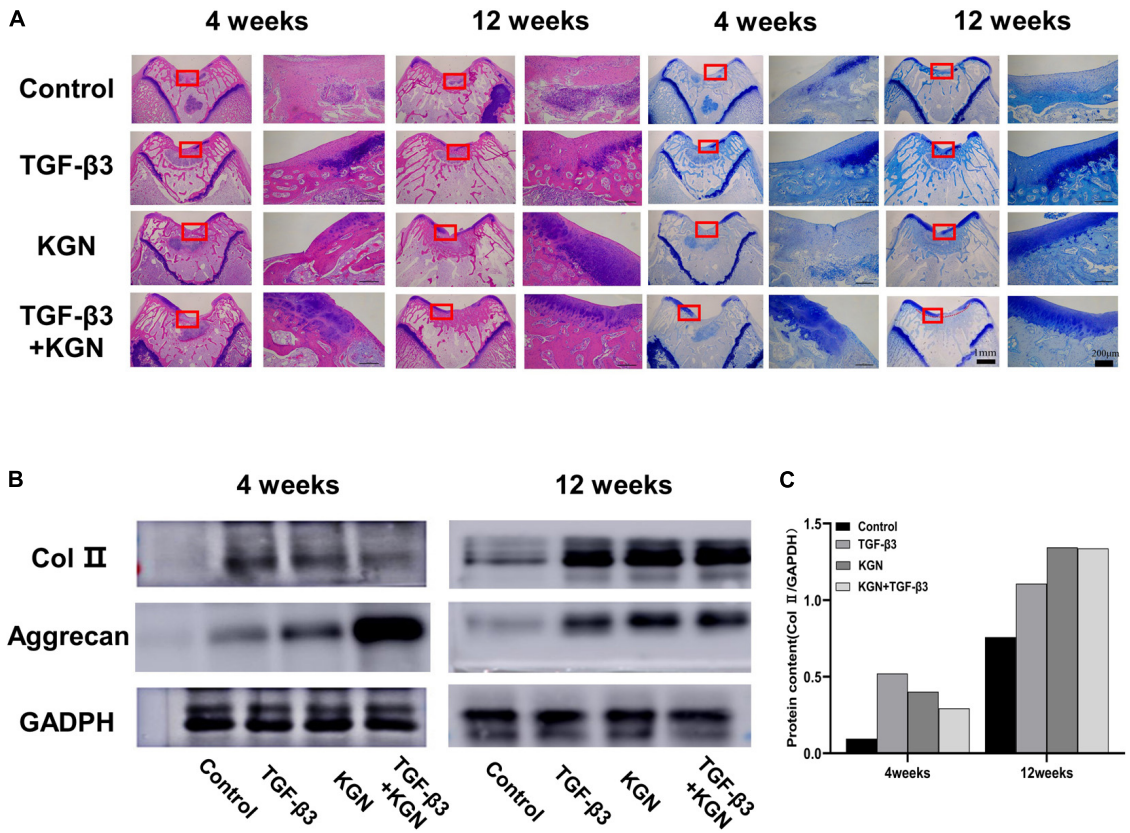

FIGURE 6 | (A) Histology of defects at 4 and 12 weeks. **(B)** Western blotting analysis of type II collagen and aggrecan at 4 and 12 weeks. **(C)** Gray value analysis of type II collagen bands.

on PLGA microspheres, which prevents the degradation of PLGA microspheres caused by rapid water entry. Therefore, in the first 5 days, only the drugs on the surface of the microspheres were released. The microspheres began to degrade in 5–10 days, which accelerated the drug release inside the microspheres. The CKP group demonstrated more robust sustained-release capability, compared to the CK group with more obvious sudden release; this implied that the composite scaffold had a double-sustained effect on KGN release, such that it may be suitable for long-acting administration of KGN in clinical applications. Notably, the PLGA microsphere-embedded scaffolds improved the diffusion path because KGN was confined to the core region of the PLGA microspheres and initially dispersed through the shell polymer before departure from the CECM. In addition, the amine groups of PLGA and the carboxyl groups of KGN exhibited strong covalent linkages, which aided in controlled release.

The bioactivity of released KGN was assessed by measuring the ability of the KGN-loaded scaffold to promote BMSC growth and chondrogenesis. Our assessment indicated that this KGN-releasing system promoted BMSC viability and proliferation (**Figure 3**); it also enhanced proteoglycan deposition and type II collagen content compared to the control group, potentially promoting the regeneration of cartilage *in vitro* (**Figure 4**). These findings were consistent with previous research demonstrating the chondrogenic effect of KGN supplementation on BMSC growth (Johnson et al., 2012). Furthermore, *in vivo* evidence indicated nearly complete repair of cartilage defects at 12 weeks after implantation of the KGN-releasing composite scaffold. Notably, the neocartilage was integrated with its surrounding tissue and subchondral bone (**Figure 6A**). The levels of type II collagen and GAG expression were elevated in the three induced groups, compared to the control group (**Figures 6B,C**), thereby improving the quantity and quality of regenerated tissue at the chondral interface. A previous study demonstrated similar improvements in proliferation and chondrogenesis of human adipose-derived MSCs or synovium-derived MSCs by treatment with KGN (Shi et al., 2016; Zhu et al., 2017). Therefore, we speculated that the cartilage repair process could be continued by recruiting other sources of MSCs when BMSCs were no longer enriched after microfracture healing. Further studies are required to examine this aspect of cartilage repair treatment.

In the present study, KGN loaded in CECM/PLGA was able to induce differentiation of BMSCs in a manner similar to that of TGF-β3 loaded in CECM, but combined treatment did not show synergistic effects. Our observations were consistent with the findings by Zhu et al., who demonstrated that KGN was a suitable replacement for TGF-β3 in terms of type II collagen induction and aggrecan deposition, but that it did not

promote or enhance the effects of TGF-β3 (Zhu et al., 2017). However, Jia et al. reported that the combination of TGF-β3 and KGN synergistically promoted chondrogenic differentiation of synovial fluid-derived MSCs via the Smad 2/3 pathway (Jia et al., 2019). Recently, Jing and colleagues also reported that KGN preconditioning could exert dually beneficial effects on TGF-β3-induced chondrogenic differentiation of human umbilical cord MSCs (Jing et al., 2019). Therefore, we speculate that the synergistic effect of combined KGN and TGF-β3 treatment may be based on sequential application consisting of KGN preconditioning with subsequent TGF-β3 induction; the synergism disappeared when the sequential application was disrupted in this study. Another possibility is that the synergistic effect may only be observed for some specific type(s) of MSCs (e.g., adipose-derived MSCs). Further studies are required to explore the mechanisms underlying these effects.

To sum up, although the CECM scaffolds and PLGA microspheres have been widely performed in the cartilage tissue engineering, the combined application of these two materials is rarely investigated. In this study, we updated the application approach of KGN through loading KGN into the CECM/PLGA scaffold. The porous CECM/PLGA scaffolds can not only cover the advantages of CECM porous scaffolds and PLGA microspheres, but also sustain the KGN release. Besides, the scaffold in the present study showed the similar cartilage regeneration efficiency with TGF-β3, hence, we hope that KGN can be a suitable replacement for TGF-β3 in cartilage tissue engineering to avoid some adverse effects caused by excessive TGF-β3 (Mi et al., 2003).

This study had some limitations. First, the biomechanical properties of the scaffold were not fully analyzed. Second, the present results were obtained in a rabbit model. Therefore, before human clinical trials, the scaffold should be examined in large-animal models that are immunologically similar to humans, which can provide evidence of its safety and efficiency.

CONCLUSION

We successfully prepared a composite scaffold by blending KGN-encapsulated PLGA microspheres and CECM. *In vitro* assessments demonstrated that the PLGA(KGN)/CECM composite scaffold prolonged the activity of KGN and supported the attachment, proliferation, and differentiation of BMSCs. Initial *in vivo* analysis indicated that the PLGA(KGN)/CECM induced superior hyaline-like neocartilage repair; the neocartilage successfully integrated with its surrounding tissue in a rabbit model. Moreover, the PLGA(KGN)/CECM system avoids difficult cell manipulation during preparation, providing a new small molecule-based strategy for cartilage tissue engineering.

DATA AVAILABILITY STATEMENT

The original contributions presented in the study are included in the article/supplementary material, further inquiries can be directed to the corresponding author/s.

ETHICS STATEMENT

The animal study was reviewed and approved by Tianjin Medical University.

AUTHOR CONTRIBUTIONS

YHZ and YMZ designed and conceptualized the work. XGZ and RZ carried out the study and collected the crucial background information. YH, YL, and XTZ collected the data. MS analyzed and interpreted the data. XGZ and YHZ wrote the manuscript. YX, MW, and YZ revised the manuscript critically. All authors have read and approved the final manuscript.

FUNDING

This work was supported by Research Foundation of the Tianjin Health Bureau (16KG114).

REFERENCES

Almeida, B., Wang, Y., and Shukla, A. (2020). Effects of nanoparticle properties on kartogenin delivery and interactions with mesenchymal stem cells. *Ann. Biomed. Eng.* 48, 2090–2102. doi: 10.1007/s10439-019-02430-x

Almeida, H., Liu, Y., Cunniffe, G., Mulhall, K., Matsiko, A., Buckley, C., et al. (2014). Controlled release of transforming growth factor-β3 from cartilage-extra-cellular-matrix-derived scaffolds to promote chondrogenesis of human-joint-tissue-derived stem cells. *Acta biomater.* 10, 4400–4409. doi: 10.1016/j.actbio.2014.05.030

Cai, J., Zhang, L., Chen, J., and Chen, S. (2019). Kartogenin and its application in regenerative medicine. *Curr. Med. Sci.* 39, 16–20. doi: 10.1007/s11596-019-1994-6

Cals, F. L., Hellingman, C. A., Koevoet, W., Baatenburg de Jong, R. J., and van Osch, G. J. (2012). Effects of transforming growth factor-beta subtypes on in vitro cartilage production and mineralization of human bone marrow stromal-derived mesenchymal stem cells. *J. Tissue Eng. Regen. Med.* 6, 68–76. doi: 10.1002/term.399

Chen, C., Huang, K., Zhu, J., Bi, Y., Wang, L., Jiang, J., et al. (2020). A novel elastic and controlled-release poly(ether-ester-urethane)urea scaffold for cartilage regeneration. *J. Mater. Chem. B* 8, 4106–4121. doi: 10.1039/c9tb02754h

Chen, Y., Green, C., Wang, K., Danesh-Meyer, H., and Rupenthal, I. (2015). Sustained intravitreal delivery of connexin43 mimetic peptide by poly(D,L-lactide-co-glycolide) acid micro- and nanoparticles–Closing the gap in retinal ischaemia. *Eur. J. Pharm. Biopharm.* 95, 378–386. doi: 10.1016/j.ejpb.2014.12.005

Danhier, F., Ansorena, E., Silva, J., Coco, R., Le Breton, A., and Préat, V. (2012). PLGA-based nanoparticles: an overview of biomedical applications. *J. Control. Release* 161, 505–522. doi: 10.1016/j.jconrel.2012.01.043

Dong, Y., Sun, X., Zhang, Z., Liu, Y., Zhang, X., and Huang, Y. (2020). Regional and sustained dual-release of growth factors from biomimetic tri-layered

scaffolds for the repair of large-scale osteochondral defects. *Appl. Mater. Today* 19:100548. doi: 10.1016/j.apmt.2019.100548

Fan, W., Li, J., Yuan, L., Chen, J., Wang, Z., Wang, Y., et al. (2018). Intra-articular injection of kartogenin-conjugated polyurethane nanoparticles attenuates the progression of osteoarthritis. *Drug. Deliv.* 25, 1004–1012. doi: 10.1080/10717544.2018.1461279

Fan, W., Yuan, L., Li, J., Wang, Z., Chen, J., Guo, C., et al. (2020). Injectable double-crosslinked hydrogels with kartogenin-conjugated polyurethane nanoparticles and transforming growth factor β3 for in-situ cartilage regeneration. *Mater. Sci. Eng. C Mater. Biol. Appl.* 110:110705. doi: 10.1016/j.msec.2020.110705

Fernando, L., Lewis, J., Evans, B., Duvall, C., and Keselowsky, B. (2018). Formulation and characterization of poly(propylacrylic acid)/poly(lactic-co-glycolic acid) blend microparticles for pH-dependent membrane disruption and cytosolic delivery. *J. Biomed. Mater. Res. A* 106, 1022–1033. doi: 10.1002/jbm.a.36298

Gupta, V., Khan, Y., Berkland, C. J., Laurencin, C. T., and Detamore, M. S. (2017). Microsphere-based scaffolds in regenerative engineering. *Annu. Rev. Biomed. Eng.* 19, 135–161. doi: 10.1146/annurev-bioeng-071516-044712

Huang, B. J., Hu, J. C., and Athanasiou, K. A. (2016). Cell-based tissue engineering strategies used in the clinical repair of articular cartilage. *Biomaterials* 98, 1–22. doi: 10.1016/j.biomaterials.2016.04.018

Jia, Z., Wang, S., Liang, Y., and Liu, Q. (2019). Combination of kartogenin and transforming growth factor-β3 supports synovial fluid-derived mesenchymal stem cell-based cartilage regeneration. *Am. J. Transl. Res.* 11, 2056–2069.

Jing, H., Zhang, X., Gao, M., Luo, K., Fu, W., and Yin, M. (2019). Kartogenin preconditioning commits mesenchymal stem cells to a precartilaginous stage with enhanced chondrogenic potential by modulating JNK and β-catenin-related pathways. *FASEB J.* 33, 5641–5653. doi: 10.1096/fj.201802137rrr

Johnson, K., Zhu, S., Tremblay, M. S., Payette, J. N., Wang, J., and Bouchez, L. C. (2012). A stem cell-based approach to cartilage repair. *Science* 336, 717–721.

Kang, M. L., Ko, J. Y., Kim, J. E., and Im, G. I. (2014). Intra-articular delivery of kartogenin-conjugated chitosan nano/microparticles for cartilage regeneration. *Biomaterials* 35, 9984–9994. doi: 10.1016/j.biomaterials.2014.08.042

Kwon, J., Lee, S., Na, H., Jung, K., Choi, J., and Cho, K. (2018). Kartogenin inhibits pain behavior, chondrocyte inflammation, and attenuates osteoarthritis progression in mice through induction of IL-10. *Sci. Rep.* 8:13832.

Li, X., Ding, J., Zhang, Z., Yang, M., Yu, J., Wang, J., et al. (2016). Kartogenin-incorporated thermogel supports stem cells for significant cartilage regeneration. *ACS Appl. Mater. Interfaces* 8, 5148–5159. doi: 10.1021/acsami.5b12212

Lih, E., Park, K. W., Chun, S. Y., Kim, H., Kwon, T. G., Joung, Y. K., et al. (2016). Biomimetic porous PLGA scaffolds incorporating decellularized extracellular matrix for kidney tissue regeneration. *ACS Appl. Mater. Interfaces* 8, 21145–21154. doi: 10.1021/acsami.6b03771

Liu, F., Xu, H., and Huang, H. (2019). A novel kartogenin-platelet-rich plasma gel enhances chondrogenesis of bone marrow mesenchymal stem cells in vitro and promotes wounded meniscus healing in vivo. *Stem Cell Res. Ther.* 10:201.

Loeser, R. F., Collins, J. A., and Diekman, B. O. (2016). Ageing and the pathogenesis of osteoarthritis. *Nat. Rev. Rheumatol.* 12, 412–420. doi: 10.1038/nrrheum.2016.65

Malfait, A. M. (2016). Osteoarthritis year in review 2015: *Biol. Osteoarthritis Cartilage* 24, 21–26. doi: 10.1016/j.joca.2015.09.010

Mi, Z., Ghivizzani, S., Lechman, E., Glorioso, J., Evans, C., and Robbins, P. (2003). Adverse effects of adenovirus-mediated gene transfer of human transforming growth factor beta 1 into rabbit knees. *Arthritis Res. Ther.* 5, R132–R139.

Monibi, F. A., and Cook, J. L. (2017). Tissue-derived extracellular matrix bioscaffolds: emerging applications in cartilage and meniscus repair. *Tissue Eng. Part B Rev.* 23, 386–398. doi: 10.1089/ten.teb.2016.0431

Ng, J., Wei, Y., Zhou, B., Burapachaisri, A., Guo, E., and Vunjak-Novakovic, G. (2016). Extracellular matrix components and culture regimen selectively regulate cartilage formation by self-assembling human mesenchymal stem cells in vitro and in vivo. *Stem Cell Res. Ther.* 7:183.

Oh, H. J., Kim, S. H., Cho, J. H., Park, S. H., and Min, B. H. (2018). Mechanically reinforced extracellular matrix scaffold for application of cartilage tissue engineering. *Tissue Eng. Regen. Med.* 15, 287–299. doi: 10.1007/s13770-018-0114-1

Ravindran, S., Kotecha, M., Huang, C. C., Ye, A., Pothirajan, P., Yin, Z., et al. (2015). Biological and MRI characterization of biomimetic ECM scaffolds for cartilage tissue regeneration. *Biomaterials* 71, 58–70. doi: 10.1016/j.biomaterials.2015.08.030

Shi, D., Xu, X., Ye, Y., Song, K., Cheng, Y., and Di, J. (2016). Photo-cross-linked scaffold with kartogenin-encapsulated nanoparticles for cartilage regeneration. *ACS Nano* 10, 1292–1299. doi: 10.1021/acsnano.5b06663

Sutherland, A. J., Converse, G. L., Hopkins, R. A., and Detamore, M. S. (2015). The bioactivity of cartilage extracellular matrix in articular cartilage regeneration. *Adv. Healthc. Mater.* 4, 29–39. doi: 10.1002/adhm.201400165

Trounson, A., and McDonald, C. (2015). Stem cell therapies in clinical trials: progress and challenges. *Cell Stem Cell* 17, 11–22. doi: 10.1016/j.stem.2015.06.007

van der Kraan, P., and van den Berg, W. (2007). Osteophytes: relevance and biology. *Osteoarthritis Cartilage* 15, 237–244. doi: 10.1016/j.joca.2006.11.006

Wang, J., Wang, Y., Sun, X., Liu, D., Huang, C., Wu, J., et al. (2019). Biomimetic cartilage scaffold with orientated porous structure of two factors for cartilage repair of knee osteoarthritis. *Artif. Cells Nanomed. Biotechnol.* 47, 1710–1721. doi: 10.1080/21691401.2019.1607866

Wang, J., Yang, Q., Cheng, N., Tao, X., Zhang, Z., and Sun, X. (2016). Collagen/silk fibroin composite scaffold incorporated with PLGA microsphere for cartilage repair. *Mater. Sci. Eng. C Mater. Biol. Appl.* 61, 705–711. doi: 10.1016/j.msec.2015.12.097

Wang, S. J., Qin, J. Z., Zhang, T. E., and Xia, C. (2019). Intra-articular injection of kartogenin-incorporated thermogel enhancing osteoarthritis treatment. *Front. Chem.* 7:677.

Wang, Z., Li, Z., Li, Z., Wu, B., Liu, Y., and Wu, W. (2018). Cartilaginous extracellular matrix derived from decellularized chondrocyte sheets for the reconstruction of osteochondral defects in rabbits. *Acta Biomater.* 81, 129–145. doi: 10.1016/j.actbio.2018.10.005

Wu, J., Kong, T., Yeung, K. W., Shum, H. C., Cheung, K. M., Wang, L., et al. (2013). Fabrication and characterization of monodisperse PLGA-alginate core-shell microspheres with monodisperse size and homogeneous shells for controlled drug release. *Acta Biomater.* 9, 7410–7419. doi: 10.1016/j.actbio.2013.03.022

Wu, M., Li, C., Zhu, G., Wang, Y., Jules, J., and Lu, Y. (2014). Deletion of core-binding factor β (Cbfβ) in mesenchymal progenitor cells provides new insights into Cbfβ/Runxs complex function in cartilage and bone development. *Bone* 65, 49–59. doi: 10.1016/j.bone.2014.04.031

Xu, X., Shi, D., Shen, Y., Xu, Z., Dai, J., and Chen, D. (2015). Full-thickness cartilage defects are repaired via a microfracture technique and intraarticular injection of the small-molecule compound kartogenin. *Arthritis Res. Ther.* 17:20. doi: 10.1177/1947603511408882

Xu, Y., Peng, J., Richards, G., Lu, S., and Eglin, D. (2019). Optimization of electrospray fabrication of stem cell-embedded alginate-gelatin microspheres and their assembly in 3D-printed poly(ε-caprolactone) scaffold for cartilage tissue engineering. *J. Orthop. Translat.* 18, 128–141. doi: 10.1016/j.jot.2019.05.003

Yang, Q., Peng, J., Guo, Q., Huang, J., Zhang, L., Yao, J., et al. (2008). A cartilage ECM-derived 3-D porous acellular matrix scaffold for in vivo cartilage tissue engineering with PKH26-labeled chondrogenic bone marrow-derived mesenchymal stem cells. *Biomaterials* 29, 2378–2387. doi: 10.1016/j.biomaterials.2008.01.037

Yang, Q., Teng, B., Wang, L., Li, K., Xu, C., and Ma, X. (2017). Silk fibroin/cartilage extracellular matrix scaffolds with sequential delivery of TGF-β3 for chondrogenic differentiation of adipose-derived stem cells. *Int. J. Nanomed.* 12, 6721–6733. doi: 10.2147/ijn.s141888

Yang, W., Zhu, P., Huang, H., Zheng, Y., Liu, J., Feng, L., et al. (2019). Functionalization of novel theranostic hydrogels with kartogenin-grafted uspio nanoparticles to enhance cartilage regeneration. *ACS Appl. Mater. Interfaces* 11, 34744–34754. doi: 10.1021/acsami.9b12288

Zhang, M., Cheng, J., Xiao, Y., Yin, R., and Feng, X. (2017). Raloxifene microsphere-embedded collagen/chitosan/β-tricalcium phosphate scaffold for effective bone tissue engineering. *Int. J. Pharm.* 518, 80–85. doi: 10.1016/j.ijpharm.2016.12.031

Zhen, G., Wen, C., Jia, X., Li, Y., Crane, J., and Mears, S. (2013). Cao, inhibition of TGF-β signaling in mesenchymal stem cells of subchondral bone attenuates osteoarthritis. *Nat. Med.* 19, 704–712. doi: 10.1038/nm.3143

Zhu, C., Peng, T., Huang, D., Feng, D., Wang, X., and Pan, X. (2019). Formation mechanism, in vitro and in vivo evaluation of dimpled exenatide loaded PLGA microparticles prepared by ultra-fine particle processing system. *AAPS PharmSciTech* 20:64.

Zhu, Y., Tan, J., Zhu, H., Lin, G., Yin, F., Wang, L., et al. (2017). Development of kartogenin-conjugated chitosan-hyaluronic acid hydrogel for nucleus pulposus regeneration. *Biomater. Sci.* 5, 784–791. doi: 10.1039/c7bm00001d

Conflict of Interest: The authors declare that the research was conducted in the absence of any commercial or financial relationships that could be construed as a potential conflict of interest.

frontiers in Bioengineering and Biotechnology

ORIGINAL RESEARCH
published: 18 December 2020
doi: 10.3389/fbioe.2020.621768

Bioconjugation of a Collagen-Mimicking Peptide Onto Poly(vinyl alcohol) Encourages Endothelialization While Minimizing Thrombosis

*Novella M. Bates[1], Heather E. Heidenreich[1], Meghan E. Fallon[1], Yuan Yao[2], Evelyn K. F. Yim[2], Monica T. Hinds[1] and Deirdre E. J. Anderson[1]**

[1] Department of Biomedical Engineering, Oregon Health & Science University, Portland, OR, United States, [2] Department of Chemical Engineering, University of Waterloo, Waterloo, ON, Canada

Poly(vinyl alcohol) hydrogel, PVA, is a suitable material for small-diameter vascular grafting. However, the bioinert properties of the material do not allow for *in situ* endothelialization, which is needed to combat common graft failure mechanisms, such as intimal hyperplasia and thrombosis. In this work, the surface of planar and tubular PVA was covalently modified with a collagen-mimicking peptide, GFPGER. The surface of modified PVA was characterized by measuring contact angle and x-ray photoelectron spectroscopy. Endothelial cell attachment to GFPGER-modified PVA was quantified and qualitatively examined using immunohistochemical staining. Then, *in vitro* hemocompatibility testing was performed by quantifying platelet attachment, coagulation factor XII activation, and initiation of fibrin formation. Finally, an established *ex vivo*, non-human primate model was employed to examine platelet attachment and fibrin formation under non-anticoagulated, whole blood flow conditions. GFPGER-modified PVA supported increased EC attachment. *In vitro* initiation of fibrin formation on the modified material was significantly delayed. *Ex vivo* thrombosis assessment showed a reduction in platelet attachment and fibrin formation on GFPGER-modified PVA. Overall, GFPGER-modified PVA encouraged cell attachment while maintaining the material's hemocompatibility. This work is a significant step toward the development and characterization of a modified-hydrogel surface to improve endothelialization while reducing platelet attachment.

Keywords: poly(vinyl alcohol), GFPGER, carbonyldiimidazole, hemocompatibility, vascular graft, platelets, fibrin, endothelial cells

OPEN ACCESS

Edited by:
Vahid Serpooshan, Emory University, United States

Reviewed by:
Atsushi Mahara, National Cerebral and Cardiovascular Center (Japan), Japan
M. Julia A. Bujan, University of Alcalá, Spain

***Correspondence:**
Deirdre E. J. Anderson
anderdei@ohsu.edu

Specialty section:
This article was submitted to Biomaterials, a section of the journal Frontiers in Bioengineering and Biotechnology

Received: *27 October 2020*
Accepted: *30 November 2020*
Published: *18 December 2020*

Citation:
Bates NM, Heidenreich HE, Fallon ME, Yao Y, Yim EKF, Hinds MT and Anderson DEJ (2020) Bioconjugation of a Collagen-Mimicking Peptide Onto Poly(vinyl alcohol) Encourages Endothelialization While Minimizing Thrombosis. Front. Bioeng. Biotechnol. 8:621768. doi: 10.3389/fbioe.2020.621768

INTRODUCTION

Development of novel, synthetic, small-diameter vascular grafts for treatment of life-threatening cardiovascular diseases has been limited by the challenge of mitigating common failure mechanisms, such as hyperplasia and thrombosis. Currently available and widely used synthetic materials include Dacron® and expanded polytetrafluoroethylene (ePTFE), which are primarily used in bypass surgeries for large diameter (>6 mm) vessels (Nakayama et al., 2004; Kumar et al., 2011; Fayol et al., 2013). Current synthetic materials fail at small diameters, likely due to a mechanical mismatch with native tissues and a lack of an endothelium to promote a healthy, blood-contacting surface. Alternatively, autologous tissues can be used for small-diameter

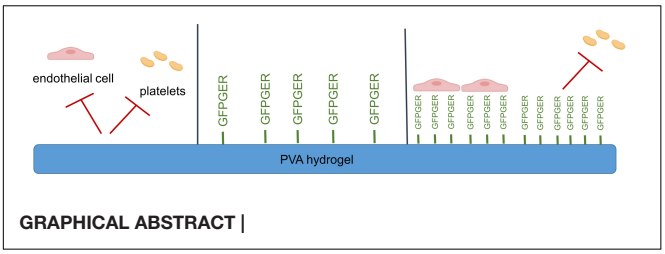

GRAPHICAL ABSTRACT |

prostheses; however, patients in need of treatment are often critically ill and may not have suitable vessels for this application. Thus, there remains an unmet clinical need for synthetic biomaterials which are hemocompatible and capable of supporting an endothelium.

One synthetic cardiovascular biomaterial under development for vascular tissue engineering applications is poly(vinyl alcohol), PVA, a hydrogel that is amenable to surface modification and has tunable mechanical properties. Previous work thoroughly characterized the mechanical properties of the PVA grafts and found that PVA hydrogels have an elastic modulus ranging from 250 to 500 kPa (Cutiongco et al., 2016a,b), which is similar to the rabbit femoral artery that has a modulus of 230 kPa (Uchida et al., 1989). These hydrogels have a modifiable circumferential compliance, which can mimic native vasculature. PVA compliance ranged between 3 and 7% (Cutiongco et al., 2016a,b), which is comparable to the rabbit femoral artery of 6% (Uchida et al., 1989). Despite PVA having suitable mechanical properties for cardiovascular applications, the bioinert surface, critical for preventing thrombosis, also prevents the material from being endothelialized *in situ* after implantation (Ino et al., 2013). The native vascular endothelium regulates thrombosis and prevents intimal hyperplasia by secreting inhibitory factors, such as nitric oxide and prostacyclin (Liu et al., 2014). Therefore, a widely accepted approach for attaining long term success of vascular grafts is to improve hemocompatibility of synthetic graft surfaces by encouraging *in situ* endothelialization. Chemical modification of bioinert devices like PVA hydrogels, can encourage endothelialization.

To generate a biomimetic tissue engineered surface, the addition of extracellular matrix (ECM)-derived peptides has been shown to increase endothelial cell (EC) attachment. However, a major drawback is that many of these peptides also support unwanted platelet attachment. For decades, work in this area focused on immobilizing peptides based on the Arg–Gly–Asp (RGD) motif in fibronectin; however, there have been mixed reports on platelet adhesion to these sequences (Schmedlen et al., 2002; Li et al., 2008; Sivaraman and Latour, 2010; Gabriel et al., 2011; Cutiongco et al., 2015a; Anderson et al., 2019). Similarly, the hexapeptide, Gly-Phe-Pro-Gly-Glu-Arg (GFPGER), based on the GFOGER motif within collagen, where the O represents hydroxyproline (Xu et al., 2000; Seo et al., 2010), has been studied for its ability to support EC attachment. Both of these sequences specifically recognize α1β1 and α2β1 integrins, which are known to bind ECs and both bind and upregulate platelet activation. The incorporation of GFPGER into materials has been shown to promote cell growth and, while in solution, the GFPGER sequence bound platelets but did not cause activation of the platelets (Munoz-Pinto et al., 2015). The effect on platelet attachment and aggregation due to a covalently linked GFPGER surface is unknown.

Previous work from our group examined the biomimetic effects of mixing ECM proteins and peptides, including GFPGER, into a hydrogel network to enhance EC attachment (Anderson et al., 2019). We found that the GFPGER peptide minimized platelet attachment *in vitro* when compared to PVA-collagen hydrogels. However, antiplatelet monotherapy was required to minimize platelet adhesion under flow in our established *ex vivo*, non-human primate, whole blood, shunt model. This was likely due to the random presentation of amino acids on the hydrogel surface. The possibility of the binding domain being buried within the hydrogel network also suggested the need for a more specific and well-controlled surface binding approach. We hypothesized that covalent attachment of GFPGER to the surface of PVA hydrogels would encourage endothelialization of the material, while mitigating thrombotic responses. The current work presents a systematic examination of this biomimetic tissue-engineered surface for cell attachment and thrombotic potential of PVA hydrogels with GFPGER at various concentrations conjugated to the surface using a 1,1′-carbonyldiimidazole (CDI) linker. This work is a significant step toward the development of hemocompatible off-the-shelf devices for the treatment of cardiovascular disease.

MATERIALS AND METHODS

PVA Film and Tube Manufacturing

Planar PVA films and tubes with an inner diameter (ID) of 4 mm were manufactured, as previously described (Cutiongco et al., 2015b, 2016b). In brief, PVA films were manufactured by adding 15% sodium trimetaphosphate (STMP, Sigma-Aldrich, St. Louis, MO, United States) to aqueous 10% PVA (Sigma-Aldrich) followed by 30% sodium hydroxide. The solution was cast into tissue culture-treated well plates at a 1.5:1 volume to surface area ratio (μL/mm^2). Films were left to crosslink in a sterile incubator at room temperature with 95% humidity followed by drying in a biosafety cabinet. Films were rehydrated under sterile conditions in 10× phosphate buffered saline (PBS, Fisher Scientific, Waltham, MA, United States) followed by 1× PBS and subsequent deionized water. Prior to modification, samples were dried in an oven overnight. PVA films were then covalently modified with GFPGER (Sigma-Aldrich) peptides. The surface of the PVA films was activated using 100 mg/mL CDI (Sigma-Aldrich) in dimethyl sulfoxide (DMSO, Sigma-Aldrich) for 1 h then briefly rinsed three times with 1× PBS before adding GFPGER (0, 15, 30, 60, and 120 μg/mL) in PBS solutions at 37°C overnight ($GFPGER_0$, $GFPGER_{15}$, $GFPGER_{30}$, $GFPGER_{60}$, and $GFPGER_{120}$, respectively). Modified films were rinsed with 1× PBS three times before use.

For the fabrication of tubular PVA samples, a cylindrical mold with an outer diameter of 3.75 mm was coated with a thin PDMS film (Dow Corning, Midland, MI, United States). The mold was treated with air plasma and then was immediately immersed in a solution of crosslinking PVA. Dip casting was performed repeatedly for 12 dips, with a drying duration of

15–30 min between each dip. The tubes were then cured at 18–20°C for 3 days before rehydration in PBS and DI water, as described above, then thoroughly rinsed in DI water overnight. For GFPGER modification, rehydrated and dried PVA tubes were immersed in a 100 mg/mL CDI solution followed by 0, 15, or 120 μg/mL GFPGER solution, as described for the films. Samples were briefly rinsed three times with PBS in between immersions. PVA films were used for surface characterization, cell attachment, and *in vitro* platelet attachment and fibrin formation assays. Tubular samples were used for *ex vivo* thrombosis testing in whole blood.

Surface Characterization

Quantification of Conjugated GFPGER Peptide on the Surface of PVA

Poly(vinyl alcohol) films in a 96-well plate were modified with GFPGER as described above ($GFPGER_0$, $GFPGER_{15}$, $GFPGER_{30}$, $GFPGER_{60}$, and $GFPGER_{120}$) with the inclusion of a five percent supplementation of each peptide concentration with fluorescent labeled GFPGER [GFPGER{Lys(5-FAM), GenScript United States, Piscataway, NJ, United States]. The modified films were rinsed with 1× PBS three times before being placed in an Infinite M200 spectrophotometer (Tecan, Männedorf, Switzerland). Fluorescent peptides conjugated to the surface of the PVA films were excited at 488 nm and emission was read at 525 nm. A standard curve of 5% fluorescent-labeled GFPGER at a range of peptide concentrations was used to quantify the peptide on the surface.

Captive Bubble Contact Angle

Static contact angle was measured by using a captive bubble method with an optical contact angle system (OCA20, Future Digital Scientific Corp). GFPGER-modified samples were immersed in DI water, and an air bubble (4 μL) was injected into the water with a syringe. The bubble was allowed to attach to the surface of the samples and imaged by a camera. The contact angle on each surface was then calculated using SCA20 software (DataPhysics Instruments United States Corp., Charlotte, NC, United States).

X-Ray Photoelectron Spectroscopy

X-ray photoelectron spectroscopy (XPS) was used to obtain the elemental composition on the surfaces of the PVA samples. XPS survey spectra were measured using a VG ESCALab 250 with a monochromatic Al K-alpha X-ray source (1486.6 eV), and high resolution spectra of C1s were obtained using a standard magnesium X-ray source (1253.6 eV) at Waterloo Advanced Technology Laboratory (University of Waterloo, Waterloo, ON, United States).

Endothelialization of Surfaces

Cell Isolation

Carotid arteries were harvested from baboons, and primary endothelial cells (ECs) were isolated, as previously described (Anderson and Hinds, 2012). Artery lumens were filled and incubated for 5 min with 600 U/mL collagenase type II (Worthington Biochemical Corp., Lakewood, NJ, United States) then massaged and flushed into collagen type I (Corning Inc., Corning, NY, United States)-coated tissue culture treated well plates containing VascuLife basal medium (Lifeline Cell Technology, Frederick, MD, United States) supplemented with 18% fetal bovine serum (FBS, Hyclone, Logan, UT, United States). Cell cultures were grown to confluence before sorting with Dynabeads (Invitrogen, Carlsbad, CA, United States) for CD31+ cells per the manufacturer's protocol. Sorted cells were expanded then stored in freezing media (50% Vasculife basal medium, 40% FBS, and 10% DMSO). Cells thawed for experimentation were maintained in 10% FBS Vasculife basal medium and used at the fourth or fifth passage.

Cell Seeding and Quantification

Rehydrated peptide-modified PVA films were incubated in FBS for 1 h at 37°C before seeding ECs at a density of 0.2 M cells/mL in 10% FBS Vasculife basal medium. For cell quantification, cells were cultured for 48 h, rinsed, and frozen dry at −20°C before further lysing with 0.02% sodium dodecyl sulfate in sodium citrate buffer. DNA in the lysate was quantified using a PicoGreen assay per the manufacturer's protocol (Invitrogen, Carlsbad, CA, United States). Cells were similarly seeded onto tissue culture treated plastic wells to serve as a positive control to the PVA films. Treatment group cell quantities were calculated as a percent confluence from this control.

Immunostaining

Cells were incubated on PVA samples for 48 h then stained, as previously described (Jurney et al., 2018). In brief, cells adhered to samples were fixed using 3.7% paraformaldehyde (PFA) then stained for VE-cadherin [primary antibody, Santa Cruz Biotechnology, mouse IgG1 monoclonal, 1:100, 1 h and IgG1 Alexa-488 as a secondary (Invitrogen, goat polyclonal, 1:500, 30 min)], and DAPI (Invitrogen, 1:10000, 5 min) as a nuclear stain. Samples were imaged with a Zeiss LSM 880 inverted confocal microscope system. Low-magnification immunofluorescent (IF) images were collected using a 10× PlanApo objective NA = 0.45. *Z*-stacks are presented in figures as maximum intensity *Z*-projections and post-processing of all images was performed using FIJI (SciJava) (Schindelin et al., 2012; Hagen and Hinds, 2019).

Thrombogenicity of Surfaces

Washed Platelet and Platelet-Rich Plasma Preparation

Human venous whole blood was drawn from healthy donors into sodium citrate, as previously described (McCarty et al., 2005). In brief, whole blood was centrifuged at 200 *g* for 20 min to obtain platelet-rich plasma (PRP). In select studies, purified platelets were isolated from PRP by further centrifugation at 1,000 *g* for 10 min in the presence of 0.1 μg/mL prostacyclin. The pellet was resuspended in HEPES/Tyrode's buffer (129 mM NaCl, 0.34 mM Na_2HPO_4, 2.9 mM KCl, 12 mM $NaHCO_3$, 20 mM HEPES, 5 mM glucose, 1 mM $MgCl_2$; pH 7.3) containing 0.1 μg/mL prostacyclin. The platelets were washed once via centrifugation (1,000 *g* for 10 min) and resuspended in HEPES-Tyrode's buffer.

Static Platelet Adhesion Quantification

Static platelet adhesion was quantified using a method modified from Vaníčková et al. (2006) to incorporate PVA films. Purified washed platelets suspensions (5.0×10^8 platelets/mL) were incubated on peptide-modified PVA films, in the absence of ECs, in a microtiter plate for 1 h at room temperature. Samples were then rinsed three times with PBS to remove all non-adherent platelets. The amount of platelets attached to the surface of each material was quantified by measuring platelet acid phosphatase activity using a calibration curve of platelet solutions ($0–5.0 \times 10^8$ platelets/mL).

Coagulation Quantification

Pooled platelet-poor plasma (PPP, ISTH SSC Lot 4) was incubated with peptide-modified PVA, in the absence of ECs, films followed by the addition of $CaCl_2$ (8 mM). Absorbance at 405 nm was documented over time. Fibrin generation lag times were defined by a 5% increase over baseline absorbance. Rates of fibrin generation were defined by maximum slopes.

Activation of coagulation factor XII (FXII, 200 nM, Haematologic Technologies, Inc., Essex Junction, VT, United States) in the presence of coagulation enzymes generated on GFPGER-modified samples, in the absence of ECs, was measured in a purified system using a chromogenic substrate, Spectrozyme-FXIIa (American Diagnostica, Inc., Stamford, CT, United States), as previously described (Bates et al., 2020).

Whole Blood Platelet and Fibrin Adhesion Under Flow Quantification

Rehydrated GFPGER-modified tubes, in the absence of ECs, (prepared from 15 or 120 μg/mL GFPGER solutions) were incorporated into a chronic, femoral arteriovenous (AV) shunt via connective silicone tubing in an established non-anticoagulated, non-human primate model (Cutiongco et al., 2015a; Anderson et al., 2019). Juvenile male baboons (9–12 kg) underwent a minor surgical procedure, cannulation of the superficial femoral artery and vein, for the placement of a chronic AV shunt. The AV shunts were composed of implanted sterilized silicone rubber tubing (3.0 mm ID, SIL-TEC, Technical Products, Inc, Lawrenceville, GA, United States). Single devices were connected to the implant with Silastic tubing (4 mm ID, Dow Chemical, Midland, MI, United States) (**Supplementary Figure 1**). Upstream of the device was a flow probe (Transonic, Ithaca, NY, United States) to measure blood velocity, and downstream of the device was a tubing clamp to control the flow at a steady rate. Autologous platelets and homologous fibrin were labeled with indium-111 (^{111}In) and iodine-125 (^{125}I), respectively. Samples were subjected to whole blood flow at 100 mL/min and platelet accumulation onto the samples was quantified in real-time by measurement of ^{111}In radiation using a Brivo NM615 nuclear imaging camera (General Electric, Boston, MA, United States). The amount of fibrin was quantified as an end-point measurement of ^{125}I radiation approximately 30 days post experiment, once the ^{111}In decayed, using a 1480 Wizard gamma counter (PerkinElmer, Waltham, MA, United States). CDI-active PVA without peptide ($GFPGER_0$) and plain PVA were used as negative controls, collagen-coated ePTFE (Collagen, 1 mg/mL equine collagen type I, Chrono-log Corp.) was used as a positive control and clinical grade ePTFE (IMPRA®, Bard Peripheral Vascular, Inc., Tempe, AZ, United States) with an ID of 4mm was used as a clinical control.

After whole blood testing, the tubes were rinsed with PBS and fixed with 3.7% PFA for 48–72 h before additional rinsing and storage. Some of the samples used in the shunt studies were examined with micro-computed tomography (MicroCT). The samples were prepared as described previously (Gupta et al., 2020). Briefly, PVA samples were filled with Microfil® polymer to render the lumens radiopaque. Since the Microfil® polymer is incompatible with ePTFE, ePTFE samples were soaked in Lugol's (Sigma-Aldrich) solution to render the thrombus radiopaque.

Shunt studies were performed in a male *Papio anubus* baboon (10.5 kg), which was under the care of the Oregon National Primate Research Center (ONPRC) staff. All studies abided by guidelines provided by the National Research Council and the Committee on Care and Use of Laboratory Animals of the Institute of Laboratory Animal Resources. All studies were approved by the ONPRC Institutional Animal Care and Use Committee.

Micro-Computed Tomography Analysis

Micro-computed tomography (Inveon, Siemens) imaging was used to analyze thrombus area over the length of the samples (volume) in the small-diameter vascular grafts formed under flow by whole blood in *ex vivo* shunts, as described previously (Gupta et al., 2020). Imaging was performed with 2×2 binning, 220 projections, at an exposure of 660 ms/projection. Thrombus physical characteristics were determined with the Amira® software package (FEI, version 5.2.2) by a trained operator blinded to specific sample treatments. The software also generated three-dimensional (3D) volume renderings of either the thrombus for ePTFE grafts or the lumen for collagen-coated and PVA grafts. The software-calculated volumes and lengths of each sample were used for subsequent analysis. Amira® was utilized, as previously described (Gupta et al., 2020), to segment specific regions of interest (ROIs) in each cross-sectional image. For PVA samples, the ROI was the luminal area of the graft. ePTFE samples were segmented for the thrombi as the ROI, and collagen-coated ePTFE samples contained ROIs of both the luminal and thrombus areas. 3D representations of either the lumen (PVA and collagen-coated ePTFE) or thrombus (ePTFE) of the grafts were generated from ROI summations, and the surface areas of each cross-sectional slice were subsequently measured. These cross-sectional data were then utilized in analyzing average thrombus generation over the entire graft surface. The cross-sectional areas obtained from each slice were used to generate topography maps of the thrombus surface for each individual sample. This allows for characterization of the thrombus surface and quantification of the intrasample variability of the thrombus over the length of a single sample.

Statistical Methods

Data are presented as mean ± standard deviation (SD) for all studies. Probability values of $p < 0.05$ were considered to be statistically significant. To determine statistical significance of captive bubble contact angle ($n = 3$), XPS ($n = 3$), peptide quantification ($n = 5$), lag time and rate of fibrin generation

(n = 3), static *in vitro* platelet adhesion (n = 3), and *ex vivo* end-point fibrin accumulation data (n = 6), one-way analysis of variance (ANOVA) tests were performed. To determine statistical significance for *ex vivo* platelet data, a repeated measures ANOVA was performed on surface modified PVA samples (n = 6). Platelet reactivity of collagen-ePTFE, ePTFE, and unmodified PVA controls samples (n = 2) were confirmed and compared to historic data, but these controls were not included in the statistical analysis. All studies were tested for ANOVA assumptions using Levene's and qqplots and, when necessary, data were natural log transformed. A subset of the *ex vivo* samples were tested with microCT (n = 4 for $GFPGER_0$, $GFPGER_{15}$, and $GFPGER_{120}$) using a one-way ANOVA between the average luminal cross-sectional area (volume/length) for each test group. SDs of the volume data generated over the entire graft length for each single sample (generated from per slice area data) were also compared with a one-way ANOVA to determine if intrasample variability was significantly different between test groups.

RESULTS

Surface Characterization

Peptide Quantification

Gly-Phe-Pro-Gly-Glu-Arg peptides were supplemented with 5% fluorescent-labeled peptide to quantify the amount of GFPGER immobilized onto the surface of PVA at each concentration. A significant increase in peptide quantity was found on $GFPGER_{30}$, $GFPGER_{60}$, and $GFPGER_{120}$ when compared to unmodified samples (**Figure 1**). Additionally, $GFPGER_{60}$ and $GFPGER_{120}$ were significantly increased from $GFPGER_{15}$, and $GFPGER_{120}$ was significantly increased from $GFPGER_{30}$.

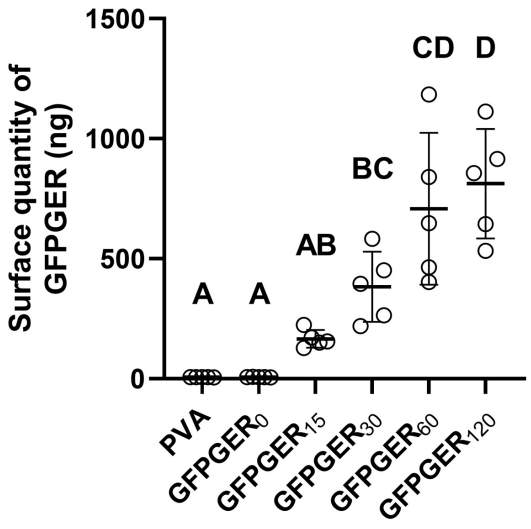

FIGURE 1 | Quantification of GFPGER peptide on the surface of modified PVA samples. The quantity of immobilized GFPGER peptide on the surface of each PVA sample was determined by fluorescent peptide supplementation and is shown as mean ± SD (n = 5). Statistical analysis was performed using a one-way ANOVA test with Tukey's HSD *post hoc* testing. Groups which do not share a letter indicate statistical significance ($p < 0.05$).

Contact Angle

Contact angle did not exhibit a significant difference among all test groups (**Figure 2**). The surfaces of PVA and GFPGER modified PVA samples all remained hydrophilic, with contact angles ranging from 44.8 to 51.7°.

XPS

X-ray photoelectron spectroscopy survey spectra of PVA and GFPGER modified PVA are shown in **Supplementary Figure 1A**. GFPGER and CDI contain nitrogen and, thus, all modified PVA groups showed significant N1s peaks. **Table 1** and **Figure 3** showed the atomic percentage of C, O, and N on different samples. $GFPGER_{120}$ had significantly higher C% than $GFPGER_{30}$ and $GFPGER_0$, and significantly lower O% than all the other groups. GFPGER modified PVA samples had significantly higher N% than $GFPGER_0$. **Supplementary Figures 2B–D** shows the high-resolution spectra of carbon on PVA, $GFPGER_0$, and $GFPGER_{120}$ samples. High-resolution spectrum of carbon on PVA showed characteristic peaks of the PVA structure at 282, 284, and 286 eV from C–C/C–H, C–O, and C=O, respectively. In addition to the characteristic PVA peaks, $GFPGER_0$ also showed a peak at 288 eV from the –O–C=O

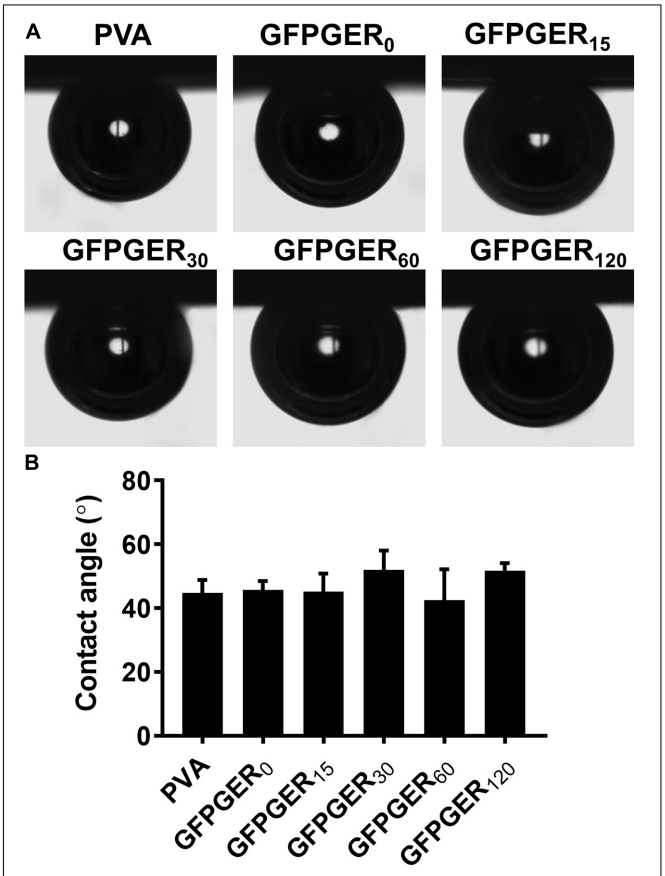

FIGURE 2 | Contact angle of PVA films modified with different concentrations of GFPGER. The contact angle was measured using a captive bubble method. Representative images **(A)** and contact angle data (n = 6) are shown as mean ± SD **(B)**. Statistical analysis was performed using a one-way ANOVA test. No significant difference was observed among all groups.

TABLE 1 | XPS results of PVA films modified with different concentration of GFPGER.

Atomic %	C	O	N
PVA	76.8 ± 2.0	23.1 ± 2.0	ND
$GFPGER_0$	73.9 ± 1.9	22.7 ± 2.1	3.3 ± 0.3
$GFPGER_{15}$	71.4 ± 1.0	23.9 ± 0.8	4.6 ± 0.2
$GFPGER_{30}$	74.0 ± 1.6	21.8 ± 1.6	4.11 ± 0.1
$GFPGER_{60}$	72.2 ± 1.7	23.2 ± 1.9	4.6 ± 0.3
$GFPGER_{120}$	78.6 ± 2.2	17.3 ± 1.9	4.17 ± 0.3

Atomic percentage of carbon, nitrogen, and oxygen. Data (n = 3) are shown as mean ± SD (ND = not detected).

bond in the imidazole carbamate intermediate groups. GFPGER contains NH-C(=O) groups, and the peak at 288.7eV observed from $GFPGER_{120}$ samples further confirmed the presence of GFPGER on the samples.

Endothelialization of Surfaces

We examined the ability of PVA to attach ECs after the hydrogel was modified with GFPGER peptide. ECs that adhered to samples were quantified using PicoGreen® as a percentage of cells adhered to tissue culture plastic and observed qualitatively using fluorescent staining. Only the GFPGER-modified samples (15, 60, and 120 μg/mL) showed a significant increase in EC attachment when compared to $GFPGER_0$ (**Figure 4A**). These results were also reflected qualitatively in the obtained stained images (**Figure 4B**). $GFPGER_{120}$ showed particularly robust VE-cadherin staining suggestive of strong cell-cell interactions. Adherent ECs were not detected nor observed on plain PVA samples, similar to results from our work (Jurney et al., 2018; Anderson et al., 2019).

Thrombogenicity of Surfaces

Static *in vitro* Platelet Adhesion Quantification

We studied the extent to which peptide-modified PVA samples supported static platelet adhesion using a solution of purified human platelets *in vitro*. There were no statistical differences found (**Figure 5**).

Fibrin Clotting Time, Rate of Fibrin Generation *in vitro*, and FXII Activation

We quantified the time to fibrin clot formation in PPP and the rate of fibrin formation on peptide-modified PVA samples. GFPGER-modified samples all had prolonged times to initiation of fibrin generation when compared to CDI only-modified samples (**Figure 6A**). There were no significant differences observed in the rate of fibrin generation in the presence of GFPGER-modified PVA films when compared to the baseline (**Figure 6B**).

To determine if the contact pathway was playing a role in the difference of time to initiation of fibrin formation, activation of FXII was measured (**Figure 6C**). There were no significant differences observed between unmodified and GFPGER-modified PVA samples.

Whole Blood Platelet and Fibrin Adhesion Under Flow Quantification

We then examined platelet and fibrin deposition onto GFPGER-modified tubes from whole, flowing blood with *ex vivo* thrombosis testing. We observed a significant decrease in platelet attachment onto GFPGER-modified samples when compared to the CDI only-modified samples for both concentrations of tested conjugated peptide, low (15 μg/mL) and high (120 μg/mL) (**Figure 7A**). Unmodified PVA samples were also quite low compared to the positive and clinical controls and consistent with both concentrations of GFPGER modifications. We observed a similar significant decrease in fibrin formation on $GFPGER_{15}$ and $GFPGER_{120}$ when compared to the CDI-only samples (**Figure 7B**).

MicroCT

Three-dimensional renderings of either the lumen (PVA and collagen-coated ePTFE) or thrombus (ePTFE) area along the length of the samples (volume) were generated based on cross-sectional ROI segmentation of each graft type (**Figure 8**).

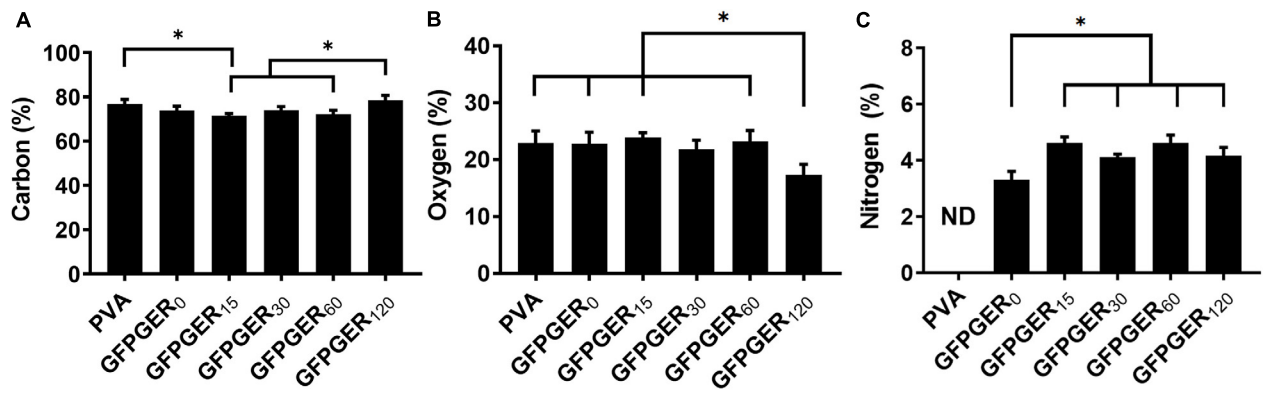

FIGURE 3 | XPS measured atomic percentages of PVA films modified with different concentrations of GFPGER. XPS was used to measure the percentage of carbon, oxygen, and nitrogen on GFPGER-modified surfaces. Atomic percentages (n = 3) are shown as mean ± SD for all samples for carbon **(A)**, oxygen **(B)**, and nitrogen **(C)**. Statistical analysis was performed using a one-way ANOVA with Tukey's HSD *post hoc* testing. *indicates statistical significance ($p < 0.05$). ND = not detected.

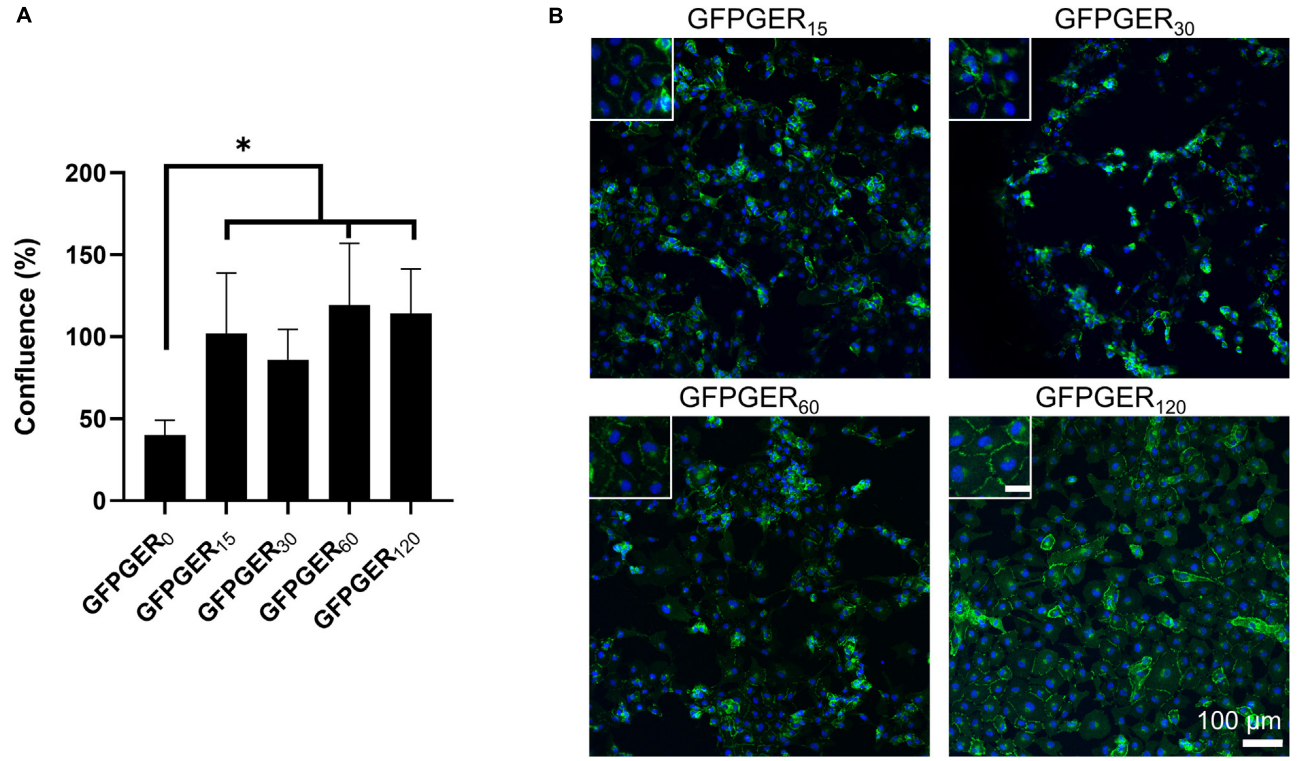

FIGURE 4 | EC quantification and visualization after 48 h on GFPGER-conjugated PVA. Cell attachment increased on modified PVA compared to unmodified PVA **(A)**. Data (n = 4–6) are presented as a percent increase from ECs adherent on a tissue culture plastic (TCP) control, where ECs were 100% confluent. Statistical analysis was performed using a one-way ANOVA with Tukey's HSD *post hoc* testing. *indicates statistical significance ($p < 0.05$). Representative staining of baboon carotid ECs on GFPGER-conjugated PVA films after 48 h showed adherent ECs on all modified PVA samples, while no cells were observed on unmodified PVA **(B)**. Green = VE-cadherin (primary antibody and IgG1 Alexa-488 as a secondary) and blue = DAPI as a nuclear stain. Inset scale bar = 30 μm.

The measurement of thrombus area along the length of each individual graft as a percentage of the maximal luminal area was evaluated and representative samples are shown in **Figure 9**.

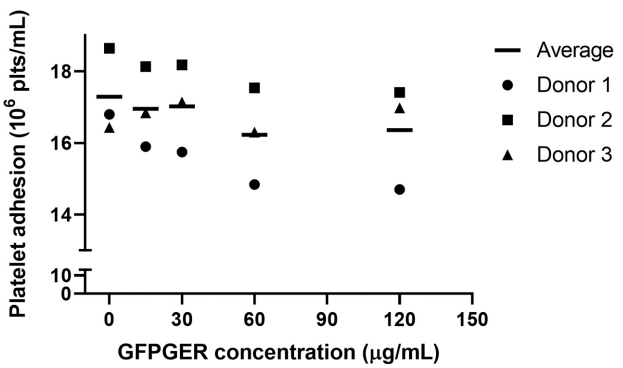

FIGURE 5 | Quantification of static platelet adhesion of purified platelets onto GFPGER-conjugated PVA samples. Platelet adhesion after 1 h, under static, purified conditions, was measured on the surface of GFPGER-modified PVA samples. Data (n = 3) are shown as individual biological replicates with means overlaid. Statistical analysis was performed using a one-way ANOVA test. No significant difference was observed among all groups.

This representative $GFPGER_0$ sample (**Figure 9A**) had an average thrombus area percentage of 12.10 ± 3.99% of the maximal luminal area, the representative $GFPGER_{15}$ sample (**Figure 9B**) had an overall thrombus area percentage of 3.66 ± 1.11%, and the representative $GFPGER_{120}$ sample (**Figure 9C**) had an overall thrombus area of 2.68 ± 1.41%. By capturing the area per sample slice, this method of analysis allows for the study of variability of an individual thrombus. The intrasample variability was quantified as the standard deviation of the individual thrombus area as a percent of the maximal luminal area of each sample type. These standard deviations were averaged and compared between all the PVA samples (n = 4) resulting in variabilities of $GFPGER_0$ (4.17 ± 0.87%), $GFPGER_{15}$ (3.10 ± 2.84%), and $GFPGER_{120}$ (4.26 ± 2.39%). These variability data were not statistically significant. The average Amira® luminal area for each type of PVA modifications (n = 4) were also compared and showed no statistical significance between the three GFPGER-modified groups (**Figure 10**).

DISCUSSION

Successful integration of synthetic small-diameter vascular grafts *in vivo* is impeded by a lack of *in situ* endothelialization and material-vessel compliance mismatch leading to neointimal

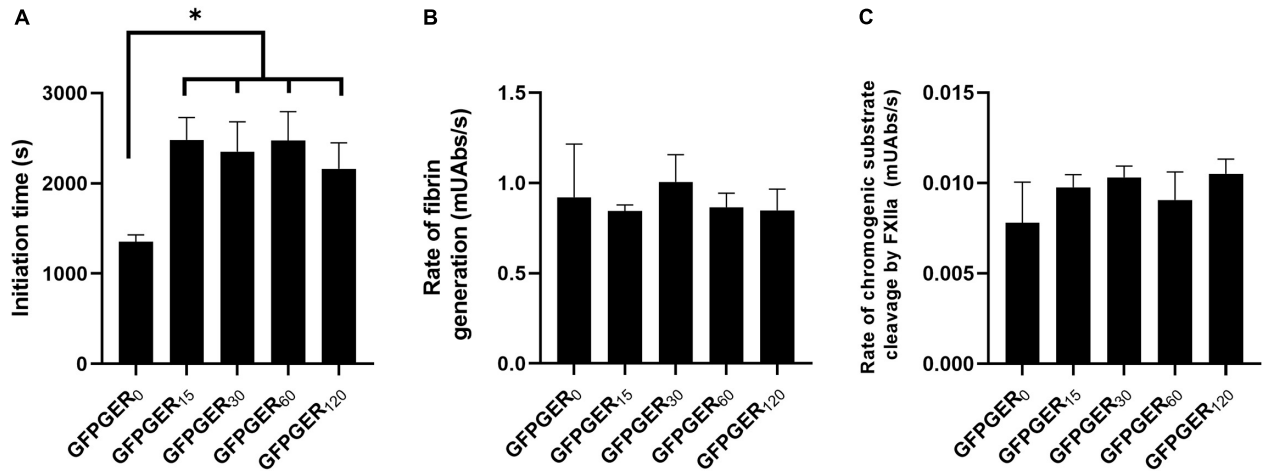

FIGURE 6 | Quantification of *in vitro* coagulation on GFPGER-conjugated PVA samples. Coagulation potential of GFPGER-modified samples was determined by measuring fibrin initiation time, rate of fibrin generation, and activity of coagulation factor XII from static coagulation assays. Fibrin initiation lag times in platelet-poor-plasma in the presence of GFPGER-conjugated PVA samples showed prolonged initiation times on GFPGER-modified samples **(A)**. No difference in rate of fibrin generation on GFPGER-conjugated PVA samples was measured **(B)**. There was no difference in FXIIa produced by GFPGER-conjugated PVA samples, shown as rate of cleavage of a chromogenic substrate, when compared to unmodified **(C)**. Data (n = 3–6) are shown as mean ± SD. Statistical analysis was performed using a one-way ANOVA with Tukey's HSD *post hoc* testing. *indicates statistical significance ($p < 0.01$).

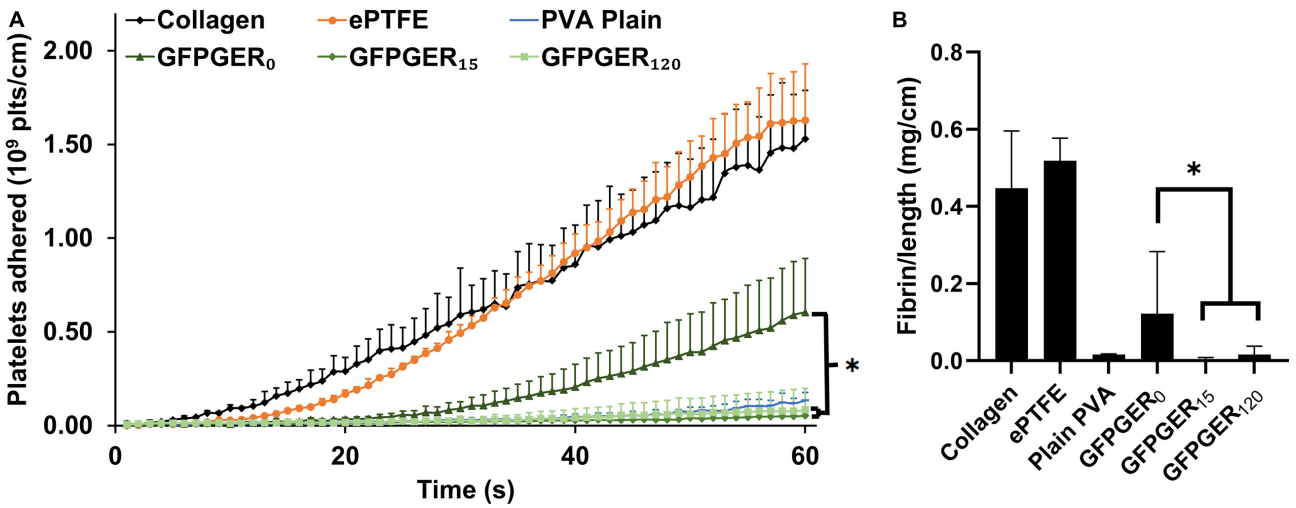

FIGURE 7 | Whole blood, *ex vivo* shunt testing. Tubular GFPGER-modified PVA (prepared from 15 or 120 μg/mL GFPGER solutions, n = 6) and unmodified but CDI-active PVA (n = 6) were tested in an *ex vivo* shunt model. Collagen-coated ePTFE (n = 2), ePTFE (n = 2), and plain PVA (n = 2) were run to compare to historical control data. **(A)** Platelet accumulation was quantified over 60 min exposure to whole blood. Data are shown as mean ± range or SD. Statistical analysis was performed only on the modified PVA samples using a repeated measures ANOVA with Tukey's HSD *post hoc* testing. $GFPGER_0$ was found to be significant from $GFPGER_{15}$ ($p < 0.001$) and from $GFPGER_{120}$ ($p = 0.001$), while $GFPGER_{15}$ was not significant from $GFPGER_{120}$. **(B)** Fibrin data were quantified and normalized per centimeter of axial length for all grafts at 60 min. Data (n = 2–6) are shown as mean ± range/SD. Statistical analysis was performed using a one-way ANOVA with Tukey's HSD *post hoc* testing ($p < 0.001$). *indicates statistical significance.

hyperplasia and thrombosis and potential loss of patency. Studies of compliant PVA biomaterials suggest that the low thrombogenicity of the material makes it a promising vascular graft material (Chaouat et al., 2008; Cutiongco et al., 2015a,b; Jurney et al., 2018; Anderson et al., 2019; Rizwan et al., 2020; Yao et al., 2020). However, in the absence of surface modifications, PVA is unable to support EC attachment and growth. We hypothesized that the covalent attachment of a collagen-mimicking peptide to PVA would enhance EC adhesion, without compromising hemocompatibility of the material. Thus, we modified PVA hydrogel surfaces using CDI chemistry with the collagen-mimetic peptide, GFPGER, a low-cost, commercially available peptide, which specifically recognizes α1β1 and α2β1 integrins. We performed characterization of this modified surface as well as thorough *in vitro* and *ex vivo* hemocompatibility testing to assess the thrombotic potential of the material.

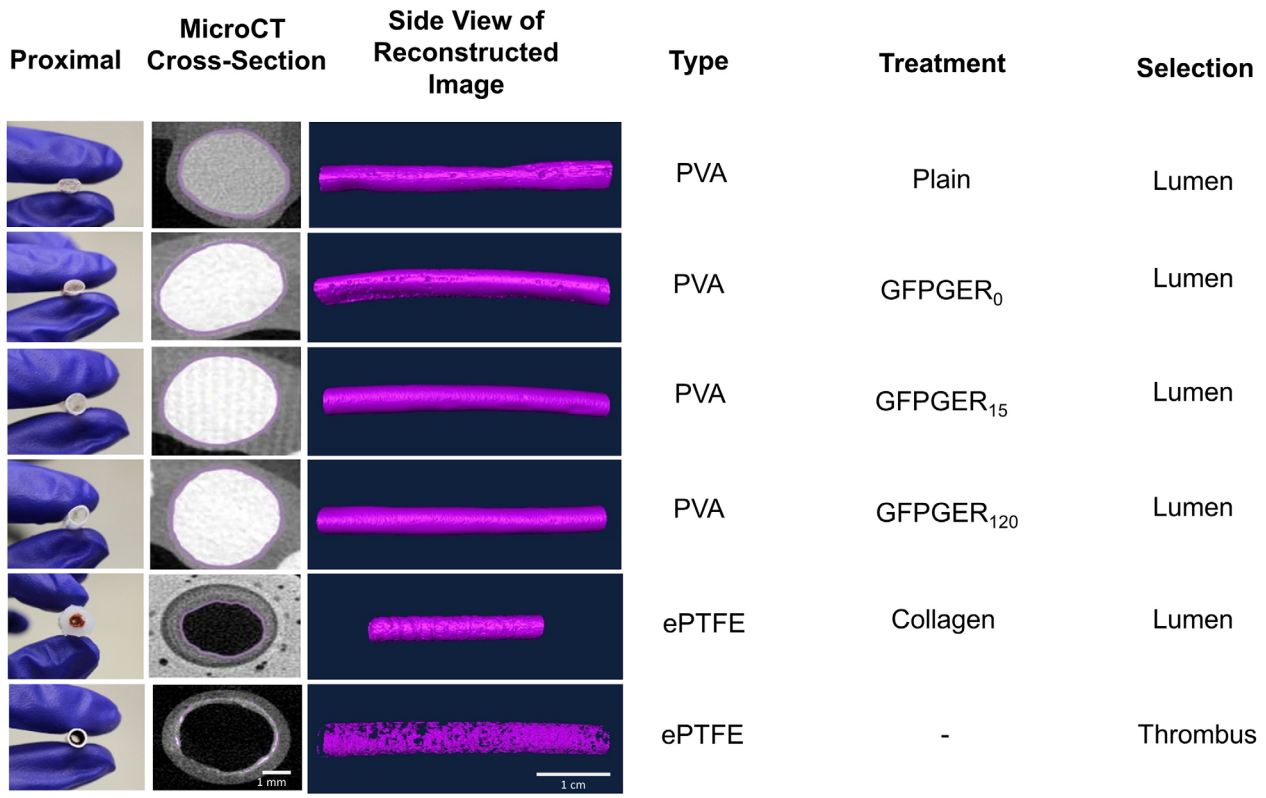

FIGURE 8 | Three-dimensional surface volume renderings of microCT cross-sectional ROI selections using Amira© showing thrombi in the lumen of tested samples. All grafts from *ex vivo* whole blood testing were 4–5 mm ID. PVA and ePTFE samples were 4 cm long and collagen-coated ePTFE samples were 2 cm long. ROI selection from a blinded, trained user is shown in purple, designating the user-selected masking range. Scale bar for microCT cross-sectional images and volume renderings are 1 mm and 1 cm, respectively.

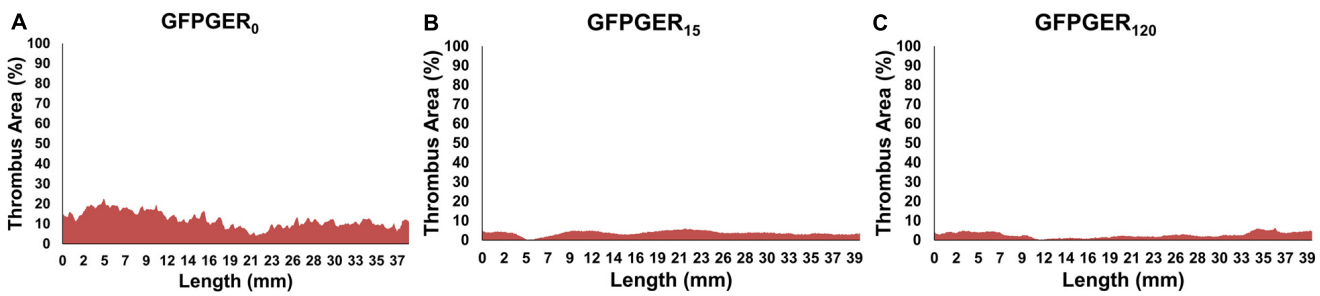

FIGURE 9 | Quantification of the cross-sectional thrombus area as a percentage of the maximal luminal area per image slice over the entire graft length for a representative sample of $GFPGER_0$ **(A)**, $GFPGER_{15}$ **(B)**, and $GFPGER_{120}$ **(C)**. Samples illustrate the variability seen in thrombus over the length of a single graft after 1 h of whole, flowing blood. Samples conjugated with GFPGER **(B, C)** had less thrombus and less observed variability than the control sample with only a vehicle control **(A)**.

Using CDI as a crosslinker enabled a concentration dependent increase in GFPGER covalently bound to the PVA surface. Upon examination of the surface chemistries present on the modified hydrogels, we found an increase in C and N%, which indicated the introduction of amine groups onto the hydrogel, while the contact angle remained unchanged when compared to unmodified PVA. CDI has been used as a chemical crosslinker to modify the surface of polymers and hydrogels, including PVA, with full length proteins (Nuttelman et al., 2001; Rizwan et al., 2020; Yao et al., 2020). CDI reacts with hydroxyl groups to form highly reactive, anchoring carbamate groups, which are then available to react with proteins or peptides for immobilization. Nuttelman et al. (2001) have previously used CDI to covalently attach fibronectin, an ECM protein found to play a role in cell adhesion and proliferation, to PVA. In their work, an 11-carbon spacer, bromoundecanoic acid, was added to the PVA

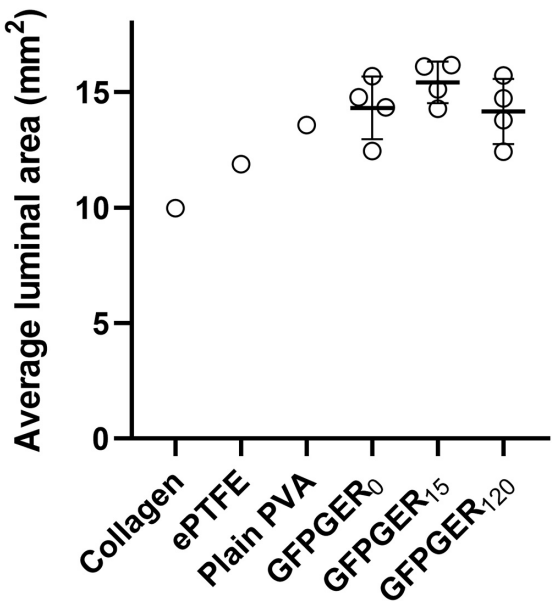

FIGURE 10 | Average luminal area of grafts after exposure to whole flowing blood in the *ex vivo* shunt. Collagen (n = 1), ePTFE (n = 1), plain PVA (n = 1), $GFPGER_0$, $GFPGER_{15}$, and $GFPGER_{120}$ (all covalently modified GFPGER PVA samples were n = 4) grafts were analyzed for the average cross-sectional area per slice of the lumen. Data are presented as the mean ± SD of the average luminal area. Statistical analysis was performed only on experimental (GFPGER) samples using a one-way ANOVA. No statistical differences were observed.

hydrogel in an intermediate step before CDI activation, followed by the addition of fibronectin. Using this chemical scheme, they found that fibroblast cell attachment, proliferation, and migration were all significantly increased on fibronectin-conjugated PVA when compared to the unmodified material. However, the additional acid wash step is cumbersome and unnecessary, as shown by Rizwan et al. (2020), in which CDI was used to covalently attach gelatin, another cell-adhesive protein, directly to PVA. In this prior study, CDI alone was used to aminate the surface of PVA before protein modification and the presence of gelatin on the PVA surface after the covalent modification was confirmed using Fourier transform infrared spectroscopy and XPS. Their surface characterization results showed a significant increase in nitrogen on the surface, which, like the results in the current study, indicate the presence of amine groups on the material surface. While some peptides, such as REDV (Lei et al., 2012), require spacers in order to retain their bioactivity, we successfully grafted GFPGER to PVA using CDI and the peptide remained active. Additionally, it is unlikely that using CDI chemistry to immobilize peptides to the surface of PVA would alter the mechanical properties of the material as was shown by previous work from our group (Rizwan et al., 2020), whereas there is more potential for physical alteration of the material when mixing peptides into the hydrogel network. To our knowledge, the work presented here is the first time that CDI has been used to covalently attach an ECM-mimicking peptide to the surface of PVA.

In our cell studies, we found that GFPGER-conjugated PVA supported the formation of an endothelial layer. This result is similar to cell attachment results obtained in our previous GFPGER-mixed PVA studies, where we found greater cell adhesion to GFPGER-mixed PVA samples when compared to PVA modified with collagen and other proteins and peptides (Anderson et al., 2019). In the current study, EC adhesion to most concentrations of GFPGER–modified PVA was significantly increased when compared to the CDI-only PVA baseline ($GFPGER_0$), and a confluent layer of ECs was seen at the lowest and highest concentrations of GFPGER-conjugated samples. Despite the surface characterization which suggested that the GFPGER had not saturated the surface at the lower concentrations, it was interesting to see that all the examined concentrations had substantially increased cell adhesion that was not significantly different from other GFPGER concentrations. Plain PVA is biologically inert and does not support cell attachment alone (Cutiongco et al., 2015a, 2016b; Rizwan et al., 2020). The EC attachment attained is likely through the α1β1 and α2β1 integrins, which are well known to interact with GFPGER (Seo et al., 2010). This cell attachment is in agreement with the work of several groups, including ours (Chaouat et al., 2008; Munoz-Pinto et al., 2015; Anderson et al., 2019). GFPGER has been shown to support cell attachment and spreading on several surfaces, including a collagen-mimetic protein with GFPGER incorporated, $Scl2_{GFPGER}$, coated onto tissue culture plastic (Seo et al., 2010) and a $Scl2_{GFPGER}$ incorporated PEG hydrogel (Cereceres et al., 2015). However, we were able to successfully conjugate GFPGER alone directly to a hydrogel surface via a simple chemical scheme, eliminating the need for site-directed mutagenesis or in-house protein synthesis.

Endothelial cells have been shown to have a distinct cobblestone appearance when cultured *in vitro* (Glynn and Hinds, 2014). Despite being cultured under identical conditions, the morphology of ECs on the different densities of GFPGER-conjugated PVA varied. ECs on $GFPGER_{15}$ were less spread and dominated by their nucleus whereas cells on $GFPGER_{120}$ appear to have spread more with a larger cytoplasm and the characteristic VE-Cadherin expression of *in vitro* cultured confluent ECs. The difference in peptide density was also demonstrated by the distinct cell wall borders observed around cells on hydrogels with the highest concentration of GFPGER. The increase in confluency and altered morphology on $GFPGER_{120}$ indicates that higher peptide concentrations may lead to phenotypic alteration of ECs. Hydrogels with a higher density of peptide have more binding sites for EC integrins, which encourages EC spreading to a greater degree than lower densities of EC adhesive peptide. However, this phenomenon was not observed in GFPGER-mixed PVA studies (Anderson et al., 2019); thus, more studies would need to be performed to understand the relationship between conjugated-peptide density and EC morphology and phenotype.

Importantly, the CDI-GFPGER modification of PVA did not increase platelet attachment and aggregation nor did the modification initiate clotting via the coagulation cascade. In our evaluation of GFPGER-conjugated PVA hydrogels, we found that all GFPGER-conjugated samples delayed the initiation time of fibrin clotting of PPP and decreased the fibrin formation

ex vivo when compared to the baseline material ($GFPGER_0$). The lack of a significance difference found in the analysis of FXII activation on PVA samples suggested that contact pathway was not a potential coagulation initiation mechanism. However, more studies will have to be done to determine the mechanism of fibrin formation inhibition on GFPGER-modified samples. *In vitro* and *ex vivo* assessment of platelet attachment onto GFPGER-conjugated samples indicated no alteration of the PVA hemocompatibility. MicroCT analysis of thrombi formed on PVA samples after *ex vivo* testing showed minimal thrombus formation. These results contrast what is known about collagen-platelet interactions (Alberio and Dale, 1998; Farndale, 2006; Ruggeri and Mendolicchio, 2007; Harrison et al., 2011) and our previous GFPGER-mixed PVA studies (Anderson et al., 2019), where we found significantly higher platelet attachment to GFPGER-mixed samples when compared to unmodified PVA. The GFPGER binding site to α2β1 integrin on platelets is known to contribute to platelet activation and aggregation (Cosemans et al., 2008; Munnix et al., 2008). The divalent cation in the α2 I-domain of the integrin coordinates with the glutamate in collagen or collagen-mimicking peptides, leading to a conformational change in the receptor followed by activation. Rich et al. (1999) predicted that the ligand-binding site in the α1 subunit, which is found on ECs, is longer and more flexible than the α2 subunit (Xu et al., 2000), which is present on the platelet surface. Previous studies found that GFPGER has slightly less affinity for the α2 subunit, when compared to GFOGER, the native integrin binding sequence in collagen (Sipilä et al., 2018). This decreased affinity may be enough to minimally bind platelets and not activate key pathways leading to aggregation. Additionally, when GFPGER is directly bonded to the surface of PVA, as with the CDI linker, the glutamate that participates in integrin coordination is always available, leading to a controlled interaction between the material and biological components. Mixing the peptide into the PVA, as was done previously (Anderson et al., 2019), buries some of the key groups needed for integrin recognition, which likely led to non-specific binding of both cells and platelets (Anderson et al., 2019). Thus, CDI-mediated binding of GFPGER is a promising surface modification of blood contacting materials, which does not activate platelets.

Ultimately, the work presented herein supported our hypothesis that covalent attachment of GFPFER to the surface of PVA hydrogels would encourage endothelialization of the material, while attenuating thrombosis. We presented a systemic characterization and evaluation of GFPGER-conjugated PVA hydrogels using *in vitro* and *ex vivo* experimentation. We have shown that covalently modifying PVA with a low cost, widely available commercial peptide, GFPGER, for use as a synthetic vascular graft material may prevent thrombosis, while promoting *in situ* endothelialization of the material. A limitation of this work is the short time duration in which thrombogenesis is studied. Future work will include longer shunt study times and implantation studies using established rabbit (small animal) carotid bypass grafting (Cutiongco et al., 2016b) and non-human primate (large animal) aortoiliac bypass grafting (Anderson et al., 2018) implant models both with an end-to-side methodology to increase pre-clinical understanding of material integration. These models provide the best approach for recapitulating clinical flow dynamics, which is frequently neglected in other vascular graft animal models (Zilla et al., 2007). Additionally, further *in vitro* work will be done to investigate specific EC phenotype and SMC proliferation on GFPGER-conjugated PVA. The promising results reported here with our novel synthetic biomaterial support the potential of this covalently linked surface modification either to coat off-the-shelf cardiovascular materials or for tissue-engineered constructs, supporting endothelialization without aggregating platelets.

DATA AVAILABILITY STATEMENT

The raw data supporting the conclusions of this article will be made available by the authors, without undue reservation.

ETHICS STATEMENT

The animal study was reviewed and approved by the ONPRC Institutional Animal Care and Use Committee.

AUTHOR CONTRIBUTIONS

NB performed *in vitro* thrombogenicity studies, peptide quantification studies, analyzed data, wrote and prepared the manuscript/figures for publication. HH performed *in vitro* thrombogenicity studies and endothelial cell attachment studies. MF performed microCT studies, associated analysis, and contributed to writing and preparing the manuscript/figures. YY performed surface characterization work, prepared tubular samples for arteriovenous shunt studies, analyzed data, and contributed to writing and preparing the manuscript/figures. EY and MH contributed to the original idea, experimental design, scientific guidance, discussions, laboratory space, and funding. DA contributed to the original idea, experimental design, scientific guidance, discussions, funding, *in vitro* thrombogenicity studies, endothelial cell attachment studies, and contributed to writing and preparing the manuscript/figures. All authors revised the manuscript.

FUNDING

This work was supported by the Achievement Rewards for College Scientists (ARCS) Foundation, the National Institutes of Health grants R01HL130274 and R01HL144113, and NSERC-CREATE, Training in Global Biomedical Technology Research and Innovation at the University of Waterloo (CREATE-509950-2018). We thank the staff at the Oregon National Primate Research Center (supported by NIH grant award P51OD011092).

ACKNOWLEDGMENTS

We appreciate the help of Mr. Alex Melrose and Ms. Stephanie Reitsma in collecting and purifying platelets. We would also like to thank Dr. Matthew Hagen, Mr. William Packwood, and

Ms. Claire Johnson for their help with fluorescent and microCT image collection. We thank Ms. Jennifer Johnson and Ms. Tiffany Burch for their technical assistance.

SUPPLEMENTARY MATERIAL

The Supplementary Material for this article can be found online at: https://www.frontiersin.org/articles/10.3389/fbioe.2020.621768/full#supplementary-material

Supplementary Figure 1 | Shunt study set up. A shunt was placed between the femoral artery and the femoral vein of a non-human primate (not pictured) using Silastic tubing. The sample to be tested was placed between the tubing using connectors, such that blood flow was continuous through the *ex vivo* shunt loop. Whole blood was used in this study without the presence of anticoagulant or antiplatelet therapies. Flow rate was controlled at 100 mL/min using the downstream flow clamp and measured using the upstream flow probe. This figure has been modified to remove all informal labeling using Photoshop.

Supplementary Figure 2 | (A) Survey XPS spectra of PVA and all GFPGER-modified PVA samples. High resolution of carbon on plain PVA **(B)**, $GFPGER_0$ **(C)**, and $GFPGER_{120}$ **(D)** samples.

REFERENCES

Alberio, L., and Dale, G. L. (1998). Flow cytometric analysis of platelet activation by different collagen types present in the vessel wall. *Br. J. Haematol.* 102, 1212–1218. doi: 10.1046/j.1365-2141.1998.00923.x

Anderson, D. E. J., and Hinds, M. T. (2012). Extracellular matrix production and regulation in micropatterned endothelial cells. *Biochem. Biophys. Res. Commun.* 427, 159–164. doi: 10.1016/j.bbrc.2012.09.034

Anderson, D. E. J., Pohan, G., Raman, J., Konecny, F., Yim, E. K. F., and Hinds, M. T. (2018). Improving surgical methods for studying vascular grafts in animal models. *Tissue Eng. C Methods* 24, 457–464. doi: 10.1089/ten.tec.2018.0099

Anderson, D. E. J., Truong, K. P., Hagen, M. W., Yim, E. K. F., and Hinds, M. T. (2019). Biomimetic modification of poly(vinyl alcohol): Encouraging endothelialization and preventing thrombosis with antiplatelet monotherapy. *Acta Biomater.* 86, 291–299. doi: 10.1016/J.ACTBIO.2019.01.008

Bates, N. M., Puy, C., Jurney, P. L., McCarty, O. J. T., and Hinds, M. T. (2020). Evaluation of the effect of crosslinking method of poly(vinyl alcohol) hydrogels on thrombogenicity. *Cardiovasc. Eng. Technol.* 11, 448–455. doi: 10.1007/s13239-020-00474-y

Cereceres, S., Touchet, T., Browning, M. B., Smith, C., Rivera, J., Hö, M., et al. (2015). Chronic wound dressings based on collagen-mimetic proteins. *Adv. Wound Care* 4, 444–456. doi: 10.1089/wound.2014.0614

Chaouat, M., Le Visage, C., Baille, W. E., Escoubet, B., Chaubet, F., Mateescu, M. A., et al. (2008). A novel cross-linked poly(vinyl alcohol) (PVA) for vascular grafts. *Adv. Funct. Mater.* 18, 2855–2861. doi: 10.1002/adfm.200701261

Cosemans, J. M. E. M., Iserbyt, B. F., Deckmyn, H., and Heemskerk, J. W. M. (2008). Multiple ways to switch platelet integrins on and off. *J. Thromb. Haemost.* 6, 1253–1261. doi: 10.1111/j.1538-7836.2008.03041.x

Cutiongco, M. F. A., Anderson, D. E. J., Hinds, M. T., and Yim, E. K. F. (2015a). In vitro and ex vivo hemocompatibility of off-the-shelf modified poly(vinyl alcohol) vascular grafts. *Acta Biomater.* 25, 97–108. doi: 10.1016/j.actbio.2015.07.039

Cutiongco, M. F. A., Choo, R. K. T., Shen, N. J. X., Chua, B. M. X., Sju, E., Choo, A. W. L., et al. (2015b). Composite scaffold of poly(vinyl alcohol) and interfacial polyelectrolyte complexation fibers for controlled biomolecule delivery. *Front. Bioeng. Biotechnol.* 3:3. doi: 10.3389/fbioe.2015.00003

Cutiongco, M. F. A., Goh, S. H., Aid-Launais, R., Le Visage, C., Low, H. Y., and Yim, E. K. F. (2016a). Planar and tubular patterning of micro and nano-topographies on poly(vinyl alcohol) hydrogel for improved endothelial cell responses. *Biomaterials* 84, 184–195. doi: 10.1016/J.BIOMATERIALS.2016.01.036

Cutiongco, M. F. A., Kukumberg, M., Peneyra, J. L., Yeo, M. S., Yao, J. Y., Rufaihah, A. J., et al. (2016b). Submillimeter diameter poly(vinyl alcohol) vascular graft patency in rabbit model. *Front. Bioeng. Biotechnol.* 4:44. doi: 10.3389/fbioe.2016.00044

Farndale, R. W. (2006). Collagen-induced platelet activation, Blood Cells. *Mol. Dis.* 36, 162–165. doi: 10.1016/j.bcmd.2005.12.016

Fayol, D., Le Visage, C., Ino, J., Gazeau, F., Letourneur, D., and Wilhelm, C. (2013). Design of biomimetic vascular grafts with magnetic endothelial patterning. *Cell Transplant.* 22, 2105–2118. doi: 10.3727/096368912X661300

Gabriel, M., Dahm, M., and Vahl, C. F. (2011). Wet-chemical approach for the cell-adhesive modification of polytetrafluoroethylene. *Biomed. Mater.* 6:035007. doi: 10.1088/1748-6041/6/3/035007

Glynn, J. J., and Hinds, M. T. (2014). Endothelial outgrowth cells: function and performance in vascular grafts. *Tissue Eng. Part B* 20, 294–303. doi: 10.1089/ten.teb.2013.0285

Gupta, A., Johnston, C. M., Hinds, M. T., and Anderson, D. E. J. (2020). Quantifying physical thrombus characteristics on cardiovascular biomaterials using microCT. *Methods Protoc.* 3:29. doi: 10.3390/mps3020029

Hagen, M. W., and Hinds, M. T. (2019). Static spatial growth restriction micropatterning of endothelial colony forming cells influences their morphology and gene expression. *PLoS One* 14:e0218197. doi: 10.1371/journal.pone.0218197

Harrison, S., Vavken, P., Kevy, S., Jacobson, M., Zurakowski, D., and Murray, M. M. (2011). Platelet activation by collagen provides sustained release of anabolic cytokines. *Am. J. Sports Med.* 39, 729–734. doi: 10.1177/0363546511401576

Ino, J. M., Sju, E., Ollivier, V., Yim, E. K. F., Letourneur, D., and Le Visage, C. (2013). Evaluation of hemocompatibility and endothelialization of hybrid poly(vinyl alcohol) (PVA)/gelatin polymer films. *J. Biomed. Mater. Res. B Appl. Biomater.* 101, 1549–1559. doi: 10.1002/jbm.b.32977

Jurney, P. L., Anderson, D. E. J., Pohan, G., Yim, E. K. F., and Hinds, M. T. (2018). Reactive ion plasma modification of poly(vinyl-alcohol) increases primary endothelial cell affinity and reduces thrombogenicity. *Macromol. Biosci.* 18:1800132. doi: 10.1002/mabi.201800132

Kumar, V. A., Brewster, L. P., Caves, J. M., and Chaikof, E. L. (2011). Tissue engineering of blood vessels: functional requirements, progress, and future challenges. *Cardiovasc. Eng. Technol.* 2, 137–148. doi: 10.1007/s13239-011-0049-3

Lei, Y., Remy, M., Labrugere, C., and Durrieu, M. C. (2012). Peptide immobilization on polyethylene terephthalate surfaces to study specific endothelial cell adhesion, spreading and migration. *J. Mater. Sci. Mater. Med.* 23, 2761–2772. doi: 10.1007/s10856-012-4736-x

Li, J., Ding, M., Fu, Q., Tan, H., Xie, X., and Zhong, Y. (2008). A novel strategy to graft RGD peptide on biomaterials surfaces for endothelization of small-diamater vascular grafts and tissue engineering blood vessel. *J. Mater. Sci. Mater. Med.* 19, 2595–2603. doi: 10.1007/s10856-007-3354-5

Liu, T., Liu, S., Zhang, K., Chen, J., and Huang, N. (2014). Endothelialization of implanted cardiovascular biomaterial surfaces: The development from in vitro to in vivo. *J. Biomed. Mater. Res. A* 102, 3754–3772. doi: 10.1002/jbm.a.35025

McCarty, O. J. T., Larson, M. K., Auger, J. M., Kalia, N., Atkinson, B. T., Pearce, A. C., et al. (2005). Rac1 is essential for platelet lamellipodia formation and aggregate stability under flow. *J. Biol. Chem.* 280, 39474–39484. doi: 10.1074/jbc.M504672200

Munnix, I. C. A., Gilio, K., Siljander, P. R. M., Raynal, N., Feijge, M. A. H., Hackeng, T. M., et al. (2008). Collagen-mimetic peptides mediate flow-dependent thrombus formation by high- or low-affinity binding of integrin α2β1 and glycoprotein VI. *J. Thromb. Haemost.* 6, 2132–2142. doi: 10.1111/j.1538-7836.2008.03167.x

Munoz-Pinto, D. J., Guiza-Arguello, V. R., Becerra-Bayona, S. M., Erndt-Marino, J., Samavedi, S., Malmut, S., et al. (2015). Collagen-mimetic hydrogels promote human endothelial cell adhesion, migration and phenotypic maturation. *J. Mater. Chem. B Mater. Biol. Med.* 3, 7912–7919. doi: 10.1039/C5TB00990A

Nakayama, Y., Ishibashi-Ueda, H., and Takamizawa, K. (2004). *In Vivo Tissue-Engineered Small-Caliber Arterial Graft Prosthesis Consisting of Autologous Tissue (Biotube)*. Available online at: www.cognizantcommunication.com (accessed April 9, 2020)

Nuttelman, C. R., Mortisen, D. J., Henry, S. M., and Anseth, K. S. (2001). Attachment of fibronectin to poly(vinyl alcohol) hydrogels promotes NIH3T3 cell adhesion, proliferation, and migration. *J. Biomed. Mater. Res.* 57, 217–223. doi: 10.1002/1097-4636(200111)57:2<217::aid-jbm1161>3.0.co;2-i

Rich, R. L., Deivanayagam, C. C. S., Owens, R. T., Carson, M., Höök, A., Moore, D., et al. (1999). Trench-shaped binding sites promote multiple classes of interactions between collagen and the adherence receptors, α1β1 integrin and Staphylococcus aureus Cna MSCRAMM. *J. Biol. Chem.* 274, 24906–24913. doi: 10.1074/jbc.274.35.24906

Rizwan, M., Yao, Y., Gorbet, M. B., Tse, J. W., Anderson, D. E. J., Hinds, M. T., et al. (2020). One-pot covalent grafting of gelatin on poly(vinyl alcohol) hydrogel to enhance endothelialization and hemocompatibility for synthetic vascular graft applications. *ACS Appl. Bio Mater.* 3, 693–703. doi: 10.1021/acsabm.9b01026

Ruggeri, Z. M., and Mendolicchio, G. L. (2007). Adhesion mechanisms in platelet function. *Circ. Res.* 100, 1673–1685. doi: 10.1161/01.RES.0000267878.97021.AB

Schindelin, J., Arganda-Carreras, I., Frise, E., Kaynig, V., Longair, M., Pietzsch, T., et al. (2012). Fiji: an open-source platform for biological-image analysis. *Nat. Methods* 9, 676–682. doi: 10.1038/nmeth.2019

Schmedlen, R. H., Masters, K. S., and West, J. L. (2002). Photocrosslinkable polyvinyl alcohol hydrogels that can be modified with cell adhesion peptides for use in tissue engineering. *Biomaterials* 23, 4325–4332. doi: 10.1016/S0142-9612(02)00177-1

Seo, N., Russell, B. H., Rivera, J. J., Liang, X., Xu, X., Afshar-Kharghan, V., et al. (2010). An engineered α1 integrin-binding collagenous sequence. *J. Biol. Chem.* 285, 31046–31054. doi: 10.1074/jbc.M110.151357

Sipilä, K. H., Drushinin, K., Rappu, P., Jokinen, J., Salminen, T. A., Salo, A. M., et al. (2018). Proline hydroxylation in collagen supports integrin binding by two distinct mechanisms. *J. Biol. Chem.* 293, 7645–7658. doi: 10.1074/jbc.RA118.002200

Sivaraman, B., and Latour, R. A. (2010). The relationship between platelet adhesion on surfaces and the structure versus the amount of adsorbed fibrinogen. *Biomaterials* 31, 832–839. doi: 10.1016/j.biomaterials.2009.10.008

Uchida, N., Emoto, H., Kambic, H., Harasaki, H., Chen, J.-F., Hsu, S.-H., et al. (1989). Compliance effect on patency of small diameter. *Trans. Am. Soc. Artif. Intern. Organs* 35, 556–558. doi: 10.1097/00002480198907000-00124

Vaníčková, M., Suttnar, J., and Dyr, J. E. (2006). The adhesion of blood platelets on fibrinogen surface: comparison of two biochemical microplate assays. *Platelets* 17, 470–476. doi: 10.1080/09537100600758875

Xu, Y., Gurusiddappa, S., Rich, R. L., Owens, R. T., Keene, D. R., Mayne, R., et al. (2000). Multiple binding sites in collagen type I for the integrins α1β1 and α2β1. *J. Biol. Chem.* 275, 38981–38989. doi: 10.1074/jbc.M007668200

Yao, Y., Zaw, A. M., Anderson, D. E. J., Hinds, M. T., and Yim, E. K. F. (2020). Fucoidan functionalization on poly(vinyl alcohol) hydrogels for improved endothelialization and hemocompatibility. *Biomaterials* 249:120011. doi: 10.1016/j.biomaterials.2020.120011

Zilla, P., Bezuidenhout, D., and Human, P. (2007). Prosthetic vascular grafts: wrong models, wrong questions and no healing. *Biomaterials* 28, 5009–5027. doi: 10.1016/j.biomaterials.2007.07.017

Conflict of Interest: The authors declare that the research was conducted in the absence of any commercial or financial relationships that could be construed as a potential conflict of interest.

frontiers in Bioengineering and Biotechnology

MINI REVIEW
published: 20 January 2021
doi: 10.3389/fbioe.2020.611936

Engineering Extracellular Matrix Proteins to Enhance Cardiac Regeneration After Myocardial Infarction

Hamid Esmaeili[1], *Chaoyang Li*[2], *Xing Fu*[2]* *and Jangwook P. Jung*[1]*

[1] Department of Biological Engineering, Louisiana State University, Baton Rouge, LA, United States, [2] School of Animal Sciences, Louisiana State University AgCenter, Baton Rouge, LA, United States

Engineering microenvironments for accelerated myocardial repair is a challenging goal. Cell therapy has evolved over a few decades to engraft therapeutic cells to replenish lost cardiomyocytes in the left ventricle. However, compelling evidence supports that tailoring specific signals to endogenous cells rather than the direct integration of therapeutic cells could be an attractive strategy for better clinical outcomes. Of many possible routes to instruct endogenous cells, we reviewed recent cases that extracellular matrix (ECM) proteins contribute to enhanced cardiomyocyte proliferation from neonates to adults. In addition, the presence of ECM proteins exerts biophysical regulation in tissue, leading to the control of microenvironments and adaptation for enhanced cardiomyocyte proliferation. Finally, we also summarized recent clinical trials exclusively using ECM proteins, further supporting the notion that engineering ECM proteins would be a critical strategy to enhance myocardial repair without taking any risks or complications of applying therapeutic cardiac cells.

Keywords: extracellular matrix, cardiomyocyte proliferation, myocardial infarction, cardiac repair, acellular therapeutics

OPEN ACCESS

Edited by:
Hae-Won Kim,
Institute of Tissue Regeneration Engineering (ITREN), South Korea

Reviewed by:
Guang-Zhen Jin,
Dankook University, South Korea
Felix B. Engel,
University Hospital Erlangen, Germany

***Correspondence:**
Jangwook P. Jung
jjung1@lsu.edu
Xing Fu
xfu1@agcenter.lsu.edu

Specialty section:
This article was submitted to Biomaterials, a section of the journal Frontiers in Bioengineering and Biotechnology

Received: *29 September 2020*
Accepted: *18 December 2020*
Published: *20 January 2021*

Citation:
Esmaeili H, Li C, Fu X and Jung JP (2021) Engineering Extracellular Matrix Proteins to Enhance Cardiac Regeneration After Myocardial Infarction. Front. Bioeng. Biotechnol. 8:611936. doi: 10.3389/fbioe.2020.611936

INTRODUCTION

Post-natal cardiomyocytes (CMs) are terminally differentiated cells in the heart and lack proliferative capacity. A withdrawal from the cell-cycle correlates with multinucleated and polyploid CMs (Derks and Bergmann, 2020). At the time of birth, the neonatal human heart comprises primarily mononucleated CMs and ∼30% binucleated CMs, and this proportion of mononucleated and binucleated CMs does not change significantly after birth. The DNA of most nuclei is duplicated to become mononucleated tetraploid in childhood when the cells undergo hypertrophy (Bergmann et al., 2009). The overall arrest in CM division is due to the downregulation of cell cycle regulators (Walsh et al., 2010; Zebrowski et al., 2015).

After myocardial infarction (MI), several strategies to replenish lost CMs have been proposed. Engraftment of exogenous cells to restore the damaged myocardium is an attractive remedy to mitigate the progression of cardiac fibrosis. Exogenous sources include stem cell-derived CMs or cardiac progenitor cells. The first-generation cell therapy employed mesenchymal stem cells (MSCs) or similar derivatives (Perin et al., 2015), and the second-generation cell therapy (Cambria et al., 2017) utilized pluripotent stem cell (PSC)-derived CM (Chong et al., 2014; Shiba et al., 2016; Liu et al., 2018), which showed a certain extent of success for cardiac repair with stem

cells. However, a major problem associated with cell therapy includes relatively low retention and integration of delivered cells, where only 10–15% are retained regardless of the source (Hou et al., 2005), and only about 1% of injected cells remained after 1 month (Nguyen et al., 2016). In addition, significant arrhythmia, excessive immunosuppression, and potential teratoma formation are the major roadblocks of applying therapeutic cells toward clinical application (Berry et al., 2019; Bolli and Wysoczynski, 2019). Alternatively, cell therapy with endogenous resources is a preferred strategy. However, the contribution of endogenous cardiac stem cells is proven to be minimal, and 31 associated publications from the Anversa laboratory were retracted (Chien et al., 2019), leading to a pause on a clinical trial involving c-kit$^+$ cardiac stem cells by the National Institutes of Health [National Heart, Lung, and Blood Institute (NHLBI)] as of October 2018. Interestingly, these results can lead to the longstanding notion that it may be possible to achieve cardiac regeneration without physically presenting cells into the injured heart (French and Holmes, 2019). The consistent mismatch between insignificant cellular engraftment and significant functional improvement has led to our assertion that the functional benefits might well be derived from paracrine actions of the transplanted cells (French and Holmes, 2019), which initiated next-generation therapies with *cell-free* approaches (Cambria et al., 2017). Here, we succinctly summarize extracellular matrix (ECM) proteins directly relevant to or instructing CM proliferation to establish better strategies for enhanced cardiac repair.

STIMULATION SIGNALS FOR CARDIOMYOCYTE PROLIFERATION

Extracellular Matrices Associated With Cardiomyocyte Proliferation

From many recent studies (Frangogiannis, 2019), the composition and mechanical properties of the ECM (Chaudhuri et al., 2020) may play a critical role in inducing the regeneration of the myocardium (Yahalom-Ronen et al., 2015). The following studies are recent investigations on ECM proteins and their roles in CM proliferation.

Fibronectin

Fibronectin is a multidomain, high-molecular-weight glycoprotein, present at low levels in the ECM of the healthy heart. Proteomics analysis of ECM compositions with developmental ages showed that collagen I and III and laminins increase gradually from fetal to adult, while fibronectin decreased with development (Williams et al., 2014). *In vivo*, fibronectin is strongly upregulated in the heart after MI (Konstandin et al., 2013a). Thus, short-term induction of fibronectin following myocardial injury may be tied to a beneficial role in cardiac repair by CM proliferation. The same group proved that fibronectin promotes CM hypertrophy by nuclear factor of activated T cell (NFAT) *in vivo* and *in vitro*, while fibronectin attenuates the activation of physiological growth *in vitro* (Konstandin et al., 2013b). Co-culture of mammalian embryonic cardiac fibroblast (cFB) and CM can promote CM proliferation, and fibronectin secreted by embryonic mouse cFB plays a pro-proliferative role in this process (Ieda et al., 2009). The mechanism of CM proliferation is only partially attributed to fibronectin or collagen type III that promoted CM proliferation by activating heparin-binding EGF-like GFs via β1 integrin signaling (Ieda et al., 2009). In zebrafish heart regeneration, loss-of-function approaches indicated that high expression of fibronectin does not remuscularize the heart (Wang et al., 2013), but fibronectin is necessary for functional regeneration by mobilizing and integrating CMs into the injured region. As such, cFB and fibronectin need additional players to proliferate CMs for cardiac repair.

Periostin

Periostin is a multimodular protein composed of a signal peptide necessary for secretion, a small cysteine-rich module for the formation of multimers via disulfide bonds, four FAS1 (fasciclin-1) domains interacting with integrins, and a hydrophilic C-terminal region known to interact with other ECM proteins (Kii et al., 2010). Periostin is primarily expressed in the developing heart, but not in healthy adult ventricular myocardium (Snider et al., 2008; Hortells et al., 2020). After acute MI, periostin is re-expressed in the infarct border zones by activated cFBs (Kanisicak et al., 2016). It was reported earlier that periostin can switch differentiated mononucleated CMs into the cell cycle and induce cardiac regeneration with improved myocardial function, as evidenced by an increase in DNA synthesis, aurora B kinase detection, and CM cytokinesis (Kühn et al., 2007). Recently, a report investigated the impact of genetic ablation of periostin in neonatal mice following MI and showed that periostin mediates PI3K/GSK3β/cyclin D1 signaling pathway for myocardial regeneration (Chen et al., 2017). However, this conclusion still remains controversial in adult mice with inducible expression of full-length periostin in that periostin is abundant in the infarcted mouse myocardium in the absence of regeneration (Lorts et al., 2009). Moreover, the periostin-induced cell cycle reentry is mediated in an integrin-dependent manner, which may impact other non-CMs expressing integrins (Kühn et al., 2007).

Agrin

Agrin is a heparan sulfate proteoglycan. It harbors three laminin-globular (LG) domains within its C-terminal region, and the first two LG domains (LG1 and LG2) are sufficient for binding to α-dystroglycan (αDG). Agrin promotes cell cycle reentry in both neonatal and adult mice (Bassat et al., 2017), and a separate study showed that Hippo/Yap signaling is a key signaling mechanism to mediate endogenous CM dedifferentiation and proliferation (Morikawa et al., 2017). *In vitro* administration of C-terminal agrin from post-natal day 1 (P1) increased CM proliferation (Bassat et al., 2017). The injection of recombinant agrin to the myocardium after MI in juvenile and adult mice also induced CM cell cycle reentry in the healthy myocardium adjacent to the infarcted regions, resulting in reduced scar size and improved cardiac function (Bassat et al., 2017). Although a single administration

of agrin promotes cardiac regeneration in adult mice after MI, the degree of CM proliferation observed in this model suggests that additional therapeutic mechanisms are required for functional regeneration of the myocardium (Bassat et al., 2017). In a preclinical porcine model of ischemia reperfusion, local (antegrade) delivery of a single dose of recombinant agrin into the infarcted heart resulted in significant improvement in heart function, infarct size, improved angiogenesis, suppressed inflammatory response, and cell cycle reentry (Baehr et al., 2020). Recent studies reported that binding of agrin to αDG could contribute to enhanced CM proliferation. To expedite such changes, modulating the stiffness of microenvironments could synergistically initiate CM proliferation via dedifferentiation–proliferation–redifferentiation of CMs (Yahalom-Ronen et al., 2015; Wang et al., 2017; Judd et al., 2019).

Slit-2 and Nephronectin

Slit-2 is a neuronal protein and is the only binding partner of αDG with a single LG domain, while two other homologous Slit-1 and Slit-3 are not yet reported to bind to αDG (Wright et al., 2012). Nephronectin is expressed in CMs throughout the heart and is secreted into the cardiac jelly (Patra et al., 2011). From embryonic cFB-derived ECMs, Slit-2 and nephronectin promote CM cytokinesis both *in vitro* and *in vivo* (Wu et al., 2020), but not cell cycle entry of post-natal CMs. The authors postulated that Slit-2 and nephronectin may act directly on CM and activate intracellular signaling pathways, such as RhoA (Backer et al., 2018).

Decellularized Extracellular Matrix

Instead of a single ECM component, decellularized zebrafish cardiac ECM (zECM) was intramyocardially injected to treat adult mice after MI (Chen et al., 2016). Given the high regenerative capacity of adult zebrafish hearts, decellularized zECM made from normal or healing hearts can induce mammalian heart regeneration. In a mouse model of acute MI, although a single injection of both normal and healing zECM improved cardiac functional recovery and repair, the healing zECM induced better improvements on heart function. Groups treated with zECM exhibited proliferation of the remaining CMs and multiple cardiac precursor cell populations and reactivation of ErbB2 expression in CMs. NRG1, a mitogen of CMs and a ligand of ErbB2/ErbB4 complex, was detected in zECM but only minimally in murine ECM. The presence of NRG1 in zECM and the reactivation of its receptor ErbB2 in zECM-treated hearts are consistent with the observed proliferation of CMs and improvement of cardiac function. In addition, decellularized porcine myocardial-derived ECM hydrogels were developed (Seif-Naraghi et al., 2013) and showed increases in cardiac muscle and improvements in cardiac function following an injection into the infarct (Christman, 2019). Application of decellularized porcine cardiac ECM to cardiac explant (post-natal day 1) with simultaneous modulation of stiffness using BAPN (3-aminopropionitrile) and ribose (stiffening) (Wang et al., 2020) presented a case that both ECM proteins and mechanical properties of microenvironments are important modulators for cardiac regeneration. Thus, these cases indicate that cardiac ECM-based therapeutics needs to combine with biomechanical modification.

Microenvironmental Contribution to Cardiomyocyte Proliferation

In addition to CM proliferation via cell cycle reentry, heart regeneration requires dedifferentiation, which indirectly initiates proliferation, and the migration of CM to the injured sites, followed by redifferentiation. Clinically, mechanical unloading of diseased hearts can improve adverse remodeling and improve metabolism (Uriel et al., 2018). The stiffness of the ECM in the myocardium increases progressively, which is correlated with CM cell cycle arrest. By modulating the stiffness of polydimethylsiloxane (PDMS) substrates, compliant (5 kPa) substrates promoted dedifferentiation and proliferation of neonatal CMs including a disorganized sarcomere network and conspicuous cell cycle reentry (Yahalom-Ronen et al., 2015). In contrast, rigid (2 MPa) substrates facilitated karyokinesis (nuclear division) leading to binucleation. Thus, the compliant microenvironment could facilitate CM dedifferentiation and proliferation via its effect on the organization of the cytoskeleton (Yahalom-Ronen et al., 2015). In addition to the first report of neonatal (up to 7 days post-partum) cardiac regeneration (Porrello et al., 2011), another recent investigation found that neonatal regeneration sharply declines within 48 h, with hearts of 2-days-old mice responding to amputation with fibrosis, rather than regeneration (Notari et al., 2018). By comparing the global transcriptomes of mouse hearts at P1 and P2, the authors reported that most differentially expressed transcripts encode ECM proteins and structural constituents of the cytoskeleton. Pharmacological inhibition of the cross-linked enzyme LOX (lysyl oxidase) using BAPN rescued the ability of heart regeneration after apical amputation in P3 neonatal mice. On the other hand, stiffer substrates (10 to 50 kPa) were shown to increase CM proliferation and Yap activity in cultures of β-catenin double-knockout CMs (αE-catenin and αT-catenin), indicating that stabilizing cytoskeleton stimulates the nuclear translocation of Yap (Vite et al., 2018). The differences between published works may be attributed to varying experimental techniques including dimensionality, tissue vs. culture conditions, and stiffness range.

CLINICAL APPLICATION OF EXTRACELLULAR MATRIX-BASED BIOMATERIALS FOR CARDIAC REPAIR

Here are a few examples for ECM-based biomaterials specifically for cardiac repair. More acellular injectable biomaterials for treating MI are reviewed elsewhere (Hernandez and Christman, 2017; Christman, 2019). In addition, commercially available ECM-based scaffolds for cardiac repair are discussed in the recent reviews therein (Swinehart and Badylak, 2016; Pattar et al., 2019)

CorMatrix is a scaffold derived from small intestinal submucosa (SIS) and is the most widely used SIS-ECM product in cardiovascular surgery, which also recently received Food and

Drug Administration (FDA) approval (Mosala Nezhad et al., 2016). CorMatrix ECM cardiac patches were tested in clinical trials (ClinicalTrials.gov identifier: NCT02887768), claiming to promote endogenous cardiac regeneration. However, a study utilizing CorMatrix patches in infants with congenital heart disease did not show evidence of native cardiac tissue ingrowth within 21 months (Nelson et al., 2016). Further complications were reported from other clinical trials with a CorMatrix patch, including patch dehiscence after atrioventricular continuity reconstruction following massive posterior annulus decalcification and mitral valve replacement for mitral stenosis due to dystrophic calcification (Poulin et al., 2013). These results suggest that CorMatrix may elicit eosinophilic inflammation in human patients after implantation, perhaps via α-gal (galactose-α-1,3-galactose) present in the porcine intestine (Mosala Nezhad et al., 2016), which probably supports the notion that completely defined therapeutics would be beneficial to avoid adverse reactions in human patients.

VentriGel is an ECM hydrogel derived from decellularized porcine myocardium (Singelyn et al., 2012; Seif-Naraghi et al., 2013; Hernandez and Christman, 2017) examined in a recently published clinical trial (ClinicalTrials.gov identifier: NCT02305602). The outcomes of the first-in-man trial highlighted the safety and efficacy of the treatment over 6 months (Traverse et al., 2019). VentriGel is a relatively weak hydrogel (Johnson et al., 2011), exhibiting two orders of magnitude lower stiffness than the stiffness (13 Pa of storage modulus at 8 mg/mL) of healthy, normal adult myocardium (around 10–15 kPa; Pandey et al., 2018). While there is yet sufficient evidence for the capability of decellularized hydrogel to promote endogenous cardiac regeneration, the ECM signals of normal healthy myocardium can prove a promising strategy for engineering biomaterials for cardiac repair.

CONCLUSIONS AND OUTLOOK

From earlier studies treating p38 mitogen-activated protein (MAP) kinase inhibitor (SB203580) for CM mitosis (Engel et al., 2005, 2006), a number of stimulation signals have been identified for CM to reenter cell cycle and to promote [cyclin A2 (Shapiro et al., 2014); a cocktail of CDK1, CDK4, cyclin D1, and B1 (Mohamed et al., 2018); Tbx20 (Xiang et al., 2016); and hypoxia-inducible factor 1α (HIF1α) (Guimarães-Camboa et al., 2015)] or inhibit [Meis1 (Mahmoud et al., 2013) and thyroid hormone (Hirose et al., 2019)] preexisting CM proliferation. Hippo (Heallen et al., 2011; Leach et al., 2017) and NRG1/ErbB4 (D'uva et al., 2015) pathways could be a molecular strategy to promote adult CM proliferation. The Hippo-DGC (dystrophin–glycoprotein complex)-agrin studies identified that viral delivery or a direct injection of CM proliferation agonist could be a viable cardiac repair strategy (Morikawa et al., 2017). More recently, ERBB2-ERK (extracellular signal-regulated kinase)-YAP mechanotransduction signaling was shown to trigger CM mitosis and epithelial-to-mesenchymal (EMT)-like transition toward phenotypic plasticity (Aharonov et al., 2020). Another important consideration is to exploit the metabolic switch from mitochondrial oxidative phosphorylation to glycolysis to induce CM proliferation. Recent studies reported that CM proliferation can be enhanced by inhibiting fatty-acid utilization with deletion of pyruvate dehydrogenase kinase-4 (PDK4) (Cardoso et al., 2020), activating Nrg1/ErbB2 signaling (Honkoop et al., 2019), and activating PPARδ/PDK1/p308Akt/GSK3β/β-catenin-pathway (Magadum et al., 2017).

Translation of technologies to augment the stimulation signals requires a thoughtful examination, especially considering the oncogenic potential of activating growth pathways (Heallen et al., 2019). Another promising strategy of activating CM proliferation is to deliver an intrinsic extracellular factor (e.g., FSTL-1) via an engineered patch to stimulate endogenous repair (Wei et al., 2015). This acellular approach reduces the laborious effort to prepare therapeutic cells, while avoiding potential tumor formation and adverse immune rejection from the

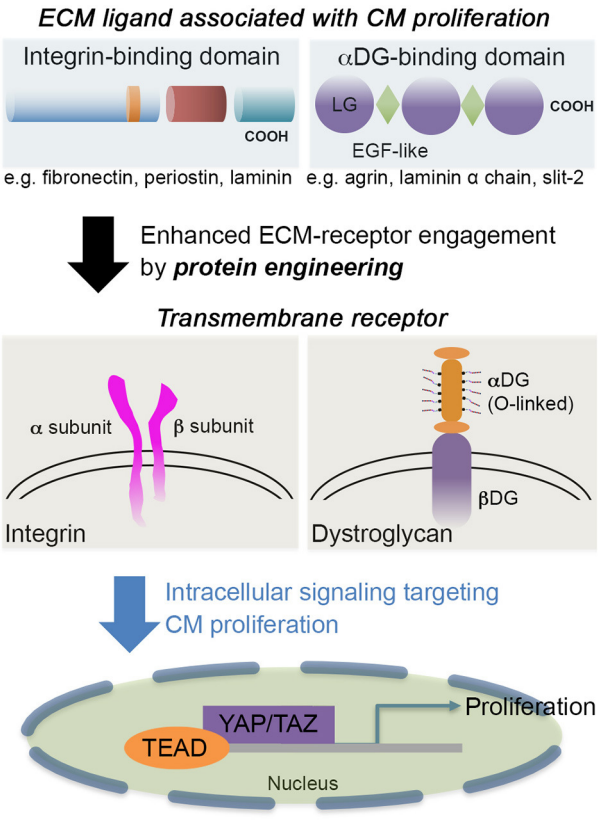

FIGURE 1 | The schematic showcases an example of integrin-binding domain, such as fibronectin, periostin, or laminin; and αDG-binding domain, such as agrin, Slit-2, or laminin α chains. The engagement of extracellular matrix (ECM) proteins via transmembrane receptors [integrin or dystroglycan (DG)] can be tuned by *engineering* the ECM proteins to further stimulate cardiomyocyte (CM) proliferation and associated pathways without penetrating CMs. Some laminin-globular (LG) domains from laminins are also interactive with integrin (Aumailley, 2013) as well as heparin (Ishihara et al., 2018), so the receptor-ligand integrations are not exclusive. For CM proliferation, active (unphosphorylated) Yap is translocated to the nucleus where the Yap interacts with TEA domain (TEAD) transcription factor to regulate cell proliferation.

patient. However, such an extracellular factor can also potentially stimulate non-CMs. Specific ligands that only allow engagement with CMs are needed to avoid adverse activation of the expansion of cFBs and their differentiation into myofibroblasts (specifically associated with fibrosis) (Fu et al., 2018).

Laminin α chains and several proteoglycans harbor a few tandem arrays of LG domains. Despite the structural similarity between agrin and laminin, binding affinity to αDG and the configuration of a tandem array of LG domains are distinct (Dempsey et al., 2019). This different feature may have conferred the different roles of ECM proteins containing LG domains in CM proliferation and differentiation. Thus, the therapeutic application of LG domain containing ECMs (agrin, laminin, and Slit-2, as depicted in **Figure 1**) needs to have further specification in their molecular nature and the receptors exclusively expressed in CM (for recent reviews on LG domain containing molecules, see Hohenester, 2019a,b; Yap et al., 2019).

ECM proteins that were applied for myocardial regeneration augmented the additional modification to enhance longevity and contribution for remuscularization (e.g., CorMatrix and VentriGel). ECM proteins binding to αDG, agrin, or Slit-2 contributed to CM proliferation (Bigotti et al., 2020), but further mechanistic understanding requires establishing a better strategy for CM proliferation. In addition to providing novel engineering strategies for cardiac repair, more critical analysis of CM proliferation assays and induction of CM proliferation by microRNA, metabolic switch, or small molecule is necessary to inform the field to efficiently reach the goal of myocardial regeneration (Leone and Engel, 2019). A recent phase I clinical trial (ESCORT, NCT02057900) with fibrin and Matrigel composites incorporating human embryonic stem cell (hESC)-derived cardiac progenitor cells ($Isl1^+$) proved the safety of the approach (Menasche et al., 2018; Menasché, 2020), which showed a synergistic contribution to the regeneration of the myocardium without apparent integration of the delivered cardiac cells. Thus, a protein engineering strategy could be a starting point to target a specific receptor and well-defined signal pathways (e.g., Hippo/Yap) (Bassat et al., 2017; Morikawa et al., 2017) (**Figure 1**). Then, engineering multifactorial, acellular biomaterials with a simple deployment strategy could be a therapeutic goal (Christman, 2019). Ideally, both mechanical compensation and biochemical definition would be necessary. In addition, what levels of complexity we have to address are an important question to answer (Ogle et al., 2016) since a small increase in the ejection fraction of 5–10% in the function of the left ventricle would be a meaningful resolution to mitigate heart failure for patients suffering from post-injury.

AUTHOR CONTRIBUTIONS

JJ and XF conceived the overall topics of discussion. All authors wrote, read, and approved the final manuscript.

FUNDING

This work was in part supported by the Louisiana Board of Regents Research Competitiveness Subprogram (JJ and XF), NIH 1R15DK122383 (XF), and the Open Access Author Fund from LSU Libraries (JJ). The authors thank Casey Chitwood for helpful discussion.

REFERENCES

Aharonov, A., Shakked, A., Umansky, K. B., Savidor, A., Genzelinakh, A., Kain, D., et al. (2020). Erbb2 drives yap activation and emt-like processes during cardiac regeneration. *Nat. Cell Biol.* 22, 1346–1356. doi: 10.1038/s41556-020-00588-4

Aumailley, M. (2013). The laminin family. *Cell Adh. Migr.* 7, 48–55. doi: 10.4161/cam.22826

Backer, S., Lokmane, L., Landragin, C., Deck, M., Garel, S., and Bloch-Gallego, E. (2018). Trio gef mediates rhoa activation downstream of slit2 and coordinates telencephalic wiring. *Development* 145:dev153692. doi: 10.1242/dev.153692

Baehr, A., Umansky, K. B., Bassat, E., Jurisch, V., Klett, K., Bozoglu, T., et al. (2020). Agrin promotes coordinated therapeutic processes leading to improved cardiac repair in pigs. *Circulation* 142, 868–881. doi: 10.1161/CIRCULATIONAHA.119.045116

Bassat, E., Mutlak, Y. E., Genzelinakh, A., Shadrin, I. Y., Baruch Umansky, K., Yifa, O., et al. (2017). The extracellular matrix protein agrin promotes heart regeneration in mice. *Nature* 547, 179–184. doi: 10.1038/nature22978

Bergmann, O., Bhardwaj, R. D., Bernard, S., Zdunek, S., Barnabé-Heider, F., Walsh, S., et al. (2009). Evidence for cardiomyocyte renewal in humans. *Science* 324, 98–102. doi: 10.1126/science.1164680

Berry, J. L., Zhu, W., Tang, Y. L., Krishnamurthy, P., Ge, Y., Cooke, J. P., et al. (2019). Convergences of life sciences and engineering in understanding and treating heart failure. *Circ. Res.* 124, 161–169. doi: 10.1161/CIRCRESAHA.118.314216

Bigotti, M. G., Skeffington, K. L., Jones, F. P., Caputo, M., and Brancaccio, A. (2020). Agrin-mediated cardiac regeneration: some open questions. *Front. Bioeng. Biotech.* 8:594. doi: 10.3389/fbioe.2020.00594

Bolli, R., and Wysoczynski, M. (2019). Human embryonic stem cell-derived cardiomyocytes. *Circ. Res.* 124, 1157–1159. doi: 10.1161/CIRCRESAHA.119.314869

Cambria, E., Pasqualini, F. S., Wolint, P., Günter, J., Steiger, J., Bopp, A., et al. (2017). Translational cardiac stem cell therapy: advancing from first-generation to next-generation cell types. *NPJ Regen. Med.* 2:17. doi: 10.1038/s41536-017-0024-1

Cardoso, A. C., Lam, N. T., Savla, J. J., Nakada, Y., Pereira, A. H. M., Elnwasany, A., et al. (2020). Mitochondrial substrate utilization regulates cardiomyocyte cell cycle progression. *Nat. Metab.* 2, 167–178. doi: 10.1038/s42255-020-0169-x

Chaudhuri, O., Cooper-White, J., Janmey, P. A., Mooney, D. J., and Shenoy, V. B. (2020). Effects of extracellular matrix viscoelasticity on cellular behaviour. *Nature* 584, 535–546. doi: 10.1038/s41586-020-2612-2

Chen, W. C., Wang, Z., Missinato, M. A., Park, D. W., Long, D. W., Liu, H. J., et al. (2016). Decellularized zebrafish cardiac extracellular matrix induces mammalian heart regeneration. *Sci. Adv.* 2:e1600844. doi: 10.1126/sciadv.1600844

Chen, Z., Xie, J., Hao, H., Lin, H., Wang, L., Zhang, Y., et al. (2017). Ablation of periostin inhibits post-infarction myocardial regeneration in neonatal mice mediated by the phosphatidylinositol 3 kinase/glycogen synthase kinase 3β/cyclin d1 signalling pathway. *Cardiovasc. Res.* 113, 620–632. doi: 10.1093/cvr/cvx001

Chien, K. R., Frisen, J., Fritsche-Danielson, R., Melton, D. A., Murry, C. E., and Weissman, I. L. (2019). Regenerating the field of cardiovascular cell therapy. *Nat. Biotech.* 37, 232–237. doi: 10.1038/s41587-019-0042-1

Chong, J. J. H., Yang, X., Don, C. W., Minami, E., Liu, Y.-W., Weyers, J. J., et al. (2014). Human embryonic-stem-cell-derived cardiomyocytes regenerate non-human primate hearts. *Nature* 510, 273–277. doi: 10.1038/nature13233

Christman, K. L. (2019). Biomaterials for tissue repair. *Science* 363, 340–341. doi: 10.1126/science.aar2955

Dempsey, C. E., Bigotti, M. G., Adams, J. C., and Brancaccio, A. (2019). Analysis of alpha-dystroglycan/lg domain binding modes: investigating protein motifs that regulate the affinity of isolated lg domains. *Front. Mol. Biosci.* 6:18. doi: 10.3389/fmolb.2019.00018

Derks, W., and Bergmann, O. (2020). Polyploidy in cardiomyocytes: roadblock to heart regeneration? *Circ. Res.* 126, 552–565. doi: 10.1161/CIRCRESAHA.119.315408

D'uva, G., Aharonov, A., Lauriola, M., Kain, D., Yahalom-Ronen, Y., Carvalho, S., et al. (2015). Erbb2 triggers mammalian heart regeneration by promoting cardiomyocyte dedifferentiation and proliferation. *Nat. Cell Biol.* 17, 627–638. doi: 10.1038/ncb3149

Engel, F. B., Hsieh, P. C., Lee, R. T., and Keating, M. T. (2006). Fgf1/p38 map kinase inhibitor therapy induces cardiomyocyte mitosis, reduces scarring, and rescues function after myocardial infarction. *Proc. Natl. Acad. Sci. U.S.A.* 103, 15546–15551. doi: 10.1073/pnas.0607382103

Engel, F. B., Schebesta, M., Duong, M. T., Lu, G., Ren, S., Madwed, J. B., et al. (2005). P38 map kinase inhibition enables proliferation of adult mammalian cardiomyocytes. *Genes Dev.* 19, 1175–1187. doi: 10.1101/gad.1306705

Frangogiannis, N. G. (2019). The extracellular matrix in ischemic and nonischemic heart failure. *Circ. Res.* 125, 117–146. doi: 10.1161/CIRCRESAHA.119.311148

French, B. A., and Holmes, J. W. (2019). Implications of scar structure and mechanics for post-infarction cardiac repair and regeneration. *Exp. Cell Res.* 376, 98–103. doi: 10.1016/j.yexcr.2019.01.001

Fu, X., Khalil, H., Kanisicak, O., Boyer, J. G., Vagnozzi, R. J., Maliken, B. D., et al. (2018). Specialized fibroblast differentiated states underlie scar formation in the infarcted mouse heart. *J. Clin. Invest.* 128, 2127–2143. doi: 10.1172/JCI98215

Guimarães-Camboa, N., Stowe, J., Aneas, I., Sakabe, N., Cattaneo, P., Henderson, L., et al. (2015). Hif1α represses cell stress pathways to allow proliferation of hypoxic fetal cardiomyocytes. *Dev. Cell* 33, 507–521. doi: 10.1016/j.devcel.2015.04.021

Heallen, T., Zhang, M., Wang, J., Bonilla-Claudio, M., Klysik, E., Johnson, R. L., et al. (2011). Hippo pathway inhibits wnt signaling to restrain cardiomyocyte proliferation and heart size. *Science* 332, 458–461. doi: 10.1126/science.1199010

Heallen, T. R., Kadow, Z. A., Kim, J. H., Wang, J., and Martin, J. F. (2019). Stimulating cardiogenesis as a treatment for heart failure. *Circ. Res.* 124, 1647–1657. doi: 10.1161/CIRCRESAHA.118.313573

Hernandez, M. J., and Christman, K. L. (2017). Designing acellular injectable biomaterial therapeutics for treating myocardial infarction and peripheral artery disease. *JACC Basic Transl. Sci.* 2, 212–226. doi: 10.1016/j.jacbts.2016.11.008

Hirose, K., Payumo, A. Y., Cutie, S., Hoang, A., Zhang, H., Guyot, R., et al. (2019). Evidence for hormonal control of heart regenerative capacity during endothermy acquisition. *Science* 364, 184–188. doi: 10.1126/science.aar2038

Hohenester, E. (2019a). Laminin g-like domains: dystroglycan-specific lectins. *Curr. Opin. Struct. Biol.* 56, 56–63. doi: 10.1016/j.sbi.2018.11.007

Hohenester, E. (2019b). Structural biology of laminins. *Essays Biochem.* 63, 285–295. doi: 10.1042/EBC20180075

Honkoop, H., De Bakker, D. E., Aharonov, A., Kruse, F., Shakked, A., Nguyen, P. D., et al. (2019). Single-cell analysis uncovers that metabolic reprogramming by erbb2 signaling is essential for cardiomyocyte proliferation in the regenerating heart. *Elife* 8:e50163. doi: 10.7554/eLife.50163.sa2

Hortells, L., Valiente-Alandi, I., Thomas, Z. M., Agnew, E. J., Schnell, D. J., York, A. J., et al. (2020). A specialized population of periostin-expressing cardiac fibroblasts contributes to postnatal cardiomyocyte maturation and innervation. *Proc. Natl. Acad. Sci. U.S.A.* 117, 21469–21479. doi: 10.1073/pnas.2009119117

Hou, D., Youssef, E. A., Brinton, T. J., Zhang, P., Rogers, P., Price, E. T., et al. (2005). Radiolabeled cell distribution after intramyocardial, intracoronary, and interstitial retrograde coronary venous delivery: implications for current clinical trials. *Circulation* 112, I150–I156. doi: 10.1161/CIRCULATIONAHA.104.526749

Ieda, M., Tsuchihashi, T., Ivey, K. N., Ross, R. S., Hong, T. T., Shaw, R. M., et al. (2009). Cardiac fibroblasts regulate myocardial proliferation through beta1 integrin signaling. *Dev. Cell* 16, 233–244. doi: 10.1016/j.devcel.2008.12.007

Ishihara, J., Ishihara, A., Fukunaga, K., Sasaki, K., White, M. J. V., Briquez, P. S., et al. (2018). Laminin heparin-binding peptides bind to several growth factors and enhance diabetic wound healing. *Nat. Commun.* 9:2163. doi: 10.1038/s41467-018-04525-w

Johnson, T. D., Lin, S. Y., and Christman, K. L. (2011). Tailoring material properties of a nanofibrous extracellular matrix derived hydrogel. *Nanotechnology* 22:494015. doi: 10.1088/0957-4484/22/49/494015

Judd, J., Lovas, J., and Huang, G. N. (2019). Defined factors to reactivate cell cycle activity in adult mouse cardiomyocytes. *Sci. Rep.* 9:18830. doi: 10.1038/s41598-019-55027-8

Kanisicak, O., Khalil, H., Ivey, M. J., Karch, J., Maliken, B. D., Correll, R. N., et al. (2016). Genetic lineage tracing defines myofibroblast origin and function in the injured heart. *Nat. Commun.* 7:12260. doi: 10.1038/ncomms12260

Kii, I., Nishiyama, T., Li, M., Matsumoto, K., Saito, M., Amizuka, N., et al. (2010). Incorporation of tenascin-c into the extracellular matrix by periostin underlies an extracellular meshwork architecture. *J. Biol. Chem.* 285, 2028–2039. doi: 10.1074/jbc.M109.051961

Konstandin, M. H., Toko, H., Gastelum, G. M., Quijada, P., De La Torre, A., Quintana, M., et al. (2013a). Fibronectin is essential for reparative cardiac progenitor cell response after myocardial infarction. *Circ. Res.* 113, 115–125. doi: 10.1161/CIRCRESAHA.113.301152

Konstandin, M. H., Völkers, M., Collins, B., Quijada, P., Quintana, M., De La Torre, A., et al. (2013b). Fibronectin contributes to pathological cardiac hypertrophy but not physiological growth. *Basic Res. Cardiol.* 108:375. doi: 10.1007/s00395-013-0375-8

Kühn, B., Del Monte, F., Hajjar, R. J., Chang, Y. S., Lebeche, D., Arab, S., et al. (2007). Periostin induces proliferation of differentiated cardiomyocytes and promotes cardiac repair. *Nat. Med.* 13, 962–969. doi: 10.1038/nm1619

Leach, J. P., Heallen, T., Zhang, M., Rahmani, M., Morikawa, Y., Hill, M. C., et al. (2017). Hippo pathway deficiency reverses systolic heart failure after infarction. *Nature* 550, 260–264. doi: 10.1038/nature24045

Leone, M., and Engel, F. B. (2019). Advances in heart regeneration based on cardiomyocyte proliferation and regenerative potential of binucleated cardiomyocytes and polyploidization. *Clin. Sci.* 133, 1229–1253. doi: 10.1042/CS20180560

Liu, Y. W., Chen, B., Yang, X., Fugate, J. A., Kalucki, F. A., Futakuchi-Tsuchida, A., et al. (2018). Human embryonic stem cell-derived cardiomyocytes restore function in infarcted hearts of non-human primates. *Nat. Biotech.* 36, 597–605. doi: 10.1038/nbt.4162

Lorts, A., Schwanekamp, J. A., Elrod, J. W., Sargent, M. A., and Molkentin, J. D. (2009). Genetic manipulation of periostin expression in the heart does not affect myocyte content, cell cycle activity, or cardiac repair. *Circ. Res.* 104, e1–e7. doi: 10.1161/CIRCRESAHA.108.188649

Magadum, A., Ding, Y., He, L., Kim, T., Vasudevarao, M. D., Long, Q., et al. (2017). Live cell screening platform identifies pparδ as a regulator of cardiomyocyte proliferation and cardiac repair. *Cell Res.* 27, 1002–1019. doi: 10.1038/cr.2017.84

Mahmoud, A. I., Kocabas, F., Muralidhar, S. A., Kimura, W., Koura, A. S., Thet, S., et al. (2013). Meis1 regulates postnatal cardiomyocyte cell cycle arrest. *Nature* 497, 249–253. doi: 10.1038/nature12054

Menasché, P. (2020). Cell therapy with human esc-derived cardiac cells: clinical perspectives. *Front. Bioeng. Biotechnol.* 8:601560. doi: 10.3389/fbioe.2020.601560

Menasche, P., Vanneaux, V., Hagege, A., Bel, A., Cholley, B., Parouchev, A., et al. (2018). Transplantation of human embryonic stem cell-derived cardiovascular progenitors for severe ischemic left ventricular dysfunction. *J. Am. Coll. Cardiol.* 71, 429–438. doi: 10.1016/j.jacc.2017.11.047

Mohamed, T. M. A., Ang, Y. S., Radzinsky, E., Zhou, P., Huang, Y., Elfenbein, A., et al. (2018). Regulation of cell cycle to stimulate adult cardiomyocyte proliferation and cardiac regeneration. *Cell* 173, 104–116.e112. doi: 10.1016/j.cell.2018.02.014

Morikawa, Y., Heallen, T., Leach, J., Xiao, Y., and Martin, J. F. (2017). Dystrophin-glycoprotein complex sequesters yap to inhibit cardiomyocyte proliferation. *Nature* 547, 227–231. doi: 10.1038/nature22979

Mosala Nezhad, Z., Poncelet, A., De Kerchove, L., Gianello, P., Fervaille, C., and El Khoury, G. (2016). Small intestinal submucosa extracellular matrix (cormatrix®) in cardiovascular surgery: a systematic review. *Interact. Cardiovasc. Thorac. Surg.* 22, 839–850. doi: 10.1093/icvts/ivw020

Nelson, J. S., Heider, A., Si, M. S., and Ohye, R. G. (2016). Evaluation of explanted cormatrix intracardiac patches in children with congenital heart disease. *Ann. Thorac. Surg.* 102, 1329–1335. doi: 10.1016/j.athoracsur.2016.03.086

Nguyen, P. K., Neofytou, E., Rhee, J. W., and Wu, J. C. (2016). Potential strategies to address the major clinical barriers facing stem cell regenerative therapy for cardiovascular disease: a review. *JAMA Cardiol.* 1, 953–962. doi: 10.1001/jamacardio.2016.2750

Notari, M., Ventura-Rubio, A., Bedford-Guaus, S. J., Jorba, I., Mulero, L., Navajas, D., et al. (2018). The local microenvironment limits the regenerative potential of the mouse neonatal heart. *Sci. Adv.* 4:eaao5553. doi: 10.1126/sciadv.aao5553

Ogle, B. M., Bursac, N., Domian, I., Huang, N. F., Menasché, P., Murry, C. E., et al. (2016). Distilling complexity to advance cardiac tissue engineering. *Sci. Transl. Med.* 8:342ps313. doi: 10.1126/scitranslmed.aad2304

Pandey, P., Hawkes, W., Hu, J., Megone, W. V., Gautrot, J., Anilkumar, N., et al. (2018). Cardiomyocytes sense matrix rigidity through a combination of muscle and non-muscle myosin contractions. *Dev. Cell* 45:661. doi: 10.1016/j.devcel.2017.12.024

Patra, C., Diehl, F., Ferrazzi, F., Van Amerongen, M. J., Novoyatleva, T., Schaefer, L., et al. (2011). Nephronectin regulates atrioventricular canal differentiation via bmp4-has2 signaling in zebrafish. *Development* 138, 4499–4509. doi: 10.1242/dev.067454

Pattar, S. S., Fatehi Hassanabad, A., and Fedak, P. W. M. (2019). Acellular extracellular matrix bioscaffolds for cardiac repair and regeneration. *Front. Cell Dev. Biol.* 7:63. doi: 10.3389/fcell.2019.00063

Perin, E. C., Borow, K. M., Silva, G. V., Demaria, A. N., Marroquin, O. C., Huang, P. P., et al. (2015). A phase II dose-escalation study of allogeneic mesenchymal precursor cells in patients with ischemic or nonischemic heart failure. *Circ. Res.* 117, 576–584. doi: 10.1161/CIRCRESAHA.115.306332

Porrello, E. R., Mahmoud, A. I., Simpson, E., Hill, J. A., Richardson, J. A., Olson, E. N., et al. (2011). Transient regenerative potential of the neonatal mouse heart. *Science* 331, 1078–1080. doi: 10.1126/science.1200708

Poulin, F., Horlick, E. M., David, T., Woo, A., and Thavendiranathan, P. (2013). 3-dimensional transesophageal echocardiography-guided closure of a gerbode shunt due to cormatrix patch dehiscence. *J. Am. Coll. Cardiol.* 62:e5. doi: 10.1016/j.jacc.2013.02.090

Seif-Naraghi, S. B., Singelyn, J. M., Salvatore, M. A., Osborn, K. G., Wang, J. J., Sampat, U., et al. (2013). Safety and efficacy of an injectable extracellular matrix hydrogel for treating myocardial infarction. *Sci. Transl. Med.* 5:173ra125. doi: 10.1126/scitranslmed.3005503

Shapiro, S. D., Ranjan, A. K., Kawase, Y., Cheng, R. K., Kara, R. J., Bhattacharya, R., et al. (2014). Cyclin a2 induces cardiac regeneration after myocardial infarction through cytokinesis of adult cardiomyocytes. *Sci. Transl. Med.* 6:224ra227. doi: 10.1126/scitranslmed.3007668

Shiba, Y., Gomibuchi, T., Seto, T., Wada, Y., Ichimura, H., Tanaka, Y., et al. (2016). Allogeneic transplantation of ips cell-derived cardiomyocytes regenerates primate hearts. *Nature* 538, 388–391. doi: 10.1038/nature19815

Singelyn, J. M., Sundaramurthy, P., Johnson, T. D., Schup-Magoffin, P. J., Hu, D. P., Faulk, D. M., et al. (2012). Catheter-deliverable hydrogel derived from decellularized ventricular extracellular matrix increases endogenous cardiomyocytes and preserves cardiac function post-myocardial infarction. *J. Am. Coll. Cardiol.* 59, 751–763. doi: 10.1016/j.jacc.2011.10.888

Snider, P., Hinton, R. B., Moreno-Rodriguez, R. A., Wang, J., Rogers, R., Lindsley, A., et al. (2008). Periostin is required for maturation and extracellular matrix stabilization of noncardiomyocyte lineages of the heart. *Circ. Res.* 102, 752–760. doi: 10.1161/CIRCRESAHA.107.159517

Swinehart, I. T., and Badylak, S. F. (2016). Extracellular matrix bioscaffolds in tissue remodeling and morphogenesis. *Dev. Dyn.* 245, 351–360. doi: 10.1002/dvdy.24379

Traverse, J. H., Henry, T. D., Dib, N., Patel, A. N., Pepine, C., Schaer, G. L., et al. (2019). First-in-man study of a cardiac extracellular matrix hydrogel in early and late myocardial infarction patients. *JACC Basic Transl. Sci.* 4, 659–669. doi: 10.1016/j.jacbts.2019.07.012

Uriel, N., Sayer, G., Annamalai, S., Kapur, N. K., and Burkhoff, D. (2018). Mechanical unloading in heart failure. *J. Am. Coll. Cardiol.* 72, 569–580. doi: 10.1016/j.jacc.2018.05.038

Vite, A., Zhang, C., Yi, R., Emms, S., and Radice, G. L. (2018). A-catenin-dependent cytoskeletal tension controls yap activity in the heart. *Development* 145:dev149823 doi: 10.1242/dev.149823

Walsh, S., Pontén, A., Fleischmann, B. K., and Jovinge, S. (2010). Cardiomyocyte cell cycle control and growth estimation *in vivo*–an analysis based on cardiomyocyte nuclei. *Cardiovasc. Res.* 86, 365–373. doi: 10.1093/cvr/cvq005

Wang, J., Karra, R., Dickson, A. L., and Poss, K. D. (2013). Fibronectin is deposited by injury-activated epicardial cells and is necessary for zebrafish heart regeneration. *Dev. Biol.* 382, 427–435. doi: 10.1016/j.ydbio.2013.08.012

Wang, W. E., Li, L., Xia, X., Fu, W., Liao, Q., Lan, C., et al. (2017). Dedifferentiation, proliferation, and redifferentiation of adult mammalian cardiomyocytes after ischemic injury. *Circulation* 136, 834–848. doi: 10.1161/CIRCULATIONAHA.116.024307

Wang, X., Senapati, S., Akinbote, A., Gnanasambandam, B., Park, P. S., and Senyo, S. E. (2020). Microenvironment stiffness requires decellularized cardiac extracellular matrix to promote heart regeneration in the neonatal mouse heart. *Acta Biomater.* 113, 380–392. doi: 10.1016/j.actbio.2020.06.032

Wei, K., Serpooshan, V., Hurtado, C., Diez-Cuñado, M., Zhao, M., Maruyama, S., et al. (2015). Epicardial fstl1 reconstitution regenerates the adult mammalian heart. *Nature* 525, 479–485. doi: 10.1038/nature15372

Williams, C., Quinn, K. P., Georgakoudi, I., and Black, L. D. III (2014). Young developmental age cardiac extracellular matrix promotes the expansion of neonatal cardiomyocytes *in vitro*. *Acta Biomater.* 10, 194–204. doi: 10.1016/j.actbio.2013.08.037

Wright, K. M., Lyon, K. A., Leung, H., Leahy, D. J., Ma, L., and Ginty, D. D. (2012). Dystroglycan organizes axon guidance cue localization and axonal pathfinding. *Neuron* 76, 931–944. doi: 10.1016/j.neuron.2012.10.009

Wu, C. C., Jeratsch, S., Graumann, J., and Stainier, D. (2020). Modulation of mammalian cardiomyocyte cytokinesis by the extracellular matrix. *Circ. Res.* 127, 896–907. doi: 10.1161/CIRCRESAHA.119.316303

Xiang, F. L., Guo, M., and Yutzey, K. E. (2016). Overexpression of tbx20 in adult cardiomyocytes promotes proliferation and improves cardiac function after myocardial infarction. *Circulation* 133, 1081–1092. doi: 10.1161/CIRCULATIONAHA.115.019357

Yahalom-Ronen, Y., Rajchman, D., Sarig, R., Geiger, B., and Tzahor, E. (2015). Reduced matrix rigidity promotes neonatal cardiomyocyte dedifferentiation, proliferation and clonal expansion. *Elife* 4:e07455. doi: 10.7554/eLife.07455.020

Yap, L., Tay, H. G., Nguyen, M. T. X., Tjin, M. S., and Tryggvason, K. (2019). Laminins in cellular differentiation. *Trends Cell Biol.* 29, 987–1000. doi: 10.1016/j.tcb.2019.10.001

Zebrowski, D. C., Vergarajauregui, S., Wu, C. C., Piatkowski, T., Becker, R., Leone, M., et al. (2015). Developmental alterations in centrosome integrity contribute to the post-mitotic state of mammalian cardiomyocytes. *Elife* 4:e05563. doi: 10.7554/eLife.05563.014

Conflict of Interest: The authors declare that the research was conducted in the absence of any commercial or financial relationships that could be construed as a potential conflict of interest.

frontiers in Bioengineering and Biotechnology

REVIEW
published: 27 January 2021
doi: 10.3389/fbioe.2021.603408

Influence of the Mechanical Environment on the Regeneration of Osteochondral Defects

Sarah Davis[1]*, *Marta Roldo*[1], *Gordon Blunn*[1], *Gianluca Tozzi*[2] and *Tosca Roncada*[1]*

[1] School of Pharmacy and Biomedical Sciences, University of Portsmouth, Portsmouth, United Kingdom, [2] Zeiss Global Centre, School of Mechanical and Design Engineering, University of Portsmouth, Portsmouth, United Kingdom

Articular cartilage is a highly specialised connective tissue of diarthrodial joints which provides a smooth, lubricated surface for joint articulation and plays a crucial role in the transmission of loads. *In vivo* cartilage is subjected to mechanical stimuli that are essential for cartilage development and the maintenance of a chondrocytic phenotype. Cartilage damage caused by traumatic injuries, ageing, or degradative diseases leads to impaired loading resistance and progressive degeneration of both the articular cartilage and the underlying subchondral bone. Since the tissue has limited self-repairing capacity due its avascular nature, restoration of its mechanical properties is still a major challenge. Tissue engineering techniques have the potential to heal osteochondral defects using a combination of stem cells, growth factors, and biomaterials that could produce a biomechanically functional tissue, representative of native hyaline cartilage. However, current clinical approaches fail to repair full-thickness defects that include the underlying subchondral bone. Moreover, when tested *in vivo*, current tissue-engineered grafts show limited capacity to regenerate the damaged tissue due to poor integration with host cartilage and the failure to retain structural integrity after insertion, resulting in reduced mechanical function. The aim of this review is to examine the optimal characteristics of osteochondral scaffolds. Additionally, an overview on the latest biomaterials potentially able to replicate the natural mechanical environment of articular cartilage and their role in maintaining mechanical cues to drive chondrogenesis will be detailed, as well as the overall mechanical performance of grafts engineered using different technologies.

Keywords: osteochondral defects, tissue engineering, biomaterials, articular cartilage, mechanobiology, stem cells, mechanical testing

OPEN ACCESS

Edited by:
Hon Fai Chan,
The Chinese University of Hong Kong, China

Reviewed by:
Marcus Mumme,
University Children's Hospital Basel, Switzerland
Lia Rimondini,
University of Eastern Piedmont, Italy

***Correspondence:**
Sarah Davis
sarah.davis@port.ac.uk
Tosca Roncada
tosca.roncada@port.ac.uk

Specialty section:
This article was submitted to Biomaterials, a section of the journal Frontiers in Bioengineering and Biotechnology

Received: *06 September 2020*
Accepted: *04 January 2021*
Published: *27 January 2021*

Citation:
Davis S, Roldo M, Blunn G, Tozzi G and Roncada T (2021) Influence of the Mechanical Environment on the Regeneration of Osteochondral Defects. Front. Bioeng. Biotechnol. 9:603408. doi: 10.3389/fbioe.2021.603408

OSTEOCHONDRAL DEFECTS

Osteochondral defects are areas of damage that involve both the articular cartilage and the underlying subchondral bone and can be caused by ageing, diseases (such as osteoarthritis and osteochondritis dissecans) or trauma. Osteoarthritis (OA) is a degenerative joint disease that affects over 250 million people worldwide (Hunter et al., 2014). Prevalence of the disease is increasing due to an ageing population and, in the US alone, 70 million people over the age of 65 are at risk of developing OA by the year 2030 (Bhatia et al., 2013). OA, originally thought to be a disease primarily affecting articular cartilage, is now considered to affect all tissues in the diarthrodial joint, including subchondral bone, ligaments, menisci, joint capsule, and synovial

membrane (Torres et al., 2006; Hunter et al., 2009; Lo et al., 2009; Krasnokutsky et al., 2011). As well as changes to the chondrocytes and the cartilage matrix, osteoarthritis is characterised by structural changes such as joint space narrowing, osteophyte formation and subchondral sclerosis that cause pain and joint immobilisation. Subtle changes to subchondral bone can be observed early, though the precise chronology of how these changes affect the OA process remains to be uncovered and the role of the subchondral bone in initiating and advancing disease progression is now receiving greater attention (Li et al., 2013). The crosstalk between subchondral bone and articular cartilage is complex and can induce biomechanical and biochemical changes in the overlying cartilage (Hu et al., 2020). The more obvious effect of changes to subchondral bone can be seen in conditions such as osteonecrosis, osteosclerosis, and Osteochondritis Dissecans (OCD). In osteonecrosis, and osteosclerosis imbalances in the bone remodelling process causes changes in bone turnover, mineralization, and subchondral bone volume, reducing overall bone density. This alters the biomechanical environment of the osteochondral unit and causes strain changes in the overlying cartilage during loading that may lead to pathological changes. OCD is a pathologic condition that affects subchondral bone formation resulting in subchondral bone fragments that disrupt the overlying articular surface. The exact causes of OCD are still unknown, yet repetitive microtrauma, abnormal endochondral ossification, and genetic factors are thought to play a role in its development (Grimm et al., 2014). Primarily, repetitive overloading or trauma is thought to disrupt the blood supply resulting in osteonecrosis. This in turn, may induce microcracks in the subchondral bone plate and underlying bone, resulting in fragmentation of bone and cartilage, causing inflammation, and joint pain. Another example is where cartilage loss adjacent to subchondral bone marrow lesions is common and is probably associated with changes in the modulation of this crosstalk (Hunter et al., 2009).

Articular cartilage is a viscoelastic tissue that provides a smooth and lubricated surface for joint movement, which also plays a key role in the absorption and dissipation of loads to the underlying subchondral bone. Healthy articular cartilage is an avascular, a-neural and a-lymphatic tissue, composed mainly of a proteoglycan rich extracellular matrix (ECM), type II collagen and chondrocytes. Mechanical properties of articular cartilage largely depend on ECM composition and organisation, however, mechanical stimulation is essential for cartilage development as well as maintaining cartilage homeostasis (Sanchez-Adams et al., 2014; Prein et al., 2016). Nevertheless, it has been demonstrated that excessive loading, either as single acute event or repetitive stresses, induces the expression of degradative enzymes such as metallopeptidase with a thrombospondin type 1 motif 5 (ADAMTS5) and matrix metalloproteinase-13 (MMP13), affecting matrix composition and hence playing a pivotal role in pathogenesis (Nakagawa et al., 2012; Buckwalter et al., 2013; Houard et al., 2013; Chang et al., 2019). Both OA (particularly post-traumatic osteoarthritis: PTOA) and OCD are associated with high-impact sports and abnormal loading/ joint injury, and therefore tend to affect highly stressed joints such as the knee and elbow. Since mechanical loading plays such a vital role in the initiation and progression of osteochondral defects and associated conditions, a deeper understanding of cartilage-bone mechanics is essential for developing better diagnosis and treatment methods.

This review will focus on the biomaterials able to replicate the natural mechanical environment of articular cartilage and the effect of mechanical cues resulting from the use of these scaffolds in directing and enhancing chondrogenesis. Importantly, osteochondral implants must be able to withstand the mechanical environment in the joint, which is responsible for these mechanical cues and that they are tested during their initial development with this environment in mind.

THE MECHANICAL ENVIRONMENT OF NATURAL CARTILAGE

Articular cartilage can be subdivided into four distinct zones: the superficial zone, the middle zone, the deep zone and the calcified zone (**Figure 1A**). Each zone exhibits a particular arrangement and organisation of chondrocytes and ECM proteins, mainly collagen type II (Col II) and proteoglycans, determining the tensile strength, flexibility and load-bearing ability of cartilage (Baumann et al., 2019). Since articular cartilage is a non-uniform structure, it presents challenges when trying to determine strain patterns and relative stiffness. This is due to variation in the orientation of collagen fibres, proteoglycan distribution, and molecular/ion content throughout the depth of native cartilage, which is a function of the anatomical location within the joint, and the type of loading applied.

The superficial zone represents the 10–20% of articular cartilage and contains flattened chondrocytes. In the superficial zone, thin collagen fibres (mainly collagen type II and IX) are tightly packed and aligned parallel to the articular surface to protect deeper layers from shear stress (Sophia Fox et al., 2009; Correa and Lietman, 2017). Moreover, the parallel arrangement of collagen provides tensile stiffness and strength providing the tissue with high mechanical stability. This thin layer acts as a barrier regulating not only the diffusion transport of nutrients and oxygen to the underlying cartilage structures but also the ingress and egress of large biomolecules (Leddy et al., 2008). Lubricin, which is responsible for reducing surface friction, is produced by chondrocytes only in this zone (Correa and Lietman, 2017). The middle zone represents 40–60% of the articular cartilage and is characterised by sparsely distributed rounded chondrocytes and a proteoglycan rich ECM (consisting mainly of aggrecan) (Fisher et al., 2019). Within the middle zone, collagen type II has thicker fibres and is obliquely distributed. The deep zone is characterised by the highest proteoglycan content and the lowest water concentration. Collagen fibres are thick and run perpendicular to the articular surface (Baumann et al., 2019). Chondrocytes are parallel to the collagen fibres and arranged in columns. Due to the high content of negatively charged proteoglycans, the deep zone is responsible for providing the greatest compressive resistance to articular cartilage (Gilbert and Blain, 2018). The deep zone is reported to have the highest stiffness, along with the superficial zone, corresponding to

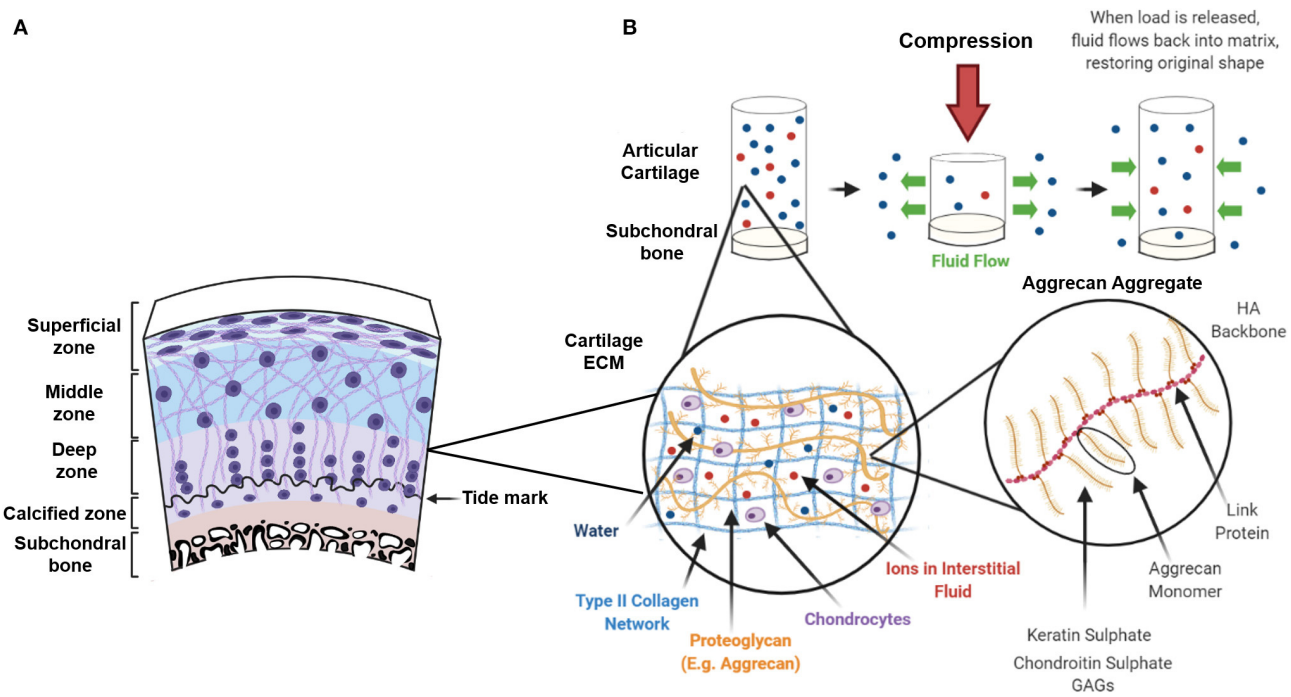

FIGURE 1 | Zonal architecture of articular cartilage and viscoelastic behaviour following compression. **(A)** Articular cartilage can be subdivided into 4 distinct zones: The superficial zone, the middle zone, the deep zone and the zone of calcified cartilage. Collagen fibre orientation in the extracellular matrix (ECM) and distribution of chondrocytes varies within each zone. **(B)** The ECM consists of a liquid phase (the interstitial fluid) and a solid phase composed of a type II collagen network interwoven with proteoglycans (predominantly aggrecan). The negative charge on the keratin sulphate and chondroitin sulphate glycosaminoglycans (GAGs) attracts positive ions that creates an osmotic pressure and retains water in the collagen network. When a compressive load is applied fluid flows out of the ECM in a time-dependent manner and similarly, when the load is removed, fluid is drawn back into the matrix restoring its original shape.

locations where the collagen fibre density is greatest, whereas the middle zone is characteristically softer (Schinagl et al., 1997; Bellucci and Seedhom, 2001). Articular cartilage stiffness has been reported to range from 0.1 to 6.2 MPa, with variabilities among studies that depend on sample type and testing setting (Boschetti et al., 2004; Robinson et al., 2016; Patel et al., 2019; Zheng et al., 2019; Guimarães et al., 2020). Within the middle and the deep zone, each chondrocyte is surrounded by a 2–4 μm thick collagen type VI rich pericellular matrix (PCM), which forms the chondron. The PCM seems to play a functional role in initiating signal transduction within the cartilage during load-bearing (Leddy et al., 2008). A study by McLeod et al. (2013) showed depth-dependent mechanical inhomogeneity of the elastic moduli of the ECM throughout the cartilage zones, yet zonal uniformity of the PCM elastic moduli in comparison. Cartilage stiffness has also shown to decrease with increasing severity of OA (Kleemann et al., 2005). The calcified zone is characterised by hypertrophic chondrocytes and has a high content of collagen type X (Col X). It anchors the collagen fibrils from the deep zone to the subchondral bone providing optimal integration and as it is infrequently penetrated by blood vessels it prevents vascularization of the articular cartilage. The zone of calcified cartilage also acts as a transitional zone and is important for reducing stress concentrations at the cartilage-bone interface (Boushell et al., 2017). The subchondral bone plate starts at the tidemark separating calcified and non-calcified cartilage. It is a supportive structure that consists of calcified cartilage and underlying subchondral bone that allows the build-up of hydrostatic pressure (Hwang et al., 2008). Damage to the integrity of the subchondral bone affects the generation of hydrostatic pressures and the repair of osteochondral defects often fails to recognise the importance of the subchondral bone plate. In its natural environment, cartilage is subject to a variety of different types of mechanical forces, including tension, compression, shear stress, and torsion. Physiological load on articular cartilage ranges from 5 to 8 MPa during walking and can reach up to 18 MPa when undergoing other activities such as rising from a chair (Clements et al., 2001). Due to the impermeable nature of the calcified cartilage and the low hydraulic permeability of the subchondral bone plate, the resistance to fluid flow within the cartilage results in the build-up of hydrostatic pressures (Hwang et al., 2008). Articular cartilage is resistant to these loads due, in part, to its viscoelastic behaviour resulting from the inter-relationship between the proteoglycan aggregates of the ECM (often referred to as the solid phase), and the interstitial fluid or liquid phase. The negatively charged carboxyl and sulphate groups of the proteoglycans attracts positive ions and creates an osmotic pressure, restrained by the tensile properties of the type II collagen network, which provides the cartilage with its compressive stiffness (Ateshian

et al., 2004). When a constant force is applied, the interstitial fluid pressure increases, forcing fluid out of the porous ECM in a time-dependent manner, creating frictional drag until equilibrium is reached. This frictional drag is inversely proportional to its permeability (Mak, 1986) and gives the cartilage its viscoelastic creep and stress-relaxation characteristics during compression (Mow et al., 1980; Halonen et al., 2014). When strain is kept constant, stress on the tissue increases until it reaches a peak which, due to redistribution of fluid within the cartilage, relaxes over time until equilibrium is reached. Similarly, when the load is removed, fluid flows back into the matrix allowing the cartilage to return to its original state, hence giving the tissue its mechanical properties and ability to withstand compressive loads (**Figure 1B**). Structural and biochemical variations relating to degenerative changes following injury or pathological conditions such as OA, alters the fluid flow dynamics throughout the tissue and can further affect load-bearing and compressive capability.

Cartilage was originally described as a biphasic material by Mow et al. (1980), composed of the liquid and solid phases as previously described. However, the model was adapted into a triphasic material by Lai et al. (1991) to include the mechano-electrochemical behaviour of monovalent ions and later the model accounted for the polyvalent ions in the interstitial fluid as forces acting as part of a separate liquid or ion phase (Gu et al., 1998). Although the triphasic model is a more recent theory that encompasses a structurally more accurate description of the composition of articular cartilage, the biphasic model highlights the importance of osmotic and hydrostatic pressure within the cartilage and how the tissue resists both compressive and tensile forces (Ateshian et al., 2004). It should be noted that any successful osteochondral implant has to accommodate these forces.

The Effect of Physiological Loading, Overuse, and Disuse on Articular Cartilage

The high and complex range of physiological loads applied to cartilage are critical for maintaining healthy joint function. Mechanical loading, in the form of moderate exercise, is one of the most important factors for maintaining a homeostatic environment and balancing the anabolic and catabolic response of chondrocytes for ECM synthesis and degradation. Numerous studies have shown reduction in pro-inflammatory cytokines (IL-1B, IL-6 TNF-α), inflammatory mediators (COX-2, PGE_2 and NO) (Chowdhury et al., 2001; Fu et al., 2019) and reduction in matrix-degrading enzymes (MMPs and ADAMTSs) in response to dynamic compression (Sun et al., 2012). *In vitro* studies also confirm anti-inflammatory effects of loading, with an increase in both gene expression, synthesis of type II collagen, aggrecan production (Buschmann et al., 1999; Waldman et al., 2006; Iseki et al., 2019) and stimulation of chondrocyte growth, differentiation, and proliferation. It is also important to note that chondrocytes from different regions of cartilage constitutively express mRNA for cartilage structural proteins in different baseline levels and respond differently to mechanical loading, suggesting that isolating chondrocytes from a non-load-bearing area might significantly affect the quality of the synthesised ECM (Bevill et al., 2009; Briant et al., 2015).

Although there is a genetic predisposition to the development of OA, loading plays a contributory role. Physiological loading is important for maintaining joint homeostasis (**Figure 2**), whilst abnormal loading caused by obesity, immobilisation, joint instability, overuse, or trauma can cause cartilage degradation and are the main risk factors linked to the development of OA (Arden and Nevitt, 2006). Overloading of the joint, either as a single impact load or cyclic loading causes increased catabolism, chondrocyte necrosis and apoptosis and damage to the collagen network in a dose-dependent manner (Chen et al., 2001; Clements et al., 2004; Hosseini et al., 2014). Most studies report a critical threshold with chondrocyte apoptosis, GAG loss and increased production of inflammatory cytokines above this threshold load (Clements et al., 2001; D'Lima et al., 2001). Kerin et al. (1998) indicated that loads above 10 MPa can result in apoptosis. In comparison, using bovine explants, Loening et al. (2000) showed that chondrocyte apoptosis can occur at 4.5 MPa as an earlier response to injury which is later followed by degradation of the collagen network at 7–12 MPa (Loening et al., 2000). On the other hand reduced mobility, which is associated with low loading conditions results in upregulation of MMPS, softening and a reduction in proteoglycan content and cartilage thinning (Jurvelin et al., 1986; Vanwanseele et al., 2002; Leong et al., 2011). Impaired joint loading significantly affects articular cartilage ECM composition and as consequence cartilage becomes thinner with reduced ability to absorb loads and shocks resulting in excessive load transmission to the underlying subchondral bone. Abnormal mechanical load can induce bone marrow oedema and subchondral sclerosis (Beckwée et al., 2015; Eriksen, 2015; Donell, 2019).

Articular cartilage is not only sensitive to the type of force applied and the magnitude of load but also to the duration, direction, and frequency of loading (Komeili et al., 2019). Párraga Quiroga et al. (2017) showed that higher strain rates cause more damage to the collagen network, while lower strain rates cause more damage to the non-fibrillar matrix components and that overall cartilage damage is both load and rate dependent. A study by Sadeghi et al. (2015) showed increases in crack length and surface damage with increasing loading frequency above a normal level of 1 Hz. There may also be variation in the material properties of the articular cartilage, in that weight-bearing areas may be more functionally prepared for loading compared to non-weight-bearing areas, and that non-weight-bearing areas may be more susceptible to damage and fibrillation when subject to the same tribological stresses (Moore and Burris, 2015). These factors highlight variability and therefore difficulty for a standard osteochondral graft material to be able to replicate native cartilage in different regions and locations within the same joint, let alone variability between different joints and that under different loading conditions.

Variations in Strain and Stiffness

In native osteochondral tissue under normal loading conditions, cartilage can experience strains of 2–9% and can reach up to 20–30% during vigorous activity, whereas the underlying

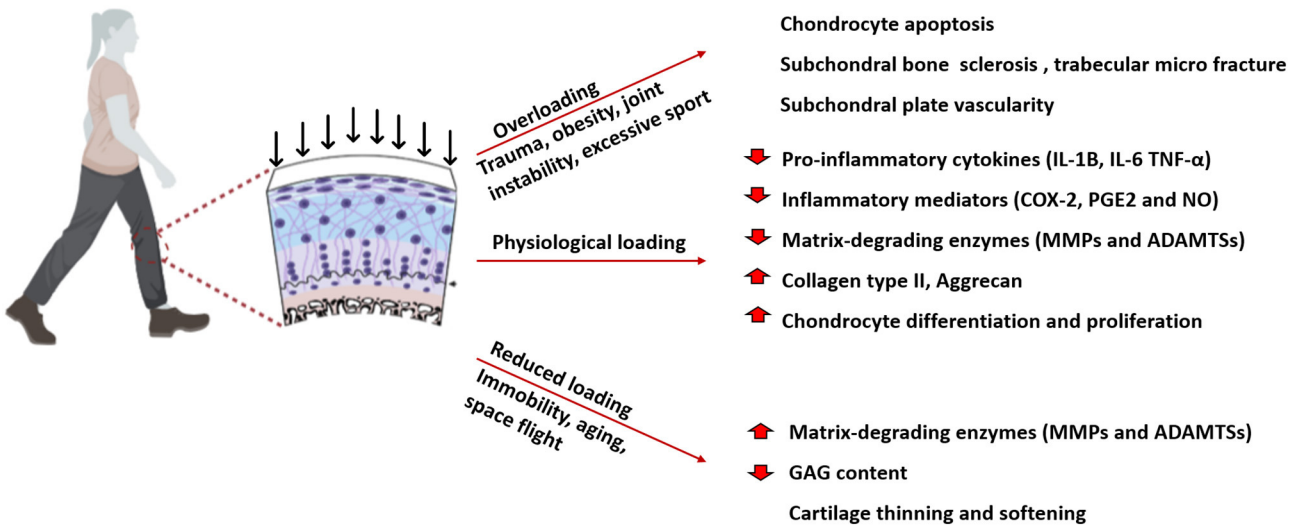

FIGURE 2 | Schematic representation of the effect of physiological, overloading, and reduced loading on articular cartilage. Physiological loading is essential for maintaining cartilage homeostasis regulating ECM synthesis and chondrocytes proliferation. Overloading, caused by trauma, obesity and joint instability, reduces collagen, and aggrecan content inducing chondrocytes apoptosis. Reduced loading increase matrix degradation leading to cartilage thinning and softening.

bone experiences strains of <1% (Sanchez-Adams et al., 2014; Steinmetz et al., 2015). In addition, calcified cartilage is ∼100 times stiffer than hyaline cartilage and 10 times less stiff than underlying subchondral bone and this transitional zone plays a crucial role in the transmission of loads between these regions (Mente and Lewis, 1994; Madi et al., 2020).

Strain distribution patterns vary depending on the type of loading, with more uniform strains during dynamic loading than static loading conditions and tension-compression non-linearity also causes variations in tensile stiffness (Huang et al., 2005; Komeili et al., 2019). Since cartilage is anisotropic material, the tensile moduli varies depending on the direction of testing and shows increased stiffness parallel to the local split-line patterns which also varies throughout the cartilage depth (Kempson et al., 1973). Variations have also been reported between anatomical locations within the joint, and differences in tensile modulus have been observed between high and low weight-bearing regions. For example, Wong and Sah (2010) showed regional variations in tibial and femoral cartilage, with more axial strain present in tibial cartilage during joint articulation. Several studies have also reported that in tibial and femoral knee condyle, higher strains are present on the medial side compared to the lateral compartment which provides an explanation for differences in mechanical stiffness and is related to contact biomechanics at these sites (Liu et al., 2010; Cotofana et al., 2011; Coleman et al., 2013; Halonen et al., 2014).

Asymmetric strain patterns of natural cartilage create numerous challenges for tissue engineers when analysing strain distribution throughout the cartilage and for replicating this mechanical environment *in vitro* in order to enhance the maturation of the tissue engineered construct. However, mechanical stimulation has successfully proven to enhance the properties of tissue engineered osteochondral grafts which will be discussed in more detail in this review. It is important to note that *in vivo* the complex interplay of other supportive tissues such as the menisci, tendons and ligaments (Halonen et al., 2014) which may also be compromised by trauma and OA.

CURRENT CLINICAL THERAPIES

Due to its avascular nature, the lack of abundant nutrients and low cell density, cartilage has limited regenerative capacity (Lo Monaco et al., 2018; Medvedeva et al., 2018). The treatment modality for repairing osteochondral injuries is dependent on the depth and area of the defect. Several clinical treatments are available to treat osteochondral defects such as microfracture (marrow stimulation), and the use of osteochondral autografts and allografts (Nukavarapu and Dorcemus, 2013; Freitag et al., 2017; Mathis et al., 2018). Microfracture is a surgical technique used to treat chondral defects, it involves perforating the subchondral bone with tiny holes allowing bone marrow mesenchymal stem cells and biomolecules to infiltrate the defect (Erggelet and Vavken, 2016). However, this often promotes the formation of mechanically inferior fibrocartilage with little evidence of type II collagen deposition (Redondo et al., 2018). For the treatment of larger osteochondral defects, where subchondral bone damage is seen tissue grafts of both cartilage and bone may be used. Osteochondral autograft transfer and mosaicplasty, have been used to treat full-thickness defects up to 4 cm^2.

During this procedure, chondral defects are replaced with plugs of the patient's own healthy articular cartilage and bone that are harvested from non-weight-bearing areas and transferred to pre-drilled holes at the defect site (Rowland et al., 2019). The outcome depends on age, sex and size of the lesion. In the case of large lesions, up to 8–9 cm^2, multiple plugs can be used but with a risk of significant donor site morbidity (Richter et al., 2016; Kato et al., 2018). Unlike autograft, allografts use full-thickness cartilage that can be harvested from locations that correlate with the defects to be filled allowing more precise matching of the size and contour of the articular surface (Assenmacher et al., 2016; Haber et al., 2019). Even though allografts can be performed as a single staged procedure and have shown good survival rate in short to medium term (5–10 years), long term follow-up has shown considerable reoperation (30.2%) and high failure rates (18.2%) over time (Familiari et al., 2018). Moreover, allografts are limited by the lack of tissue supply, low cell viability due to graft storage and possible immunorejection (Yang et al., 2017; Mathis et al., 2018).

Among the current clinical therapies, multi-layered cell-free scaffolds have been considered and are currently under pre-clinical and clinical evaluation. TruFit CB (Smith and Nephew) is a synthetic plug designed to be used with microfracture in order to improve the mechanical stability of the defect. Initial studies showed positive results with the regeneration of cartilage in a goat model, however, clinical studies revealed that 70% of patients required reoperation and the plug failed specifically in restoring the subchondral bone (Williams and Gamradt, 2008; Joshi et al., 2012). The bone-layer of TruFit CB is made of PGA and calcium phosphate, two materials that degrade quickly post-implantation and mechanical failure has resulted in the plug being withdrawn from the market (Fraser et al., 2016; Tseng et al., 2020). D'Ambrosi et al. (2019), investigated the clinical and radiological efficacy of MaioRegen, a try-layered collagen-based scaffold, in restoring osteochondral knee defects. Despite the promising satisfactory and reliable results at mid-term follow-up, this systematic review revealed that, in terms of clinical improvement at follow-up, MaioRegen is not superior to conservative treatment or other cartilage techniques. Therefore, there is still an unmet need for an optimal biomaterial system that favours simultaneous bone and cartilage regeneration. Although current clinical approaches can reduce pain and improve the quality of a patient's life, none of them has routinely achieved complete healing of the osteochondral lesion. Non-biological man-made materials can be used to partially replace the joint (e.g., unicompartmental knee replacement) or when the whole joint is severely affected it is likely that a total joint replacement (TJR) will be required as an end-stage intervention. In the elderly TJR is a successful end stage treatment for OA however, younger patients have a significantly higher risk of undergoing revision due to implant limited lifespan (25 years), periprosthetic joint infection or aseptic mechanical failure (Meehan et al., 2014; Stambough et al., 2014; Bayliss et al., 2017; Evans et al., 2019). To overcome these limitations, in the last two decades, research has focused on tissue engineering (TE) as a possible solution for osteochondral regeneration and repair of cartilage.

TISSUE ENGINEERING APPROACHES

The most common tissue engineering approach involves the use of a biocompatible scaffold, cells (e.g., stem cells) and/or a combination of bioactive molecules such as growth factors and cytokines. Autologous chondrocyte implantation (ACI) is a procedure for the regeneration of cartilage introduced by Brittberg et al. (1994), where autologous chondrocytes are isolated from a non-load-bearing site of the cartilage, expanded *in vitro* for 4–6 weeks and subsequently injected under a periosteal flap that is sutured onto the cartilage positioned over the defect (Könst et al., 2012). Although this technique has been used for two decades with successful surgical outcomes, the main issue is that two operations are required, one to obtain the cells, using arthroscopy and the other usually an open procedure to implant the cells (Minas et al., 2014; Mistry et al., 2017; Zikria et al., 2019). Matrix-induced autologous chondrocytes implantation (MACI) was originally developed to improve the biological performance of autologous chondrocytes cells and simplify surgical procedures (Andriolo et al., 2020). As with ACI, chondrocytes are isolated from a non-load-bearing area and cultured *in vitro*, however, this approach aims to deliver autologous chondrocytes in a biopolymer membrane. MACI® is also the name of a commercially available membrane of porcine collagen type I/III (Genzyme, United States). Several types of membranes and scaffolds have been developed for MACI procedures such as Novocart®3D (TETEC Tissue Engineering Technologies AG, Germany) a collagen-chondroitin-sulphate based membrane, CaRes®–Cartilage Regeneration System (Arthro-Kinetics, Germany) a collagen type I matrix and Cartipatch® (Tissue Bank of France, France) a monolayer agarose-alginate hydrogel (Vilela et al., 2018). However, MACI failed to prevent fibrocartilaginous healing and the integration of the scaffold into host hyaline cartilage is still unsatisfactory due to the intrinsic features of fully differentiated chondrocytes with their poor capability of tissue remodelling. Moreover, MACI still requires a two-step surgery, cartilage biopsy and cell cultivation, thus increasing the total cost (Behrens et al., 2006; Zikria et al., 2019). To further improve ACI outcomes and obtain a more reliable tissue repair, third generation of ACI has been developed, in which autologous chondrocytes are cultured in 3D to form spherical aggregates with a self-synthesised extracellular matrix. Spheroids of human autologous matrix-associated chondrocytes (Spherox) is an advanced tissue medicinal product with European Medicines Agency (EMA) market approval for the treatment of osteochondral defects up to 10 cm^2 (Niemeyer et al., 2020). However, due to differences in cartilage phenotype isolating chondrocytes from a non-load-bearing area might significantly affect the quality of the synthesised ECM (Bevill et al., 2009; Briant et al., 2015).

So far there appears to be little difference in outcomes of these cell therapies and tissue engineering approaches when compared with osteochondral autograft transfer system, mosaicplasty or microfracture surgery. Further, when harvested *in vitro*, chondrocytes undergo dedifferentiation exhibiting a flattened, fibroblast-like morphology. In these conditions they

produce a higher amount of collagen type I and collagen type X inducing the formation of fibrocartilage. An advantage of growing spheroids of chondrocytes isolated from biopsies is that the cartilage phenotype is better maintained than when cells are grown on flat tissue culture plastic. However, all of these approaches fail to fully repair the lesion in severe osteochondral defects, where both subchondral bone and articular cartilage are damaged (Davies and Kuiper, 2019). A significant proportion of research is focusing on the use of stem cells for cartilage repair since a large number of cells can be obtained from different sources such as bone marrow, peripheral blood, adipose tissue, dental pulp, placenta, and the umbilical cord (Tozzi et al., 2016). However, selectively promoting stem cell differentiation into appropriate cell lineages *in situ* is still challenging. An expanding field of research has demonstrated that mechanical cues from the environment could drive tissue formation and maturation, suggesting that combining scaffolds with mechanical properties that can drive stem cell differentiation could provide a solution for osteochondral defects where both bone and cartilage formation is required.

OSTEOCHONDRAL GRAFTS MATERIALS THAT CAN BE USED TO REPLICATE THE NATURAL MECHANICAL ENVIRONMENT

The development of an osteochondral implant that replicates the structure of articular cartilage and subchondral bone remains challenging for tissue engineers. Material selection plays a pivotal role in the development of osteochondral grafts as it potentially contributes to the mechanical properties of the scaffold (Jahr, 2017; Bonani et al., 2018).

Natural Materials

Natural materials such as collagen, chitosan, hyaluronic acid, silk, and alginate have been extensively used in TE for their biocompatibility, degradability and bioactivity (Jeuken et al., 2016; Li et al., 2018b). Natural materials are often used in the form of hydrogels with a highly hydrated viscoelastic matrix, tunable swelling behaviour and mechanical properties depending on the type and degree of crosslinking (Catoira et al., 2019; Mantha et al., 2019). Moreover, natural materials provide multiple binding sites for cell-ECM interaction. Multiple scaffolds for osteochondral TE in the clinical market are mainly composed of collagen type I (NOVOCART®3D, MACI®, CaReS®, NeoCart®, Maioregen®) (Kon et al., 2009; Crawford et al., 2012; Petri et al., 2013; Saris et al., 2014; Zak et al., 2014). Collagen can be extracted from various tissues and sources, for example, studies have reported that purified collagen can be isolated from vertebrate (generally rat, bovine, porcine and sheep) skin, tendon, cartilage and bone as well as from marine invertebrates (jellyfish, sponges, octopus, squid, cuttlefish, starfish) (Barzideh et al., 2014; Langasco et al., 2017). Even though collagen type I does not represent the main component of articular cartilage, several studies have demonstrated its pro-chondrogenic effects (Calabrese et al., 2017a,b; Xia et al., 2018). Preference of type I collagen in TE is largely attributed to its availability, its general biocompatibility and safety approvals granted by various agencies; however, high production costs and poor mechanical properties of pure collagen scaffolds are still major limitations (**Table 1**) (Dong and Lv, 2016; Ghodbane and Dunn, 2016). In comparison, Gelatin is derived by thermal denaturation of collagen and can be manufactured at a much lower cost and in larger quantities (Grover et al., 2012). Gelatin shows low antigenicity, it possesses integrin-binding sites, and it is completely resorbable *in vivo*. However, at body temperature gelatin hydrogels are not stable, limiting their possible use as a biomaterial. Van Den Bulcke et al. (2000) first described gelatin methacrylate (GelMA), a chemically modified form of gelatin that can be stabilised through photo-crosslinking allowing the formation of a hydrogel that is stable at body temperature. The modulus of GelMA-based biomaterial can be controlled by varying the degree of substitution and macromer concentration (Sadeghi et al., 2017), for example, Gan et al. (2019) has modified GelMA hydrogels by intercalating oligomers of dopamine methacrylate obtaining flexible hydrogels with compressive modulus of 2.5 MPa and shape-recovery ability. GelMA has also been used in combination with hyaluronic acid (HA), which forms the backbone of aggrecan and therefore plays a critical role in maintaining the viscoelastic and mechanical properties of cartilage (Hemmati-Sadeghi et al., 2018). HA acts also as a biochemical cue enhancing chondrogenic differentiation of MSCs, promoting chondrocyte proliferation and preventing chondrocyte de-differentiation by activating CD 44 (Chen et al., 2018; Li et al., 2018a; Yamagata et al., 2018). The use of HA in TE affects matrix deposition by cells, thus enhancing the dynamic and equilibrium moduli during *in vitro* culture (Levett et al., 2014). Recently silk fibroin (SF) has also been investigated in the context of osteochondral TE due to its biocompatibility, low immunogenicity, slow degradation rate, and remarkable mechanical properties (Qi et al., 2017). Silk has a high tensile strength (around 300–740 MPa) and depending on the source and production method, it is possible to obtain elastic moduli ranging from 1 MPa to 17 GPa, making it a favourable biomaterial not only for cartilage repair but also for subchondral bone (Koh et al., 2015; Peng et al., 2019). Li J. J. et al. (2015), developed a bi-layered scaffolds for osteochondral regeneration using silk fibroin for the cartilage layer and a silk-coated strontium-hardystonite-gahnite ceramic scaffold for the bone layer. The silk layer exhibited highly elastic behaviour showing 91% strain at failure, indicating that the silk scaffold could stretch to approximately twice its original length before breakage, which is desirable for the cartilage phase. When tested under compression the biphasic scaffold approximated the biomechanical behaviour of osteochondral tissue, as it could maintain structural integrity under large compressive stresses while retaining the ability for shape recovery when hydrated, in addition the stiff bone phase could withstand large compressive stresses with minimal deformation.

Among natural polysaccharides, both alginate and chitosan have potential for cartilage repair (Xu et al., 2008; Yao et al., 2016; Ewa-Choy et al., 2017; Henrionnet et al., 2017; Merlin Rajesh Lal et al., 2017; Ruvinov et al., 2018; Huang et al., 2019). Alginate is a biodegradable and biocompatible material, derived

TABLE 1 | Summary of advantages, disadvantages, and mechanical properties of naturally-derived materials.

Natural materials	Advantages	Disadvantages	Mechanical properties	References
Collagen type I	Low immunogenicity Degraded *in vivo* by MMPs	High production cost Low mechanical properties	Permeability 0.044–0.072 mm4/Ns Compressive modulus 3.5–3.7 kPa	Ghodbane and Dunn, 2016
Gelatin	Manufactured at a lower cost and in large quantities Low antigenicity Resorbable	Not stable at body temperature	Compressive modulus 0.75–6 kPa	Chen S. et al., 2016
GelMA	Stabilised form of gelatin Photocrosslinkable Varying the degree of substitution is possible to vary mechanical properties	UV crosslinking may have a negative effects on encapsulated cells	Compressive modulus 2–30 kPa	Sadeghi et al., 2017 Klotz et al., 2016
Hyaluronic acid (HA)	Enache MSCs chondrogenic differentiation Maintaining viscoelastic and mechanical properties in native cartilage Can be physically and chemically modified	Rapid degradation and poor mechanical properties	Elastic modulus of modified HA 1–70 kPa	Chen C. H. et al., 2016; Li et al., 2018a; Yamagata et al., 2018 Lee et al., 2018 Trombino et al., 2019
Silk fibroin	Biocompatibility Low immunogenicity Slow degradation rate Remarkable mechanical properties	Brittleness and swelling behaviour limits its applications in tissue engineering	High tensile strength 300–700 MPa and elastic modulus ranging from 1MPa to 17GPa	Koh et al., 2015; Chen et al., 2018; Peng et al., 2019
Alginate	Biodegradable Biocompatible Re-differentiate chondrocytes after monolayer culture Support chondrogenic phenotype Tunable mechanical properties	Lack of adhesion ligands	Elastic modulus 0.15-0.55MPa	Kaklamani et al., 2014
Chitosan	Biocompatibility Biodegradability Antibacterial properties	Display poor mechanical properties	0.13–0.199 MPa	Thomas et al., 2017

from seaweed that is composed of α-*D*-mannuronic acid and β-l-glucuronic acid. Studies have shown that it can support chondrogenic phenotype promoting a rounded morphology of isolated chondrocytes and the synthesis of type II collagen and proteoglycans (Homicz et al., 2003; Caron et al., 2012; Angelozzi et al., 2017; Aurich et al., 2018). Chondrogenic differentiation of stem cells isolated from bone marrow, adipose tissues, Wharton's Jelly, and dental pulp has been promoted by growing cells within alginate gels (Huang et al., 2015; Reppel et al., 2015; Ewa-Choy et al., 2017; Mata et al., 2017; Baba et al., 2018). Although much lower than the compressive modulus of native cartilage the mechanical properties of alginate scaffolds can be modified to give values of 0.15–0.55 MPa using divalent ions (Mg^{2+}, Ca^{2+}, and Sr^{2+}) (Kaklamani et al., 2014). However, the main limitation of alginate-based materials is the lack of adhesion ligands that are essential for cell-attachment and to overcome this, bioactive components such as collagen may be incorporated (Bian et al., 2011; Lee and Mooney, 2012; Ganesh et al., 2013).

Another natural polymer employed is chitosan, derived from partial deacetylation of chitin, used in TE for its biocompatibility, *in vivo* degradation and antibacterial properties (Cheung et al., 2015; Varun et al., 2017; Huang et al., 2019). Chitosan hydrogels have been shown to support the proliferation of chondrocytes and MSCs *in vitro* and to improve the deposition of cartilaginous ECM both *in vitro* and *in vivo* (Griffon et al., 2006; Elder et al., 2013; Faikrua et al., 2013; Sheehy et al., 2015; Huang et al., 2019; Scalzone et al., 2019). However, since chitosan display poor mechanical properties, crosslinking or combination with other materials is required to optimise the elastic modulus for osteochondral TE (Muzzarelli et al., 2015; De Mori et al., 2019; Kusmono and Abdurrahim, 2019; Scalzone et al., 2019). Thomas et al. (2017) tuned the stiffness of chitosan-hydrogels by blending increasing concentrations of hyaluronic acid dialdehyde and the degree of crosslinking to obtain hydrogels with a Young's modulus of 0.13 MPa and 0.199 MPa. However, a reinforced chitosan-based scaffold failed to regenerate bone and cartilage *in vivo* suggesting that the crosslinking treatment may have affected its overall degradation (Roffi et al., 2019). Therefore, a careful balance between the mechanical properties and degradation rate should be considered when designing osteochondral scaffolds using this material.

Synthetic Materials

Synthetic materials are attractive substitutes for load-bearing tissues, since the mechanical properties can be tailored by altering the molecular weight and/or via the use of different processing methods (Grigore, 2017). Synthetic polymers, including poly(ethylene glycol) (PEG), polylactide (PLA) and its derivatives poly(L-lactide) (PLLA) and poly(lactic-co-glycolic acid) (PLGA), polyglycolic acid (PGA), poly(ε-caprolactone)

TABLE 2 | Summary of advantages, disadvantages, and mechanical properties of synthetic materials.

Synthetic materials	Advantages	Disadvantages	Mechanical properties	References
PEG	High solubility in water Hydrophilicity Biocompatibility Inertness Non-immunogenicity	Lack of specific binding motifs for cell attachment	Equilibrium modulus 0.01–2.46 MPa Hydraulic permeability 10–13–10–16 m2/Pa Tensile modulus 0.02–3.5 MPa	Nguyen et al., 2012 Zhu, 2010
PGA	Biocompatible Bioresorbable	Loses its mechanical integrity between 2–4 weeks *in vivo*	Tensile modulus 7 GPa	Woodard and Grunlan, 2018; Gorth and Webster, 2011
PLA	PLA is more hydrophobic compared to PGA, leading to a slower hydrolysis rate.	Lack of specific binding motifs for cell attachment	Tensile modulus 3 GPa Tensile strength 50–70 MPa	Narayanan et al., 2016 Samavedi et al., 2013
PLGA	Modulation of Young's modulus and degradation rate, Sustained mechanical integrity after implantation	Lack of specific binding motifs for cell attachment	Compression storage modulus 3.2–4.6 MPa	Baker et al., 2009 Gentile et al., 2014
PVA	Biodegradable Biocompatible Adjustable mechanical properties	Lack of specific binding motifs for cell attachment	Tensile strength 1–17 MPa Elastic modulus 0.0012–0.85 MPa Low friction coefficients (μ) 0.02–0.05	Lin et al., 2017 Teixeira et al., 2019 Sánchez-Téllez et al., 2017
PCL	Adjustable mechanical strength Possibility to produce hydrogel, porous scaffold, electrospun nanofibers	Lack of specific binding motifs for cell attachment	Compressive modulus 6.63–56.46 MPa Tensile Modulus 6.03–46.04 MPa	Olubamiji et al., 2016

(PCL) and poly(vinyl alcohol) (PVA), are used to form hydrogels, porous scaffolds and nanofibrous scaffolds (Sánchez-Téllez et al., 2017; Yang et al., 2017; Castilho et al., 2018; Dai et al., 2018; Kudva et al., 2018; Critchley et al., 2020). The main disadvantage of these materials is the lack of specific binding motifs for cell attachment, but this can be improved through functionalization or by combining with more bioactive materials. PEG hydrogels have been used in TE due to their high solubility in water, hydrophilicity, biocompatibility, inertness, and non-immunogenicity (**Table 2**). They have also shown to maintain cell viability and promote chondrogenic ECM synthesis (Bryant and Anseth, 2002). By varying the molecular weight and the concentration of PEG precursors, Nguyen et al. (2012) obtained hydrogels with equilibrium modulus (0.01–2.46 MPa), hydraulic permeability [ranging from 10^{-13} to 10^{-16} (m^2/Pa s)] and tensile modulus (0.02–3.5 MPa) similar to articular cartilage. Steinmetz et al. (2015) also developed a multi-layer PEG hydrogel resembling the zonal organisation of the osteochondral tissue. Although the compressive modulus did not match that of the native cartilage and bone when subject to mechanical loading, the strain distribution pattern was similar to osteochondral tissue with higher strain in the cartilage-like layer. When 7.5% apparent strains were applied to the hydrogel the local strains in the cartilage-like layer and in the bone-like layer were 15 and 2% respectively.

PGA exerts high tensile modulus (7 GPa) but due to its relatively hydrophilic nature and instability in aqueous solution loses its mechanical integrity between two and four weeks *in vivo* (Gunatillake and Adhikari, 2003; Gorth and Webster, 2011; Woodard and Grunlan, 2018). PLA exists in several isoforms and the presence of one extra methyl group makes it more hydrophobic compared to PGA, leading to a slower hydrolysis rate. PLA possesses a high tensile modulus (3 GPa) and strength (50–70 MPa) (Gorth and Webster, 2011; Samavedi et al., 2013). PLGA can be synthesised using a different ratio of PGA and PLA that allows modulation of both Young's modulus and the degradation rate which can be, from a few weeks up to months, resulting in sustained mechanical integrity after implantation (Félix Lanao et al., 2013; Samavedi et al., 2013; Gentile et al., 2014). PVA is a biodegradable and biocompatible polymer, from which hydrogels can be prepared at different polymer concentrations to obtain tensile strengths in the cartilage range of 1–17 MPa as well as an elastic modulus up to 0.85 MPa (Karimi and Navidbakhsh, 2014; Lin et al., 2017; Teixeira et al., 2019). PVA hydrogels exhibit limited swelling when tested at osmotic pressures similar to that of articular cartilage, which is desirable for soft tissue engineering to preserve the initial size and shape and to prevent interfacial debonding (Holloway et al., 2011; Oliveira et al., 2019). A non-biodegradable PVA based hydrogel (Cartiva®) exerts biphasic behaviour similar to normal articular cartilage under compression and it is currently under clinical trial for first metatarsophalangeal joint hemiarthroplasty (Brandao et al., 2020).

PCL is an FDA approved biodegradable aliphatic linear polyester and it is one of the most investigated polymers for tissue engineering applications due to its adjustable mechanical strength. PCL can be used to produce porous scaffolds as well as electrospun nanofibers (Zhu et al., 2014; Panadero et al., 2016). Visser et al. (2015) incorporated PCL microfibers into GelMA obtaining reinforced hydrogels with mechanical properties similar to articular cartilage. Castilho et al. (2019) also used PCL to successfully develop a bi-layered construct that mimics the zonal structure as well as the functional properties of native cartilage. This construct incorporated a thin superficial tangential layer, mimicking the collagen organisation in the superficial layer of the cartilage, that improved the load-bearing properties of the micro-fibre reinforced hydrogel with a peak modulus of 473 kPa under unconfined compression as well as

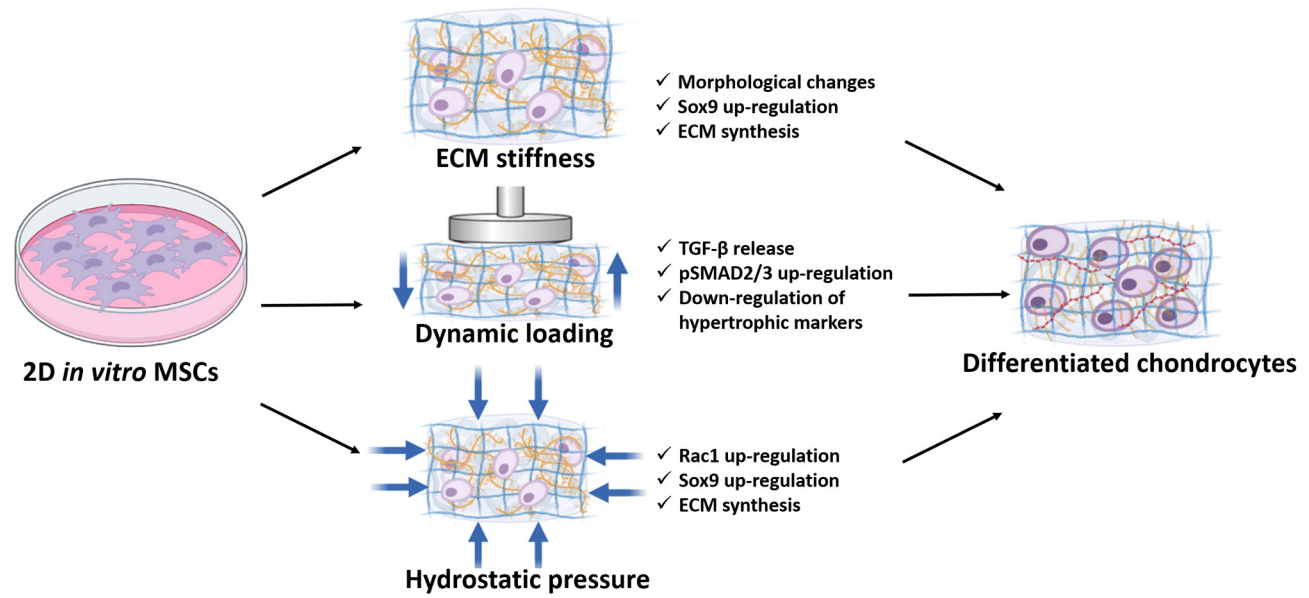

FIGURE 3 | Schematic representation of the mechanical cues affecting stem cell differentiation down the chondrogenic lineage. MSCs are mechanosensitive in response to ECM stiffness, dynamic loading, and hydrostatic pressures which activates various signalling pathways necessary to drive differentiation down the chondrocytic lineage.

exhibiting relaxation rates similar to those for native cartilage (Castilho et al., 2019). Controlling the mechanical properties of scaffolds for osteochondral TE is essential, not only to maintain structural integrity and withstand high mechanical loading *in vivo*, but also to provide environmental mechanical cues to selectively guide stem cell differentiation into the appropriate osteochondral phenotypes.

MECHANICAL CUES AFFECTING STEM CELL DIFFERENTIATION

MSC commitment to the chondrocytic lineage is governed by TGF-β and WNT/ß-catenin signalling (Usami et al., 2016). In particular, the activation of TGF-β/SMAD2/3 pathways is essential for the intracellular phosphorylation of Smad2 and Smad3, which then translocate to the nucleus to activate and stabilise the transcription factor Sex determining region Y (SRY) Box 9 (SOX9), that is the master regulator of chondrogenesis (Furumatsu et al., 2009; Coricor and Serra, 2016; Pfeifer et al., 2019). SOX9, along with SOX5 and SOX6 expression is required during embryonic development as well as in post-natal maintenance of articular cartilage regulating expression of ECM molecules, such as collagen (mainly types II, IX, XI) and proteoglycans (aggrecan, decorin).

To differentiate MSCs into chondrocytes the use of growth factors, such as TGF-β, is usually required. However, its use in the clinic is limited as it leads to the expression of hypertrophic markers such as Col X, MMP13 and alkaline phosphatase (ALP), which will eventually lead to cartilage mineralization. There is increasing evidence that environmental (such as low oxygen tension) and mechanical cues control stem cell fate. In particular (as described in **Figure 3**), MSCs are highly mechanosensitive and respond to both passive stimuli such as stiffness, and dynamic stimulation such as mechanical loading and hydrostatic pressure that signals through integrins and focal adhesion (FA) protein complex, transducing physical signals into biochemical signals.

Regulation of MSCs Differentiation by ECM Stiffness

In vivo each tissue is characterised by a specific stiffness, which regulates tissue development and homeostasis by affecting cell migration, proliferation, morphology, cell phenotype and ECM protein production (Ehrbar et al., 2011; Handorf et al., 2015; Hwang et al., 2015; Du et al., 2016; Sun et al., 2017; Xia et al., 2017; Abbas et al., 2019; Chu et al., 2019; d'Angelo et al., 2019; Saidova and Vorobjev, 2020). Engler et al. (2006) originally explored the effect of stiffness on MSCs using polyacrylamide hydrogels mimicking the native elasticity of brain, muscle and osteoid. This work demonstrated that stiffness not only affects MSC morphology showing that the expression of the neurogenic marker ß tubulin 3 was enhanced on soft substrates and Runx2 on stiff substrates. Interestingly, this work showed that growth factors tend to be less selective compared to matrix stiffness in driving lineage specification. MSCs pre-conditioned on a matrix with a specific stiffness for 3 weeks cannot be reprogrammed,

TABLE 3 | Summary of the effect of mechanical cues on MSCs differentiation.

EFFECT OF MECHANICAL CUES ON MSCs				
Substrate stiffness	**Soft substrates (1–30 kPa)**	**Intermediate substrate (0.1–5MPa)**	**Stiff substrates (5–300 MPa)**	**References**
	MSCs on soft substrates exhibit a rounded chondrocyte-like morphology Higher expression levels of chondrogenic markers Unable to withstand mechanical loads	Mechanically competent Stiffness in the range of native cartilage MSCs found to express high level of SOX9 and Col II on substrates stiffness of 0.8MPa and 4.7MPa	Highly organised cytoskeleton Spindle-shape morphology	Engler et al., 2006; Park et al., 2011; Wang et al., 2016; Olivares-Navarrete et al., 2017
Dynamic loading	**0.15–1.5% compressive strain 1Hz**	**10% compressive strain 1 Hz from day 0**	**10% compressive strain 1 Hz after 1 week of pre-culture**	
	Dynamic loading, delayed osteogenesis. Mineral deposits was diffuse in the unloaded condition while under dynamic loading was concentrated and spatially restricted to the central region	Compression from day 0 has negative effects on MSC chondrogenesis	Dynamic culture increase synthesis of GAG aggrecan, Col II and increase expression SOX9 Upregulation of phosphorylated-SMAD2/3 MSCs under static culture MSCs exhibited higher of hypertrophic markers	Thorpe et al., 2010; Zhang et al., 2015; Sawatjui et al., 2018; Aziz et al., 2019; Cao et al., 2019
Hydrostatic pressure	**Low HP stimulation 100–300 kPa**	**Physiological HP stimulation in the cartilage layer 1–10 MPa**	**High HP 25 MPa**	
	IHP upregulate osteogenic markers Increase expression of Runx2, ALP and osteopontin	HP applied continuously it negatively affects SOX9, Coll II and aggrecan gene expression IHP positively affects SOX9 and Col II expression even without external growth factors and enhances cartilaginous matrix deposition	Inhibited aggrecan and Col II Pro-osteoarthritic effects	Correia et al., 2012; Li et al., 2016; Montagne et al., 2017; Stavenschi et al., 2018; Stavenschi and Hoey, 2019

suggesting that modulation of ECM modulus could be a powerful tool to drive stem cell differentiation. When cultured on stiff substrates, MSCs develop a highly organised cytoskeleton showing a spindle-shape morphology (**Table 3**). Conversely, MSCs on soft substrates exhibit a rounded chondrocyte-like morphology and express higher levels of chondrogenic markers. Park et al. (2011) compared collagen type II and GAG synthesis on a soft collagen hydrogel, on plastic coated with a thin layer of collagen and on polyacrylamide hydrogels with different stiffnesses (1 and 15 kPa). They showed an increase in expression of chondrogenic markers both on the soft collagen hydrogel and on the 1 kPa substrate. The effect of substrate stiffness together with biochemical cues was investigated by Wang et al. (2016). They showed that HA enhanced MSC chondrogenesis, evidenced by upregulated of aggrecan and Col II expression and this effect was more distinct when cells were grown in soft hydrogels (3 kPa), while this effect was reversed in the stiff hydrogel (90 kPa). It is important to note that cartilage stiffness varies between 0.1 and 6.2 MPa, and soft hydrogels will fail to maintain their structural integrity after implantation (Wang et al., 2016; Zheng et al., 2019; Guimarães et al., 2020). Olivares-Navarrete et al. (2017) compared both cytoskeletal organisation and gene expression of MSCs and auricular chondrocytes grown on methyl acrylate/methyl methacrylate (MA/MMA) polymer surfaces with elastic moduli ranging from 0.8 to 310 MPa mimicking the stiffness of articular cartilage and cortical bone. MSCs appeared to be elongated on the less stiff surfaces with a higher number of adhesion plaques on the 4.7 MPa substrate. After 7 days without exogenous stimuli by cytokines or other factors associated with cartilage differentiation, the expression of SOX9, Col II, aggrecan and cartilage oligomeric matrix protein (COMP) in MSCs showed an increasing trend with decreasing stiffness. This work showed that mimicking the native elasticity of cartilage enhances chondrogenic phenotype without exogenous stimuli. Nevertheless, it is also important to consider that osteochondral tissue exhibits different stiffness among the different layers, and an implant displaying a layering or gradient approach with varying stiffness, might be more effective in reproducing the native architecture of the tissue as well as selectively promoting ECM synthesis.

Role of Dynamic Loading in MSCs

During ambulation mechanical load plays an important role in maintenance and degeneration of articular cartilage affecting gene expression of Col II, aggrecan, and degenerative enzymes (MMPs). Interestingly dynamic stimulation also affects MSC differentiation and the quality of ECM synthesised. A study from Thorpe et al. (2008) revealed a negative effect of long term dynamic compression on MSCs cultured in agarose hydrogels. This study reported that unconfined compression at 10% strain and 0.5 Hz for 1 h/day significantly reduced GAG production and Col II synthesis compared to static culture. Interestingly, the application of dynamic compression from day 0 inhibits chondrogenesis even in the presence of TGF-β3 (Thorpe et al., 2010). In contrast, the inhibition of chondrogenesis in response to dynamic compression was not observed if the MSCs were

first allowed to undergo chondrogenesis. Consistent with these results, Sawatjui et al. (2018) studied the effect of dynamic compression of both MSCs and chondrocytes derived from osteoarthritic joints seeded on silk fibroin scaffold, pre-cultured for 1 week, and subsequently subjected to compression with 10% dynamic strain at 1 Hz, 1 h/day for 2 weeks. This study showed that dynamic compression significantly enhanced the synthesis of Col II and aggrecan along with an increase of compressive modulus. Cao et al. (2019) seeded rabbit derived MSCs into collagen scaffolds under 10% compressive sinusoidal strain at 1 Hz frequency, for 2 h/day for 21 days. Starting from the second week of culture, the morphology of MSCs in the dynamic culture group exhibited a rounded chondrocyte-like morphology, whereas cells remained spindle shaped in static culture. Dynamic culture also promoted GAG synthesis as well as aggrecan, Col II and SOX9 expression compared to the static culture. Zhang et al. (2015) demonstrated that delayed dynamic compression positively affected MSC chondrogenesis through phosphorylated-SMAD2/3 enhancing matrix deposition and suppressing hypertrophy. Further MSCs under free swelling condition exhibited higher expression of ERK (involved in chondrocyte hypertrophy) along with upregulation of MMP13, Runx2, and Col X. In addition, Gardner et al. (2017) demonstrated that multiaxial loads on MSC led to endogenous production and secretion of TGF-β1 as well as the activation of the secreted latent TGF-β1. Taken together these data suggest that dynamic load positively affects MSC chondrogenesis, however, MSCs should first be differentiated before applying loads. Consequently *in vitro* differentiation of stem cells prior to implantation could be critical for osteochondral tissue engineering.

Hydrostatic Pressure and MSCs Differentiation

Cartilage ECM is characterised by a high water content and low permeability, and as a consequence when a load is applied the resistance of fluid flow generates hydrostatic pressure (HP). *In vivo* HP varies between 2 and 10 MPa with peaks of 18 MPa during intense activities such as jumping or running (Elder and Athanasiou, 2009; Correia et al., 2012). Several studies have demonstrated that the application of HP on MSCs might have a pro-chondrogenic effect. Angele et al. (2003) examined the effects of cyclic hydrostatic pressure on MSCs aggregates showing a significant increase in GAG and collagen content at days 14 and 28 compared to the unloaded control. Furthermore, Miyanishi et al. (2006a) studied MSCs in pellet culture exposed to intermittent hydrostatic pressure (IHP) and demonstrated an increase in expression of SOX9, Col II, and aggrecan with or without the addition of TGF-β3. In a second study the authors also demonstrated that the magnitude of loading modulated chondrogenic gene expression and cartilage matrix protein deposition in MSCs pellets in the presence of TGF-β3 suggesting that the magnitude of the load could enhance MSCs chondrogenesis (Miyanishi et al., 2006b). In fact, physiological levels of HP (5MPa) significantly enhance cartilaginous matrix deposition (Correia et al., 2012; Li et al., 2016). Conversely, high HP (25 MPa up to 24 h) on the ATDC5 cell line markedly affecting the expression of matrix remodelling related genes, apoptosis-related genes and strongly inhibited aggrecan and Col II, suggesting that excessive loads induce pro-osteoarthritic effects (Montagne et al., 2017). Interestingly the use of low HP, in the range of 100–300 kPa, has been demonstrated to direct MSCs differentiation into the osteogenic lineage upregulating the expression of Runx2, ALP and osteopontin (Stavenschi et al., 2018; Stavenschi and Hoey, 2019). Not only the magnitude of load, but also the length of the stimulation affects matrix deposition. In fact, it has been shown that when the load is applied continuously, it negatively affects SOX9, Col II and aggrecan gene expression (Correia et al., 2012; Li et al., 2016).

One of the major limitations of cartilage tissue engineering is the formation of fibrocartilage, which has inferior mechanical properties compared to articular cartilage. HP appears to affect hypertrophic genes, increasing Col I, Col X and MMP13 (Ogawa et al., 2009, 2015; Li et al., 2016). Conversely, other studies revealed decreasing levels of Col I and Col X under IHP (Vinardell et al., 2012; Saha et al., 2017; Rieder et al., 2018). Freeman et al. (2017) demonstrated that HP without any external growth factors resulted in enhanced chondrogenesis along with reduction in hypertrophic markers. Additionally, when MSCs were stimulated with HP alone and subsequently induced to undergo osteogenic differentiation without any external mechanical stimulation, the production of hypertrophic markers was reduced compared to those exposed to chondrogenic growth factors alone. These studies suggested that the application of intermittent hydrostatic pressure could potentially lead to a stable differentiation of MSCs into the chondrogenic lineage without the use of growth factors. However, it is important to note that the intensity and the frequency of HP applied differ among studies, suggesting that standardisation is required to obtain consistent results.

TESTING OSTEOCHONDRAL GRAFT MATERIALS

The success of osteochondral grafts depends on the restoration of surfaces representative of native articular cartilage to provide smooth joint movement during joint articulation. Implanted grafts also need to be structurally stable to withstand physiological loading conditions of up to 4–5 times body weight during walking (Morrison, 1970; Bellucci and Seedhom, 2001) with peak stresses in the knee ranging from 2 to 10 MPa and at a loading frequency of approximately 1 Hz (Brand, 2005; Sadeghi et al., 2015). Osteochondral defects cause high contact stresses at the rim, that vary depending on the size of the defect causing uneven strain distribution (Brown et al., 1991; Kock et al., 2008). These abnormal contact stresses and strains at the defect perimeter cause damage and chondrocyte death that could impair integration and healing of the graft, leading to reduced functionality of the joint, or cartilage damage (D'Lima et al., 2001; Wu et al., 2002). However, contact stresses can be restored to pre-operative levels, resembling intact cartilage depending on appropriate fitting, alignment, length and surface

of the graft (D'Lima et al., 2001; Koh et al., 2004; Kock et al., 2006, 2008). One of the major issues is that post-implantation osteochondral implants will be subject to continual cyclic loads, encompassing a range of shear and tensile forces which will affect the biological response of the graft and test the integration with the surrounding native cartilage. However, specific test methods to demonstrate the performance of these grafts have not yet been defined.

Standardisation

Osteochondral grafts are classed by the International Standard Organisation (ISO) as implantable medical devices that as defined in ISO 13485, 2016, are implanted into the human body via surgical intervention and are intended to remain in place after the procedure. ISO 14630:2012 specifies the general requirements for non-active surgical implants, whereas ISO 21536:2007 is the level 3 standard referring more specifically to knee joint replacement implants. These standards include performance, design, materials, evaluation and sterilisation and the tests needed to demonstrate compliance with these regulations. More specific standards relating to tissue engineered cartilage constructs include the quantification of sulfated glycosaminoglycans (sGAG) (ISO 13019: 2018), and the evaluation of tissue morphology including collagen fibre orientation and anisotropy *in vivo* (ISO/TR 16379:2014) have also been defined. Despite these biological and clinical evaluation there are no specific requirements for mechanical testing, and there is uncertainty as to whether articular cartilage implants are classified as partial joint replacement implants and should therefore be subject to mechanical characterisation (Marchiori et al., 2019).

In contrast, the FDA provides more specific mechanical testing criteria for the use of tissue engineered cartilage constructs, which highlights inconsistencies with regard to global standardisation. The FDA guidance document for products intended to repair or replace knee cartilage includes specifications for *in vivo* animal studies (that will be discussed later in this review) and various *in vitro* mechanical tests. It states that "mechanical testing should address the following: the ability of the implant to withstand expected *in vivo* static and dynamic loading (i.e., compression, shear, and tension); analysis of fixation method (i.e., strength of integration between the product and surrounding native tissue); and propensity to generate wear debris." It is also recommended that static mechanical behaviour such as the maximum recoverable compressive strain, the aggregate modulus (HA), the shear modulus (G), and permeability (κ) as well as the dynamic complex shear modulus are included. Degradable scaffolds should also include assessment of failure properties over time and some examples of confined or unconfined compression and indentation are suggested for analysing the mechanical properties of implants.

In vitro Compressive Testing (Confined, Unconfined and Indentation)

The most frequent *in vitro* test are usually biological assays to evaluate the biocompatibility (ISO 1099), cytotoxicity (ISO 10993-5), gene expression and matrix deposition (ISO 13019 quantification of sulfated glycosaminoglycans for evaluation of chondrogenesis) (Keong and Halim, 2009; Li W. et al., 2015). However, mechanical evaluation of osteochondral scaffolds are essential to ensure graft stability in the initial period following implantation (Bowland et al., 2015). As reviewed by Patel et al. (2019), compression testing is the most common test performed both on cartilage and tissue engineered construct. Compression test can be performed using unconfined and confined compression and indentation (**Figure 4**). For unconfined compression testing, the sample is placed between two impermeable steel plates allowing the Young's modulus to be measured directly from the linear portion of the stress-strain curve produced (Korhonen et al., 2002; Griffin et al., 2016). For confined compression the sample is either tested using a porous indenter or placed in a porous chamber with an impermeable indenter to ensure fluid flow. Confined compression allows the measurement of both the aggregate modulus (determined when fluid flow stops) of the specimen as well as the permeability (Boschetti et al., 2004). While unconfined and confined compression require the cartilage sample or the scaffold to be tested within a chamber, indentation allows the test to be performed on a whole osteochondral specimen (Griffin et al., 2016; Tozzi et al., 2020). Compression tests can be performed by applying a strain at a constant rate (ramp), by applying a strain to a target level and holding the strain constant (stress-relaxation) or applying a cyclic strain (dynamic) (Scholten et al., 2011; Vikingsson et al., 2015; Coluccino et al., 2016; Kundanati et al., 2016). Compression tests can be also load-controlled, applying a rapid load that is then kept constant, measuring sample strain over time (Oyen, 2014; Patel et al., 2019). Both the FDA and International Cartilage Repair Society (ICRS) recommend both static and dynamic compression tests to assess the mechanical behaviour of the osteochondral graft. However, specific guidelines on how to perform each test have not been agreed, which leads to inconsistent or non-physiologically relevant data. Cartilage and osteochondral grafts should be tested under the same conditions, as the strain rate influences the stress-strain curves, implying that the higher the strain rate the higher the modulus will be. As reviewed by Patel et al. (2019), 48% of the studies that analysed cartilage repair constructs under ramp mechanical testing, were tested to more than 20% strain, more than double the compressive strain that articular cartilage was tested to. Considering that the physiological average strain is 10% the data produced using higher strain might not be reliable (Chan et al., 2016).

In addition to the standard mechanical tests previously mentioned, implants need to be tested after periods *in vivo* (for dynamic and static loading) and under loading conditions of compression, tension, and shear. Analysis of fixation within the defect is also required (e.g., mechanical push-out tests to assess integration) and assessment of the bioreactivity of any device-generated wear debris.

In vivo Animal Models

In vivo animal models are crucial preliminary studies to assess the safety and efficacy of newly developed cartilage TE implants. However, currently there are no exact guidelines

TEST	CONFIGURATION	RESULT	
Confined compression	The sample is either tested using a porous indenter or placed in a porous chamber with an impermeable indenter to ensure fluid flow	Aggregate modulus and permeability	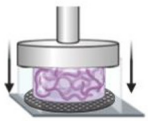
Unconfined compression	The sample is placed between two impermeable steel plates allowing to measure Young's modulus directly from the linear portion of the stress-strain curve	Elastic modulus (Young's modulus)	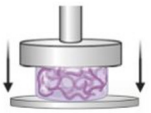
Indentation	The test can be performed in situ allowing to test the whole osteochondral plug	Elastic modulus (Young's modulus)	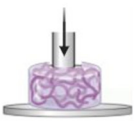

FIGURE 4 | Standard mechanical tests for assessing osteochondral grafts. Confined compression tests using either an impermeable chamber and porous indenter; or porous chamber with an impermeable indenter, are useful for defining the aggregate modulus. Unconfined compression tests and indentation tests can determine the elastic modulus (Young's modulus).

for the comparison of animal models, assessment of defect size/location and description of appropriate mechanical tests for the assessment of implantable devices such as osteochondral grafts to repair and regenerate articular cartilage. The FDA recommends using combined animal studies with appropriate mechanical testing to assess biological response, durability (using large animal models) and toxicology (U. S. Food Drug Administration, 2011). In addition, dose response (of bioactive scaffolds), lesion size and location, appropriate endpoints, and continual arthroscopic/MRI evaluation should also be taken into consideration (U. S. Food Drug Administration, 2011). Nevertheless, despite these recommendations there are no clearly defined protocols, test criteria, or test parameters for mechanical testing. It is also acknowledged that there is no optimal animal model for cartilage repair, which may also lead to variability between studies.

Small animal models (mouse, rat and rabbit) are mainly used for "proof of concept" studies as a translational step between *in vitro* tests and larger animal/human studies. Rabbit models have spontaneous intrinsic healing capabilities of cartilage defects that must be taken into consideration, therefore, they usually require additional validation in other animal models (Shapiro et al., 1993). Other variables to consider when choosing the most appropriate animal model are thickness of cartilage and joint suitability, skeletal/ cartilage maturity, defect type, size and location of the defect, availability and post-operative care (Hurtig et al., 2011). Canine models, like humans, often suffer from diseases such as OA and OCD which makes them useful for assessing cartilage regeneration in pathologic conditions (Chu et al., 2010). Large animal models (goat, sheep, pig and horse) more closely reflect intended clinical use for assessing toxicity, integrity and inflammatory responses for both small and larger defects in load bearing environments. Since cartilage thickness in equine stifle joints (1.5–2.0 mm) is the most similar to human cartilage thickness (2.2–2.5 mm) the horse is the closest approximation for creating both partial and full thickness defects for preclinical cartilage repair studies (Frisbie et al., 2006; McIlwraith et al., 2011). Nevertheless, in most animal models the loading, thickness and geometry of the joint surface is very different to that of humans.

Mechanical Push-Out Tests for Assessing Integration

Mechanical push-out tests are useful pre-clinical studies to evaluate the maximum forces needed for graft failure and for assessing integrative repair with host cartilage over time (Theodoropoulos et al., 2011). A biopsy punch is normally used to create a cylindrical defect filled with the TE scaffold or osteochondral graft to be tested. After a culture and/or treatment period to allow a certain amount of integration with the host tissue, the inner core is pushed out of the outer ring using a mechanical push-out rod. The calculated amount of force needed for displacement (or failure of the graft) allows an assessment of integrative strength at the interface to be assessed. A recent study

by Bowland et al. (2020) performed a series of push-in and push-out tests to assess the mechanical stability of bovine and porcine osteochondral grafts. Interestingly, the results showed that the harvesting method (using a trephine drill or chisel) showed no significant differences in graft stability (Bowland et al., 2020). However, preparation of the recipient site, the depth of insertion and dilation had more of an effect, showing that grafts with equal lengths to the site of insertion were more stable, and that dilation of grafts reduces the stability particularly in more skeletally immature tissue (Bowland et al., 2020). This research also highlights the importance of the underlying subchondral bone and the interrelationship between these tissues on regeneration and durability of focal defects consistent with other studies (Chan et al., 2012).

Whole Joint Simulation Models to Mimic Joint Articulation

In contrast, *in vitro* whole joint simulations can be used to assess the tribological performance of osteochondral grafts, taking into consideration the interactions and biomechanical properties of the joint as a whole under physiological loading conditions. These types of test are relevant for comparing the efficacy of osteochondral grafts to other surgical interventions such as scaffolds and cell-based approaches (Bowland et al., 2018b). Bowland et al. (2018a) used an adapted method from Liu et al. (2015) using a whole joint simulator with six degrees of freedom and five controlled axes of motion to mechanically test grafts. The axial load was force controlled, tibial rotation (1.6–1.6°) and flexion/extension (0–21°) were displacement controlled at a frequency of 1 Hz. Anterior-posterior displacement was constrained using springs that generated rolling and sliding motions of the femur against the tibia, and mimicked ligament function. The medial-lateral axis was fully constrained and abduction/adduction was under passive motion. The main finding of this study was that allograft plugs fitted flush with the defect site to restore the articular surface caused the least wear and damage on the opposing joint surface after applying a complex range of motions. Similarly, Nebelung et al. (2017) combined a whole-knee joint loading device with MRI imaging to non-invasively assess the structural and functional responses of human articular osteochondral grafts in defect sites during *in situ* compressive loading. Whole joint simulation models highlight the importance of restoring the congruence of articular surfaces during an experimental setting that mimics more closely the physiological environment of joint articulation. However, the use of cadaveric tissue with diluted serum replicating the joint's synovial fluid is a useful approach but it fails to replicate large numbers of walking cycles due to limitations regarding the continual sterility and viability of the tissue.

Shear Stress to Assess Tribology

Chondrocytes in the superficial layer produce lubricin that maintains low coefficients of friction of joints. Maintaining a low frictional interface is essential to prevent mechanical wear and erosion of the articular surface. The application of frictional shear stress has been shown to cause damage such as cracking and peeling in cartilage TE constructs, which are not seen in native cartilage controls (Whitney et al., 2017). Therefore, assessing the tribology of osteochondral grafts is essential to ensure adequate integration and longevity. To measure the frictional coefficient, three different configurations of tribometer can be used: pin-on-disc, pin-on-plate, or rolling-ball-on-disc. In the first two settings a pin is glued to the sample and a disc or a plate are in motion, while for the rolling-ball-on-disc the disc and the ball can be moved independently. In each configuration a normal force is applied and a sensor measures the frictional force, the frictional coefficient can be derived by dividing the frictional force for the normal force applied. Different types of lubricant can be used (i.e., PBS or foetal bovine serum) which combined with the different testing configurations often lead to variable results, highlighting the need of standardisation procedure to test both cartilage samples and osteochondral TE constructs. Other mechanical tests such as frictional shear stress testing can assess the tribology, pressure distribution and the response to damage of osteochondral grafts and TE constructs in whole joint models under a complex range of sliding and torsional motions (Walter et al., 2013; Bobrowitsch et al., 2014).

CONCLUSIONS

Despite tremendous advances in the field of tissue engineering, an optimal biomaterial system for osteochondral defects that is able to direct stem cell differentiation into chondrocytes for the cartilage and osteoblast for bone without the use of exogenous stimuli is elusive. Material selection is essential for creating a graft able to withstand the multiple forces that cartilage is subject to. Synthetic materials not only provide high tensile stress and compressive modulus, but they are easily modified, facilitating the creation of layered scaffolds which is a requirement for osteochondral grafts. However, the lack of cellular binding sites require them to be combined with natural materials, which are highly biocompatible and can provide biochemical cues for stem cell differentiation. The natural architecture of cartilage and the impermeable subchondral plate enhances the development of hydrostatic stress in the cartilage which promotes and maintains the chondrocytic phenotype, however few osteochondral implant designs replicate this subchondral barrier.

Although suitable mechanical properties are essential for ensuring graft stability *in vivo*, the optimal range of stiffnesses is yet to be determined. Conflicting results have been reported, as to whether high stiffness could enhance chondrogenic differentiation of MSCs or upregulate hypertrophic markers. The use of dynamic stimulation, such as hydrostatic pressure or dynamic loading, could promote a stable differentiation of MSCs into chondrocytes and enhance matrix deposition, thus preventing the use of TGF-β which lead to the formation of hypertrophic cartilage.

Mechanical testing of TE constructs *in vitro* are essential to ensure graft stability *in vivo,* however, the lack of standardised procedures questions the reliability of the published data in providing an understanding of the long term endurance and

suitability of osteochondral grafts. In addition, only a small fraction of studies on cartilage constructs tests all of the mechanical properties requested from the FDA or the ICRS and this might, in part, explain why many scaffolds fail when tested *in vivo*.

AUTHOR CONTRIBUTIONS

SD and TR completed a literature search, wrote the manuscript and critically revised the manuscript. MR, GB, and GT contributed ideas, content to the manuscript, and critically revised the manuscript. All authors contributed to the article and approved the submitted version.

FUNDING

This work was supported by the Faculty of Science and Health of the University of Portsmouth.

ACKNOWLEDGMENTS

All figures were created with Biorender.com.

REFERENCES

Abbas, Y., Carnicer-Lombarte, A., Gardner, L., Thomas, J., Brosens, J. J., Moffett, A., et al. (2019). Tissue stiffness at the human maternal-fetal interface. *Human Reproduct.* 34, 1999–2008. doi: 10.1093/humrep/dez139

Andriolo, L., Reale, D., Di Martino, A., De Filippis, R., Sessa, A., Zaffagnini, S., et al. (2020). Long-term results of arthroscopic matrix-assisted autologous chondrocyte transplantation: a prospective follow-up at 15 years. *Am. J. Sports Med.* 48, 2994–3001. doi: 10.1177/0363546520949849

Angele, P., Yoo, J. U., Smith, C., Mansour, J., Jepsen, K. J., Nerlich, M., et al. (2003). Cyclic hydrostatic pressure enhances the chondrogenic phenotype of human mesenchymal progenitor cells differentiated *in vitro*. *J. Orthopaed. Res.* 21, 451–457. doi: 10.1016/S0736-0266(02)00230-9

Angelozzi, M., Penolazzi, L., Mazzitelli, S., Lambertini, E., Lolli, A., Piva, R., et al. (2017). Dedifferentiated chondrocytes in composite microfibers as tool for cartilage repair. *Front. Bioeng. Biotechnol.* 5:35. doi: 10.3389/fbioe.2017.00035

Arden, N., and Nevitt, M. C. (2006). Osteoarthritis: epidemiology. *Best Pract. Res. Clin. Rheumatol.* 20, 3–25. doi: 10.1016/j.berh.2005.09.007

Assenmacher, A. T., Pareek, A., Reardon, P. J., Macalena, J. A., Stuart, M. J., and Krych, A. J. (2016). Long-term outcomes after osteochondral allograft: a systematic review at long-term follow-up of 12.3 years. *Arthroscopy* 32, 2160–2168. doi: 10.1016/j.arthro.2016.04.020

Ateshian, G. A., Chahine, N. O., Basalo, I. M., and Hung, C. T. (2004). The correspondence between equilibrium biphasic and triphasic material properties in mixture models of articular cartilage. *J.Biomechan.* 37, 391–400. doi: 10.1016/S0021-9290(03)00252-5

Aurich, M., Hofmann, G. O., Best, N., and Rolauffs, B. (2018). Induced redifferentiation of human chondrocytes from articular cartilage lesion in alginate bead culture after monolayer dedifferentiation: an alternative cell source for cell-based therapies? *Tissue Eng.* 24, 275–286. doi: 10.1089/ten.tea.2016.0505

Aziz, A. H., Eckstein, K., Ferguson, V. L., and Bryant, S. J. (2019). The effects of dynamic compressive loading on human mesenchymal stem cell osteogenesis in the stiff layer of a bilayer hydrogel. *J. Tissue Eng. Regenerat. Med.* 13, 946–959. doi: 10.1002/term.2827

Baba, R., Onodera, T., Matsuoka, M., Hontani, K., Joutoku, Z., Matsubara, S., et al. (2018). Bone marrow stimulation technique augmented by an ultrapurified alginate gel enhances cartilage repair in a canine model. *Am. J. Sports Med.* 46, 1970–1979. doi: 10.1177/0363546518770436

Baker, S. C., Rohman, G., Southgate, J., and Cameron, N. R. (2009). The relationship between the mechanical properties and cell behaviour on PLGA and PCL scaffolds for bladder tissue engineering. *Biomaterials* 30, 1321–1328. doi: 10.1016/j.biomaterials.2008.11.033

Barzideh, Z., Latiff, A. A., Gan, C. Y., Abedin, M. Z., and Alias, A. K. (2014). ACE inhibitory and antioxidant activities of collagen hydrolysates from the ribbon jellyfish (*Chrysaora* sp.). *Food Tech. Biotechnol.* 52, 495–504. doi: 10.17113/ftb.52.04.14.3641

Baumann, C. A., Hinckel, B. B., Bozynski, C. C., and Farr, J. (2019). "Articular cartilage: structure and restoration," in *Joint Preservation of the Knee*, eds A. Yanke and B. Cole (Cham: Springer). doi: 10.1007/978-3-030-01491-9_1

Bayliss, L. E., Culliford, D., Monk, A. P., Glyn-Jones, S., Prieto-Alhambra, D., Judge, A., et al. (2017). The effect of patient age at intervention on risk of implant revision after total replacement of the hip or knee: a population-based cohort study. *Lancet* 389, 1424–1430. doi: 10.1016/S0140-6736(17)30059-4

Beckwée, D., Vaes, P., Shahabpour, M., Muyldermans, R., Rommers, N., and Bautmans, I. (2015). The influence of joint loading on bone marrow lesions in the knee: a systematic review with meta-analysis. *Am. J. Sports Med.* 43, 3093–3107. doi: 10.1177/0363546514565092

Behrens, P., Bitter, T., Kurz, B., and Russlies, M. (2006). Matrix-associated autologous chondrocyte transplantation/implantation (MACT/MACI)-5-year follow-up. *Knee* 13, 194–202. doi: 10.1016/j.knee.2006.02.012

Bellucci, G., and Seedhom, B. B. (2001). Mechanical behaviour of articular cartilage under tensile cyclic load, *Rheumatology* 40, 1337–1345. doi: 10.1093/rheumatology/40.12.1337

Bevill, S. L., Briant, P. L., Levenston, M. E., and Andriacchi, T. P. (2009). Central and peripheral region tibial plateau chondrocytes respond differently to in vitro dynamic compression. *Osteoarthrit. Cartilage* 17, 980–987. doi: 10.1016/j.joca.2008.12.005

Bhatia, D., Bejarano, T., and Novo, M. (2013). Current interventions in the management of knee osteoarthritis. *J. Pharmacy Bioallied Sci.* 5:30. doi: 10.4103/0975-7406.106561

Bian, L., Zhai, D. Y., Tous, E., Rai, R., Mauck, R. L., and Burdick, J. A. (2011). Enhanced MSC chondrogenesis following delivery of TGF-β3 from alginate microspheres within hyaluronic acid hydrogels *in vitro* and *in vivo*. *Biomaterials* 32, 6425–6434. doi: 10.1016/j.biomaterials.2011.05.033

Bobrowitsch, E., Lorenz, A., Jörg, J., Leichtle, U. G., Wülker, N., and Walter, C. (2014). Changes in dissipated energy and contact pressure after osteochondral graft transplantation. *Med. Eng. Phys.* 36. 1156–1161. doi: 10.1016/j.medengphy.2014.06.015

Bonani, W., Singhatanadgige, W., Pornanong, A., and Motta, A. (2018). "Natural Origin Materials for Osteochondral Tissue Engineering," in *Osteochondral Tissue Engineering. Advances in Experimental Medicine and Biology*, Vol. 1058. eds J. Oliveira, S. Pina, R. Reis, J. San Roman (Cham: Springer). doi: 10.1007/978-3-319-76711-6_1

Boschetti, F., Pennati, G., Gervaso, F., Peretti, G. M., and Dubini, G. (2004). Biomechanical properties of human articular cartilage under compressive loads. *Biorheology* 41, 159–166.

Boushell, M. K., Hung, C. T., Hunziker, E. B., Strauss, E. J., and Lu, H. H. (2017). Current strategies for integrative cartilage repair. *Connect. Tissue Res.* 58, 393–406. doi: 10.1080/03008207.2016.1231180

Bowland, P., Cowie, R. M., Ingham, E., Fisher, J., and Jennings, L. M. (2020). Biomechanical assessment of the stability of osteochondral grafts implanted in porcine and bovine femoral condyles. *Proc. Inst. Mech. Eng. H.* 234, 163–170. doi: 10.1177/0954411919891673

Bowland, P., Ingham, E., Fisher, J., and Jennings, L. M. (2018a). Development of a preclinical natural porcine knee simulation model for the tribological assessment of osteochondral grafts *in vitro*. *J. Biomech.* 77, 91–98. doi: 10.1016/j.jbiomech.2018.06.014

Bowland, P., Ingham, E., Fisher, J., and Jennings, L. M. (2018b). Simple geometry tribological study of osteochondral graft implantation in the knee. *Proc. Inst. Mech. Eng. H.* 232, 249–256. doi: 10.1177/0954411917751560

Bowland, P., Ingham, E., Jennings, L., and Fisher, J. (2015). Review of the biomechanics and biotribology of osteochondral grafts used for surgical

interventions in the knee. *Proc. Insti. Mech. Eng. J. Eng. Med.* 229, 879–888. doi: 10.1177/0954411915615470

Brand, R. A. (2005). Joint contact stress: a reasonable surrogate for biological processes? *Iowa Orthopaed. J.* 25, 82–94.

Brandao, B., Aljawadi, A., Hall, A., Fox, A., and Pillai, A. (2020). Cartiva case series: the efficacy of the cartiva synthetic cartilage implant interpositional arthroplasty at one year. *J. Orthopaed.* 20, 338–341. doi: 10.1016/j.jor.2020.05.009

Briant, P., Bevill, S., and Andriacchi, T. (2015). Cartilage strain distributions are different under the same load in the central and peripheral tibial plateau regions. *J. Biomech. Eng.* 137:121009. doi: 10.1115/1.4031849

Brittberg, M., Lindahl, A., Nilsson, A., Ohlsson, C., Isaksson, O., and Peterson, L. (1994). Treatment of deep cartilage defects in the knee with autologous chondrocyte transplantation. *N. Engl. J. Med.* 331, 889–895. doi: 10.1056/NEJM199410063311401

Brown, T. D., Pope, D. F., Hale, J. E., Buckwalter, J. A., and Brand, R. A. (1991). Effects of osteochondral defect size on cartilage contact stress. *J. Orthop. Res.* 9, 559–567. doi: 10.1002/jor.1100090412

Bryant, S. J., and Anseth, K. S. (2002). Hydrogel properties influence ECM production by chondrocytes photoencapsulated in poly(ethylene glycol) hydrogels. *J. Biomed. Mater. Res.* 59, 63–72. doi: 10.1002/jbm.1217

Buckwalter, J. A., Anderson, D. D., Brown, T. D., Tochigi, Y., and Martin, J. A. (2013). The roles of mechanical stresses in the pathogenesis of osteoarthritis: implications for treatment of joint injuries. *Cartilage* 4, 286–294. doi: 10.1177/1947603513495889

Buschmann, M. D., Kim, Y. J., Wong, M., Frank, E., Hunziker, E. B., and Grodzinsky, A. J. (1999). Stimulation of aggrecan synthesis in cartilage explants by cyclic loading is localized to regions of high interstitial fluid flow. *Arch. Biochem. Biophys.* 366, 1–7. doi: 10.1006/abbi.1999.1197

Calabrese, G., Forte, S., Gulino, R., Cefalì, F., Figallo, E., Salvatorelli, L., et al. (2017a). Combination of collagen-based scaffold and bioactive factors induces adipose-derived mesenchymal stem cells chondrogenic differentiation *in vitro*. *Front. Physiol.* 8:50. doi: 10.3389/fphys.2017.00050

Calabrese, G., Gulino, R., Giuffrida, R., Forte, S., Figallo, E., Fabbi, C., et al. (2017b). *In vivo* evaluation of biocompatibility and chondrogenic potential of a cell-free collagen-based scaffold. *Front. Physiol.* 8:984. doi: 10.3389/fphys.2017.00984

Cao, W., Lin, W., Cai, H., Chen, Y., Man, Y., Liang, J., et al. (2019). Dynamic mechanical loading facilitated chondrogenic differentiation of rabbit BMSCs in collagen scaffolds. *Regenerat. Biomater.* 6, 99–106. doi: 10.1093/rb/rbz005

Caron, M. M., Emans, P. J., Coolsen, M. M., Voss, L., Surtel, D. A., Cremers, A., et al. (2012). Redifferentiation of dedifferentiated human articular chondrocytes: comparison of 2D and 3D cultures. *Osteoarthritis Cartilage* 20, 1170–1178. doi: 10.1016/j.joca.2012.06.016

Castilho, M., Hochleitner, G., Wilson, W., van Rietbergen, B., Dalton, P. D., Groll, J., et al. (2018). Mechanical behavior of a soft hydrogel reinforced with three-dimensional printed microfibre scaffolds. *Sci. Rep.* 8:1245. doi: 10.1038/s41598-018-19502-y

Castilho, M., Mouser, V., Chen, M., Malda, J., and Ito, K. (2019). Bi-layered micro-fibre reinforced hydrogels for articular cartilage regeneration. *Acta Biomaterialia* 95, 297–306. doi: 10.1016/j.actbio.2019.06.030

Catoira, M. C., Fusaro, L., Di Francesco, D., Ramella, M., and Boccafoschi, F. (2019). Overview of natural hydrogels for regenerative medicine applications. *J. Mater. Sci.* 30:115. doi: 10.1007/s10856-019-6318-7

Chan, D. D., Cai, L., Butz, K. D., Trippel, S. B., Nauman, E. A., and Neu, C. P. (2016). *In vivo* articular cartilage deformation: noninvasive quantification of intratissue strain during joint contact in the human knee. *Sci. Rep.* 6:19220. doi: 10.1038/srep19220

Chan, E. F., Liu, I. L., Semler, E. J., Aberman, H. M., Simon, T. M., Chen, A. C., et al. (2012). Association of 3-dimensional cartilage and bone structure with articular cartilage properties in and adjacent to autologous osteochondral grafts after 6 and 12 months in a Goat Model. *Cartilage* 3, 255–266. doi: 10.1177/1947603511435272

Chang, S. H., Mori, D., Kobayashi, H., Mori, Y., Nakamoto, H., Okada, K., et al. (2019). Excessive mechanical loading promotes osteoarthritis through the gremlin-1-NF-κB pathway. *Nat. Commun.* 10:1442. doi: 10.1038/s41467-019-09491-5

Chen, C. H., Kuo, C. Y., Wang, Y. J., and Chen, J. P. (2016). Dual function of glucosamine in gelatin/hyaluronic acid cryogel to modulate scaffold mechanical properties and to maintain chondrogenic phenotype for cartilage tissue engineering. *Int. J. Mol. Sci.* 17:1957. doi: 10.3390/ijms17111957

Chen, C. T., Burton-Wurster, N., Borden, C., Hueffer, K., Bloom, S. E., and Lust, G. (2001). Chondrocyte necrosis and apoptosis in impact damaged articular cartilage. *J. Orthopaed. Res.* 19, 703–711. doi: 10.1016/S0736-0266(00)00066-8

Chen, S., Zhang, Q., Nakamoto, T., Kawazoe, N., and Chen, G. (2016). Gelatin scaffolds with controlled pore structure and mechanical property for cartilage tissue engineering. *Tissue Eng.* 22, 189–198. doi: 10.1089/ten.tec.2015.0281

Chen, Z., Zhong, N., Wen, J., Jia, M., Guo, Y., Shao, Z., et al. (2018). Porous three-dimensional silk fibroin scaffolds for tracheal epithelial regeneration *in vitro* and *in vivo*. *ACS Biomater. Sci. Eng.* 4, 2977–2985. doi: 10.1021/acsbiomaterials.8b00419

Cheung, R. C., Ng, T. B., Wong, J. H., and Chan, W. Y. (2015). Chitosan: an update on potential biomedical and pharmaceutical applications. *Marine Drugs* 13, 5156–5186. doi: 10.3390/md13085156

Chowdhury, T. T., Bader, D. L., and Lee, D. A. (2001). Dynamic compression inhibits the synthesis of nitric oxide and PGE(2) by IL-1beta-stimulated chondrocytes cultured in agarose constructs. *Biochem. Biophys. Res. Commun.* 285, 1168–1174. doi: 10.1006/bbrc.2001.5311

Chu, C. R., Szczodry, M., and Bruno, S. (2010). Animal models for cartilage regeneration and repair. *Tissue Eng. Part B Rev.* 16, 105–115. doi: 10.1089/ten.teb.2009.0452

Chu, G., Yuan, Z., Zhu, C., Zhou, P., Wang, H., Zhang, W., et al. (2019). Substrate stiffness- and topography-dependent differentiation of annulus fibrosus-derived stem cells is regulated by Yes-associated protein. *Acta Biomaterial.* 92, 254–264. doi: 10.1016/j.actbio.2019.05.013

Clements, K., Bee, Z., Crossingham, G., Adams, M., and Sharif., M (2001). How severe must repetitive loading be to kill chondrocytes in articular cartilage? *Osteoarthrit. Cartilage* 9, 499–507. doi: 10.1053/joca.2000.0417

Clements, K. M., Hollander, A. P., Sharif, M., and Adams, M. A. (2004). Cyclic loading can denature type II collagen in articular cartilage. *Connect Tissue Res.* 45, 174–180. doi: 10.1080/03008200490514121

Coleman, J. L., Widmyer, M. R., Leddy, H. A., Utturkar, G. M., Spritzer, C. E., Moorman, C. T. III, et al. (2013). Diurnal variations in articular cartilage thickness and strain in the human knee. *J. Biomechan.* 46, 541–547. doi: 10.1016/j.jbiomech.2012.09.013

Coluccino, L., Stagnaro, P., Vassalli, M., and Scaglione, S. (2016). Bioactive TGF-β1/HA alginate-based scaffolds for osteochondral tissue repair: design, realization and multilevel characterization. *J. Appl. Biomater. Funct. Mater.* 14, e42–e52. doi: 10.5301/jabfm.5000249

Coricor, G., and Serra, R. (2016). TGF-β regulates phosphorylation and stabilization of Sox9 protein in chondrocytes through p38 and Smad dependent mechanisms. *Sci. Rep.* 6:38616. doi: 10.1038/srep38616

Correa, D., and Lietman, S. A. (2017). Articular cartilage repair: current needs, methods and research directions. *Semin. Cell Dev. Biol.,* 62, 67–77. doi: 10.1016/j.semcdb.2016.07.013

Correia, C., Pereira, A. L., Duarte, A. R., Frias, A. M., Pedro, A. J., Oliveira, J. T., et al. (2012). Dynamic culturing of cartilage tissue: the significance of hydrostatic pressure. *Tissue Eng.* 18, 1979–1991. doi: 10.1089/ten.tea.2012.0083

Cotofana, S., Eckstein, F., Wirth, W., Souza, R. B., Li, X., Wyman, B., et al. (2011). *In vivo* measures of cartilage deformation: patterns in healthy and osteoarthritic female knees using 3T MR imaging. *Eur. Radiol.* 21, 1127–1135. doi: 10.1007/s00330-011-2057-y

Crawford, D. C., DeBerardino, T. M., and Williams, R. J. III (2012). NeoCart, an autologous cartilage tissue implant, compared with microfracture for treatment of distal femoral cartilage lesions: an FDA phase-II prospective, randomized clinical trial after two years. *J. Bone Joint Surgery* 94, 979–989. doi: 10.2106/JBJS.K.00533

Critchley, S., Sheehy, E. J., Cunniffe, G., Diaz-Payno, P., Carroll, S. F., Jeon, O., et al. (2020). 3D printing of fibre-reinforced cartilaginous templates for the regeneration of osteochondral defects. *Acta Biomaterial.* S1742-7061(20)30319-6. doi: 10.1016/j.actbio.2020.05.040

Dai, Y., Shen, T., Ma, L., Wang, D., and Gao, C. (2018). Regeneration of osteochondral defects in vivo by a cell-free cylindrical poly(lactide-co-glycolide) scaffold with a radially oriented microstructure. *J. Tissue Eng. Regenerat. Med.* 12, e1647–e1661. doi: 10.1002/term.2592

D'Ambrosi, R., Valli, F., De Luca, P., Ursino, N., and Usuelli, F. G. (2019). MaioRegen osteochondral substitute for the treatment of knee defects: a systematic review of the literature. *J. Clin. Med.* 8:783. doi: 10.3390/jcm8060783

d'Angelo, M., Benedetti, E., Tupone, M. G., Catanesi, M., Castelli, V., Antonosante, A., et al. (2019). The role of stiffness in cell reprogramming: a potential role for biomaterials in inducing tissue regeneration. *Cells* 8:1036. doi: 10.3390/cells8091036

Davies, R. L., and Kuiper, N. J. (2019). Regenerative medicine: a review of the evolution of autologous chondrocyte implantation (ACI) Therapy. *Bioengineering* 6:22. doi: 10.3390/bioengineering6010022

De Mori, A., Hafidh, M., Mele, N., Yusuf, R., Cerri, G., Gavini, E., et al. (2019). Sustained release from injectable composite gels loaded with silver nanowires designed to combat bacterial resistance in bone regeneration applications. *Pharmaceutics* 11:116. doi: 10.3390/pharmaceutics11030116

D'Lima, D. D., Hashimoto, S., Chen, P. C., Colwell, C. W. Jr, and Lotz, M. K. (2001). Human chondrocyte apoptosis in response to mechanical injury. *Osteoarthritis Cartilage* 9, 712–719. doi: 10.1053/joca.2001.0468

Donell, S. (2019). Subchondral bone remodelling in osteoarthritis. *EFORT Open Rev.* 4, 221–229. doi: 10.1302/2058-5241.4.180102

Dong, C., and Lv, Y. (2016). Application of collagen scaffold in tissue engineering: recent advances and new perspectives. *Polymers* 8:42. doi: 10.3390/polym8020042

Du, J., Zu, Y., Li, J., Du, S., Xu, Y., Zhang, L., et al. (2016). Extracellular matrix stiffness dictates Wnt expression through integrin pathway. *Sci. Rep.* 6:20395. doi: 10.1038/srep20395

Ehrbar, M., Sala, A., Lienemann, P., Ranga, A., Mosiewicz, K., Bittermann, A., et al. (2011). Elucidating the role of matrix stiffness in 3D cell migration and remodeling. *Biophys. J.* 100, 284–293. doi: 10.1016/j.bpj.2010.11.082

Elder, B. D., and Athanasiou, K. A. (2009). Hydrostatic pressure in articular cartilage tissue engineering: from chondrocytes to tissue regeneration. *Tissue Eng.* 15, 43–53. doi: 10.1089/ten.teb.2008.0435

Elder, S., Gottipati, A., Zelenka, H., and Bumgardner, J. (2013). Attachment, proliferation, and chondroinduction of mesenchymal stem cells on porous chitosan-calcium phosphate scaffolds. *Open Orthopaed. J.* 7, 275–281. doi: 10.2174/1874325001307010275

Engler, A. J., Sen, S., Sweeney, H. L., and Discher, D. E. (2006). Matrix elasticity directs stem cell lineage specification. *Cell* 126, 677–689. doi: 10.1016/j.cell.2006.06.044

Erggelet, C., and Vavken, P. (2016). Microfracture for the treatment of cartilage defects in the knee joint - a golden standard? *J. Clin. Orthop. Trauma.* 7, 145–152. doi: 10.1016/j.jcot.2016.06.015

Eriksen, E. F. (2015). Treatment of bone marrow lesions (bone marrow edema). *BoneKEy Rep.* 4:755. doi: 10.1038/bonekey.2015.124

Evans, J. T., Evans, J. P., Walker, R. W., Blom, A. W., Whitehouse, M. R., and Sayers, A. (2019). How long does a hip replacement last? A systematic review and meta-analysis of case series and national registry reports with more than 15 years of follow-up. *Lancet* 393, 647–654. doi: 10.1016/S0140-6736(18)31665-9

Ewa-Choy, Y. W., Pingguan-Murphy, B., Abdul-Ghani, N. A., Jahendran, J., and Chua, K. H. (2017). Effect of alginate concentration on chondrogenesis of co-cultured human adipose-derived stem cells and nasal chondrocytes: a biological study. *Biomater. Res.* 21:19. doi: 10.1186/s40824-017-0105-7

Faikrua, A., Wittaya-areekul, S., Oonkhanond, B., and Viyoch, J. (2013). In vivo chondrocyte and transforming growth factor-β1 delivery using the thermosensitive chitosan/starch/β-glycerol phosphate hydrogel. *J. Biomater. Appl.* 28, 175–186. doi: 10.1177/0885328212441847

Familiari, F., Cinque, M. E., Chahla, J., Godin, J. A., Olesen, M. L., Moatshe, G., et al. (2018). Clinical outcomes and failure rates of osteochondral allograft transplantation in the knee: a systematic review. *Am. J. Sports Med.* 46, 3541–3549. doi: 10.1177/0363546517732531

Félix Lanao, R. P., Jonker, A. M., Wolke, J. G., Jansen, J. A., van Hest, J. C., and Leeuwenburgh, S. C. (2013). Physicochemical properties and applications of poly(lactic-co-glycolic acid) for use in bone regeneration. *Tissue Eng.* 19, 380–390. doi: 10.1089/ten.teb.2012.0443

Fisher, M., Ackley, T., Richard, K., Oei, B., and Dealy, C. N. (2019). *Osteoarthritis at the Cellular Level: Mechanisms, Clinical Perspectives, and Insights From Development. Reference Module in Biomedical Sciences Encyclopedia of Biomedical Engineering*. Amsterdam: Elsevier, 660–676.

Fraser, E. J., Savage-Elliott, I., Yasui, Y., Ackermann, J., Watson, G., Ross, K. A., et al. (2016). Clinical and MRI donor site outcomes following autologous osteochondral transplantation for talar osteochondral lesions. *Foot Ankle Int.* 37, 968–976. doi: 10.1177/1071100716649461

Freeman, F. E., Schiavi, J., Brennan, M. A., Owens, P., Layrolle, P., and McNamara, L. M. (2017). * Mimicking the biochemical and mechanical extracellular environment of the endochondral ossification process to enhance the *in vitro* mineralization potential of human mesenchymal stem cells. *Tissue Eng. Part A*, 23, 1466–1478. doi: 10.1089/ten.tea.2017.0052

Freitag, J., Shah, K., Wickham, J., Boyd, R., and Tenen, A. (2017). The effect of autologous adipose derived mesenchymal stem cell therapy in the treatment of a large osteochondral defect of the knee following unsuccessful surgical intervention of osteochondritis dissecans - a case study. *BMC Musculoskeletal Disord.* 18:298. doi: 10.1186/s12891-017-1658-2

Frisbie, D. D., Cross, M. W., and McIlwraith, C. W. (2006). A comparative study of articular cartilage thickness in the stifle of animal species used in human pre-clinical studies compared to articular cartilage thickness in the human knee. *Vet. Comparat. Orthopaed. Traumatol.* 19, 142–146. doi: 10.1055/s-0038-1632990

Fu, S., Thompson, C. L., Ali, A., Wang, W., Chapple, J.P., Mitchison, H. M., et al. (2019). Mechanical loading inhibits cartilage inflammatory signalling via an HDAC6 and IFT-dependent mechanism regulating primary cilia elongation. *Osteoarthritis Cartilage* 27, 1064–1074. doi: 10.1016/j.joca.2019.03.003

Furumatsu, T., Ozaki, T., and Asahara, H. (2009). Smad3 activates the Sox9-dependent transcription on chromatin. *Int. J. Biochem. Cell Biol.* 41, 1198–1204. doi: 10.1016/j.biocel.2008.10.032

Gan, D., Xu, T., Xing, W., Wang, M., Fang, J., Wang, K., et al. (2019). Mussel-inspired dopamine oligomer intercalated tough and resilient gelatin methacryloyl (GelMA) hydrogels for cartilage regeneration. *J. Mater. Chem.* 7, 1716–1725. doi: 10.1039/C8TB01664J

Ganesh, N., Hanna, C., Nair, S. V., and Nair, L. S. (2013). Enzymatically cross-linked alginic-hyaluronic acid composite hydrogels as cell delivery vehicles. *Int. J. Biol. Macromolecules* 55, 289–294. doi: 10.1016/j.ijbiomac.2012.12.045

Gardner, O., Fahy, N., Alini, M., and Stoddart, M. J. (2017). Joint mimicking mechanical load activates TGFβ1 in fibrin-poly(ester-urethane) scaffolds seeded with mesenchymal stem cells. *J. Tissue Eng. Regenerative Med.* 11, 2663–2666. doi: 10.1002/term.2210

Gentile, P., Chiono, V., Carmagnola, I., and Hatton, P. V. (2014). An overview of poly(lactic-co-glycolic) acid (PLGA)-based biomaterials for bone tissue engineering. *In. J. Mol. Sci.* 15, 3640–3659. doi: 10.3390/ijms15033640

Ghodbane, S. A., and Dunn, M. G. (2016). Physical and mechanical properties of cross-linked type I collagen scaffolds derived from bovine, porcine, and ovine tendons. *J. Biomed. Mater. Re. Part A*, 104, 2685–2692. doi: 10.1002/jbm.a.35813

Gilbert, S. J., and Blain, E. J. (2018). "Cartilage mechanobiology: how chondrocytes respond to mechanical load," in *Mechanobiology in Health and Disease*, ed S. Verbruggen, Mechanobiology in Health and Disease (Elsevier), 99–126. doi: 10.1016/B978-0-12-812952-4.00004-0

Gorth, D., and Webster, T. J. (2011). *10-Matrices for Tissue Engineering and Regenerative Medicine Biomaterials for Artificial Organs*, Woodhead Publishing Series in Biomaterials, ed M. L. J. Webster. Sawston: Woodhead Publishing, 270–286.

Griffin, M., Premakumar, Y., Seifalian, A., Butler, P. E., and Szarko, M. (2016). Biomechanical characterization of human soft tissues using indentation and tensile testing. *J. Visualized Exp.* 118:54872. doi: 10.3791/54872

Griffon, D. J., Sedighi, M. R., Schaeffer, D. V., Eurell, J. A., and Johnson, A. L. (2006). Chitosan scaffolds: interconnective pore size and cartilage engineering. *Acta Biomaterial.* 2, 313–320. doi: 10.1016/j.actbio.2005.12.007

Grigore, M. E. (2017). Biomaterials for cartilage tissue engineering. *J. Tiss. Sci. Eng.* 8, 4–9. doi: 10.4172/2157-7552.1000192

Grimm, N. L., Weiss, J. M., Kessler, J. I., and Aoki, S. K. (2014). Osteochondritis dissecans of the knee: pathoanatomy, epidemiology, and diagnosis. *Clin. Sports Med.* 33, 181–188. doi: 10.1016/j.csm.2013.11.006

Grover, C. N., Gwynne, J. H., Pugh, N., Hamaia, S., Farndale, R. W., Best, S. M., et al. (2012). Crosslinking and composition influence the surface properties, mechanical stiffness and cell reactivity of collagen-based films. *Acta Biomaterial.* 8, 3080–3090. doi: 10.1016/j.actbio.2012.05.006

Gu, W. Y., Lai, W. M., and Mow, V. C. (1998). A mixture theory for charged-hydrated soft tissues containing multi-electrolytes: passive transport and swelling behaviors. *J. Biomechan. Eng.* 120, 169–180. doi: 10.1115/1.2798299

Guimarães, C. F., Gasperini, L., Marques, A. P., and Reis, L. R. (2020). The stiffness of living tissues and its implications for tissue engineering. *Nat. Rev. Mater.* 5, 351–370 doi: 10.1038/s41578-019-0169-1

Gunatillake, P. A., and Adhikari, R. (2003). Biodegradable synthetic polymers for tissue engineering. *Eur. Cells Mater.* 5, 1–16. doi: 10.22203/eCM.v005a01

Haber, D. B., Logan, C. A., Murphy, C. P., Sanchez, A., LaPrade, R. F., and Provencher, M. T. (2019). Osteochondral allograft transplantation for the knee: post-operative rehabilitation. *Int. J. Sports Phys. Ther.* 14, 487–499. doi: 10.26603/ijspt20190487

Halonen, K. S., Mononen, M. E., Jurvelin, J. S., Töyräs, J., Salo, J., and Korhonen, R. K. (2014). Deformation of articular cartilage during static loading of a knee joint – Experimental and finite element analysis. *J. Biomechan.* 47, 2467–2474. doi: 10.1016/j.jbiomech.2014.04.013

Handorf, A. M., Zhou, Y., Halanski, M. A., and Li, W. J. (2015). Tissue stiffness dictates development, homeostasis, and disease progression. *Organogenesis* 11, 1–15. doi: 10.1080/15476278.2015.1019687

Hemmati-Sadeghi, S., Ringe, J., Dehne, T., Haag, R., and Sittinger, M. (2018). Hyaluronic acid influence on normal and osteoarthritic tissue-engineered cartilage. *Int. J. Mol. Sci.* 19:1519. doi: 10.3390/ijms19051519

Henrionnet, C., Liang, G., Roeder, E., Dossot, M., Wang, H., Magdalou, J., et al. (2017). * Hypoxia for mesenchymal stem cell expansion and differentiation: the best way for enhancing TGFß-induced chondrogenesis and preventing calcifications in alginate beads. *Tissue Eng.* 23, 913–922. doi: 10.1089/ten.tea.2016.0426

Holloway, J. L., Spiller, K. L., Lowman, A. M., and Palmese, G. R. (2011). Analysis of the *in vitro* swelling behavior of poly(vinyl alcohol) hydrogels in osmotic pressure solution for soft tissue replacement. *Acta Biomaterial.* 7, 2477–2482. doi: 10.1016/j.actbio.2011.02.016

Homicz, M. R., Chia, S. H., Schumacher, B. L., Masuda, K., Thonar, E. J., Sah, R. L., et al. (2003). Human septal chondrocyte redifferentiation in alginate, polyglycolic acid scaffold, and monolayer culture. *Laryngoscope* 113, 25–32. doi: 10.1097/00005537-200301000-00005

Hosseini, S. M., Wilson, W., Ito, K., and Van Donkelaar, C. C. (2014). A numerical model to study mechanically induced initiation and progression of damage in articular cartilage. *Osteoarthr. Cartil.* 22, 95–103. doi: 10.1016/j.joca.2013.10.010

Houard, X., Goldring, M. B., and Berenbaum, F. (2013). Homeostatic mechanisms in articular cartilage and role of inflammation in osteoarthritis. *Curr. Rheumatol. Rep.* 15:375. doi: 10.1007/s11926-013-0375-6

Hu, W., Chen, Y., Dou, C., and Dong, S. (2020). *Microenvironment in Subchondral Bone: Predominant Regulator for the Treatment of Osteoarthritis*. Annals of the rheumatic diseases, annrheumdis-2020-218089. Advance online publication. doi: 10.1136/annrheumdis-2020-218089

Huang, C. Y., Stankiewicz, A., Ateshian, G. A., and Mow, V. C. (2005). Anisotropy, inhomogeneity, and tension-compression nonlinearity of human glenohumeral cartilage in finite deformation. *J. Biomechan.* 38, 799–809. doi: 10.1016/j.jbiomech.2004.05.006

Huang, Y., Seitz, D., König, F., Müller, P. E., Jansson, V., and Klar, R. M. (2019). Induction of articular chondrogenesis by chitosan/hyaluronic-acid-based biomimetic matrices using human adipose-derived stem cells. *Int. J. Mol. Sci.* 20:4487. doi: 10.3390/ijms20184487

Huang, Z., Nooeaid, P., Kohl, B., Roether, J. A., Schubert, D. W., Meier, C., et al. (2015). Chondrogenesis of human bone marrow mesenchymal stromal cells in highly porous alginate-foams supplemented with chondroitin sulfate. *Mater. Sci. Eng.* 50, 160–172. doi: 10.1016/j.msec.2015.01.082

Hunter, D., Schofield, D., and Callander, E. (2014). The individual and socioeconomic impact of osteoarthritis. *Nat. Rev. Rheumatol.* 10, 437–441. doi: 10.1038/nrrheum.2014.44

Hunter, D. J., Gerstenfeld, L., Bishop, G., Davis, A. D., Mason, Z. D., Einhorn, T. A., et al. (2009). Bone marrow lesions from osteoarthritis knees are characterized by sclerotic bone that is less well mineralized. *Arthrit. Res. Therapy* 11:R11. doi: 10.1186/ar2601

Hurtig, M. B., Buschmann, M. D., Fortier, L. A., Hoemann, C. D., Hunziker, E. B., Jurvelin, J. S., et al. (2011). Preclinical studies for cartilage repair: recommendations from the international cartilage repair society. *Cartilage* 2, 137–152. doi: 10.1177/1947603511401905

Hwang, J., Bae, W. C., Shieu, W., Lewis, C. W., Bugbee, W. D., and Sah, R. L. (2008). Increased hydraulic conductance of human articular cartilage and subchondral bone plate with progression of osteoarthritis. *Arthritis Rheumat.* 58, 3831–3842. doi: 10.1002/art.24069

Hwang, J. H., Byun, M. R., Kim, A. R., Kim, K. M., Cho, H. J., Lee, Y. H., et al. (2015). Extracellular matrix stiffness regulates osteogenic differentiation through MAPK activation. *PLoS ONE* 10:e0135519. doi: 10.1371/journal.pone.0135519

Iseki, T., Rothrauff, B. B., Kihara, S., Sasaki, H., Yoshiya, S., Fu, F. H., et al. (2019). Dynamic compressive loading improves cartilage repair in an in vitro model of microfracture: comparison of 2 mechanical loading regimens on simulated microfracture based on fibrin gel scaffolds encapsulating connective tissue progenitor cells. *Am. J. Sports Med.* 47, 2188–2199. doi: 10.1177/0363546519855645

Jahr, H. (2017). "Tissue engineering strategies for cartilage repair," in *Cartilage*, eds S. Grässel and A. Aszódi (Cham: Springer). doi: 10.1007/978-3-319-53316-2_10

Jeuken, R. M., Roth, A. K., Peters, R., Van Donkelaar, C. C., Thies, J. C., Van Rhijn, L. W., et al. (2016). Polymers in cartilage defect repair of the knee: current status and future prospects. *Polymers* 8:219. doi: 10.3390/polym8060219

Joshi, N., Reverte-Vinaixa, M., Díaz-Ferreiro, E. W., and Domínguez-Oronoz, R. (2012). Synthetic resorbable scaffolds for the treatment of isolated patellofemoral cartilage defects in young patients: magnetic resonance imaging and clinical evaluation. *Am. J. Sports Med.* 40, 1289–1295. doi: 10.1177/0363546512441585

Jurvelin, J., Kiviranta, I., Tammi, M., and Helminen, J. H. (1986). Softening of canine articular cartilage after immobilization of the knee joint. *Clin. Orthop. Relat. Res.* 207, 246–252. doi: 10.1097/00003086-198606000-00042

Kaklamani, G., Cheneler, D., Grover, L. M., Adams, M. J., and Bowen, J. (2014). Mechanical properties of alginate hydrogels manufactured using external gelation. *J. Mech. Behav. Biomed. Mater.* 36, 135–142. doi: 10.1016/j.jmbbm.2014.04.013

Karimi, A., and Navidbakhsh, M. (2014). Mechanical properties of PVA material for tissue engineering applications. *Mater. Technol.* 29:2, 90–100. doi: 10.1179/1753555713Y.0000000115

Kato, Y., Chavez, J., Yamada, S., Hattori, S., Takazawa, S., and Ohuchi, H. (2018). A large knee osteochondral lesion treated using a combination of osteochondral autograft transfer and second-generation autologous chondrocyte implantation: a case report. *Regenerat. Ther.* 10, 10–16. doi: 10.1016/j.reth.2018.10.002

Kempson, G. E., Muir, H., Pollard, C., and Tuke, M. (1973). The tensile properties of the cartilage of human femoral condyles related to the content of collagen and glycosaminoglycans. *Biochim. Biophys. Acta* 297, 456–472. doi: 10.1016/0304-4165(73)90093-7

Keong, L. C., and Halim, A. S. (2009). In vitro models in biocompatibility assessment for biomedical-grade chitosan derivatives in wound management. *Int. J. Mol. Sci.* 10, 1300–1313. doi: 10.3390/ijms10031300

Kerin, A. J., Wisnom, M. R., and Adams, M. A. (1998). The compressive strength of articular cartilage. *Proc. Inst. Mech. Eng. H* 212, 273-280. doi: 10.1243/0954411981534051

Kleemann, R. U., Krocker, D., Cedraro, A., Tuischer, J., and Duda, G. N. (2005). Altered cartilage mechanics and histology in knee osteoarthritis: relation to clinical assessment (ICRS Grade). *Osteoarthrit. Cartilage* 13, 958–963. doi: 10.1016/j.joca.2005.06.008

Klotz, B. J., Gawlitta, D., Rosenberg, A., Malda, J., and Melchels, F. (2016). Gelatin-methacryloyl hydrogels: towards biofabrication-based tissue repair. *Trends Biotechnol.* 34, 394–407. doi: 10.1016/j.tibtech.2016.01.002

Kock, N. B., Smolders, J. M., van Susante, J. L., Buma, P., van Kampen, A., and Verdonschot, N. (2008). A cadaveric analysis of contact stress restoration after osteochondral transplantation of a cylindrical cartilage defect. *Knee Surg Sports Traumatol Arthrosc.* 16, 461–468. doi: 10.1007/s00167-008-0494-1

Kock, N. B., Van Susante, J. L., Buma, P., Van Kampen, A., and Verdonschot, N. (2006). Press-fit stability of an osteochondral autograft: influence of different plug length and perfect depth alignment. *Acta Orthop.* 77, 422–428. doi: 10.1080/17453670610046352

Koh, J. L., Wirsing, K., Lautenschlager, E., and Zhang, L. O. (2004). The effect of graft height mismatch on contact pressure following osteochondral

grafting: a biomechanical study. *Am. J. Sports Med.* 32, 317–320. doi: 10.1177/0363546503261730

Koh, L. D., Cheng, Y., Teng, C. P., Khin, Y. W., Loh, X. J., Tee, S. Y., et al. (2015). Structures, mechanical properties and applications of silk fibroin materials. *In Progress in Polymer Science*. 46, 86–110. doi: 10.1016/j.progpolymsci.2015.02.001

Komeili,A., Abusara, Z., Federico, S., and Herzog, W. (2019). Effect of strain rate on transient local strain variations in articular cartilage. *J. Mech. Behav. Biomed. Mater.* 95, 60–66. doi: 10.1016/j.jmbbm.2019.03.022

Kon, E., Delcogliano, M., Filardo, G., Altadonna, G., and Marcacci, M. (2009). Novel nano-composite multi-layered biomaterial for the treatment of multifocal degenerative cartilage lesions. *Knee Surgery Sports Traumatol. Arthroscopy* 17, 1312–1315. doi: 10.1007/s00167-009-0819-8

Könst, Y. E., Benink, R. J., Veldstra, R., van der Krieke, T. J., Helder, M. N., and van Royen, B. J. (2012). Treatment of severe osteochondral defects of the knee by combined autologous bone grafting and autologous chondrocyte implantation using fibrin gel. *Knee Surgery Sports Traumatol Arthroscopy* 20, 2263–2269. doi: 10.1007/s00167-012-1891-z

Korhonen, R. K., Laasanen, M. S., Töyräs, J., Rieppo, J., Hirvonen, J., Helminen, H. J., et al. (2002). Comparison of the equilibrium response of articular cartilage in unconfined compression, confined compression and indentation. *J. Biomechan.* 35, 903–909. doi: 10.1016/S0021-9290(02)00052-0

Krasnokutsky, S., Belitskaya-Lévy, I., Bencardino, J., Samuels, J., Attur, M., Regatte, R., et al. (2011). Quantitative magnetic resonance imaging evidence of synovial proliferation is associated with radiographic severity of knee osteoarthritis. *Arthritis Rheumat.* 63, 2983–2991. doi: 10.1002/art.30471

Kudva, A. K., Luyten, F. P., and Patterson, J. (2018). *In vitro* screening of molecularly engineered polyethylene glycol hydrogels for cartilage tissue engineering using periosteum-derived and ATDC5 cells. *Int. J. Mol. Sci.* 19:3341. doi: 10.3390/ijms19113341

Kundanati, L., Singh, S. K., Mandal, B. B., Murthy, T. G., Gundiah, N., and Pugno, N. M. (2016). Fabrication and mechanical characterization of hydrogel infused network silk scaffolds. *Int. J. Mol. Sci.* 17:1631. doi: 10.3390/ijms17101631

Kusmono, and Abdurrahim, I. (2019). Water sorption, antimicrobial activity, and thermal and mechanical properties of chitosan/clay/glycerol nanocomposite films. *Heliyon* 5:e02342. doi: 10.1016/j.heliyon.2019.e02342

Lai, W. M., Hou, J. S., and Mow, V. C. (1991). A triphasic theory for the swelling and deformation behaviors of articular cartilage. *J. Biomechan. Eng.* 113, 245–258. doi: 10.1115/1.2894880

Langasco, R., Cadeddu, B., Formato, M., Lepedda, A. J., Cossu, M., Giunchedi, P., et al. (2017). Natural collagenic skeleton of marine sponges in pharmaceutics: Innovative biomaterial for topical drug delivery. *Mater. Sci. Eng.* 70(Pt 1), 710–720. doi: 10.1016/j.msec.2016.09.041

Leddy, H. A., Christensen, S. E., and Guilak, F. (2008). Microscale diffusion properties of the cartilage pericellular matrix measured using 3D scanning microphotolysis. *J. Biomechan. Eng.* 130:061002. doi: 10.1115/1.2979876

Lee, H. Y., Hwang, C. H., Kim, H. E., and Jeong, S. H. (2018). Enhancement of bio-stability and mechanical properties of hyaluronic acid hydrogels by tannic acid treatment. *Carbohydrate Polymers* 186, 290–298. doi: 10.1016/j.carbpol.2018.01.056

Lee, K. Y., and Mooney, D. J. (2012). Alginate: properties and biomedical applications. *Progr. Polymer Sci.* 37, 106–126. doi: 10.1016/j.progpolymsci.2011.06.003

Leong, D. J., Li, Y. H., Gu, X. I., Sun, L., Zhou, Z., Nasser, P., et al. (2011). Physiological loading of joints prevents cartilage degradation through CITED2. *FASEB J.* 25, 182–191. doi: 10.1096/fj.10-164277

Levett, P. A., Hutmacher, D. W., Malda, J., and Klein, T. J. (2014). Hyaluronic acid enhances the mechanical properties of tissue-engineered cartilage constructs. *PLoS ONE* 9:e113216. doi: 10.1371/journal.pone.0113216

Li, G., Yin, J., Gao, J., Cheng, T. S., Pavlos, N. J., Zhang, C., et al. (2013). Subchondral bone in osteoarthritis: insight into risk factors and microstructural changes. *Arthritis Res. Therapy* 15:223. doi: 10.1186/ar4405

Li, J. J., Kim, K., Roohani-Esfahani, S. I., Guo, J., Kaplan, D. L., and Zreiqat, H. (2015). A biphasic scaffold based on silk and bioactive ceramic with stratified properties for osteochondral tissue regeneration. *J. Materials Chem. B* 3, 5361–5376. doi: 10.1039/C5TB00353A

Li, L., Duan, X., Fan, Z., Chen, L., Xing, F., Xu, Z., et al. (2018a). Mesenchymal stem cells in combination with hyaluronic acid for articular cartilage defects. *Sci. Rep.* 8:9900. doi: 10.1038/s41598-018-27737-y

Li, L., Yu, F., Zheng, L., Wang, R., Yan, W., Wang, Z., et al. (2018b). Natural hydrogels for cartilage regeneration: Modification, preparation and application. *J. Orthopaed. Translat.* 17, 26–41. doi: 10.1016/j.jot.2018.09.003

Li, W., Zhou, J., and Xu, Y. (2015). Study of the *in vitro* cytotoxicity testing of medical devices. *Biomed. Rep.* 3, 617–620. doi: 10.3892/br.2015.481

Li, Y., Zhou, J., Yang, X., Jiang, Y., and Gui, J. (2016). Intermittent hydrostatic pressure maintains and enhances the chondrogenic differentiation of cartilage progenitor cells cultivated in alginate beads. *Dev. Growth Differentiation* 58, 180–193. doi: 10.1111/dgd.12261

Lin, H. Y., Tsai, W. C., and Chang, S. H. (2017). Collagen-PVA aligned nanofiber on collagen sponge as bi-layered scaffold for surface cartilage repair. *J. Biomater. Sci.* 28, 664–678. doi: 10.1080/09205063.2017.1295507

Liu, A., Jennings, L. M., Ingham, E., and Fisher, J. (2015). Tribology studies of the natural knee using an animal model in a new whole joint natural knee simulator. *J. Biomechan.* 48, 3004–3011. doi: 10.1016/j.jbiomech.2015.07.043

Liu, F., Kozanek, M., Hosseini, A., Van de Velde, S. K., Gill, T. J., Rubash, H. E., et al. (2010). *In vivo* tibiofemoral cartilage deformation during the stance phase of gait. *J. Biomechan.* 43, 658–665. doi: 10.1016/j.jbiomech.2009.10.028

Lo Monaco, M., Merckx, G., Ratajczak, J., Gervois, P., Hilkens, P., Clegg, P., et al. (2018). Stem cells for cartilage repair: preclinical studies and insights in translational animal models and outcome measures. *Stem Cells Int.* 2018:9079538. doi: 10.1155/2018/9079538

Lo, G. H., Hunter, D. J., Nevitt, M., Lynch, J., McAlindon, T. E., and OAI Investigators Group (2009). Strong association of MRI meniscal derangement and bone marrow lesions in knee osteoarthritis: data from the osteoarthritis initiative. *Osteoarthritis and cartilage*, *17*, osteoarthritis knees are characterized by sclerotic bone that is less well mineralized. *Arthritis Res. Ther.* 11:R11. doi: 10.1016/j.joca.2008.11.014

Loening, A. M., James, I. E., Levenston, M. E., Badger, A. M., Frank, E. H., Kurz, B., et al. (2000). Injurious mechanical compression of bovine articular cartilage induces chondrocyte apoptosis. *Arch. Biochem. Biophys.* 381 205–212. doi: 10.1006/abbi.2000.1988

Madi, K., Staines, K. A., Bay, B. K., Javaheri, B., Geng, H., Bodey, A. J., et al. (2020). *In situ* characterization of nanoscale strains in loaded whole joints via synchrotron X-ray tomography. *Nat. Biomed. Eng.* 4, 343–354. doi: 10.1038/s41551-019-0477-1

Mak, A. F. (1986). The apparent viscoelastic behavior of articular cartilage–the contributions from the intrinsic matrix viscoelasticity and interstitial fluid flows. *J. Biomechan. Eng.* 108, 123–130. doi: 10.1115/1.3138591

Mantha, S., Pillai, S., Khayambashi, P., Upadhyay, A., Zhang, Y., Tao, O., et al. (2019). Smart hydrogels in tissue engineering and regenerative medicine. *Materials* 12:3323. doi: 10.3390/ma12203323

Marchiori, G., Berni, M., Boi, M., and Filardo, G. (2019). Cartilage mechanical tests: evolution of current standards for cartilage repair and tissue engineering. A literature review. *Clin. Biomechan.* 68, 58–72. doi: 10.1016/j.clinbiomech.2019.05.019

Mata, M., Milian, L., Oliver, M., Zurriaga, J., Sancho-Tello, M., de Llano, J., et al. (2017). *In vivo* articular cartilage regeneration using human dental pulp stem cells cultured in an alginate scaffold: a preliminary study. *Stem Cells Int.* 2017:8309256. doi: 10.1155/2017/8309256

Mathis, D. T., Kaelin, R., Rasch, H., Arnold, M. P., and Hirschmann, M. T. (2018). Good clinical results but moderate osseointegration and defect filling of a cell-free multi-layered nano-composite scaffold for treatment of osteochondral lesions of the knee. *Knee Surgery Sports Traumatol Arthroscopy.* 26, 1273–1280. doi: 10.1007/s00167-017-4638-z

McIlwraith, C. W., Fortier, L. A., Frisbie, D. D., and Nixon, A. J. (2011). Equine models of articular cartilage repair. *Cartilage* 2, 317–326. doi: 10.1177/1947603511406531

McLeod, M. A., Wilusz, R. E., and Guilak, F. (2013). Depth-dependent anisotropy of the micromechanical properties of the extracellular and pericellular matrices of articular cartilage evaluated via atomic force microscopy. *J. Biomech.* 46, 586–592. doi: 10.1016/j.jbiomech.2012.09.003

Medvedeva, E. V., Grebenik, E. A., Gornostaeva, S. N., Telpuhov, V. I., Lychagin, A. V., Timashev, P. S., et al. (2018). Repair of damaged articular

cartilage: current approaches and future directions. *Int. J. Mol. Sci.* 19:2366. doi: 10.3390/ijms19082366

Meehan, J., Danielsen, B. H., Kim, S. H., Jamali, A. A., and White, R. H. (2014). Younger age is associated with a higher risk of early periprosthetic joint infection and aseptic mechanical failure after total knee arthroplasty. *J. Bone Joint Surg.* 96, 529–535. doi: 10.2106/JBJS.M.00545

Mente, P. L., and Lewis, J. L. (1994). Elastic modulus of calcified cartilage is an order of magnitude less than that of subchondral bone. *J. Orthopaed. Res.* 12, 637–647. doi: 10.1002/jor.1100120506

Merlin Rajesh Lal, L. P., Suraishkumar, G. K., and Nair, P. D. (2017). Chitosan-agarose scaffolds supports chondrogenesis of Human Wharton's Jelly mesenchymal stem cells. *J. Biomed. Mater. Res. Part A* 105, 1845–1855. doi: 10.1002/jbm.a.36054

Minas, T., Von Keudell, A., Bryant, T., and Gomoll, A. H., (2014). The John Insall Award: a minimum 10-year outcome study of autologous chondrocyte implantation. *Clin. Orthopaed. Relat. Res.* 472, 41–51. doi: 10.1007/s11999-013-3146-9

Mistry, H., Connock, M., Pink, J., Shyangdan, D., Clar, C., Royle, P., et al. (2017). Autologous chondrocyte implantation in the knee: systematic review and economic evaluation. *Health Technol. Assess.* 21, 1–294. doi: 10.3310/hta21060

Miyanishi, K., Trindade, M. C., Lindsey, D. P., Beaupr,é, G. S., Carter, D. R., Goodman, S. B., et al. (2006a). Effects of hydrostatic pressure and transforming growth factor-beta 3 on adult human mesenchymal stem cell chondrogenesis *in vitro*. *Tissue Eng.* 12, 1419–1428. doi: 10.1089/ten.2006.12.1419

Miyanishi, K., Trindade, M. C., Lindsey, D. P., Beaupr,é, G. S., Carter, D. R., Goodman, S. B., et al. (2006b). Dose- and time-dependent effects of cyclic hydrostatic pressure on transforming growth factor-beta3-induced chondrogenesis by adult human mesenchymal stem cells *in vitro*. *Tissue Eng.* 12, 2253–2262. doi: 10.1089/ten.2006.12.2253

Montagne, K., Onuma, Y., Ito, Y., Aiki, Y., Furukawa, K. S., and Ushida, T. (2017). High hydrostatic pressure induces pro-osteoarthritic changes in cartilage precursor cells: a transcriptome analysis. *PLoS ONE* 12:e0183226. doi: 10.1371/journal.pone.0183226

Moore, A. C., and Burris, D. L. (2015). Tribological and material properties for cartilage of and throughout the bovine stifle: support for the altered joint kinematics hypothesis of osteoarthritis. *Osteoarthritis Cartilage* 23, 161–169. doi: 10.1016/j.joca.2014.09.021

Morrison, J. B. (1970). The mechanics of the knee joint in relation to normal walking. *J. Biomech.* 3, 51–61. doi: 10.1016/0021-9290(70)90050-3

Mow, V. C., Kuei, S. C., Lai, W. M., and Armstrong, C. G. (1980). Biphasic creep and stress relaxation of articular cartilage in compression? Theory and experiments. *J. Biomech. Eng.* 102, 73–84. doi: 10.1115/1.3138202

Muzzarelli, R. A., El Mehtedi, M., Bottegoni, C., Aquili, A., and Gigante, A. (2015). Genipin-crosslinked chitosan gels and scaffolds for tissue engineering and regeneration of cartilage and bone. *Marine Drugs* 13, 7314–7338. doi: 10.3390/md13127068

Nakagawa, K., Teramura, T., Takehara, T., Onodera, Y., Hamanishi, C., Akagi, M., et al. (2012). Cyclic compression-induced p38 activation and subsequent MMP13 expression requires Rho/ROCK activity in bovine cartilage explants. *Inflammation Res.* 61, 1093–1100. doi: 10.1007/s00011-012-0500-4

Narayanan, G., Vernekar, V. N., Kuyinu, E. L., and Laurencin, C. T. (2016). Poly (lactic acid)-based biomaterials for orthopaedic regenerative engineering. *Adv. Drug Delivery Rev.* 107, 247–276. doi: 10.1016/j.addr.2016.04.015

Nebelung, S., Post, M., Raith, S., Fischer, H., Knobe, M., Braun, B., et al. (2017). Functional *in situ* assessment of human articular cartilage using MRI: a whole-knee joint loading device. *Biomech. Model Mechanobiol.* 16, 1971–1986. doi: 10.1007/s10237-017-0932-4

Nguyen, Q. T., Hwang, Y., Chen, A. C., Varghese, S., and Sah, R. L. (2012). Cartilage-like mechanical properties of poly (ethylene glycol)-diacrylate hydrogels. *Biomaterials* 33, 6682–6690. doi: 10.1016/j.biomaterials.2012.06.005

Niemeyer, P., Laute, V., Zinser, W., John, T., Becher, C., Diehl, P., et al. (2020). Safety and efficacy of matrix-associated autologous chondrocyte implantation with spheroid technology is independent of spheroid dose after 4 years. *Knee Surgery Sports Traumatol. Arthroscop.* 28, 1130–1143. doi: 10.1007/s00167-019-05786-8

Nukavarapu, S. P., and Dorcemus, D. L. (2013). Osteochondral tissue engineering: current strategies and challenges. *Biotechnology. Adv.* 31, 706–721. doi: 10.1016/j.biotechadv.2012.11.004

Ogawa, R., Mizuno, S., Murphy, G. F., and Orgill, D. P. (2009). The effect of hydrostatic pressure on three-dimensional chondroinduction of human adipose-derived stem cells. *Tissue Eng. Part A* 15, 2937–2945. doi: 10.1089/ten.tea.2008.0672

Ogawa, R., Orgill, D. P., Murphy, G. F., and Mizuno, S. (2015). Hydrostatic pressure-driven three-dimensional cartilage induction using human adipose-derived stem cells and collagen gels. *Tissue Eng. Part A*, 21, 257–266. doi: 10.1089/ten.tea.2013.0525

Olivares-Navarrete, R., Lee, E. M., Smith, K., Hyzy, S. L., Doroudi, M., Williams, J. K., et al. (2017). Substrate stiffness controls osteoblastic and chondrocytic differentiation of mesenchymal stem cells without exogenous stimuli. *PLoS ONE* 12:e0170312. doi: 10.1371/journal.pone.0170312

Oliveira, A. S., Seidi, O., Ribeiro, N., Colaço, R., and Serro, A. P. (2019). Tribomechanical comparison between PVA hydrogels obtained using different processing conditions and human cartilage. *Materials* 12:3413. doi: 10.3390/ma12203413

Olubamiji, A. D., Izadifar, Z., Si, J. L., Cooper, D. M., Eames, B. F., and Chen, D. X. (2016). Modulating mechanical behaviour of 3D-printed cartilage-mimetic PCL scaffolds: influence of molecular weight and pore geometry. *Biofabrication* 8:025020. doi: 10.1088/1758-5090/8/2/025020

Oyen, M. L. (2014). Mechanical characterisation of hydrogel materials. *Int. Mater. Rev.* 59, 44–59. doi: 10.1179/1743280413Y.0000000022

Panadero, J. A., Sencadas, V., Silva, S. C., Ribeiro, C., Correia, V., Gama, F. M., et al. (2016). Mechanical fatigue performance of PCL-chondroprogenitor constructs after cell culture under bioreactor mechanical stimulus. *J. Biomed. Mater. Res. Appl. Biomater.* 104, 330–338. doi: 10.1002/jbm.b.33386

Park, J. S., Chu, J. S., Tsou, A. D., Diop, R., Tang, Z., Wang, A., et al. (2011). The effect of matrix stiffness on the differentiation of mesenchymal stem cells in response to TGF-β. *Biomaterials* 32, 3921–3930. doi: 10.1016/j.biomaterials.2011.02.019

Párraga Quiroga, J. M., Wilson, W., Ito, K., and van Donkelaar, C. C. (2017). The effect of loading rate on the development of early damage in articular cartilage. *Biomechan. Model. Mechanobiol.* 16, 263–273. doi: 10.1007/s10237-016-0815-0

Patel, J. M., Wise, B. C., Bonnevie, E. D., and Mauck, R. L. (2019). A systematic review and guide to mechanical testing for articular cartilage tissue engineering. *Tissue Eng.* 25, 593–608. doi: 10.1089/ten.tec.2019.0116

Peng, Z., Yang, X., Liu, C., Dong, Z., Wang, F., Wang, X., et al. (2019). Structural and mechanical properties of silk from different instars of *Bombyx mori*. *Biomacromolecules* 20, 1203–1216. doi: 10.1021/acs.biomac.8b01576

Petri, M., Broese, M., Simon, A., Liodakis, E., Ettinger, M., Guenther, D., et al. (2013). CaReS (MACT) versus microfracture in treating symptomatic patellofemoral cartilage defects: a retrospective matched-pair analysis. *J. Orthopaedic Sci.* 18, 38–44. doi: 10.1007/s00776-012-0305-x

Pfeifer, C. G., Karl, A., Kerschbaum, M., Berner, A., Lang, S., Schupfner, R., et al. (2019). TGF-β signalling is suppressed under pro-hypertrophic conditions in MSC chondrogenesis due to TGF-β receptor downregulation. *Int. J. Stem Cells* 12, 139–150. doi: 10.15283/ijsc18088

Prein, C., Warmbold, N., Farkas, Z., Schieker, M., Aszodi, A., and Clausen-Schaumann, H. (2016). Structural and mechanical properties of the proliferative zone of the developing murine growth plate cartilage assessed by atomic force microscopy. *Matrix Biol.* 50, 1–15. doi: 10.1016/j.matbio.2015.10.001

Qi, Y., Wang, H., Wei, K., Yang, Y., Zheng, R. Y., Kim, I. S., et al. (2017). A review of structure construction of silk fibroin biomaterials from single structures to multi-level structures. *Int. J. Mol. Sci.* 18:237. doi: 10.3390/ijms18030237

Redondo, M. L., Naveen, N. B., Liu, J. N., Tauro, T. M., Southworth, T. M., and Cole, B. J. (2018). Preservation of knee articular cartilage. *Sports Med. Arthrosc. Rev.* 26:e23-e30. doi: 10.1097/JSA.0000000000000226

Reppel, L., Schiavi, J., Charif, N., Leger, L., Yu, H., Pinzano, A., et al. (2015). Chondrogenic induction of mesenchymal stromal/stem cells from Wharton's jelly embedded in alginate hydrogel and without added growth factor: an alternative stem cell source for cartilage tissue engineering. *Stem Cell Res. Ther.* 6:260. doi: 10.1186/s13287-015-0263-2

Richter, D. L., Schenck, R. C. Jr, Wascher, D. C., and Treme, G. (2016). Knee articular cartilage repair and restoration techniques: a review of the literature. *Sports Health* 8, 153–160. doi: 10.1177/1941738115611350

Rieder, B., Weihs, A. M., Weidinger, A., Szwarc, D., Nürnberger, S., Redl, H., et al. (2018). Hydrostatic pressure-generated reactive oxygen species

induce osteoarthritic conditions in cartilage pellet cultures. *Sci. Rep.* 8:17010. doi: 10.1038/s41598-018-34718-8

Robinson, D. L., Kersh, M. E., Walsh, N. C., Ackland, D. C., de Steiger, R. N., and Pandy, M. G. (2016). Mechanical properties of normal and osteoarthritic human articular cartilage. *J. Mech. Behav. Biomed. Mater.* 61, 96–109. doi: 10.1016/j.jmbbm.2016.01.015

Roffi, A., Kon, E., Perdisa, F., Fini, M., Di Martino, A., Parrilli, A., et al. (2019). A composite chitosan-reinforced scaffold fails to provide osteochondral regeneration. *Int. J. Mol. Sci.* 20:2227. doi: 10.3390/ijms20092227

Rowland, R., Colello, M., and Wyland, D. J. (2019). Osteochondral autograft transfer procedure: arthroscopic technique and technical pearls. *Arthroscopy Techniques* 8, e713–e719. doi: 10.1016/j.eats.2019.03.006

Ruvinov, E., Tavor Re'em, T., Witte, F., and Cohen, S. (2018). Articular cartilage regeneration using acellular bioactive affinity-binding alginate hydrogel: a 6-month study in a mini-pig model of osteochondral defects. *J. Orthopaed. Translat.* 16, 40–52. doi: 10.1016/j.jot.2018.08.003

Sadeghi, A. H., Shin, S. R., Deddens, J. C., Fratta, G., Mandla, S., Yazdi, I. K., et al. (2017). Engineered 3D cardiac fibrotic tissue to study fibrotic remodeling. *Adv. Healthcare Mater.* 6:1601434. doi: 10.1002/adhm.201601434

Sadeghi, H., Shepherd, D. E. T., and Espino, D. M. (2015). Effect of the variation of loading frequency on surface failure of bovine articular cartilage. *Osteoarthrit. Cartilage* 23. 2252–2258. doi: 10.1016/j.joca.2015.06.002

Saha, A., Rolfe, R., Carroll, S., Kelly, D. J., and Murphy, P. (2017). Chondrogenesis of embryonic limb bud cells in micromass culture progresses rapidly to hypertrophy and is modulated by hydrostatic pressure. *Cell Tissue Res.* 368, 47–59. doi: 10.1007/s00441-016-2512-9

Saidova, A. A., and Vorobjev, I. A. (2020). Lineage commitment, signaling pathways, and the cytoskeleton systems in mesenchymal stem cells. *Tissue Eng. Part B Rev.* 26, 13–25. doi: 10.1089/ten.teb.2019.0250

Samavedi, S., Poindexter, L., Dyke, M., and Goldstein, A. (2013). "Synthetic Biomaterials for Regenerative Medicine Applications." in *the Regenerative Medicine Applications in Organ Transplantation*, 81–99. doi: 10.1016/B978-0-12-398523-1.00007-0

Sanchez-Adams, J., Leddy, H. A., McNulty, A. L., O'Conor, C. J., and Guilak, F. (2014). The mechanobiology of articular cartilage: bearing the burden of osteoarthritis. *Curr. Rheumatol. Rep.* 16:451. doi: 10.1007/s11926-014-0451-6

Sánchez-Téllez, D. A., Téllez-Jurado, L., and Rodríguez-Lorenzo, L. M. (2017). Hydrogels for cartilage regeneration, from polysaccharides to hybrids. *Polymers* 9:671. doi: 10.3390/polym9120671

Saris, D., Price, A., Widuchowski, W., Bertrand-Marchand, M., Caron, J., Drogset, J. O., et al. (2014). Matrix-applied characterized autologous cultured chondrocytes versus microfracture: two-year follow-up of a prospective randomized trial. *Am. J. Sports Med.* 42, 1384–1394. doi: 10.1177/0363546514528093

Sawatjui, N., Limpaiboon, T., Schrobback, K., and Klein, T. (2018). Biomimetic scaffolds and dynamic compression enhance the properties of chondrocyte- and MSC-based tissue-engineered cartilage. *J. Tissue Eng. Regenerat. Med.* 12, 1220–1229. doi: 10.1002/term.2653

Scalzone, A., Ferreira, A. M., Tonda-Turo, C., Ciardelli, G., Dalgarno, K., and Gentile, P. (2019). The interplay between chondrocyte spheroids and mesenchymal stem cells boosts cartilage regeneration within a 3D natural-based hydrogel. *Sci. Rep*, 9:14630. doi: 10.1038/s41598-019-51070-7

Schinagl, R. M., Gurskis, D., Chen, A. C., and Sah, R. L. (1997). Depth-dependent confined compression modulus of full-thickness bovine articular cartilage. *J. Orthopaedic Res.* 15, 499–506. doi: 10.1002/jor.1100150404

Scholten, P. M., Ng, K. W., Joh, K., Serino, L. P., Warren, R. F., Torzilli, P. A., et al. (2011). A semi-degradable composite scaffold for articular cartilage defects. *J. Biomed. Mater. Res.* 97A, 8–15. doi: 10.1002/jbm.a.33005

Shapiro, F., Koide, S., and Glimcher, M. J. (1993). Cell origin and differentiation in the repair of full-thickness defects of articular cartilage. *J. Bone Joint Surg. Am.* 75, 532–553. doi: 10.2106/00004623-199304000-00009

Sheehy, E. J., Mesallati, T., Vinardell, T., and Kelly, D. J. (2015). Engineering cartilage or endochondral bone: a comparison of different naturally derived hydrogels. *Acta Biomaterial.* 13, 245–253. doi: 10.1016/j.actbio.2014.11.031

Sophia Fox, A. J., Bedi, A., and Rodeo, S. A. (2009). The basic science of articular cartilage: structure, composition, and function. *Sports Health* 1, 461–468. doi: 10.1177/1941738109350438

Stambough, J. B., Clohisy, J. C., Barrack, R. L., Nunley, R. M., and Keeney, J. A. (2014). Increased risk of failure following revision total knee replacement in patients aged 55 years and younger. *Bone Joint J.* 96-B, 1657–1662. doi: 10.1302/0301-620X.96B12.34486

Stavenschi, E., Corrigan, M. A., Johnson, G. P., Riffault, M., and Hoey, D. A. (2018). Physiological cyclic hydrostatic pressure induces osteogenic lineage commitment of human bone marrow stem cells: a systematic study. *Stem Cell Res. Ther.* 9:276. doi: 10.1186/s13287-018-1025-8

Stavenschi, E., and Hoey, D. A. (2019). Pressure-induced mesenchymal stem cell osteogenesis is dependent on intermediate filament remodeling. *FASEB J.* 33, 4178–4187. doi: 10.1096/fj.201801474RR

Steinmetz, N. J., Aisenbrey, E. A., Westbrook, K. K., Qi, H. J., and Bryant, S. J. (2015). Mechanical loading regulates human MSC differentiation in a multi-layer hydrogel for osteochondral tissue engineering. *Acta Biomaterial.* 21, 142–153. doi: 10.1016/j.actbio.2015.04.015

Sun, A. X., Lin, H., Fritch, M. R., Shen, H., Alexander, P. G., DeHart, M., et al. (2017). Chondrogenesis of human bone marrow mesenchymal stem cells in 3-dimensional, photocrosslinked hydrogel constructs: effect of cell seeding density and material stiffness. *Acta Biomaterial.* 58, 302–311. doi: 10.1016/j.actbio.2017.06.016

Sun, H. B., Zhao, L., Tanaka, S., and Yokota, H. (2012). Moderate joint loading reduces degenerative actions of matrix metalloproteinases in the articular cartilage of mouse ulnae. *Connective Tissue Res.* 53, 180–186. doi: 10.3109/03008207.2011.628765

Teixeira, M. A., Amorim, M., and Felgueiras, H. P. (2019). Poly(Vinyl Alcohol)-based nanofibrous electrospun scaffolds for tissue engineering applications. *Polymers* 12:7. doi: 10.3390/polym12010007

Theodoropoulos, J. S., De Croos, J. N. A., Park, S. S., Pilliar, R., and Kandel, R. A., (2011). Integration of tissue-engineered cartilage with host cartilage: an *in vitro* model. *Clin. Orthop. Relat. Res.* 469:2785. doi: 10.1007/s11999-011-1856-4

Thomas, L., Vg, R., and Nair, P. R.(2017). Effect of stiffness of chitosan-hyaluronic acid dialdehyde hydrogels on the viability and growth of encapsulated chondrocytes. *Int. J. Biol. Macromolecules* 104(Pt B), 1925–1935. doi: 10.1016/j.ijbiomac.2017.05.116

Thorpe, S. D., Buckley, C. T., Vinardell, T., O'Brien, F. J., Campbell, V. A., and Kelly, D. J. (2008). Dynamic compression can inhibit chondrogenesis of mesenchymal stem cells. *Biochem. Biophys. Res.* 377, 458–462. doi: 10.1016/j.bbrc.2008.09.154

Thorpe, S. D., Buckley, C. T., Vinardell, T., O'Brien, F. J., Campbell, V. A., and Kelly, D. J. (2010). The response of bone marrow-derived mesenchymal stem cells to dynamic compression following TGF-beta3 induced chondrogenic differentiation. *Annals Biomed. Eng.* 38, 2896–2909. doi: 10.1007/s10439-010-0059-6

Torres, L., Dunlop, D. D., Peterfy, C., Guermazi, A., Prasad, P., Hayes, K. W., et al. (2006). The relationship between specific tissue lesions and pain severity in persons with knee osteoarthritis. *Osteoarthritis Cartilage* 14, 1033–1040. doi: 10.1016/j.joca.2006.03.015

Tozzi, G., de Mori, A., Oliveira, A., and Roldo, M. (2016). Composite hydrogels for bone regeneration. *Materials* 9:267. doi: 10.3390/ma9040267

Tozzi, G., Peña Fernández, M., Davis, S., Karali, A., Kao, A. P., and Blunn, G. (2020). Full-Field Strain Uncertainties and Residuals at the cartilage-bone interface in unstained tissues using propagation-based phase-contrast XCT and digital volume correlation. *Materials* 13:2579. doi: 10.3390/ma13112579

Trombino, S., Servidio, C., Curcio, F., and Cassano, R. (2019). Strategies for hyaluronic acid-based hydrogel design in drug delivery. *Pharmaceutics* 11:407. doi: 10.3390/pharmaceutics11080407

Tseng, T. H., Jiang, C. C., Lan, H. H., Chen, C. N., and Chiang, H. (2020). The five year outcome of a clinical feasibility study using a biphasic construct with minced autologous cartilage to repair osteochondral defects in the knee. *Int. Orthopaedics* 44, 1745–1754. doi: 10.1007/s00264-020-04569-y

Usami, Y., Gunawardena, A. T., Iwamoto, M., and Enomoto-Iwamoto, M. (2016). Wnt signaling in cartilage development and diseases: lessons from animal studies. *Lab. Investigat.* 96, 186–196. doi: 10.1038/labinvest.2015.142

U. S. Food and Drug Administration (2011). *Guidance for Industry: Preparation of IDEs and INDs for Products Intended to Repair Or Replace Knee Cartilage*. Available online at: https://www.fda.gov/media/82562/download.

Van Den Bulcke, A. I., Bogdanov, B., De Rooze, N., Schacht, E. H., Cornelissen, M., and Berghmans, H. (2000). Structural and rheological properties of

methacrylamide modified gelatin hydrogels. *Biomacromolecules* 1, 31–38. doi: 10.1021/bm990017d

Vanwanseele, B., Eckstein, F., Knecht, H., Stüssi, E., and Spaepen, A. (2002). Knee cartilage of spinal cord-injured patients displays progressive thinning in the absence of normal joint loading and movement. *Arthritis Rheum*. 46, 2073–2078. doi: 10.1002/art.10462

Varun, T. K., Senani, S., Jayapal, N., Chikkerur, J., Roy, S., Tekulapally, V. B., et al. (2017). Extraction of chitosan and its oligomers from shrimp shell waste, their characterization and antimicrobial effect. *Vet. World* 10, 170–175. doi: 10.14202/vetworld.2017.170-175

Vikingsson, L., Gómez-Tejedor, J. A., Gallego Ferrer, G., and Gómez Ribelles, J. L. (2015). An experimental fatigue study of a porous scaffold for the regeneration of articular cartilage. *J. Biomechan*. 48, 1310–1317. doi: 10.1016/j.jbiomech.2015.02.013

Vilela, C. A., da Silva Morais, A., Pina, S., Oliveira, J. M., Correlo, V. M., Reis, R. L., et al. (2018). Clinical trials and management of osteochondral lesions. *Adv. Exp. Med. Biol.* 1058, 391–413. doi: 10.1007/978-3-319-76711-6_18

Vinardell, T., Rolfe, R. A., Buckley, C. T., Meyer, E. G., Ahearne, M., Murphy, P., et al. (2012). Hydrostatic pressure acts to stabilise a chondrogenic phenotype in porcine joint tissue derived stem cells. *Eur. Cells Mater.* 23, 121–134. doi: 10.22203/eCM.v023a09

Visser, J., Melchels, F. P., Jeon, J. E., van Bussel, E. M., Kimpton, L. S., Byrne, H. M., et al. (2015). Reinforcement of hydrogels using three-dimensionally printed microfibres. *Nat. Commun.* 6:6933. doi: 10.1038/ncomms7933

Waldman, S. D., Couto, D. C., Grynpas, M. D., Pilliar, R. M., and Kandel, R. A. (2006). A single application of cyclic loading can accelerate matrix deposition and enhance the properties of tissue-engineered cartilage. *Osteoarthritis Cartilage* 14, 323–330. doi: 10.1016/j.joca.2005.10.007

Walter, C., Leichtle, U., Lorenz, A., Mittag, F., Wülker, N., Müller, O., et al. (2013). Dissipated energy as a method to characterize the cartilage damage in large animal joints: an *in vitro* testing model. *Med. Eng. Phys.* 35, 1251–1255. doi: 10.1016/j.medengphy.2013.01.002

Wang, T., Lai, J. H., and Yang, F. (2016). Effects of hydrogel stiffness and extracellular compositions on modulating cartilage regeneration by mixed populations of stem cells and chondrocytes *in vivo*. *Tissue Eng. Part A*, 22, 1348–1356. doi: 10.1089/ten.tea.2016.0306

Whitney, G. A., Jayaraman, K., Dennis, J. E., and Mansour, J. M. (2017). Scaffold-free cartilage subjected to frictional shear stress demonstrates damage by cracking and surface peeling. *J. Tissue Eng. Regenerat. Med.* 11, 412–424. doi: 10.1002/term.1925

Williams, R. J., and Gamradt, S. C. (2008). Articular cartilage repair using a resorbable matrix scaffold. *Instructional Course Lectures* 57, 563–571.

Wong, B. L., and Sah, R. L. (2010). Mechanical asymmetry during articulation of tibial and femoral cartilages: local and overall compressive and shear deformation and properties. *J. Biomechanics* 43, 1689–1695. doi: 10.1016/j.jbiomech.2010.02.035

Woodard, L. N., and Grunlan, M. A. (2018). Hydrolytic degradation and erosion of polyester biomaterials. *ACS Macro Lett.* 7, 976–982. doi: 10.1021/acsmacrolett.8b00424

Wu, J. Z., Herzog, W., and Hasler, E. M. (2002). Inadequate placement of osteochondral plugs may induce abnormal stress-strain distributions in articular cartilage –finite element simulations. *Med. Eng. Phys.* 24, 85–97. doi: 10.1016/S1350-4533(01)00122-9

Xia, H., Liang, C., Luo, P., Huang, J., He, J., Wang, Z., et al. (2018). Pericellular collagen I coating for enhanced homing and chondrogenic differentiation of mesenchymal stem cells in direct intra-articular injection. *Stem Cell Res. Therapy* 9:174. doi: 10.1186/s13287-018-0916-z

Xia, T., Liu, W., and Yang, L. (2017). A review of gradient stiffness hydrogels used in tissue engineering and regenerative medicine. *J. Biomed. Mater. Res. Part A* 105, 1799–1812. doi: 10.1002/jbm.a.36034

Xu, J., Wang, W., Ludeman, M., Cheng, K., Hayami, T., Lotz, J. C., et al. (2008). Chondrogenic differentiation of human mesenchymal stem cells in three-dimensional alginate gels. *Tissue Eng. Part A*. 14, 667–680. doi: 10.1089/tea.2007.0272

Yamagata, K., Nakayamada, S., and Tanaka, Y. (2018). Use of mesenchymal stem cells seeded on the scaffold in articular cartilage repair. *Inflammation Regenerat.* 38:4. doi: 10.1186/s41232-018-0061-1

Yang, J., Zhang, Y. S., Yue, K., and Khademhosseini, A. (2017). Cell-laden hydrogels for osteochondral and cartilage tissue engineering. *Acta Biomaterial.* 57, 1–25. doi: 10.1016/j.actbio.2017.01.036

Yao, Y., Zeng, L., and Huang, Y. (2016). The enhancement of chondrogenesis of ATDC5 cells in RGD-immobilized microcavitary alginate hydrogels. *J. Biomater. Appl.* 31, 92–101. doi: 10.1177/0885328216640397

Zak, L., Albrecht, C., Wondrasch, B., Widhalm, H., Vekszler, G., Trattnig, S., et al. (2014). Results 2 years after matrix-associated autologous chondrocyte transplantation using the novocart 3D Scaffold: an analysis of clinical and radiological data. *Am. J. Sports Med.* 42, 1618–1627. doi: 10.1177/0363546514532337

Zhang, T., Wen, F., Wu, Y., Goh, G. S., Ge, Z., Tan, L. P., et al. (2015). Cross-talk between TGF-beta/SMAD and integrin signaling pathways in regulating hypertrophy of mesenchymal stem cell chondrogenesis under deferral dynamic compression. *Biomaterials*. (2015) 38:72–85. doi: 10.1016/j.biomaterials.2014.10.010

Zheng, L., Liu, S., Cheng, X., Qin, Z., Lu, Z., Zhang, K., et al. (2019). Intensified stiffness and photodynamic provocation in a collagen-based composite hydrogel drive chondrogenesis. *Adv. Sci.* 6:1900099. doi: 10.1002/advs.201900099

Zhu, J. (2010). Bioactive modification of poly(ethylene glycol) hydrogels for tissue engineering. *Biomaterials* 31, 4639–4656. doi: 10.1016/j.biomaterials.2010.02.044

Zhu, Y., Wu, H., Sun, S., Zhou, T., Wu, J., and Wan, Y. (2014). Designed composites for mimicking compressive mechanical properties of articular cartilage matrix. *J. Mech. Behav. Biomed. Mater.* 36, 32–46. doi: 10.1016/j.jmbbm.2014.04.003

Zikria, B., Hafezi-Nejad, N., Patten, I., Johnson, A., Haj-Mirzaian, A., Wilckens, J. H., et al. (2019). Image-guided chondrocyte harvesting for autologous chondrocyte implantation: initial feasibility study with human cadaver and pilot clinical experience. *JB JS Open Access* 4:e0039. doi: 10.2106/JBJS.OA.18.00039

Conflict of Interest: The authors declare that the research was conducted in the absence of any commercial or financial relationships that could be construed as a potential conflict of interest.

frontiers in Bioengineering and Biotechnology

MINI REVIEW
published: 11 March 2021
doi: 10.3389/fbioe.2021.603608

Metal-Organic Framework (MOF)-Based Biomaterials for Tissue Engineering and Regenerative Medicine

*Moldir Shyngys[1], Jia Ren[1], Xiaoqi Liang[1], Jiechen Miao[1], Anna Blocki[2,3,4] and Sebastian Beyer[1,2]**

[1] Department of Biomedical Engineering, The Chinese University of Hong Kong, Shatin, Hong Kong, [2] Institute for Tissue Engineering & Regenerative Medicine, The Chinese University of Hong Kong, Shatin, Hong Kong, [3] School of Biomedical Sciences, Faculty of Medicine, The Chinese University of Hong Kong, Shatin, Hong Kong, [4] Department of Orthopaedics & Traumatology, Faculty of Medicine, The Chinese University of Hong Kong, Shatin, Hong Kong

The synthesis of Metal-organic Frameworks (MOFs) and their evaluation for various applications is one of the largest research areas within materials sciences and chemistry. Here, the use of MOFs in biomaterials and implants is summarized as narrative review addressing primarely the Tissue Engineering and Regenerative Medicine (TERM) community. Focus is given on MOFs as bioactive component to aid tissue engineering and to augment clinically established or future therapies in regenerative medicine. A summary of synthesis methods suitable for TERM laboratories and key properties of MOFs relevant to biomaterials is provided. The use of MOFs is categorized according to their targeted organ (bone, cardio-vascular, skin and nervous tissue) and whether the MOFs are used as intrinsically bioactive material or as drug delivery vehicle. Further distinction between *in vitro* and *in vivo* studies provides a clear assessment of literature on the current progress of MOF based biomaterials. Although the present review is narrative in nature, systematic literature analysis has been performed, allowing a concise overview of this emerging research direction till the point of writing. While a number of excellent studies have been published, future studies will need to clearly highlight the safety and added value of MOFs compared to established materials for clinical TERM applications. The scope of the present review is clearly delimited from the general 'biomedical application' of MOFs that focuses mainly on drug delivery or diagnostic applications not involving aspects of tissue healing or better implant integration.

Keywords: metal-organic frameworks, biomaterial, tissue engineering, regenerative medicine, bone, cardio-vascular, nervous tissue

OPEN ACCESS

Edited by:
Xin Zhao,
Hong Kong Polytechnic University,
Hong Kong

Reviewed by:
Jose Mauro Granjeiro,
National Institute of Metrology, Quality and Technology, Brazil
Junling Guo,
Sichuan University, China
Dariusz Matoga,
Jagiellonian University, Poland

***Correspondence:**
Sebastian Beyer
sebastian.beyer@cuhk.edu.hk

Specialty section:
This article was submitted to Biomaterials, a section of the journal Frontiers in Bioengineering and Biotechnology

Received: *07 September 2020*
Accepted: *27 January 2021*
Published: *11 March 2021*

Citation:
Shyngys M, Ren J, Liang X, Miao J, Blocki A and Beyer S (2021) Metal-Organic Framework (MOF)-Based Biomaterials for Tissue Engineering and Regenerative Medicine. Front. Bioeng. Biotechnol. 9:603608. doi: 10.3389/fbioe.2021.603608

INTRODUCTION

MOFs are new synthetic materials that emerged over the past three decades (Yaghi and Li, 1995; Yaghi et al., 1995). MOFs comprise of organic ligands that bridge metal ions. This leads to highly ordered, porous and 3-dimensional crystalline structures. The pore size and aperture is significantly smaller compared to polymeric structures (Pan et al., 2013) and can be accurately controlled (Eddaoudi et al., 2002; Banerjee et al., 2009). This accurate control makes MOFs predestined for drug loading and sustained or triggered release from nano-particulate

drug formulations or coatings (Wang et al., 2020). This has led to the classical understanding of "biomedical MOF applications" that primarily focused on diagnostic applications (Chaparteguí-Arias et al., 2019) or drug delivery (Keskin and Kizilel, 2011; Banerjee et al., 2020). The present review is clearly delimited from these established fields of investigation by focusing on MOFs for TERM applications. In particular, the present review addresses MOFs that modulate the foreign body response to implants, MOFs that influence the inflammatory wound environment, or MOFs that improve the host tissue-implant interface and aid healing.

A systematic literature analysis was performed using Clarivate Analytics Web of Science database in combination with a structured key word search. In brief, a comprehensive list of works on MOFs was generated and those interfacing with biomaterials, tissue engineering, regenerative medicine or MOFs interfacing with neuronal repair were identified. Works solely focusing on drug-delivery or cancer treatment were excluded if not reporting aspect of tissue healing, integration or improvement of the foreign body response.

In addition to the drug loading capacity, the present review aims to highlight that MOFs may also have intrinsic bioactivity through delivering specific metal ions (Su et al., 2019), ligands (Rojas et al., 2017) or through catalytically generating messenger molecules such as nitric oxide in copper-based MOFs (Harding and Reynolds, 2012). Beyond individual components, structural aspects of MOFs are essential since they determine release kinetics as well as the accessibility of the metal centers providing catalytic effects. Most studies investigating MOFs for TERM application focused on orthopedic applications, followed by cardiovascular treatment, cutaneous wound healing, and applications in nervous tissue (**Figure 1**). Beyond these targeted organs, a specialized MOF was proposed for treatment of periodontitis (Li et al., 2019), while materials for other organs seem not yet to have been evaluated. In summary, the use of MOFs for TERM applications is an emerging field of research with only very few works published before the year 2018.

Parallels of MOFs to Natural Minerals in TERM Applications

The concept of MOFs originates from natural minerals, which have a substantial track record in TERM applications. Calcium phosphate has intrinsic osteogenic effect (Albee, 1920) and its admixtures to biodegradable polymers led to clinical implants (de Groot, 1993). A calcium and strontium based MOF with bisphosphonate linker (Matlinska et al., 2019) appears to be the evolution of minerals with engineered bioactivity.

Another naturally occurring mineral is zinc oxide (ZnO), a non-porous solid devoid of any drug loading capacity, that has long been used to treat cutaneous wounds and pathological skin conditions (Lansdown et al., 2007). In contrast to ZnO, versatile drug loading, release and disintegration rate of porous Zeolitic Imidazolate Frameworks (ZIFs) can be designed leading to various envisioned biomedical applications (Maleki et al., 2020). The most prominent member of the ZIF family is ZIF-8, which is a polymorph of zinc(II)2-methylimidazolate and has a ligand-metal-ligand bonding angle similar to that of O-Si-O. In addition, ZIF-8 shares the crystal topology (SOD) with Sodalite, a naturally occurring zeolite of the sodium aluminum silicate framework family.

PREPARATION METHODS OF MOFs SUITABLE FOR TERM LABORATORIES AND THEIR KEY PROPERTIES

Solution Precipitation Synthesis of ZIF-8 and Loading of Bioactive Agents

ZIF-8 is easily synthesized through simple precipitation reactions facilitated by mixing the ligand (2-methylimidazole) and zinc salt solution at room temperature (Park et al., 2006; Beyer et al., 2016, 2018b; Kulow et al., 2019). ZIF-8 can be engineered to acquire bioactivity beyond that of zinc ions through encapsulation of drugs. Admixtures of Dexamethasone (Sarkar et al., 2019) or non-steroidal anti-inflammatory drugs (Ho et al., 2020) to these precursor mixtures during precipitation reactions led to their firm entrapment within ZIF-8. ZIF-8 shows a sustained release behavior for small molecules up to several weeks (Liédana et al., 2012). An interesting aspect of ZIF-8 is the observation that it crystallizes around biomacromolecules in aqueous solution by a process termed biomimetic mineralization (Liang et al., 2015a,b; Gao et al., 2019). This approach has been used for delivery of insulin (Duan et al., 2018) and may provide opportunities for e.g., growth factor delivery.

Mechanochemical Synthesis of MOFs and Potential Use as Filler in Polymer Composites

MOFs may also be synthesized mechanochemically (Stolar and Užarevíæ, 2020) by mixing organic linkers and metal precursors in a small planetary ball-mill (Akhmetova et al., 2019), immediately yielding MOF powder in large quantities and short time. So far, the mechanochemical synthesis of calcium and strontium MOFs has been reported (Al-Terkawi et al., 2017), which is an excellent route to produce MOFs as bioactive fillers for e.g., polymeric biomaterials. However, mechanochemical syntheses routes for earth alkaline metal MOFs specifically for TERM applications have yet to be developed.

Solvothermal Synthesis of CU-BTC

During solvo-thermal synthesis, two precursor solutions of organic ligands and metal ions are mixed and heated in a micro-autoclave beyond the boiling point of the solvent (Ni and Masel, 2006). Copper(II)1,3,5-benzenetricarboxylate (Cu-BTC), also known as HKUST-1 (Chui, 1999) is typically synthesized under solvo-thermal conditions. The porous structure of Cu-BTC makes the copper metal center accessible to solutes. This renders Cu-BTC an interesting catalyst for the conversion of blood borne nitrosothiols to continuously release nitric oxide (NO) (Harding and Reynolds, 2012). Nitric oxide is a key

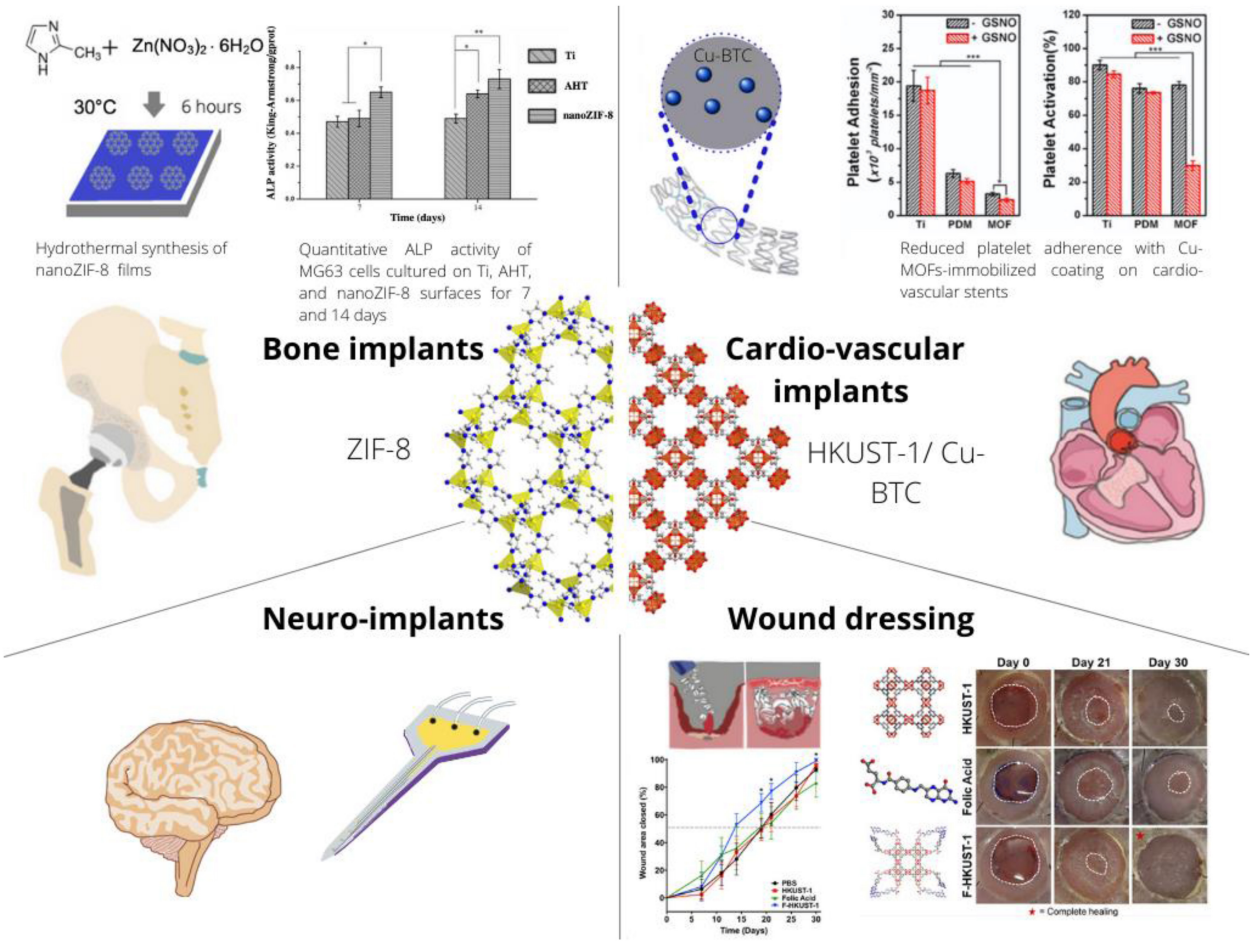

FIGURE 1 | Schematic on the present and envisioned use of MOFs as a component of implants or biomaterial compositions with applications in Tissue Engineering and Regenerative Medicine (TERM). The crystal structure of the prototypical MOF Zeolitic Imidazolate Framework 8 (ZIF-8) is depicted along the [111] crystallographic direction (left side) and HKUST-1 also known as Cu-BTC is depicted along the [001] crystallographic direction. These two different structures have been most frequently applied to TERM research and represent the diverse class of MOFs. In particular, simple exposure of osteoblast like cells to ZIF-8 increases ALP activity (Chen et al., 2017a), Cu-BTC can decrease adherence and activation of platelets (Fan et al., 2019) and also accelerates skin wound closure (Xiao et al., 2018).

messenger molecule during inflammation (Sharma et al., 2007), platelet adhesion (Radomski et al., 1987), ECM deposition (Myers and Tanner, 1998), angiogenesis and other aspects of tissue healing and foreign body response (Schäffer et al., 1996). Beyond the intrinsic catalytic activity, constant release of copper ions is crucial for the biological activity of Cu-BTC. Copper ions are known to stimulate angiogenesis (Sen et al., 2002) and to increase extracellular matrix (ECM) deposition (Gérard et al., 2010). These properties together hold potential to benefit TERM applications of copper-based MOFs when correctly dosed for the intended application.

Electrochemical MOF Coating With Potential Use in Sensors or Electrodes

Electro-deposition of MOFs (Campagnol et al., 2016) may be useful for coating of conductive, implantable electrodes and sensors especially with future applications in neuro-interface engineering.

APPLICATIONS OF MOFs OR MOF BASED BIOMATERIALS IN TERM

MOFs for Orthopedic Implants

Most reports on use of MOFs in TERM applications focus on the improvement of structural bone implants. Indeed, a small but significant fraction of clinical implants fail due to an unfavorable, non-healing wound environment that may be aggravated by bacterial infection (Inacio et al., 2013).

Intrinsic Bioactivity of MOFs and Influence on Bone Tissue Biology

In vitro studies showed significantly improved corrosion resistance of magnesium alloys upon coating with bio-MOF-1, comprising of zinc ions and adenine as well as interconnections of 4,4-biphenyldicarboxylate linkers (Liu et al., 2019). Besides engineering corrosion resistance for better structural integrity, the ability to prevent bacterial infection

is crucial for successful integration of bone implants. Sr-HA (Sr-substituted hydroxyapatite) with MOF74 has demonstrated excellent abilities to inhibit *S. Aureus* and *E. Coli* bacteria and simultaneously induced apoptosis in Saos-2 cancer cells while promoting proliferation and maturation of primary osteoblasts (Zhang et al., 2019).

The effect of different metal ions on bone mineralization and osteogenesis is long known and mechanistic insights have been obtained e.g., for zinc (Kwun et al., 2010) or magnesium (Zhang et al., 2016). Consequently, MOFs were shown to promote osteogenic differentiation *in vitro*, an indicator for a better osteointegration of bone implants. ZIF-8 coatings on titanium implants enhanced ALP activity, better extracellular matrix mineralization and upregulation of osteogenic gene expression in MG63 cells, while suppressing Streptococcus Mutans proliferation (Chen et al., 2017a). Beyond zinc and magnesium, Ca-Sr MOFs could upregulate the expression of ALP, whereas simultaneous release of Ca and Sr provided osteo-inductive signals (Joseph et al., 2019). Further, simultaneous delivery of calcium and strontium ions as well as bisphosphonate linkers was noted to allow better bone mineralization (Matlinska et al., 2019). In the context of regenerative medicine, Mg/HCOOH-MOF was investigated for the treatment of osteoarthritis. This MOF was shown to up-regulate the expression of OCN, Axin2 and down-regulate iNOS and IL-1β, indicating a potentially favorable effect to ease osteoarthritis (Li et al., 2020).

In vivo investigations were less frequently reported, indicating that the field of MOFs for orthopedic applications is just at the beginning of being explored. Mg/Zn-MOF74, was demonstrated to have low toxicity, intrinsic anti-inflammatory and antibacterial features, while improving early osteogenic promotion and angiogenesis *in vivo* (Zhu et al., 2020).

Acquired Bioactivity of MOFs Through Drug Loading for Enhanced Bone Regeneration

Acquired bioactivity refers to any additional biological effect that does not originate from the MOF itself, which can be acquired through encapsulation of drugs, ions or other bioactive agents. MOF-based drug carriers are interesting for orthopedic implant coatings due to their high drug encapsulation capacity with a negligible premature release (Tan et al., 2016).

In vitro studies showed that Poly-l-lactic acid (PLLA) scaffolds coated with copper loaded ZIF-8 promoted osteogenic differentiation as compared to pure PLLA scaffolds while preventing bacterial infection in the presence of Zn^{2+} and Cu^{2+} ions (Telgerd et al., 2019).

Beyond the release of ions, MOFs have unique sustained release abilities for small molecular weight drugs. A sustained release of dexamethasone for 4 weeks was achieved through integrating dexamethasone loaded ZIF-8 into cellulose-hydroxyapatite nanocomposites envisioned for load bearing orthopedic applications (Sarkar et al., 2019). A similar approach has led to silk fibroin-dexamethasone@zeolitic imidazolate framework-8-titanium (SF-DEX@ZIF-8-Ti) composite materials. MC3T3-E1 osteoblast precursor cells cultured on the SF-DEX@ZIF-8-Ti showed enhanced osteo-differentiation (Ran et al., 2018). Hence, current research indicates a good potential of MOFs to facilitate osteointegration of bone implants, thereby improving their clinical outcome. Examples for treating bone diseases include the release of naringin, which improves osseointegration and prevents bacterial infection (Yu et al., 2017), delivery of antitubercular drug for treatment of osteoarticular tuberculosis (Pei et al., 2018) and release of vancomycin for treatment of osteomyelitis (Karakeçili et al., 2019). The versatility of MOF-based drug carriers principally allow the design of elaborate drug release mechanisms tailored to specific triggers. However, only one study describes pH and Ca^{2+} ion dependent release of drugs into the bone environment using a Zr-MOFs capped with CP5-based pseudorotaxanes (Tan et al., 2016).

In vivo studies are less frequently reported. One study investigated implant materials modified with levofloxacin loaded ZIF-8 particles, that resulted in better attachment, proliferation, and differentiation of osteoblasts *in vitro*. Special focus was given on the pH-triggered release in slightly acidic environments resulting from inflammation and bacterial infection. The effectiveness of this implant material was confirmed in terms of osseointegration and antibacterial properties in a rat infected femur model (Tao et al., 2020).

In conclusion, MOFs have been shown to be promising to enhance bone healing through intrinsic and/or acquired properties (**Figure 2**). While the here presented initial studies provide excellent perspectives for the use of MOFs for bone healing, more studies are needed toward their clinical applicability.

MOFs for Cardio-Vascular Implants

Approximately 4% of the population in industrialized societies suffer from coronary artery disease (CAD) requiring intervention (Sanchis-Gomar et al., 2016). Traditionally, anti-thrombotic medication and small molecular weight nitric oxide donors acting as vasodilators are administrated to prevent artery occlusion. In more severe cases, drug-eluting stents are implanted into the artery to prevent occlusion permanently. Copper-based MOFs recently emerged as component in anti-thrombotic coatings for cardio-vascular implants.

In vitro: Cu-BTC was established to be an efficient catalyst for the conversion of blood borne s-nitroso-cysteine to nitric oxide and cysteine (Harding and Reynolds, 2012). More complex Cu-MOFs have subsequently been investigated for catalytic conversion of s-ntirosoglutathione (Neufeld et al., 2017b). This has led to works on MOF/polymer composite materials for nitric oxide release as suitable leads for novel implant materials (Harding and Reynolds, 2014; Neufeld et al., 2015, 2016, 2017a; Zang et al., 2020). In addition to these initial studies, Cu-BTC was directly grown on stent surfaces as SURMOF and investigated *in vitro* showing favorable hemocompatibility (Zhao et al., 2019).

Evaluating non-copper based MOFs for cardiovascular implants, a MIL-101 (Fe) poly(ε−caprolactone) composite was investigated as material for metal free stents, using the MOF as mechanical re-enforcement, sustained drug release vehicle and Magnetic Resonance Imaging (MRI) contrast agent (Hamideh et al., 2020). Further, few studies exist that address the interaction of MOFs with cardiomyocytes (Al-Ansari et al., 2020).

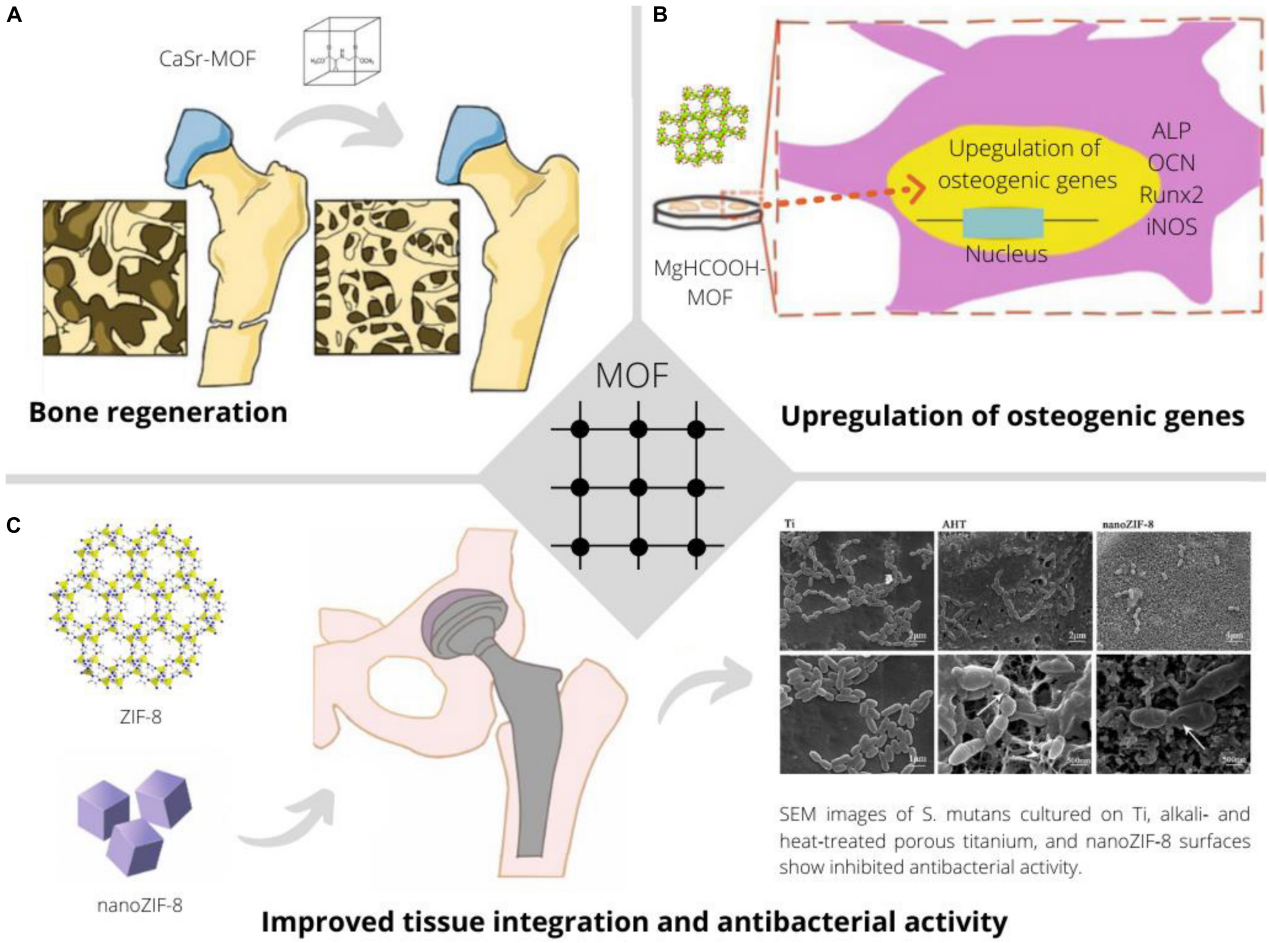

FIGURE 2 | Application of MOFs to improve bone implants through continuous release of earth alkaline ions promoting bone regeneration and biomineralization (Joseph et al., 2019) **(A)**, facilitating osteo-induction and -integration through favorable upregulation of relevant genes in presence of specific MOFs (Li et al., 2020) **(B)** and providing improved tissue integration and an anti-bacterial effect (Chen et al., 2017a) **(C)**.

In vivo, Cu-BTC was shown effective as cardiovascular stent surface modification through coating together with polydopamine (Fan et al., 2019). This significantly reduced protein absorption, thrombus formation, platelet adhesion and an increased vasodilating effect, especially upon systemic injection of nitric oxide donors requiring catalytic degradation. Using a 5-(1H-tetrazol-5-yl)isophthalic acid based MOF with Ni^{2+} and K^{+} ions in another study prevented arrhythmia through reducing the sympathetic excitability in a rat model (Ding et al., 2020). Future studies will need to compare the effectiveness and safety of MOFs with that of clinically used materials.

MOF-Based Biomaterials for Cutaneous Wound Care

The clinical healing outcome of chronic wounds arising from pressure ulcers or injuries of diabetic patients is often unsatisfactory, which motivates research for better cutaneous wound care material. In addition, achieving fast hemostasis and antibacterial properties is important for emergency care equipment and the potential role of MOFs for these two applications is elucidated in the following.

In vitro studies investigated polymer meshes with enclosed Cu-BTC (Zhang et al., 2020) and cellulose based biomaterials with the ability to release nitric oxide (Darder et al., 2020) as wound dressing. To ascribe increased mitochondrial respiration solely to nitric oxide, a titanium-based MOF devoid of intrinsic bioactivity and with controlled release of pre-loaded nitric oxide was proposed to be a copper free alternative (Pinto et al., 2020).

In vivo studies have shown the positive effect of Cu-BTC on skin healing using full-thickness splinted skin wounds in rodents. Dosage forms included folate stabilized Cu-BTC crystal suspensions (Xiao et al., 2018) and hydrogel compositions (Xiao et al., 2017).

Supplementation of zinc ions from ZIF-8 has shown to be similarly effective in a ZIF-8 hydrogel composite membrane (Yao et al., 2020) for wound healing. Combination of zinc and copper ions in MOFs that further encapsulated bioactive molecules promised to be most effective. Along this line of

thought, the encapsulation of niacin loaded copper-/zinc MOFs within alginate shells has shown antibacterial, antioxidant and angiogenic properties, which resulted in significant improvement of wound closure in an infected full-thickness skin defect model (Chen et al., 2019).

Future studies are necessary to ascribe these effects to the synergistic potential of MOFs and not to the presence of its individual components upon dissolution.

MOFs for Neuronal Tissue Engineering and Implants

Traumatic injuries to the nervous system result in dysfunctional regeneration and glial scaring in an inflammatory process leading to loss of nervous tissue. The consequences include physical paralysis of muscles, neurosensory or mental impairment. This has motivated the development of biomaterials for nervous tissue regeneration (Liu and Hsu, 2020), and MOFs may be suitable to further augment positive materials characteristic toward this goal.

In vitro studies focused on assessing the response of sensory neurons to nano-particulate MOFs by employing a neurite outgrowth assay, indicating the potential of a material to promote axonal outgrowth, thus nervous regeneration (Wuttke et al., 2017). The MOFs investigated included iron and chromium salts of trimesic acid (MIL-100) and Zirconium fumarate MOFs. These MOFs did not show reduction in neurite outgrowth at a concentration of 100 μg/ml, indicating their suitability for drug delivery applications. In line with the thought that MOFs are compatible with neuronal biology, treatment of neuronal stem cells with a cobalt MOF having 3,3',5,5' -azobenzenetetracarboxylic acid as linker was envisioned to benefit therapies for spinal cord injury. This was due to molecular docking studies revealing potential binding of the MOF with the trkA receptor, which led to activation of PI3K/Akt signaling and enhanced nerve growth factor (NGF) production *in vitro*. NGF is responsible for neuron growth and survival (Cao et al., 2020).

MOF based drug delivery vehicles include cationic MOF-74-Fe(III) with low cytotoxicity on PC12 neuron cells and high drug loading due to electrostatic accumulation (Hu et al., 2014) of ibuprofen, which is known to reduce neuroinflammation (Wixey et al., 2019) and is passively released from the MOF. An example for actively triggered dopamine release by magnetophoretic means was demonstrated using MIL-88A (iron(III) fumarate) encapsulated iron oxide particles (Pinna et al., 2018). A drug delivery mechanism that is triggered upon synaptic transmission can be achieved using adenosine triphosphate (ATP) responsive release of drugs. Here, a MOF based on Zr^{4+} ions and amino-triphenyldicarboxylic acid was capped with aptamers specific for ATP, leading to an un-locking effect upon binding and drug release (Chen et al., 2017b). These three examples of passive-, triggered- and targeted drug release show the versatility of MOF based drug delivery for neurobiological applications. Systemic injection requires MOF particles to cross the blood-brain barrier. This ability was assessed for e.g., ZIF-8 particles through crossing an hCMEC/D3 brain endothelial cell membrane (Chiacchia et al., 2015). Future studies in this direction would benefit from microfluidic vascular transport models for nanoparticles (Ho et al., 2017) involving pericytes to better emulate the blood-brain barrier and to study the biological response of further cell types in inflammation and healing (Beyer et al., 2018a; Blocki et al., 2018).

In vivo studies reported the use of a Cu(II) MOF in a mixed linker approach with 5-methylisophthalic acid and 1,3-bis(5,6-dimethylbenzimidazol-1-yl)propane (Tian and Tian, 2020). This MOF inhibited dopaminergic neurons, decreased expression of dopamine reporters, decreased dopamine release, reduced apoptosis and increased Wnt1-Nkx2.2 activation. The MOF was presumably injected on a systemic level into LgDel ± mice and biological effects were observed in a dose dependent manner up to 5 mg/kg body weight. No comparison of the biological effect upon injection of the MOF or a solution containing only the ligand was made.

A very inspiring study used MIL-100 (Fe) as a drug carrier for siSOX9 and retinoic acid in combination with co-encapsulated ceria based nanozymes to reduce oxidative stress (Yu et al., 2020). This complex drug formulation was incubated with neuronal stem cells (NSCs) isolated from newborn mice prior to NSC transplantation at sites of lesions. The co-release of soSOX9 and retinoic acid promoted neuro-differentiation and reduced oxidative stress prevented newborn neurons from apoptosis. The studies were carried out with 11-month old APPswe/PS1M146V/TauP301L triple transgenic mice, a model for Alzheimer's disease. The positive effect of the MOF based drug combination was shown through cognitive improvements in a Morris Water Maze test and histopathological improvements.

These inspiring *in vitro* and *in vivo* works have highlighted a clear potential of MOFs to treat neurological disorders. Very few macroscopic biomaterials have been developed along this thought and future studies should include evaluating the opportunity to improve implant-nervous tissue interfaces with these materials.

CONCLUSION AND OUTLOOK

The presented *in vitro* and *in vivo* data are impressive in terms of the strong biological response that MOFs elicit toward a positive healing outcome in various tissues and applications. However, more efforts are required to understand the basic dose dependent response of individual cell types and tissues to different MOFs. In addition, concerns about the safety of some organic linkers of MOFs need to be eliminated or alternative linkers considered save for clinical applications must be shown effective in yielding MOFs with similar properties. This is essential before MOF based biomaterials for TERM applications will commence improving healing outcomes in the treatment of human patients.

AUTHOR CONTRIBUTIONS

MS reviewed literature related to orthopedic implants and cutaneous wound care and designed the figures. JR reviewed

literature related to neuronal TERM applications. XL reviewed literature related to nitric oxide producing biomaterials. JM reviewed literature related to MOF & polymer composite materials. AB and SB wrote the manuscript. SB guided the review process. All authors contributed to the article and approved the submitted version.

FUNDING

This work was supported by grant 4055120 to SB through Faculty of Engineering of The Chinese University of Hong Kong (CUHK). SB appreciates the research budget provided by the Department of Biomedical Engineering of CUHK.

REFERENCES

Akhmetova, I., Beyer, S., Schutjajew, K., Tichter, T., Wilke, M., Prinz, C., et al. (2019). Cadmium benzylphosphonates – the close relationship between structure and properties. *Cryst. Eng. Comm.* 21, 5958–5964. doi: 10.1039/C9CE00776H

Al-Ansari, D. E., Mohamed, N. A., Marei, I., Zekri, A., Kameno, Y., Davies, R. P., et al. (2020). Internalization of metal–organic framework nanoparticles in human vascular cells: implications for cardiovascular disease therapy. *Nanomaterials* 10:1028. doi: 10.3390/nano10061028

Albee, F. H. (1920). Studies in bone growth triple calcium phosphate as a stimulus to osteogenesis. *Ann. Surg.* 71, 32–39.

Al-Terkawi, A.-A., Scholz, G., Buzanich, A. G., Reinsch, S., Emmerling, F., and Kemnitz, E. (2017). Ca- and Sr-tetrafluoroisophthalates: mechanochemical synthesis, characterization, and ab initio structure determination. *Dalt. Trans.* 46, 6003–6012. doi: 10.1039/C7DT00734E

Banerjee, R., Furukawa, H., Britt, D., Knobler, C., O'Keeffe, M., and Yaghi, O. M. (2009). Control of pore size and functionality in isoreticular zeolitic imidazolate frameworks and their carbon dioxide selective capture properties. *J. Am. Chem. Soc.* 131, 3875–3877. doi: 10.1021/ja809459e

Banerjee, S., Lollar, C. T., Xiao, Z., Fang, Y., and Zhou, H. C. (2020). Biomedical integration of metal–organic frameworks. *Trends Chem.* 2, 467–479. doi: 10.1016/j.trechm.2020.01.007

Campagnol, N., Van Assche, T. R. C., Li, M., Stappers, L., Dinca, M., Denayer, J. F. M., et al. (2016). On the electrochemical deposition of metal-organic frameworks. *J. Mater. Chem. A* 4, 3914–3925. doi: 10.1039/c5ta10782b

Beyer, S., Koch, M., Lee, Y., Jung, F., and Blocki, A. (2018a). An in vitro model of angiogenesis during wound healing provides insights into the complex role of cells and factors in the inflammatory and proliferation phase. *Int. J. Mol. Sci.* 19:2913. doi: 10.3390/ijms19102913

Beyer, S., Schürmann, R., Feldmann, I., Blocki, A., Bald, I., Schneider, R. J., et al. (2018b). Maintaining stable Zeolitic Imidazolate Framework (ZIF) templates during polyelectrolyte multilayer coating. *Colloids Interface Sci. Commun.* 22, 14–17. doi: 10.1016/j.colcom.2017.11.004

Beyer, S., Prinz, C., Schürmann, R., Feldmann, I., Zimathies, A., Blocki, A. M., et al. (2016). Ultra-Sonication of ZIF-67 crystals results in ZIF-67 nano-flakes. *ChemistrySelect* 1, 5905–5908. doi: 10.1002/slct.201601513

Blocki, A., Beyer, S., Jung, F., and Raghunath, M. (2018). The controversial origin of pericytes during angiogenesis - implications for cell-based therapeutic angiogenesis and cell-based therapies. *Clin. Hemorheol. Microcirc.* 69, 215–232. doi: 10.3233/CH-189132

Cao, C., Li, Z. Z., Zhang, Z. Q., and Chen, X. H. (2020). A new porous cationic metal–organic framework: selective sorption of organic dyes and treatment on neural stem cells during spinal cord injury treatment. *J. Iran. Chem. Soc.* 17, 2933–2942. doi: 10.1007/s13738-020-01969-1960

Chapartegui-Arias, A., Villajos, J. A., Myxa, A., Beyer, S., Falkenhagen, J., Schneider, R. J., et al. (2019). Covalently fluorophore-functionalized ZIF-8 colloidal particles as a sensing platform for endocrine-disrupting chemicals such as phthalates plasticizers. *ACS Omega* 4, 17090–17097. doi: 10.1021/acsomega.9b01051

Chen, G., Yu, Y., Wu, X., Wang, G., Gu, G., Wang, F., et al. (2019). Microfluidic electrospray niacin metal-organic frameworks encapsulated microcapsules for wound healing. *Research* 2019:6175398. doi: 10.34133/2019/6175398

Chen, J., Zhang, X., Huang, C., Cai, H., Hu, S., Wan, Q., et al. (2017a). Osteogenic activity and antibacterial effect of porous titanium modified with metal-organic framework films. *J. Biomed. Mater. Res. - Part A.* 105, 834–846. doi: 10.1002/jbm.a.35960

Chen, W.-H., Yu, X., Liao, W.-C., Sohn, Y. S., Cecconello, A., Kozell, A., et al. (2017b). ATP-Responsive aptamer-based metal-organic framework nanoparticles (NMOFs) for the controlled release of loads and drugs. *Adv. Funct. Mater.* 27:1702102. doi: 10.1002/adfm.201702102

Chiacchia, M., Cerutti, C., Gromnicova, R., Rietdorf, K., Romero, I. A., and Bradshaw, D. (2015). Zinc-imidazolate polymers (ZIPs) as a potential carrier to brain capillary endothelial cells. *J. Mater. Chem. B* 3, 9053–9059. doi: 10.1039/C5TB01814E

Chui, S. S. Y. (1999). A chemically functionalizable nanoporous material [Cu3(TMA)2(H2O)3]n. *Science* 283, 1148–1150. doi: 10.1126/science.283.5405.1148

Darder, M., Karan, A., Real, G., del, and DeCoster, M. A. (2020). Cellulose-based biomaterials integrated with copper-cystine hybrid structures as catalysts for nitric oxide generation. *Mater. Sci. Eng. C* 108:110369. doi: 10.1016/j.msec.2019.110369

de Groot, K. (1993). Clinical applications of calcium phosphate biomaterials: a review. *Ceram. Int.* 19, 363–366. doi: 10.1016/0272-8842(93)90050-90052

Ding, C., Zhang, W., Xu, Z., Zhang, H., and Zheng, J. (2020). A new heterometallic MOF with 1D nano-sized channels for cyanosilylation reaction and prevention effect against arrhythmia by reducing the sympathetic excitability. *J. Exp. Nanosci.* 15, 87–96. doi: 10.1080/17458080.2020.1729356

Duan, Y., Ye, F., Huang, Y., Qin, Y., He, C., and Zhao, S. (2018). One-pot synthesis of a metal–organic framework-based drug carrier for intelligent glucose-responsive insulin delivery. *Chem. Commun.* 54, 5377–5380. doi: 10.1039/C8CC02708K

Eddaoudi, M., Kim, J., Rosi, N., Vodak, D., Wachter, J., O'Keeffe, M., et al. (2002). Systematic design of pore size and functionality in isoreticular MOFs and their application in methane storage. *Science* 295, 469–472. doi: 10.1126/science.1067208

Fan, Y., Zhang, Y., Zhao, Q., Xie, Y., Luo, R., Yang, P., et al. (2019). Immobilization of nano Cu-MOFs with polydopamine coating for adaptable gasotransmitter generation and copper ion delivery on cardiovascular stents. *Biomaterials* 204, 36–45. doi: 10.1016/j.biomaterials.2019.03.007

Gao, S., Hou, J., Deng, Z., Wang, T., Beyer, S., Buzanich, A. G., et al. (2019). Improving the acidic stability of zeolitic imidazolate frameworks by biofunctional molecules. *Chemistry* 5, 1597–1608. doi: 10.1016/j.chempr.2019.03.025

Gérard, C., Bordeleau, L. J., Barralet, J., and Doillon, C. J. (2010). The stimulation of angiogenesis and collagen deposition by copper. *Biomaterials* 31, 824–831. doi: 10.1016/j.biomaterials.2009.10.009

Hamideh, R. A., Akbari, B., Fathi, P., Misra, S. K., Sutrisno, A., Lam, F., et al. (2020). Biodegradable MRI visible drug eluting stent reinforced by metal organic frameworks. *Adv. Healthc. Mater.* 9:2000136. doi: 10.1002/adhm.202000136

Harding, J. L., and Reynolds, M. M. (2012). Metal organic frameworks as nitric oxide catalysts. *J. Am. Chem. Soc.* 134, 3330–3333. doi: 10.1021/ja210771m

Harding, J. L., and Reynolds, M. M. (2014). Composite materials with embedded metal organic framework catalysts for nitric oxide release from bioavailable S-nitrosothiols. *J. Mater. Chem. B* 2, 2530–2536. doi: 10.1039/C3TB21458C

Ho, Y. T., Adriani, G., Beyer, S., Nhan, P. T., Kamm, R. D., and Kah, J. C. Y. (2017). A facile method to probe the vascular permeability of nanoparticles in nanomedicine applications. *Sci. Rep.* 7:707. doi: 10.1038/s41598-017-00750-753

Ho, P. H., Salles, F., Di Renzo, F., and Trens, P. (2020). One-pot synthesis of 5-FU@ZIF-8 and ibuprofen@ZIF-8 nanoparticles. *Inorganica Chim. Acta* 500:119229. doi: 10.1016/j.ica.2019.119229

Hu, Q., Yu, J., Liu, M., Liu, A., Dou, Z., and Yang, Y. (2014). A low cytotoxic cationic metal–organic framework carrier for controllable drug release. *J. Med. Chem.* 57, 5679–5685. doi: 10.1021/jm5004107

Inacio, M. C. S., Ake, C. F., Paxton, E. W., Khatod, M., Wang, C., Gross, T. P., et al. (2013). Sex and risk of hip implant failure. *JAMA Intern. Med.* 173:435. doi: 10.1001/jamainternmed.2013.3271

Joseph, N., Lawson, H. D., Overholt, K. J., Damodaran, K., Gottardi, R., Acharya, A. P., et al. (2019). Synthesis and characterization of CaSr-Metal organic frameworks for biodegradable orthopedic applications. *Sci. Rep.* 9:13024. doi: 10.1038/s41598-019-49536-49539

Karakeçili, A., Topuz, B., Korpayev, S., and Erdek, M. (2019). Metal-organic frameworks for on-demand pH controlled delivery of vancomycin from chitosan scaffolds. *Mater. Sci. Eng. C* 105:110098. doi: 10.1016/j.msec.2019.110098

Keskin, S., and Kizilel, S. (2011). Biomedical applications of metal organic frameworks. *Ind. Eng. Chem. Res.* 50, 1799–1812. doi: 10.1021/ie101312k

Kulow, A., Witte, S., Beyer, S., Guilherme Buzanich, A., Radtke, M., Reinholz, U., et al. (2019). A new experimental setup for time- and laterally-resolved X-ray absorption fine structure spectroscopy in a 'single shot.'. *J. Anal. At. Spectrom.* 34, 239–246. doi: 10.1039/C8JA00313K

Kwun, I.-S., Cho, Y.-E., Lomeda, R.-A. R., Shin, H.-I., Choi, J.-Y., Kang, Y.-H., et al. (2010). Zinc deficiency suppresses matrix mineralization and retards osteogenesis transiently with catch-up possibly through Runx 2 modulation. *Bone* 46, 732–741. doi: 10.1016/j.bone.2009.11.003

Lansdown, A. B. G., Mirastschijski, U., Stubbs, N., Scanlon, E., and Ågren, M. S. (2007). Zinc in wound healing: theoretical, experimental, and clinical aspects. *Wound Repair Regen.* 15, 2–16. doi: 10.1111/j.1524-475X.2006.00179.x

Li, X., Qi, M., Li, C., Dong, B., Wang, J., Weir, M. D., et al. (2019). Novel nanoparticles of cerium-doped zeolitic imidazolate frameworks with dual benefits of antibacterial and anti-inflammatory functions against periodontitis. *J. Mater. Chem. B* 7, 6955–6971. doi: 10.1039/C9TB01743G

Li, Z., Peng, Y., Pang, X., and Tang, B. (2020). Potential therapeutic effects of Mg/HCOOH metal organic framework on relieving osteoarthritis. *Chem. Med. Chem.* 15, 13–16. doi: 10.1002/cmdc.201900546

Liang, K., Coghlan, C. J., Bell, S. G., Doonan, C., and Falcaro, P. (2015a). Enzyme encapsulation in zeolitic imidazolate frameworks: a comparison between controlled co-precipitation and biomimetic mineralisation. *Chem. Commun.* 52, 473–476. doi: 10.1039/c5cc07577g

Liang, K., Ricco, R., Doherty, C. M., Styles, M. J., Bell, S., Kirby, N., et al. (2015b). Biomimetic mineralization of metal-organic frameworks as protective coatings for biomacromolecules. *Nat. Commun.* 6:7240. doi: 10.1038/ncomms8240

Liédana, N., Galve, A., Rubio, C., Téllez, C., and Coronas, J. (2012). CAF@ZIF-8: one-step encapsulation of caffeine in MOF. *ACS Appl. Mater. Interfaces* 4, 5016–5021. doi: 10.1021/am301365h

Liu, W., Yan, Z., Zhang, Z., Zhang, Y., Cai, G., and Li, Z. (2019). Bioactive and anti-corrosive bio-MOF-1 coating on magnesium alloy for bone repair application. *J. Alloys Compd.* 788, 705–711. doi: 10.1016/j.jallcom.2019.02.281

Liu, Y., and Hsu, S. (2020). Biomaterials and neural regeneration. *Neural Regen. Res.* 15:1243. doi: 10.4103/1673-5374.272573

Maleki, A., Shahbazi, M., Alinezhad, V., and Santos, H. A. (2020). The progress and prospect of zeolitic imidazolate frameworks in cancer therapy, antibacterial activity, and biomineralization. *Adv. Healthc. Mater.* 9:2000248. doi: 10.1002/adhm.202000248

Matlinska, M. A., Ha, M., Hughton, B., Oliynyk, A. O., Iyer, A. K., Bernard, G. M., et al. (2019). Alkaline earth metal–organic frameworks with tailorable ion release: a path for supporting biomineralization. *ACS Appl. Mater. Interfaces* 11, 32739–32745. doi: 10.1021/acsami.9b11004

Myers, P. R., and Tanner, M. A. (1998). Vascular endothelial cell regulation of extracellular matrix collagen: role of nitric oxide. *Arterioscler. Thromb. Vasc. Biol.* 18, 717–722. doi: 10.1161/01.ATV.18.5.717

Neufeld, M. J., Harding, J. L., and Reynolds, M. M. (2015). Immobilization of metal-organic framework copper(II) benzene-1,3,5-tricarboxylate (CuBTC) onto cotton fabric as a nitric oxide release catalyst. *ACS Appl. Mater. Interfaces* 7, 26742–26750. doi: 10.1021/acsami.5b08773

Neufeld, M. J., Lutzke, A., Jones, W. M., and Reynolds, M. M. (2017a). Nitric oxide generation from endogenous substrates using metal-organic frameworks: inclusion within poly(vinyl alcohol) membranes to investigate reactivity and therapeutic potential. *ACS Appl. Mater. Interfaces.* 9, 35628–35641. doi: 10.1021/acsami.7b11846

Neufeld, M. J., Lutzke, A., Tapia, J. B., and Reynolds, M. M. (2017b). Metal-Organic framework/chitosan hybrid materials promote nitric oxide release from S-nitrosoglutathione in aqueous solution. *ACS Appl. Mater. Interfaces.* 9, 5139–5148. doi: 10.1021/acsami.6b14937

Neufeld, M. J., Ware, B. R., Lutzke, A., Khetani, S. R., and Reynolds, M. M. (2016). Water-Stable metal-organic framework/polymer composites compatible with human hepatocytes. *ACS Appl. Mater. Interfaces.* 8, 19343–19352. doi: 10.1021/acsami.6b05948

Ni, Z., and Masel, R. I. (2006). Rapid production of metal-organic frameworks via microwave-assisted solvothermal synthesis. *J. Am. Chem. Soc.* 128, 12394–12395. doi: 10.1021/ja0635231

Pan, H. M., Beyer, S., Zhu, Q., and Trau, D. (2013). Inwards interweaving of polymeric layers within hydrogels: assembly of spherical multi-shells with discrete porosity differences. *Adv. Funct. Mater.* 23, 5108–5115. doi: 10.1002/adfm.201300733

Park, K. S., Ni, Z., Côté, A. P., Choi, J. Y., Huang, R., Uribe-Romo, F. J., et al. (2006). Exceptional chemical and thermal stability of zeolitic imidazolate frameworks. *Proc. Natl. Acad. Sci. U S A.* 103, 10186–10191. doi: 10.1073/pnas.0602439103

Pei, P., Tian, Z., and Zhu, Y. (2018). 3D printed mesoporous bioactive glass/metal-organic framework scaffolds with antitubercular drug delivery. *Microporous Mesoporous Mater.* 272, 24–30. doi: 10.1016/j.micromeso.2018.06.012

Pinna, A., Ricco', R., Migheli, R., Rocchitta, G., Serra, P. A., Falcaro, P., et al. (2018). A MOF-based carrier for in situ dopamine delivery. *RSC Adv.* 8, 25664–25672. doi: 10.1039/C8RA04969F

Pinto, R. V., Wang, S., Tavares, S. R., Pires, J., Antunes, F., Vimont, A., et al. (2020). Tuning cellular biological functions through the controlled release of NO from a porous Ti-MOF. *Angew. Chemie Int. Ed.* 59, 5135–5143. doi: 10.1002/anie.201913135

Radomski, M. W., Palmer, R. M. J., and Moncada, S. (1987). Endogenous nitric oxide inhibits human platelet adhesion to vascular endothelium. *Lancet* 2, 1057–1058. doi: 10.1016/S0140-6736(87)91481-91484

Ran, J., Zeng, H., Cai, J., Jiang, P., Yan, P., Zheng, L., et al. (2018). Rational design of a stable, effective, and sustained dexamethasone delivery platform on a titanium implant: an innovative application of metal organic frameworks in bone implants. *Chem. Eng. J.* 333, 20–33. doi: 10.1016/j.cej.2017.09.145

Rojas, S., Devic, T., and Horcajada, P. (2017). Metal organic frameworks based on bioactive components. *J. Mater. Chem. B* 5, 2560–2573. doi: 10.1039/C6TB03217F

Sanchis-Gomar, F., Perez-Quilis, C., Leischik, R., and Lucia, A. (2016). Epidemiology of coronary heart disease and acute coronary syndrome. *Ann. Transl. Med.* 4:256. doi: 10.21037/atm.2016.06.33

Sarkar, C., Chowdhuri, A. R., Garai, S., Chakraborty, J., and Sahu, S. K. (2019). Three-dimensional cellulose-hydroxyapatite nanocomposite enriched with dexamethasone loaded metal–organic framework: a local drug delivery system for bone tissue engineering. *Cellulose* 26, 7253–7269. doi: 10.1007/s10570-019-02618-2613

Schäffer, M. R., Tantry, U., Gross, S. S., Wasserkrug, H. L., and Barbul, A. (1996). Nitric oxide regulates wound healing. *J. Surg. Res.* 63, 237–240. doi: 10.1006/jsre.1996.0254

Sen, C. K., Khanna, S., Venojarvi, M., Trikha, P., Christopher Ellison, E., Hunt, T. K., et al. (2002). Copper-induced vascular endothelial growth factor expression and wound healing. *Am. J. Physiol. - Hear. Circ. Physiol.* 282, H1821–H1827. doi: 10.1152/ajpheart.01015.2001

Sharma, J. N., Al-Omran, A., and Parvathy, S. S. (2007). Role of nitric oxide in inflammatory diseases. *Inflammopharmacology* 15, 252–259. doi: 10.1007/s10787-007-0013-x

Stolar, T., and Užareviæ, K. (2020). Mechanochemistry: an efficient and versatile toolbox for synthesis, transformation, and functionalization of porous metal-organic frameworks. *CrystEngComm* 22, 4511–4525. doi: 10.1039/d0ce00091d

Su, Y., Cockerill, I., Wang, Y., Qin, Y.-X., Chang, L., Zheng, Y., et al. (2019). Zinc-Based biomaterials for regeneration and therapy. *Trends Biotechnol.* 37, 428–441. doi: 10.1016/j.tibtech.2018.10.009

Tan, L.-L., Song, N., Zhang, S. X.-A., Li, H., Wang, B., and Yang, Y.-W. (2016). Ca 2+, pH and thermo triple-responsive mechanized Zr-based MOFs for on-command drug release in bone diseases. *J. Mater. Chem. B* 4, 135–140. doi: 10.1039/C5TB01789K

Tao, B., Zhao, W., Lin, C., Yuan, Z., He, Y., Lu, L., et al. (2020). Surface modification of titanium implants by ZIF-8@Levo/LBL coating for inhibition of bacterial-associated infection and enhancement of in vivo osseointegration. *Chem. Eng. J.* 390:124621. doi: 10.1016/j.cej.2020.124621

Telgerd, M. D., Sadeghinia, M., Birhanu, G., Daryasari, M. P., Zandi-Karimi, A., Sadeghinia, A., et al. (2019). Enhanced osteogenic differentiation of

mesenchymal stem cells on metal–organic framework based on copper, zinc, and imidazole coated poly- l -lactic acid nanofiber scaffolds. *J. Biomed. Mater. Res. Part A* 107, 1841–1848. doi: 10.1002/jbm.a.36707

Tian, S., and Tian, D. (2020). A water-stable Cu(II)-based coordination polymer for clinical nursing effect on schizophrenia by inhibiting over-activity of the dopaminergic neurons. *Supramol. Chem.* 32, 365–372. doi: 10.1080/10610278.2020.1739285

Wang, Y., Yan, J., Wen, N., Xiong, H., Cai, S., He, Q., et al. (2020). Metal-organic frameworks for stimuli-responsive drug delivery. *Biomaterials* 230:119619. doi: 10.1016/j.biomaterials.2019.119619

Wixey, J. A., Sukumar, K. R., Pretorius, R., Lee, K. M., Colditz, P. B., Bjorkman, S. T., et al. (2019). Ibuprofen treatment reduces the neuroinflammatory response and associated neuronal and white matter impairment in the growth restricted newborn. *Front. Physiol.* 10:541. doi: 10.3389/fphys.2019.00541

Wuttke, S., Zimpel, A., Bein, T., Braig, S., Stoiber, K., Vollmar, A., et al. (2017). Validating metal-organic framework nanoparticles for their nanosafety in diverse biomedical applications. *Adv. Healthc. Mater.* 6:1600818. doi: 10.1002/adhm.201600818

Xiao, J., Chen, S., Yi, J., Zhang, H. F., and Ameer, G. A. (2017). A cooperative copper metal–organic framework-hydrogel system improves wound healing in diabetes. *Adv. Funct. Mater.* 27:1604872. doi: 10.1002/adfm.201604872

Xiao, J., Zhu, Y., Huddleston, S., Li, P., Xiao, B., Farha, O. K., et al. (2018). Copper metal-organic framework nanoparticles stabilized with folic acid improve wound healing in diabetes. *ACS Nano* 12, 1023–1032. doi: 10.1021/acsnano.7b01850

Yaghi, O. M., Li, G., and Li, H. (1995). Selective binding and removal of guests in a microporous metal–organic framework. *Nature* 378, 703–706. doi: 10.1038/378703a0

Yaghi, O. M., and Li, H. (1995). Hydrothermal synthesis of a metal-organic framework containing large rectangular channels. *J. Am. Chem. Soc.* 117, 10401–10402. doi: 10.1021/ja00146a033

Yao, X., Zhu, G., Zhu, P., Ma, J., Chen, W., Liu, Z., et al. (2020). Omniphobic ZIF-8@Hydrogel membrane by microfluidic-emulsion-templating method for wound healing. *Adv. Funct. Mater.* 30:1909389. doi: 10.1002/adfm.201909389

Yu, D., Ma, M., Liu, Z., Pi, Z., Du, X., Ren, J., et al. (2020). MOF-encapsulated nanozyme enhanced siRNA combo: control neural stem cell differentiation and ameliorate cognitive impairments in Alzheimer's disease model. *Biomaterials* 255:120160. doi: 10.1016/j.biomaterials.2020.120160

Yu, M., You, D., Zhuang, J., Lin, S., Dong, L., Weng, S., et al. (2017). Controlled release of naringin in metal-organic framework-loaded mineralized collagen coating to simultaneously enhance osseointegration and antibacterial activity. *ACS Appl. Mater. Interfaces* 9, 19698–19705. doi: 10.1021/acsami.7b05296

Zang, Y., Roberts, T. R., Batchinsky, A. I., and Reynolds, M. M. (2020). Metal–Organic framework polymer coating inhibits staphylococcus aureus attachment on medical circulation tubing under static and dynamic flow conditions. *ACS Appl. Bio Mater.* 3, 3535–3543. doi: 10.1021/acsabm.0c00151

Zhang, P., Li, Y., Tang, Y., Shen, H., Li, J., Yi, Z., et al. (2020). Copper-Based metal–organic framework as a controllable nitric oxide-releasing vehicle for enhanced diabetic wound healing. *ACS Appl. Mater. Interfaces* 12, 18319–18331. doi: 10.1021/acsami.0c01792

Zhang, Y., Shen, X., Ma, P., Peng, Z., and Cai, K. (2019). Composite coatings of Mg-MOF74 and Sr-substituted hydroxyapatite on titanium substrates for local antibacterial, anti-osteosarcoma and pro-osteogenesis applications. *Mater. Lett.* 241, 18–22. doi: 10.1016/j.matlet.2019.01.033

Zhang, Y., Xu, J., Ruan, Y. C., Yu, M. K., O'Laughlin, M., Wise, H., et al. (2016). Implant-derived magnesium induces local neuronal production of CGRP to improve bone-fracture healing in rats. *Nat. Med.* 22, 1160–1169. doi: 10.1038/nm.4162

Zhao, Q., Fan, Y., Zhang, Y., Liu, J., Li, W., and Weng, Y. (2019). Copper-Based SURMOFs for nitric oxide generation: hemocompatibility, vascular cell growth, and tissue response. *ACS Appl. Mater. Interfaces* 11, 7872–7883. doi: 10.1021/acsami.8b22731

Zhu, Z., Jiang, S., Liu, Y., Gao, X., Hu, S., Zhang, X., et al. (2020). Micro or nano: evaluation of biosafety and biopotency of magnesium metal organic framework-74 with different particle sizes. *Nano Res.* 13, 511–526. doi: 10.1007/s12274-020-2642-y

Conflict of Interest: The authors declare that the research was conducted in the absence of any commercial or financial relationships that could be construed as a potential conflict of interest.

frontiers in Bioengineering and Biotechnology

ORIGINAL RESEARCH
published: 14 June 2021
doi: 10.3389/fbioe.2021.674384

Ultra-Thin Porous PDLLA Films Promote Generation, Maintenance, and Viability of Stem Cell Spheroids

*Ya An Tsai[1], Tianshu Li[2], Lucia A. Torres-Fernández[3], Stefan C. Weise[3], Waldemar Kolanus[3] and Shinji Takeoka[1,2]**

[1] Department of Life Science and Medical Bioscience, Graduate School of Advanced Science and Engineering, Waseda University (TWIns), Tokyo, Japan, [2] Institute for Advanced Research of Biosystem Dynamics, Research Institute for Science and Engineering, Waseda University, Tokyo, Japan, [3] Life and Medical Sciences Institute (LIMES), University of Bonn, Bonn, Germany

OPEN ACCESS

Edited by:
Xin Zhao,
Hong Kong Polytechnic University,
Hong Kong

Reviewed by:
Pei Feng,
Central South University, China
Giovanni Vozzi,
University of Pisa, Italy
Jiashen Li,
The University of Manchester,
United Kingdom

***Correspondence:**
Shinji Takeoka
takeoka@waseda.jp

Specialty section:
This article was submitted to Biomaterials, a section of the journal Frontiers in Bioengineering and Biotechnology

Received: 01 March 2021
Accepted: 05 May 2021
Published: 14 June 2021

Citation:
Tsai YA, Li T, Torres-Fernández LA, Weise SC, Kolanus W and Takeoka S (2021) Ultra-Thin Porous PDLLA Films Promote Generation, Maintenance, and Viability of Stem Cell Spheroids. Front. Bioeng. Biotechnol. 9:674384. doi: 10.3389/fbioe.2021.674384

Three-dimensional (3D) culture bridges and minimizes the gap between *in vitro* and *in vivo* states of cells and various 3D culture systems have been developed according to different approaches. However, most of these approaches are either complicated to operate, or costive to scale up. Therefore, a simple method for stem cell spheroid formation and preservation was proposed using poly(D,L-lactic acid) porous thin film (porous nanosheet), which were fabricated by a roll-to-roll gravure coating method combining a solvent etching process. The obtained porous nanosheet was less than 200 nm in thickness and had an average pore area of 6.6 μm^2 with a porosity of 0.887. It offered a semi-adhesive surface for stem cells to form spheroids and maintained the average spheroid diameter below 100 μm for 5 days. In comparison to the spheroids formed in suspension culture, the porous nanosheets improved cell viability and cell division rate, suggesting the better feasibility to be applied as 3D culture scaffolds.

Keywords: ultra-thin film, porous nanosheet, PDLLA, 3D spheroid culture, cell viability, cell division

INTRODUCTION

Two-dimensional (2D) cell culture on tissue plates is commonly performed in *in vitro* cell biology studies, allowing researchers to study how cells expand, behave under various stresses, proliferate and/or differentiate in response to stimuli. Monolayer incubation, however, lacks fundamental cell-cell and cell-matrix interactions as well as direct cell-to-cell exchange of chemical cues, thus limiting our understanding on how cells behave *in vivo*. Compared to 2D cell culture, three-dimensional (3D) culture bridges the gap between cell physiology and *in vitro* cell culture and improves *in vitro* to close-to-*in vivo* research. It provides more practical tool in basic and applied research to broaden the perspective of cell biology.

3D cell aggregates (spheroids) generate an inherent nutrient and oxygen gradient within their structure and constitute an *in vivo* microenvironment. Previous studies using 3D arranged cells uncovered mechanisms involved in tumorigenesis (Lv et al., 2017) and in maintaining expression of specific biomarkers due to enhanced extracellular matrix (ECM) (Bazou, 2010), and demonstrated the ability of spheroids to serve for drug evaluation and development. Stem cell spheroids are especially promising to improve the therapeutic effects of stem cell therapy through raised

cell viability, cell secretomes and differentiation ability (Park et al., 2017). Embryonic stem cell spheroids have shown multiple functional capabilities in development and differentiation (McKee and Chaudhry, 2017). In addition, mesenchymal stem cells cultured in 3D systems exhibit secretion of anti-inflammatory factors (Bartosh et al., 2010), enhanced cell survival (Emmert et al., 2013) and the osteogenic differentiation ability for bone regeneration application (Yamaguchi et al., 2014).

3D cultures made in different culture environments aid in our understanding of cell physiology changes by cell morphology observation, cytoskeleton examination, and cell-cell junction visualization within aggregates. Numerous techniques have been published for 3D cell cultures and classified according to the methodology of scaffold-free or scaffold-based systems. Scaffold-free techniques based on non- or limited support provide low-cost, simple and rapid cell aggregation via gravitation from the hanging drop and pellet culture methods (Santos et al., 2015; Xu et al., 2016) to form spheroids. These spheroids are easy to harvest but difficult to expand in a continuous passage (Lv et al., 2017). On the other hand, scaffold-based systems could construct a culture environment that is much closer to the *in vivo* conditions. For example, chitosan-based scaffolds or gel-supported embeddings chemically interact with cell spheroids, provide dense ECM signal connections and induce focal adhesion protein expressions (Huang et al., 2011; Zujur et al., 2017). However, these techniques require relatively complicated chemical reactions (Kim et al., 2013) and are costly in large-scale production (Lv et al., 2017). Therefore, economic biomaterials and easy-to-handle procedures are desired to achieve large-scale 3D cultures.

We have developed nanosheets with biocompatible and biodegradable organic polymers which are free-standing thin films, with tens or hundreds of nanometers in thinness (Fujie, 2016). They are suitable to be applied in a variety of biomedical applications such as an alternative to bio-membranes, for drug loading or as wound dressing materials (Fujie, 2016). They were also applied as wrapping materials to achieve high-quality live imaging of tissue and suspension cells (Zhang et al., 2017, 2018).

The tissue-biomaterial interface is pivotal in regulating the cellular interactions, for example cell adhesion, morphology, orientation, motility, proliferation, and differentiation as well as other intracellular events. Conventional lithographic techniques using photoresists and micro-patterned molds provide a feasible way to fabricate the nanomaterials, however, it may be not a suitable methodology to produce biomedical-use materials due to the necessary irradiate process. To address this problem, we previously proposed a convenient method to pattern murine fibroblasts by engineering the physiochemical properties of free-standing nanosheet (Fujie et al., 2011). Since then, various kinds of surface-modified polymeric nanosheets have been developed as novel scaffolds for cell organization, cell delivery, and cell hierarchical construction (Fujie et al., 2013, 2015; Shi et al., 2014; Otomo et al., 2020). Microporous thin films (referred to as porous nanosheets) were previously introduced to induce cell construction and cell alignment (Suzuki et al., 2016). ECM proteins such as fibronectin, collagen and laminin penetrate through the micropores to stabilize cell hierarchies constructed between multi-layered porous nanosheets. Additionally, it has been reported that porous nanosheets facilitated long-term cell culture (up to 2 weeks) with more than 80% cell viability and oriented cell arrangement (Nishiwaki et al., 2019). Most recently, we reported for the first time that porous nanosheets prepared by a solvent etching method could support the adipose-tissue derived stem cell (ASC) spheroids for high-magnification imaging owing to its transparency (Suematsu et al., 2020). In this study, we further verified that free-standing poly(D,L-lactic acid) (PDLLA) porous nanosheet could improve the 3D spheroid cell viability and proliferation in comparison with the conventional suspension culture, demonstrating its potential to be applied as a novel 3D culture scaffold, which is cost-effective and easy-to-handle.

MATERIALS AND METHODS

Materials

The polymers, solvents and reagents used in this study were purchased from the following suppliers: Poly(D,L-lactic acid) (PDLLA, Mw = 300,000–600,000) from Polysciences, Inc. (Warrington, PA); Poly(vinyl alcohol) (PVA, Mw = 13,000–23,000), ethyl acetate and cyclohexane from Kanto Chemical, Co., Inc. (Tokyo, Japan); Polystyrene (PS, Mw = ∼280,000) and bovine fibronectin from Sigma-Aldrich Co., LLC. (St. Louis, MO); poly (ethylene terephthalate) (PET) film (Lumirror 25T60) from Panac Co., Ltd. (Tokyo, Japan).

Preparation of Porous Nanosheet

Using the approach proposed by Suzuki et al. (2016), the porous nanosheet were generated by Micro Gravure TM coater ML-120 (Yasui Seiki Co., Ltd., Kanagawa, Japan), a gravure coating method combining the roll-to-roll process. PVA solution (20 mg/mL) was coated first on the PET film to serve as a sacrificial layer, which could be dissolved and detach nanosheets from the PET substrate. From the polymer solution, the PET film runs through the coater, which rotates at 30 rpm, with a 1.3 m/min line speed over 7 meters. The solvent-coated film was high temperature air-dried (100°C) for about 5 min until the remaining solution has been evaporated. PDLLA and PS were then mixed in a 1:1 weight ratio and dissolved in ethyl acetate to make the polymer concentration of 20 mg/mL, which was optimized for cell culture purpose in terms of pore uniformity and diameters, porosity and thickness of nanosheets (Suzuki et al., 2016). This polymer solution was topped on PVA-coated film, and it went through the same coating process as the PVA layer except for a lower temperature (80°C) for drying. The obtained nanosheet was cut into 2 cm × 2 cm pieces, and then immersed into cyclohexane to selectively dissolve and remove PS regions by solvent etching. Without the PS regions, a random porous topography was produced on the remaining PDLLA nanosheet.

Measurement of Thickness and Porous Diameter

Before the measurements, the substrate supported porous nanosheet was placed in deionized water to dissolve the PVA layer between the PET film and the porous nanosheet. Then the free-standing porous nanosheet was collected and reattached on a silicon wafer in deionized water in order to measure the thickness of porous nanosheet and porous diameter. The porous and non-porous nanosheets were examined with a profilometer (Dektak XT-S, Bruker BioSpin Co., Kanagawa, Japan), which uses two scarred scratches on the nanosheet attaching on a silicon wafer as the base to compare and obtain the relative height to represent nanosheet thickness. An atomic force microscope (AFM; VN-8000, Keyence Co., Ltd., Osaka, Japan) was applied to characterize the topographical surface. For the porous area, the ImageJ software package (U.S. National Institutes of Health, Bethesda, MD) was employed to measure the diameter using the phase-contrast images of porous nanosheets.

Cell Culture

Murine adipose-derived stem cells (mASCs) (<10 passages; Cyagen Biosciences, Santa Clara, CA) were incubated at 37°C, 5% CO_2 atmosphere in a cell culture media [Dulbecco's Modified Eagle Medium: Nutrient Mixture F-12 (DMEM/F-12)] containing 10% (v/v) fetal bovine serum (FBS) and 1% (v/v) penicillin streptomycin. When the confluence reached 80%, cells were detached from the tissue-culture dish by using 0.25% (w/v) trypsin/0.1% (w/v) ethylenediaminetetraacetic acid (EDTA) after washing with Dulbecco's phosphate-buffered saline (DPBS; Thermo Fisher Scientific, Inc., Carlsbad, CA). Murine embryonic stem cells (mESCs) were cultured in DMEM-knockout medium containing 15% FBS, 1% PS, 1% Glutamax, 1% NEAA, 0.1% β-mercaptoethanol, 0.2% leukemia inhibitory factor (LIF) and two inhibitors (PD0325901 and CHIR99021) at 37°C, 5% CO_2 atmosphere.

Spheroids Formation and Characterization

Collected stem cells (2×10^5 cells) were seeded on the porous nanosheet, which had been fixed on a glass-based dish (thickness: 0.15–0.18 mm, 35 ø glass base dish, AGC Inc., Tokyo, Japan) with silicone elastomer: poly(dimethyl-siloxane) (PDMS). The same cell density was applied to non-adherent 12-well plate as well. The culture media would be changed every 2 days to keep cell survival. Cell aggregations were observed and the images were captured using an inverted microscope (IX-71; Olympus) from day 1 to 5 after cell seeding. According to the phase-contrast images, the diameter of cell aggregations was analyzed on ImageJ.

Live/Dead Staining

After 72 h of cell seeding, Live/Dead viability/cytotoxicity test kit (Thermo Fisher Scientific) was used to observe the living and dead cells distribution within the spheroids. The kit includes two staining solutions, calcein AM targeting living cells and ethidium homodimer labeling dead cells. Calcein AM is hydrolyzed by esterase in living cells to become calcein, which retains in the cell cytoplasm and strongly emits green fluorescence; while ethidium homodimer only penetrates cells with disrupted plasma membrane and intercalates into DNA. Calcein AM and ethidium homodimer were mixed and diluted in PBS as instructed by the manual. After washing mASC spheroids collected from the nanosheet and the suspension culture media with PBS, 1 mL staining solution were added to each culture dish, followed by 15 min incubation at 37°C. Then, suspension cells were transferred into a glass-based dish prior to the observation under a confocal laser-scanning microscope (FV1000, Olympus Life Science). The green and red fluorescence intensity was separately analyzed by ImageJ and the ratio of living and dead cells in spheroids was compared between different groups. The corrected total cell fluorescence (CTCF) value was calculated using the formula (1) shown below:

$$\text{CTCF} = \text{Integrated density} - (\text{area of the selected cells} \times \text{mean fluorescence of background readings}) \quad (1)$$

Cytoskeleton Staining

On day 3 after seeding, mASC spheroids were first fixed with 4% paraformaldehyde for 10 min and followed by treatment with 5% Trition X-100 (Wako Pure Chemical Industries, Osaka, Japan) in PBS for 15 min to disrupt the cell membrane after washing. In order to prevent background fluorescence, cells were treated with 10% bovine serum albumin (BSA, Sigma-Aldrich, United States) at room temperature for about 30 min for blocking of non-specific binding of antibodies. A dilution (1:500) of anti-Vinculin antibody (ab18058, Abcam, Cambridge, United Kingdom) was then used as the primary antibody to mark vinculin for overnight incubation at 4°C. After washing away the free anti-vinculin antibodies, a mixture of staining solution, containing Alexa Fluor 488-conjugated goat anti-mouse IgG (H + L) secondary antibody (A11001, Thermo Fisher Scientific), DAPI (4',6-diamidino-2-phenylindole, Invitrogen™) and Alexa Fluor 594 Phalloidin (Invitrogen™) were added and incubated with cells at room temperature for at least 45 min. DAPI and Phalloidin were used to label the nuclei and filamentous actin (F-actin), respectively. The suspension spheroids were transferred into glass-based dish prior to the observation using a confocal microscope.

Proliferation Assay

Spheroid cell proliferation assays were performed by using eBioscience™ Cell Proliferation Dye eFluor™ 670 (ThermoFisher). 1×10^6 stem cells were counted and stained before seeding. The culture medium containing serum were first washed away with DPBS, and then cells were resuspended in 1mL DPBS complemented with 5 μL cell proliferation eFluor™ 670 dye. After incubating and staining in dark at 37°C, the staining reaction was stopped by adding 4–5 mL cold FBS and incubating the cells on ice for 5 min. Cells were spun down (280 g, 5 min, 4°C) and washed once with culture medium. Then, 2×10^5 cells were seeded in non-adherent 12-well plate as suspension culture or on a porous nanosheet to form spheroid. On day 3,

the spheroids were harvested and dispersed into single cells with 100 μL trypsin/EDTA. After 5–8 min incubation at 37°C, the fluorescent intensity was monitored with a Cytomics FC500 flow cytometer (Beckman Coulter). The initial signal on day 0 was measured right after the staining process as the basis for the cell division calculation. The eFluor^{TM} 670 dye specifically binds to primary amines in cellular proteins and it would be dispensed evenly when the cell divides. According to the fading fluorescence, number of cell divisions and cell cycle duration were calculated using the following formula (2) and (3):

$$\text{Number of cell divisions} = \text{Log}_2\left[(F_0 - F_{unstained}) / \left(F_{samples} - F_{unstained}\right)\right] \quad (2)$$

$$\text{Cell cycle duration (hours)} = \text{cell culture duration (hours)} / \text{number of cell divisions} \quad (3)$$

Where F_0 and $F_{samples}$ indicate the median fluorescence intensities of spheroid cells on day 0 and day 3, respectively; $F_{unstained}$ indicates the background signal of unstained cells.

Apoptosis Analysis

PE Annexin V Apoptosis Detection Kit I (BD Bioscience) was used to analyze the spheroid cell apoptosis cultured as suspension and on porous nanosheets. PE Annexin V detects the loss of membrane integrity accompanying the latest stage of cell death. It is often used in combination with 7-AAD, which labels dead or damaged cells without intact membranes, to identify viable cells (double negative), early apoptotic cells (PE annexin V positive, 7-AAD negative) and dead cells (double positive). The cells collected from both culture systems were washed with DPBS and treated with trypsin/EDTA in 37°C water-bath for 5–8 min to deconstruct the spheroids into single cells. Next, culture medium was added to stop the trypsinization, and the single cells were washed with DPBS. As the instruction describes, PE annexin V and 7-AAD were mixed and diluted in 1X Annexin V binding buffer, and samples were added to the staining solution. The cells were incubated and protected from light at room temperature for 15 min and then diluted with 1X Annexin V binding buffer before analyzing with the Cytomics FC500 Flow cytometer. For the positive control, cells were exposed under UV-light for 3–4 h.

Statistical Analysis

All statistical analyses were performed using one-way ANOVA by StatsPlus software. *P*-value significance was determined as <0.005 (***), <0.01 (**), and <0.05 (*).

RESULTS

Preparation and Characterization of Porous Nanosheet

Porous nanosheets were integrated from two immiscible polymers, PS and PDLLA (1:1 in weight) via a gravure-coating method (**Figure 1A**), followed by a solvent etching process with cyclohexane to remove the phase-separated PS regions (**Figure 1B**).

As indicated by the phase-contrast images in **Figures 2A,B**, the porous nanosheet obtained after cyclohexane treatment showed bubble-like, shiny and porous topography, whereas the PS regions remaining in the non-porous nanosheet block the light from optical microscopy and exhibited as little black circles. The thickness of nanosheet was calculated from the relative height of nanosheet surface to the substrate surface using a stylus profilometer (**Figures 2C,D**). The resulting porous nanosheets were 168 nm in thickness and had an average porous area of 6.6 μm^2 with a porosity of 0.887, whereas the non-porous nanosheet was 228 nm in thickness (**Table 1**).

Spheroid Formation on Porous Nanosheet

The edges of porous nanosheets were fixed on a glass-based dish with a silicone elastomer; poly-dimethyl-siloxane (PDMS), to proceed *in vitro* experiments. To observe how porous nanosheets affect the morphology of mASCs, phase-contrast images were captured every day after cell seeding. Representative images of day 1, 3, and 5 were chosen to demonstrate the differences in spheroid size and morphology among mASCs seeded on porous nanosheets and those in non-adherent dishes as suspension culture (Fang and Eglen, 2017; Lv et al., 2017).

Within the first 24 h, mASCs aggregated as spheroids both in suspension culture and on the porous nanosheet (**Figure 3A**). Spheroids in suspension culture tended to cluster together (represented by black arrows) as compared to spheroids on the porous nanosheet, which were evenly distributed. On day l, spheroids had grown to an average diameter of 225 μm in suspension culture and 90 μm for spheroids on the porous nanosheet (**Figure 3B**). Furthermore, the spheroids cultured on the porous nanosheet started developing as a tethered state to the porous surface as indicated by the white arrows. Until day 5, the spheroids in suspension culture had grown to an average diameter of 250 μm in irregular shapes, whereas spheroid size on the porous nanosheet remained below 100 μm in average while keeping a spherical shape. Taken together, the porous nanosheets promoted a stable generation of mASC spheroids with a better homogeneity in size and shape.

Live/Dead Staining of Spheroids

To evaluate cell viability within the spheroids, Live/Dead cell staining was conducted on day 3. Confocal images of spheroids on the porous nanosheet were captured through the porous nanosheet owing to its ultra-thin and transparent characteristics, which does not interfere with focusing the spheroids (Suematsu et al., 2020). It was found that dead cells mostly presented in the core region of spheroids regardless of culture environment (**Figures 4A,B**). Then, the fluorescence intensity was analyzed to confirm the Live/Dead cell ratio within the spheroids (**Figure 4C**). After eliminating the background intensity, the correlated total cell fluorescence (CTCF) indicates that the proportion of living and dead cells was approximately 9:1 in both culture systems. It is suggested that cell viability of spheroids was not affected by the external stress from the two

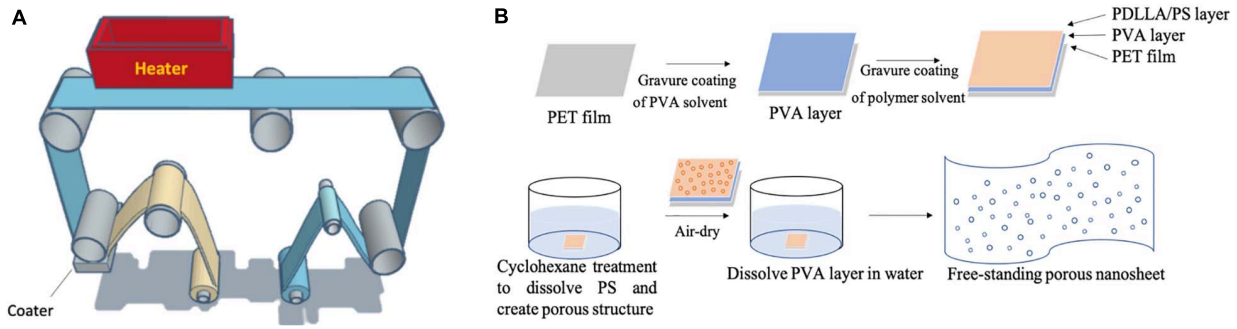

FIGURE 1 | (A) Image of the gravure-coating method combining with roll-to-roll process to prepare nanosheet. **(B)** Schematic illustration of free-standing porous nanosheet preparation.

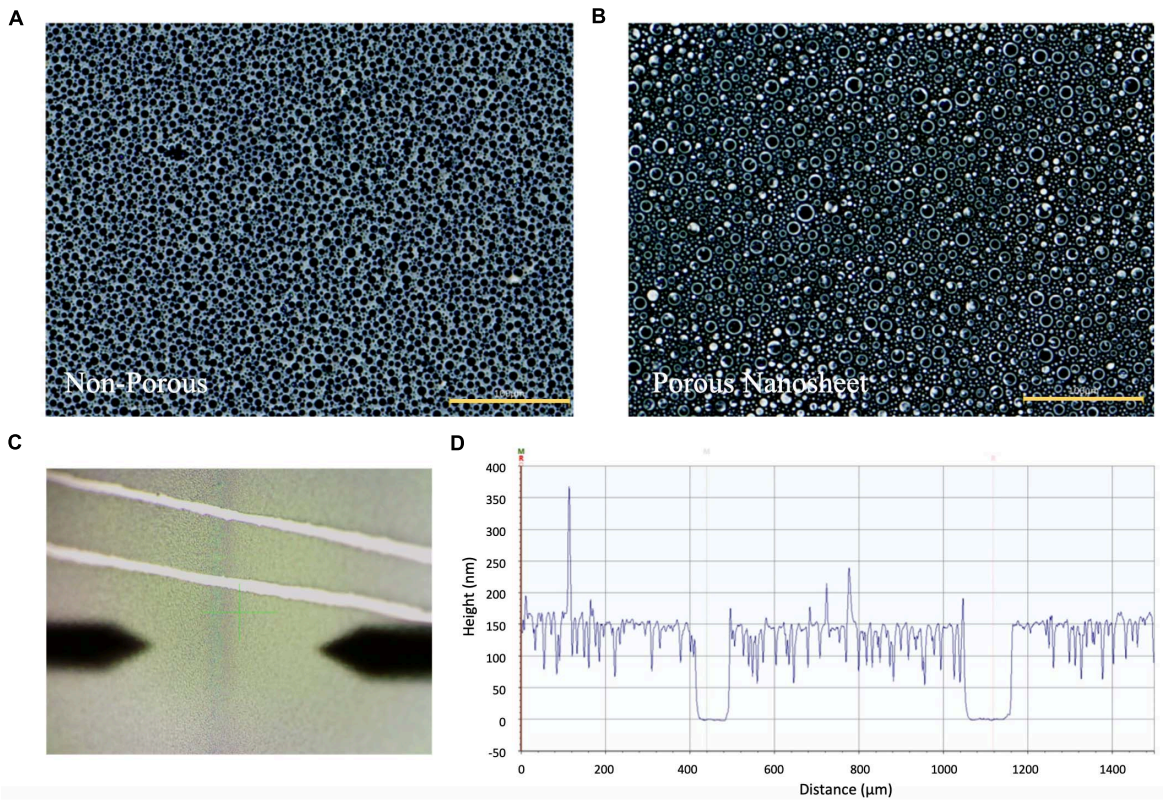

FIGURE 2 | The phase-contrast images of **(A)** non-porous nanosheet and **(B)** porous nanosheet (scale bar: 100 μm). Measurement of the thickness of nanosheet. **(C)** Image of nanosheet obtained from the profilometer. Two parallel scratches were gently made to expose the silicon substrate. The surface topography was profiled to obtain the height difference to represent film thickness **(D)**.

different culture environments and they supported cell viability to a similar extent. Note that spheroids of similar sizes were analyzed for comparison.

Cytoskeleton Observation

In order to confirm spheroid attachments on the porous nanosheets, vinculin and f-actin were visualized. Vinculin, a globular protein associated with cell adhesion and lamellipodia formation, interacts with f-actin and is identified as a mechano-transducer when developing focal adhesion (Tolbert et al., 2013). When cells anchor down on the substrate and spread like a monolayer culture, f-actin expands radially and

TABLE 1 | Characterization of non-porous nanosheet and porous nanosheet.

Sample	Thickness (nm)	Porous area (μm^2)	Porosity
Non-porous nanosheet	228	N/A	N/A
Porous nanosheet	168	6.6	0.887

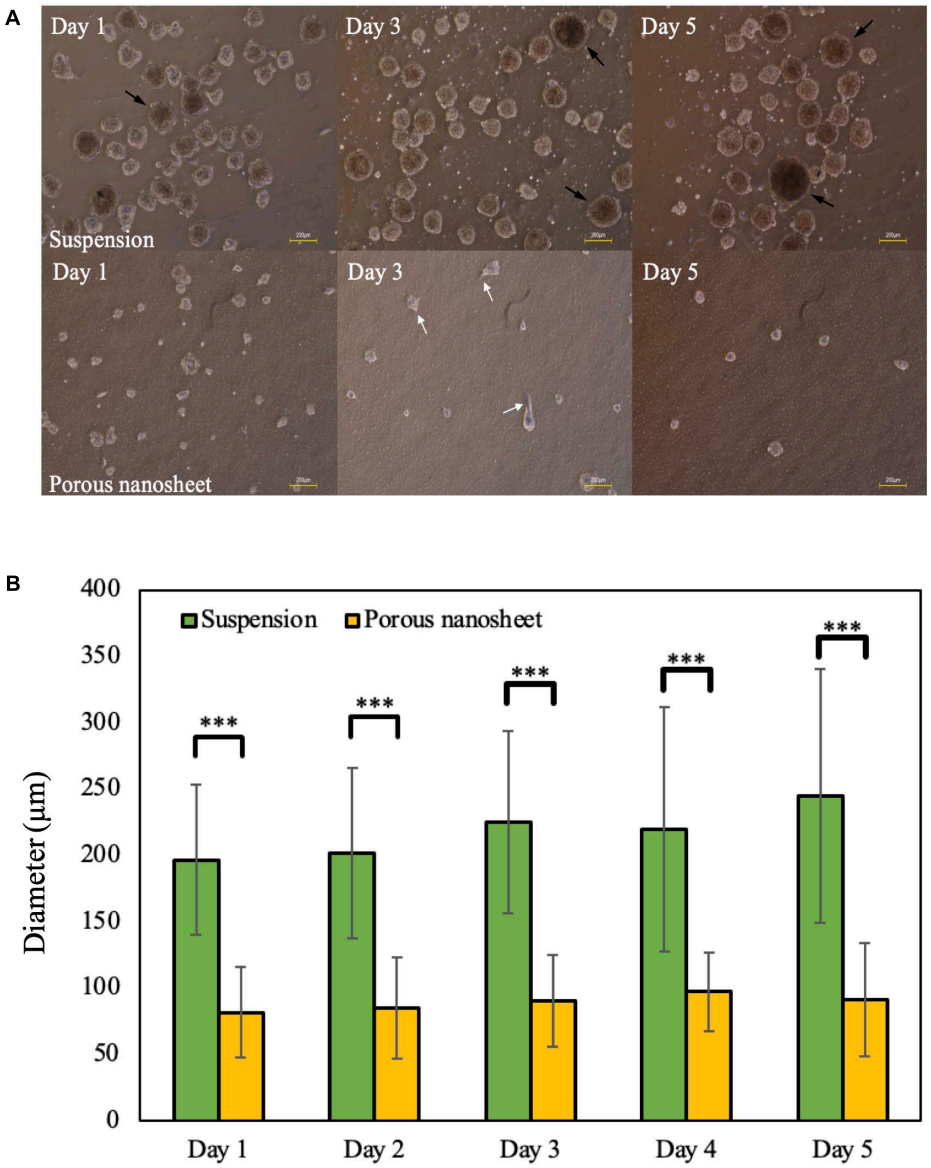

FIGURE 3 | (A) The morphology of mASC spheroids cultured in suspension (top) and on porous nanosheets (bottom) on days 1, 3, and 5. Spheroids showed the attachment on porous nanosheet on day 3 as indicated by white arrows and representative spheroid clusters formed in suspesnsion culture were indicated by black arrows. Scale bar: 200 μm. **(B)** The average diameter of spheroids formed in suspension and on porous nanosheets. Data show the mean ± SD ($n = 5$, $^{***}p < 0.005$).

colocalizes with vinculin at the pointed end of actin filaments (Noriega and Subramanian, 2011). A confocal laser scanning microscope was used to capture z-stack images of the spheroids obtained from suspension culture or a porous nanosheet, starting on the bottom part of spheroids (i) and ending at the apex of spheroids (iv) (**Figure 5**). F-actin filaments in spheroids from the porous nanosheet noticeably expanded two-dimensionally and adhered on the nanosheet illustrated by the strongest intensity at the bottom half of the sphere. In contrast, focal adhesions were not observed for spheroids cultured in suspension and the f-actin fluorescence was mainly apparent in the central part and on the edge of the spheroid. It is also interesting to find that the cell (nuclei) orientation is different. The spheroid cells in suspension culture appeared to be circumferentially oriented and tightly compressed, whereas those generated on the porous nanosheet did not show uniformed orientation at the bottom part and only the cells at the apex part tended to be circumferentially oriented. Additionally, the colocalization of f-actin and vinculin was clearly observed in a circumferential manner surrounding the suspension spheroids. In comparison, when seeded on the porous nanosheet, f-actin seemed to be evenly distributed and

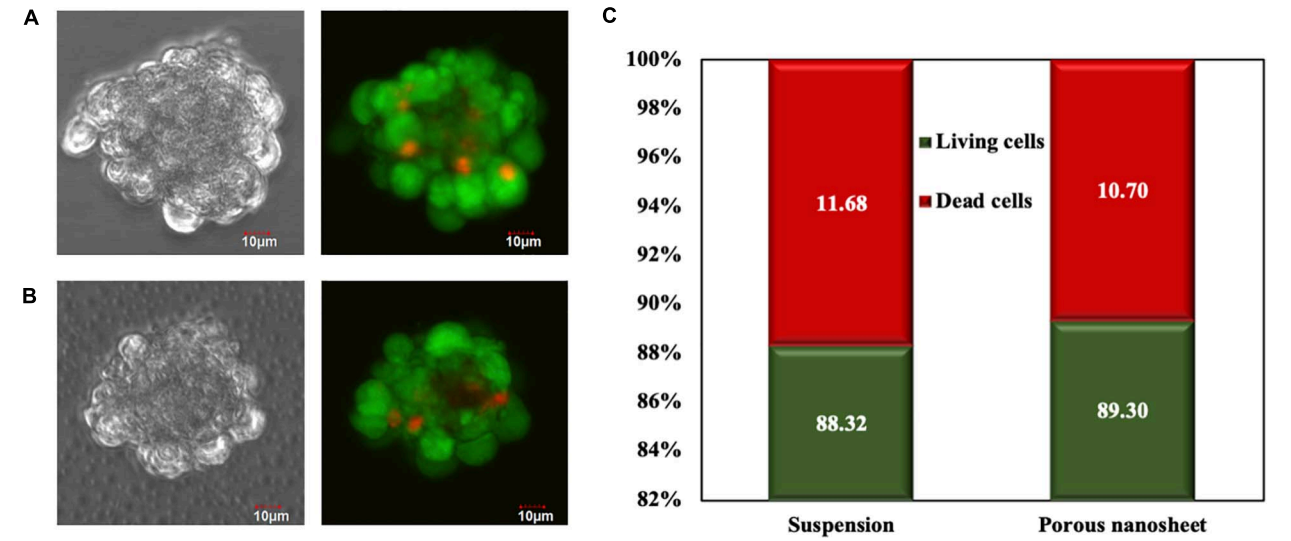

FIGURE 4 | Live/Dead cell staining of mASC spheroids of a similar size formed in suspension **(A)** and on the porous nanosheet **(B)** on day 3. Scale bar: 10 μm. **(C)** The percentage of living and dead cells in spheroids was calculated by the corrected total cell fluorescence (CTCF) intensity.

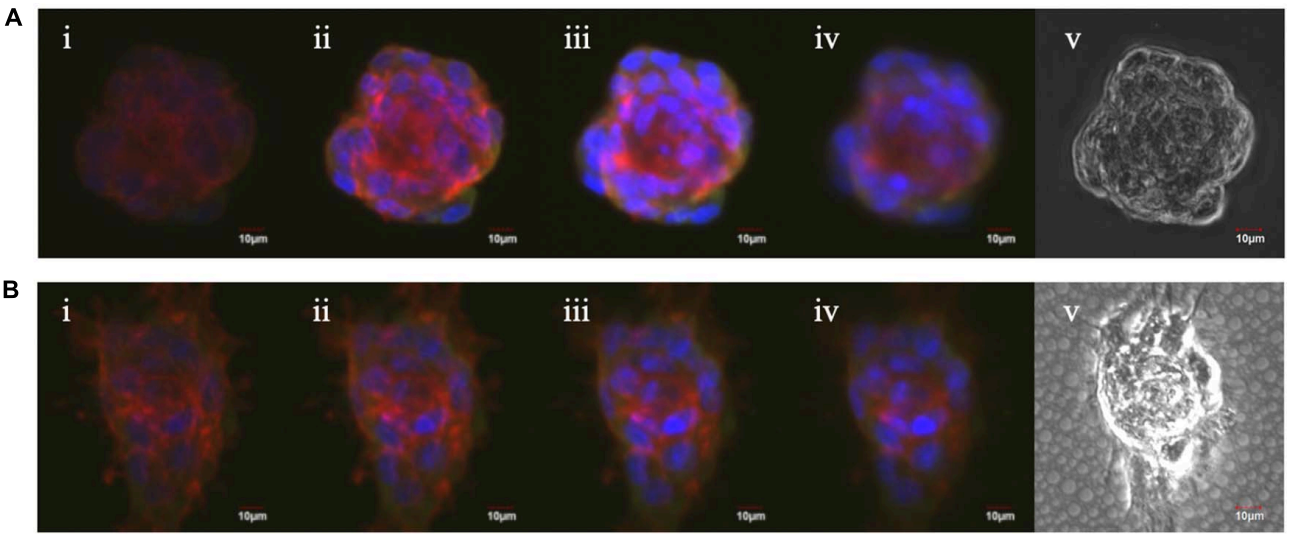

FIGURE 5 | The Z-stack fluorescent images of mASC spheroids in suspension culture **(A)** and on the porous nanosheet **(B)** from the bottom (i) to the top (iv) view and the phase-contrast images (v). Red: Alexa Fluor 594 Phalloidin; green: Anti-Vinculin antibody; blue: DAPI.

appeared with relatively weak signals only at the cell-junctions within the spheroids.

Proliferation Assay

As mentioned above, the spheroids in both culture systems continued to develop during the culturing period, which might be due to the aggregation and fusion of spheroids or cell proliferation within the spheroid itself. Thus, a cell proliferation dye that binds to cellular proteins was used to analyze cell divisions overtime by flow cytometry, assuming that upon every cell division, the dye fluorescence intensity decreases to the half. As shown in **Figures 6A,B**, the cell division profiles of two culture systems were remarkably different on day 3. In suspension culture, there was a portion of spheroid cells that have decelerated or terminated the division; whereas most of those seeded on the porous nanosheets continued to proliferate from day 2 to 3. It was estimated that the mASC of spheroids in suspension culture divided about 2.5 times while those adhered on the porous nanosheet divided approximately 4 times after 3 days of incubation (**Figure 6C**). From the number of cell divisions in this time frame, the cell cycle duration could be roughly gauged. It took nearly 30 h for the spheroid cells in suspension culture to divide once, whereas it took about 20 h for those seeded on the porous nanosheets (**Figure 6D**).

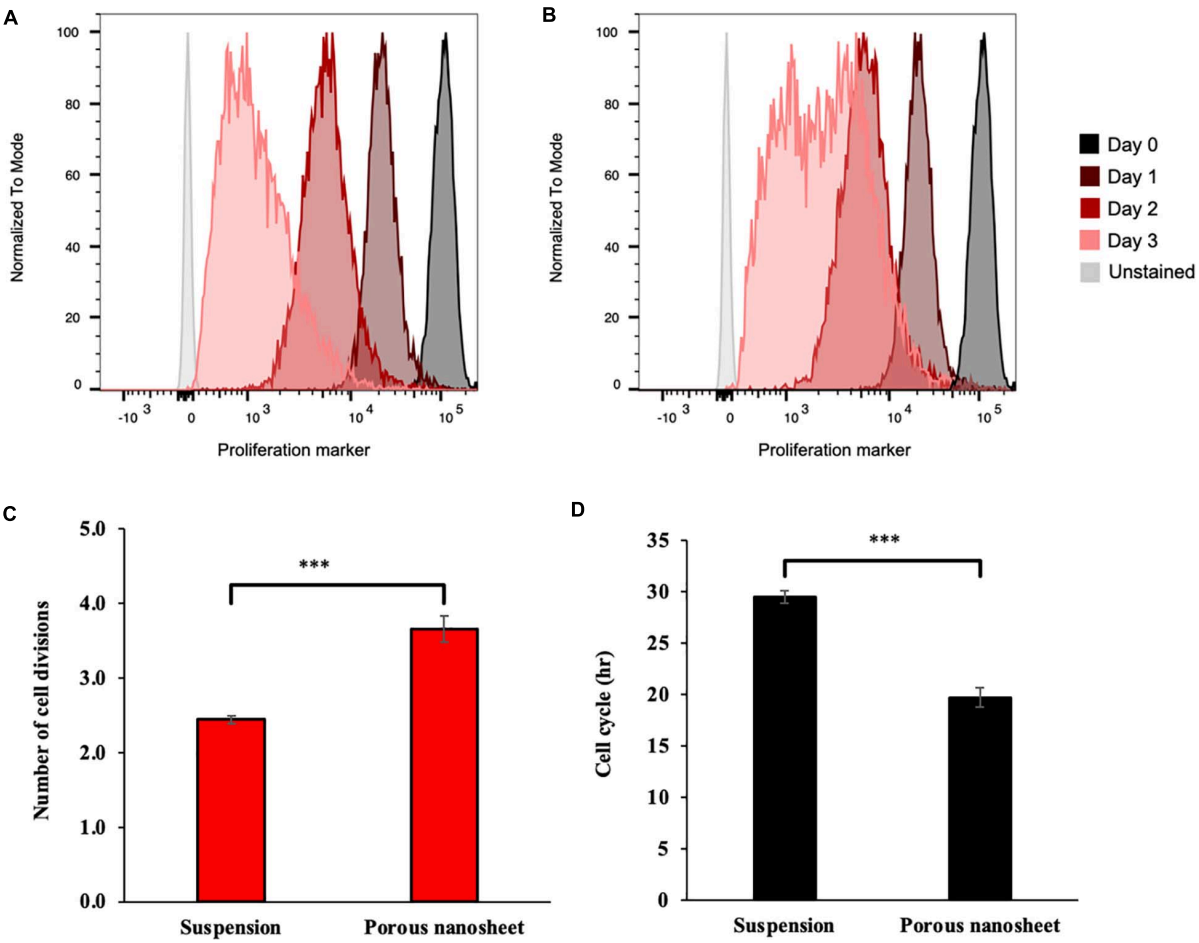

FIGURE 6 | Representative flow cytometry histograms of the proliferation assay, showing fluorescence reduction of cells from spheroids cultured on porous nanosheet **(A)** and in suspension **(B)** from day 1 to 3. Number of cell divisions **(C)** and average cell cycle duration **(D)** in hours (h) of mASC spheroids were calculated according to the loss of fluorescence on day 3 relative to initial fluorescence on day 0. Data show the mean ± SD ($n = 3$, $^{***}p < 0.005$).

The mESC spheroids constructed on the porous nanosheets also showed a similar trend, with shorter, though not statistically significant, estimated cell cycle durations than the suspension culture (**Supplementary Figure 1**). Overall, these results showed that the porous nanosheet could sustain the spheroids in a prosperous state with higher proliferation rates than those in the suspension culture.

Apoptosis Analysis

The Live/Dead staining allowed the visualization of cell viability in the spheroids of similar sizes; however, it is difficult to give an overall evaluation including all the spheroids. Therefore, cell apoptosis assay was performed by using PE annexin V and 7-AAD double staining in order to comprehensively analyze the cell death without size discrimination and investigate the progress of apoptosis.

The cells were harvested from mASC spheroids on day 3 and 5, dissociated by trypsinization of spheroids, labeled and analyzed by flow cytometry. PE annexin V and 7-AAD double negative cells were gated in Q4 on the scatter plots (**Figures 7A–F**) to represent living cells. Early apoptotic cells were defined in Q1 gates (PE annexin V positive, 7-AAD negative) while double positive cells were identified in Q2 gates as dead cells. On day 3, the mASC spheroids in suspension contained almost 20% of dead cells whereas less than 3% of dead cells existed on the porous nanosheet (**Figure 7G**). On day 5, the population of living cells in the suspension spheroids shrank to 58%; in comparison, 93% of the spheroid cells on porous nanosheet remained alive (**Figure 7H**), the difference of which was remarkably significant. Notably, suspension culture also resulted in a small portion of early apoptotic cells on day 5, implying the progress of apoptosis. Similarly, it was confirmed with mESC spheroids that the porous nanosheet enhanced the cell viability with over 50% of living cells on day 5 in contrast to mESCs suspension spheroids, which contained about 40% of living cells (**Supplementary Figures 2, 3**). With the support of porous nanosheet, spheroids could be better preserved from apoptosis/necrosis than suspension culture and possibly used for long-term culture for comprehensive studies.

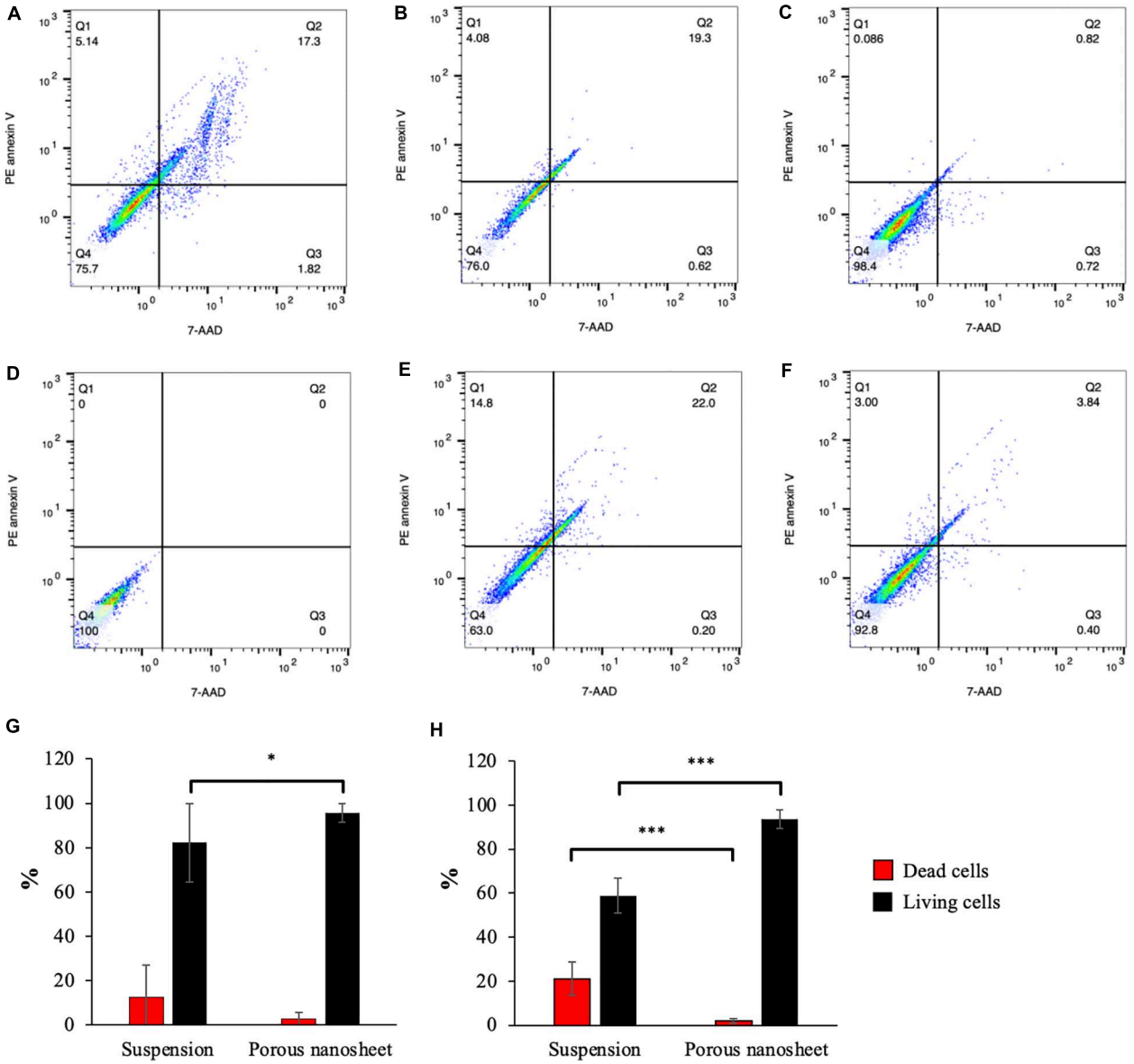

FIGURE 7 | Apoptosis analyses of cells from spheroids cultured on porous nanosheets or in suspension. Representative PE annexin V apoptosis scatter plots of positive control treated with UV-light **(A)**, spheroids in suspension **(B,E)** and on porous nanosheet **(C,F)** harvested on day3 **(B,C)** and day 5 **(E,F)**, and unstained negative control **(D)**. Percentage of dead cells (Q2) and living cells (Q4) in mASC spheroids on day 3 **(G)** and day 5 **(H)**. Data show the mean ± SD ($n = 3$, $^{*}p < 0.05$, $^{***}p < 0.005$).

DISCUSSION

PDLLA is a hydrophobic polymer with high biocompatibility and biodegradability. Due to its amorphous nature, it exhibits a lower mechanical strength and a faster degradation rate than the crystalline poly(L-lactic acid) (PLLA), making it more preferrable to engineer soft tissue scaffold (Ulery et al., 2011). In contrast, PLLA is widely applied for bone tissue engineering after blending with hydrophilic polymers such as poly (glycolic acid) (PGA) to accelerate the degradation (Shuai et al., 2021). We previously reported that PDLLA porous nanosheets could induce the generation of mASC spheroids owing to their porous topology and hydrophobic property (water contact angle: 74°), which provides a weakly adhesive surface to allow the cell attachment as well as migration (Suematsu et al., 2020). In this study, we further demonstrated that this 3D culture scaffold had several advantages over the conventional suspension culture, as it better promoted cell viability and cell proliferation, as well as a better homogeneity of spheroid's size and shape.

3D culture provides a close-to-*in vivo* microenvironment to study cell-cell interaction and spatial effects. However, due to the lack of angiogenesis, radial gradients of nutrients, gasses

and growth factors are generated, reducing the viability of spheroid cells toward the core by decreased accessibility to nutrients and stimuli (Mehta et al., 2012; Cui et al., 2017). Therefore, the diameter of spheroids is thought to be a key factor in determining the cell viability. To verify whether the porous nanosheet imposes additional disturbance to affect the homeostasis, the spheroids of similar sizes were used for comparable quantifications, i.e., in the Live/Dead staining and cytoskeleton observation.

The mechanical properties within spheroids depend on the spatial position. In the core region, cells are progressively compressed in the radical direction, while the cells in the peripheral area further bear an increased circumferential stress, forming a contractile outer shell with more nuclei to drive the spheroid compaction (Lee et al., 2019). At an early stage of spheroid formation, cell-cell contact is relatively loose, and cells are either circumferentially, radially, or not oriented within the spheroids. Following the increase of spheroid size, structural anisotropy is generated, transducing compression forces toward the core which imposes mechanical anisotropy as a response of the cells. Such mechanical stress would lead to remodeling and changes in cell orientations, with the circumferentially oriented cells dominating the edge of spheroids, while the radially oriented cells occupying the central region (Dolega et al., 2017; Lee et al., 2019). Surprisingly, the cell orientation and the distribution of vinculin and f-actin were different in the two culture systems, indicating that the spheroids were bearing different kinds of mechanical stress and undergoing different fates. The porous nanosheet controlled the diameter of mASC spheroid by offering the porous scaffold for spheroids to cling on, which reduced cell aggregations. Therefore, the porous nanosheet might provide a culture system that favors the early stage of spheroid formation through proper size control.

In general, both the porous nanosheet and the non-adherent dish showed 3D spheroid construction capability. The suspended mASC spheroids had aggregated rapidly in the first 24 h, yet they developed into uneven sizes during the 5 days incubation. From Live/Dead cell staining, it was revealed that cell death started from the central region of the spheroids of both suspension and porous nanosheet culture systems, which may be caused by the shortage of oxygen and nutrition supplies; however, there was no distinguishable difference when analyzing by similar sizes. Living and dead cell ratios were almost 9:1 from both culture systems (**Figure 4**), in this regard, 20% of dead cells in suspended spheroids analyzed by flow cytometry (**Figure 7**) might have resulted from relatively large spheroids. Given the fact that the porous nanosheet provides limited area of attachment, stem cells could loosely and sparsely adhere to it to form spheroids instead of a monolayer (Suematsu et al., 2020). Meanwhile, the spheroid size would be controlled by lowering the opportunity of spheroid fusion or aggregation in terms of collision frequency and movement speed of spheroids. The crawling-like f-actin fluorescence depicts the spheroid attachments on the porous nanosheets, verifying the semi-adhesive property of porous nanosheet, which is crucial to control the spheroid size. As a result, the spheroids anchoring on the porous nanosheet reduce interaction with each other so that preventing further development into larger spheroids as those floating in the suspension. The different culture environments contribute to the spheroid formation with different sizes, and the size difference affects spheroid biological performances including cell proliferation and apoptosis. Stem cells are characterized by a high potential of proliferation throughout the lifetime of organisms, and a high proliferation rate is thought to be crucial in maintaining human embryonic stem cell identity (Ruiz et al., 2011). It is no doubt that a sustained stem cell proliferation is a favorable feature for its application in tissue engineering and regeneration (Zhao et al., 2013; Zhou et al., 2016). Overall, mASC spheroids cultured on the porous nanosheet proliferated faster and survived longer when comparing to those forming in the suspension, implying a higher potential of PDLLA porous nanosheet in maintaining the stem cell functions and applicability for tissue engineering. However, further investigations on the pluripotency and differentiation potential of spheroid stem cells are necessary for a comprehensive evaluation. In addition to mASCs, porous nanosheets are also applicable to generate and sustain mESC spheroids although the improvement was not statistically significant. Note that advanced coating such as Matrigel is commonly used to support mESC culture *in vitro*, its lack on the porous nanosheet was likely to compromise the spheroid formation. Therefore, a combination of Matrigel and the porous nanosheet is expected to further improve the preservation of mESC spheroids.

In conclusion, porous nanosheets have shown its improvement in 3D cell constructions by providing efficient semi-attachment, which appears to limit the spheroid size. With preserved spheroids, porous nanosheets could be a promising scaffold for advanced long-term spheroid culture and close-to-*in vivo* study.

DATA AVAILABILITY STATEMENT

The original contributions presented in the study are included in the article/**Supplementary Material**, further inquiries can be directed to the corresponding author/s.

AUTHOR CONTRIBUTIONS

YT, LT-F, and SW conducted the experiments and performed data analysis. YT wrote the first draft of the manuscript. TL guided the experiments, organized the manuscript, and performed data analysis. WK and ST conceived and supervised the study. All authors contributed to manuscript revision.

FUNDING

This work was supported by Japan Society for the Promotion of Science (JSPS) KAKENHI Grant Nos. JP19K20700,

JP20K12656, and a Waseda University Grant for Special Research Projects (2018B-214).

ACKNOWLEDGMENTS

The authors would like to thank the Leading Graduate Program in Science and Engineering, Waseda University from MEXT, Japan, and Japan Student Services Organization (JASSO) for promoting the international academic collaboration.

SUPPLEMENTARY MATERIAL

The Supplementary Material for this article can be found online at: https://www.frontiersin.org/articles/10.3389/fbioe.2021.674384/full#supplementary-material

REFERENCES

Bartosh, T. J., Ylostalo, J. H., Mohammadipoor, A., Bazhanov, N., Coble, K., Claypool, K., et al. (2010). Aggregation of human mesenchymal stromal cells (MSCs) into 3D spheroids enhances their antiinflammatory properties. *Proc. Natl. Acad. Sci. U.S.A.* 107, 13724–13729. doi: 10.1073/pnas.1008117107

Bazou, D. (2010). Biochemical properties of encapsulated high-density 3-D HepG2 aggregates formed in an ultrasound trap for application in hepatotoxicity studies : biochemical responses of encapsulated 3-D HepG2 aggregates. *Cell. Biol. Toxicol.* 26, 127–141. doi: 10.1007/s10565-009-9123-0

Cui, X., Hartanto, Y., and Zhang, H. (2017). Advances in multicellular spheroids formation. *J. R. Soc. Interface* 14:20160877. doi: 10.1098/rsif.2016.0877

Dolega, M. E., Delarue, M., Ingremeau, F., Prost, J., Delon, A., and Cappello, G. (2017). Cell-like pressure sensors reveal increase of mechanical stress towards the core of multicellular spheroids under compression. *Nat. Commun.* 8:14056.

Emmert, M. Y., Wolint, P., Winklhofer, S., Stolzmann, P., Cesarovic, N., Fleischmann, T., et al. (2013). Transcatheter based electromechanical mapping guided intramyocardial transplantation and in vivo tracking of human stem cell based three dimensional microtissues in the porcine heart. *Biomaterials* 34, 2428–2441. doi: 10.1016/j.biomaterials.2012.12.021

Fang, Y., and Eglen, R. M. (2017). Three-dimensional cell cultures in drug discovery and development. *SLAS Discov.* 22, 456–472. doi: 10.1177/1087057117696795

Fujie, T. (2016). Development of free-standing polymer nanosheets for advanced medical and health-care applications. *Polym. J.* 48, 773–780. doi: 10.1038/pj.2016.38

Fujie, T., Ahadian, S., Liu, H., Chang, H., Ostrovidov, S., Wu, H., et al. (2013). Engineered nanomembranes for directing cellular organization toward flexible biodevices. *Nano Lett.* 13, 3185–3192. doi: 10.1021/nl401237s

Fujie, T., Haniuda, H., and Takeoka, S. (2011). Convenient method for surface modification by patching a freestanding anti-biofouling nanosheet. *J. Mater. Chem.* 21, 9112–9120. doi: 10.1039/c1jm10156k

Fujie, T., Shi, X., Ostrovidov, S., Liang, X., Nakajima, K., Chen, Y., et al. (2015). Spatial coordination of cell orientation directed by nanoribbon sheets. *Biomaterials* 53, 86–94. doi: 10.1016/j.biomaterials.2015.02.028

Huang, G. S., Dai, L. G., Yen, B. L., and Hsu, S. H. (2011). Spheroid formation of mesenchymal stem cells on chitosan and chitosan-hyaluronan membranes. *Biomaterials* 32, 6929–6945. doi: 10.1016/j.biomaterials.2011.05.092

Kim, J., Kim, Y. R., Kim, Y., Lim, K. T., Seonwoo, H., Park, S., et al. (2013). Graphene-incorporated chitosan substrata for adhesion and differentiation of human mesenchymal stem cells. *J. Mater. Chem. B* 1, 933–938. doi: 10.1039/c2tb00274d

Lee, W., Kalashnikov, N., Mok, S., Halaoui, R., Kuzmin, E., Putnam, A. J., et al. (2019). Dispersible hydrogel force sensors reveal patterns of solid mechanical stress in multicellular spheroid cultures. *Nat. Commun.* 10:144.

Lv, D., Hu, Z., Lu, L., Lu, H., and Xu, X. (2017). Three-dimensional cell culture: a powerful tool in tumor research and drug discovery. *Oncol. Lett.* 14, 6999–7010.

McKee, C., and Chaudhry, G. R. (2017). Advances and challenges in stem cell culture. *Colloids Surf B Biointerfaces* 159, 62–77. doi: 10.1016/j.colsurfb.2017.07.051

Mehta, G., Hsiao, A. Y., Ingram, M., Luker, G. D., and Takayama, S. (2012). Opportunities and challenges for use of tumor spheroids as models to test drug delivery and efficacy. *J. Control Release* 164, 192–204. doi: 10.1016/j.jconrel.2012.04.045

Nishiwaki, K., Aoki, S., Kinoshita, M., Kiyosawa, T., Suematsu, Y., Takeoka, S., et al. (2019). In situ transplantation of adipose tissue-derived stem cells organized on porous polymer nanosheets for murine skin defects. *J. Biomed. Mater. Res. B Appl. Biomater.* 107, 1363–1371. doi: 10.1002/jbm.b.34228

Noriega, S. E., and Subramanian, A. (2011). Consequences of neutralization on the proliferation and cytoskeletal organization of chondrocytes on chitosan-based matrices. *Int. J. Carbohydrate Chem.* 2011:809743.

Otomo, A., Ueda, M. T., Fujie, T., Hasebe, A., Suematsu, Y., Okamura, Y., et al. (2020). Efficient differentiation and polarization of primary cultured neurons on poly(lactic acid) scaffolds with microgrooved structures. *Sci. Rep.* 10:6716.

Park, I. S., Chung, P. S., and Ahn, J. C. (2017). Adipose-derived stem cell spheroid treated with low-level light irradiation accelerates spontaneous angiogenesis in mouse model of hindlimb ischemia. *Cytotherapy* 19, 1070–1078. doi: 10.1016/j.jcyt.2017.06.005

Ruiz, S., Panopoulos, A. D., Herrerias, A., Bissig, K. D., Lutz, M., Berggren, W. T., et al. (2011). A high proliferation rate is required for cell reprogramming and maintenance of human embryonic stem cell identity. *Curr. Biol.* 21, 45–52. doi: 10.1016/j.cub.2010.11.049

Santos, J. M., Camoes, S. P., Filipe, E., Cipriano, M., Barcia, R. N., Filipe, M., et al. (2015). Three-dimensional spheroid cell culture of umbilical cord tissue-derived mesenchymal stromal cells leads to enhanced paracrine induction of wound healing. *Stem Cell Res. Ther.* 6:90.

Shi, X., Fujie, T., Saito, A., Takeoka, S., Hou, Y., Shu, Y., et al. (2014). Periosteum-mimetic structures made from freestanding microgrooved nanosheets. *Adv. Mater.* 26, 3290–3296. doi: 10.1002/adma.201305804

Shuai, C., Yang, W., Feng, P., Peng, S., and Pan, H. (2021). Accelerated degradation of HAP/PLLA bone scaffold by PGA blending facilitates bioactivity and osteoconductivity. *Bioact Mater.* 6, 490–502. doi: 10.1016/j.bioactmat.2020.09.001

Suematsu, Y., Tsai, Y. A., Takeoka, S., Franz, C. M., Arai, S., and Fujie, T. (2020). Ultra-thin, transparent, porous substrates as 3D culture scaffolds for engineering ASC spheroids for high-magnification imaging. *J. Mater. Chem. B* 8, 6999–7008. doi: 10.1039/d0tb00723d

Suzuki, S., Nishiwaki, K., Takeoka, S., and Fujie, T. (2016). Large-Scale fabrication of porous polymer nanosheets for engineering hierarchical cellular organization. *Adv. Mater. Technol-Us* 1:1600064. doi: 10.1002/admt.201600064

Tolbert, C. E., Burridge, K., and Campbell, S. L. (2013). Vinculin regulation of F-actin bundle formation: what does it mean for the cell? *Cell. Adh. Migr.* 7, 219–225. doi: 10.4161/cam.23184

Ulery, B. D., Nair, L. S., and Laurencin, C. T. (2011). Biomedical applications of biodegradable polymers. *J. Polym. Sci. B Polym. Phys.* 49, 832–864.

Xu, Y., Shi, T., Xu, A., and Zhang, L. (2016). 3D spheroid culture enhances survival and therapeutic capacities of MSCs injected into ischemic kidney. *J. Cell. Mol. Med.* 20, 1203–1213. doi: 10.1111/jcmm.12651

Yamaguchi, Y., Ohno, J., Sato, A., Kido, H., and Fukushima, T. (2014). Mesenchymal stem cell spheroids exhibit enhanced in-vitro and in-vivo osteoregenerative potential. *BMC Biotechnol.* 14:105. doi: 10.1186/s12896-014-0105-9

Zhang, H., Aoki, T., Hatano, K., Kabayama, K., Nakagawa, M., Fukase, K., et al. (2018). Porous nanosheet wrapping for live imaging of suspension cells. *J. Mater. Chem. B* 6, 6622–6628. doi: 10.1039/c8tb01943f

Zhang, H., Masuda, A., Kawakami, R., Yarinome, K., Saito, R., Nagase, Y., et al. (2017). Fluoropolymer nanosheet as a wrapping mount for high-quality tissue imaging. *Adv. Mater.* 29:1703139. doi: 10.1002/adma.201703139

Zhao, C. Y., Tan, A., Pastorin, G., and Ho, H. K. (2013). Nanomaterial scaffolds for stem cell proliferation and differentiation in tissue engineering. *Biotechnol. Adv.* 31, 654–668. doi: 10.1016/j.biotechadv.2012.08.001

Zhou, C. C., Grottkau, B. E., and Zou, S. J. (2016). Regulators of stem cells proliferation in tissue regeneration. *Curr. Stem. Cell Res. T* 11, 177–187. doi: 10.2174/1574888x10666150531172108

Zujur, D., Kanke, K., Lichtler, A. C., Hojo, H., Chung, U. I., and Ohba, S. (2017). Three-dimensional system enabling the maintenance and directed differentiation of pluripotent stem cells under defined conditions. *Sci. Adv.* 3:e1602875. doi: 10.1126/sciadv.1602875

Conflict of Interest: ST was an inventor of patent (PCT/JP2013/056823) of porous nanosheets and collaborating with Nanotheta Co., Ltd., which is holding the patent.

The remaining authors declare that the research was conducted in the absence of any commercial or financial relationships that could be construed as a potential conflict of interest.

frontiers in Bioengineering and Biotechnology

REVIEW
published: 20 July 2021
doi: 10.3389/fbioe.2021.592118

Intervertebral Disk Degeneration: The Microenvironment and Tissue Engineering Strategies

Yiming Dou[1†], Xun Sun[1†], Xinlong Ma[1], Xin Zhao[2] and Qiang Yang[1]*

[1] Department of Spine Surgery, Tianjin Hospital, Tianjin University, Tianjin, China, [2] Department of Biomedical Engineering, The Hong Kong Polytechnic University, Kowloon, Hong Kong

Intervertebral disk degeneration (IVDD) is a leading cause of disability. The degeneration is inevitable, and the mechanisms are complex. Current therapeutic strategies mainly focus on the relief of symptoms, not the intrinsic regeneration of the intervertebral disk (IVD). Tissue engineering is a promising strategy for IVDD due to its ability to restore a healthy microenvironment and promote IVD regeneration. This review briefly summarizes the IVD anatomy and composition and then sets out elements of the microenvironment and the interactions. We rationalized different scaffolds based on tissue engineering strategies used recently. To fulfill the complete restoration of a healthy IVD microenvironment, we propose that various tissue engineering strategies should be combined and customized to create personalized therapeutic strategies for each individual.

Keywords: intervertebral disk degeneration, microenvironment, tissue engineering, scaffold, regeneration, disk herniation, low back pain

OPEN ACCESS

Edited by:
Chien-Wen Chang, National Tsing Hua University, Taiwan

Reviewed by:
Jennifer Patterson, Instituto IMDEA Materiales, Spain
Nihal Engin Vrana, Spartha Medical, France

***Correspondence:**
Qiang Yang
yangqiang1980@126.com

† These authors have contributed equally to this work

Specialty section:
This article was submitted to Biomaterials, a section of the journal Frontiers in Bioengineering and Biotechnology

Received: *06 August 2020*
Accepted: *18 May 2021*
Published: *20 July 2021*

Citation:
Dou Y, Sun X, Ma X, Zhao X and Yang Q (2021) Intervertebral Disk Degeneration: The Microenvironment and Tissue Engineering Strategies. Front. Bioeng. Biotechnol. 9:592118. doi: 10.3389/fbioe.2021.592118

INTRODUCTION

Low back pain is prevalent in the society and is the number one cause of disability globally; 60–80% of adults experience varying degrees of low back pain (Murray et al., 2012; Hartvigsen et al., 2018). Although the etiology and pathology of low back pain are complex, evidence suggests that low back pain is strongly associated with intervertebral disk degeneration (IVDD) (Luoma et al., 1976). The intervertebral disk (IVD) is a fibrous cartilaginous tissue that connects two adjacent vertebral bodies consisting of three parts: the nucleus pulposus (NP), the annulus fibrosus (AF), and the cartilage endplate (CEP). The NP is a centrally located highly hydrated gel-like tissue surrounded by the AF, comprised of layer-by-layer collagen fiber lamellas. The CEPs are situated at the top and bottom of the vertebral bodies, and they interface the IVDs with the adjacent vertebrae (Lawson and Harfe, 2017). This complex structure plays a vital role in transmitting and absorbing mechanical loading onto the spine and maintaining motor function.

The IVD gradually degenerates due to aging and tissue damage caused by multiple stressors, resulting in vertebral instability, spinal canal stenosis, and spinal segment deformity, causing low back pain and mobility disability (Wang et al., 2016). There are three main events in IVDD: (1) inflammation and catabolic cascades, (2) continuous loss of cells, and (3) decline in cellular functions and anabolic activities (Frapin et al., 2019). NP gradually degenerates under the influence

of these events. The AF ruptures as the degree of degeneration increases, while the degenerated NP is extruded and oppresses nerve roots due to abnormal stress, resulting in nerve compression symptoms. The CEP becomes more calcified, which adversely affects the transport of nutrients and metabolites, making it difficult to maintain sagittal stress balance. Inflammatory factors stimulate nerve roots, causing or aggravating pain, and enhancing mobility disability. The deteriorating microenvironment further aggravates IVDD.

Traditional therapeutic strategies (surgical and non-surgical treatments) focus on solving the symptoms. Surgical treatments focus more on physically relieving symptoms at the organ level, such as decompressing nerve roots (discectomy) and removing the degenerated disk (fusion and disk replacement). Non-surgical treatments (non-pharmacological therapy, pharmacological therapy, and interventional therapies) perform limited intervention for the microenvironment through anti-inflammatory, analgesic, and spasmolysant effects. Traditional therapeutic strategies do not promote disk regeneration at the cell level and, therefore, do not reverse the progress of disk degeneration (Harmon et al., 2020). Some patients relapse after treatment, and the disk degeneration might even accelerate the degeneration of adjacent segments (Harper and Klineberg, 2019).

In the early stage of IVDD, the enclosed environment makes it difficult for the external stem cells to exert potential regenerative ability on the NP. In the later stage when the degeneration is severe, the AF will tear, and neovascularization and neoinnervation will occur in the NP. Inflammation caused by newly colonized immune cells further harms the microenvironment and accelerates degeneration. Thus, the deteriorating microenvironment and low self-regenerative ability of the IVD are primary obstacles for regeneration. How to customize suitable regenerative strategies for IVD has become a hot topic of recent research. Tissue engineering strategies combining material science, engineering, and life science will become new clinical therapeutic approaches in the future. Tissue engineering strategies contain three key elements: cells, scaffolds, and biomechanical or biochemical signals (Mhanna and Hasan, 2017). These elements have been applied and extended in IVD tissue engineering. Applications of stem cells in IVD and derivative methods (gene therapy and extracellular vesicle therapy) have shown promising therapeutic potential for IVDD. Illustrating the interactive mechanisms between the components [IVD cells, biological factors, extracellular matrix (ECM) components, and environmental factors] in the IVD microenvironment makes therapeutic strategies more rational. Scaffolds mimic the microstructure of the IVD ECM and provide proper structural support for IVD cells. Scaffolds can carry and release therapeutic biological factors. These findings contribute to IVD tissue engineering strategies. Tissue engineering strategies should be devised, considering the pathological changes of IVDD with the aim to reverse degeneration, namely: (1) cell proliferation should be promoted and cell apoptosis should be inhibited to ensure cell density; (2) the IVD microenvironment should be ameliorated to mitigate cellular stress and inhibit inflammation; and (3) anabolic/catabolic balance should be mediated to ensure the quality and the quantity of the ECM.

IVD AND THE MICROENVIRONMENT

Anatomy and Composition of the IVD

The IVD is an articular cartilage structure located between the vertebral bodies and accounts for 25–30% of the overall length (height) of the spine. An IVD consists of the NP, the AF, and the CEP. The primary function of the IVD is to provide mechanical support for the vertebral body and allow movement of the spine (flexion, extension, and rotation) (Devereaux, 2007).

The NP is a centrally located highly hydrated gel-like structure consisting of NP cells and the ECM. The cell density in the NP is low (3,000/mm^3), and the cell types are not completely clear, mainly containing small chondrocyte-like nucleopulpocytes (NPCs) and large vacuolated notochord cells (NCs) (Wang et al., 2014). The ECM of the NP is quite different comparing to that of hyaline cartilage and is mainly synthesized by the NPCs. It contains mostly aggrecan [a large proteoglycan (PG) aggregate], a high ratio of type II/type I collagen, hyaluronic acid (HA), and secondary components (type IX/VI/V collagen and small proteoglycans). PGs are widely found in cartilage, the brain, IVDs, tendons, and corneal tissues. They provide viscoelastic properties, retain water, maintain osmotic pressure, and arrange collagen tissue. Aggrecan in the IVD contains more keratin sulfated (a highly hydrated sulphated glycosaminoglycan). Thus, it provides more hydration ability (Iozzo and Schaefer, 2015; Frapin et al., 2019; Harmon et al., 2020). HA is a widely expressed glycosaminoglycan (GAG) located in the ECM, intracellular environment, and the cell surface that interacts with specific proteins, such as aggrecan, versican, lymphatic vessel endothelial HA receptor-1, tumor necrosis factor (TNF)-inducible gene-6 protein, and thrombospondin as well as membrane receptors, such as CD44, HA-mediated motility receptor, and Toll-like receptor 4/2. Thus, it plays a role in morphogenesis, cell migration, cell survival, apoptosis, inflammation, and tumorigenesis (Dicker et al., 2014). HA binds to PGs to form aggrecan, which highly hydrates NP and generates a hydrostatic pressure to effectively absorb stress, reduce vibration, and maintain the osmotic pressure and disk height of healthy IVDs (Raj, 2008; Brown et al., 2012; Wang et al., 2014). A small part of small leucine-rich proteoglycans (SLRPs) in PGs, which mediate tissue order, cell proliferation, matrix adhesion, and the responses between cell and biological factors, is an important signal transduction factor and receptor for the development, morphogenesis, and immunization activities of IVDs. Recent research has reported that SLRPs are related to IVDD, where the asporin gene in the SLRP family rapidly upregulates after the age of 22. SLRPs also exhibit an increased expression in degenerated IVDs (Song et al., 2008; Gruber et al., 2009). Type II collagen is the most critical collagen in the NP for forming irregular networks to support PGs and water. The distinctive arrangement equalizes the NP stress in different directions and, together with water, makes the NP elastic

(Colombier et al., 2014). As IVD degeneration progresses, type II collagen is gradually replaced by low-elasticity type I collagen, and the fibrotic NP gradually loses its biomechanical function.

The AF is comprised of 15–25 layers of angle-ply collagen fiber lamellas containing PGs, arranged in concentric circles outside the NP (Chu et al., 2018), and contains AF cells (AFCs) and ECM. The AF is divided into the outer AF and the inner AF. The outer AF mainly consists of dense and organized type I collagen. Thus, it has robust tensile strength, while the inner AF contains a lower ratio of type I collagen as the transition zone between the AF and NP. The density of AFCs is about 9,000/mm^3 and mainly consists of fibroblast cells (Raj, 2008). NP generates a hydrostatic pressure when IVDs are under axial stress and releases fluid shear stress to the AF. The multi-lamellated AF structure effectively converts the axial stress to interlamellar stress and produces annular stress to resist it (Liu et al., 2001; Iu et al., 2017). The AF can withstand compression and tensile stress during movement of IVDs.

The CEP is a hyaline cartilage structure that connects the vertebral bodies to the IVD. The CEP is comprised of hyaline cartilage cells and chondrocytes that produce PGs and type II collagen to transport nutrients and metabolites to the IVD, which is avascular tissue. The blood supply ends in the CEP, making the CEP a critical transportation junction. The CEP also bears the stress from the IVD to protect the vertebral bodies (McFadden and Taylor, 1989; Roberts et al., 1989; Fontana et al., 2015; Frapin et al., 2019).

As the core of this structure, the stable and enclosed microenvironment of the NP guarantees the expression of the ECM, which supports and separates the vertebrae, absorbs shock, permits transient compression, and allows for movement. NPCs also affect the expression of the AFC ECM. A healthy ECM (mainly type 1 collagen in the outer AF) is comprised of dense AF lamella, which provides protection for the NP microenvironment. Besides bearing sagittal stress, the CEP is the sole pathway of metabolite exchange for the avascular NP. These three parts together form a unique anatomical structure, which maintains homeostasis of the IVD microenvironment in unity and maintains healthy IVD function.

Physiological Microenvironment

The IVD is in a unique microenvironment: avascular, hypoxic, hyperosmotic, acidic, and with low diffusion of metabolites and restricted by biomechanics (Roberts et al., 1996; Bartels et al., 1998; Wuertz et al., 2008). During early embryonic development, a rod-like notochord is located in the central area of the embryo and guides the ectoderm folds in on itself over the notochord to form neural tube mesenchymal cells (MSCs) to form vertebral bodies and the AF. NCs are trapped inside and participate in the formation of the NP. NCs are considered to be involved in the regeneration of the NP through cellular dialogue with other cells. NCs disappear in most human adults before the bone matures, but signs of IVDD occur not long after their disappearance (Hunter et al., 2003).

The cellular dialog between NCs and NP cells, which is triggered by multiple biological factors, maintains IVD homeostasis. These biological factors can also mediate the IVD microenvironment.

One of the critical factors mediating cell metabolism is hypoxia-inducible factor (HIF) (Semenza et al., 1994). HIF is a transcription factor that initiates a coordinated cellular cascade in response to a low-oxygen tension environment, including the regulation of numerous enzymes in response to hypoxia (Li et al., 2013). The HIF-1 α-subunits remain stable in hypoxic conditions but rapidly degrade under normoxic conditions. At the same time, HIF-1α and HIF-2α activities are stable in IVD, which illustrates that these two factors are positively related to IVD activity (Wang et al., 1995; Agrawal et al., 2008; Li et al., 2013).

Hypoxia-inducible factor is associated with most cell activities in the IVD. HIF-1α regulates the glycolytic activity of NPCs to ensure an energy supply under hypoxia, which results in the acidic microenvironment in the IVD (Agrawal et al., 2007; Kalson et al., 2008). HIF promotes the synthesis of PGs, type II collagen, and GAGs by direct or indirect pathways (Agrawal et al., 2007; Li et al., 2013; Liu et al., 2017). It also inhibits Fas/FasL-mediated apoptosis of NPCs by inducing the expression of Galectin-3. The expression of HIF-1α increases significantly in degenerated IVDs and is correlated with cell apoptosis (Ha et al., 2006; Li et al., 2013). HIF-2α regulates the expression of aggrecan and type II collagen by regulating the expression of catabolic factors (MMPs-13 and ADAMTS-4). The expression of HIF-2α, MMP-13, and ADAMTS-4 increases significantly, while the expression of aggrecan and type II collagen decreases significantly in degenerated IVDs (Huang et al., 2019), indicating that HIF plays an essential role in maintaining the IVD ECM. The hypoxic environment is destroyed after IVDD occurs; the absence of HIF can further accelerate degeneration (Meng et al., 2018).

Vascular endothelial growth factor (VEGF) is important during vasculogenesis and angiogenesis and mainly targets endothelial cells (Apte et al., 2019). Interestingly, the VEGF protein and its receptors are expressed in the avascular NP (Fujita et al., 2008). VEGF-A has a strong angiogenic activity and specific effects of mitosis and chemotaxis on endothelial cells (Risau, 1997). The expression of VEGF-A can be induced by hypoxia, leading to a local vascular invasion, but, typically, VEGF-A expressed by NPCs will not cause neovascularization. The reason may depend on the inhibition of endothelial cell adhesion and migration by the high aggrecan content in the IVD (Johnson et al., 1976). The complex of VEGF-A and its receptor VEGFR-1 also inhibit NP cell apoptosis (Fujita et al., 2008).

Nucleus pulposus cells stimulate NCs to secrete connective tissue growth factor (CTGF) and sonic hedgehog (Shh) by secreting transforming growth factor (TGF-β). CTGF and Shh together inhibit the expression of MMPs and stimulate the expression of tissue inhibitors of metalloproteinases (TIMPs), which inhibit MMPs, thereby suppressing the degradation of the ECM (Erwin et al., 2006; Erwin, 2008; Frapin et al., 2019). CTGF and Shh also stimulate the anabolism of the NP ECM and inhibit NP neovascularization and apoptosis by inhibiting VEGF, interleukin (IL)-6, and IL-8. Shh also promotes the proliferation of AF and CEP cells.

The bone morphogenetic protein (BMP) family promotes ECM synthesis by impacting the cellular dialog between NCs and NP cells and regulates the production of MMPs

(Leung et al., 2017; Frapin et al., 2019). BMP-2 and osteogenic protein-1 (BMP-7) upregulate the expression of aggrecan and type II collagen, promote the synthesis of GAGs, and concomitantly inhibit the expression of profibrotic genes. BMP-2 and BMP-7 are the most effective factors in the family stimulating the accumulation of PGs, while BMP-4 and growth differentiation factor-5 GDF-5 (BMP-14) stimulate the accumulation of collagen (Zhang et al., 2006; Leung et al., 2017; Li et al., 2017).

The characteristics of high osmotic pressure and high hydration ensure the biomechanical function of the IVD. As a weight-bearing organ, the metabolic and cellular activities of the IVD are closely related to the biomechanical microenvironment (Neidlinger-Wilke et al., 2014). External loads on the spine result in intense pressure on the disk. Intradiscal pressure varies from 0.1 to 2.3 MPa in different locations (Wilke et al., 1999; Neidlinger-Wilke et al., 2014). Severe degeneration can unbalance sagittal/coronal stress, resulting in abnormal stress of degenerated segments (Le Huec et al., 2011). NP cells in the IVD are mainly under extensive hydrostatic pressure, AF cells are under tensile strain, and the CEP is under compression due to its location at the interface (Le Maitre et al., 2004; Setton and Chen, 2006). The cytoskeleton of the IVD cells responds to the mechanical microenvironment. High osmotic pressure has positive effects on metabolic activity and matrix gene expression by IVD cells, and changes in hydrostatic pressure affect the synthesis of PGs by regulating the production of nitric oxide (Liu et al., 2001).

Interactions between different components in the IVD microenvironment maintain the homeostasis of the microenvironment (**Figure 1**). Due to aging, impaired disk function, loss of cells, and imbalance of ECM anabolism/catabolism, the homeostasis of the microenvironment breaks down, eventually resulting in pathological IVDD.

Pathological Environment

The degenerative mechanisms are very complex and are related to various causes, such as age, genetics, the microenvironment, and biomechanics (Frapin et al., 2019). Early degeneration may be asymptomatic. Signs may be detectable by radiography, while the reduction in water content of NP can be visualized by magnetic resonance imaging due to the reduced synthesis of PGs and reduced disk height of the IVD on a computed tomography scan (Modic et al., 1988). Four main changes occur during degeneration: (1) cell senescence, (2) imbalance of ECM anabolism/catabolism, (3) inflammatory microenvironment, and (4) abnormal biomechanics (**Figure 2**).

Cell Senescence

Cellular senescence, which is a fundamental mechanism that mediates age-related dysfunctions and chronic diseases, accumulates in human, bovine, and rat degenerative IVDs during aging (Roberts et al., 2006; Gruber et al., 2007; Kim et al., 2009; Muñoz-Espín and Serrano, 2014; van Deursen, 2014; Sharpless and Sherr, 2015). Unlike apoptosis, senescent cells are metabolically viable and arrest at the cell cycle transition, cease proliferation, and exhibit an altered expression of various catabolic cytokines and degrading enzymes (Campisi, 2005; Davalos et al., 2010; Muñoz-Espín and Serrano, 2014; van Deursen, 2014; Sharpless and Sherr, 2015). Two intrinsic pathways are related to cellular senescence in IVDs: the p53-p21-RB pathway in a telomere-dependent manner and stress-induced premature senescence that activates the p16INK4a -RB pathway independently of telomere length (Ben-Porath and Weinberg, 2005). A stimulus from the microenvironment can cause damage to IVD cells, resulting in early senescence.

Senescent cells in degenerated disks can form senescent cell clusters, which can cause inflammatory stress by secreting pro-inflammatory cytokines and accelerate the senescence of neighboring cells (Wang et al., 2016). As a result, cellular senescence, impaired self-repair capacity, increased inflammation, and enhanced catabolism gradually lead to deterioration of the microenvironment and cause disorder in the cellular dialogue and an imbalance of anabolism/catabolism.

Imbalance of ECM Anabolism/Catabolism

The ECM provides mechanical support for the IVD and is essential for maintaining the relatively avascular and aneural nature of a healthy disk. Proteoglycans, which are a primary component of the ECM, retain water and contribute to the osmotic pressure responsible for NP biomechanical properties. In the early stage of degeneration, proteoglycan content gradually decreases and is a sign of early degeneration. Type I collagen makes IVDs fibrotic, while type II collagen makes IVDs elastic. The proportions of collagen in the disk change with degeneration of the matrix. The absolute quantity of collagen changes little, but the type and distribution of the collagen can be altered. The ratio of collagen type II/type I decreases, and fibronectin content increases with increasing degeneration. As a result, the disk becomes more fibrotic and less elastic (Raj, 2008; Wang et al., 2016).

The balance between anabolism and catabolism is positively related to the IVD microenvironment, and the cellular dialogue, metabolic enzyme activity, and biomechanical changes affect this balance. As the population of NCs decreases with age, the cellular dialogue between NCs and NPCs gradually diminishes. Anabolic activity is mediated by biological factor disorders, while catabolic activity continuously progresses (Freemont, 2009).

MMPs, disintegrin, and metalloproteinase with thrombospondin motifs (ADAMTS) are important catabolic factors in disk degeneration. ADAMTS1, 4, 5, 9, and 15 are aggrecanases that degrade aggrecan, while MMP1, 8, and 13 are collagenases that cleave fibrillar collagen (Weiler et al., 2002; Le Maitre et al., 2004; Bachmeier et al., 2009; Vo et al., 2013). Upregulation of MMP and ADAMTS expression and enzymatic activity is implicated in the destruction of the disk ECM, leading to the development of IVDD (Bachmeier et al., 2009; Pockert et al., 2009; Vo et al., 2013). TIMP, which is a specific inhibitor of MMPs, binds to the active forms of MMPs to suppress catabolic enzyme activity. However, the activities of MMPs, ADAMTS, and TIMP are all regulated by inflammation-related factors, particularly pro-inflammatory factors. PGs in the IVD are proposed as a barrier to vascular and neural ingrowth into the NP (Khan et al., 2017). As PG contents decrease, the inhibiting effect for the neovascularization function

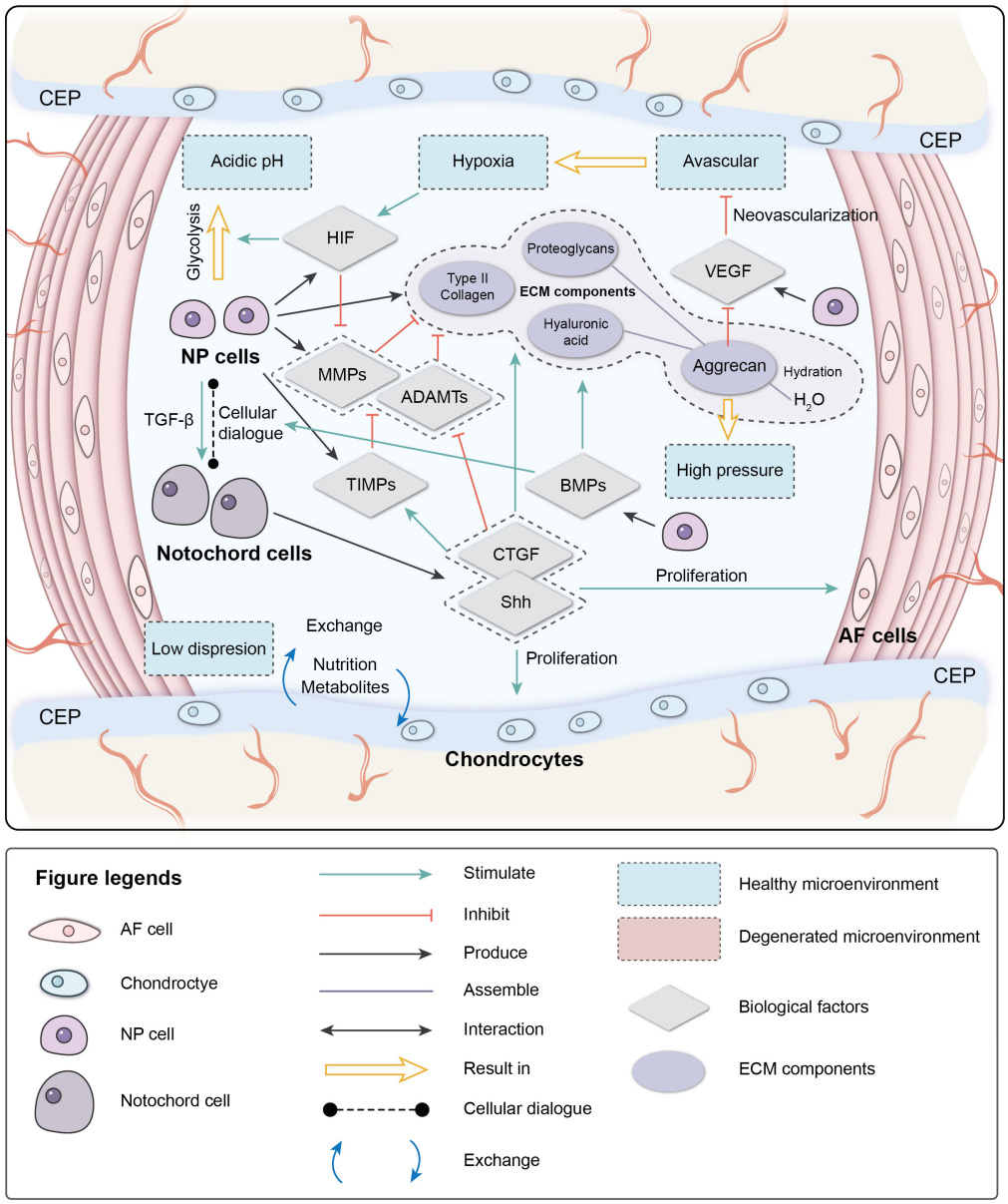

FIGURE 1 | Physiological microenvironment of intervertebral disk (IVD). AF, annulus fibrosus; NP, nucleus pulposus; CEP, cartilage endplate; ECM, extracellular matrix; HIF, hypoxia-inducible factor; MMPs, metalloproteinases; ADAMTs, metalloproteinase with thrombospondin motifs; TIMPs, tissue inhibitors of metalloproteinases; CTGF, connective tissue growth factor; Shh, sonic hedgehog; BMPs, bone morphogenetic protein; VEGF, vascular endothelial growth factor.

of VEGF weakens. Moreover, AF fissures caused by abnormal biomechanics allow neovascularization and neoinnervation from a lack of PG production. As a result, NP is invaded by immune cells transported by new blood vessels. Immune cells respond to the deteriorating microenvironment, eventually leading to inflammation.

Inflammatory Microenvironment

Inflammation is an adaptive response triggered by noxious stimuli and conditions, such as infection and tissue injury. Regardless of the cause, inflammation presumably evolved as an adaptive response to restore homeostasis. If the acute inflammatory response fails to eliminate the pathogen, the inflammatory process persists and acquires new characteristics (Majno and Joris, 2004; Medzhitov, 2008). The IVD is an avascular tissue until neovascularization occurs due to degeneration. Crystals and ECM breakdown products may be responsible for causing the IVD inflammatory response (Medzhitov, 2008). When anabolism/catabolism becomes unbalanced, degradation products trigger inflammation. In human IVD cells, HA fragments upregulate the mRNA expression levels of the inflammatory and catabolic genes IL-1β,

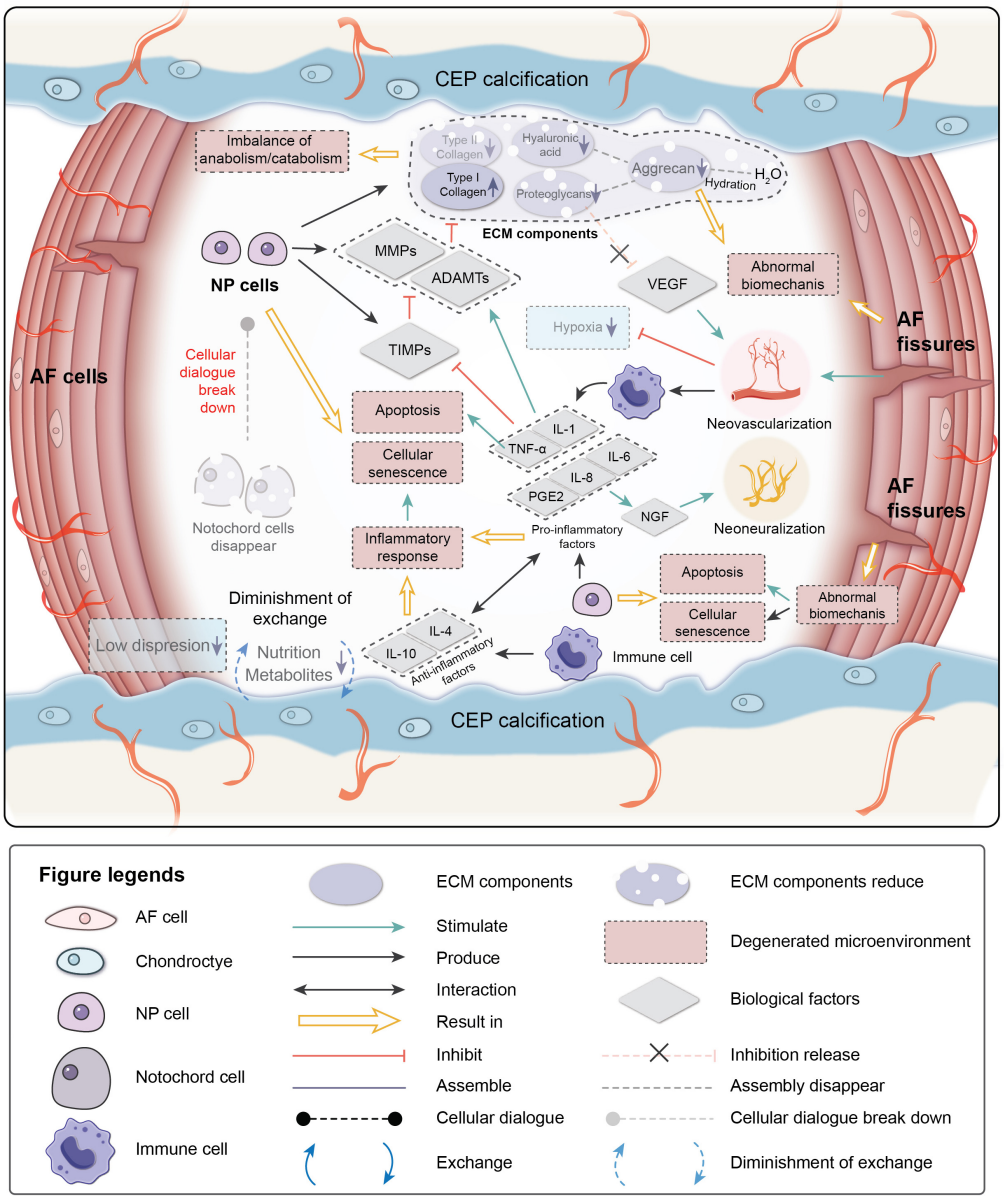

FIGURE 2 | Pathological microenvironment of intervertebral disk (IVD). AF, annulus fibrosus; NP, nucleus pulposus; CEP, cartilage endplate. ECM, extracellular matrix; MMPs, metalloproteinases; ADAMTs, metalloproteinase with thrombospondin motifs; TIMPs, tissue inhibitors of metalloproteinases; VEGF, vascular endothelial growth factor; NGF, nerve growth factor; IL-1,4,6,8,10, interleukin-1,4,6,8,10; TNF-a, tumor necrosis factor; PGE2, prostaglandin E2.

IL-6, IL-8, cyclooxygenase-2, MMP-1, and MMP-13 (Quero et al., 2013). After neovascularization occurs, immune cells migrate to the NP to respond to the microenvironment. NP embryologically develops in an enclosed structure, which makes NP an avascular and immune-privileged tissue. Hence, immune cells invade when disk degeneration progresses to a certain stage, making IVD inflammation a chronic process. Inflammatory factors play essential roles in mediating IVD homeostasis and degeneration.

TNF-α, IL-1β, and IL-1α are expressed by healthy IVD cells and immune cells (macrophages, monocytes, dendritic cells, B cells, and natural killer cells) (Le Maitre et al., 2005; Richardson et al., 2009; Wang et al., 2013), where they have been observed at increased levels along with other inflammatory mediators in degenerated IVDs (Le Maitre et al., 2005, 2007). TNF-α is a cytokine that stimulates the inflammatory response, induces nerve swelling and neuropathic pain, and promotes cellular apoptosis *via* its cytotoxic effect (Pedersen et al., 2015). IL-1β induces a catabolic response by NP cells at the molecular level (Smith et al., 2011). Together they stimulate the production of MMPs and ADAMTS by NPCs and suppress the expression of TIMPs, resulting in decreased synthesis of aggrecan and type II collagen by NPCs (Frapin et al., 2019). Pro-inflammatory

factors are also related to pain. IL-6, IL-8, and prostaglandin E2 synthesis by NPCs stimulate nerve growth factor production, which induces abnormal nerve ingrowth and causes pain (Frapin et al., 2019). IL-6 and IL-8 are both higher in severe sciatica patients, and IL-6 is correlates to low back pain frequency (Khan et al., 2017). A herniated disk impinging on the nerve root is painless in 70% of patients, and it is likely that the secretion of products involved in the inflammation cascade in a torn AF sensitizes the nerve root or increases the number of innervations, thereby causing pain (Sharifi et al., 2015). Anti-inflammatory activity is also part of the IVD microenvironment. IL-4 and IL-10 are anti-inflammatory factors produced by activated macrophages and monocytes. They participate in pro-inflammatory/anti-inflammatory balance and inhibit the synthesis of pro-inflammatory cytokines (Khan et al., 2017).

Abnormal Biomechanics

Intervertebral disk degeneration can also be affected by the biomechanical environment. A positive dose-response relationship is observed between cumulative lumbar load and early onset of symptomatic lumbar disk space narrowing: the disk disease onset time of workers with the highest exposure to heavy physical constraints is significantly advanced compared to others (Petit and Roquelaure, 2015). Xing et al. (1976) designed an amputated-leg rat model. Due to the forelimb amputation, the IVDs underwent abnormal mechanical loading. The results of senescence-associated β-galactosidase-positive staining showed that IVD cell senescence accelerates due to the abnormal loading of rat lumbar IVDs (Xing et al., 1976). Constant pressure on the disk can cause degeneration, which may be related to the upregulation of matrix degradation-related enzymes (Yurube et al., 2012; Neidlinger-Wilke et al., 2014). The mechanical load can also induce IVD cell apoptosis through the mitochondrial pathway (Rannou et al., 2004; Kuo et al., 2014).

Briefly, IVDs are continually adapting to changes in the microenvironment from embryogenesis to degeneration under the regulation of numerous factors (Colombier et al., 2014). The avascular and immune-privileged NPs regulate cell activity *via* cellular dialogue (Fontana et al., 2015; Henry et al., 2018). ECM synthesized by IVD cells ensures the biomechanical function of IVD. The CEP ensures transport of nutrients and metabolites (Zhang et al., 2018). When degeneration begins, interactions between components in the microenvironment break down, resulting in cascades of degeneration (Freemont, 2009). Therefore, therapeutic strategies should first consider how to relieve pain and regain IVD function in patients and, furthermore, correct the factors causing degeneration to eventually achieve ideal IVD regeneration and functional restoration.

CURRENT IVDD TREATMENTS

Non-surgical Treatments

Intervertebral disk degeneration is inevitable; 60–90% of patients can be treated non-surgically as long as no symptoms occur or mild symptoms that occur do not affect daily life (el Barzouhi et al., 2013; Chiu et al., 2015). Non-surgical treatments include non-pharmacological treatments, pharmacological treatments, and interventional treatments. Non-pharmacological treatments, such as exercise, traction, acupuncture, massage, physical therapy, and spinal manipulation, are applied in daily life, but only for second-line or adjunctive treatment options with insufficient evidence for cure (Kreiner et al., 2014; Foster et al., 2018). More than 50% of patients with IVDD have used drugs. Non-steroidal anti-inflammatory drugs are most applied drugs for pain relief and improved function. Oral glucocorticoids alleviate the inflammation of nerve roots. At the same time, muscle relaxants can be useful to relieve muscle spasms, but these drugs are discouraged for lack of sufficient evidence (Kreiner et al., 2014; Ramaswami et al., 2017; Foster et al., 2018; Benzakour et al., 2019; Lee et al., 2019).

A meta-analysis reported that the therapeutic effect of an epidural injection intervention treatment is better than an intradiscal injection, percutaneous discectomy, traction, physical therapy/exercise, radiofrequency therapy, or chemonucleolysis (Lewis et al., 2015). However, interventional treatments are discouraged in the guidelines (Foster et al., 2018).

The goal of non-surgical treatments is to relieve symptoms and improve function, but they cannot halt the degeneration. Surgical treatments are required when non-surgical treatments are unable to relieve symptoms.

Surgical Treatments

Mixter and Barr (1934) reported that a tumor in the spinal canal, which causes sciatica, was a herniated NP. Laminectomy, combined with excision of the NP, was performed, and satisfactory results were obtained (Mixter and Barr, 1934). Since then, surgical treatments to treat disk herniation have been developed. Four main types of surgical procedures are used: (1) decompression for neurological problems, (2) fusion to abolish motion at a functional spinal unit, (3) motion preservation/modifying surgery in the form of disk replacement/dynamic fixation devices, and (4) deformity surgery to realign the biomechanics between a large number of functional spinal units (Eisenstein et al., 2020). The purpose of decompression surgery is to relieve pain and numbness caused by nerve compression, and the most common procedure is discectomy.

A discectomy removes disk tissue that oppresses nerve roots in the intervertebral space. An emergency discectomy is required for patients who already have cauda equina syndrome and a new motor disorder. Selective discectomy is required for patients with persistent neurological symptoms that cannot be relieved by non-surgical treatments (Butler and Donnally, 2020).

Discectomy can be open or minimally invasive. Open discectomy is performed in a wide range of operations but with more tissue damage. Minimally invasive discectomy causes less tissue damage, but indications are limited. A meta-analysis showed that the incidence of postoperative complications and reoperations is similar, while less blood loss, shorter operating time, and shorter hospital stay are common after minimally invasive discectomy (Alvi et al., 2018;

Li et al., 2018a; Butler and Donnally, 2020). Discectomy relieves nerve root compression, relieves pain while retaining some of the structure, and restores some of the biomechanical functions of the disk. However, discectomy cannot change the deteriorating microenvironment. Therefore, further progression of degeneration cannot be prevented, and postoperative complications may occur (12.5, 13.3, and 10.8% for open microdiscectomy, microendoscopic discectomy, and percutaneous microdiscectomy, respectively) (Shriver et al., 2015). The AF must be broken to perform this surgery, and no new AF tissue is formed, so the opening remains open or is closed with the formation of scar tissue, which might cause reherniation (Sharifi et al., 2015).

Spinal fusion is a classic procedure. Hibbs and Albee treated Pott disease using fusion. Fusion abolishes pain by abolishing the motion of adjacent segments (Hibbs, 1964). Spinal fusion is widely used to treat many spinal diseases and is the gold standard for treating significant, chronic axial low back pain due to IVDD. About 60–65% of lumbar fusion procedures are performed for degenerative disk disease (Lee and Langrana, 2004; Auerbach et al., 2009). Spinal fusion completely removes the IVD and entirely relieves the oppression on the nerve roots, where the degenerated segments become integrated and lose motor function. Although the pain symptoms are relieved, the native IVD microenvironment is destroyed. The motor function is abolished, which may cause long-term complications. The mechanical environment of adjacent segments is affected and may develop into adjacent segmental disease (Lee and Langrana, 1984; Hilibrand and Robbins, 2004; Virk et al., 2014; Hashimoto et al., 2019).

Artificial disk prosthesis replacement surgery is performed to restore disk height, biomechanical structure, and motor function of the IVD and overcomes some deficiencies of spinal fusion. This procedure was first applied in the 1950s. As more and more prostheses have been developed, disk replacement surgery has developed quickly (Guyer and Ohnmeiss, 2003; Zhao et al., 2019). Disk replacement surgery effectively relieves pain and improves the quality of life, but it is not a superior substitute surgery for fusion. The average reoperation rate is 12.1% during follow-up after lumbar disk replacement or cervical disk replacement. Postoperative complications, such as prosthesis failure, infection, adjacent segmental disease, and pain, can occur, yet no evidence demonstrates that the surgical effect of disk replacement is better than fusion (Thavaneswaran and Vandepeer, 2014; Cui et al., 2018; MacDowall et al., 2019). The effect of disk replacement surgery greatly depends on the type of prosthesis and surgical technique of the surgeon. An artificial disk prosthesis replicates the anatomical structure of the IVD and attempts to mimic its biomechanical properties. The risk of adjacent segmental disease is reduced compared with fusion (Findlay et al., 2018). However, it is similar to fusion surgery in that the native IVD microenvironment is destroyed. Further follow-up studies are needed to investigate the long-term efficacy and safety of disk replacement surgery.

Several experimental surgeries have been developed. AF sutures strengthen the intensity of AF; thus, they restrict NP from herniating but cannot prevent the progression of IVDD (Marcolongo et al., 2011). Annuloplasty is a minimally invasive method in which heat produced by electricity or radiofrequency radiation strengthens the collagen fibers and seals fissures in a process similar to tissue soldering (Helm Ii et al., 2017). Nucleoplasty releases the pressure on the outer AF, allowing the disk to return to normal size, thereby decompressing the nerve, with better therapeutic effects than non-surgical treatments. This procedure can be performed in the clinic, and the patient recovers quickly after the procedure, but the indications of this procedure are limited (Eichen et al., 2014; Liliang et al., 2016; de Rooij et al., 2017).

Patients who undergo surgery may have better pain relief, functional improvement, and satisfaction than those who receive non-surgical treatments. Nevertheless, long-term follow-up shows that disability outcomes are similar regardless of which treatment a patient receives (Atlas et al., 2001, 2005), suggesting that current strategies can only alleviate symptoms and that regenerative strategy is key to solving IVDD.

TISSUE ENGINEERING STRATEGIES

Surgical treatments for IVDD have developed rapidly, but the limitations of surgical treatments are becoming apparent. Thus, researchers have turned their attention to tissue engineering strategies. Tissue engineering is "an interdisciplinary field that applies the principles of engineering and life sciences toward the development of biological substitutes that restore, maintain, or improve tissue function or a whole organ," as defined by Langer and Vacanti (1993). Mizuno et al. (2004) fabricated the first documented IVD scaffold of polyglycolic acid and polylactic acid. The scaffold was seeded with AF cells. NP cells were injected into the center after 1 day. Then, the scaffolds were implanted in the subcutaneous space of the dorsum of athymic mice. The results showed that the engineered disks strongly resembled native IVDs and synthesized similar collagen components as native NP and AF (Mizuno et al., 2004; Hukins, 2005). This attempt was initially intended to identify an alternative strategy for IVD replacement due to its long-term deficiencies. The flaws in that study included the cell source, immunological rejection, and fixation of the scaffold, but that study inspired researchers to try tissue engineering strategies for IVDD. Various strategies have been formulated based on different treatment principles. It is important to note that there are no separate strategies, only those that are focused on in the study.

Scaffold Strategy: From Natural ECM Mimetic to Multifunctional Platform

Scaffolds were initially designed as cell substrates to mimic the microenvironment where cells live. An ECM scaffold is similar to the native microenvironment of cells and has excellent biocompatibility and immunogenicity, which are beneficial for cell proliferation and metabolic activities. Yang et al. (2008) fabricated a decellularized ECM scaffold derived from human cartilage, and the scaffold successfully generated cartilaginous tissue in nude mice. As the AF is a fibrous cartilage structure and has a similar ECM

composition to cartilage, an ECM scaffold might be feasible to regenerate AF. McGuire et al. (2017) fabricated an ECM scaffold made of decellularized pericardial tissue. Collagen patches were obtained from treated pericardial tissue. These patches were assembled into a multi-laminate angle-ply scaffold. This scaffold mimicked the structure of AF, provided similar mechanical support, and supported cell viability, infiltration, and proliferation for bovine AF *in vitro* (McGuire et al., 2017).

Complete AF regeneration requires the recovery of biomechanical and structural properties of healthy AF and the restoration of the biological behavior of resident cells in AF (Driscoll et al., 2013). The alignment and organization of AF cells determine their biomechanical functions. As manufacturing technology develops, fabricating methods, such as electrospinning and 3-D printing, provide the possibility for microstructural scaffolds. Microstructural scaffolds guide the cells to form a specific order and are widely applied in AF tissue engineering due to their unique structure. Ma et al. (2018) developed a hybrid scaffold for AF tissue engineering. This hybrid scaffold consisted of traditional electrospun aligned nanofibrous scaffolds (AFS) as a baseline scaffold and electrospun aligned nanoyarn scaffolds (AYS). Morphological measurements showed that this hybrid scaffold replicates the tensile strength, axial compression, and anisotropic properties of AF tissues to some degree. Mechanical testing demonstrated that the tensile properties of AFS and AYS were qualitatively similar to those of native AF tissue. *In vitro* biocompatibility analyses demonstrated that the AYS and HS yield improved bone marrow mesenchymal stem cell (BMSC) proliferation (Ma et al., 2018). Gluais et al. (2019) fabricated electrospun aligned microfibrous scaffolds that recruit neighboring healthy AF cells to migrate to the scaffold, which promotes cell colonization and proliferation. The results showed that, in addition to numerous dense collagen fibers in the aligned scaffolds, the fibers were arranged in the same direction as the scaffold (Gluais et al., 2019). Kang et al. (2018) combined electrospinning and 3D printing techniques to fabricate a biomimetic biodegradable scaffold that consisted of multi-lamella nano/microfibers. Each lamella contained one layer of aligned electrospun nanofibers and one layer of supporting 3D printed microfibers on each side, which were all aligned in the same direction, and the angle of the fibers between adjacent layers was 60°. The nano/microfibres aligned as native collagen tissue of AF. These results show that these scaffolds can form and integrate collagen fibers (Kang et al., 2018).

However, electrospun scaffolds often face several limitations, including low porosity that restricts uniform cell infiltration and a discrepancy of mechanical properties compared with native AF. To recapitulate the form and function of the complex anatomy of AF, Bhunia et al. (2018) adopted a directional freezing technique to fabricate silk-based multi-layered disk-like angle-ply (±30° of successive layers) bio-artificial scaffolds. The fabricated bio-discs supported the primary AF or human mesenchymal stem cell proliferation, differentiation, and deposition of a sufficient amount of specific ECM *in vitro*. The subcutaneous implantation results showed a negligible immune response (Bhunia et al., 2018).

Three-dimensional printing precisely fabricates the scaffold structure. To generate a scaffold with angle-ply architecture similar to natural AF, Christiani et al. (2019) printed laminar constructs comprised of polycaprolactone (PCL) struts oriented at alternating angles of ±30°. The mechanical characterization results showed that the mechanical properties of the scaffolds were similar to native AF tissue. They also cultured bovine AFCs with smooth-surface PCL and unidirectional channel-etched PCL to further study cell arrangement and ECM deposition, respectively. The SEM micrographs of the scaffolds showed that cells cultured on etched PCL had a tendency to align along the underlying surface, and the alignment of proteins with the underlying surface texture can be observed (Christiani et al., 2019).

However, PCL materials have poor hydrophilicity, have a long degradation time, and lack cell recognition sites. PCL materials bind poorly to surrounding host tissues after implantation *in vivo* (Cheng et al., 2017). Three-dimensional bioprinting achieves precise bionics according to the structure and size of native tissues and organs (Kang et al., 2016). As a novel technology, 3D bioprinting shows great potential and enormous advantages in the repair of IVDs. Sun et al. (2021) fabricated a dual growth-factor-releasing IVD scaffold using 3D bioprinting. They loaded CTGF and transforming growth factor-β3 (TGF-β3) on polydopamine nanospheres (PDA NPs). Then, CTGF@PDA and TGF-β3@PDA were mixed with rat BMSCs as the 3D bioprinting ink. A 3D model of the IVD scaffold was designed using AutoCAD software, and the support structures of CEP and AF were printed using a PCL polymer, while the parts of the model corresponding to AF and NP were printed using 3D bioprinting ink. *In vitro* experiments confirmed that the growth factors were released from the IVD scaffolds in a spatially controlled manner and induced the corresponding BMSCs to differentiate into NP-like cells and AF-like cells. After being implanted subcutaneously into the dorsum of nude mice, the reconstructed IVDs exhibited a zone-specific matrix: primarily type II collagen and glycosaminoglycan in the core zone and type I collagen in the surrounding zone (Sun et al., 2021).

In addition to providing mechanical support and topographic stimulus for cells, scaffolds can also be loaded with therapeutic drugs or cells. Cheng et al. (2011) fabricated an injectable thermosensitive chitosan/gelatin/glycerol phosphate hydrogel as a controlled release system for ferulic acid (FA) delivery. FA is an excellent antioxidant drug. The scaffolds were incorporated with FA, added to Transwells, and incubated with H_2O_2-induced NP cells *in vitro*. The results showed that these scaffolds achieved excellent antioxidant properties after loading with FA (Cheng et al., 2011).

Scaffolds are a crucial element of this strategy, as they provide a similar microenvironment for IVD cells by mimicking the structure of native IVDs. The scaffold strategy can also be combined with other strategies, such as delivery of therapeutic drugs or cells.

Cell Therapy Strategy and Derivative Strategies

Cell Therapy Strategy

Cell therapy is a classic strategy. An increasing number of studies have shown the efficacy of therapeutic cells in several IVDD animal models (Hiyama et al., 2008; Jeong et al., 2009; Henriksson et al., 2019). One study reported that stem cells and stem-like cells are found in almost all adult tissues (da Silva Meirelles et al., 2006).

Due to the potential of stem cells to differentiate, replacing damaged cells in target tissues, stem cells are ideal therapeutic cells for IVD tissue engineering (Krause, 2008; Meirelles Lda et al., 2009). Mesenchymal stem cells and induced pluripotent stem cells (iPSCs) are the most widely used in IVD cell therapy (Wei et al., 2014; Vickers et al., 2019). Several studies have demonstrated the ability of BMSCs and adipose-derived stem cells to differentiate into an NP-like phenotype, and *in vivo* studies have demonstrated the ability of implanted MSCs to enhance matrix production, particularly GAG synthesis, and increase disk height and hydration (Richardson et al., 2006; Gantenbein-Ritter et al., 2011; Stoyanov et al., 2011; Clarke et al., 2014). iPSCs differentiate into NCs or NP-like cells and reduce IVDD after transplantation *in vivo* (Sheyn et al., 2019; Xia K. et al., 2019).

Researchers have attempted different methods to transport therapeutic cells to diseased areas, such as direct injection of therapeutic cells or loading of cells onto scaffolds. Hiyama et al. (2008), Jeong et al. (2009), and Henriksson et al. (2019) injected human MSCs into rat, dog, and pig disk degeneration models, respectively. The results showed that transplantation of human MSCs has a positive repair effect on the xenogeneic animal disk degeneration model. Sheyn et al. (2019) induced human iPSCs to differentiate into notochordal cells *in vitro* and proved their regenerative capacity *in vivo* in an annular puncture pig model.

However, direct injection by needle puncture causes damage to the AF, and implanted cells could leak out through annular fissures. AF damage can lead to further degeneration and an increased risk of disk herniation (Oehme et al., 2015). Scaffolds could be pivotal to provide transplanted cells with a supportive environment. Bhunia et al. (2018) seeded MSCs on AF structure-like scaffolds and reported ideal results as mentioned above. GDF-5 inhibits IVDD and promotes NP-like differentiation of stem cells (Taylor et al., 2011). However, such a factor could require multiple injections due to its short life *in vivo* (Jin et al., 2016). Xia C. et al. (2019) generated polymeric gelatin microspheres, which can release growth and differentiation factor-5 and act as a cell delivery vehicle for iPSC-derived NP-like cells. Then, they injected these cell-seeded polymeric microspheres into rat coccygeal IVDs, and the results indicated that disk height was recovered, water content was increased, and the NP ECM was partially restored (Xia K. et al., 2019). This study utilized growth factors to enhance the therapeutic efficacy of cells and prolong the life of growth factors *via* a polymeric gelatin microsphere as a sustained release platform. Multiple strategies complementing each other will become more important in IVD tissue engineering.

Recent studies have also revealed the existence of endogenous stem/progenitor cells in the IVD (Hu et al., 2018). Ying et al. (2019) found that stromal cell-derived factor-1α expression is higher in the degenerative IVD microenvironment and showed a positive effect on enhancing the proliferation and recruitment of endogenous NP-derived stem cells into IVDs *in vitro* and *in vivo*. These cells might be a promising source for cell therapy.

Cell-based therapies have the advantages of modulating inflammation and concomitantly affecting the remodeling process, without presenting toxicity or immunosuppression (Lopes-Pacheco et al., 2016). These properties make cell therapy an exceptionally advantageous therapeutic approach for IVD tissue engineering. Nevertheless, various complications occur with stem cells, including tumorigenesis and immune reactions. Certain cases of tumorigenesis and immune reaction of iPSCs and embryonic stem cells (which are also a cell source for iPSCs) have been reported, and the application risks are always discussed (Pera et al., 2000; Taylor et al., 2011; Lee et al., 2013; Kim, 2014; Jin et al., 2016). Compared to iPSCs and embryonic stem cells, MSCs seem to be safer, as no case of tumorigenesis has been reported after MSC transplantation *in vivo* (Oryan et al., 2017).

Although the transplantation of stem cells may have risks, their efficacy cannot be denied. Risks may be hedged by enhancing the immune compatibility of stem cells. Immune rejection is caused by HLA mismatching. Xu et al. (2019) generated HLA pseudo-homozygous iPSCs through CRISPR-Cas9, with allele-specific editing of HLA heterozygous iPSCs and HLA-C-retained iPSCs, which evade T and NK cells *in vitro* and *in vivo*. HLA-C-retained iPSCs combined with HLA-class II knockout are immunologically compatible with >90% of the world's population, greatly facilitating iPSC-based regenerative medicine applications (Xu et al., 2019). Cell strategies have potential in tissue engineering, but improving safety and avoiding risks should be given more attention in future studies.

Therapy Strategies Using Biological Factors

Biological factors are promising therapeutic drugs for IVDD as native mediators in the IVD microenvironment since they are key signaling factors in the cellular dialogue. Unlike conventional drugs, biological factors are secreted by IVD cells and have fewer side effects. Therapeutic biological factors

should be able to restore the healthy microenvironment of IVD. Therefore, biological factors should have at least one therapeutic function as follows: (1) pro-anabolism/anti-catabolism, (2) anti-inflammation, and (3) regulate cell activity. The application of biological factors is limited by their short life *in vivo*. Thus, biological factors are often used in conjunction with other strategies.

Researchers can customize biological factor scaffolds according to different conditions, with the key concept of restoring the balance of the microenvironment. Several widely used factors are introduced in **Table 1**.

Gene Therapy Strategy

Biological factors intercellularly mediate cell activities, while microRNAs (miRNAs) mediate intracellularly. Gene therapy is a strategy to achieve the durable expression of a therapeutic gene or "transgene" at a level sufficient to ameliorate or cure disease symptoms with minimal adverse events. Two basic strategies have been proposed. An integrating vector is introduced into a precursor or stem cell so the gene is passed to every daughter cell or the gene is delivered in a non-integrating vector to long-lived post-mitotic or slowly dividing cells, ensuring the expression of that gene for the life of the cell (High and Roncarolo, 2019).

Although the application of gene therapy to the IVD has lagged behind other tissues, gene therapy shows excellent potential and safety for IVD tissue engineering. As an encapsulated and avascular tissue, the sealing property of IVD effectively prevents leakage of the disk contents to other sites in the body (Levicoff et al., 2005). Some researchers are using gene-editing techniques, such as CRISPR, to precisely alter DNA sequences or genetically modify immune cells to imbue them with the ability to fight cancer. TNF-α and IL-1β are inflammatory cytokines related to the inflammatory microenvironment in IVDD through TNFR1/IL1R1 signaling. To regulate this signaling, Farhang et al. (2019) produced CRISPR epigenome-edited lentiviral vectors based on TNFR1/IL1R1 targeted screens and delivered the genes into human NPCs by lentiviral transduction. The expression of the editing vectors was confirmed by qRT-PCR. Measurement of NF-κB activity (which is a downstream transcription factor that mediates TNFR1/IL1R1 signaling), apoptosis, and anabolic/catabolic changes in gene expression demonstrated that the lentiviral vectors significantly downregulated TNFR1 and IL1R1 and significantly attenuated the deleterious microenvironment (Farhang et al., 2019).

Gene therapy provides a potentially ideal tool for many diseases by delivering synthetic miRNAs to regulate gene expression (Deverman et al., 2018). However, there are obstacles to delivering miRNAs directly to target tissues due to their inactivation, low transfection efficiency, and short half-life. Chen W. et al. (2020) synthesized agomir, which is cholesterol-, methyl-, and phosphorothioate-modified miRNA, with good stability and enhanced transfection efficiency, in animals. Agomir penetrates the barriers of the cell membrane and tissues *in vivo* to enrich target cells. Agomir874 downregulates the expression of MMPs in NP by mimicking miRNA874. Chen et al. loaded agomir on an injectable polyethylene glycol hydrogel and injected it into a rat IVD. After 8 weeks, the rat IVD was gradually restored to normal height, similar to the healthy group. These results show that agomir874 regulates the balance of synthesis/decomposition of the NP ECM and inhibits IVDD (Chen W. et al., 2020).

Six gene therapy products have been approved since 2016 (High and Roncarolo, 2019). Gene therapy is promising to be performed "one time," with long-term and high-value therapeutic effects. However, there are still some problems to be solved, such as safety issues and high treatment expense. Gene therapy is aimed at specific targets, which have been studied thoroughly, to regulate cell activities. Thus, gene therapy cannot be used to regulate a series of therapeutic targets or pathways as in cell therapy. Due to the encapsulated microenvironment of the IVD, gene therapy is still promising and not fully explored for IVDD treatment. Studies on safety and therapeutic mechanisms should be conducted in the future.

Extracellular Vesicle Therapeutic Strategy

Studies have confirmed that the mechanism of action of MSCs is predominantly paracrine (Lu et al., 2017; Zhu et al., 2020). Almost all types of cells secrete extracellular vesicles (EVs). As the main components of paracrine activity, EVs derived from MSCs achieve regenerative functions. The three main kinds of EVs are exosomes, microvesicles, and apoptotic bodies (El Andaloussi et al., 2013). Exosomes from MSCs have various effects on IVD regeneration, such as antioxidant, anti-inflammatory, anti-apoptosis, and proliferation-promoting effects (El Andaloussi et al., 2013; Lu et al., 2017; Xia C. et al., 2019). Due to the low immunogenicity and high efficiency of exosomes compared to MSCs, exosomes are promising substitutes for MSCs in cell therapy. The mechanism of its regenerative ability remains unclear, but it is very likely to be related to miRNAs. The level of miR-532-5p was observed to be decreased in TNF-α induced apoptotic NPCs but abundant in bone marrow mesenchymal stem cell (BMSC)-derived exosomes. Zhu et al. (2020) demonstrated that exosomes from BMSCs could deliver miR-532-5p and suppress the IVDD *via* targeting RASSF5. Cheng et al. (2018) also reported that exosomes from BMSCs could deliver miR-21, which could activate the PI3K/Akt pathway in apoptotic NPCs, and further inhibit IVDD.

Exosomes were also confirmed to be associated with pathological changes in IVDD. circRNA_0000253 has the maximum upregulation in degenerative NPC exosomes. Song et al. (2020) found that exosomes in NPCs were differentially expressed in degenerative and normal NPCs. The circRNA_0000253 levels notably increased and the miRNA-141-5p levels markedly reduced in degenerative NPCs compared with normal NPCs. Further research confirmed that the circRNA_0000253 could increase IVDD by adsorbing miRNA-141-5p and downregulating SIRT1 *in vivo* and *in vitro* (Song et al., 2020). This study also demonstrated that, in a degenerative microenvironment of IVD, communication between NPCs by secreting exosomes may aggravate degeneration. Utilizing or blocking degeneration-related exosomes might become a promising therapeutic strategy for IVD degeneration.

TABLE 1 | Several widely used therapeutic biological factors.

Factors	Targets	Scaffolds	Effects	Functions
GDF-5	Rat adipose-derived mesenchymal stem cells(ADSCs) *in vitro* and rat tail puncture model *in vivo*	Gelatin methacryloyl (GelMA) microspheres	(1) Exhibited good mechanical properties, biocompatibilities and enhanced the ADSCs differentiation into NP-like phenotypes *in vitro*. (2) Maintained NP tissue integrity and accelerated the synthesis of ECM *in vivo*.	Pro-anabolism and induce differentiation (Xu et al., 2020)
IGF-1	Human NPCs *in vitro*		IGF-1 protein treatment upregulated the IFG-1R and ER-α expression and promoted NP cell proliferation, collagen-II, and PCNA expression.	Pro-anabolism, promote proliferation and anti-inflammation (Chen R. S. et al., 2020)
SDF-1	Rat BMSCs *in vitro* and rat tail puncture model *in vivo*	Albumin/heparin nanoparticles (BHNPs)	(1) Induce migration of BMSCs *in vitro*. (2) Induce regeneration of annulus fibrosus and nucleus pulposus *in vivo*.	Pro-anabolism and induce migration (Zhang H. et al., 2018)
CCL5	Bovine AFCs and organ-cultured IVDs *in vitro*. Sheep AF rupture model *in vivo*.	Fibrin Gel	(1) Dose-dependent recruitment effect of CCL5 on AF cells were confirmed. (2) In the organ culture study CCL5 did not stimulate homing of AF cells toward the defect sites. (3) The pilot animal study did not show any repair effect of CCL5.	Induce migration (Zhou et al., 2020)
KGN	Human ADSCs *in vitro* and rat tail puncture model *in vivo*	Amphiphilic copolymer PEG-PAPO	(1) Enhanced the viability, autophagic activation (P62, LC3 II), ECM-related transcription factor (SOX9), and ECM (Collagen II, Aggrecan) maintenance in human ADSCs *in vitro*. (2) The injection of PAKM with human ADSCs yielded higher disk height and water content in rats.	Pro-anabolism and induce differentiation (Yu et al., 2021)
BMP-2	Human NPCs and AFCs *in vitro*		BMP-2 antagonized the IL-18 induced upregulation of aggrecan, type II collagen, and SOX6, resulting in reversal of IL-18 mediated disk degeneration.	Anti-catabolism (Ye et al., 2016)
BMP-7	Human NPCs *in vitro*	Self-assembled peptide RADA-KPSS	Attenuate the expression of MMP-3, MMP-9, ADAMTS-4, NF-κB-p65, IL-1, IL-6, and PGE2, promote the accumulation of ECM proteins and suppress apoptosis of NP cells treated with TNF-α *in vitro*	Pro-anabolism/anti-catabolism, anti-apoptosis, and anti-inflammation (Li et al., 2018b)
Anti-TNF-α	Rat lumbar IVD puncture model *in vivo*		Prevents long-term upregulation of intradiscal TNFα	Anti-inflammation (vashwick-Rogler et al., 2018)
Combination of CCL5, TGF-β1, and GDF-5	Human ADSCs and lumbar ovine IVD organ *in vitro*	Pullulan microbeads	(1) Induced Human ADSCs migration *in vitro* (2) The overall NP cellularity, the collagen type II and aggrecan staining intensity, and the Tie2-positive progenitor cell density in the NP were increased at day 28 compared to the control groups.	Pro-anabolism and induce migration (Frapin et al., 2020)

GDF-5, growth and differentiation factor 5. IGF-1, insulin-like growth factor 1. TGF-β1, transforming growth factor beta1. SDF-1, stromal cell-derived factor-1. CCL5, chemokine receptor type 5. KGN, kartogenin. BMP-2, bone morphogenetic protein 2. BMP-7, bone morphogenetic protein 7. TNF-α, tumor necrosis factor-alpha.

The components of exosomes should be thoroughly studied. EVs can also be used to carry therapeutic drugs. Dou et al. (2020) fabricated engineered EVs to deliver drugs targeting inflammation. EVs have also been proven to have therapeutic effects on IVDD, but they have not been applied in IVD tissue engineering. The combination of EVs and tissue engineering is prospective. The study of EVs is still a hot research field. As research progresses, EVs will be a promising therapeutic drug or targeted drug delivery system for regenerating IVDs.

CONCLUSION

Intervertebral disk degeneration is a complex and common disease, and tissue engineering strategies provide many

innovative methods, but most are still in the experimental stage. Surgical and non-surgical treatments are the most effective and safest strategies to relieve pain and regain mobility for patients with IVDD. However, there are obvious limitations in intervertebral discs: toward engineering tissue the current therapeutic strategies, and relief of symptoms do not mean that degeneration has stopped, as IVDs remain in a hostile microenvironment. Regenerative strategies are key to the reversal of degeneration and need to be further studied.

The application of genes, biological factors, and EV are research hotspots. These applications are better substitutes for therapeutic cells, but their long-term viability and efficacy remain uncertain, and the mechanisms are not fully understood. The analysis of active components and illustration of mechanisms should be emphasized in the next stage to achieve precise therapies. Tissue-engineered scaffolds are more like multifunctional platforms, which may be able to simultaneously regulate cellular activities, load, and the controlled release of therapeutic drugs or cells while providing proper structural support, anti-inflammation, and antibiosis. Compared to traditional materials, such as decellularized ECM and classic synthetic materials, manufacturing technology utilizes superior materials to most traditional materials. Although many biomaterials have been proven to be safe and stable, researchers must develop novel materials and adjust their characteristics according to other strategies.

Every therapeutic strategy has a deficiency. Researchers should combine different strategies to restore the healthy IVD microenvironment and try to customize the best treatment strategy for individual patients according to their personalized microenvironments in the future.

AUTHOR CONTRIBUTIONS

YD read the manuscript and wrote the draft. XS reviewed and improved the manuscript. QY set up the framework of this review. XM and XZ provided guidance for YD and XS as consultants. YD and XS contributed equally to this work. All the authors contributed to the article and approved the submitted version.

FUNDING

This study was supported by the National Key R&D Program of China (2020YFC1107402), National Natural Science Foundation of China (81871782, 31900968, and 81871777), and Tianjin Science Fund for Distinguished Young Scholars (18JCJQJC47900). Research Foundation of the Tianjin Health Commision (KJ20052).

SUPPLEMENTARY MATERIAL

The Supplementary Material for this article can be found online at: https://www.frontiersin.org/articles/10.3389/fbioe.2021.592118/full#supplementary-material

REFERENCES

Agrawal, A., Gajghate, S., Smith, H., Anderson, D. G., Albert, T. J., Shapiro, I. M., et al. (2008). Cited2 modulates hypoxia-inducible factor-dependent expression of vascular endothelial growth factor in nucleus pulposus cells of the rat intervertebral disc. *Arthritis Rheum.* 58, 3798–3808. doi: 10.1002/art.24073

Agrawal, A., Guttapalli, A., Narayan, S., Albert, T. J., Shapiro, I. M., and Risbud, M. V. (2007). Normoxic stabilization of HIF-1alpha drives glycolytic metabolism and regulates aggrecan gene expression in nucleus pulposus cells of the rat intervertebral disk. *Am. J. Physiol. Cell Physiol.* 293, C621–C631.

Alvi, M. A., Kerezoudis, P., Wahood, W., Goyal, A., and Bydon, M. (2018). Operative approaches for lumbar disc herniation: a systematic review and multiple treatment meta-analysis of conventional and minimally invasive surgeries. *World Neurosurg.* 114, 391–407.e2.

Apte, R. S., Chen, D. S., and Ferrara, N. (2019). VEGF in signaling and disease: beyond discovery and development. *Cell* 176, 1248–1264. doi: 10.1016/j.cell.2019.01.021

Atlas, S. J., Keller, R. B., Chang, Y., Deyo, R. A., and Singer, D. E. (2001). Surgical and nonsurgical management of sciatica secondary to a lumbar disc herniation: five-year outcomes from the maine lumbar spine study. *Spine (Phila Pa 1976)* 26, 1179–1187. doi: 10.1097/00007632-200105150-00017

Atlas, S. J., Keller, R. B., Wu, Y. A., Deyo, R. A., and Singer, D. E. (2005). Long-term outcomes of surgical and nonsurgical management of sciatica secondary to a lumbar disc herniation: 10 year results from the maine lumbar spine study. *Spine (Phila Pa 1976)* 30, 927–935. doi: 10.1097/01.brs.0000158954.68522.2a

Auerbach, J. D., Jones, K. J., Milby, A. H., Anakwenze, O. A., and Balderston, R. A. (2009). Segmental contribution toward total lumbar range of motion in disc replacement and fusions: a comparison of operative and adjacent levels. *Spine (Phila Pa 1976)* 34, 2510–2517. doi: 10.1097/brs.0b013e3181af2622

Bachmeier, B. E., Nerlich, A., Mittermaier, N., Weiler, C., Lumenta, C., Wuertz, K., et al. (2009). Matrix metalloproteinase expression levels suggest distinct enzyme roles during lumbar disc herniation and degeneration. *Eur. Spine J.* 18, 1573–1586. doi: 10.1007/s00586-009-1031-8

Bartels, E. M., Fairbank, J. C., Winlove, C. P., and Urban, J. P. (1998). Oxygen and lactate concentrations measured in vivo in the intervertebral discs of patients with scoliosis and back pain. *Spine (Phila Pa 1976)* 23, 1–7; discussion 8.

Ben-Porath, I., and Weinberg, R. A. (2005). The signals and pathways activating cellular senescence. *Int. J. Biochem. Cell Biol.* 37, 961–976. doi: 10.1016/j.biocel.2004.10.013

Benzakour, T., Igoumenou, V., Mavrogenis, A. F., and Benzakour, A. (2019). Current concepts for lumbar disc herniation. *Int. Orthop.* 43, 841–851.

Bhunia, B. K., Kaplan, D. L., and Mandal, B. B. (2018). Silk-based multilayered angle-ply annulus fibrosus construct to recapitulate form and function of the intervertebral disc. *Proc. Natl. Acad. Sci. U.S.A.* 115, 477–482. doi: 10.1073/pnas.1715912115

Brown, S., Melrose, J., Caterson, B., Roughley, P., Eisenstein, S. M., and Roberts, S. (2012). A comparative evaluation of the small leucine-rich proteoglycans of pathological human intervertebral discs. *Eur. Spine J.* 21(Suppl. 2), S154–S159.

Butler, A. J., and Donnally, I. C. (2020). *Discectomy*. Treasure Island (FL): StatPearls Publishing.

Campisi, J. (2005). Senescent cells, tumor suppression, and organismal aging: good citizens, bad neighbors. *Cell* 120, 513–522. doi: 10.1016/j.cell.2005.02.003

Chen, R. S., Zhang, X. B., Zhu, X. T., and Wang, C. S. (2020). The crosstalk between IGF-1R and ER-α in the proliferation and anti-inflammation of nucleus pulposus cells. *Eur. Rev. Med. Pharmacol. Sci.* 24, 5886–5894.

Chen, W., Chen, H., Zheng, D., Zhang, H., Deng, L., Cui, W., et al. (2020). Gene-hydrogel microenvironment regulates extracellular matrix metabolism balance in nucleus pulposus. *Adv. Sci. (Weinh.)* 7:1902099. doi: 10.1002/advs.201902099

Cheng, S., Jin, Y., Wang, N., Cao, F., Zhang, W., Bai, W., et al. (2017). Self-adjusting, polymeric multilayered roll that can keep the shapes of the blood vessel scaffolds during biodegradation. *Adv. Mater.* 29:1700171. doi: 10.1002/adma.201700171

Cheng, X., Zhang, G., Zhang, L., Hu, Y., Zhang, K., Sun, X., et al. (2018). Mesenchymal stem cells deliver exogenous miR-21 via exosomes to inhibit nucleus pulposus cell apoptosis and reduce intervertebral disc degeneration. *J. Cell. Mol. Med.* 22, 261–276. doi: 10.1111/jcmm.13316

Cheng, Y. H., Yang, S. H., and Lin, F. H. (2011). Thermosensitive chitosan-gelatin-glycerol phosphate hydrogel as a controlled release system of ferulic acid for nucleus pulposus regeneration. *Biomaterials* 32, 6953–6961. doi: 10.1016/j.biomaterials.2011.03.065

Chiu, C. C., Chuang, T. Y., Chang, K. H., Wu, C. H., Lin, P. W., and Hsu, W. Y. (2015). The probability of spontaneous regression of lumbar herniated disc: a systematic review. *Clin. Rehabil.* 29, 184–195. doi: 10.1177/0269215514540919

Christiani, T. R., Baroncini, E., Stanzione, J., and Vernengo, A. J. (2019). In vitro evaluation of 3D printed polycaprolactone scaffolds with angle-ply architecture for annulus fibrosus tissue engineering. *Regen. Biomater.* 6, 175–184. doi: 10.1093/rb/rbz011

Chu, G., Shi, C., Wang, H., Zhang, W., Yang, H., and Li, B. (2018). Strategies for annulus fibrosus regeneration: from biological therapies to tissue engineering. *Front. Bioeng. Biotechnol.* 6:90.

Clarke, L. E., McConnell, J. C., Sherratt, M. J., Derby, B., Richardson, S. M., and Hoyland, J. A. (2014). Growth differentiation factor 6 and transforming growth factor-beta differentially mediate mesenchymal stem cell differentiation, composition, and micromechanical properties of nucleus pulposus constructs. *Arthritis Res. Ther.* 16:R67.

Colombier, P., Clouet, J., Hamel, O., Lescaudron, L., and Guicheux, J. (2014). The lumbar intervertebral disc: from embryonic development to degeneration. *Joint Bone Spine* 81, 125–129. doi: 10.1016/j.jbspin.2013.07.012

Cui, X. D., Li, H. T., Zhang, W., Zhang, L. L., Luo, Z. P., and Yang, H. L. (2018). Mid- to long-term results of total disc replacement for lumbar degenerative disc disease: a systematic review. *J. Orthop. Surg. Res.* 13:326.

da Silva Meirelles, L., Chagastelles, P. C., and Nardi, N. B. (2006). Mesenchymal stem cells reside in virtually all post-natal organs and tissues. *J. Cell Sci.* 119, 2204–2213. doi: 10.1242/jcs.02932

Davalos, A. R., Coppe, J. P., Campisi, J., and Desprez, P. Y. (2010). Senescent cells as a source of inflammatory factors for tumor progression. *Cancer Metastasis Rev.* 29, 273–283. doi: 10.1007/s10555-010-9220-9

de Rooij, J. D., Gadjradj, P. S., Soria van Hoeve, J. S., Huygen, F. J., Aukes, H. A., and Harhangi, B. S. (2017). Percutaneous nucleoplasty for the treatment of a contained cervical disk herniation. *Clin. Spine Surg.* 30, 389–391. doi: 10.1097/bsd.0000000000000583

Devereaux, M. W. (2007). Anatomy and examination of the spine. *Neurol. Clin.* 25, 331–351. doi: 10.1016/j.ncl.2007.02.003

Deverman, B. E., Ravina, B. M., Bankiewicz, K. S., Paul, S. M., and Sah, D. W. Y. (2018). Gene therapy for neurological disorders: progress and prospects. *Nat. Rev. Drug Discov.* 17, 641–659.

Dicker, K. T., Gurski, L. A., Pradhan-Bhatt, S., Witt, R. L., Farach-Carson, M. C., and Jia, X. (2014). Hyaluronan: a simple polysaccharide with diverse biological functions. *Acta Biomater.* 10, 1558–1570. doi: 10.1016/j.actbio.2013.12.019

Dou, G., Tian, R., Liu, X., Yuan, P., Ye, Q., Liu, J., et al. (2020). Chimeric apoptotic bodies functionalized with natural membrane and modular delivery system for inflammation modulation. *Sci. Adv.* 6:eaba2987. doi: 10.1126/sciadv.aba2987

Driscoll, T. P., Nakasone, R. H., Szczesny, S. E., Elliott, D. M., and Mauck, R. L. (2013). Biaxial mechanics and inter-lamellar shearing of stem-cell seeded electrospun angle-ply laminates for annulus fibrosus tissue engineering. *J. Orthop. Res.* 31, 864–870. doi: 10.1002/jor.22312

Eichen, P. M., Achilles, N., Konig, V., Mosges, R., Hellmich, M., Himpe, B., et al. (2014). Nucleoplasty, a minimally invasive procedure for disc decompression: a systematic review and meta-analysis of published clinical studies. *Pain Physician* 17, E149–E173.

Eisenstein, S. M., Balain, B., and Roberts, S. (2020). Current treatment options for intervertebral disc pathologies. *Cartilage* 11, 143–151. doi: 10.1177/1947603520907665

El Andaloussi, S., Mäger, I., Breakefield, X. O., and Wood, M. J. (2013). Extracellular vesicles: biology and emerging therapeutic opportunities. *Nat. Rev. Drug Discov.* 12, 347–357. doi: 10.1038/nrd3978

el Barzouhi, A., Vleggeert-Lankamp, C. L., Lycklama à Nijeholt, G. J., Van der Kallen, B. F., van den Hout, W. B., Jacobs, W. C., et al. (2013). Magnetic resonance imaging in follow-up assessment of sciatica. *N. Engl. J. Med.* 368, 999–1007. doi: 10.1056/nejmoa1209250

Erwin, W. M. (2008). The notochord, notochordal cell and CTGF/CCN-2: ongoing activity from development through maturation. *J. Cell Commun. Signal.* 2, 59–65. doi: 10.1007/s12079-008-0031-5

Erwin, W. M., Ashman, K., O'Donnel, P., and Inman, R. D. (2006). Nucleus pulposus notochord cells secrete connective tissue growth factor and up-regulate proteoglycan expression by intervertebral disc chondrocytes. *Arthritis Rheum.* 54, 3859–3867. doi: 10.1002/art.22258

Farhang, N., Ginley-Hidinger, M., Berrett, K. C., Gertz, J., Lawrence, B., and Bowles, R. D. (2019). Lentiviral CRISPR epigenome editing of inflammatory receptors as a gene therapy strategy for disc degeneration. *Hum. Gene Ther.* 30, 1161–1175. doi: 10.1089/hum.2019.005

Findlay, C., Ayis, S., and Demetriades, A. K. (2018). Total disc replacement versus anterior cervical discectomy and fusion: a systematic review with meta-analysis of data from a total of 3160 patients across 14 randomized controlled trials with both short- and medium- to long-term outcomes. *Bone Joint J.* 100-b, 991–1001. doi: 10.1302/0301-620x.100b8.bjj-2018-0120.r1

Fontana, G., See, E., and Pandit, A. (2015). Current trends in biologics delivery to restore intervertebral disc anabolism. *Adv. Drug Deliv. Rev.* 84, 146–158. doi: 10.1016/j.addr.2014.08.008

Foster, N. E., Anema, J. R., Cherkin, D., Chou, R., Cohen, S. P., Gross, D. P., et al. (2018). Prevention and treatment of low back pain: evidence, challenges, and promising directions. *Lancet* 391, 2368–2383.

Frapin, L., Clouet, J., Chédeville, C., Moraru, C., Samarut, E., Henry, N., et al. (2020). Controlled release of biological factors for endogenous progenitor cell migration and intervertebral disc extracellular matrix remodelling. *Biomaterials* 253:120107. doi: 10.1016/j.biomaterials.2020.120107

Frapin, L., Clouet, J., Delplace, V., Fusellier, M., Guicheux, J., and Le Visage, C. (2019). Lessons learned from intervertebral disc pathophysiology to guide rational design of sequential delivery systems for therapeutic biological factors. *Adv. Drug Deliv. Rev.* 149-150, 49–71. doi: 10.1016/j.addr.2019.08.007

Freemont, A. J. (2009). The cellular pathobiology of the degenerate intervertebral disc and discogenic back pain. *Rheumatology (Oxford)* 48, 5–10. doi: 10.1093/rheumatology/ken396

Fujita, N., Imai, J., Suzuki, T., Yamada, M., Ninomiya, K., Miyamoto, K., et al. (2008). Vascular endothelial growth factor-a is a survival factor for nucleus pulposus cells in the intervertebral disc. *Biochem. Biophys. Res. Commun.* 372, 367–372. doi: 10.1016/j.bbrc.2008.05.044

Gantenbein-Ritter, B., Benneker, L. M., Alini, M., and Grad, S. (2011). Differential response of human bone marrow stromal cells to either TGF-β(1) or rhGDF-5. *Eur. Spine J.*20, 962–971. doi: 10.1007/s00586-010-1619-z

Gluais, M., Clouet, J., Fusellier, M., Decante, C., Moraru, C., Dutilleul, M., et al. (2019). In vitro and in vivo evaluation of an electrospun-aligned microfibrous implant for Annulus fibrosus repair. *Biomaterials* 205, 81–93. doi: 10.1016/j.biomaterials.2019.03.010

Gruber, H. E., Ingram, J. A., Hoelscher, G. L., Zinchenko, N., Hanley, E. N. Jr., and Sun, Y. (2009). Asporin, a susceptibility gene in osteoarthritis, is expressed at higher levels in the more degenerate human intervertebral disc. *Arthritis Res. Ther.* 11:R47.

Gruber, H. E., Ingram, J. A., Norton, H. J., and Hanley, E. N. Jr. (2007). Senescence in cells of the aging and degenerating intervertebral disc: immunolocalization of senescence-associated beta-galactosidase in human and sand rat discs. *Spine (Phila Pa 1976)* 32, 321–327. doi: 10.1097/01.brs.0000253960.57051.de

Guyer, R. D., and Ohnmeiss, D. D. (2003). Intervertebral disc prostheses. *Spine (Phila Pa 1976)* 28, S15–S23.

Ha, K. Y., Koh, I. J., Kirpalani, P. A., Kim, Y. Y., Cho, Y. K., Khang, G. S., et al. (2006). The expression of hypoxia inducible factor-1alpha and apoptosis in herniated discs. *Spine (Phila Pa 1976)* 31, 1309–1313. doi: 10.1097/01.brs.0000219493.76081.d6

Harmon, M. D., Ramos, D. M., Nithyadevi, D., Bordett, R., Rudraiah, S., Nukavarapu, S. P., et al. (2020). Growing a backbone - functional biomaterials and structures for intervertebral disc (IVD) repair and regeneration: challenges, innovations, and future directions. *Biomater. Sci.* 8, 1216–1239. doi: 10.1039/c9bm01288e

Harper, R., and Klineberg, E. (2019). The evidence-based approach for surgical complications in the treatment of lumbar disc herniation. *Int. Orthop.* 43, 975–980. doi: 10.1007/s00264-018-4255-6

Hartvigsen, J., Hancock, M. J., Kongsted, A., Louw, Q., Ferreira, M. L., Genevay, S., et al. (2018). What low back pain is and why we need to pay attention. *Lancet* 391, 2356–2367.

Hashimoto, K., Aizawa, T., Kanno, H., and Itoi, E. (2019). Adjacent segment degeneration after fusion spinal surgery-a systematic review. *Int. Orthop.* 43, 987–993. doi: 10.1007/s00264-018-4241-z

Helm Ii, S., Simopoulos, T. T., Stojanovic, M., Abdi, S., and El Terany, M. A. (2017). Effectiveness of thermal annular procedures in treating discogenic low back pain. *Pain Phys.* 20, 447–470. doi: 10.36076/ppj/447

Henriksson, H. B., Papadimitriou, N., Hingert, D., Baranto, A., Lindahl, A., and Brisby, H. (2019). The traceability of mesenchymal stromal cells after injection into degenerated discs in patients with low back pain. *Stem Cells Dev.* 28, 1203–1211. doi: 10.1089/scd.2019.0074

Henry, N., Clouet, J., Le Bideau, J., Le Visage, C., and Guicheux, J. (2018). Innovative strategies for intervertebral disc regenerative medicine: from cell therapies to multiscale delivery systems. *Biotechnol. Adv.* 36, 281–294. doi: 10.1016/j.biotechadv.2017.11.009

Hibbs, R. (1964). An operation for progressive spinal deformities. *Clin. Orthop. Relat. Res.* 35, 4–8.

High, K. A., and Roncarolo, M. G. (2019). Gene therapy. *N. Engl. J. Med.* 381, 455–464.

Hilibrand, A. S., and Robbins, M. (2004). Adjacent segment degeneration and adjacent segment disease: the consequences of spinal fusion? *Spine J.* 4, 190s–194s.

Hiyama, A., Mochida, J., Iwashina, T., Omi, H., Watanabe, T., Serigano, K., et al. (2008). Transplantation of mesenchymal stem cells in a canine disc degeneration model. *J. Orthop. Res.* 26, 589–600. doi: 10.1002/jor.20584

Hu, B., He, R., Ma, K., Wang, Z., Cui, M., Hu, H., et al. (2018). Intervertebral disc-derived stem/progenitor cells as a promising cell source for intervertebral disc regeneration. *Stem Cells Int.* 2018:7412304.

Huang, Y., Wang, Y., Wu, C., and Tian, W. (2019). Elevated expression of hypoxia-inducible factor-2alpha regulated catabolic factors during intervertebral disc degeneration. *Life Sci.* 232:116565. doi: 10.1016/j.lfs.2019.116565

Hukins, D. W. (2005). Tissue engineering: a live disc. *Nat. Mater.* 4, 881–882.

Hunter, C. J., Matyas, J. R., and Duncan, N. A. (2003). The notochordal cell in the nucleus pulposus: a review in the context of tissue engineering. *Tissue Eng.* 9, 667–677. doi: 10.1089/107632703768247368

Iozzo, R. V., and Schaefer, L. (2015). Proteoglycan form and function: a comprehensive nomenclature of proteoglycans. *Matrix Biol.* 42, 11–55. doi: 10.1016/j.matbio.2015.02.003

Iu, J., Massicotte, E., Li, S. Q., Hurtig, M. B., Toyserkani, E., Santerre, J. P., et al. (2017). (*) In vitro generated intervertebral discs: toward engineering tissue integration. *Tissue Eng. Part A* 23, 1001–1010. doi: 10.1089/ten.tea.2016.0433

Jeong, J. H., Jin, E. S., Min, J. K., Jeon, S. R., Park, C. S., Kim, H. S., et al. (2009). Human mesenchymal stem cells implantation into the degenerated coccygeal disc of the rat. *Cytotechnology* 59, 55–64. doi: 10.1007/s10616-009-9192-1

Jin, X., Lin, T., and Xu, Y. (2016). Stem cell therapy and immunological rejection in animal models. *Curr. Mol. Pharmacol.* 9, 284–288. doi: 10.2174/1874467208666150928153511

Johnson, W. E., Caterson, B., Eisenstein, S. M., and Roberts, S. (1976). Human intervertebral disc aggrecan inhibits endothelial cell adhesion and cell migration in vitro. *Spine (Phila Pa 1976)* 30, 1139–1147. doi: 10.1097/01.brs.0000162624.95262.73

Kalson, N., Richardson, S., and Hoyland, J. (2008). Strategies for regeneration of the intervertebral disc. *Regen. Med.* 3, 717–729. doi: 10.2217/17460751.3.5.717

Kang, H. W., Lee, S. J., Ko, I. K., Kengla, C., Yoo, J. J., and Atala, A. (2016). A 3D bioprinting system to produce human-scale tissue constructs with structural integrity. *Nat. Biotechnol.* 34, 312–319. doi: 10.1038/nbt.3413

Kang, R., Li, H., Xi, Z., Ringgard, S., Baatrup, A., Rickers, K., et al. (2018). Surgical repair of annulus defect with biomimetic multilamellar nano/microfibrous scaffold in a porcine model. *J. Tissue Eng. Regen. Med.* 12, 164–174. doi: 10.1002/term.2384

Khan, A. N., Jacobsen, H. E., Khan, J., Filippi, C. G., Levine, M., Lehman, R. A. Jr., et al. (2017). Inflammatory biomarkers of low back pain and disc degeneration: a review. *Ann. N. Y. Acad. Sci.* 1410, 68–84. doi: 10.1111/nyas.13551

Kim, C. (2014). Disease modeling and cell based therapy with iPSC: future therapeutic option with fast and safe application. *Blood Res.* 49, 7–14. doi: 10.5045/br.2014.49.1.7

Kim, K. W., Chung, H. N., Ha, K. Y., Lee, J. S., and Kim, Y. Y. (2009). Senescence mechanisms of nucleus pulposus chondrocytes in human intervertebral discs. *Spine J.* 9, 658–666. doi: 10.1016/j.spinee.2009.04.018

Krause, D. S. (2008). Bone marrow-derived cells and stem cells in lung repair. *Proc. Am. Thorac. Soc.* 5, 323–327.

Kreiner, D. S., Hwang, S. W., Easa, J. E., Resnick, D. K., Baisden, J. L., Bess, S., et al. (2014). evidence-based clinical guideline for the diagnosis and treatment of lumbar disc herniation with radiculopathy. *Spine J.* 14, 180–191.

Kuo, Y. J., Wu, L. C., Sun, J. S., Chen, M. H., Sun, M. G., and Tsuang, Y. H. (2014). Mechanical stress-induced apoptosis of nucleus pulposus cells: an in vitro and in vivo rat model. *J. Orthop. Sci.* 19, 313–322. doi: 10.1007/s00776-013-0510-2

Langer, R., and Vacanti, J. P. (1993). Tissue engineering. *Science (New York, N.Y.)* 260, 920–926.

Lawson, L. Y., and Harfe, B. D. (2017). Developmental mechanisms of intervertebral disc and vertebral column formation. *Wiley Interdiscip. Rev. Dev. Biol.* 6:e283. doi: 10.1002/wdev.283

Le Huec, J. C., Saddiki, R., Franke, J., Rigal, J., and Aunoble, S. (2011). Equilibrium of the human body and the gravity line: the basics. *Eur. Spine J.* 20(Suppl. 5), 558–563. doi: 10.1007/s00586-011-1939-7

Le Maitre, C. L., Freemont, A. J., and Hoyland, J. A. (2004). Localization of degradative enzymes and their inhibitors in the degenerate human intervertebral disc. *J. Pathol.* 204, 47–54. doi: 10.1002/path.1608

Le Maitre, C. L., Freemont, A. J., and Hoyland, J. A. (2005). The role of interleukin-1 in the pathogenesis of human intervertebral disc degeneration. *Arthritis Res. Ther.* 7, R732–R745.

Le Maitre, C. L., Hoyland, J. A., and Freemont, A. J. (2007). Catabolic cytokine expression in degenerate and herniated human intervertebral discs: IL-1beta and TNFalpha expression profile. *Arthritis Res. Ther.* 9:R77.

Lee, A. S., Tang, C., Rao, M. S., Weissman, I. L., and Wu, J. C. (2013). Tumorigenicity as a clinical hurdle for pluripotent stem cell therapies. *Nat. Med.* 19, 998–1004. doi: 10.1038/nm.3267

Lee, C. K., and Langrana, N. A. (1984). Lumbosacral spinal fusion. A biomechanical study. *Spine (Phila Pa 1976)* 9, 574–581. doi: 10.1097/00007632-198409000-00007

Lee, C. K., and Langrana, N. A. (2004). A review of spinal fusion for degenerative disc disease: need for alternative treatment approach of disc arthroplasty? *Spine J.* 4, 173s–176s.

Lee, J. H., Choi, K. H., Kang, S., Kim, D. H., Kim, D. H., Kim, B. R., et al. (2019). Nonsurgical treatments for patients with radicular pain from lumbosacral disc herniation. *Spine J.* 19, 1478–1489.

Leung, V. Y. L., Zhou, L., Tam, W. K., Sun, Y., Lv, F., Zhou, G., et al. (2017). Bone morphogenetic protein-2 and -7 mediate the anabolic function of nucleus pulposus cells with discrete mechanisms. *Connect. Tissue Res.* 58, 573–585. doi: 10.1080/03008207.2017.1282951

Levicoff, E. A., Gilbertson, L. G., and Kang, J. D. (2005). Gene therapy for disc repair. *Spine J.* 5, 287s–296s.

Lewis, R. A., Williams, N. H., Sutton, A. J., Burton, K., Din, N. U., Matar, H. E., et al. (2015). Comparative clinical effectiveness of management strategies for sciatica: systematic review and network meta-analyses. *Spine J.* 15, 1461–1477. doi: 10.1016/j.spinee.2013.08.049

Li, H., Liang, C. Z., and Chen, Q. X. (2013). Regulatory role of hypoxia inducible factor in the biological behavior of nucleus pulposus cells. *Yonsei Med. J.* 54, 807–812. doi: 10.3349/ymj.2013.54.4.807

Li, X., Chang, H., and Meng, X. (2018a). Tubular microscopes discectomy versus conventional microdiscectomy for treating lumbar disk herniation: systematic review and meta-analysis. *Medicine* 97:e9807. doi: 10.1097/md.0000000000009807

Li, X., Cheng, S., Wu, Y., Ying, J., Wang, C., Wen, T., et al. (2018b). Functional self-assembled peptide scaffold inhibits tumor necrosis factor-alpha-induced inflammation and apoptosis in nucleus pulposus cells by suppressing nuclear

factor-κB signaling. *J. Biomed. Mater. Res. Part A* 106, 1082–1091. doi: 10.1002/jbm.a.36301

Li, Z., Lang, G., Karfeld-Sulzer, L. S., Mader, K. T., Richards, R. G., Weber, F. E., et al. (2017). Heterodimeric BMP-2/7 for nucleus pulposus regeneration-In vitro and ex vivo studies. *J. Orthop. Res.* 35, 51–60. doi: 10.1002/jor.23351

Liliang, P. C., Lu, K., Liang, C. L., Chen, Y. W., Tsai, Y. D., and Tu, Y. K. (2016). Nucleoplasty for treating lumbar disk degenerative low back pain: an outcome prediction analysis. *J. Pain Res.* 9, 893–898. doi: 10.2147/jpr.s116533

Liu, G. Z., Ishihara, H., Osada, R., Kimura, T., and Tsuji, H. (2001). Nitric oxide mediates the change of proteoglycan synthesis in the human lumbar intervertebral disc in response to hydrostatic pressure. *Spine (Phila Pa 1976)* 26, 134–141. doi: 10.1097/00007632-200101150-00005

Liu, Z., Li, C., Meng, X., Bai, Y., Qi, J., Wang, J., et al. (2017). Hypoxia-inducible factor-lα mediates aggrecan and collagen ΠI expression via NOTCH1 signaling in nucleus pulposus cells during intervertebral disc degeneration. *Biochem. Biophys. Res. Commun.* 488, 554–561. doi: 10.1016/j.bbrc.2017.05.086

Lopes-Pacheco, M., Bandeira, E., and Morales, M. M. (2016). Cell-based therapy for silicosis. *Stem Cells Int.* 2016:5091838.

Lu, K., Li, H. Y., Yang, K., Wu, J. L., Cai, X. W., Zhou, Y., et al. (2017). Exosomes as potential alternatives to stem cell therapy for intervertebral disc degeneration: in-vitro study on exosomes in interaction of nucleus pulposus cells and bone marrow mesenchymal stem cells. *Stem Cell Res. Ther.* 8:108.

Luoma, K., Riihimäki, H., Luukkonen, R., Raininko, R., Viikari-Juntura, E., and Lamminen, A. (1976). Low back pain in relation to lumbar disc degeneration. *Spine (Phila Pa 1976)* 25, 487–492. doi: 10.1097/00007632-200002150-00016

Ma, J., He, Y., Liu, X., Chen, W., Wang, A., Lin, C. Y., et al. (2018). A novel electrospun-aligned nanoyarn/three-dimensional porous nanofibrous hybrid scaffold for annulus fibrosus tissue engineering. *Int. J. Nanomed.* 13, 1553–1567. doi: 10.2147/ijn.s143990

MacDowall, A., Canto Moreira, N., Marques, C., Skeppholm, M., Lindhagen, L., Robinson, Y., et al. (2019). Artificial disc replacement versus fusion in patients with cervical degenerative disc disease and radiculopathy: a randomized controlled trial with 5-year outcomes. *J. Neurosurg. Spine* 30, 323–331. doi: 10.3171/2018.9.spine18659

Majno, G., and Joris, I. (2004). *Cells, Tissues, and Disease Principles of General Pathology. Part II: Inflammation*. 2nd Edn.Cary: Oxford University Press.

Marcolongo, M., Sarkar, S., and Ganesh, N. (2011). Trends in materials for spine surgery. *Compr. Biomater.* 6, 127–145. doi: 10.1016/b978-0-08-055294-1.00208-7

McFadden, K. D., and Taylor, J. R. (1989). End-plate lesions of the lumbar spine. *Spine (Phila Pa 1976)* 14, 867–869. doi: 10.1097/00007632-198908000-00017

McGuire, R., Borem, R., and Mercuri, J. (2017). The fabrication and characterization of a multi-laminate, angle-ply collagen patch for annulus fibrosus repair. *J. Tissue Eng. Regen. Med.* 11, 3488–3493. doi: 10.1002/term.2250

Medzhitov, R. (2008). Origin and physiological roles of inflammation. *Nature* 454, 428–435. doi: 10.1038/nature07201

Meirelles Lda, S., Fontes, A. M., Covas, D. T., and Caplan, A. I. (2009). Mechanisms involved in the therapeutic properties of mesenchymal stem cells. *Cytokine Growth Factor Rev.* 20, 419–427. doi: 10.1016/j.cytogfr.2009.10.002

Meng, X., Zhuang, L., Wang, J., Liu, Z., Wang, Y., Xiao, D., et al. (2018). Hypoxia-inducible factor (HIF)-1alpha knockout accelerates intervertebral disc degeneration in mice. *Int. J. Clin. Exp. Pathol.* 11, 548–557.

Mhanna, R., and Hasan, A. (2017). "Introduction to Tissue Engineering," in *Regenerative Medicine, Smart Diagnostics and Personalized Medicine, Tissue Engineering for Artificial Organs*, ed. A. Hasan (Hoboken NJ: Wiley-VCH).

Mixter, W., and Barr, J. (1934). Rupture of the intervertebral disc with involvement of the spinal canal. *Ed. N. Engl. J. Med.* 211, 210–215. doi: 10.1056/nejm193408022110506

Mizuno, H., Roy, A. K., Vacanti, C. A., Kojima, K., Ueda, M., and Bonassar, L. J. (2004). Tissue-engineered composites of anulus fibrosus and nucleus pulposus for intervertebral disc replacement. *Spine (Phila Pa 1976)* 29, 1290–7; discussion 1297–8.

Modic, M. T., Steinberg, P. M., Ross, J. S., Masaryk, T. J., and Carter, J. R. (1988). Degenerative disk disease: assessment of changes in vertebral body marrow with MR imaging. *Radiology* 166, 193–199. doi: 10.1148/radiology.166.1.3336678

Muñoz-Espín, D., and Serrano, M. (2014). Cellular senescence: from physiology to pathology. *Nat. Rev. Mol. Cell Biol.* 15, 482–496. doi: 10.1038/nrm3823

Murray, C. J., Vos, T., Lozano, R., Naghavi, M., Flaxman, A. D., Michaud, C., et al. (2012). Disability-adjusted life years (DALYs) for 291 diseases and injuries in 21 regions, 1990-2010: a systematic analysis for the global burden of disease study 2010. *Lancet* 380, 2197–2223.

Neidlinger-Wilke, C., Galbusera, F., Pratsinis, H., Mavrogonatou, E., Mietsch, A., Kletsas, D., et al. (2014). Mechanical loading of the intervertebral disc: from the macroscopic to the cellular level. *Eur. Spine J.* 23(Suppl. 3), S333–S343.

Oehme, D., Goldschlager, T., Ghosh, P., Rosenfeld, J. V., and Jenkin, G. (2015). Cell-based therapies used to treat lumbar degenerative disc disease: a systematic review of animal studies and human clinical trials. *Stem Cells Int.* 2015:946031.

Oryan, A., Kamali, A., Moshiri, A., and Baghaban Eslaminejad, M. (2017). Role of mesenchymal stem cells in bone regenerative medicine: what is the evidence? *Cells Tissues Organs* 204, 59–83. doi: 10.1159/000469704

Pedersen, L. M., Schistad, E., Jacobsen, L. M., Røe, C., and Gjerstad, J. (2015). Serum levels of the pro-inflammatory interleukins 6 (IL-6) and -8 (IL-8) in patients with lumbar radicular pain due to disc herniation: a 12-month prospective study. *Brain Behav. Immun.* 46, 132–136. doi: 10.1016/j.bbi.2015.01.008

Pera, M. F., Reubinoff, B., and Trounson, A. (2000). Human embryonic stem cells. *J. Cell Sci.* 113(Pt 1), 5–10.

Petit, A., and Roquelaure, Y. (2015). Low back pain, intervertebral disc and occupational diseases. *Int. J. Occup. Saf. Ergon.* 21, 15–19. doi: 10.1080/10803548.2015.1017940

Pockert, A. J., Richardson, S. M., Le Maitre, C. L., Lyon, M., Deakin, J. A., Buttle, D. J., et al. (2009). Modified expression of the ADAMTS enzymes and tissue inhibitor of metalloproteinases 3 during human intervertebral disc degeneration. *Arthritis Rheum.* 60, 482–491. doi: 10.1002/art.24291

Quero, L., Klawitter, M., Schmaus, A., Rothley, M., Sleeman, J., Tiaden, A. N., et al. (2013). Hyaluronic acid fragments enhance the inflammatory and catabolic response in human intervertebral disc cells through modulation of toll-like receptor 2 signalling pathways. *Arthritis Res. Ther.* 15:R94.

Raj, P. P. (2008). Intervertebral disc: anatomy-physiology-pathophysiology-treatment. *Pain Pract.* 8, 18–44. doi: 10.1111/j.1533-2500.2007.00171.x

Ramaswami, R., Ghogawala, Z., and Weinstein, J. N. (2017). Management of sciatica. *N. Engl. J. Med.* 376, 1175–1177.

Rannou, F., Lee, T. S., Zhou, R. H., Chin, J., Lotz, J. C., Mayoux-Benhamou, M. A., et al. (2004). Intervertebral disc degeneration: the role of the mitochondrial pathway in annulus fibrosus cell apoptosis induced by overload. *Am. J. Pathol.* 164, 915–924.

Richardson, S. M., Curran, J. M., Chen, R., Vaughan-Thomas, A., Hunt, J. A., Freemont, A. J., et al. (2006). The differentiation of bone marrow mesenchymal stem cells into chondrocyte-like cells on poly-L-lactic acid (PLLA) scaffolds. *Biomaterials* 27, 4069–4078. doi: 10.1016/j.biomaterials.2006.03.017

Richardson, S. M., Doyle, P., Minogue, B. M., Gnanalingham, K., and Hoyland, J. A. (2009). Increased expression of matrix metalloproteinase-10, nerve growth factor and substance P in the painful degenerate intervertebral disc. *Arthritis Res. Ther.* 11:R126.

Risau, W. (1997). Mechanisms of angiogenesis. *Nature* 386, 671–674.

Roberts, S., Evans, E. H., Kletsas, D., Jaffray, D. C., and Eisenstein, S. M. (2006). Senescence in human intervertebral discs. *Eur. Spine J.* 15(Suppl. 3), S312–S316.

Roberts, S., Menage, J., and Urban, J. P. (1989). Biochemical and structural properties of the cartilage end-plate and its relation to the intervertebral disc. *Spine (Phila Pa 1976)* 14, 166–174. doi: 10.1097/00007632-198902000-00005

Roberts, S., Urban, J. P., Evans, H., and Eisenstein, S. M. (1996). Transport properties of the human cartilage endplate in relation to its composition and calcification. *Spine (Phila Pa 1976)* 21, 415–420. doi: 10.1097/00007632-199602150-00003

Semenza, G. L., Roth, P. H., Fang, H. M., and Wang, G. L. (1994). Transcriptional regulation of genes encoding glycolytic enzymes by hypoxia-inducible factor 1. *J. Biol. Chem.* 269, 23757–23763. doi: 10.1016/s0021-9258(17)31580-6

Setton, L. A., and Chen, J. (2006). Mechanobiology of the intervertebral disc and relevance to disc degeneration. *J. Bone Joint Surg. Am.* 88(Suppl. 2), 52–57. doi: 10.2106/00004623-200604002-00011

Sharifi, S., Bulstra, S. K., Grijpma, D. W., and Kuijer, R. (2015). Treatment of the degenerated intervertebral disc; closure, repair and regeneration of the annulus fibrosus. *J. Tissue Eng. Regen. Med.* 9, 1120–1132.

Sharpless, N. E., and Sherr, C. J. (2015). Forging a signature of in vivo senescence. *Nat. Rev. Cancer* 15, 397–408. doi: 10.1038/nrc3960

Sheyn, D., Ben-David, S., Tawackoli, W., Zhou, Z., Salehi, K., Bez, M., et al. (2019). Human iPSCs can be differentiated into notochordal cells that reduce intervertebral disc degeneration in a porcine model. *Theranostics* 9, 7506–7524. doi: 10.7150/thno.34898

Shriver, M. F., Xie, J. J., Tye, E. Y., Rosenbaum, B. P., Kshettry, V. R., Benzel, E. C., et al. (2015). Lumbar microdiscectomy complication rates: a systematic review and meta-analysis. *Neurosurg. Focus* 39:E6.

Smith, L. J., Chiaro, J. A., Nerurkar, N. L., Cortes, D. H., Horava, S. D., Hebela, N. M., et al. (2011). Nucleus pulposus cells synthesize a functional extracellular matrix and respond to inflammatory cytokine challenge following long-term agarose culture. *Eur. Cells Mater.* 22, 291–301. doi: 10.22203/ecm.v022a22

Song, J., Chen, Z. H., Zheng, C. J., Song, K. H., Xu, G. Y., Xu, S., et al. (2020). Exosome-transported circRNA_0000253 competitively adsorbs MicroRNA-141-5p and increases IDD. *Mol. Ther. Nucleic Acids* 21, 1087–1099. doi: 10.1016/j.omtn.2020.07.039

Song, Y. Q., Cheung, K. M., Ho, D. W., Poon, S. C., Chiba, K., Kawaguchi, Y., et al. (2008). Association of the asporin D14 allele with lumbar-disc degeneration in Asians. *Am. J. Hum. Gen.* 82, 744–747. doi: 10.1016/j.ajhg.2007.12.017

Stoyanov, J. V., Gantenbein-Ritter, B., Bertolo, A., Aebli, N., Baur, M., Alini, M., et al. (2011). Role of hypoxia and growth and differentiation factor-5 on differentiation of human mesenchymal stem cells towards intervertebral nucleus pulposus-like cells. *Eur. Cells Mater.* 21, 533–547. doi: 10.22203/ecm.v021a40

Sun, B., Lian, M., Han, Y., Mo, X., Jiang, W., Qiao, Z., et al. (2021). A 3D-bioprinted dual growth factor-releasing intervertebral disc scaffold induces nucleus pulposus and annulus fibrosus reconstruction. *Bioact. Mater.* 6, 179–190. doi: 10.1016/j.bioactmat.2020.06.022

Taylor, C. J., Bolton, E. M., and Bradley, J. A. (2011). Immunological considerations for embryonic and induced pluripotent stem cell banking. *Philos. Trans. R. Soc. Lond. Ser. B Biol. Sci.* 366, 2312–2322. doi: 10.1098/rstb.2011.0030

Thavaneswaran, P., and Vandepeer, M. (2014). Lumbar artificial intervertebral disc replacement: a systematic review. *ANZ J. Surg.* 84, 121–127. doi: 10.1111/ans.12315

van Deursen, J. M. (2014). The role of senescent cells in ageing. *Nature* 509, 439–446. doi: 10.1038/nature13193

vashwick-Rogler, T. W. E., Lai, A., Watanabe, H., Salandra, J. M., Winkelstein, B. A., Cho, S. K., et al. (2018). Inhibiting tumor necrosis factor-alpha at time of induced intervertebral disc injury limits long-term pain and degeneration in a rat model. *JOR Spine* 1:e1014. doi: 10.1002/jsp2.1014

Vickers, L., Thorpe, A. A., Snuggs, J., Sammon, C., and Le Maitre, C. L. (2019). Mesenchymal stem cell therapies for intervertebral disc degeneration: consideration of the degenerate niche. *JOR Spine* 2:e1055.

Virk, S. S., Niedermeier, S., Yu, E., and Khan, S. N. (2014). Adjacent segment disease. *Orthopedics* 37, 547–555.

Vo, N. V., Hartman, R. A., Yurube, T., Jacobs, L. J., Sowa, G. A., and Kang, J. D. (2013). Expression and regulation of metalloproteinases and their inhibitors in intervertebral disc aging and degeneration. *Spine J.* 13, 331–341. doi: 10.1016/j.spinee.2012.02.027

Wang, F., Cai, F., Shi, R., Wang, X. H., and Wu, X. T. (2016). Aging and age related stresses: a senescence mechanism of intervertebral disc degeneration. *Osteoarthritis Cartilage* 24, 398–408. doi: 10.1016/j.joca.2015.09.019

Wang, G. L., Jiang, B. H., Rue, E. A., and Semenza, G. L. (1995). Hypoxia-inducible factor 1 is a basic-helix-loop-helix-PAS heterodimer regulated by cellular O2 tension. *Proc. Natl. Acad. Sci. U.S.A.* 92, 5510–5514. doi: 10.1073/pnas.92.12.5510

Wang, H., Tian, Y., Wang, J., Phillips, K. L., Binch, A. L., Dunn, S., et al. (2013). Inflammatory cytokines induce NOTCH signaling in nucleus pulposus cells: implications in intervertebral disc degeneration. *J. Biol. Chem.* 288, 16761–16774.

Wang, S. Z., Rui, Y. F., Lu, J., and Wang, C. (2014). Cell and molecular biology of intervertebral disc degeneration: current understanding and implications for potential therapeutic strategies. *Cell Prolif.* 47, 381–390. doi: 10.1111/cpr.12121

Wei, A., Shen, B., Williams, L., and Diwan, A. (2014). Mesenchymal stem cells: potential application in intervertebral disc regeneration. *Transl. Pediatr.* 3, 71–90.

Weiler, C., Nerlich, A. G., Zipperer, J., Bachmeier, B. E., and Boos, N. (2002). 2002 SSE award competition in basic science: expression of major matrix metalloproteinases is associated with intervertebral disc degradation and resorption. *Eur. Spine J.* 11, 308–320. doi: 10.1007/s00586-002-0472-0

Wilke, H. J., Neef, P., Caimi, M., Hoogland, T., and Claes, L. E. (1999). New in vivo measurements of pressures in the intervertebral disc in daily life. *Spine (Phila Pa 1976)* 24, 755–762. doi: 10.1097/00007632-199904150-00005

Wuertz, K., Godburn, K., Neidlinger-Wilke, C., Urban, J., and Iatridis, J. C. (2008). Behavior of mesenchymal stem cells in the chemical microenvironment of the intervertebral disc. *Spine (Phila Pa 1976)* 33, 1843–1849. doi: 10.1097/brs.0b013e31817b8f53

Xia, C., Zeng, Z., Fang, B., Tao, M., Gu, C., Zheng, L., et al. (2019). Mesenchymal stem cell-derived exosomes ameliorate intervertebral disc degeneration via anti-oxidant and anti-inflammatory effects. *Free Radic. Biol. Med.* 143, 1–15. doi: 10.1016/j.freeradbiomed.2019.07.026

Xia, K., Zhu, J., Hua, J., Gong, Z., Yu, C., Zhou, X., et al. (2019). Intradiscal injection of induced pluripotent stem cell-derived nucleus pulposus-like cell-seeded polymeric microspheres promotes rat disc regeneration. *Stem Cells Int.* 2019:6806540.

Xing, Q. J., Liang, Q. Q., Bian, Q., Ding, D. F., Cui, X. J., Shi, Q., et al. (1976). Leg amputation accelerates senescence of rat lumbar intervertebral discs. *Spine (Phila Pa 1976)* 35, E1253–E1261.

Xu, H., Sun, M., Wang, C., Xia, K., Xiao, S., Wang, Y., et al. (2020). GDF5-GelMA injectable microspheres laden with adipose-derived stem cells for disc degeneration repair. *Biofabrication* [Epub ahead of print].

Xu, H., Wang, B., Ono, M., Kagita, A., Fujii, K., Sasakawa, N., et al. (2019). Targeted Disruption of HLA Genes via CRISPR-Cas9 Generates iPSCs with Enhanced Immune Compatibility. *Cell Stem Cell* 24, 566–578.e7.

Yang, Q., Peng, J., Guo, Q., Huang, J., Zhang, L., Yao, J., et al. (2008). A cartilage ECM-derived 3-D porous acellular matrix scaffold for in vivo cartilage tissue engineering with PKH26-labeled chondrogenic bone marrow-derived mesenchymal stem cells. *Biomaterials* 29, 2378–2387. doi: 10.1016/j.biomaterials.2008.01.037

Ye, S., Ju, B., Wang, H., and Lee, K. B. (2016). Bone morphogenetic protein-2 provokes interleukin-18-induced human intervertebral disc degeneration. *Bone Joint Res.* 5, 412–418. doi: 10.1302/2046-3758.59.bjr-2016-0032.r1

Ying, J., Han, Z., Pei, S., Su, L., and Ruan, D. (2019). Effects of stromal cell-derived factor-1α secreted in degenerative intervertebral disc on activation and recruitment of nucleus pulposus-derived stem cells. *Stem Cells Int.* 2019:9147835.

Yu, C., Li, D., Wang, C., Xia, K., Wang, J., Zhou, X., et al. (2021). Injectable kartogenin and apocynin loaded micelle enhances the alleviation of intervertebral disc degeneration by adipose-derived stem cell. *Bioact. Mater.* 6, 3568–3579. doi: 10.1016/j.bioactmat.2021.03.018

Yurube, T., Takada, T., Suzuki, T., Kakutani, K., Maeno, K., Doita, M., et al. (2012). Rat tail static compression model mimics extracellular matrix metabolic imbalances of matrix metalloproteinases, aggrecanases, and tissue inhibitors of metalloproteinases in intervertebral disc degeneration. *Arthritis Res. Ther.* 14:R51.

Zhang, H., Yu, S., Zhao, X., Mao, Z., and Gao, C. (2018). Stromal cell-derived factor-1α-encapsulated albumin/heparin nanoparticles for induced stem cell migration and intervertebral disc regeneration in vivo. *Acta Biomater.* 72, 217–227. doi: 10.1016/j.actbio.2018.03.032

Zhang, J. F., Wang, G. L., Zhou, Z. J., Fang, X. Q., Chen, S., and Fan, S. W. (2018). Expression of matrix metalloproteinases, tissue inhibitors of metalloproteinases, and interleukins in vertebral cartilage endplate. *Orthop. Surg.* 10, 306–311. doi: 10.1111/os.12409

Zhang, Y., An, H. S., Thonar, E. J., Chubinskaya, S., He, T. C., and Phillips, F. M. (2006). Comparative effects of bone morphogenetic proteins and sox9

overexpression on extracellular matrix metabolism of bovine nucleus pulposus cells. *Spine (Phila Pa 1976)* 31, 2173–2179. doi: 10.1097/01.brs.0000232792.66632.d8

Zhao, L., Manchikanti, L., Kaye, A. D., and Abd-Elsayed, A. (2019). Treatment of discogenic low back pain: current treatment strategies and future options-a literature review. *Curr. Pain Headache Rep.* 23: 86.

Zhou, Z., Zeiter, S., Schmid, T., Sakai, D., Iatridis, J. C., Zhou, G., et al. (2020). Effect of the CCL5-releasing fibrin gel for intervertebral disc regeneration. *Cartilage* 11, 169–180. doi: 10.1177/1947603518764263

Zhu, G., Yang, X., Peng, C., Yu, L., and Hao, Y. (2020). Exosomal miR-532-5p from bone marrow mesenchymal stem cells reduce intervertebral disc degeneration by targeting RASSF5. *Exp. Cell Res.* 393:112109. doi: 10.1016/j.yexcr.2020.112109

Conflict of Interest: The authors declare that the research was conducted in the absence of any commercial or financial relationships that could be construed as a potential conflict of interest.

Advantages of publishing in Frontiers

OPEN ACCESS
Articles are free to read for greatest visibility and readership

FAST PUBLICATION
Around 90 days from submission to decision

HIGH QUALITY PEER-REVIEW
Rigorous, collaborative, and constructive peer-review

TRANSPARENT PEER-REVIEW
Editors and reviewers acknowledged by name on published articles

Frontiers
Avenue du Tribunal-Fédéral 34
1005 Lausanne | Switzerland

Visit us: www.frontiersin.org
Contact us: frontiersin.org/about/contact

REPRODUCIBILITY OF RESEARCH
Support open data and methods to enhance research reproducibility

DIGITAL PUBLISHING
Articles designed for optimal readership across devices

FOLLOW US
@frontiersin

IMPACT METRICS
Advanced article metrics track visibility across digital media

EXTENSIVE PROMOTION
Marketing and promotion of impactful research

LOOP RESEARCH NETWORK
Our network increases your article's readership